THE UNIVERSITY OF CALGARY

Equalizer Structures for Spread Spectrum Multiuser Systems

by

Ramon Schlagenhaufer

A THESIS

SUBMITTED TO THE FACULTY OF GRADUATE STUDIES

IN PARTIAL FULFILMENT OF THE REQUIREMENTS FOR THE

DEGREE OF DOCTOR OF PHILOSOPHY

DEPARTMENT OF ELECTRICAL AND COMPUTER ENGINEERING

CALGARY, ALBERTA

APRIL, 2001

THE UNIVERSITY OF CALGARY
FACULTY OF GRADUATE STUDIES

The undersigned certify that they have read, and recommend to the Faculty of Graduate Studies for acceptance, a thesis entitled "Equalizer Structures for Spread Spectrum Multiuser Systems" submitted by Ramon Schlagenhaufer in partial fulfilment of the requirements for the degree of Doctor of Philosophy.

Supervisor, Dr. A. B. Sesay
Department of Electrical and Computer Engineering

Co-supervisor, Dr. B. R. Petersen
University of New Brunswick

Dr. M. Fattouche
Department of Electrical and Computer Engineering

Dr. R. J. Davies
Department of Electrical and Computer Engineering

Dr. K.-P. Schwarz
Department of Geomatics Engineering

External Reader, Dr. S. D. Blostein
Queen's University at Kingston

Date

Abstract

The topic of this dissertation is a digital multiuser communications system whose structure is identical to a single cell of a typical cellular telephone system. It consists of several spatially distributed portables (users) which communicate simultaneously with a central base station. The general objective is to investigate and improve the central receiver which detects the signals of all in-cell portables.

In order to support several users, a multiple access scheme combining frequency diversity (SSMA – spread spectrum multiple access) with receive antenna diversity (SDMA – space division multiple access) is considered. The system is designed for high data rates, frequency selective and quasi-stationary radio channels.

A vector model of the system is developed, which incorporates frequency diversity as well as multiple receive antennas. In addition to simplifying the mathematical analysis, it provides precious insight into the behavior of the system.

A new approach to approximate and bound the error probability in linear systems is described, which is accurate, numerically very efficient and easy to use. The results show that it compares very well with the existing state-of-the-art approximations.

Promising detectors for multiuser systems are numerically efficient and take the signals of *all* users into account for the estimation process. One of the candidates strongly considered for a practical implementation in future systems is the equalizer family with multiple inputs (from multiple receive antennas) and multiple outputs (one for the signal of each user). This detector type is analyzed here. Although significantly less complex than the optimum detectors, multiple-input multiple-output (MIMO) equalizers require a total number of operations which is too heavy a burden

for present systems. For that reason, numerically more efficient approaches for the optimization of the equalizer coefficients are considered.

In addition, an extension of the standard MIMO equalizer with decision feedback is analyzed. This detector addresses the special situation of cellular systems in which the received signal strengths differ significantly. It is shown that the inclusion of simple delay elements may strongly reduce the requirements for power control, a technique that adds considerable complexity but is crucial to current cellular systems.

Acknowledgements

moments of this journey made it so much easier.

Table of Contents

List of Tables

List of Figures

List of Abbreviations

Abbreviation	Meaning
ACI	adjacent channel interference
AMPS	Advanced Mobile Phone System
AWGN	additive white Gaussian noise
BER	bit error rate
BPSK	binary phase shift keying
C-DDFE	conventional delayed-decision-feedback equalizer
C-DFE	conventional decision-feedback equalizer
cdf	complementary distribution function
CDMA	code-division multiple access
CIR	channel impulse response
CCI	co-channel interference
CTF	channel transfer function
dB	decibel
DDFE	delayed-decision-feedback equalizer
DFE	decision-feedback equalizer
DFS	discrete Fourier series
DS-CDMA	direct sequence code-division multiple access
DTFT	discrete-time Fourier transform
EDGE	Enhanced Data Rates for Global Evolution

Abbreviation	Meaning
FDMA	frequency-division multiple access
FF	forward filter
FFT	fast Fourier transform
FIR	finite impulse response
FS	Fourier series
FT	Fourier transform
GSM	Global System for Mobile Communication
Hz	Hertz
IC	interference canceller
IFFT	inverse fast Fourier transform
IIR	infinite impulse response
INR	interference-to-noise ratio
ISI	intersymbol interference
LE	linear equalizer
LMS	least mean square
LSSE	least sum of square errors
MAI	multiple access interference
MFB	matched filter bound
MIMO	multiple-input multiple-output
MLSE	maximum likelihood sequence estimation
MMSE	minimum mean-square error
MSE	mean-square error
NP-DDFE	noise-predictive delayed-decision-feedback equalizer
NP-DFE	noise-predictive decision-feedback equalizer
op	operations
PAM	pulse amplitude modulation

Abbreviation	Meaning
pdf	probability density function
PN	pseudo-random noise
PSD	power spectral density
PSK	phase shift keying
QAM	quadrature amplitude modulation
RLS	recursive least square
RMS	root mean square
ROS	region of support
RV	random variable
s	seconds
S-DFE	successive decision-feedback equalizer
SC-DFE	successive conventional decision-feedback equalizer
SINR	signal-to-interference-and-noise ratio
SISO	single-input single-output
SNR	signal-to-noise ratio
SSMA	spread spectrum multiple access
SVD	singular value decomposition
TDMA	time-division multiple access
WCDMA	wide-band CDMA
ZF	zero-forcing

List of Mathematical Symbols

Latin Symbols

Symbol	Meaning	Page	Reference
A	number of receive antennas	55	
$\mathcal{A}_i$	finite alphabet of complex numbers containing all possible data symbols of user i	60	
$\boldsymbol{a}$	$1 \times N$ data input signal vector	76	Eqn. (2.50)
$\tilde{\boldsymbol{a}}$	$1 \times N$ continuous-valued data estimate at the input to the decision device	137	Fig. 4.1
$\hat{\boldsymbol{a}}$	$1 \times N$ final quantized data estimate	137	Fig. 4.1
$\breve{\boldsymbol{a}}$	$1 \times N$ linear data estimate at the output of the MIMO forward filter	137	Fig. 4.1
a_i	data sequence transmitted by user i	60	
a_i^{im}	imaginary part of a_i	61	Eqn. (2.5)
a_i^{re}	real part of a_i	61	Eqn. (2.5)
$\tilde{a}_k$	continuous-valued data estimate for user k at the input of the decision device	87	Eqn. (3.5)
$\tilde{a}_k^{\text{im}}$	imaginary part of the input signal $\tilde{a}_k$ to the k-th decision element	88	Eqn. (3.7)

Symbol	Meaning	Page	Reference
$\tilde{a}_k^{\mathrm{re}}$	real part of the input signal $\tilde{a}_k$ to the k-th decision element	88	Eqn. (3.7)
$\hat{a}_k$	k-th component of $\hat{\boldsymbol{a}}$		
$\breve{a}_k$	k-th component of $\breve{\boldsymbol{a}}$		
B	double-sided Nyquist bandwidth	10	
B_C	transfer function of the lowpass filter at the output of each receive antenna	70	
B_h	double-sided bandwidth of the radio channel impulse responses	67	Eqn. (2.19)
B_s	3 dB double-sided signal bandwidth	64	Tab. 2.1
B_T	minimally required double-sided bandwidth to transmit a discrete-time signal with a symbol period of T [s] over a continuous-time channel (according to the Nyquist criterion)	81	
$\boldsymbol{B}$	$N \times N$ feedback filter of the MIMO DFE		
$\boldsymbol{B}_{\mathrm{mmse}}$	optimal feedback filter of the MIMO DFE with respect to the MMSE criterion	162	Eqn. (4.56)
$\boldsymbol{B}_{\mathrm{c,mmse}}$	optimal feedback matrix filter of the MMSE MIMO C-DFE	165	Eqn. (4.63)
$\boldsymbol{B}_{\mathrm{c,zf}}$	optimal feedback matrix filter of the ZF MIMO C-DFE	178	Eqn. (4.111)
$\boldsymbol{B}_{\mathrm{c\Delta}}$	$N \times N$ causal feedback filter of the MIMO C-DDFE	221	Fig. 5.7
$\boldsymbol{B}_{\mathrm{np,mmse}}$	optimal feedback matrix filter of the MMSE MIMO NP-DFE	176	Eqn. (4.106)

Symbol	Meaning	Page	Reference
$\boldsymbol{B}_{\mathrm{np,zf}}$	optimal feedback matrix filter of the ZF MIMO NP-DFE	178	Eqn. (4.114)
$\boldsymbol{B}_{\mathrm{np}\Delta}$	feedback matrix filter of the MIMO NP-DDFE	225	
$\bar{\boldsymbol{B}}_{\mathrm{np}\Delta}$	extended feedback filter matrix	229	Eqn. (5.36)
$\bar{\boldsymbol{B}}_{\mathrm{np}\Delta,\mathrm{mmse}}$	optimal value of $\bar{\boldsymbol{B}}_{\mathrm{np}\Delta}$ for the MMSE MIMO NP-DDFE	230	Eqn. (5.45)
$\boldsymbol{B}_{\mathrm{sc0}}$	optimal feedback matrix filter of the MMSE MIMO SC-DFE (without feedback of the currently detected signal)	239	Eqn. (5.87)
$\boldsymbol{B}_{\mathrm{sc+}}$	optimal feedback matrix filter of the MMSE MIMO SC-DFE (including feedback of the currently detected signal)	241	Eqn. (5.101)
b_C	impulse response of the continuous-time lowpass filter at the output of each receive antenna	69	Fig. 2.8
b_{ik}	(i,k)-th component of the decision-feedback matrix filter $\boldsymbol{B}$	180	Eqn. (4.120)
b_{ik}^{im}	imaginary part of b_{ik}	88	Eqn. (3.9)
b_{ik}^{re}	real part of b_{ik}	88	Eqn. (3.9)
b_k	maximum number of bits that user k can transmit while still maintaining a bit error rate (BER) of less than P_b	184	
$\boldsymbol{b}_k^H$	$L_k \times 1$ subvector of the matrix $\bar{\boldsymbol{B}}_{\mathrm{np}\Delta}$	229	Eqn. (5.38)
$\boldsymbol{b}_{k,\mathrm{mmse}}^H$	optimal value of $\boldsymbol{b}_k^H$ for the MMSE MIMO NP-DDFE	230	Eqn. (5.44)

Symbol	Meaning	Page	Reference
$\boldsymbol{C}_{\mathrm{np\Delta}}$	forward matrix filter of the MIMO NP-DDFE	225	Eqn. (5.26)
$\mathbb{C}$	set of all complex numbers	291	Tab. A.7
$c_{a,ik}[m]$	cross-covariance of the data sequences $a_i[n]$ and $a_k[n]$	60	Eqn. (2.3)
c_{mp}	(m,p)-th element of the equalizer forward matrix filter $\boldsymbol{C}$	140	Fig. 4.2
c_n	n-th coefficient of the Taylor series expansion of $\ln Q(x)$	103	Eqn. (3.88)
$c_{\nu,lm}(t,\tau)$	cross-covariance of the noise signals $\nu_{CGl}(t)$ and $\nu_{CGm}(t)$	63	Eqn. (2.13)
$\cos(\dots)$	cosine function	284	Tab. A.3
$\cosh(\dots)$	hyperbolic cosine	284	Tab. A.3
$\cot(\dots)$	cotangent	284	Tab. A.3
$\coth(\dots)$	hyperbolic cotangent	284	Tab. A.3
D	dummy complex variable describing the parameter of the D-transform (everywhere except Chapter 3)	49	
D	relative peak distortion (only Chapter 3)	120	Eqn. (3.138)
$\mathcal{D}\{\dots\}$	D-transform of $\dots$	49	Eqn. (1.18)
$\mathcal{D}^{-1}\{\dots\}$	inverse D-transform of $\dots$	49	Eqn. (1.19)
d	decision order function	214	
d_k	interfering, normalized data symbol ($k \neq 0$)	101	Eqn. (3.77)
d_0	normalized data symbol to be estimated	101	Eqn. (3.79)
$\det\{\dots\}$	determinant of the matrix $\dots$	284	Tab. A.3

Symbol	Meaning	Page	Reference
$\mathbf{D}\mathrm{iag}\langle\ldots\rangle$	diagonal hypermatrix	284	Tab. A.3
$E[\ldots]$	statistical expectation	284	Tab. A.3
$E_M[\ldots]$	statistical cross-power spectrum	51	Def. 1.3
$\mathcal{E}_{a,i}^{\mathrm{im}}$	variance of the quadrature PAM data signal of user i	62	Eqn. (2.11)
$\mathcal{E}_{a,i}^{\mathrm{re}}$	variance of the inphase PAM data signal of user i	62	Eqn. (2.10)
$\mathcal{E}_{\mathrm{IN},k}$	distortion energy in the data estimate $\tilde{a}_k$	98	Eqn. (3.68)
$\mathcal{E}_{\mathrm{IN},k}^{\mathrm{im}}$	distortion energy in $\tilde{a}_k^{\mathrm{im}}$	95	Eqn. (3.52)
$\mathcal{E}_{\mathrm{IN},k}^{\mathrm{re}}$	distortion energy in $\tilde{a}_k^{\mathrm{re}}$	95	Eqn. (3.51)
$\mathcal{E}_{\mathrm{S},k}$	signal energy in the data estimate $\tilde{a}_k$	98	Eqn. (3.67)
$\mathcal{E}_{\mathrm{S},k}^{\mathrm{im}}$	signal energy in $\tilde{a}_k^{\mathrm{im}}$	94	Eqn. (3.50)
$\mathcal{E}_{\mathrm{S},k}^{\mathrm{re}}$	signal energy in $\tilde{a}_k^{\mathrm{re}}$	94	Eqn. (3.49)
$\mathcal{E}_{z,M}$	combined energy of the small interference components	107	Eqn. (3.98)
$\mathcal{E}_{z,0}$	interference-to-noise ratio (INR) of the decision variable	110	Eqn. (3.112)
$\mathcal{E}_{\alpha,i}$	variance of the data symbols α_i	92	Eqn. (3.39)
$\mathcal{E}_{\zeta}$	variance of the Gaussian noise random variable ζ_0	92	Eqn. (3.41)
$\mathcal{E}_{\zeta,k}$	variance of the complex noise component ζ_k in the linear data estimate of user k	90	Eqn. (3.22)
$\mathcal{E}_{\zeta,k}^{\mathrm{im}}$	variance of the imaginary part of ζ_k	90	Eqn. (3.24)
$\mathcal{E}_{\zeta,k}^{\mathrm{re}}$	variance of the real part of ζ_k	90	Eqn. (3.23)
e	constant ($e \triangleq 2.7182\ldots$, $\ln\{e\} = 1$)	291	Tab. A.7

Symbol	Meaning	Page	Reference
$\boldsymbol{e}$	$1 \times N$ estimation error at the input to the decision device	137	Fig. 4.1
$\tilde{\boldsymbol{e}}$	$1 \times N$ estimate of the error signal $\breve{\boldsymbol{e}}$ obtained from the feedback filter	137	Fig. 4.1
$\hat{\boldsymbol{e}}$	$1 \times N$ approximation of the estimation error $\breve{\boldsymbol{e}}$	172	Eqn. (4.81)
$\breve{\boldsymbol{e}}$	$1 \times N$ estimation error at the output of the MIMO forward filter	137	Fig. 4.1
e_k	k-th component of $\boldsymbol{e}$	137	Eqn. (4.3)
$\tilde{e}_k$	k-th component of $\tilde{\boldsymbol{e}}$		
$\hat{e}_k$	k-th component of $\hat{\boldsymbol{e}}$		
$\breve{e}_k$	k-th component of $\breve{\boldsymbol{e}}$	137	Eqn. (4.4)
$\exp\{\dots\}$	exponent with base e	284	Tab. A.3
$F_1(z_0)$	general first-order upper bound on the threshold probability	107	Eqn. (3.99)
$\mathcal{F}_{cc}\{\dots\}$	Fourier transform (FT) of ...	293	Tab. A.9
$\mathcal{F}_{cc}^{-1}\{\dots\}$	inverse Fourier transform of ...	293	Tab. A.9
$\mathcal{F}_{cd}\{\dots\}$	Fourier series (FS) of ...	293	Tab. A.9
$\mathcal{F}_{cd}^{-1}\{\dots\}$	inverse Fourier series of ...	293	Tab. A.9
$\mathcal{F}_{dc}\{\dots\}$	discrete-time Fourier transform (DTFT) of ...	293	Tab. A.9
$\mathcal{F}_{dc}^{-1}\{\dots\}$	inverse discrete-time Fourier transform of ...	293	Tab. A.9
$\mathcal{F}_{dd}\{\dots\}$	discrete Fourier series (DFS) of ...	293	Tab. A.9
$\mathcal{F}_{dd}^{-1}\{\dots\}$	inverse discrete Fourier series of ...	293	Tab. A.9

Symbol	Meaning	Page	Reference
f	dummy variable describing frequency ($f \in \mathbb{R}$, unit: Hz)		
f_{car}	carrier frequency	305	
f_k	normalized channel weight for the interfering data symbol d_k, $k \neq 0$ (only Chapter 3)	101	Eqn. (3.76)
f_{max}	frequency above which all signal components vanish for all practical purposes	303	
f_0	normalized channel weight for the desired data symbol d_0 (only Chapter 3)	101	Eqn. (3.78)
f_{3dB}	3 dB cut-off frequency	302	
$\check{f}$	normalized frequency (with respect to T)	139	Eqn. (4.9)
$\check{f}_c$	normalized frequency (with respect to T_c)	68	Eqn. (2.26)
$\check{f}_s$	normalized frequency (with respect to T_s)	292	Eqn. (A.16)
$\boldsymbol{G}$	constant diagonal matrix obtained in the matrix spectral factorization of $\boldsymbol{Q}$	164	Eqn. (4.61)
$\boldsymbol{G}_{\mathrm{zf}}$	constant diagonal matrix obtained in the matrix spectral factorization of $\boldsymbol{S}_x$	177	Eqn. (4.108)
$\boldsymbol{G}_\Delta$	constant diagonal matrix obtained in the matrix spectral factorization of $\boldsymbol{Q}_\Delta$	223	Eqn. (5.20)
$g(z_0)$	special function	107	Eqn. (3.101)
$\boldsymbol{H}$	$N \times N$ linear matrix filter representing the total system part between the original data signal and the input to decision elements	86	Eqn. (3.1)
$\ldots^{H}$	conjugate transposition	284	Tab. A.3
$\ldots^{-H}$	inverse conjugate transpose	284	Tab. A.3

Symbol	Meaning	Page	Reference
H_{Cil}	transfer function of the radio channel between user i and receive antenna l of the base station	66	
$\check{H}_{Cil}$	discrete-time Fourier transform of the discrete-time radio channel impulse response h_{il}	68	
H_{il}	discrete Fourier series of the discrete-time radio channel impulse response h_{il}	68	
h	continuous-time pulse waveform representing the total impulse response between data input and final receiver output before the decision device	118	
h_{Cil}	impulse response of the radio channel between user i and receive antenna l of the base station	55	Fig. 2.2
h_i	channel weight for the interfering data symbol α_i, $i \neq 0$ (only Chapter 3)	92	Eqn. (3.38)
h_{ik}	(i, k)-th component of the matrix filter $\boldsymbol{H}$ (everywhere except for Chapter 2)	180	Eqn. (4.119)
h_{ik}^{im}	imaginary part of h_{ik} (everywhere except for Chapter 2)	88	Eqn. (3.8)
h_{ik}^{re}	real part of h_{ik} (everywhere except for Chapter 2)	88	Eqn. (3.8)
h_{il}	discrete-time sequence approximating the continuous-time radio channel impulse response h_{Cil} (only Chapter 2)	67	Eqn. (2.24)

Symbol	Meaning	Page	Reference
$h_{kk}^{\mathrm{re}}[0]$	bias coefficient for user k (everywhere except for Chapter 2)	89	
h_0	channel weight for the desired data symbol α_0 (only Chapter 3)	92	Eqn. (3.38)
Hz	physical unit 'Hertz': $\mathrm{Hz} \triangleq 1/s$		
[Hz]	indicating that the unit of the preceding quantity is 'Hertz' (Hz)		
$\boldsymbol{I}_N$	$N \times N$ identity matrix	291	Tab. A.7
$\mathcal{I}_A$	set of all integer numbers between and including 1 and A	291	Tab. A.7
$\mathcal{I}_K$	set of all integer numbers between and including 1 and K	291	Tab. A.7
$\mathcal{I}_N$	set of all integer numbers between and including 1 and N	291	Tab. A.7
$\mathcal{I}_M$	set of all integer numbers between and including 1 and M	291	Tab. A.7
$\Im\{\dots\}$	imaginary part of ...	284	Tab. A.3
i	dummy variable ($i \in \mathbb{Z}$)		
J_k	mean-square error (MSE) in the data estimate $\tilde{a}_k$ for the k-th user	139	Eqn. (4.10)
$J_{k,\mathrm{c,mmse}}$	MMSE of the k-th user's signal estimate for the MMSE MIMO C-DFE	166	Eqn. (4.65)
$J_{k,\mathrm{c}\Delta}$	MMSE of the k-th user's signal estimate for the MMSE MIMO C-DDFE	224	Eqn. (5.24)
$J_{k,\mathrm{dfe,zf}}$	MMSE of the k-th user's signal estimate for the ZF MIMO C-DFE and NP-DFE	178	Eqn. (4.115)

Symbol	Meaning	Page	Reference
$J_{k,\mathrm{le,mmse}}$	MMSE of the k-th user's signal estimate for the MMSE MIMO LE	144	Eqn. (4.23)
$J_{k,\mathrm{mfb}}$	matched filter bound MMSE	315	Eqn. (D.8)
$J_{k,\mathrm{mmse}}$	MMSE of the k-th user's signal estimate for optimal MMSE equalizer filters	182	
$J_{k,\mathrm{np}\Delta}$	MMSE of the k-th user's signal estimate for the MMSE MIMO NP-DDFE	230	Eqn. (5.41)
$J_{k,\mathrm{sc0}}$	MMSE of the k-th user's signal estimate for the optimal MMSE MIMO SC-DFE (without feedback of the k-th signal)	239	Eqn. (5.90)
$J_{k,\mathrm{sc+}}$	MMSE of the k-th user's signal estimate for the optimal MMSE MIMO SC-DFE (including feedback of the k-th signal)	241	Eqn. (5.103)
$J_{k,\mathrm{zf}}$	MSE of the k-th user's signal estimate for optimal ZF equalizer filters		
$\bar{J}$	algebraic average of the MMSE over all N users	156	Eqn. (4.47)
$\bar{J}_\Pi$	geometric average of the MMSE over all N users	166	Eqn. (4.66)
j	imaginary unit (square root of "-1")	291	Tab. A.7
K	processing gain (spreading factor)	55	
K_{3dB}	3 dB normalized system bandwidth, $K_{\mathrm{3dB}} = B_s T = 2 f_{\mathrm{3dB}} T$	64	Tab. 2.1
k	dummy integer variable ($k \in \mathbb{N}$)		

Symbol	Meaning	Page	Reference
L_c	number of necessary samples to approximate accurately the continuous-time radio channel impulse responses by a discrete-time model	67	Eqn. (2.22)
L_i	number of PAM levels for the inphase and quadrature data signal of user i provided that the modulation scheme is square QAM	97	Eqn. (3.62)
L_i^{im}	number of PAM levels for the quadrature data signal of user i	61	
L_i^{re}	number of PAM levels for the inphase data signal of user i	61	
L_k	vector length (only Chapter 5)	229	Eqn. (5.39)
$\boldsymbol{L}$	$N \times N$ matrix filter; one part of the equalizer forward filter $\boldsymbol{C}$		
$\boldsymbol{L}_{\mathrm{c,mmse}}$	optimal matrix filter for the MMSE MIMO C-DFE	165	Eqn. (4.62)
$\boldsymbol{L}_{\mathrm{c,zf}}$	optimal matrix filter for the ZF MIMO C-DFE	178	Eqn. (4.110)
$\boldsymbol{L}_{\mathrm{c\Delta}}$	$N \times N$ forward filter of the MIMO C-DDFE	221	Fig. 5.7
$\boldsymbol{L}_{\mathrm{le,mmse}}$	optimal matrix filter for the MMSE MIMO LE	143	Eqn. (4.17)
$\boldsymbol{L}_{\mathrm{le,zf}}$	optimal matrix filter for the ZF MIMO LE	158	Eqn. (4.52)
$\boldsymbol{L}_{\mathrm{np,mmse}}$	optimal matrix filter for the MMSE MIMO NP-DFE	175	Eqn. (4.104)
$\boldsymbol{L}_{\mathrm{np,zf}}$	optimal matrix filter for the ZF MIMO NP-DFE	178	Eqn. (4.113)

Symbol	Meaning	Page	Reference
$\boldsymbol{L}_{\mathrm{np}\Delta}$	$N \times N$ filter of the MIMO NP-DDFE	225	Eqn. (5.26)
$\boldsymbol{L}_{\mathrm{sc0}}$	optimal matrix filter of the MMSE MIMO SC-DFE (without feedback of the currently detected signal)	239	Eqn. (5.88)
$\boldsymbol{L}_{\mathrm{sc+}}$	optimal matrix filter of the MMSE MIMO SC-DFE (including feedback of the currently detected signal)	241	Eqn. (5.102)
l	dummy integer variable ($l \in \mathbb{N}$)		
$\log_r\{\dots\}$	logarithm to the base r	284	Tab. A.3
$\ln\{\dots\}$	natural logarithm	284	Tab. A.3
M	number of interfering symbols with a large contribution to the decision variable (only Chapter 3)	106	
M_C	length of the finite equalizer's forward filter in samples	150	
M_B	length of the finite equalizer's feedback filter in samples	228	
M_i	number of nonzero samples in the impulse response of user i's spreading filter $q_i[n]$	64	
m	dummy integer variable ($m \in \mathbb{Z}$)		
N	number of users	54	
N_h	number of selected nonzero interference samples	118	
N_0	double-sided power spectral density of the white, complex noise	63	

Symbol	Meaning	Page	Reference
$N_{0,l}$	double-sided power spectral density of the white, complex noise added to receive antenna l	314	
$\mathbb{N}$	set of all positive integer numbers	291	Tab. A.7
$\mathbb{N}_0$	set of all nonnegative integer numbers	291	Tab. A.7
n	dummy integer variable ($n \in \mathbb{N}$)		
$\boldsymbol{O}_{N \times M}$	$N \times M$ null matrix	291	Tab. A.7
P_b	bit error rate (BER) for the desired user	93	Eqn. (3.44)
$P_{b,k}$	bit error rate (BER) for the received signal of user k provided that the modulation scheme is square QAM	90	Eqn. (3.21)
$P_{b,k}^{\mathrm{im}}$	bit error rate (BER) for the quadrature component of the received signal of user k	96	
$P_{b,k}^{\mathrm{re}}$	bit error rate (BER) for the inphase component of the received signal of user k	96	
$P_{b,k}^{(\mathrm{mfb})}$	matched filter bound BER for the received signal of user k provided that the modulation scheme is square QAM	317	Eqn. (D.13)
P_C	transfer function of the waveform produced by the transmitter pulse generators	302	
P_{ex}	probability of exceeding one decision threshold for the desired user (threshold probability)	93	Eqn. (3.43)
$\tilde{P}_{\mathrm{ex}}$	estimate of the threshold probability P_{ex}		

Symbol	Meaning	Page	Reference
$P_{\mathrm{ex},k}$	probability of exceeding one decision threshold for the inphase or quadrature signal of user k provided that the modulation scheme is square QAM	90	
$P_{\mathrm{ex},k}^{\mathrm{im}}$	probability of exceeding one decision threshold for the quadrature signal of user k	89	Eqn. (3.20)
$P_{\mathrm{ex},k}^{\mathrm{re}}$	probability of exceeding one decision threshold for the inphase signal of user k	89	Eqn. (3.18)
$P_{\mathrm{ex}}^{\mathrm{(mfb)}}$	matched filter bound probability of exceeding one decision threshold for square QAM	317	Eqn. (D.12)
$P_{\mathrm{ex},k,\mathrm{zf}}$	exact threshold probability for the k-th signal estimate of a ZF equalizer	183	Eqn. (4.134)
P_{out}	outage probability	201	
$\hat{P}_{\mathrm{out}}$	estimate of the outage probability	201	Eqn. (4.145)
$\tilde{P}_{\mathrm{ex},k}^{\mathrm{(Gauss)}}$	Gaussian approximation of the threshold probability for the k-th signal estimate of a MMSE equalizer	183	Eqn. (4.133)
$\tilde{P}_{\mathrm{ex},k}^{\mathrm{(Saltz)}}$	Saltzberg upper bound of the threshold probability for the k-th signal estimate of a MMSE equalizer	183	Eqn. (4.132)
$\tilde{P}_{\mathrm{Gauss}}$	Gaussian approximation of the threshold probability	115	Eqn. (3.129)
$\tilde{P}_{\mathrm{Saltz}}$	Saltzberg upper bound of the threshold probability	115	Eqn. (3.131)
$\boldsymbol{P}$	constant diagonal matrix obtained by the spectral factorization of $\boldsymbol{V}^{-1}$	240	Eqn. (5.95)

Symbol	Meaning	Page	Reference
p_C	waveform of the transmitter pulse generators	64	Fig. 2.6
$\text{Prob}\{\dots\}$	probability that the expression in the brackets is satisfied		
$Q(\dots)$	Q-function	284	Tab. A.3
$\boldsymbol{Q}$	$N \times N$ matrix function	143	Eqn. (4.18)
$\boldsymbol{Q}_\Delta$	delay transform of the matrix spectrum $\boldsymbol{Q}$	223	Eqn. (5.18)
$\mathbb{Q}$	set of all rational numbers	291	Tab. A.7
q_i	impulse response of the discrete-time spreading filter of transmitter i	64	Fig. 2.5
$\boldsymbol{R}_a$	$N \times N$ autocorrelation of the data input signal $\boldsymbol{a}$	79	Eqn. (2.64)
$\boldsymbol{R}_{ae}$	$N \times N$ cross-correlation of the vector signals $\boldsymbol{a}$ and $\boldsymbol{e}$	234	Eqn. (5.60)
$\boldsymbol{R}_{a\nu}$	$N \times AK$ cross-correlation of the data input signal $\boldsymbol{a}$ and the noise signal $\boldsymbol{\nu}$	79	Eqn. (2.66)
$\boldsymbol{R}_e$	$N \times N$ autocorrelation of the estimation error $\boldsymbol{e}$	138	Eqn. (4.5)
$\boldsymbol{R}_{\breve{e}}$	$N \times N$ autocorrelation of the estimation error $\breve{\boldsymbol{e}}$	232	
$\boldsymbol{R}_{\breve{e}e}$	cross-correlation of the vector signals $\breve{\boldsymbol{e}}$ and $\boldsymbol{e}$	173	Eqn. (4.89)
$\boldsymbol{R}_{ue}$	$N \times N$ cross-correlation of the vector signals $\boldsymbol{u}$ and $\boldsymbol{e}$	234	Eqn. (5.59)
$\boldsymbol{R}_{uv}$	cross-correlation of the vector functions $\boldsymbol{u}$ and $\boldsymbol{v}$	52	Eqn. (1.30)

Symbol	Meaning	Page	Reference
$\boldsymbol{R}_y$	autocorrelation of the equalizer input signal $\boldsymbol{y}$		
$\boldsymbol{R}_{ya}$	cross-correlation between the equalizer input signal $\boldsymbol{y}$ and the transmitted data $\boldsymbol{a}$		
$\boldsymbol{R}_{ye}$	cross-correlation of the vector signals $\boldsymbol{y}$ and $\boldsymbol{e}$	173	Eqn. (4.88)
$\boldsymbol{R}_{\breve{\varepsilon}}$	autocorrelation matrix sequence of the vector signal $\breve{\boldsymbol{\varepsilon}}$	231	Eqn. (5.50)
$\boldsymbol{R}_{\epsilon}$	autocorrelation matrix of the vector $\boldsymbol{\epsilon}$	231	Eqn. (5.49)
$\boldsymbol{R}_{\epsilon,k}$	$L_k \times L_k$ autocorrelation matrix of the signal $\boldsymbol{\epsilon}_k$	230	Eqn. (5.43)
$\boldsymbol{R}_{\nu}$	$AK \times AK$ autocorrelation of the noise signal $\boldsymbol{\nu}$	79	Eqn. (2.65)
$\mathbb{R}$	set of all real numbers	291	Tab. A.7
$\mathbb{R}^+$	set of all positive real numbers	291	Tab. A.7
r_{Cl}	complex baseband signal received at base antenna l	69	Eqn. (2.29)
$r_{\breve{\varepsilon},ik}$	(i,k)-th element of the matrix $\boldsymbol{R}_{\breve{\varepsilon}}[m]$	232	Eqn. (5.54)
$\boldsymbol{r}_{\breve{\varepsilon}\epsilon,k}^H$	$L_k \times 1$ crosscorrelation vector of the signals $\boldsymbol{\epsilon}_k$ and $\breve{\varepsilon}_k$	230	Eqn. (5.42)
$\Re\{\dots\}$	real part of …	284	Tab. A.3
SNR_k	output SNR of a maximal ratio combiner for user k for an interference-free system	314	Eqn. (D.2)
$\boldsymbol{S}_a$	$N \times N$ power spectrum of the data input signal $\boldsymbol{a}$	79	Eqn. (2.61)
$\boldsymbol{S}_{ae}$	$N \times N$ cross-power spectrum of the vector signals $\boldsymbol{a}$ and $\boldsymbol{e}$	234	Eqn. (5.62)

Symbol	Meaning	Page	Reference
$\boldsymbol{S}_{az}$	$N \times N$ cross-power spectrum of the vector signals $\boldsymbol{a}$ and $\boldsymbol{z}$	235	Eqn. (5.72)
$\boldsymbol{S}_{a\nu}$	$N \times AK$ cross-power spectrum of the data input signal $\boldsymbol{a}$ and the noise signal $\boldsymbol{\nu}$	79	Eqn. (2.63)
$\boldsymbol{S}_{e}$	$N \times N$ power spectrum of the estimation error $\boldsymbol{e}$	138	Eqn. (4.6)
$\boldsymbol{S}_{\breve{e}}$	$N \times N$ power spectrum of the estimation error $\breve{\boldsymbol{e}}$	232	
$\boldsymbol{S}_{\breve{e}e}$	cross-power spectrum of the vector signals $\breve{\boldsymbol{e}}$ and $\boldsymbol{e}$	173	Eqn. (4.94)
$\boldsymbol{S}_{u}$	$N \times N$ power spectrum of the vector signal $\boldsymbol{u}$	235	Eqn. (5.73)
$\boldsymbol{S}_{ua}$	$N \times N$ cross-power spectrum of the vector signals $\boldsymbol{u}$ and $\boldsymbol{a}$	235	Eqn. (5.74)
$\boldsymbol{S}_{ue}$	$N \times N$ cross-power spectrum of the vector signals $\boldsymbol{u}$ and $\boldsymbol{e}$	234	Eqn. (5.61)
$\boldsymbol{S}_{uv}$	cross-power spectrum of the vector functions $\boldsymbol{u}$ and $\boldsymbol{v}$	52	
$\boldsymbol{S}_{x}$	$N \times N$ equivalent channel	143	Eqn. (4.16)
$\boldsymbol{S}_{y}$	power spectrum of the equalizer input signal $\boldsymbol{y}$	147	Eqn. (4.27)
$\boldsymbol{S}_{ya}$	cross-power spectrum between the equalizer input signal $\boldsymbol{y}$ and the transmitted data $\boldsymbol{a}$	147	Eqn. (4.28)
$\boldsymbol{S}_{ye}$	cross-power spectrum of the vector signals $\boldsymbol{y}$ and $\boldsymbol{e}$	173	Eqn. (4.93)
$\boldsymbol{S}_{z}$	power spectrum of the noise signal $\boldsymbol{z}$	164	Eqn. (4.59)

Symbol	Meaning	Page	Reference
$\boldsymbol{S}_\alpha$	power spectrum of the delayed data signal	221	Eqn. (5.6)
$\boldsymbol{S}_{\breve{\varepsilon}}$	power spectrum of the vector signal $\breve{\varepsilon}$	232	Eqn. (5.51)
$\boldsymbol{S}_\zeta$	power spectrum of the delayed noise signal ζ	223	Eqn. (5.17)
$\boldsymbol{S}_\nu$	$AK \times AK$ power spectrum of the noise signal $\boldsymbol{\nu}$	79	Eqn. (2.62)
$\boldsymbol{S}_{\nu,lm}$	$K \times K$ cross-power spectrum of the noise signals $\boldsymbol{\nu}_l$ and $\boldsymbol{\nu_m}$	80	Eqn. (2.70)
$\mathcal{S}_i^{\mathrm{im}}$	set of PAM constellation points for the quadrature data signal of user i	62	Eqn. (2.9)
$\mathcal{S}_i^{\mathrm{re}}$	set of PAM constellation points for the in-phase data signal of user i	62	Eqn. (2.8)
$\mathcal{S}_L$	set of integer values between and including 0 and L	345	Eqn. (I.3)
s	physical unit 'seconds'		
[s]	indicating that the unit of the preceding quantity is 'seconds' (s)		
s_{Ci}	transmitted continuous-time signal of user i	65	Eqn. (2.17)
s_i	data symbol sequence of user i after up-sampling	64	Eqn. (2.15)
$\tilde{s}_i$	output signal of the i-th user's spreading filter	64	Eqn. (2.16)
$\sin(\dots)$	sine function	284	Tab. A.3
$\sinh(\dots)$	hyperbolic sine	284	Tab. A.3

Symbol	Meaning	Page	Reference
[symbols/s]	indicating that the unit of the preceding quantity is 'symbols per second' (symbols/s)		
T	symbol period	64	Tab. 2.1
T_c	sampling period of the channel impulse response	67	Eqn. (2.21)
T_h	maximal time duration of the radio channel impulse responses	67	Eqn. (2.20)
T_s	sampling or chip period	64	Tab. 2.1
T_0	time period of periodic signal	292	
$\ldots^T$	transposition	284	Tab. A.3
$\ldots^{-T}$	inverse transposition	284	Tab. A.3
t	dummy variable describing time ($t \in \mathbb{R}$, unit: s)		
t_0	sampling phase in seconds	118	
t_0/T	sampling instant	118	
$\check{t}_0$	normalized time (with respect to T_0)	292	Eqn. (A.18)
$\tan(\ldots)$	tangent	284	Tab. A.3
$\tanh(\ldots)$	hyperbolic tangent	284	Tab. A.3
$\mathrm{tr}\{\ldots\}$	trace of the square matrix $\ldots$	284	Tab. A.3
U_{div}	number of diversity channels in the system	81	Eqn. (2.74)
u_i	i-th component of the vector signal $\boldsymbol{u}$	234	
$\boldsymbol{u}$	$1 \times N$ input signal to the forward filter matrix $\boldsymbol{L}$	234	
$\boldsymbol{V}$	arbitrary matrix function (Chapter 1)	49	

Symbol	Meaning	Page	Reference
$\boldsymbol{V}$	diagonal matrix function obtained by performing Cholesky factorizations of $\boldsymbol{Q}$ (Chapter 5)	238	Eqn. (5.84)
W	double-sided spread spectrum bandwidth	11	
$\boldsymbol{W}$	positive definite, Hermitian matrix that results from the matrix spectral factorization of $\boldsymbol{Q}(e^{-j2\pi\frac{k}{L}})$	346	Eqn. (I.5)
w_K	discrete basis function ($w_K \triangleq e^{-j2\pi/K}$)	291	Tab. A.7
$\boldsymbol{X}$	$N \times AK$ overall channel matrix	77	Eqn. (2.57)
X_{Cil}	Fourier transform of x_{Cil}	73	
$\check{X}_{Cil}$	discrete-time Fourier transform of x_{il}	73	Eqn. (2.44)
$\boldsymbol{X}_l$	$N \times K$ combined channel matrix for the l-th receiver input	76	Eqn. (2.53)
x	dummy variable ($x \in \mathbb{R}$)		
x_{Cil}	impulse response of the combined channel	71	Eqn. (2.36)
x_{il}	impulse response of the combined channel in the equivalent discrete-time model	73	Eqn. (2.43)
x_{il}^m	partitioned channel impulse response for user i, receiver branch l and demultiplexer output m	75	Eqn. (2.47)
x_0	dummy parameter ($x_0 \in \mathbb{R}$)	103	
$\boldsymbol{y}$	$1 \times AK$ overall output signal vector of the first receiver stage	77	Eqn. (2.55)
y_{Cl}	output signal of the lowpass filter in receiver branch l	69	Eqn. (2.30)
y_l	discrete-time signal at the output of branch l of the first receiver stage	70	Eqn. (2.31)

Symbol	Meaning	Page	Reference
$\boldsymbol{y}_l$	$1 \times K$ output signal vector at receiver branch l	76	Eqn. (2.51)
y_l^m	m-th output of the demultiplexer in receiver branch l	74	Eqn. (2.46)
y_{li}	The component in the receiver output signal y_l which stems from user i	73	Fig. 2.9
$\mathbb{Z}$	set of all integer numbers	291	Tab. A.7
z	interference random variable	101	Eqn. (3.81)
z_0	parameter for the first- and second-order bounds ($z_0 \in \mathbb{R}$)	105	
$\bar{z}_0$	parameter which yields the tightest first-order upper bound for the threshold probability ($\bar{z}_0 \in \mathbb{R}$)	108	Eqn. (3.109)
$\boldsymbol{z}$	Gaussian noise component in the output signal of the channel matched filter	164	Eqn. (4.58)

Greek Symbols

Symbol	Meaning	Page	Reference
α_i	interfering data symbol transmitted by one of the users $(i \neq 0)$	92	Eqn. (3.38)
α_0	data symbol to be estimated of the desired user	92	Eqn. (3.38)
$\tilde{\alpha}_0$	linear estimate of the desired data symbol α_0 for the desired user	92	Eqn. (3.38)
$\boldsymbol{\alpha}$	delayed data signal	221	Eqn. (5.4)
$\breve{\boldsymbol{\alpha}}$	linear estimate of the delayed data signal at the output of the delay matrix in the MIMO DDFE	221	Eqn. (5.8)
$\tilde{\boldsymbol{\alpha}}$	continuous-valued estimate of the delayed data signal $\boldsymbol{\alpha}$ at the input to the decision device	222	Eqn. (5.11)
$\hat{\boldsymbol{\alpha}}$	final, quantized estimate of the delayed data signal $\boldsymbol{\alpha}$	221	Eqn. (5.5)
Γ_k	expected value of the matched filter bound (MFB) SNR for user k	315	Eqn. (D.7)
$\boldsymbol{\Gamma}$	normalized upper triangular matrix function obtained by performing Cholesky factorizations of $\boldsymbol{Q}$	238	Eqn. (5.84)
Δ	time delay in symbols $(\Delta \in \mathbb{N})$	50	
Δ_k	indicates by how many symbols the k-th signal estimate is delayed at the output of the DDFE forward filter $(\Delta_k \in \mathbb{N}_0)$	216	
Δf	frequency difference between two samples	67	Eqn. (2.23)

Symbol	Meaning	Page	Reference
$\boldsymbol{\Delta}$	delay matrix	220	Eqn. (5.3)
$\delta(\dots)$	Dirac delta distribution	284	Tab. A.3
$\delta_K[\dots]$	Kronecker delta sequence	284	Tab. A.3
ε	relative error between the approximation and the exact value of the threshold probability	116	Eqn. (3.132)
ε_k	k-th component of the vector $\boldsymbol{\varepsilon}$	230	Eqn. (5.40)
$\breve{\varepsilon}_k$	k-th component of the vector $\breve{\boldsymbol{\varepsilon}}$	228	
$\tilde{\varepsilon}$	k-th component of the vector $\tilde{\boldsymbol{\varepsilon}}$	230	
$\hat{\varepsilon}$	k-th component of the vector $\hat{\boldsymbol{\varepsilon}}$		
$\boldsymbol{\varepsilon}$	error signal in the estimate of the delayed data at the input to the decision device	222	Eqn. (5.12)
$\breve{\boldsymbol{\varepsilon}}$	error signal in the linear estimate $\breve{\boldsymbol{\alpha}}$ of the delayed data	222	Eqn. (5.9)
$\tilde{\boldsymbol{\varepsilon}}$	estimate of the error signal $\breve{\boldsymbol{\varepsilon}}$	222	Eqn. (5.10)
$\hat{\boldsymbol{\varepsilon}}$	estimate of the error signal $\breve{\boldsymbol{\varepsilon}}$ using the quantized decisions $\hat{\boldsymbol{\alpha}}$	226	Eqn. (5.27)
$\boldsymbol{\epsilon}$	extended noise vector	229	Eqn. (5.35)
$\boldsymbol{\epsilon}_k$	$1 \times L_k$ subvector of $\boldsymbol{\epsilon}$	229	Eqn. (5.37)
$\boldsymbol{\zeta}$	delayed noise signal	222	Eqn. (5.14)
$\boldsymbol{\zeta}$	$1 \times N$ noise component of the input signal to the decision elements	180	Eqn. (4.118)
ζ_k	k-th component of the noise vector signal $\boldsymbol{\zeta}$	180	Eqn. (4.121)
ζ_k^{im}	imaginary part of ζ_k	88	Eqn. (3.10)
ζ_k^{re}	real part of ζ_k	88	Eqn. (3.10)

Symbol	Meaning	Page	Reference
ζ_0	Gaussian noise component in the linear estimate $\tilde{\alpha}_0$	92	Eqn. (3.38)
$\bar{\zeta}_0$	Gaussian noise component in the normalized decision variable	101	
$\boldsymbol{\Theta}$	causal, diagonal matrix function obtained by the spectral factorization of $\boldsymbol{V}^{-1}$	240	Eqn. (5.95)
κ_i	distance between two adjacent constellation points of the PAM/QAM data signal of user i	62	Eqn. (2.12)
Λ	parameter for the second-order bound ($\Lambda \in \mathbb{C}$)	104	Eqn. (3.89)
$\bar{\Lambda}$	parameter which yields a tight second-order upper bound for the threshold probability ($\bar{\Lambda} \in \mathbb{C}$)	114	Eqn. (3.126)
$\boldsymbol{\Lambda}_{\mathrm{c}}$	delay transform of the C-DDFE forward filter $\boldsymbol{L}_{\mathrm{c}\Delta}$	222	Eqn. (5.16)
$\boldsymbol{\Lambda}_{\mathrm{np}}$	delay transform of the C-DDFE forward filter $\boldsymbol{L}_{\mathrm{np}\Delta}$	226	Eqn. (5.29)
λ	real part of the parameter Λ	105	Eqn. (3.96)
$\bar{\lambda}$	parameter which yields the tightest first-order upper bound for the threshold probability ($\bar{\lambda} \in \mathbb{R}$)	108	Eqn. (3.108)
μ	imaginary part of the parameter Λ	113	Eqn. (3.124)
$\bar{\mu}$	parameter which yields a tight second-order upper bound for the threshold probability ($\bar{\lambda} \in \mathbb{R}$)	114	Eqn. (3.127)

Symbol	Meaning	Page	Reference
$\boldsymbol{\nu}$	$1 \times AK$ overall noise signal vector after the first receiver stage	77	Eqn. (2.56)
ν_{CGl}	complex Gaussian, white noise added at antenna l	63	
ν_{Cl}	colored, complex Gaussian noise after low-pass filtering in receiver branch l	71	Eqn. (2.38)
ν_l	sampled, discrete-time noise signal in receiver branch l	73	Eqn. (2.41)
$\boldsymbol{\nu}_l$	$1 \times K$ noise signal vector at receiver branch l	76	Eqn. (2.52)
ν_l^m	partitioned noise signal for receiver branch l and demultiplexer output m	75	Eqn. (2.48)
ξ	overpopulation number	156	Eqn. (4.46)
π	Ludolphian number ($\pi \triangleq 3.141592\dots$)	291	Tab. A.7
ρ	function depending on the number of PAM levels	96	Eqn. (3.59)
$\boldsymbol{\Sigma}_x$	delay transform of the equivalent channel $\boldsymbol{S}_x$	222	Eqn. (5.15)
τ	dummy variable describing time ($\tau \in \mathbb{R}$, unit: s)		
$\boldsymbol{\Upsilon}$	causal whitening filter for the equalizer input signal $\boldsymbol{y}$	149	Eqn. (4.35)
Φ	signal-to-interference-and-noise ratio (SINR) at the input of the decision device		
Φ_k	total SINR of the complex data estimate $\tilde{a}_k$ at the input of the decision device	98	Eqn. (3.69)

Symbol	Meaning	Page	Reference
Φ_k^{im}	SINR for the quadrature signal of user k at the input to the decision device	95	Eqn. (3.54)
Φ_k^{re}	SINR for the inphase signal of user k at the input to the decision device	95	Eqn. (3.53)
$\Phi_{k,\mathrm{mmse}}$	SINR of the complex data estimate $\tilde{a}_k$ at the input to the decision device for an optimal MMSE equalizer	182	Eqn. (4.130)
$\Phi_{k,\mathrm{zf}}$	SINR of the complex data estimate $\tilde{a}_k$ at the input to the decision device for an optimal ZF equalizer	182	Eqn. (4.131)
$\boldsymbol{\Phi}$	causal factor of the sampled matrix spectrum $\boldsymbol{Q}(e^{-j2\pi\breve{f}})$	347	Eqn. (I.7)
$\boldsymbol{\Phi}_{\mathrm{FIR}}$	causal factor of the sampled matrix spectrum $\boldsymbol{Q}(e^{-j2\pi\frac{k}{L}})$	346	Eqn. (I.5)
φ_{Ci}	signature waveform of user i	70	Eqn. (2.32)
$\chi_{\mathrm{IN},k}$	distortion component of the complex data estimate $\tilde{a}_k$	97	Eqn. (3.66)
$\chi_{\mathrm{IN},k}^{\mathrm{im}}$	distortion component of $\tilde{a}_k^{\mathrm{im}}$	94	Eqn. (3.48)
$\chi_{\mathrm{IN},k}^{\mathrm{re}}$	distortion component of $\tilde{a}_k^{\mathrm{re}}$	94	Eqn. (3.47)
$\chi_{\mathrm{S},k}$	signal component of the complex data estimate $\tilde{a}_k$	97	Eqn. (3.65)
$\chi_{\mathrm{S},k}^{\mathrm{im}}$	signal component of $\tilde{a}_k^{\mathrm{im}}$	94	Eqn. (3.46)
$\chi_{\mathrm{S},k}^{\mathrm{re}}$	signal component of $\tilde{a}_k^{\mathrm{re}}$	94	Eqn. (3.45)
$\boldsymbol{\Psi}$	purely causal factor of the matrix function $\boldsymbol{Q}$	164	Eqn. (4.61)
$\boldsymbol{\Psi}_{\mathrm{FIR}}$	matrix sequence that is a finite impulse response approximation of $\boldsymbol{\Psi}$	345	Eqn. (I.4)

l

Symbol	Meaning	Page	Reference
$\boldsymbol{\Psi}_x$	purely causal factor of the matrix function $\boldsymbol{S}_x$	177	Eqn. (4.108)
$\boldsymbol{\Psi}_\Delta$	purely causal factor of the matrix function $\boldsymbol{Q}_\Delta$	223	Eqn. (5.20)
ψ_{Cil}	overall channel waveform	70	Eqn. (2.33)

Miscellaneous Symbols

Symbol	Meaning	Page	Reference
$\mathbf{0}_N$	all zero row vector with N components	291	Tab. A.7
$\mathbf{1}_N$	all ones row vector with N components	291	Tab. A.7
$+$	addition	288	Tab. A.4
$-$	subtraction	288	Tab. A.4
$\cdot$	multiplication	288	Tab. A.4
$/$	division	288	Tab. A.4
$\star$	convolution	288	Tab. A.4
$\oslash$	modulus	288	Tab. A.4
$=$	is equal to	282	Tab. A.2
$\neq$	is not equal to	282	Tab. A.2
$\triangleq$	is defined by	282	Tab. A.2
$\equiv$	is equivalent to	282	Tab. A.2
$>$	is greater than	282	Tab. A.2
$<$	is smaller than	282	Tab. A.2
$\gg$	is much greater than	282	Tab. A.2
$\ll$	is much smaller than	282	Tab. A.2
$\geq$	is greater than or equal to	282	Tab. A.2
$\leq$	is smaller than or equal to	282	Tab. A.2
$\approx$	is approximately the same as	282	Tab. A.2
$\in$	is an element of the set	282	Tab. A.2
$\notin$	is not an element of the set	282	Tab. A.2
$\cup$	union	290	Tab. A.6
$\cap$	intersection	290	Tab. A.6
$\setminus$	set minus	290	Tab. A.6

Symbol	Meaning	Page	Reference
$\mid$	such that	282	Tab. A.2
$\forall$	for all	282	Tab. A.2
∞	infinity	282	Tab. A.2
$\mapsto$	is mapped into	282	Tab. A.2
$\lvert \ldots \rvert$	absolute value	284	Tab. A.3
$\lfloor \ldots \rfloor$	*floor* function	284	Tab. A.3
$\lceil \ldots \rceil$	*ceil* function	284	Tab. A.3
$[f(s)l]$	row vector defined by the numbers f (start value), s (step size) and l (end value)	291	Tab. A.7
$[\ldots]_i$	i-th element of vector	284	Tab. A.3
$[\ldots]_{i,k}$	(i,k)-th element of matrix	284	Tab. A.3
$[\ldots]_{ik}$	(i,k)-th element of matrix (identical to $[\ldots]_{i,k}$)	284	Tab. A.3
$[\ldots]_{\imath_1,\imath_2}$	submatrix of a matrix defined by the vectors $\boldsymbol{\imath}_1$ and $\boldsymbol{\imath}_2$	284	Tab. A.3
$!$	factorial	284	Tab. A.3
$\ldots'$	first derivative	284	Tab. A.3
$\ldots''$	second derivative	284	Tab. A.3
$\ldots'''$	third derivative	284	Tab. A.3
$\ldots^*$	complex conjugation	284	Tab. A.3
$\ldots^{-1}$	inversion	284	Tab. A.3
$\ldots^{-*}$	complex conjugated inversion	284	Tab. A.3
$\ldots^{\blacktriangleleft}$	upper triangular part of a matrix	284	Tab. A.3
$\ldots^{\blacktriangleright}$	lower triangular part of a matrix	284	Tab. A.3
$\ldots^{\triangleleft}$	diagonal part of a matrix	284	Tab. A.3

Symbol	Meaning	Page	Reference
$\ldots^+$	purely causal part of a function or matrix function	284	Tab. A.3
$\ldots^-$	purely anticausal part of a function or matrix function	284	Tab. A.3

Chapter 1

Introduction

1.1 Overview

Exchanging information with other individuals or the environment is one of the basic human needs. In particular, it is very important for many of us to find out and be aware of certain events within reasonable time. This means, very often, that information has to be exchanged over long distances; and it has to be done, if not for necessity at least for convenience, as soon as possible. However, it has not been until the late nineteenth century that the speed of a horse or a train limited not only the traveling time but also the form of the message. By that time, a major breakthrough in the evolution of communications means occurred. For the first time, electromagnetic signals were used for the transport of information. This initiated, starting with the invention of telegraphy, a new area of communication, *telecommunication*, which has been changing our ethics, philosophy, knowledge and perception of the world irreversibly. Since then, telecommunications has and will become increasingly faster, more powerful and enabling ever new products and lifestyles. Some of the most important include broadcast radio, the telephone, television, to name only a few. The *world wide web* and *cellular telephony* are the current hot products fuelling an unprecedented growth of the telecommunications market. The preliminary climax was reached in the middle of the year 2000 with the auction of third generation cellular phone licences in several European countries. For example, the licence fees filled the treasury of England

with more than 38 billion EURO (US\$ 36 billion) and that of Germany with more than 51 billion EURO (US\$ 48 billion) [23]. Moreover, telecommunication companies spent these large sums without yet having the third generation wireless products and applications using the licenced bandwidth. The financial pressure to develop these products fast will add to the already strong activities of telecommunications hardware and software manufacturers. An end to this long-term trend cannot be foreseen at this point of time.

Presently, envisioned capabilities of future telecommunications systems are very often far ahead of current products and even research results. Not surprisingly, the research is very active in this field. Among others, four important areas within communications are *networks*, *digital*, *broadband* and *wireless systems*.

The trend towards networks is as old as electrical communication and stems from the fact that some systems need to connect many different locations and individuals. A great deal of work has been carried out on this subject during the twentieth century. Not surprisingly, many existing communication systems are examples of mature and reliable networks. At this time, probably the most sophisticated network is the global telephone system. Nonetheless, new systems are emerging which offer more and better services as well as an integration of voice, video, and data. These networks have to be designed for the specific requirements of the intended services and the characteristics and constraints of the system. A very simple type of network is a multiuser system consisting of several portables and one base station. In the down- or forward link, the base station sends data simultaneously to all users. While in uplink or reverse mode, the portables transmit information to the base station. The base station can be used as a control and/or switching unit, and it may be connected to a larger network.

Digital data became popular with the invention and development of computers. In parallel, it was observed that the inherently analog signals of our real world can be time sampled and coded with negligible loss of information. Consequently, the foundation for the digital representation of analog signals was laid. The final breakthrough of digital systems was based on two properties. Firstly, data compression, also called source coding, enables the extraction of relevant information only; secondly, digital systems can easily integrate different data formats and offer more and

better services.

Compression techniques are able to discard redundant parts of the signal. This reduces the total amount of data to be transmitted and increases the capacity of communication systems. Due to a large amount of redundancy in real world signals, digital systems are nowadays usually far more efficient than analog systems.

The integration of different data formats such as still and moving images, text, voice and data has already been achieved in applications for the world wide web. Products with similar abilities are currently under development for third generation cellular systems. The digital data representation is ideal for this kind of integration since all formats are coded into symbol sequences using the same binary alphabet. At the basic data level, all signals, whether they are voice, images or any other format, look the same. Moreover, additional user services are easily included with appropriate protocols and software.

Recent technological advances paved the way for a variety of new services and applications, among them digital television/radio, video on demand and world wide web services. In spite of highly effective compression methods, these applications have in common that they require the transmission of enormous amounts of data. Moreover, the required data quantities are constantly increasing. In order to be able to use these services without unacceptable delay and waiting periods, it is necessary to develop sufficiently fast broadband systems which are able to keep pace with the growing information transfer.

In many communication applications, wireless systems are preferable. Firstly, the cost of systems may be reduced if no cables are required. The installation of wireless systems is easier and more convenient. Even more important is that wireless systems enable the mobility of users. People become instantly accessible and are able to access information "anywhere at any time". Whether or not the hereby inspired culture is necessary or desirable, many people are willing to spend money for this service. The recent success of cellular phones has been a direct consequence. In the near future, new wireless systems will emerge and existing products will become more powerful.

The combination of network, digital, broadband and wireless properties is necessary for many envisioned products. It is also the basis for the type of system

investigated in this work.

Important aspects for the system design are performance, efficiency and complexity. The most reasonable quality or performance measure for digital systems is the *bit error rate* (BER), which expresses the probability that a received information bit is detected wrongly. The system must guarantee that a certain BER value, which is dictated by the type of application, not be exceeded. More efficient systems require less resources and achieve a higher capacity for the same properties. For example, more users are supportable and/or higher data rates are possible. Simpler systems are usually less expensive, more reliable and easier to design than more complex ones. Interestingly, there exists a trade-off among performance, efficiency and complexity. For example, a higher efficiency or performance is often achieved by adding additional complexity (error correction codes, multiple antennas, sophisticated receivers/detectors). System resources like bandwidth or transmit power may be sacrificed for higher performance and vice versa. Consequently, a reasonable compromise has to be found by taking all system requirements and resources into account.

Two other important factors for the design are system properties and application requirements. The system properties include the amount of available bandwidth, transmit power, interference, the channel characteristics, noise level and so forth. Resources like bandwidth and transmit power are more or less restricted; other effects like interference, noise, time-varying and frequency selective channels may require special attention. In addition, the type of application determines the requirements for capacity, data rate and performance. As a consequence, each system requires different solutions and techniques in order to meet all objectives most efficiently.

Let us illustrate the practical differences with two examples. Ordinary telephone systems operating over twisted pair cables are mainly bandwidth limited because of the physical characteristics of the twisted pair cable. The noise in the system is usually small and the transmitter may send the signals with a relatively high power. The channel may be approximated very accurately as time invariant. Consider now a cellular phone system. The portables are mostly operating on batteries. This puts a strong constraint on the transmitter power. The parameters of the radio channel are time varying, especially if the portables are moving. Another characteristic of

the radio channel is multipath signal propagation which spreads the signal in time and may cause an overlap of adjacent symbols (intersymbol interference). The detrimental effect of intersymbol interference (ISI) can only be mitigated by employing more complex receivers and/or transmitters. Additional interference may be caused by other system portables or different radio systems accessing the same or adjacent frequency bands. The bandwidth of the radio channel is usually higher than that of a twisted pair cable, but it is by no means unlimited. This example shows that the transceiver solutions for a telephone and cellular phone system will be different. Each solution has to be considered individually depending on the system properties. The requirements in terms of capacity and performance depend mainly on the signals being transmitted. A voice signal, for example, needs only low data rates in the order of kbits/s. It may tolerate relatively high bit error rates, but it is very sensitive to time delays. On the other hand, data signals require usually a high performance transmission with BER's lower than 10^{-7}. Digital video signals convey a lot of information and need high data rates in the order of Mbits/s for real time applications.

1.2 This Work in the Context

The evolution of cellular telephone systems into an affordable popular service can be roughly described by three main steps. The introduction of analog systems during the 1980s, so called *first generation* (1G) cell phones, made it possible to offer wireless phone services at low prices and it became affordable and attractive to people with average income. However, the enormously increasing customer base soon became a problem because the capacity of the systems needed to be strongly increased in urban areas. This triggered strong efforts to improve the system efficiency, leading to move from analog to digital solutions. Currently, these digital *second generation* (2G) systems dominate the cellular market. They offer, for now, only circuit-switched voice and very low speed (≈ 10 kbit/s) circuit-switched data services. However, standards for the next generation of cellular systems have been under development since the late 1980s and are expected to enter the market in Europe by mid 2001, in North America a little later. These *third generation* (3G) systems will offer higher data rates and the

support for packet-switched data in addition to circuit-switched voice signals. While telecommunications equipment manufacturers are working hard to provide reliable 3G systems, research and standard bodies envision already even higher speed systems, currently called *fourth generation* (4G) or *beyond 3G* systems.

Tables 1.1 and 1.2 show some characteristics and specifications of the different systems [19, 100]. With the introduction of the cellular telephone standard *IS-95*, the spread spectrum technique CDMA[1] became a popular multiple access alternative to TDMA. Both TDMA and CDMA have proven to be significantly more efficient than conventional FDMA used in the public switched telephone network (PSTN) and early first generation cell phone standards (e.g. AMPS). In spite of a hot discussion in the research community as to which technique, TDMA or CDMA, is the better, both multiple access schemes turn out to be in practice approximately equally efficient in terms of data rate per bandwidth. Used in different existing cell phone networks, both TDMA and CDMA achieve spectral efficiencies between 0.04 and 0.07 bits/s per Hz per sector [19]. Consequently, both TDMA and CDMA are considered in future 3G standards, while tending slightly more to CDMA. Especially in Europe and the rest of the world excluding North America, the 3G standard WCDMA (wideband CDMA) seems to be the dominating future standard. In North America, the situation will be different as not sufficient spectrum is available for the realization WCDMA. As a consequence, three other standards are being considered, namely EDGE (TDMA), IS-2000 (CDMA) and HDR (hybrid TDMA/CDMA). In essence, the spread spectrum technique CDMA is and will be an important multiple access scheme for cellular and wireless systems. This dissertation considers a spread spectrum multiple access system (SSMA) which is a generalization of CDMA.

As shown in Table 1.2, the required data rates and spectral efficiencies grow by going from one cellular generation to the next. Current second generation CDMA systems achieve spectral efficiencies of only 0.04–0.07 bits/s per Hz and sector. The

---

[1]CDMA stands for *code-division multiple access* and refers in this context exclusively to direct sequence (DS) CDMA as opposed to frequency hopping (FH) CDMA. Other multiple access schemes are FDMA (frequency-division multiple access) and TDMA (time-division multiple access). Detailed definitions and descriptions of CDMA, TDMA and FDMA may be found, for example, in the books of Rappaport [101] or Proakis [99].

Table 1.1: Characteristics of different generations of cellular telephone systems.

System	Type	Multiple Access	Signals	Switching
1G	analog	FDMA	only voice	circuit
2G	digital	TDMA, CDMA	mainly voice	circuit
3G	digital	TDMA, CDMA	voice and data	circuit and packet
4G	digital	OFDM?, TDMA, CDMA	data (incl. voice)	packet

main reason is a simple receiver which is in essence a filter matched to the received signal waveform (rake receiver plus despreader). The matched filter receiver is unable to reduce interference caused by other users (portables). Higher spectral efficiencies can only be achieved by employing more complex detectors which take special statistical properties of the interference into account in order to reduce or cancel its effects. An excellent detector is based on maximum likelihood sequence estimation (MLSE), however, it requires a known channel and an amount of operations that grows exponentially with the number of system users times the channel memory. As a consequence, the MLSE detector requires, very often, too many computations to be implemented. This is especially the case when more than only a handful of users are to be detected in a frequency-selective environment. Possible alternatives are equalizers with multiple input and multiple output signals (MIMO equalizers). Their performance has been proven to be significantly superior to the matched filter receiver. Although not achieving the same quality as the MLSE detector, equalizers are able to perform almost as well at a numerical complexity only growing linearly with both the number of users and the channel memory. Thus, one practically realizable solution to the increasing demands for performance, capacity and spectral efficiency are MIMO equalizers. This kind of detector, which exists in both linear and nonlinear (decision-feedback) form, is the subject of this work.

The dissertation consists of two main parts:

1. efficient approximation of error probabilities (Chapter 3);

2. analysis and evaluation of existing and new equalizer structures for spread spectrum multiuser systems (Chapters 4 and 5).

Table 1.2: Specifications for different generations of cellular telephone systems.

System	Data Rates in kbit/s per user			Efficiency Target
	Outdoor		Indoor	in bit/s per Hz per sector
	high speed	low speed		
1G	analog 3.1 kHz voice signal		—	N/A
2G	≈ 10		—	$0.04 - 0.07$
3G	≥ 144	≥ 384	≥ 2000	$0.1 - 0.5$
4G	larger than 3G			> 0.5

The equalizer structures considered in this dissertation are designed for a specific spread spectrum system. A detailed description of the system characteristics is given in Chapter 2.

The systems investigated (including transmitter, channel and equalizer) are either linear or can be fairly approximated by linear models. Nevertheless, the calculation of error probabilities becomes complex or difficult unless the interference part is eliminated in the output signal of the equalizer. Since this is not necessarily the case, special methods have to be used in order to approximate the error probability efficiently. A new approach is described in Section 3.4, which is very accurate, efficient and easy to use.

The equalizer structures described in the second part of this work have certain special characteristics. They are designed for use in the reverse link of a spread spectrum (SSMA, CDMA) multiuser system consisting of multiple portables and one base station. The equalizers are MIMO structures whose theoretical description is suited for the accommodation of an arbitrary number of receive antennas or antenna elements. It is the main purpose of the equalizers to combat and mitigate interference caused by frequency selective channels (intersymbol interference, ISI) and other portables (co-channel interference, CCI). The main properties of these suboptimal multiuser detectors are capability to achieve high performance and bandwidth efficiency for a moderate degree of complexity.

There are three main objectives with respect to the investigated MIMO equalizers. The first is a general analysis and description of these detectors, including the determination of the optimal parameters and expressions for their performance. It is

intended to evaluate and compare the performance, complexity and capacity of the different structures. Finally, alternative approaches and new equalizer structures are introduced and explored in order to further improve the performance, increase the capacity and/or reduce the complexity.

Equalizers may be analyzed in either the time or the frequency domain. The time-domain approach is better suited to time-varying systems while a frequency-domain analysis requires, usually, stationary or quasi-stationary[2] environments. On the other hand, the optimal equalizer and expressions for the performance may be determined more efficiently in the frequency-domain. In spite of that, most publications within the field of multiuser detection perform a time-domain analysis. This work concentrates on the frequency-domain approach.

Let us finally outline the system for which the investigated equalizers are suited. The MIMO equalizers perform inherently a joint detection of several signals. This implies that they be used in the receiver of a base station which detects the data signals of multiple users. Although similar structures may also be used in the forward link, the investigation concentrates solely on the reverse link. One characteristic of the reverse link is that the signals of different users are received asynchronously, i.e. the data sequences are delayed relatively to each other. The special structure of the equalizers considered here is able to deal with asynchronous signals. The equalizers are space-time filters and can be viewed as a bank of discrete-time filters. This makes them suitable for mitigating frequency-selective channels and implies that the symbol period is on the order of or shorter than the impulse response of the channel. In other words, the data rate is relatively high and the system is broadband. The frequency-domain analysis requires quasi-stationary channels. This is especially reasonable for high data rate systems, whose symbol period and thus block duration is short and whose portables are stationary or slowly moving. It will be shown that MIMO equalizers are highly bandwidth efficient and that they may achieve a very

---

[2]In practice, data is transmitted in blocks or frames of a specified length rather than continuously without interruption. A system will be called *quasi-stationary* if its characteristics are time-variant but do not, for all practical purposes, change during the length of one data block. The system can then be described as long term time-variant with respect to several data blocks, but short term stationary within each block.

good performance. That makes them appropriate for a wide application of services. Taking the possible large data rates into account, even broadband services such as video and high speed data may be supported (especially for indoor systems). In summary, a possible application of the equalizers investigated here is as detectors in the reverse link of a wireless multiuser system with the following characteristics and requirements:

- spread spectrum multiple access (SSMA, DS-CDMA),

- multiple receive antennas (optional),

- asynchronous signal reception,

- frequency selective channels (high data rate),

- quasi-stationary channels (slowly moving portables, high data rates),

- high bandwidth efficiency,

- low error probabilities,

- moderate complexity.

1.3   Background

1.3.1   Frequency and Antenna Diversity

A multiuser system requires a multiple access scheme in order to support several users (portables) simultaneously. The scheme *spread spectrum multiple access* (SSMA) realizes this by using the principle of *frequency diversity*.

Consider a discrete-time signal to be transmitted over a continuous-time channel at a symbol period of T [s]. This requires, according to the well known Nyquist criterion, a double-sided bandwidth[3] of at least $B = 1/T$ [Hz]. A spread spectrum system,

---

[3]In baseband systems, the double-sided bandwidth comprises both negative and positive frequencies of the signal. In contrast, the double-sided bandwidth of a passband (modulated) system includes only the signal bandwidth around the carrier frequency in the positive frequency region.

however, converts the information sequence to a continuous-time signal with a larger bandwidth of $W = KB$ [Hz], where the integer $K > 1$ is called the *spreading factor* or the *processing gain*. The bandwidth spreading may be realized in different ways[4]. The process of spreading introduces K-fold diversity into the transmitted signal. In particular, the complete information is contained in any connected subband of bandwidth B [Hz] within the total spread spectrum signal bandwidth $W = KB$ [Hz]. The process of spreading may therefore be interpreted by producing K (different) copies of the original information and transmitting them in K parallel subbands of bandwidth B [Hz] over the channel. Since the resource of diversity is additional frequency, spread spectrum systems provide *frequency diversity*.

In multiuser systems, each user generates a spread spectrum signal by using a different code or filter characteristic. Although the signals of all users overlap and interfere with each other, the receiver may recover any individual signal. This can be done by correlating and despreading the received, combined signal with the code of the desired user. If all codes are mutually uncorrelated, the original signal will be ideally regenerated without residual interference. One way to achieve this is by choosing *orthogonal codes*. However, even initially orthogonal signals may become correlated at the receiver when the channel is sufficiently time dispersive. In this case, residual interference from other user's signals remains in the desired signal after correlation and despreading (matched filtering). This can be avoided by applying a linear transformation to the despreaded signal which inverts the correlation characteristic of the received signals or, alternatively, which minimizes the combined signal distortion caused by interference and noise. A publication of Shnidman [113] is one of the first works recognizing that different signals overlapping both temporally and spectrally can be recovered completely. He derived the *generalized Nyquist criterion*, which is an extension of the Nyquist criterion for zero ISI in a system that modulates only one waveform (single user systems) to a system that modulates several different

---

[4]One method of bandwidth spreading is to multiply each symbol of the original information sequence with a *code sequence* whose sample period is $T_s = T/K$ (chip period). In another technique, the information sequence is K-times *upsampled* (expanded), i.e. $K - 1$ zeros are inserted between either two information symbols, and the resulting expanded sequence is fed into an arbitrary linear, time-invariant filter.

waveforms. It is a necessary and sufficient condition for minimizing the noise variance under the constraint of zero interference.

A fundamental result is that all individual signals from different users may be totally recovered without any residual interference by a linear *transformation if the number of users (N) does not exceed the processing gain:*

$$N \leq K. \tag{1.1}$$

This result was foretold by Shnidman [113]. It has been derived by Gardner in the context of cyclostationarity, [37, 38], which represents an alternative way to describe spread spectrum signals. Note that condition (1.1) is necessary but not sufficient since, even for $N \leq K$, some original signals may not be recovered if the set of all codes (or received signal waveforms) is linearly dependent, which is equivalent to a singular correlation matrix.

The above discussion implies that the multiple access scheme SSMA relies on bandwidth expansion in order to support several users. In essence, each user's signal bandwidth is expanded to K times the fundamental (single user) Nyquist bandwidth such that a maximum of $N = K$ users may transmit information simultaneously. Since each user may send data at a rate of $B = 1/T$ [symbols/s], the maximal system capacity is $C = KB$ [symbols/s]. The important thing to note is that each individual signal occupies the whole bandwidth $W = KB$ [Hz] at all times.

Interestingly, other schemes like *frequency-division multiple access* (FDMA) and *time-division multiple access* (TDMA) also use bandwidth expansion for the support of multiple users. FDMA reserves a separate frequency band of at least B [Hz] for each user transmitting symbols at a rate of $B = 1/T$ [symbols/s]. Assuming that the FDMA system provides K frequency bands, up to $N = K$ users may transmit data simultaneously and the maximal system capacity is $C = KB$ [symbols/s]. The required system bandwidth is in this case at least $W = KB$ [Hz]. Hence, formally FDMA and SSMA achieve the same capacity. Note that FDMA is an orthogonal multiple access scheme since all transmitted signals occupy different frequency bands and do not interfere with each other as long as the individual bands are spaced

sufficiently apart. In TDMA, a certain user is allowed to send data during a specific time period while all other users are silent. Each user is assigned a different time period in order to share the system resources. This prevents that signals from different users interfere with each other; consequently TDMA is an orthogonal multiple access scheme. Assuming that the total system bandwidth is W [Hz], the active user may transmit data according to the Nyquist criterion at a symbol rate of W [symbols/s]. The system capacity is thus $C = W$ [symbols/s], which turns out to be theoretically the same as for FDMA or SSMA. In practice, however, FDMA systems achieve a lower capacity than SSMA or TDMA since frequency bands have to be reserved at all times, even when the number of active users is smaller than the maximum. In this case, the unused bands are wasted, which reduces the effective capacity of the system [101].

Another way of supporting several users simultaneously is by using several individual, physically separated channels between the transmitters and the receiver. This principle is obvious for wired systems. Suppose a system similar to the one described above connects N users to a central base station and there is one cable used between each user and the base. If the bandwidth of each cable is B [Hz], up to B [symbols/s] may be transmitted by each user. This results in a total system capacity of $C = NB$ [symbols/s]. Note that the capacity is increased by a factor of N when N separate cables are used, even if each cable uses the same frequency band. The capacity gain will not be diminished if there exists serious crosstalk among the different cables. In this case, a linear transformation, similar to that discussed above for SSMA systems, may be used at the receiver in order to invert the crosstalk characteristics caused by the channels.

The same principle can now be applied to wireless radio channels by using multiple transmit[5] and receive antennas. Suppose that the base station employs $A \geq 1$ receive antennas. Then, there are A signal paths between each user and the receiver, which results in an A-fold antenna diversity. Whether the paths are realized by a cable or the radio channel is not important. In both cases, the receiver may be able to recover

---

[5]Note that the total number of transmit antennas in the whole system is N when each of the N users has a single transmit antenna.

each signal completely for

$$N \leq A \tag{1.2}$$

users sending different data simultaneously in the same frequency band of bandwidth B [Hz]. This results in maximal system capacity of $C = AB$ [symbols/s], even though the total system bandwidth is only $W = B$ [Hz]. Hence, the number of supportable users and thus the capacity of a multiuser system may increase linearly with the number of receive antennas. A necessary condition for a linear capacity increase is that, for all users, the channel impulse responses between a certain user and all receive antennas are distinct. This implies that the receive antennas must be sufficiently spaced. If this is not the case and the channel impulse responses are not distinct, the capacity increase will be less than linear in the number of receive antennas.

The phenomenon of increasing the system capacity (number of users) by adding receive antennas while keeping the bandwidth constant has been described in several publications of Winters. He derived the above result (1.2) initially for frequency non-selective (flat) fading channels [128, 129]. In a later paper, it was verified through simulations that the same result also holds in frequency selective environments [130]. The linear transformation required for the complete recovery of each individual signal has been termed *optimum combining*.

If not used for increasing the system capacity, the methods of frequency and antenna diversity can be employed to improve the performance. This concept is particularly beneficial in systems with flat fading channels [99, 128, 129]. In particular, Winters *et al.* [130] showed theoretically for flat fading channels with a linear antenna diversity receiver that an N user, A antenna system can null out all interferers and $A-N+1$ path diversity improvement can be achieved by each of the users. The impact of antenna diversity on the performance of a single user system with a frequency selective channel was investigated by Scott *et al.* [111]. They showed that a lower bit error rate (BER) can be achieved with more than one antenna at the receiver. Similar results have been obtained by Balaban and Salz [10], who examined the impact of

dual antenna diversity on the performance of a single user system.

Several authors have investigated approaches that use both frequency and antenna diversity in an effort to increase the number of system users or to improve the performance. Using a linear transformation of the received signals, it was shown analytically that the number of completely suppressible interferers increases linearly by the product of the number of receive antennas and the processing gain [93, 33]. In other words, all transmitted signals may be recovered without residual interference as long as the number of users is smaller than or equal to the product of antenna and frequency diversity (processing gain):

$$N \leq AK. \tag{1.3}$$

Similar results have been observed for an alternative optimization criterion which minimizes the overall distortion energy caused by interference and noise in the receiver output (minimum mean-square error, MMSE). Qualitative simulation results for a nonlinear detector using the MMSE criterion, [114, 63], indicate that the combination of frequency and antenna diversity improves the system performance and capacity. Another publication shows the derivation of a lower bound for the MMSE of a multiuser system with a linear detector [108]. This bound exists only in the region where the number of users exceeds the product AK. This implies that a linear transformation has a basic performance limitation if $N > AK$. On the other hand, the system performance is merely noise limited when $N \leq AK$. In addition, it is shown that the number of diversity channels in the system is equal to AK.

The important thing to note is that the benefits from antenna and frequency diversity increase with their product. For example, in order to realize a 16-fold diversity, one may use either 16 receive antennas or a 16-fold bandwidth expansion. Alternatively, the same result may be achieved by applying 4 receive antennas in combination with a 4-fold bandwidth expansion.

1.3.2 Optimization Criteria

This dissertation considers a combination of SSMA and antenna diversity as multiple access scheme. Both methods have a very similar characteristic as the transmitted signals from different users do not remain orthogonal. In contrast, they overlap and interfere with each other. Hence, the received signals are a linear combination of all transmitted signals. Still, the original data may be recovered, as discussed in the previous section, provided that certain conditions are satisfied. For this purpose, a detector is required at the receiver which uses the interference-distorted receiver signals as input and provides, based on linear or nonlinear operations, estimates of the original data. The detector used here has a defined structure with variable coefficients which have to be optimized to obtain the best possible estimate. What "best possible" exactly means is determined by the *optimization criterion* for the detector.

The ultimate performance criterion of any communications system with discrete-valued and discrete-time input signals is the error probability. This justifies its application for detector optimization. However, its value is strongly diminished by the fact that it leads to mathematically intractable optimization problems for some detectors. This is, for example, the case for equalizers, which are used in the following chapters as multiuser detectors. Thus, other criteria are required for the optimization of equalizers, which are both mathematically convenient and also good indicators of the system performance. Two of the most commonly used optimization rules that meet both conditions are the *zero-forcing* (ZF) and the *minimum mean-square error* (MMSE) criterion.

The ZF rule minimizes the noise variance in the detector output under the constraint that all interference be completely removed. The MMSE criterion, on the other hand, minimizes the variance of the overall distortion consisting of residual interference and noise. A theoretical advantage of the ZF equalizers is that the distortion in the detector output signal is Gaussian distributed (provided that the noise at the receiver input is Gaussian distributed, too). Thus, the error probability of these equalizers can be calculated with a very simple expression. This is not the case

for MMSE detectors since their output signals include residual interference.

The mathematical complexity required for the detector optimization is approximately the same when using the MMSE or ZF rule. However, the performance is significantly different in both cases. It is well known that the ZF rule may cause a strong amplification of the noise signal in the detector output. As a result, optimizing the detector according to the MMSE criterion results generally in a better system performance. In addition, the MMSE exhibits a strong correlation with the error probability. In particular, decreasing the MMSE translates almost exclusively into a reduction of the error rate. It will be shown in Chapter 4 that a certain upper bound of the error probability is a strictly monotonically increasing function of the MMSE. Moreover, the MMSE criterion lends itself to adaptive equalization, in which the detector coefficients are constantly updated. The MMSE equalizer may also be used for a blind reduction of unknown interference. On the other hand, adaptive and blind equalizers are not as straightforwardly realized based on the ZF criterion. Therefore, for all practical purposes, the MMSE rule should be preferred.

1.3.3 Receiver Structures for Spread Spectrum Multiuser Systems

A common characteristic of the SSMA scheme and multiple receive antenna structures is the overlapping of received signals from different users in both frequency and time which causes interference among all signals. It is, therefore, crucial to apply a detector at the receiver which is able to reconstruct the signal of interest.

An overview on multiuser detectors, for the special application in CDMA systems, can be found in several tutorial publications [30, 79, 124]. Possible detector types include the matched filter detector, the optimum MLSE detector, multistage detectors, successive and parallel interference cancelers, linear decorrelating (ZF) and MMSE detectors, and multiuser decision-feedback equalizers (DFE).

The simplest detector for SSMA systems is the matched filter receiver. It consists simply of a filter that is matched to the waveform of the transmitted signal followed by a despreader (integrator) and a decision element (quantizer). The term

waveform describes the pulse shape of a symbol measured at the receiver. It may be obtained by a convolution of the impulse responses of all system parts that the original data sequence passes before it arrives at the receiver. For a practical system, the waveform is the convolution of the impulse responses of spreading filter (code sequence), transmit filter, radio channel and receive filter [108]. The matched filter effectively enhances the signal of interest and reduces all other signals. In fact, it is the optimal detector for systems with only stationary noise and no interference because it maximizes the signal-to-noise ratio (SNR) at the filter output. However, the received signals of SSMA and multiple antenna systems include a large amount of nonorthogonal interference. Since the cross correlations between the signal of interest and all other signals are typically nonzero for asynchronous and frequency selective channels, the output of the matched filter and despreader still contains components of the interfering signals which lead to signal distortion. Note that the matched filter detector is effectively a *single user detector* because it does not take into account any information about the interferers and treats their signals like stationary noise. As a result, the performance of the matched filter detector is significantly suboptimal.

Particularly sensitive is the matched filter receiver to the *near-far effect*. In this case, the received power of an interfering signal is much higher than that of the signal of interest. The remaining cochannel interference[6] (CCI) after the matched filter is proportional to the received power of the interfering signal. A strong near-far effect may cause a low signal-to-interference ratio (SIR) which results in a high error probability, even when the cross correlations between the desired and the interfering signals are small. One way to mitigate the near-far effect is to use *power control*, i.e. each user adjusts its transmit power such that all signals are received at approximately the same power level. A disadvantage of power control is additional system complexity.

The optimal detector[7] for multiuser systems has been described by Verdú [122]. It consists of a bank of matched filters, where each filter is matched to one of the

---

[6]Cochannel interference (CCI) is the interference caused by other system users.

[7]The term *optimal detector* refers in this context to the detector that maximizes the joint posterior distribution (maximum-likelihood sequence estimation). Note that this is different from the detector that minimizes the marginal posterior distributions of each symbol (minimum probability of error detection) [122].

transmitted waveforms, followed by a MLSE[8] or Viterbi algorithm [99]. It is shown in another publication of Verdú, [123], that unlike the matched filter detector, the optimal detector is near-far resistant. However, the complexity of the optimum detector may become very high. It increases exponentially by the product of the number of users and the channel memory. This prevents a practical implementation of the MLSE detector in many systems, especially when the number of users is on the order of or larger than 10 and when the channels are frequency selective.

The poor performance of the conventional matched filter and the enormous complexity of the optimum detector in many practical situations motivated many researchers to look for suboptimal, high-performance detectors. The objective was to find receivers that are near-far resistant, perform significantly better than the conventional matched filter and have a complexity that might be implemented in systems with many users and/or highly frequency selective channels. Indeed, an enormous amount of suboptimal detectors has been described in the literature. Most of them may be assigned to one of three main classes:

- multistage detectors,

- interference cancelers, and

- equalizers.

The general structure of *multistage detectors*, [120, 121], consists of several identical blocks. In the first stage, decisions are made on the symbols of all users based on the received signals only. Possible choices for the first stage are, for example, the conventional matched filter detectors, ZF- or MMSE- type receivers. The second stage is very similar to the first except that it uses the preliminary decisions from the first stage in conjunction with the received signals in order to make decisions of improved quality. The following stages are identical to the second. In particular, the k-th stage uses preliminary decisions made in the previous stage $k-1$ and the received signals. Note that multistage detectors are nonlinear since they use hard-decisions in the estimation process. Obviously, the detection delay as well as the receiver complexity

---

[8]MLSE is the abbreviation for *maximum likelihood sequence estimation*.

increases with every additional stage. It is therefore desirable to limit the detector to only a few stages. This is justified by results that show diminishing returns for additional stages.

Interference cancelers (IC) use available soft- or hard-decisions of previous symbols in order to cancel intersymbol and cochannel interference in the received signals. If soft-decisions, obtained from a linear transformation, are used, the IC will be considered a linear detector. On the other hand, the IC is nonlinear when hard-decisions from the output of the quantizer are employed.

Successive IC's, [50], perform the decisions on a user-by-user basis. The individual signals are ordered according to their received powers. At first, the (soft or hard) decisions for the strongest user are made conventionally using a matched filter with or without an additional linear transformation. The decisions are appropriately weighted in order to remodulate the interference terms that this user caused in all other signals. These terms are then subtracted from the weaker signals. The same procedure is repeated for the second strongest signal and so on. The successive IC processes the different signals successively, hence its name.

Conversely, parallel interference cancelers subtract simultaneously from all signals the interference caused by all other signals. For this, only the decisions of previous (past) symbols may be used.

The hard decisions of weaker users are less reliable. Hence, they may deteriorate instead of enhancing the signal of stronger users when they are used for interference cancellation. This inspired the IC with *partial cancellation* [24] which does not remove the interference completely. Instead, the decisions are weighted according to their quality with a weight factor between 0 (completely unreliable) to 1 (very reliable) before they are remodulated and removed from the received signals.

It has been found, [90], that successive interference cancelers perform better when the received signal powers are significantly different while parallel IC's yield better results when the received signal energies are similar.

The combination of successive interference cancelers and multistage detectors results in the multistage successive interference cancellation (MSIC) receiver [82, 56]. Provided that the channel estimate is sufficiently accurate, this receiver may yield

performance improvements. The combined structure, however, increases the receiver complexity, hardware requirements (memory) and the overall delay.

Equalizers used for multiuser signal detection have to be generalized to *multiple-input multiple-output* (MIMO) structures [55, 27] in order to be able to reduce or cancel cochannel interference and to detect several signals simultaneously. The equalizer structure contains coefficients (tap weights). Equations and methods to calculate the coefficients are derived mathematically based on an optimization criterion. In contrast, the coefficients of the previously described structures, multistage detectors and interference cancelers, are directly obtained from the channel information according to intuitive reasoning (cancel interference) rather than by optimization. MIMO equalizers exist as linear or nonlinear (decision-feedback) structures. They are the main subject of this dissertation. A detailed literature discussion is included in the following section.

1.4 Literature Survey

1.4.1 Calculation of the Error Probability

It is important in the analysis and design of digital communication systems to determine the system performance. The most intuitive and important performance criterion is the probability of error. A nonzero error probability is, due to system imperfections, caused by a distortion component in the receiver output signal. The probability distribution of the distortion signal is not Gaussian for most receivers, including the MMSE equalizer. Even for zero-forcing equalizers with an ideally Gaussian distributed noise component, system imperfections such as erroneous channel estimation, finite-length filters or a non-ideal sampling time may cause an interference component in the output signal, which is not Gaussian. In addition, a Gaussian approximation for the interference has been shown in many cases to lead to significantly inaccurate results for the error probability [21, 94]. Thus, it is desirable to describe the statistical properties of the interference accurately.

Problem Statement Consider a communication system with a linear time-invariant channel. For the sake of clarity, the input signal is assumed to be a sequence of binary symbols. Stationary noise is added at the receiver front end. After sampling at the symbol rate $1/T$, the unquantized equivalent baseband signal at the output of the receiver is

$$\tilde{\alpha}(t_0) = \alpha_0 h(t_0) + \sum_{\substack{i=-\infty \\ i\neq 0}}^{\infty} \alpha_i h(t_0 - iT) + \zeta(t_0) \tag{1.4}$$

where t_0 is the sampling instant, $\alpha_i \in \{-1; 1\}$ is the transmitted sequence of binary symbols, $h(t)$ is the overall channel impulse response between the transmitter and the receiver and $\zeta(t)$ is the additive stationary noise signal with variance $\mathcal{E}_\zeta$. Note that the first term in Equation (1.4) is the signal component and the second term is intersymbol interference (ISI). For simplicity, let us define $\tilde{\alpha}_0 \triangleq \tilde{\alpha}(t_0)$, $h_i \triangleq h(t_0 - iT)$ and $\zeta_0 \triangleq \zeta(t_0)$. In addition, consider the ISI random variable (RV)

$$Z \triangleq \sum_{\substack{i=-\infty \\ i\neq 0}}^{\infty} \alpha_i h_i \tag{1.5}$$

and the overall signal distortion RV

$$X \triangleq Z + \zeta_0 \tag{1.6}$$

which consists of ISI and noise.

Based on Equation (1.4), the decision variable can be expressed as

$$\tilde{\alpha}_0 = \alpha_0 h_0 + Z + \zeta_0 = \alpha_0 h_0 + X. \tag{1.7}$$

Note that the error probability of the system can be calculated by considering only the decision variable $\tilde{\alpha}_0 \triangleq \tilde{\alpha}(t_0)$ obtained at time $t = t_0$ because the system is assumed to be stationary. Consequently, the statistics of all other receiver samples taken at previous or subsequent times are identical.

Assuming that the symbols 1 and -1 occur with equal probability, the optimal

decision threshold is the midpoint 0 between the binary symbols.

Considering the symbol $\alpha_0 = -1$ has been sent, the first class of expressions for the error probability is obtained with Equation (1.7) by [72, 134]

$$P_e = \text{Prob}\{\tilde{\alpha}_0 > 0\}$$

$$= \text{Prob}\{\zeta_0 > h_0 - Z\} \tag{1.8}$$

$$= \int_{-\infty}^{\infty} q\left(\frac{h_0 - z}{\sqrt{\mathcal{E}_\zeta}}\right) P_Z(z)\, dz \tag{1.9}$$

$$= \int_{-\infty}^{\infty} Q\left(\frac{h_0 - z}{\sqrt{\mathcal{E}_\zeta}}\right) p_Z(z)\, dz \tag{1.10}$$

$$= E_Z\left[Q\left(\frac{h_0 - z}{\sqrt{\mathcal{E}_\zeta}}\right)\right] \tag{1.11}$$

where $q(z/\sqrt{\mathcal{E}_\zeta})$ and $p_Z(z)$ are the probability density functions (pdf) of the noise RV ζ_0 and the ISI RV Z, respectively. The corresponding complementary distribution function (cdf) of the noise is $Q(z/\sqrt{\mathcal{E}_\zeta}) = \int_{z/\sqrt{\mathcal{E}_\zeta}}^{\infty} q(u)\, du$, while the cdf of the ISI RV Z is $P_Z(z) = \int_z^{\infty} p_Z(u)\, du$. Note that in the case of Gaussian noise, the noise pdf is $q(u) = 1/\sqrt{2\pi} \exp\{-u^2/2\}$. $E_Z[\ldots]$ is the expectation operator, where the subscript 'Z' indicates that the expectation is taken over the RV Z.

In order to obtain the second class of expressions for the probability of error, let us assume for simplicity that $\alpha_0 = 1$ and substitute again Equation (1.7):

$$P_e = \text{Prob}\{\tilde{\alpha}_0 < 0\}$$

$$= \text{Prob}\{X < -h_0\}$$

$$= \int_{-\infty}^{-h_0} p_X(x)\, dx \tag{1.12}$$

where $p_X(x)$ is the pdf of the overall distortion RV X. Define the characteristic function of X by $\psi_X(s) \triangleq E_X[e^{-sx}] = \int_{-\infty}^{\infty} e^{-sx} p_X(x)\, dx$. Since X is the sum of the independent RV's Z and ζ_0, its characteristic function is the product of the characteristic functions of Z ($\psi_Z(s)$) and ζ_0 ($\psi_{\zeta_0}(s)$) [99]: $\psi_X(s) = \psi_Z(s)\psi_{\zeta_0}(s)$. The pdf of X can then be obtained through an inverse Laplace transformation by

the contour integral $1/(2\pi j) \int_C \psi_X(s) e^{sx} \, ds$. Substituting the last expression into Equation (1.12), exchanging both integrations and noting that $\int_{-\infty}^{-h_0} e^{sx} \, dx = s^{-1} e^{-h_0 s}$ yields the probability of error expressed by an inverse Laplace transform [47]

$$P_{\mathrm{e}} = \frac{1}{2\pi j} \int_C \psi_Z(s) \psi_{\zeta_0}(s) \frac{1}{s} e^{-h_0 s} \, ds. \tag{1.13}$$

If the noise is Gaussian distributed, $\psi_{\zeta_0}(s)$ will be given by a simple expression. In addition, an expression for $\psi_Z(s)$ may also be obtained easily provided that the interfering symbols are statistically independent. Nevertheless, a closed-form solution of the equations (1.9), (1.10), (1.11) or (1.13) has not been found and does most probably not exist. The more accurate and efficient methods used to approximate or bound the error probability start with one of these expressions and perform an approximation in order to achieve a mathematically tractable formulation.

Basic Approaches   The most straightforward approach to calculate the error probability is the *truncated pulse train approximation* [66]. While small interference pulses are neglected, all possible combinations of the dominant interference samples are evaluated in order to calculate the probability density of the interference. In particular, assume that the ISI is caused by M neighboring symbols. In this case, the RV Z takes on, with equal probability, 2^M discrete values, one for each combination of the binary, interfering symbols. Let us denote these possible values of Z by Z_m, where $m = 1, 2, \ldots, 2^M$. The error probability can then be calculated from Equation (1.8) by averaging over all values Z_m

$$\begin{aligned}
P_{\mathrm{e}} &= \mathrm{Prob}\{\zeta_0 > h_0 - Z\} \\
&= \frac{1}{2^M} \sum_{m=1}^{2^M} \mathrm{Prob}\{\zeta_0 > h_0 - Z_m\} \\
&= \frac{1}{2^M} \sum_{m=1}^{2^M} Q\left(\frac{h_0 - Z_m}{\sqrt{\mathcal{E}_\zeta}}\right).
\end{aligned} \tag{1.14}$$

If the noise is Gaussian distributed, $Q(x)$ will be the well-known Q-function and the above expression can readily be solved. However, its evaluation is only economical

if M is very small. It becomes inefficient for moderate to large M as the required amount of operations grows exponentially with the number of interfering symbols. Very often, not all but only the M largest interferers are included in the calculation in order to reduce the computational effort (*truncated pulse train*). For most cases of practical interest, the result can be shown to be a lower bound of the true error probability [52].

The *worst case bound* [66] is a more efficient method. It always assumes the largest possible amount of interference, i.e. $Z_{\max} = \max\{Z_m\}$. This leads to the very simple expression

$$P_{\mathrm{e}} < Q\left(\frac{h_0 - Z_{\max}}{\sqrt{\mathcal{E}_\zeta}}\right). \tag{1.15}$$

However, this upper bound is in most cases rather loose.

Chernoff Bounds Define the complementary step function $S(x) \triangleq 1, \ \forall x < 0$; $S(x) \triangleq 0, \ \forall x \geq 0$. With this, the probability of error in Equation (1.12) can equivalently be expressed as

$$
\begin{aligned}
P_{\mathrm{e}} &= \int_{-\infty}^{\infty} S(x + h_0) p_X(x) \, dx \\
&= E_X[S(X + h_0)]
\end{aligned} \tag{1.16}
$$

where $E_X[\ldots]$ denotes the statistical expectation taken over the RV X. Since the step function can be upper bounded by the negative exponential $e^{-\lambda x} \geq S(x), \ \forall x \in \mathbb{R}, \ \lambda > 0$, the following inequality for the error probability holds

$$P_{\mathrm{e}} < e^{-\lambda h_0} E_X\left[e^{-\lambda X}\right]. \tag{1.17}$$

The second term on the right hand side is the *exponential moment* of X, which can be expressed in closed form because X consists of a sum of independent RV's. λ is an arbitrary positive real number, that is usually optimized to determine the tightest

upper bound. The above bounding technique is called the *Chernoff bound*.

The first application of the Chernoff bound for the calculation of the error probability can be found in Saltzberg's publication [103]. Instead of using the exact expression for the exponential moment of the ISI RV Z, he introduced two exponential functions which are always larger than $E_Z[e^{-\lambda Z}]$ in order to simplify the mathematical formulation further. In his most general result for the error probability, both approximations are used. The interference samples h_i have to be assigned to either of two sets which correspond to the two exponential approximations. The assignment of the h_i as well as the determination of λ is done such that the tightest bound is achieved. Hence, in general all h_i have to be known, the noise is restricted to be Gaussian and the data symbols α_i have to be statistically independent. However, an important special case is obtained by assigning all h_i to one set. Although suboptimal, this leads to a very simple bound, often referred to as the *Saltzberg bound*, which requires knowledge only about the variance of the combined distortion consisting of ISI and noise. Foschini *et al.* [34] applied this bound to SISO MMSE equalizers, which leads to an upper bound on the error probability that depends only on the value of the MMSE.

Saltzberg's approach has been extended and refined by Lugannani [67]. The resulting upper bound never exceeds the worst case bound. However, the bound exceeds the true error probability, depending on the channel impulse response, by at least two to more than ten times.

Worst-Case Distribution Bounds   Glave [41] determined the worst-case distribution of the ISI RV Z that maximizes the error probability. This resulted in an upper bound on P_e, which is valid for both correlated and uncorrelated input data α_i and requires an "open eye" (i.e. the peak distortion Z_{max} is smaller than the distance between the decision threshold and h_0). The noise needs to be Gaussian and the only quantities required for the calculation of the very simple expression are the peak distortion Z_{max}, the signal sample h_0, the variance of the Gaussian noise $E[\zeta_0^2]$ and the variance of the ISI $E_Z[Z^2]$. Results suggest that Glave's approximation is somewhat tighter than Lugannani's Chernoff bound. Matthews [71] extended Glave's method

and derived both upper and lower bounds for different cases.

Other Simple Bounds   McLane [73] presented two simple lower bounds on the error probability which hold for an open eye and in some cases when the source symbols α_i are correlated. The calculation of the bounds requires the value of the peak distortion and the second moment of the ISI RV Z. For one bound, also the fourth moment of Z is needed. The bounds are given by a simple expression which is independent of the number of interfering symbols. They are reasonably accurate considering their simplicity.

Milewski [76] derived upper and lower bounds for systems with an open eye, whose computation requires the knowledge of all interference samples h_i. His results showed that they were tighter than the Chernoff and worst-case distribution bounds. The number of necessary operations increases linearly with the number of interfering symbols (M).

A lower and an approximate upper bound, which are fairly tight, are described by Jenq *et al.* [53]. The approximation to the upper bound is twice the lower bound and their expression is very simple. The noise is not restricted to be Gaussian, but its cdf is required. One needs to know all interference samples and the number of operations grows linearly with M. The published results show that the bounds are significantly tighter than the Chernoff bounds of Saltzberg and Lugannani.

Another class of upper and lower bounds, which are based on bounds on the distribution function of the sum of two random variables, is presented by Prabhu [95]. They can be used to calculate the error probability with arbitrarily small error. Their application is, however, more complex than the above methods.

Approximations and Bounds on the Error Integral   This class of methods starts with either of the two equivalent expressions (1.10) or (1.11) for the error probability and approximates a certain part of it in order to solve the problem analytically or numerically. Since the expectation over the noise cdf with respect to the ISI RV Z, $E_Z[Q([h_0 - z]/\mathcal{E}_\zeta^{1/2})]$, normally cannot be solved, one usually tries to manipulate this expression such that it reduces to the moments $E_Z[Z^n]$ ($n = 2, 4, 6, \dots$) or the ex-

ponential moment $E_Z[e^{-\lambda Z}]$. These moments can be calculated. The computational complexity for the following methods generally increases linearly with the number of interfering symbols. Nevertheless, the exact number of operations required as well as the complexity of applying the different algorithms varies significantly.

One of the first approaches to yield high precision results for the error probability has been proposed by Ho and Yeh [48]. Considering expression (1.10), they developed the Gaussian noise cdf $Q([h_0 - z]/\mathcal{E}_\zeta^{1/2})$ into a Taylor series around $z = 0$ and obtained the error probability in terms of the even ISI moments $E_Z[Z^n]$. Theoretically, the accuracy of the result can be made arbitrarily small by increasing the number of series terms. In practice, however, the truncated series expansion for the error probability tends to oscillate occasionally when additional higher order terms are included. This is in particular the case when the signal-to-noise ratio (SNR) is high and/or when the peak distortion $Z_{\max}$ becomes large. Later, the above method, valid for binary modulation, was extended to multilevel pulse amplitude modulation (PAM) by the same authors [49].

The main problem of the series expansion used by Ho and Yeh is that the Taylor approximation is locally optimal around the point of development and becomes increasingly inaccurate for growing distances. Similarly, Murphy [84] proposed a polynomial approximation of $Q([h_0 - z]/\mathcal{E}_\zeta^{1/2})$, but he used a Legendre polynomial which minimizes the L_2-norm. Hence, this approximation is globally optimal within the region of support (ROS) of the RV Z, i.e. it minimizes the error variance between the approximation and the original function. Consequently, this method does not oscillate and converges fast towards the exact value for additional polynomial terms. In the same paper, he also introduced the approximation of $Q([h_0 - z]/\mathcal{E}_\zeta^{1/2})$ by a series of negative exponentials whose parameters are determined according to the same strategy of global approximation.

In a similar approach, Nakhla [85, 86] approximated the noise cdf $Q([h_0 - z]/\mathcal{E}_\zeta^{1/2})$ by a polynomial which is globally optimal in a minimax sense (Chebyshev approximation) within the ROS of Z. Again, an evaluation of the ISI moments is required. The method does not oscillate with additional polynomial terms, converges fast and promises very accurate results.

The previous methods are all based on a polynomial approximation of the noise cdf with respect to different optimization criteria. Consequently, the moments of the ISI RV Z are required. In comparison, a calculation of the exponential moment $E_Z[e^{-\lambda Z}]$ may be done more efficiently. This suggests to approximate $Q([h_0-z]/\mathcal{E}_\zeta^{1/2})$ by a linear combination of exponentials.

One approach is to use a Fourier series expansion for the noise cdf, which minimizes the variance of the approximation error within the ROS of Z and is thus globally optimal. This idea was introduced by Levy [65] and extended by Beaulieu [11]. The latter also derived several bounds for the approximation errors. Obtained are approximations for the error probability rather than bounds. Later, the method was generalized by Reuter [102] in order to apply it to arbitrary modulation formats.

Amadesi [7] used only one exponential which is a "good" approximation of the noise cdf within the ROS of Z. The parameters of the approximation are given by an empirical expression rather then being optimized in a strict sense. Only one exponential moment has to be determined and the number of required operations is consequently significantly smaller than in the Fourier series approach. However, the accuracy of the approximation for the error probability is lower.

In the same manner, McGee [72] applied only one exponential in order to bound the noise cdf. For this purpose, he developed the natural logarithm of the noise cdf into a Taylor series and truncated it after the linear term. Hence, the approximation is locally optimal around the point of development, which may be chosen arbitrarily. In practice, the choice of this point should be optimized to obtain the tightest upper bound. However, McGee outlined the method only briefly and suggested to use a crude approximation of $Q(x)$ in order to find a good point of development.

Yao and Tobin [134] obtained upper and lower bounds for the error probability by replacing the noise cdf with functions whose expectations over the ISI RV Z can be calculated. Their approach was to apply an isomorphism theorem from the theory of moment spaces. Functions used were the absolute value of Z, Z^2, Z^4, and an exponential in Z. It was found that the absolute value leads to the same lower bound as that derived by McLane [73] and that Z^2 results in the worst-case distribution bounds of Glave [41] and Matthews [71]. In addition to an analytical approach, the

bounds can be obtained with a graphical method. Yao [132] used the same method for calculating error probabilities for asynchronous SSMA/CDMA systems with a matched filter receiver. In this publication, he also applied a linear combination of (real) exponentials as approximation to the noise cdf. The parameters of the exponentials were chosen such that the approximation is identical to the noise cdf at several points within the ROS of Z.

Instead of directly evaluating the expectation over the noise cdf (1.11), Yao and Biglieri applied the principal representation of Krein in the theory of approximation in order to upper or lower bound the error probability [133]. The tightest bounds have been obtained with this method. However, their computation is extremely complicated [47].

Benedetto *et al.* [15] found an approximation for the whole integral (1.10) by expressing it as a linear combination of values of the noise cdf. The parameters of the linear combination are determined by the method of Gauss quadrature rules, which requires the moments $E_Z[Z^n]$. The noise is not restricted to be Gaussian, very accurate results are obtained and the method converges very fast, but the computations are long and intricate [47].

The methods described previously all use a similar approach in that they approximate either the noise cdf or the whole error integral. For that, the moments or exponential moments of the ISI RV Z have to be calculated. In contrast, Metzger [75] described a numerical algorithm in order to approximate the pdf of the ISI RV, $p_Z(z)$, by a staircase function. With this knowledge, an approximation of the error probability can be computed by numerically evaluating the integral (1.10). The accuracy as well as the number of required operations depends on the resolution chosen for the representation of the ISI pdf.

Approximations and Bounds on the Inverse Laplace Integral   Shimbo and Celebiler [112] developed a very similar method to that of Ho and Yeh [48] at about the same time. The difference is that they start with the representation of the error probability as an inverse Fourier transform, which is practically identical to expression (1.13). After that, they developed the characteristic function of the ISI RV Z,

$\psi_Z(s)$, into a Taylor series around the origin $s = 0$. The remaining integral expression can then be solved by calculating the even ISI moments. Like Ho and Yeh's approach, their method can be made arbitrarily accurate in theory by including additional series terms. In practice, however, the truncated series tends to oscillate for a growing number of terms. The problem is again the use of a locally optimal approximation around a nonoptimal point of development ($s = 0$).

Upper and lower bounds have been derived by Prabhu [96]. The upper bound was obtained by realizing that the absolute value of the integral (1.13), which is identical to the error probability, is smaller than or equal to the integral over the absolute value of its integrand. A parameter search and the determination of the exponential moment of the ISI RV is required for the calculation of the result.

Starting with Equation (1.13), Yue [135] expanded the natural logarithm of the product $\psi_Z(s)\psi_{\zeta_0}(s)e^{-h_0 s}$ into a Taylor series around the saddle point of the integrand. He truncated the series after the linear term and solved the remaining integral. The resulting approximation for the probability of error is very accurate and requires a relatively low number of operations. In addition, his expression is easy to use. The main reason for the accuracy of the method is that the locally optimal Taylor expansion is developed around a well chosen rather than an arbitrary point. Although not shown analytically, the result is almost exclusively smaller than the true error probability. In addition, less accurate upper and lower bounds were derived.

Helstrom [47] proposed to solve the inverse Laplace integral (1.13) by numerical quadrature. He applied the trapezoidal rule and evaluated the integrand at equally spaced points. The truncation of the integration interval as well as the integration step size are chosen such that a desired accuracy is achieved. A bound for the truncation error in the case of Gaussian noise is given. The method is applicable to arbitrary noise as long as the characteristic function of the noise pdf is known. A very useful feature is a term which upper bounds the effects of neglected ISI symbols based on their energy. Generally, the method can be made arbitrarily accurate. However, the number of necessary operations usually exceeds that of Yue's method for the same accuracy because Helstrom's approach requires the calculation of one complex exponential moment for each integration point.

1.4.2 MIMO Equalizers for Spread Spectrum Systems

This section reviews findings and results in the area of multiple-input multiple-output (MIMO) equalizers, a structure which is able to detect several signals simultaneously. In general, the MIMO structure is a generalization of the well-known single-input single-output (SISO) equalizer, which is mainly used in order to reduce intersymbol interference (ISI) caused by time-dispersive channels.

MIMO Linear Equalizers The earliest MIMO equalizer structure proposed as a detector for SSMA/CDMA multiuser systems is the *decorrelating detector* [68, 110] for synchronous signal reception. It is identical to the MIMO linear equalizer (LE) optimized according to the zero-forcing (ZF) criterion. The first part of the decorrelating detector is identical to the matched filter detector and consists of a bank of filters matched to each of the received signal waveforms. The structure detects simultaneously a block of data symbols and is similar for synchronous, flat fading [68] and asynchronous/frequency selective fading channels [60]. In the case of synchronous data reception and flat fading channels, the N outputs[9] of the matched filters are multiplied by a $N \times N$ matrix which is the inverse of the autocorrelation matrix for all received signal waveforms. If the data is received asynchronously or if the channels are strongly frequency selective, the autocorrelation matrix is of dimension NL, where L denotes the total number of symbols per transmitted data block. The realization of the block decorrelator [60, 131], which requires the inversion of the autocorrelation matrix, may thus be computationally intensive. Alternatively, a continuous signal detector following the matched filters may be employed [29]. The N matched filter outputs are fed into a matrix filter with N inputs and N outputs. The matrix filter can be interpreted as a matrix in which each element is a linear discrete-time filter rather than a simple scalar value.

The decorrelating detector eliminates effectively all remaining interference (ISI and CCI) components in the output signals of the matched filters. In other words, it cancels interference resulting from correlated waveforms of different users. Hence the

---

[9]The variable N denotes the number of users in the system.

name *decorrelating detector*.

Lupas *et al.* [68] have shown that the decorrelating detector exhibits the same degree of near-far resistance as the optimum MLSE detector. For synchronously received data, its complexity per detected symbol is shown to increase only linearly with the number of users. This characteristic makes the decorrelating detector attractive for practical implementation. An alternative structure of the decorrelating receiver for synchronous, frequency selective (multipath fading) channels is described by Zvonar [137]. This detector can be extended to a receiver using multiple receive antennas in asynchronous, frequency selective channels [138].

It is important to note that the price for completely cancelled (zero-forced) interference is amplified noise in all output signals. For this reason, the decorrelating detector performs generally worse than the MIMO linear equalizer (LE) optimized according to the minimum mean-square error (MMSE) criterion. MMSE MIMO equalizers minimize the variance of the combined distortion consisting of both interference and noise. The MMSE MIMO LE structure has been described and investigated by several authors [16, 27, 51, 105, 131].

The optimal single-input single-output (SISO) MMSE linear receiver for nonlinear channels has been derived by Biglieri *et al.* [16]. However, it is possible to apply their results to multiuser systems with linear channels. The equalizer is optimal even if the the Gaussian noise signal is not white.

The system described by Salz [105] consists of a continuous-time channel with N inputs (users) and N outputs (receive antennas). An expression for the MMSE averaged over all N signals is derived. Using a time-domain analysis, it is shown that the optimal continuous-time MMSE receiver consists of the same bank of matched filters that is part of the decorrelating detector followed by symbol rate samplers and a discrete-time $N \times N$ matrix filter. The structures of the linear decorrelating and MMSE LE detectors are therefore the same.

The most general case has been considered by Honig *et al.* [51]. The solution for the MMSE MIMO LE is applicable for correlated input signals, colored Gaussian noise, an arbitrary linear continuous-time $N \times N$ channel and N receiver inputs. Mean-square error (MSE) expressions for the MMSE and zero-forcing (decorrelating)

LE were derived. Almost identical results have been obtained independently by Duel-Hallen [27] for an $N \times N$ discrete-time channel model, which implicitly assumes a waveform matched filter front-end structure of the detector.

A surprisingly early work about an adaptive version of the MMSE MIMO LE has been described by Harrison in his Masters thesis [44]. An extension to the MMSE MIMO DFE with feedback of the signal of interest is also outlined. The equalizer structure was based on an implementation initially derived by Kaye and George [57], which seems to be the first description of the optimal MMSE MIMO LE. Interestingly, his work already considered potentially a multiuser system, multiple receiver inputs (antenna diversity) and he showed that the optimal structure may be realized by a bank of filters matched to each signal waveform followed by symbol-rate samplers and tapped delay-lines.

Madhow *et al.* [70] analyze another adaptive implementation of the MMSE LE. This structure does not require a priori knowledge of the channel and can be used in a time-varying environment. However, in the case of strong cochannel interference, the convergence performance and speed of the adaptive algorithm are a major concern. Miller [77] performed a time-domain analysis of an adaptive MMSE LE consisting of a chip matched filter followed by an adaptive, chip-spaced equalizer structure. The adaption may be performed with a standard LMS or RLS algorithm. Only a training sequence for the user of interest is required in order to adapt the tap weights. The detector is immune to the near-far problem and shows good performance in the presence of both narrowband and multipath interference. This structure can easily be extended to a receiver with multiple antenna elements [63], which improves the performance and increases the capacity (larger number of possible users). However, the dimension of the matrix to be inverted, either directly or by using an adaptive algorithm, increases linearly with each additional equalizer coefficient. The number of coefficients may easily become large for this structure and the number of required operations grows rapidly.

While the previous MMSE equalizers are continuous signal structures (matrix filters), Xie *et al.* describe a block implementation of the MIMO MMSE LE for an additive white Gaussian noise (AWGN) channel and asynchronously received CDMA

signals [131]. Instead of processing the signals symbol by symbol, all symbols within one block are detected simultaneously. The detector is realized in the time domain by inverting the modified autocorrelation matrix. It is practically identical to the MMSE block linear equalizer used for frequency-selective channels [61]. Note that the dimension of the matrix to be inverted is equal to the product of the number of users and the block length of the transmitted symbols, which may be a very large number. Some reduction in the number of operations is achieved by using a LU decomposition.

An implementation of the block decorrelator and MMSE block LE which avoids a direct inversion or decomposition is based on the polynomial expansion of the inverse autocorrelation matrix [80, 81]. This approach may reduce the number of required operations significantly.

MIMO Decision-Feedback Equalizers   An improvement to the linear equalizer can be achieved by feeding previous decisions back into a linear filter in order to reduce interference in the present symbol. The resulting *decision-feedback equalizer* (DFE) is nonlinear since nonlinear decisions are used in the detection process. Analytical treatments and performance evaluations of the single user SISO DFE have been published already more than three decades ago [6, 9, 39, 58, 98, 104]. Later, this structure has been extended to receivers with multiple inputs and outputs. There exists now a wide variety of different implementations for the multiuser DFE, which all share the concept of feeding back symbols from the outputs of the nonlinear decision elements.

The continuous signal DFE consists of a linear feedforward matrix filter with U_{div} inputs and N outputs, where U_{div} is the number of receiver inputs (diversity paths) and N is the number of users or waveforms. Subtracted from each output is a noise estimate that is obtained from a linear transformation of previous (nonlinear) decisions. This linear transformation is in general a linear, causal $N \times N$ feedback matrix filter. In the case of flat fading channels and synchronous data reception, the matrix filters reduce to conventional matrices with scalar values as elements; in this case, half of the elements of the feedback matrix including the main diagonal elements

are constrained to zero in order to satisfy the causality requirement.

The block DFE consists of two matrices, one in the forward and the other in the feedback section, which are obtained from a Cholesky factorization of the (modified) autocorrelation matrix. In the synchronous, flat fading channel case, the matrices are of size $N \times N$. However, their dimension will increase to[10] $NL \times NL$ if the signal reception is asynchronous or if the channels are time-dispersive.

It has been shown in the single user case that the DFE achieves, depending on the channel, more or less significant performance gains over the linear receivers provided that the error rate in the output signals is sufficiently low [104]. The difference among various multiuser DFE structures and descriptions is a result of

- block structure or continuous signal structure,

- different optimization criteria (MMSE, ZF),

- different analysis domains (time, frequency),

- continuous- or discrete-time implementation of the forward filter,

- different channel characteristics (flat, frequency selective fading),

- synchronous or asynchronous data reception,

- the feedback of all possible or only some output signals,

- adaptive or nonadaptive implementation, and

- different feedback structures (noise-predictive or conventional).

Belfiore *et al.* [14] described an alternative implementation of the single user DFE which feeds back the noise component in the output signal of the forward filter rather than the decisions. Since the feedback filter estimates the noise component in the present symbol before quantization from the known noise components of past symbols, it is in fact a linear prediction filter. Hence, this structure of the DFE has been named *noise-predictive* (NP) DFE. The output of the predictor is added to the output of

---

[10]L is the number of symbols per data block and N is the number of users in the system.

the forward filter and the error signal at the input of the decision element is equal to the prediction error provided that all previous decisions are correct. It can easily be shown that the conventional DFE and the NP-DFE are equivalent and that their performance is identical. In fact, the feedback filters of both structures are the same. Only the forward filters are different. Interestingly, the forward filters of the NP-DFE and the LE (with respect to either MMSE or ZF criterion) are identical. These results also hold for the corresponding MIMO structures.

Let us now discuss some specific MIMO DFE structures. The decorrelating (ZF) decision-feedback equalizer [28] minimizes the MSE under the constraint of zero interference in the input signals to the decision elements. A CDMA system, flat fading channels and synchronous signal reception have been considered. The DFE structure has one input and consists of a bank of code matched filters followed by a $N \times N$ upper triangular matrix, which has been obtained from Cholesky factorization of the code autocorrelation matrix. The output signal of the strongest user is directly connected to a decision element. The hard decision is appropriately weighted and subtracted from the remaining outputs of the forward matrix. Then, a decision on the second strongest user signal is made, which is also weighted and fed back to the remaining weaker signals. This procedure is continued for all other signals until the complete cochannel interference in the weakest user's signal is cancelled. Provided that all previous decisions are correct, the decorrelating DFE eliminates completely the cochannel interference in all input signals to the decision element. It can be shown that the performance of the LE and DFE decorrelating detectors are identical for the strongest user. For the DFE, however, the error probability of the weakest user is equal to the single user case, i.e. the hypothetical situation when only the weakest user's signal is transmitted over the channel. Thus, for all but the strongest user, the decorrelating DFE performs better than the decorrelating LE.

Decorrelating (zero-forcing) DFE structures suited for asynchronous and/or frequency-selective channels have been described by Duel-Hallen [29] (continuous signal version with matrix filters) and Klein *et al.* [61] (block version with scalar matrices).

The MMSE DFE structure described by Petersen *et al.* [92] consists of a single-input single-output continuous-time forward filter whose output is sampled at the

symbol rate. Only the signal of interest is detected and fed back to an infinite-length discrete-time filter. The results are valid for asynchronous as well as synchronous data reception over flat or frequency selective fading channels. It is shown that the optimal structure of the forward filter may be realized with the well known bank of matched filters[11] followed by symbol-rate samplers and a $N \times 1$ vector filter whose components are anti-causal, infinite-length, discrete-time filters. An expression for the MMSE performance of this equalizer is derived. In addition, it is shown for a generalized ZF LE (decorrelating detector) that the number of supportable users[12] has to be smaller than or equal to the signal bandwidth in terms of the data rate. The same author [91] has performed a frequency-domain analysis of this DFE structure. He derived expressions for the optimal filters and the MMSE. In addition, it is shown that the performance will be significantly better if the cyclostationary nature of the interference is taken into account rather than modeling it by equal energy stationary noise.

The same DFE structure as before has been used by Abdulrahman *et al.* [2] with the exception that the continuous-time forward filter [92] is replaced by a sampler followed by a fractionally-spaced discrete-time filter. The output of the forward filter is downsampled to the symbol rate, which is equivalent to the symbol-rate samplers in Petersen's structure [92]. If aliasing is avoided by sampling the input signal at a rate of at least twice the signal bandwidth, both structures will have the same performance. It has been found that cyclostationary interference can be effectively suppressed and that the fractionally-spaced DFE (FS-DFE) is not sensitive to the sampling phase. A suboptimum structure with a symbol-rate spaced forward filter was also investigated. This structure shows sensitivity to the sampling phase and performs significantly worse. The performance of the FS-DFE, depending on the number of system users and forward filter taps, has been simulated by the same authors [3]. This investigation was performed for a CDMA system with processing gain 8 and slow fading frequency selective channels. The issues of convergence time, birth/death of interferers and decision-directed convergence for an adaptive implementation of

---

[11]The filters are matched to the waveform of the received signal.
[12]The users are interferers that operate at the same symbol rate as the user of interest.

the FS-DFE are addressed in other publications of Abdulrahman *et al.* [1, 4]. The results show that the parameters converge relatively slowly. The convergence time varies between several hundred and several thousand symbols in a system with 4 to 6 interferers.

A generalization of the above DFE to a structure with multiple receive antenna elements can be found in publications of Subramanian [114] and Legnain *et al.* [62]. Their results confirm that the performance and capacity of the system improved significantly with additional antennas.

DFE detectors that feed back decisions from all signals have been described and analyzed by Kavehrad *et al.* [55] and Duel-Hallen [27]. These fully connected MIMO structures are suited for systems with frequency-selective channels and asynchronous data reception. They consist of a linear forward matrix filter and a feedback block. The feedback part is essentially a linear $N \times N$ matrix filter whose inputs are the N output signals of the decision elements for each user. The outputs of the feedback filter are added to the output signals of the forward filter. The first detection approach [55] can be described as completely parallel in time. All symbols transmitted at the time $n = n_0$ are detected simultaneously based on previously detected symbols transmitted at $n < n_0$ only. Thus, all symbols transmitted at the same time are detected with the same amount of available information provided by the feedback filter.

The second detection approach [27] is slightly different. Rather than using only previous symbols as feedback inputs, the output signals of the feedback matrix are based on both previous and some present symbols. For that, the received signals are ordered according to their strength or performance. The signal with the largest received power is *signal 1*, the second strongest is *signal 2*, and so on. At time $n = n_0$, the decision is made on the symbol of user 1 first. Then follows the decision on the symbol of user 2, until finally user N's symbol is detected. Note that, for the detection of user i's symbol ($i = 2, 3, \ldots, N$), not only are all previous decisions available but also the decisions of the present symbols from users 1 to $i - 1$. Despite this time-sequential element, the described detector operates mainly parallel in time. The optimal MMSE MIMO DFE for a N-input N-output discrete-time channel is derived in the same paper [27]. A frequency-domain method is used which requires

the spectral factorization of a matrix spectrum. The channel model implies that the receiver front end consists of filters matched to the received signal waveforms (codes plus channels).

The DFE with feedback from all users may also be applied to receivers with multiple receive antennas [64]. The system capacity increases and the performance improves with each additional antenna. However, the numerical complexity will strongly increase with the number of antennas, especially if the equalizer coefficients are determined according to the conventional time-domain approach [64, 46]. Another method to calculate a fixed structure, realizable MIMO MMSE DFE is outlined by Tidestav *et al.* [115].

Eleftheriou *et al.* [31] have described a MMSE MIMO DFE based on the noise-predictive structure. The optimal forward and feedback matrix filters are determined using a frequency-domain approach similar to that of Duel-Hallen [27]. The solution is expressed in terms of a matrix filter obtained through spectral factorization. As the detector described before [27], this equalizer detects the N signals predominantly parallel in time. The predicted noise is calculated from all past and some present decisions.

In contrast to the above DFE realizations, which are continuous signal structures, Klein *et al.* [61] derived a block implementation of the DFE. Both ZF and MMSE block DFE are described. Basically, these structures are an extension of the decorrelating DFE for flat fading channels and synchronous signal reception to systems with time-dispersive and/or asynchronous channels.

Optimal Detector Structures Let us review optimal structures for the class of linear and decision-feedback equalizers. Using a time-domain approach, one obtains the optimal equalizer usually directly in a "one-block" realization. In the frequency-domain analysis, however, it is often advantageous to split the equalizer into different blocks. To my knowledge, Kaye *et al.* [57] were the first to observe that the optimal structure of a linear equalizer, using several inputs (antenna diversity) and arbitrary signal bandwidth, may be obtained by a bank of filters matched to each of the received signal waveforms followed by symbol rate samplers and a discrete-time matrix filter.

If the additive noise signals at the receiver input are colored or correlated, a noise-whitening matched matrix filter has to precede the bank of (waveform) matched filters [117]. Interestingly, the front-end part of the MLSE detector consists as well of the matched noise-whitening, waveform matched filters and symbol rate samplers [99]. In fact, the discrete-time outputs of this combined front-end structure constitute a set of sufficient statistics. Recently, it has been shown by Vandendorpe *et al.* [118] that the same front-end structure is also a possible realization of the optimal MMSE MIMO DFE.

Block Detectors Versus Continuous Signal Detectors   This section shall be concluded by a different method of categorizing equalizers. Firstly, it is important to distinguish between detectors used in two different systems:

- synchronous signal reception *and* flat (frequency-nonselective) fading channels, and

- asynchronous signal reception *or* frequency selective fading channels.

Equalizers for the first case of synchronous reception and flat fading channels reduce to relatively simple structures because only $N - 1$ "same time" symbols of cochannel users interfere with the symbol of the desired user. In fact, the task of estimating all symbols transmitted at different times decouples into successively estimating the N symbols of all users transmitted at time n, after that those transmitted at time $n + 1$ and so on. Each time instant is independent of symbols transmitted at other times and can be treated separately. The problem becomes effectively one of inverting or decomposing a $N \times N$ matrix. Thus, the total number of required operations per symbol depends on the number of users, N. Among the above mentioned equalizers, other approaches fall into this category [28, 68, 110].

On the other hand, if either the signals are received asynchronously or the channels are time dispersive (frequency selective), each symbol to be detected not only depends on those of other users but also on previously and subsequently transmitted data. In this situation, the symbol detection cannot be decoupled anymore and the problem

becomes more complex. Generally, two main types of detectors can be distinguished for this situation:

- signal block detectors, and

- continuous signal detectors.

Note that in the special case of synchronous, flat fading channels, both the signal block and the continuous signal detectors reduce to the $N \times N$ matrix equalizers mentioned before.

Normally, it is assumed that the system uses a block transmission scheme. In this case, a certain number of symbols, say L, is transmitted over the channel. A straightforward extension of the synchronous detectors to asynchronous or time-dispersive systems lead to *signal block detectors*. Instead of estimating N symbols at each time instant, all LN symbols transmitted in the whole data block are detected simultaneously. Block detectors [60, 61, 131] may realize the decorrelator, MMSE LE or DFE exactly for the transmitted data block. Additionally, the effect of time-varying channels can easily be incorporated in the problem formulation provided that the channel impulse responses are known at all times. However, the correlation matrix is now of size $LN \times LN$, which may be large if there are many symbols per data block. Although the correlation matrix is more or less sparse, its inversion or decomposition may be numerically very complex. The total number of operations per symbol depends in most cases on the matrix dimension LN. This inspired a search for alternative methods avoiding a direct inversion or decomposition of the correlation matrix and thus reducing the number of required operations [79, 80, 81]. Another method of reducing the number of operations is to consider only a finite data window of length $M \ll L$ [54]. The resulting truncated detectors are suboptimal due to *edge effects*, however, it has been demonstrated that moderate window sizes are sufficient to obtain almost the same performance as the ideal block detectors even under severe near-far conditions [54]. The complexity then reduces to inverting or decomposing a matrix of size $MN \times MN$.

Continuous signal detectors are usually implemented as time-domain filters (tapped delay-line structure), but they can also be described by linear frequency-domain

transformations. Rather than realizing the ZF (MMSE) LE or DFE exactly, they approximate these equalizers by truncating their time length (delay-line) for all practical purposes to a certain number of symbol periods, say M. Although theoretically derived for continuous, infinite-length signals, continuous signal detectors may also be used in block transmission systems which have many symbols per block (compared to the channel memory). The parameters of these equalizers can be determined via time- or frequency-domain analysis.

The time-domain approach [1, 4, 57, 63, 62, 64, 70, 77, 105, 114, 115] is better suited to channels varying during the block duration. For example, the equalizer coefficients may be adaptively updated. The complexity of calculating the optimal equalizer coefficients is roughly on the order of $(NM)^3$ operations per data block. In addition, the detection process requires (MN) operations per symbol.

The equalizer coefficients may only be determined with a frequency-domain analysis [27, 29, 51, 91, 92] if the channels are at least quasi-stationary. In other words, the channel impulse response must be constant for the whole block duration, but it might change from one block to another. The main advantage of this approach is that the number of operations can be significantly reduced. There are approximately only N^3M operations per block required for the calculation of the equalizer coefficients and only on the order of N operations[13] for the detection of each symbol.

Note that continuous-time detectors become attractive from the viewpoint of numerical efficiency when the truncated equalizer length M is significantly smaller than the block length L.

1.4.3 Delayed-Decision-Feedback Equalization

Consider the reverse link of a multiuser system with frequency selective channels or asynchronously received signals at the base station. Spatially distributed portables and fading channel conditions may cause more or less severe near-far conditions. At the base station, a continuous signal MIMO DFE is employed in order to detect the SSMA multiplexed signals of all intracellular users. As discussed before, the common

---

[13]It is considered that all calculations are performed in the frequency domain. The number of operations required for the time/frequency signal transformation (FFT/IFFT) is not included.

MIMO DFE structures operate mainly parallel in time [27, 55], i.e. only decisions of all previous and some present symbols of all N users may be used in the purely causal feedback filter[14] in order to reduce interference.

Monsen [78] noticed that the parallel operation may be relaxed by "introducing delay into the desired signal channel to allow time for formation" of fed back decisions from cochannel users. This would make it possible to use decisions of subsequent (future) symbols from other users for an improved reduction of cochannel interference in the desired signal. The same idea was formulated by Duel-Hallen [29] who proposed the *partial feedback detector with delay*. With this detector, some users may apply decisions of future symbols from other users in the feedback process.

An adaptive version of the partial DFE with delay has been employed by Fulghum *et al.* [35, 36] in a two user, narrowband system with twofold spatial (antenna) diversity. It was found that the common, parallel feedback of only past and present symbols will yield a better performance if the received powers from both signals are similar. With an increasing difference between the received powers, the partial DFE with delay will eventually perform better than the parallel DFE if a detection delay is added to the weaker signal. This behavior can be explained as follows:

- In a system with a strong near-far effect, the decisions on the stronger user's symbols are significantly more reliable than the decisions from the weaker signals. Feeding back less reliable decisions with a larger error probability from weaker users to cancel interference in the strong signals may actually cause a performance degradation. No or less feedback of decisions from weaker signals may be the better choice.

- If the received powers are significantly different, the weaker users will have a much larger error probability. It is thus the weaker users who limit the overall system performance. Improving the quality of the weaker users by using more (past and future) decisions of stronger users thus results in a higher system performance.

---

[14]For the definition of "purely causal" see publication [27].

- The performance difference among strong and weak users may be large. Thus, putting more effort into an improvement of the weaker signals while sacrificing potential enhancement of stronger signals is a good strategy. Exactly this is achieved by delaying the detection process of weaker users, since more information (past and future decisions) is available in the feedback part for interference reduction.

Schlagenhaufer *et al.* [107, 106] introduced a mathematical model of the MIMO DFE with delay, called the *delayed-decision-feedback equalizer* (DDFE). The DDFE has a variable number of delay elements at each output of the forward matrix filter, just before the interference estimates provided by the feedback filter are canceled. DDFE structures are found for both the conventional and the noise-predictive MIMO DFE [106]. The DDFE is analyzed in the frequency-domain. Expressions for the individual MMSE's as well as the optimal forward and feedback filters are derived [107].

1.5   Thesis Contributions

System Model (Chapter 2)   An equivalent symbol-rate discrete-time model for the reverse link of a spread spectrum multiuser system is derived. It is suited for receivers with an arbitrary number of antennas. The system equations may be formulated conveniently in vector form. The description unifies the concepts of spread spectrum (frequency diversity) and input (antenna) diversity. It is shown that a system with processing gain K and A receiver inputs provides effectively $U_{\mathrm{div}} = AK$ parallel diversity channels. The mathematical treatment shows that there is no conceptual difference between frequency and antenna diversity. Both lead, in a similar manner, to an increase in the number of diversity channels.

Calculation of Error Probabilities (Chapter 3)   For systems using arbitrary rectangular quadrature amplitude modulation (QAM) whose inphase and quadrature signals are independent, expressions of the Saltzberg upper bound on the error probability have been derived. These expressions depend only on the signal-to-interference-

and-noise ratio (SINR) at the input of the decision device and the number of modulation levels.

A new class of bounds and approximations for the error probability is described. It includes a first and a second order approximation which provide very accurate results. The algorithms require the explicit knowledge of all interference symbols and they are both efficient and easy to use. As a special case, an energy upper bound, requiring information of the noise and interference variance only, is obtained.

Numerical results are presented which verify that the derived bounds and approximations are very accurate in all situations of practical interest. In addition, the algorithms are significantly more efficient than other very accurate methods such as those of Helstrom [47] and Beaulieu [11].

Equalizers for Spread Spectrum Multiuser Systems (Chapter 4) An extensive analysis is performed for multiple-input multiple-output (MIMO) linear and decision-feedback equalizers. The analysis is done in the frequency domain in order to reduce the number of operations required to calculate the optimal parameters of MIMO equalizers used in stationary or quasi-stationary systems.

Different equations for the optimal linear equalizer coefficients are presented, among them an expression for a direct realization of the linear equalizer (LE). This expression, which can be interpreted as a multidimensional extension of the non-causal Wiener filter from estimation theory, requires knowledge only about the power spectrum of the received signal and the cross-power spectrum of the received signal and the desired data. Provided that the desired data is known (for example from training or pilot symbols), the optimal coefficients may be calculated from quantities directly available at the receiver. In contrast, the current literature describes the LE in the frequency-domain by a cascade of noise-whitening matched filter, channel matched filter and symbol rate equalizer. For this formulation, explicit knowledge of the channel transfer matrix and the noise statistics are required.

The time- and frequency-domain approaches for the calculation of the optimal equalizer coefficients are compared. The result shows that the number of necessary operations increases linearly with the (time-) length (M) of the equalizer for the

frequency-domain based methods, while it grows cubically in M when a time-domain approach is applied.

A new lower bound for the average minimum mean-square error (MMSE) of a MMSE MIMO LE is derived. It is valid for overpopulated systems, i.e. for systems with more users than diversity channels. The bound becomes very tight for high SNR scenarios.

It is shown for the MMSE MIMO decision feedback equalizer (DFE) that its optimal structure may be realized by a cascade consisting of a noise-whitening matched filter, a channel matched filter and a symbol rate matrix filter. A different formal proof for this optimal structure has been found only recently by Vandendorpe *et al.* [118].

It is well known that there exists a unique relationship between the signal-to-interference-and-noise ratio (SINR) and the MMSE of the single-input single-output MMSE LE and DFE [99]. This dissertation provides a proof that the same relationship holds also for both the MIMO MMSE LE and DFE. This enables the application of Foschini's *et al.* [34] and Saltzberg's [103] upper bound on the error probability to multiuser systems with MIMO linear or decision-feedback equalizers.

A lower capacity bound is derived for multiuser systems using square quadrature amplitude modulation (QAM). The inphase and quadrature signals have to be independently pulse amplitude modulated with an equal number of signal levels.

Finally, numerical results are provided for the performance of the MIMO LE and DFE in terms of the MMSE, bit error rate (BER), outage probability and capacity. It is found that the LE will be able to perform well only if the number of system users is smaller than the number of diversity channels. On the other hand, a MIMO DFE may perform satisfactorily even in overloaded systems with more users than diversity channels.

Delayed-Decision-Feedback Equalization (Chapter 5)   Monsen [78] and Duel-Hallen [29] initially formulated the idea that the performance of a MIMO DFE may be improved by delaying the decisions on the weaker signals with respect to the stronger ones. Simulation results published by Fulghum [35, 36] verify this assumption for an adaptive MIMO DFE applied in a multiuser system, in which the received powers

from the users differ significantly. However, a mathematical analysis of the problem has not been performed yet.

This dissertation introduces a model for the MIMO delayed-decision-feedback equalizer (DDFE). The delay elements for each signal are described by a diagonal matrix. This enables the mathematical analysis of the system. A closed-form solution for the optimal coefficients of the MIMO DDFE is derived and expressions for the equalizer performance are found.

It is generally necessary to perform a matrix spectral factorization in order to determine the optimal MIMO DDFE. This procedure is, however, numerically complex and requires many operations. A hybrid algorithm for the noise-predictive structure of the MIMO DDFE is developed, which does not need a matrix spectral factorization. In the first step, the forward filter is calculated in the frequency domain. After that, the optimal coefficients of the feedback filter are determined in the time domain.

The MIMO successive decision-feedback equalizer (S-DFE) is a special case of the DDFE. It is obtained by increasing the delays between two consecutive signals hypothetically to infinity. In other words, the signals from different users are completely processed one after another. At first, all symbols of the first user are detected, then all symbols of the second user and so on. The concept of the S-DFE is introduced and a model is described. A mathematical analysis is performed and the optimal equalizer coefficients are derived. Compared to the DDFE, the optimal S-DFE can be calculated with a less complex and numerically significantly more efficient method. It requires solely Cholesky factorizations of several matrices rather than a matrix spectral factorization.

Numerical data are presented which compare the MIMO DFE, DDFE and S-DFE detectors. The results show that the equalizer versions with delay perform superior in near-far situations when the received powers of different signals differ significantly. In particular, the DDFE and S-DFE versions are able to mitigate the malicious consequences of the near-far effect, either eliminating the necessity for power control or requiring a less stringent and simpler power control technique.

1.6   Notation

The notation used in this dissertation is discussed in Appendix A. Section A.1 explains the general symbol notation. Arguments supporting a row vector notation are provided in Section A.2. Functions, operators, constants and sets are defined and explained in Sections A.3 to A.5. Section A.6 includes some statistical definitions. A short section about a specific set of orthogonal basis functions can be found in A.7. Finally, four different kinds of Fourier transforms are described in Section A.8.

1.7 D-Transform

The D-transform provides a powerful tool to analyze systems. It is regularly used in this thesis. This section defines the transform and states some important properties.

Let $\boldsymbol{V}[n]$ be an arbitrary dimensional matrix, vector or scalar whose elements $[\boldsymbol{V}[n]]_{ik}$ are scalar, complex sequences ($[\boldsymbol{V}[n]]_{ik} \in \mathbb{C}$).

Definition 1.1 *D-transform.*
The D-transform of the matrix sequence $\boldsymbol{V}[n]$ is

$$\boldsymbol{V}(D) = \mathcal{D}\left\{\boldsymbol{V}[n]\right\} \triangleq \sum_{n=-\infty}^{\infty} \boldsymbol{V}[n]D^n \tag{1.18}$$

where D belongs to the set of complex numbers ($D \in \mathbb{C}$).

Accordingly, the inverse D-transform is denoted by

$$\boldsymbol{V}[n] = \mathcal{D}^{-1}\left\{\boldsymbol{V}(D)\right\}. \tag{1.19}$$

An alternative notation for the transform pair $\boldsymbol{V}[n], \boldsymbol{V}(D)$ is

$$\boldsymbol{V}[n] \xleftarrow{\mathcal{D}} \boldsymbol{V}(D). \tag{1.20}$$

The D-transform is very similar to the z-transform [88]. They are related by $D = z^{-1}$.

There are numerous properties of the D-transform, most of which are identical or almost identical to those of the z-transform. A good reference is Oppenheim and Schafer's book [88] for scalar sequences. In many cases, the properties are easily extended to matrix sequences. Some important properties are assumed explicitly or implicitly throughout this dissertation and are mentioned in the following.

Let $n, \Delta \in \mathbb{Z}$, $c_1, c_2 \in \mathbb{C}$ and $\boldsymbol{V}[n], \boldsymbol{U}[n]$ be arbitrary dimensional complex matrix sequences with corresponding D-transforms $\boldsymbol{V}(D) = \mathcal{D}\{\boldsymbol{V}[n]\}, \boldsymbol{U}(D) = \mathcal{D}\{\boldsymbol{U}[n]\}$.

Property 1.1 *Linearity.*

The D-transform is a linear transformation, i.e.

$$c_1 \boldsymbol{V}[n] + c_2 \boldsymbol{U}[n] \overset{\mathcal{D}}{\longleftrightarrow} c_1 \boldsymbol{V}(D) + c_2 \boldsymbol{U}(D). \tag{1.21}$$

Property 1.2 *Time-shift.*

$$\boldsymbol{V}[n - \Delta] \overset{\mathcal{D}}{\longleftrightarrow} \boldsymbol{V}(D)D^\Delta. \tag{1.22}$$

Property 1.3 *Time reversal of the conjugate transpose matrix sequence.*

$$\boldsymbol{V}^H[-n] \overset{\mathcal{D}}{\longleftrightarrow} \boldsymbol{V}^H(D^{-*}). \tag{1.23}$$

For convenience, the notation D^{-*} is defined as $D^{-*} \triangleq (D^{-1})^* = (D^*)^{-1}$ (see Table A.3).

Definition 1.2 *Time-Shift Notation.*

The notation "$\boldsymbol{V}[n]D^\Delta$" denotes a delay of the sequence $\boldsymbol{V}[n]$ by Δ symbols.

$$\boldsymbol{V}[n]D^\Delta \triangleq \boldsymbol{V}[n - \Delta] \tag{1.24}$$

where $\Delta \in \mathbb{N}$.

With this notation, the delay operator D^Δ becomes invariant with respect to the

D-transform, i.e.

$$\boldsymbol{V}[n]D^\Delta \xleftrightarrow{\mathcal{D}} \boldsymbol{V}(D)D^\Delta. \tag{1.25}$$

Note that there is a direct connection between the discrete-time Fourier transform (DTFT) and the *D*-transform. Comparing the definitions of both transforms in Equation 1.18 and Table A.9, it can immediately be seen that the DTFT can directly be obtained by evaluating the *D*-domain signal on the unit circle $D = e^{-j2\pi\check{f}}$:

$$\check{\boldsymbol{V}}_C(e^{-j2\pi\check{f}}) = \boldsymbol{V}(D)|_{D=e^{-j2\pi\check{f}}} \tag{1.26}$$

The power spectrum of a signal plays an important role in system analysis. It is directly related to the cross- or auto-correlation sequence. Let the complex row vector sequence $\boldsymbol{u} = [u_1, u_2, \ldots, u_N]$ be composed of N scalar sequences $u_k[n]$ ($k \in \mathcal{I}_N$, $u_k[n] \in \mathbb{C}$). The corresponding truncated sequence $\boldsymbol{u}_M[n]$ be restricted to $(2M+1)$ nonzero samples

$$\boldsymbol{u}_M[n] \triangleq \begin{cases} \boldsymbol{u}[n], & \text{for } |n| \leq M \\ \boldsymbol{0}_N, & \text{for } |n| > M. \end{cases} \tag{1.27}$$

Let $\boldsymbol{v}[n]$ be another row vector signal whose truncated sequence is $\boldsymbol{v}_M[n]$. Denote the *D*-transforms of the signals $\boldsymbol{u}[n]$, $\boldsymbol{v}[n]$, $\boldsymbol{u}_M[n]$ and $\boldsymbol{v}_M[n]$ by $\boldsymbol{u}(D)$, $\boldsymbol{v}(D)$, $\boldsymbol{u}_M(D)$ and $\boldsymbol{v}_M(D)$,respectively.

Definition 1.3 *Cross-power spectrum.*
The cross-power spectrum of the signals $\boldsymbol{u}[n]$ and $\boldsymbol{v}[n]$ is

$$E_M[\boldsymbol{u}^H(D^{-*})\boldsymbol{v}(D)] \triangleq \lim_{M\to\infty} \frac{1}{2M+1} E[\boldsymbol{u}_M^H(D^{-*})\boldsymbol{v}_M(D)]. \tag{1.28}$$

Denote $\boldsymbol{S}_{M,uv}(D) = \boldsymbol{u}_M^H(D^{-*})\boldsymbol{v}_M(D)$ and let $\boldsymbol{X}_l(D)$, $\boldsymbol{X}_r(D)$ be time-invariant matrix filters.

Lemma 1.1

$$E_M[\boldsymbol{X}_l(D)\boldsymbol{S}_{M,uv}(D)\boldsymbol{X}_r(D)] = \boldsymbol{X}_l(D)E_M[\boldsymbol{S}_{M,uv}(D)]\boldsymbol{X}_r(D). \qquad (1.29)$$

Proof.

$$
\begin{aligned}
E_M[\boldsymbol{X}_l(D)\boldsymbol{S}_{M,uv}(D)\boldsymbol{X}_r(D)] &= \lim_{M\to\infty} \frac{1}{2M+1} E[\boldsymbol{X}_l(D)\boldsymbol{S}_{M,uv}(D)\boldsymbol{X}_r(D)] \\
&= \boldsymbol{X}_l(D) \lim_{M\to\infty} \frac{1}{2M+1} E[\boldsymbol{S}_{M,uv}(D)]\boldsymbol{X}_r(D) \\
&= \boldsymbol{X}_l(D)E_M[\boldsymbol{S}_{M,uv}(D)]\boldsymbol{X}_r(D).
\end{aligned}
$$

The matrix filters $\boldsymbol{X}_l(D)$ and $\boldsymbol{X}_r(D)$ can be moved out of the expectation because they are assumed to be constant; the expectation $E[\ldots]$ is only taken over the stochastic signals $\boldsymbol{u}_M$ and $\boldsymbol{v}_M$.

■

Define the *cross-correlation matrix* of the wide-sense stationary signals $\boldsymbol{u}$ and $\boldsymbol{v}$ as

$$\boldsymbol{R}_{uv}[m] \triangleq E[\boldsymbol{u}^H[n-m]\boldsymbol{v}[n]]. \qquad (1.30)$$

The relationship between the cross-correlation $\boldsymbol{R}_{uv}[m]$ and the cross-power spectrum $\boldsymbol{S}_{uv}(D) = E_M[\boldsymbol{u}^H(D^{-*})\boldsymbol{v}(D)]$ is then given by

Lemma 1.2

$$\boldsymbol{S}_{uv}(D) = \mathcal{D}\left\{\boldsymbol{R}_{uv}[m]\right\}. \qquad (1.31)$$

Proof. Since the signals $\boldsymbol{u}$ and $\boldsymbol{v}$ are wide-sense stationary, the Definition (1.30) may

be expressed in the alternative form

$$\boldsymbol{R}_{uv}[m] = \lim_{M\to\infty} \frac{1}{2M+1-m} \sum_{n=-\infty}^{\infty} E[\boldsymbol{u}_M^H[n-m]\boldsymbol{v}_M[n]]$$

$$= \lim_{M\to\infty} \frac{1}{2M+1} \sum_{n=-\infty}^{\infty} E[\boldsymbol{u}_M^H[n-m]\boldsymbol{v}_M[n]]. \qquad (1.32)$$

Taking the D-transform of $\boldsymbol{R}_{uv}[m]$, substituting the above equation and applying Property 1.3 yields

$$\sum_{m=-\infty}^{\infty} \boldsymbol{R}_{uv}[m]D^m = \sum_{m=-\infty}^{\infty} \left\{ \lim_{M\to\infty} \frac{1}{2M+1} \sum_{n=-\infty}^{\infty} E[\boldsymbol{u}_M^H[n-m]\boldsymbol{v}_M[n]] \right\} D^m$$

$$= \lim_{M\to\infty} \frac{1}{2M+1} E\left[\sum_{n=-\infty}^{\infty} \left\{ \sum_{m=-\infty}^{\infty} \boldsymbol{u}_M^H[-(m-n)]D^{m-n} \right\} \boldsymbol{v}_M[n]D^n \right]$$

$$= \lim_{M\to\infty} \frac{1}{2M+1} E[\boldsymbol{u}_M^H(D^{-*})\boldsymbol{v}_M(D)]$$

$$= \boldsymbol{S}_{uv}(D). \qquad (1.33)$$

■

Chapter 2

System Model

2.1 General Description and Assumptions

The main contributions of this chapter are the derivation of a simple discrete-time vector model and the finding that frequency and antenna diversity are conceptually equivalent. The presented discrete-time model completely describes the mixed discrete/continuous-time multiuser system. It integrates frequency and antenna diversity using a simple notation. Overall, the whole system, which includes a multitude of components, is described by a vector model merely consisting of a channel, an input and a noise signal.

In the description of the system model, the concepts of spread spectrum (frequency diversity) and input (antenna) diversity are unified. It is shown that a system with processing gain K and A receiver inputs provides effectively $U_{\mathrm{div}} = AK$ parallel diversity channels. The mathematical treatment shows that there is no conceptual difference between frequency and antenna diversity. Both lead, in a similar manner, to an increase in the number of diversity channels. These findings allow predictions of the system capacity merely based on the introduced model.

The investigated system consists of the reverse link of a multiuser system with N ($N \in \mathbb{N}$) users and a single base station. Each user is equipped with one transmit antenna and employs quadrature amplitude modulation (QAM) or phase shift keying (PSK). The transmitted data symbols are considered to have statistically zero mean

and may be correlated in an arbitrary fashion. The base station receives the signals at A ($A \in \mathbb{N}$) different antennas. It is assumed that the receive antennas are spaced sufficiently apart to ensure distinct impulse responses between a certain user and different base antennas. Additive white Gaussian noise (AWGN) with zero mean distorts the signals received at each antenna. The noise signals at different base antennas are considered to be mutually uncorrelated. An additional assumption is that the transmitted data signals and the noise signals are independent. The frequency selective, quasi-stationary radio channels are assumed to be known. The multiuser system is, in general, asynchronous unless the impulse responses of all individual channels start at the same time (in which case the system is synchronous). Spread spectrum multiple access (SSMA) is employed in order to support several users simultaneously. For this, each user spreads the signal to K times the Nyquist bandwidth before transmission ($K \in \mathbb{N}$). In particular, if T denotes the symbol period of the data sequence, the double-sided bandwidth of the transmitted signal will be K/T.

Figure 2.1 shows the physical structure of the system. Since the base station is equipped with A receive antennas, there are exactly A different physical connections (wireless channels) between each user and the base (Figure 2.2). The channel impulse response between user i ($i \in \mathcal{I}_N$) and the l-th ($l \in \mathcal{I}_A$) receive antenna is denoted $h_{Cil}(t)$.

The research in this thesis is centered around the data transfer from the users to the base station, which is also called the reverse link. The reasoning behind this is the fact that simultaneous or multiuser detection of all signals at a centralized station may yield considerably better performance than conventional single user detection [30]. On the other hand, for the forward link (data transmission from the base station to the users), multiuser detection is either not possible or not practical [30].

Since the modulation scheme is QAM or PSK, the signals consist of inphase and quadrature components. In order to circumvent a complicated notation and eliminate the carrier modulation process in the mathematical analysis, the complex baseband model is used [40]. As a consequence, all signals and impulse responses are in general complex functions.

The system is expected to detect and process the data transmitted by several users.
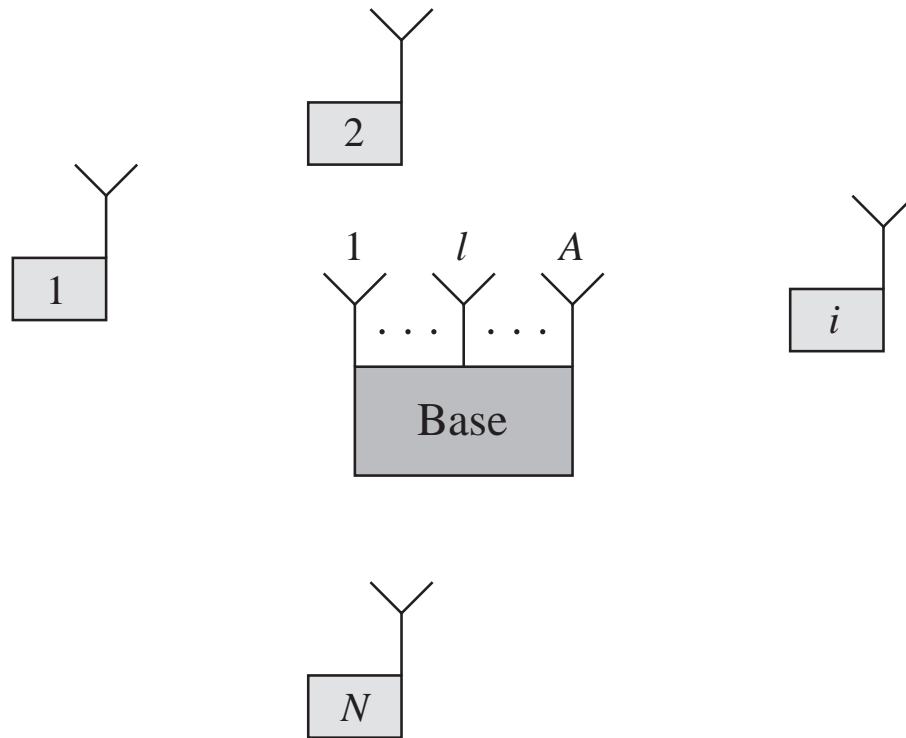
Figure 2.1: Multiuser system with N users and one base station.
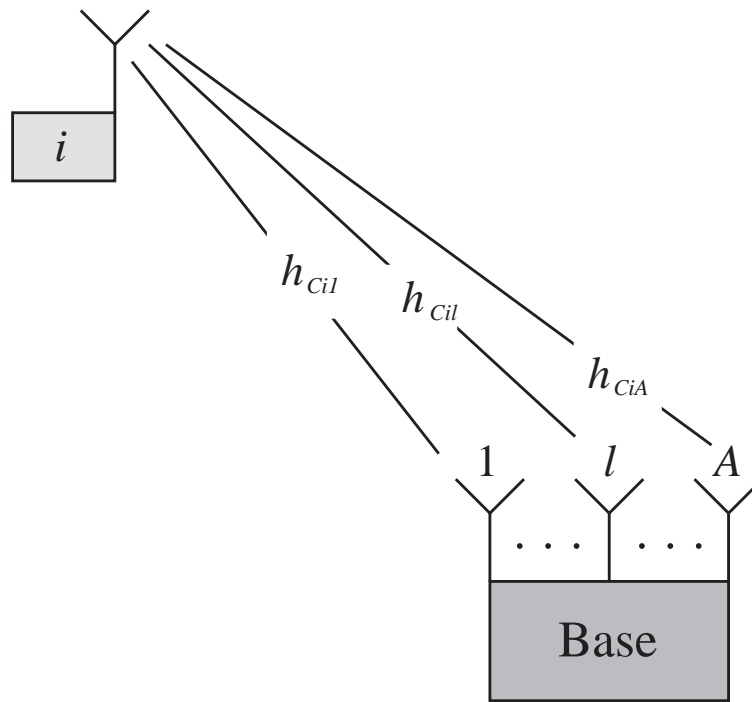
Figure 2.2: Radio links between user i and the base station.

In order to do this successfully, diversity is necessary in one form or another. The system described derives the required diversity from two sources: the first is frequency diversity introduced through spread spectrum modulation; the second is antenna diversity by receiving the signals at several inputs. As will be shown subsequently, the degree of frequency and antenna diversity is equal to K and A, respectively. Moreover, the *number of diversity channels* in the system, U_{div}, is given by the product of frequency and antenna diversity: $U_{\mathrm{div}} = AK$. Finally, the *effective degree of diversity* in the system is frequency dependent. It is equal to $U_{\mathrm{div}} - N$ for a given frequency provided that the N row vectors of the channel transfer matrix are linearly independent at that frequency.

High data rates are considered. In particular, it is assumed that the multipath delay spread is comparable to or larger than the symbol period. This leads to a significant amount of intersymbol interference (ISI) and frequency selective channels, i.e. the channel gain magnitude and phase shift vary over frequency. In addition, the system model implicitly takes into account relative time delays among different channels. The time delay of the channel between a certain user and a receive antenna may be defined as the time of the first nonzero sample in the channel impulse response. If these time delays are not the same for all channels, the system will be asynchronous.

The channel characteristics vary over time due to a changing environment or alternating transmitter and receiver locations. A measure for the speed of these variations is the *coherence time* [99]. If we consider a transfer protocol that transmits blocks of data symbols (frames), changes in the channel impulse response (CIR) between the beginning and the end of the frame determine the overall effect on the performance. When the data rate becomes higher, the frame duration decreases provided that the number of frame symbols stays constant. As a consequence, the CIR's are varying less between the start and the end of a frame and the system is less affected by the time-variant channel. If the frame duration is significantly shorter than the channel coherence time, varying CIR's will hardly affect the system performance and might be neglected. This situation is considered for the following analysis. The CIR's are thus assumed to be stationary within the duration of one frame and the system is described as "quasi-stationary".

2.2 Conventional CDMA Multiuser Model

A special case of SSMA, *direct sequence code-division multiple access* (DS-CDMA) enjoys by far the largest popularity in both research and commercial systems among all spread spectrum schemes. It is very often combined with binary phase-shift keying (BPSK) modulation. In order to clearly show the relationship and common properties between the SSMA technique used throughout the remainder of this dissertation and the ubiquitous CDMA/BPSK scheme, the latter is described in this section.

Let a_i denote the data sequence of user i ($i \in \mathcal{I}_N$) to be transmitted to the base station. Since BPSK is used as modulation scheme, each symbol of the data sequence may assume either of the two values '-1' or '+1' ($a_i[n] \in \{-1, +1\}, \forall n \in \mathbb{Z}$). Each user is assigned an individual signature waveform $\varphi_{Ci}(t)$ ($i \in \mathcal{I}_N$), which is used to modulate all transmitted symbols $a_i[n]$. As a consequence, the transmitted analog signal entering the radio channel is given by

$$s_{Ci}(t) = \sum_{n=-\infty}^{\infty} a_i[n]\varphi_{Ci}(t - nT) \tag{2.1}$$

where T is the symbol period. The transmitted signal s_{Ci} ($i \in \mathcal{I}_N$) travels through the radio channel with impulse response $h_{Cil}(t)$ before it is received at the l-th base antenna ($l \in \mathcal{I}_A$). In order to reduce adjacent channel interference (ACI) and noise $\nu_{CGl}(t)$ added at each antenna front end, the received signals are processed by a lowpass filter $b_C(t)$. Finally, the signals are sampled at the chip rate $1/T_s = K/T$, where K is the processing gain (spreading factor). The sampler output sequences y_l constitute the inputs to the centralized detector, which produces estimates of the original input data $a_i[n]$ $\forall i \in \mathcal{I}_N, n \in \mathbb{Z}$.

The process of modulating the data symbols with a signature waveform can be subdivided into two parts: multiplication with a code sequence and modulation. In the first part, each symbol $a_i[n]$ is multiplied with a code q_i consisting of $M = K$ samples (chips). The chips are usually chosen from the binary alphabet of plus/minus one ($q_i[n] \in \{-1, +1\}$, $\forall n \in \{0, 1, 2, \ldots, M-1\}$). It is customary to choose the code duration to be equal to the symbol duration T, i.e. the chip period is $T_s = T/M$.
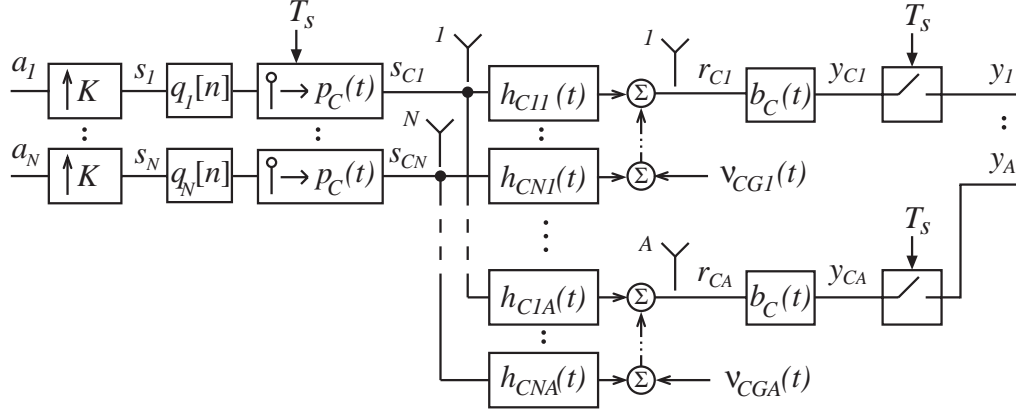
Figure 2.3: Block diagram of the multiuser system.

After coding, each chip is modulated with a pulse waveform $p_C(t)$. The signature waveform can thus be expressed as

$$\varphi_{Ci}(t) = \sum_{m=0}^{M-1} q_i[m]p_C(t - mT_s). \tag{2.2}$$

It is easy to show that the multiplication of the data symbols with the code sequence may equivalently be described by upsampling $a_i[n]$ K times and feeding the resulting sequence into a discrete-time filter with impulse response $q_i[n]$. The resulting system model is shown in Figure 2.3.

2.3 Practical SSMA System Model

2.3.1 Introduction

This section describes the system model, on which the analysis in the remaining chapters is based, from a practical point of view. The objective is to model each system component realistically bearing a real implementation in mind. Nonetheless, the complex baseband notation is still applied, enabling a clear and simple description and eliminating the carrier frequency modulation/demodulation processes.

As shown subsequently, the described model is very similar to the CDMA system outlined in Section 2.2. In fact, the arrangement of the system blocks and signals

stays identical, only the discrete-time transmit filters and the input data signals are generalized. Therefore, Figure 2.3 represents the system block diagram for this section. The signals of the block diagram are defined in the following Section 2.3.2 and the system blocks are thoroughly described in Section 2.3.3. Section 2.3.4, finally, summarizes the mathematical description of the combined discrete-time/continuous-time system.

2.3.2 Definition of Signals and Quantities

2.3.2.1 Transmitted Signal

User i ($i \in \mathcal{I}_N$) transmits the discrete-time, discrete-valued symbol sequence a_i. The individual symbols $a_i[n]$ are drawn from a finite alphabet of complex numbers, $\mathcal{A}_i$ ($a_i[n] \in \mathcal{A}_i$). The contents of the alphabet $\mathcal{A}_i$ depend on the modulation scheme. The a_i are assumed to be wide-sense stationary, discrete-time stochastic processes with zero mean. Thus, the individual data symbols $a_i[n]$ are random variables with zero mean and cross-covariance

$$c_{a,ik}[m] \triangleq E[a_i^*[n-m]a_k[n]] \tag{2.3}$$

where $i, k \in \mathcal{I}_N$ and $n, m \in \mathbb{Z}$.

For some analyses, it is additionally assumed that the data signals of all users, $a_i \; \forall i \in \mathcal{I}_N$ are mutually independent (Definition A.1) and temporally independent (Definition A.2). In this case, the data signals satisfy Equations (A.9) and (A.10).

In the following chapters, the system analysis and performance evaluation is based on two different criteria: The mean-square error (MSE) and the error probability. The MSE analysis and results are valid for *any* linear modulation scheme, i.e. they are the same for PAM, PSK or QAM. In contrast, the error probability of the system depends critically on the modulation format. For this reason, the following paragraphs specify the considered modulation schemes in more detail.

For the *probability of error analysis*, the modulation scheme will be restricted to pulse amplitude modulation (PAM) or quadrature amplitude modulation (QAM). In

the case of QAM, it is assumed that the inphase and quadrature signals are independent and that the distance between adjacent constellation points is the same for all points. This means that QAM is identical to independent PAM of the inphase and quadrature signal components. The distance between adjacent modulation levels is constant for both inphase and quadrature PAM, whereas the number of PAM levels may be different for the inphase and quadrature signals.

The distance between constellation points is chosen such that the variance of the transmitted data symbols is equal to unity:

$$E[|a_i[n]|^2] = 1, \quad \forall i \in \mathcal{I}_N. \tag{2.4}$$

This property ensures that the transmit power is constant while switching from one modulation scheme to another (e.g. from 4-QAM to 16-QAM). Thus, a meaningful performance comparison of modulation schemes with different alphabet sizes (capacities) is possible.

Each QAM symbol may be expressed in terms of its real and imaginary part:

$$a_i[n] = a_i^{\mathrm{re}}[n] + ja_i^{\mathrm{im}}[n]. \tag{2.5}$$

According to the above assumptions, both real and imaginary parts are independently pulse amplitude modulated. Let us assume that L_i^{re} and L_i^{im} denote the number of PAM levels for the inphase and quadrature signal, respectively. Both L_i^{re} and L_i^{im} are constrained to be positive, even integer numbers. Thus, the number of QAM constellation points is given by the product $L_i^{\mathrm{re}} L_i^{\mathrm{im}}$ and the real and imaginary parts of the data signal $a_i[n]$ belong to the sets

$$a_i^{\mathrm{re}}[n] \in \mathcal{S}_i^{\mathrm{re}} \tag{2.6}$$

$$a_i^{\mathrm{im}}[n] \in \mathcal{S}_i^{\mathrm{im}} \tag{2.7}$$

where the sets are defined by

$$\mathcal{S}_i^{\mathrm{re}} \triangleq \left\{ \pm\frac{\kappa_i}{2}, \pm3\frac{\kappa_i}{2}, \pm5\frac{\kappa_i}{2}, \ldots, \pm(L_i^{\mathrm{re}} - 1)\frac{\kappa_i}{2} \right\} \tag{2.8}$$

$$\mathcal{S}_i^{\mathrm{im}} \triangleq \left\{ \pm\frac{\kappa_i}{2}, \pm3\frac{\kappa_i}{2}, \pm5\frac{\kappa_i}{2}, \ldots, \pm(L_i^{\mathrm{im}} - 1)\frac{\kappa_i}{2} \right\} \tag{2.9}$$

and κ_i is the distance between adjacent constellation points. Under the assumption that the data symbols assume all elements in the sets (2.8) and (2.9) with equal probability, the variance of the inphase and quadrature PAM signals is

$$\mathcal{E}_{a,i}^{\mathrm{re}} \triangleq E[|a_i^{\mathrm{re}}[n]|^2] = \frac{\kappa_i^2}{12} \left[(L_i^{\mathrm{re}})^2 - 1 \right] \tag{2.10}$$

$$\mathcal{E}_{a,i}^{\mathrm{im}} \triangleq E[|a_i^{\mathrm{im}}[n]|^2] = \frac{\kappa_i^2}{12} \left[(L_i^{\mathrm{im}})^2 - 1 \right]. \tag{2.11}$$

In order to guarantee unit variance of the complex QAM data symbols $a_i[n]$ (Equation (2.4)), the value of the distance κ_i has to be chosen such that $E[|a_i[n]|^2] = \mathcal{E}_{a,i}^{\mathrm{re}} + \mathcal{E}_{a,i}^{\mathrm{im}} = 1$. This is satisfied for

$$\kappa_i = \sqrt{\frac{12}{(L_i^{\mathrm{re}})^2 + (L_i^{\mathrm{im}})^2 - 2}}. \tag{2.12}$$

Note that for a given number of constellation points $(L_i^{\mathrm{re}} L_i^{\mathrm{im}})$, the distance is maximized for $L_i^{\mathrm{re}} = L_i^{\mathrm{im}}$. Thus, square QAM constellations (4-, 16-, 36-QAM, etc.), which have the same number of modulation levels for both inphase and quadrature signals, obtain the largest distance and best performance among all other QAM schemes with the same number of constellation points.

Not only QAM but also PAM of the transmitted data $a_i[n]$ can be described with the above notation. For that, one has to set $L_i^{\mathrm{im}} = 1$ and $a_i^{\mathrm{im}}[n] = 0$, $\forall n \in \mathbb{Z}$. With this, all equations derived for QAM are also valid for PAM.

The modulation format described above will be used in the following chapters whenever the error probability criterion is considered. It allows to choose freely the number of PAM levels for both inphase and quadrature signal. Thus, the number of bits/symbol can be varied while the variance of the transmitted data is constant. This enables a fair performance comparison of QAM schemes with a different number

of constellation points since the transmit power is kept constant. As a result, the distance is constrained to the value in expression (2.12).

2.3.2.2 Noise

Noise is added to the received signals at the front end of each receiving antenna. The noise signal at antenna l ($l \in \mathcal{I}_A$), ν_{CGl}, is a complex Gaussian distributed random variable with zero mean. The noise signals ν_{CGl} and ν_{CGm} received at different antennas ($l \neq m; l, m \in \mathcal{I}_A$) are considered to be uncorrelated. Additionally, each noise signal is assumed to be complex, stationary and white with a double-sided power spectral density (PSD) of N_0, i.e. the cross-covariance function of the noise process is given by

$$c_{\nu,lm}(t, \tau) = E[\nu_{CGl}(t)\nu_{CGm}^*(t - \tau)] = \begin{cases} N_0\delta(\tau), & \text{for } l = m \\ 0, & \text{for } l \neq m \end{cases}, \forall l, m \in \mathcal{I}_A. \quad (2.13)$$

As stated in Section 2.1, the noise signals and the transmitted data signals are independent. This results in

$$E[a_i[n]\nu_{CGl}(t)] = 0, \quad \forall i \in \mathcal{I}_N, \forall l \in \mathcal{I}_A, \forall n \in \mathbb{Z}, \forall t \in \mathbb{R}. \quad (2.14)$$

2.3.2.3 Quantities

Table 2.1 summarizes and defines the system quantities.

2.3.3 System Components

2.3.3.1 Transmitter

The transmitter of each user consists of three elements: upsampler, spreading filter, and pulse generator. Figure 2.4 shows the symbol of the upsampler. Consider the transmitter of the i-th user. The input signal to the upsampler is the data sequence

Table 2.1: System quantities.

Symbol	Meaning
T	symbol period, $T \in \mathbb{R}^+$
N	number of system users, $N \in \mathbb{N}$
A	number of receive antennas at the base station, $A \in \mathbb{N}$
K	processing gain, spreading factor, upsampling factor, $K \in \mathbb{N}$
$K_{3\text{dB}}$	3 dB normalized system bandwidth, $K_{3\text{dB}} \in \mathbb{R}^+$
T_s	modulation/sampling period of the transmitter/receiver, $T_s = T/K$
N_0	double-sided power spectral density of the complex noise, $N_0 \in \mathbb{R}^+$
B_s	3 dB double-sided signal bandwidth, $B_s = K_{3\text{dB}}/T$

a_i. According to Section B.1, the output signal is given by

$$s_i[Kn + m] = \begin{cases} a_i[n], & \text{for } m = 0 \\ 0, & \text{for } m \in \{1, 2, 3, \dots, K-1\} \end{cases} \tag{2.15}$$

where the parameter m_0 has been set for convenience, and without loss of generality, to $m_0 = 0$.

Each user may apply a different discrete-time spreading filter (Figure 2.5) to convolve the transmitted data with a unique code. The impulse response q_i of the spreading filter is a sequence consisting of M_i samples ($q_i[n] = 0$, for $n < 0$ or $n \geq M_i$, $M_i \in \mathbb{N}$). In contrast to conventional CDMA (Section 2.2), there are no restrictions placed on the sequence length M_i. It may be smaller or even larger than the processing gain K. The samples of q_i are chosen from the set of complex numbers ($q_i[n] \in \mathbb{C}, \forall n \in \{0, 1, 2, \dots, M_i - 1\}$). This is also in contrast to the CDMA case where the $q_i[n]$ were restricted to the binary alphabet $\{-1, +1\}$. The output signal of the linear time-invariant spreading filter is

$$\tilde{s}_i[n] = s_i[n] \star q_i[n]. \tag{2.16}$$

The pulse generator (Figure 2.6) takes, at a period of T_s, the current sample $\tilde{s}_i[n]$ of the input sequence and multiplies it with the pulse waveform $p_C(t)$ to form the

$$a[n] \quad\longrightarrow\quad \boxed{\uparrow \mathrm{K}} \quad\longrightarrow\quad s[n]$$

Figure 2.4: Block diagram of a K-times upsampler.

transmitted signal

$$s_{Ci}(t) = \sum_{n=-\infty}^{\infty} \tilde{s}_i[n] p_C(t - nT_s). \tag{2.17}$$

$p_C(t)$ has a lowpass characteristic in order to limit the bandwidth of the transmitted signal.

2.3.3.2 Radio Channel

Theoretical Model The radio channel is characterized by the fact that multiple copies of the transmitted signal arrive at the receiver, each with a different gain, phase and time delay. This may be explained with the existence of different paths (*multipath*) in the environment over which the signal travels. These paths are a result of effects like scattering, diffraction and reflection that occur in the propagation of electromagnetic waves [101].

In the most common model, the radio channel is described as a linear filter that takes the above characteristics into account [101]. In general, the channel impulse response (CIR) is time varying since the environment and the locations of transmitter and receiver may change. In many applications, however, these changes are relatively slow compared to the symbol period and data block duration (frame) of the communications system. It is assumed throughout the following chapters that the change of the CIR during one frame is negligible. In this case, the channel impulse response between user i and receive antenna l can be expressed in complex baseband representation as [101]

$$h_{Cil}(t) = \sum_{u=0}^{L_c-1} h_{Cil}^{(u)} \delta(t - t_u) \tag{2.18}$$

where $L_c \in \mathbb{N}$ is the number of paths, $h_{Cil}^{(u)} \in \mathbb{C}$ is the complex gain, $t_u \in \mathbb{R}$ is the time

$$s_i \longrightarrow \boxed{q_i[n]} \longrightarrow \tilde{s}_i$$
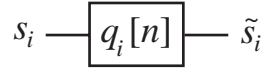
Figure 2.5: Block diagram of the discrete-time spreading filter.

delay of the u-th path, and $\delta(t)$ is the Dirac delta distribution (Table A.3). Thus, the radio channel model is equivalent to a linear time-invariant and non-recursive filter with complex coefficients.

Discrete Representation of the Radio Channel Measured channel impulse responses are used for the numerical calculations in the following chapters. The basis for these measurements is the multipath channel model (see above) which is completely described by the CIR in Equation (2.18).

The real radio channel is a continuous-time system. In order to avoid errors, it is generally necessary that the CIR be measured for a continuous time-range which consists of an infinite number of points. This means that infinite information is required to describe an arbitrary system accurately. In practice, however, it is possible to exploit the properties of real systems for a reduction of the necessary information to a finite amount of data.

Real systems are bandwidth limited. It can be shown that this property allows it to completely describe the continuous-time impulse response by a discrete-time sequence (sampling theorem). If the impulse response has most of its energy in a limited time window, the system can be described for all practical purposes by a finite number of samples.

For the following, it is assumed that

1. the channel is causal,

2. the channel is linear and can be completely described by its impulse response, and

3. the CIR is truly bandwidth and practically time limited.

Let $h_{Cil}(t)$ and $H_{Cil}(f)$ denote the continuous-time CIR and CTF[1], respectively.

---

[1]CTF is the abbreviation for *channel transfer function*.

$$\tilde{s}_i[n] \longrightarrow \boxed{\begin{array}{c} T_S \\ \downarrow \\ \text{P} \rightarrow p_C(t) \end{array}} \longrightarrow s_{Ci}(t)$$
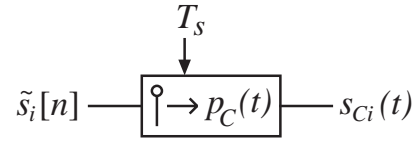
Figure 2.6: Block diagram of the pulse generator.

CIR and CTF are connected through the *Fourier Transform* $H_{Cil}(f) = \mathcal{F}_{cc}\{h_{Cil}(t)\}$ (Table A.9). Define B_h and T_h as the double-sided bandwidth and duration of the CIR, respectively:

$$H_{Cil}(f) = 0, \quad \text{for } |f| > B_h/2 \tag{2.19}$$

$$h_{Cil}(t) \approx 0, \quad \text{for } t < 0 \text{ or } t > T_h. \tag{2.20}$$

According to the *Nyquist sampling theorem* [87], no information will be lost if the CIR is sampled at a rate $1/T_c$ with

$$T_c \leq \frac{1}{B_h}. \tag{2.21}$$

It follows that the number of samples necessary to represent the CIR for all practical purposes is

$$L_c = \left\lceil \frac{T_h}{T_c} \right\rceil \tag{2.22}$$

where $\lceil x \rceil$ is the smallest integer greater than or equal to x (Table A.3). The frequency step shall be defined as

$$\Delta f = \frac{1}{L_c T_c}. \tag{2.23}$$

There are two objectives that have to be considered when defining the discrete-time sequence h_{il} representing the CIR:

- it must be possible to obtain the complete channel information from the sequence h_{il},

- the sequence h_{il} shall be the discrete-time analogy of the continuous-time CIR.

The first objective is achieved by applying the Nyquist sampling theorem. The second means in other words that the output sequence of the channel, which fully represents the continuous-time output of the real channel, is obtained by convolving the input sequence, representing the continuous-time input signal, with h_{il}. It can be shown that this is the case if every sample of the continuous-time CIR, taken at a period of T_c, is multiplied by the constant factor T_c [88]. Therefore, provided that the condition in Equation (2.21) is fulfilled, the relationship between discrete- and continuous-time channel impulse responses is

$$h_{il}[n] = \begin{cases} T_c h_{Cil}(nT_c), & \text{for } n = 0, 1, 2, \ldots, L_c - 1 \\ 0, & \text{for } n < 0 \text{ or } n > L_c - 1 \end{cases} \tag{2.24}$$

or equivalently

$$h_{il}[n] = T_c \sum_{k=0}^{L_c-1} h_{Cil}(kT_c)\, \delta_K[n - k] \tag{2.25}$$

where $\delta_K[n]$ denotes the Kronecker delta function (Table A.3). For all practical purposes, the values of $h_{il}[n]$ have been set to zero for $n < 0$ and $n > L_c - 1$ since the magnitude of $h_{Cil}(t)$ is assumed to be negligibly small for $t < 0$ and $t > T_h$.

More properties of the discrete-time CIR (2.25) are described in the following discussion. Introduce for the discrete Fourier series (DFS) the transformation pair $H_{il}[k] = \mathcal{F}_{dd}\{h_{il}[n]\}$ and for the discrete-time Fourier transform (DTFT) the transformation pair $\check{H}_{Cil}(e^{-j2\pi \check{f}_c}) = \mathcal{F}_{dc}\{h_{il}[n]\}$ (Table A.9), where $\check{f}_c$ is the normalized frequency:

$$\check{f}_c \triangleq f T_c. \tag{2.26}$$

It can then be shown that the CTF is given by

$$H_{Cil}(f) = \begin{cases} \check{H}_{Cil}(e^{-j2\pi f T_c}), & \text{for } |f| \leq 1/(2T_c) \\ 0, & \text{for } |f| > 1/(2T_c) \end{cases} \tag{2.27}$$

$$r_{Cl} \longrightarrow \boxed{b_C(t)} \longrightarrow y_{Cl}$$

(a) lowpass filter

$$y_{Cl}(t) \longrightarrow \boxed{\nearrow} \longrightarrow y_l[n] \quad (T_s)$$
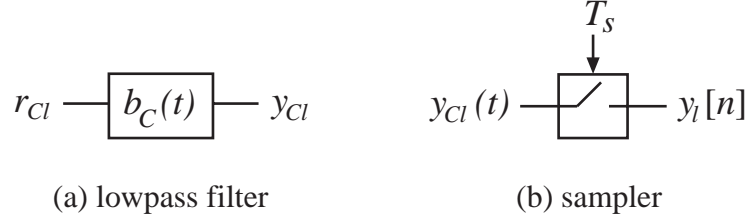
(b) sampler

Figure 2.7: Block diagrams of the receive lowpass filter and the sampler.

if and only if the conditions in Equations (2.19), (2.20) and (2.21) are fulfilled. In this case, using the transform equations of the DFS and the DTFT in Table A.9 and Equation (2.27) yields

$$H_{Cil}(k\Delta f) = \begin{cases} H_{il}[k], & \text{for } |f| \leq 1/(2T_c) \\ 0, & \text{for } |f| > 1/(2T_c) \end{cases}. \tag{2.28}$$

Thus, the sequence $H_{il}[k]$ represents the frequency-sampled CTF.

2.3.3.3 Receiver

The base station receiver contains $A \in \mathbb{N}$ identical branches. Each branch consists of a receive antenna followed by a lowpass filter b_C (Figure 2.7(a)) and a rate $1/T_s$ sampler (Figure 2.7(b)).

Consider branch $l \in \mathcal{I}_A$. According to the system model in Figure 2.3, the received signal can be expressed as

$$r_{Cl}(t) = \sum_{i=1}^{N} s_{Ci}(t) \star h_{Cil}(t) + \nu_{CGl}(t). \tag{2.29}$$

After lowpass filtering, the signal becomes

$$y_{Cl}(t) = r_{Cl}(t) \star b_C(t). \tag{2.30}$$

Finally, the signal is sampled at a period T_s and the output of the receiver front-end
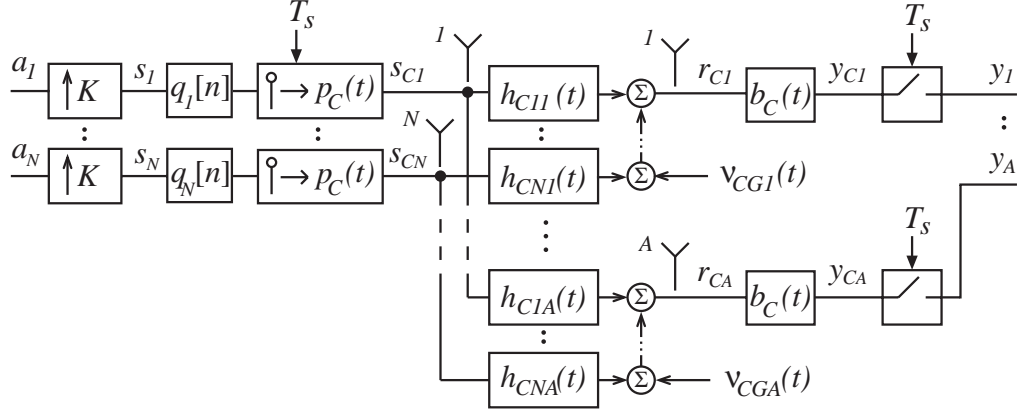
Figure 2.8: Block diagram of the multiuser system.

is

$$y_l[n] = y_{Cl}(nT_s). \tag{2.31}$$

The sequences y_l $(\forall l \in \mathcal{I}_A)$ serve as inputs to the centralized multiuser detector.

In the following simulations, a fifth-order Butterworth lowpass filter has been chosen for b_C. The characteristics of this filter have been identical to the transmitter pulse p_C. Refer to Appendix C.1 for a detailed description of $B_C(f) = \mathcal{F}_{cc}\{b_C(t)\}$.

2.3.4 System Description

The current Section shall be concluded with a summary of the mathematical system description. As shown in Figure 2.8, the system contains continuous-time as well as discrete-time parts.

Starting at the transmitter, each user is assigned a *signature waveform* or *code*

$$\varphi_{Ci}(t) = \sum_{m=0}^{M_i-1} q_i[m]p_C(t - mT_s). \tag{2.32}$$

Define the *overall channel waveform* between user i and the l-th base antenna as

$$\psi_{Cil}(t) \triangleq \varphi_{Ci}(t) \star h_{Cil}(t). \tag{2.33}$$

The signal received at antenna l is then given by

$$r_{Cl}(t) = \sum_{i=1}^{N} \sum_{n=-\infty}^{\infty} a_i[n]\psi_{Cil}(t - nT) + \nu_{CGl}(t). \tag{2.34}$$

If we are interested in the input signal to the sampler, it is convenient to define the *combined channel*

$$x_{Cil}(t) \triangleq \psi_{Cil}(t) \star b_C(t) \tag{2.35}$$

$$= \varphi_{Ci}(t) \star h_{Cil}(t) \star b_C(t). \tag{2.36}$$

With that, the input to the sampler of receiver branch l may be expressed as

$$y_{Cl}(t) = \sum_{i=1}^{N} \sum_{n=-\infty}^{\infty} a_i[n]x_{Cil}(t - nT) + \nu_{Cl}(t) \tag{2.37}$$

where

$$\nu_{Cl}(t) = \nu_{CGl}(t) \star b_C(t) \tag{2.38}$$

is the colored Gaussian noise after lowpass filtering. Finally, the discrete-time output of the l-th receiver branch is

$$y_l[n] = y_{Cl}(nT_s). \tag{2.39}$$

2.4   Equivalent Discrete-Time Model

2.4.1   System

This section introduces a discrete-time model completely equivalent to the model described previously. Three main properties characterize the new model, which significantly simplify notation and complexity, and additionally provide precious insight into understanding the important characteristics of the system. The first property is that it is a completely discrete-time model. This simplifies representation by elim-

(a)

(b)

(c)
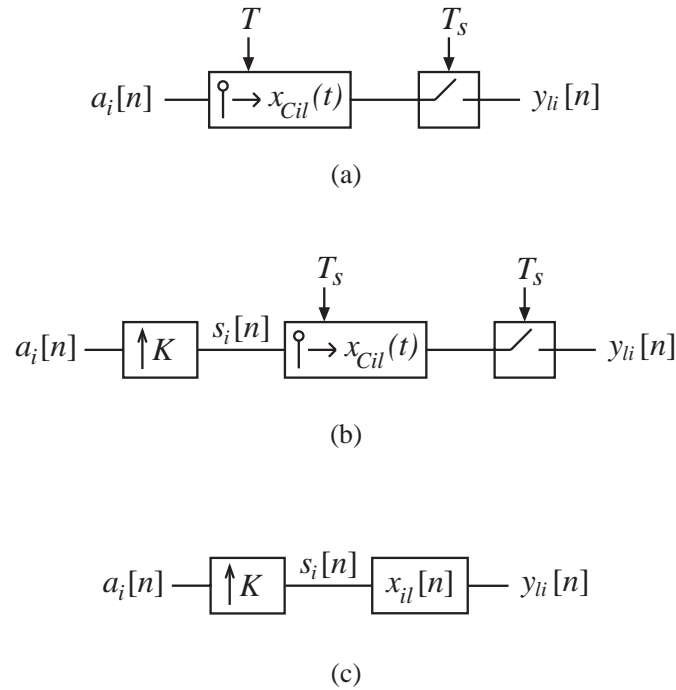
Figure 2.9: Equivalent models for the connection between user i and receiver output l.

inating the pulse generator and sampler elements. Secondly, a $(1{:}K)$ demultiplexer will be added to each branch of the receiver in order to obtain a model with AK signal outputs instead of only A. It will be shown that this structure suits the general behavior of the system and enables a deeper understanding of the performance properties. Finally, vector notation will be introduced in order to describe the model in a compact mathematical form.

Let us start by replacing the continuous-time system parts, impulse generators and samplers by ordinary discrete-time filters. According to Equation (2.37), the connection between user i's data signal and the l-th receiver branch output may be described by a pulse generator modulating the input sequence with the pulse $x_{Cil}(t)$ at a symbol rate of T followed by a sampler operating at a sample period of $T_s = T/K$ (Figure 2.9(a)). The overall branch output y_l can be expressed in terms of the signals

y_{li} stemming from user i, $\forall i \in \mathcal{I}_N$, and noise, i.e.

$$y_l[n] = \sum_{i=1}^{N} y_{li}[n] + \nu_l[n] \tag{2.40}$$

where

$$\nu_l[n] = \nu_{Cl}(nT_s) \tag{2.41}$$

is the sampled noise signal. A K-times upsampler may be added in front of the pulse modulator without changing the system behavior (Figure 2.9(b)). For convenience, the output of the upsampler shall be expressed in the form

$$s_i[Kn + m] = \begin{cases} a_i\left[n + \frac{m}{K}\right], & \text{for } m = 0, \pm K, \pm 2K, \ldots \\ 0, & \text{otherwise} \end{cases} \tag{2.42}$$

which is equivalent to Equation (2.15). Note that the symbol rates of the pulse generator and the sampler are now identical $(1/T_s)$. This enables us, without changing the input/output relationship, to replace pulse generator and sampler by a discrete-time filter x_{il}, which is given by

$$x_{il}[n] = T_s x_{Cil}(nT_s) \tag{2.43}$$

$$\check{X}_{Cil}(e^{-j2\pi f T_s}) = \sum_{v=-\infty}^{\infty} X_{Cil}\left(f - \frac{v}{T_s}\right) \tag{2.44}$$

where $\check{X}_{Cil}(e^{-j2\pi \check{f}}) = \mathcal{F}_{dc}\{x_{il}[n]\}$ and $X_{Cil}(f) = \mathcal{F}_{cc}\{x_{Cil}(t)\}$ are the discrete-time Fourier transform (DTFT) of x_{il} and the Fourier transform (FT) of x_{Cil}, respectively (see Appendix A.8). The final, completely discrete-time, model for the path connection is shown in Figure 2.9(c). It can be used in conjunction with Equation (2.42) to arrive at the *equivalent discrete-time system model* shown in Figure 2.10. The output
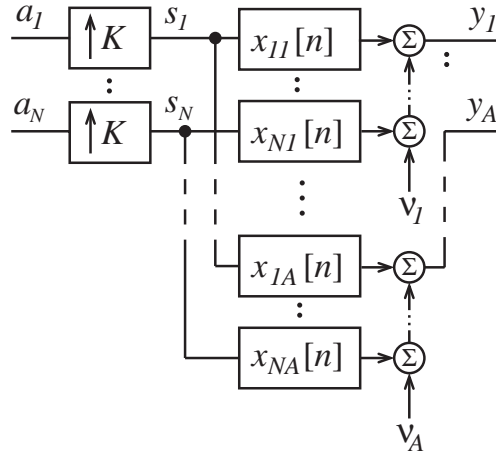
Figure 2.10: Equivalent discrete-time system model.

signal of the l-th receiver branch may now be written as

$$y_l[n] = \sum_{i=1}^{N} s_i[n] \star x_{il}[n] + \nu_l[n].\tag{2.45}$$

The input/output relationship of the system is therefore completely described by Equations (2.42) and (2.45).

The following changes to the system representation are motivated by the objective to find a direct relationship between the rate $1/T$ input data a_i and the receiver output signals. The disadvantage of the system model shown in Figure 2.10 is the expression of the upsampled signals s_i by Equation (2.42). A mathematically significantly simplified model can be obtained by feeding each receiver output signal $y_l[n]$ ($\forall l \in \mathcal{I}_A$) into a (1:$K$) serial to parallel demultiplexer (Figure 2.11). The m-th ($m \in \mathcal{I}_K$) output of the demultiplexer in branch l is then given by

$$y_l^m[n] \triangleq y_l[Kn + m - 1].\tag{2.46}$$

Figure 2.12 shows the equivalent discrete-time system with demultiplexers, which has a total of AK output signals y_l^m ($l \in \mathcal{I}_A, m \in \mathcal{I}_K$). Define the partitioned impulse
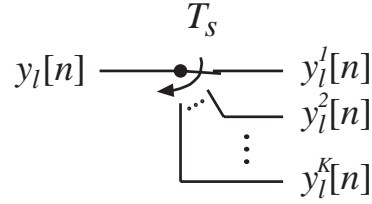
Figure 2.11: Block diagram of $(1{:}K)$ demultiplexer.

responses x_{il}^m and noise signals ν_l^m according to

$$x_{il}^m[n] \triangleq x_{il}[Kn + m - 1] \tag{2.47}$$

$$\nu_l^m[n] \triangleq \nu_l[Kn + m - 1]. \tag{2.48}$$

It can then be shown that the final output signals are given by

$$y_l^m[n] = \sum_{i=1}^{N} a_i[n] \star x_{il}^m[n] + \nu_l^m[n]. \tag{2.49}$$

Proof. Starting with Definition (2.46), substituting Equation (2.45), using the definition of the discrete-time convolution operator '$\star$' (Table A.4), substituting Expression (2.42) for $s_i[n]$, introducing the new variable $w = (v+1-m)/K$, and applying the Definitions (2.47), (2.48) results in Equation (2.49) from

$$
\begin{aligned}
y_l^m[n] \quad &= \quad y_l[Kn + m - 1] \\
&\overset{(2.45)}{=} \quad \sum_{i=1}^{N} \sum_{v=-\infty}^{\infty} s_i[Kn + m - 1 - v] x_{il}[v] + \nu_l[Kn + m - 1] \\
&\overset{(2.42)}{=} \quad \sum_{i=1}^{N} \sum_{w=-\infty}^{\infty} a_i[n - w] x_{il}[Kw + m - 1] + \nu_l[Kn + m - 1] \\
&\overset{\substack{(2.47)\\(2.48)}}{=} \quad \sum_{i=1}^{N} \sum_{w=-\infty}^{\infty} a_i[n - w] x_{il}^m[w] + \nu_l^m[n] \\
&= \quad \sum_{i=1}^{N} a_i[n] \star x_{il}^m[n] + \nu_l^m[n].
\end{aligned}
$$

■
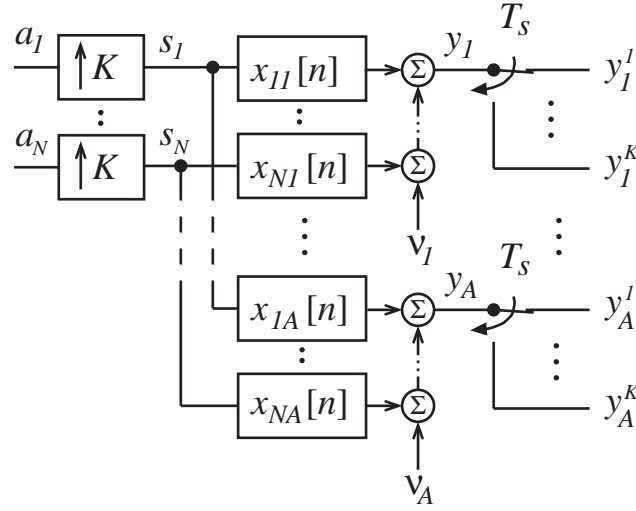
Figure 2.12: Equivalent discrete-time system model with demultiplexers.

Based on Equation (2.49), the final equivalent discrete-time system model is easily obtained. It is shown in Figure 2.13.

Let us now describe the system in vector form. The input signal vector is defined as

$$\boldsymbol{a} \triangleq [a_1, a_2, \ldots, a_N]. \tag{2.50}$$

The equalizer input and noise signal of receive antenna l are given by

$$\boldsymbol{y}_l \triangleq [y_l^1, y_l^2, \ldots, y_l^K] \tag{2.51}$$

$$\boldsymbol{\nu}_l \triangleq [\nu_l^1, \nu_l^2, \ldots, \nu_l^K]. \tag{2.52}$$

The combined channel matrix for the l-th receiver input shall be defined as

$$\boldsymbol{X}_l \triangleq \begin{bmatrix} x_{1l}^1 & x_{1l}^2 & \cdots & x_{1l}^K \\ x_{2l}^1 & x_{2l}^2 & \cdots & x_{2l}^K \\ \vdots & \vdots & \ddots & \vdots \\ x_{Nl}^1 & x_{Nl}^2 & \cdots & x_{Nl}^K \end{bmatrix}. \tag{2.53}$$

According to Equation (2.49) and the definition of matrix convolution in Table A.5,
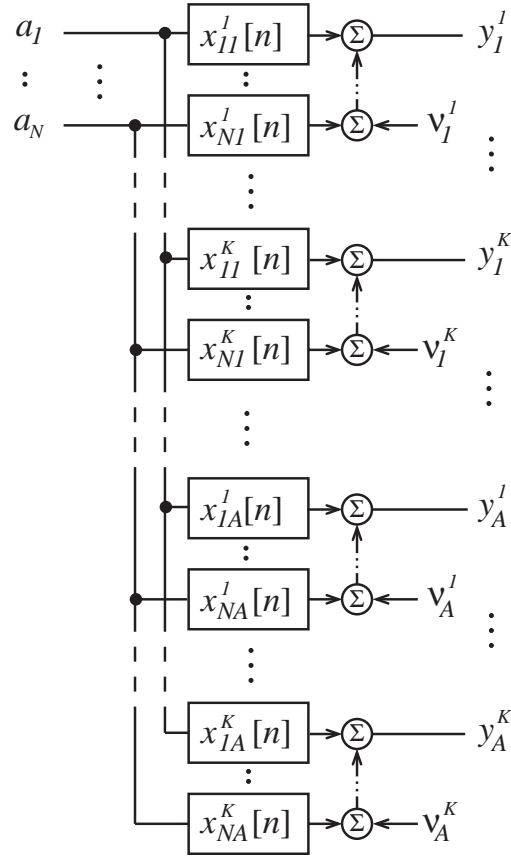
Figure 2.13: Equivalent discrete-time system model.

the output signal at the l-th receiver branch may be expressed as

$$\boldsymbol{y}_l[n] = \boldsymbol{a}[n] \star \boldsymbol{X}_l[n] + \boldsymbol{\nu}_l[n].\tag{2.54}$$

Define the *overall output signal*, *noise signal* and *channel matrix* by

$$\boldsymbol{y} \triangleq [\boldsymbol{y}_1, \boldsymbol{y}_2, \dots, \boldsymbol{y}_A]\tag{2.55}$$

$$\boldsymbol{\nu} \triangleq [\boldsymbol{\nu}_1, \boldsymbol{\nu}_2, \dots, \boldsymbol{\nu}_A]\tag{2.56}$$

$$\boldsymbol{X} \triangleq [\boldsymbol{X}_1, \boldsymbol{X}_2, \dots, \boldsymbol{X}_A],\tag{2.57}$$

respectively. Thus, the overall received signal, consisting of AK scalar sequences y_l^m
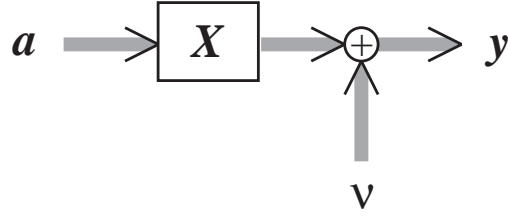
Figure 2.14: Vector system model.

$(l \in \mathcal{I}_A, m \in \mathcal{I}_K)$ can be expressed as

$$\boldsymbol{y}[n] = \boldsymbol{a}[n] \star \boldsymbol{X}[n] + \boldsymbol{\nu}[n]. \tag{2.58}$$

Figure 2.14 shows the corresponding system model.

The system behavior may also be expressed in the D-domain. Let the D-transform of an arbitrary matrix or vector signal $\boldsymbol{V}$ be defined by $\boldsymbol{V}(D) = \sum_{n=-\infty}^{\infty} \boldsymbol{V}[n] D^n$ (see Section 1.7). The output signal of the l-th receiver branch is

$$\boldsymbol{y}_l(D) = \boldsymbol{a}(D)\boldsymbol{X}_l(D) + \boldsymbol{\nu}_l(D) \tag{2.59}$$

where $\boldsymbol{a}(D) = \mathcal{D}\{\boldsymbol{a}[n]\}$, $\boldsymbol{\nu}_l(D) = \mathcal{D}\{\boldsymbol{\nu}_l[n]\}$, $\boldsymbol{y}_l(D) = \mathcal{D}\{\boldsymbol{y}_l[n]\}$, and $\boldsymbol{X}_l(D) = \mathcal{D}\{\boldsymbol{X}_l[n]\}$ are the D-transforms of the input signal vector, noise signal vector, output signal vector of receiver branch l, and combined channel matrix for the l-th receiver input, respectively. Finally, the overall received signal is

$$\boldsymbol{y}(D) = \boldsymbol{a}(D)\boldsymbol{X}(D) + \boldsymbol{\nu}(D) \tag{2.60}$$

where $\boldsymbol{\nu}(D) = \mathcal{D}\{\boldsymbol{\nu}[n]\}$, $\boldsymbol{y}(D) = \mathcal{D}\{\boldsymbol{y}[n]\}$, and $\boldsymbol{X}(D) = \mathcal{D}\{\boldsymbol{X}[n]\}$ are the D-transforms of the overall noise signal vector, overall output signal vector, and overall channel matrix, respectively.

2.4.2 Signals

As a result of the assumptions made in Section 2.1, the input signal vector and the overall noise signal are zero mean random processes. Let us define their power spectra

by

$$\boldsymbol{S}_a(D) \triangleq E_M[\boldsymbol{a}^H(D^{-*})\boldsymbol{a}(D)] \tag{2.61}$$

$$\boldsymbol{S}_\nu(D) \triangleq E_M[\boldsymbol{\nu}^H(D^{-*})\boldsymbol{\nu}(D)] \tag{2.62}$$

where the expectation operator 'E_M' is defined in Equation (1.28).

Noise and input signals are considered to be uncorrelated. It follows from Equation (2.14) that

$$\boldsymbol{S}_{a\nu}(D) \triangleq E_M[\boldsymbol{a}^H(D^{-*})\boldsymbol{\nu}(D)] = \boldsymbol{O}_{N \times AK}, \quad \forall D \in \mathbb{C} \tag{2.63}$$

where $\boldsymbol{O}_{N \times AK}$ is the $N \times AK$ all zero matrix (Table A.7).

The corresponding quantities in the time-domain are the autocorrelation of the input signal vector, $\boldsymbol{R}_a[m]$, the autocorrelation of the overall noise signal, $\boldsymbol{R}_\nu[m]$, and the cross-correlation of the input and noise signals, $\boldsymbol{R}_{a\nu}[m]$:

$$\boldsymbol{R}_a[m] \triangleq E[\boldsymbol{a}^H[n-m]\boldsymbol{a}[n]] \tag{2.64}$$

$$\boldsymbol{R}_\nu[m] \triangleq E[\boldsymbol{\nu}^H[n-m]\boldsymbol{\nu}[n]] \tag{2.65}$$

$$\boldsymbol{R}_{a\nu}[m] \triangleq E[\boldsymbol{a}^H[n-m]\boldsymbol{\nu}[n]] = \boldsymbol{O}_{N \times AK}, \quad \forall m \in \mathbb{Z} \tag{2.66}$$

where the last relation is a result of the fact that noise and input signals are uncorrelated. The time- and frequency-domain quantities are related by the D-transform:

$$\boldsymbol{S}_a(D) = \mathcal{D}\{\boldsymbol{R}_a[m]\} \tag{2.67}$$

$$\boldsymbol{S}_\nu(D) = \mathcal{D}\{\boldsymbol{R}_\nu[m]\} \tag{2.68}$$

$$\boldsymbol{S}_{a\nu}(D) = \mathcal{D}\{\boldsymbol{R}_{a\nu}[m]\}. \tag{2.69}$$

2.4.3   Noise

An expression for the power spectrum of the noise signal $\boldsymbol{\nu}$ will be required in the system analysis of the following chapters. The noise power spectrum is defined in Equation (2.62). It is possible to divide the power spectrum $\boldsymbol{S}_\nu(D)$ into A^2 subma-

trices

$$\boldsymbol{S}_{\nu,lm}(D) \triangleq E_M[\boldsymbol{\nu}_l^H(D^{-*})\boldsymbol{\nu}_m(D)] \tag{2.70}$$

of size $K \times K$ ($l, m \in \mathcal{I}_A$). Since the noise signals at different receiver branches are uncorrelated with zero mean (Section 2.3.2.2), the cross-power spectrum between $\boldsymbol{\nu}_l$ and $\boldsymbol{\nu}_m$ is zero for $l \neq m$:

$$\boldsymbol{S}_{\nu,lm}(D) = \boldsymbol{O}_{K \times K}, \quad \text{for } l \neq m, \tag{2.71}$$

where $\boldsymbol{O}_{K \times K}$ denotes the $K \times K$ all zero matrix (Table A.7). Only the submatrices $\boldsymbol{S}_{\nu,ll}(D)$ ($l \in \mathcal{I}_A$) are nonzero. It can be shown that the (u, v)-th component of $\boldsymbol{S}_{\nu,ll}(D)$, evaluated on the unit circle $D = e^{-j2\pi fT}$, is given by

$$\left[\boldsymbol{S}_{\nu,ll}(e^{-j2\pi fT})\right]_{uv} = \frac{N_0}{T} \sum_{m=-\infty}^{\infty} \left| B_C\left(f - \frac{m}{T}\right) \right|^2 e^{-j\frac{2\pi}{K}(fT-m)(u-v)} \tag{2.72}$$

where $B_C(f) = \mathcal{F}_{cc}\{b_C(t)\}$ is the transfer function of the receive lowpass filter.

Proof. See Appendix E.

∎

Considering Equation (2.71), the overall noise power spectrum may be expressed as

$$\boldsymbol{S}_{\nu}(D) = \mathbf{Diag}\langle \boldsymbol{S}_{\nu,ll}(D) \rangle, \quad l \in \mathcal{I}_A, \tag{2.73}$$

where $\mathbf{Diag}\langle \boldsymbol{S}_{\nu,ll}(D) \rangle$, $l = 1, 2, \ldots, A$, is a diagonal hypermatrix with the matrix $\boldsymbol{S}_{\nu,ll}(D)$ on the l-th diagonal position and zeros otherwise (see Table A.3). The components of $\boldsymbol{S}_{\nu,ll}(D)$ are given in Equation (2.72).

If the receive filter has a double-sided bandwidth of at least $2/T$, the summation on the right hand side of Equation (2.72) includes at least two nonzero terms for each frequency f. The magnitude of the sum will be equal to the sum of magnitudes of each summation term if a main diagonal element ($u = v$) is calculated. For $u \neq v$,

the phases of the individual summation terms differ by $2\pi m(u - v)/K$. Thus, the magnitude of the sum is less than the sum of magnitudes of the individual terms. In conclusion, the magnitude of the side diagonal elements of $\boldsymbol{S}_{\nu,ll}(D)$ will always be smaller than that of the main diagonal elements if the receive filter bandwidth is at least $2/T$. Hence, both $\boldsymbol{S}_{\nu,ll}(D)$ and $\boldsymbol{S}_\nu(D)$ are regular. Equation (2.62) shows that $\boldsymbol{S}_\nu(D)$ is positive semi-definite. Combined with the fact that it is regular, it follows that $\boldsymbol{S}_\nu(D)$ is positive definite. In the special case when the receive filter has an ideal rectangular shape and a double-sided bandwidth of K/T, the side diagonal elements of $\boldsymbol{S}_{\nu,ll}(D)$ are zero. In this case, the overall noise spectrum matrix $\boldsymbol{S}_\nu(D)$ is diagonal. Additional characteristics of the matrices $\boldsymbol{S}_{\nu,ll}(D)$ and $\boldsymbol{S}_\nu(D)$, which follow from Equation (2.72), are that they are both Toeplitz and Hermitian.

2.5   Concluding Remarks – Diversity

Cancellation of cochannel and intersymbol interference (CCI, ISI) and detection relies on a sufficient degree of diversity in the transmitted signals. This diversity is introduced into the investigated system by a combination of antenna diversity and frequency diversity. Antenna diversity is realized by receiving the signals at $A > 1$ antennas at the base station. Frequency diversity is obtained by spreading the transmitted signals by a factor of $K > 1$. If the symbol period of the transmitted signals is T, the minimum required double-sided bandwidth (Nyquist criterion) is $B_T = 1/T$. After spreading, the signal bandwidth is K/T. The *number of diversity channels* is defined as the product of antenna and frequency diversity:

$$U_{\mathrm{div}} = AK. \tag{2.74}$$

As long as no more than U_{div} users are present, the system is referred to as *well populated*. If the number of users N exceeds the number of diversity channels, we will call the system *overpopulated*.

The basis of Definition (2.74) is the fact that the system may be viewed as one with AK different channel outputs and detector inputs. Hence, there are exactly

U_{div} diversity channels in the system. This can be verified mathematically through Equation (2.58): the input signal vector $\boldsymbol{a}$ has N components, one for each user. The overall channel matrix $\boldsymbol{X}$ consists of N inputs and AK outputs. Thus, the overall output signal vector $\boldsymbol{y}$ has AK components. Each component can be interpreted as a separate diversity input signal to the detector.

The effective degree of diversity in the system depends on the number of diversity channels and the number of users. Moreover, it also depends on the frequency.

Let the effective degree of diversity at the normalized frequency $\check{f}$ be defined as U_{div} minus the number of users in the system (N) if the rank of the channel matrix $\boldsymbol{X}(D)$ evaluated at $D = e^{-j2\pi\check{f}}$ is equal to N. On the other hand, if the rank of $\boldsymbol{X}(D)$ is smaller than N, the system will be under-determined at this frequency and it will not be possible to estimate the data input signal $\boldsymbol{a}(D)$ at $D = e^{-j2\pi\check{f}}$ from the observation $\boldsymbol{y}(D)$ with a linear detector. It follows from the above that each additional user reduces the effective degree of diversity generally by one unless it causes the row vectors of the channel matrix to become linearly dependent. In the latter case, the system becomes singular at this particular frequency, which corresponds to a spectral null in a single-input single-output system.

The above discussion implies that the data input signals $\boldsymbol{a}$ may be estimated from the observation $\boldsymbol{y}$ with a linear detector as long as the number of users (N) is smaller than or equal to the number of diversity channels (U_{div}). This is a necessary but not a sufficient condition for the feasibility of estimating $\boldsymbol{a}$. A sufficient condition is that the rank of the channel matrix $\boldsymbol{X}(D)$ is equal to N for all D on the unit circle.

Chapter 3

Calculation of the Error Probability

3.1 Introduction

Consider a communications system which transmits periodically pulses chosen from a finite set of waveforms. It is the objective of the detector to decide which waveform has been sent. The quality of the detector is determined by the number of errors it produces.

The detection process is impaired by two effects: noise and interference. Random noise originates normally at the receiver front end. It is usually added to the information signal. Its probability characteristic is very often modeled as a Gaussian distribution, however certain processes may be described more accurately by other distributions. The second impairment is interference and encompasses malicious interaction among other communication signals with the signal of interest or between the signal with itself. The former is often referred to as *adjacent channel interference* (ACI) and *cochannel interference* (CCI). ACI occurs because of leaking from communication signals sent over adjacent frequency bands. CCI is interference from signals using the same frequency band as the desired signal. Other forms of interference are narrow and broadband interferers from different communications systems or devices generating electromagnetic waves. The signal of interest may also interfere

with itself and cause *intersymbol interference* (ISI). This will happen if waveforms sent at different times interact with and distort each other. Causes of that kind of self-interference are bandwidth limitations of the communications system, imperfect design of the transmitted signals and receive filters, distortion due to dispersive or multipath channels, and nonideal sampling instants. If the interfering signals of adjacent and co-channels are uncorrelated with, and sent at the same symbol rate as, the desired signal, the effect of ACI, CCI and ISI on the system will be comparable and they can be described identically in mathematical terms. This is shown subsequently for the case of a multiuser system, in which several users communicate simultaneously.

The error probability is the ultimate performance criterion of the described communications system. However, it becomes very difficult to calculate the exact value when interference is contained in the signal. An easy solution is to approximate the interference term by a Gaussian distributed random variable with the same variance. However, interference is in many cases described inaccurately by a Gaussian probability distribution and leads under these circumstances to wrong results when the error rate is determined. It is therefore necessary to take the specific statistical properties of the interference into account.

Several methods have been proposed in the literature for the accurate calculation or approximation of the error probability. It turns out that conceptual simple approaches are either inaccurate or computationally complex and inefficient. On the other hand, more sophisticated methods have been developed that are both very accurate and efficient.

In this chapter, the Saltzberg upper bound on the error probability is extended to multiple-input multiple-output (MIMO) systems and equalizers. A new class of error probability bounds and approximations, based on McGee's approximation of the Q-function [72], is derived and introduced. It consists of a first- and second-order approximation. The first-order approximation results in an exact upper bound and an energy upper bound solely based on the signal-to-interference-and-noise ratio (SINR) and the interference-to-noise ratio (INR). The second-order approximation leads to an approximate upper bound.

The new error probability approximations are efficient and very accurate. Nu-

merical results obtained through extensive simulations yielded for the second-order approximation relative errors[1] below 0.1% in situations of most practical interest. In the most extreme cases, the relative errors approached 100%. The corresponding relative errors for the exact first-order bound were 10% and below 1000%, respectively. The first-order energy upper bound performed comparable to a Gaussian approximation[2].

3.2   Model

The following analysis and results will be restricted to pulse amplitude modulation (PAM) and rectangular quadrature amplitude modulation (QAM), which is essentially PAM of both inphase and quadrature signals. The objective in the case of PAM is basically to find the probability that a real random variable with one-dimensional range exceeds a certain threshold. QAM may be reduced to two independent one-dimensional random variables and can be solved in the same fashion. One basic assumption for the QAM analysis is that the inphase and quadrature components of the modulated signal are independent.

Consider a multiuser system consisting of N users and a single base station with a receiver front end as described in Chapter 2. Each user transmits a data sequence a_i ($i \in \mathcal{I}_N$), after spreading with a code of processing gain K, over a communication channel. The signals are received at A different antennas and white Gaussian noise is added to each element. The receiver filters, demodulates and samples the signals. As shown in Figure 3.1, the system parts consisting of channel and receiver front end can be described completely by a discrete-time complex baseband vector model (Chapter 2), whose output signal is the vector sequence $\boldsymbol{y}$ with AK components.

---

[1]The relative error is defined as the difference between the approximation and the true probability of error normalized by the smaller of these two values (see Equation (3.132)).

[2]For the Gaussian approximation, it is assumed that the interference is Gaussian distributed. Although this is obviously not correct, the assumption is made in order to obtain a very simple expression. The error caused by the assumption may or may not be small depending on the situation. Note that the first-order energy upper bound always yields an estimate which is larger than the true error probability while this is not necessarily the case for the Gaussian approximation.
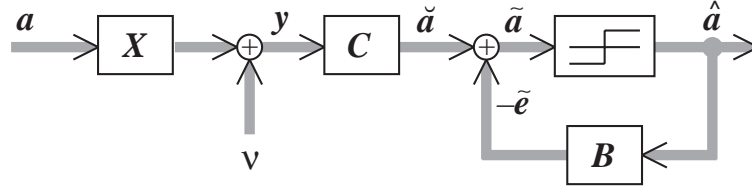
Figure 3.1: System block diagram including channel, equalizer and decision-feedback loop.

Let us consider optional data processing by an equalizer[3] with or without a decision-feedback loop. The forward filter may be described by an $AK \times N$ matrix filter $\boldsymbol{C}$, whose elements c_{lk} define a discrete-time filter between input l and output k. Previous decisions $\hat{a}_k$ may be fed into a causal $N \times N$ feedback matrix filter $\boldsymbol{B}$ in order to reconstruct and cancel remaining interference from the output signal of the forward filter.

Let us describe the linear system part by the $N \times N$ matrix filter

$$\boldsymbol{H}[n] \triangleq \boldsymbol{X}[n] \star \boldsymbol{C}[n]. \tag{3.1}$$

The input signal to the decision element can then be written as

$$\tilde{\boldsymbol{a}}[n] = \boldsymbol{a}[n] \star \boldsymbol{H}[n] + \hat{\boldsymbol{a}}[n] \star \boldsymbol{B}[n] + \boldsymbol{\zeta}[n] \tag{3.2}$$

where $\boldsymbol{\zeta}[n] = \boldsymbol{\nu}[n] \star \boldsymbol{C}[n]$ is a vector consisting of N colored Gaussian noise sequences $\zeta_k \triangleq [\boldsymbol{\zeta}]_k$.

The quantized decisions $\hat{a}_k[n] \triangleq [\hat{\boldsymbol{a}}[n]]_k$ ($k \in \mathcal{I}_N$) belong to the same alphabet of complex numbers as the input data ($a_k[n], \hat{a}_k[n] \in \mathcal{A}_k$). The modulation scheme is restricted to quadrature amplitude modulated (QAM) systems with rectangular signal constellations (see Section 2.3.2.1). The inphase and the quadrature signals of user k are then pulse amplitude modulated with an even number of signal levels L_k^{re} and L_k^{im}, respectively[4].

---

[3]The results obtained by the following analysis are valid for equalization as well as any other kind of linear combination of the received signal.

[4]This includes the general case that different users may apply modulation schemes with a different number of levels.

The output signal shall be formulated by a simple expression. Let us start with the system output which may be described equivalently by N scalar equations

$$\tilde{a}_k[n] = \sum_{i=1}^{N} \sum_{m=-\infty}^{\infty} a_i[n-m]h_{ik}[m] + \sum_{i=1}^{N} \sum_{m=-\infty}^{\infty} \hat{a}_i[n-m]b_{ik}[m] + \zeta_k[n], \quad \forall k \in \mathcal{I}_N$$

(3.3)

where $h_{ik} \triangleq [\boldsymbol{H}]_{ik}$ and $b_{ik} \triangleq [\boldsymbol{B}]_{ik}$ are the (i,k)-th components of $\boldsymbol{H}$ and $\boldsymbol{B}$, respectively. The feedback filter impulse responses are causal, i.e. $b_{ik}[n] = 0$ for $n \leq 0, \forall i, k \in \mathcal{I}_N$.

Let us, from this point on, make the fundamental assumption that all decisions provided to the feedback filter are correct, i.e.

$$\hat{a}_i[n] = a_i[n], \quad \forall i \in \mathcal{I}_N, \ n \in \mathbb{Z}.$$

(3.4)

Formally, this assumption is wrong since the combination of interference and noise will eventually cause erroneous decisions. However, in situations when the error probability is low, the mistake caused by this assumption may be small or even negligible. Thus, for the decision-feedback equalizer (DFE), the following results are reasonable only when the effect of wrong decisions in the feedback loop is small. On the other hand, the assumption turns out to be crucial for the mathematical tractability of the DFE. Note that this problem does not arise for linear receivers.

Under the assumption of correct decisions (3.4), the input to the k-th decision device (3.3) becomes

$$\tilde{a}_k[n] = \sum_{i=1}^{N} \sum_{m=-\infty}^{\infty} a_i[n-m] \left(h_{ik}[m] + b_{ik}[m] \right) + \zeta_k[n], \quad \forall k \in \mathcal{I}_N$$

(3.5)

As a result of the modulation scheme and the complex baseband representation, all quantities are in general complex. They may be expressed in terms of their real

and imaginary parts

$$a_i[n] \triangleq a_i^{\text{re}}[n] + j a_i^{\text{im}}[n] \tag{3.6}$$

$$\tilde{a}_k[n] \triangleq \tilde{a}_k^{\text{re}}[n] + j \tilde{a}_k^{\text{im}}[n] \tag{3.7}$$

$$h_{ik}[n] \triangleq h_{ik}^{\text{re}}[n] + j h_{ik}^{\text{im}}[n] \tag{3.8}$$

$$b_{ik}[n] \triangleq b_{ik}^{\text{re}}[n] + j b_{ik}^{\text{im}}[n]. \tag{3.9}$$

$$\zeta_k[n] \triangleq \zeta_k^{\text{re}}[n] + j \zeta_k^{\text{im}}[n] \tag{3.10}$$

The real and imaginary parts of the input signal to the decision element are obtained by substituting Equations (3.6) to (3.9) into (3.3):

$$\tilde{a}_k^{\text{re}}[n] = \sum_{i=1}^{N} \sum_{m=-\infty}^{\infty} \left\{ a_i^{\text{re}}[n-m] \left(h_{ik}^{\text{re}}[m] + b_{ik}^{\text{re}}[m] \right) \right.$$
$$\left. - a_i^{\text{im}}[n-m] \left(h_{ik}^{\text{im}}[m] + b_{ik}^{\text{im}}[m] \right) \right\} + \zeta_k^{\text{re}}[n] \tag{3.11}$$

$$\tilde{a}_k^{\text{im}}[n] = \sum_{i=1}^{N} \sum_{m=-\infty}^{\infty} \left\{ a_i^{\text{im}}[n-m] \left(h_{ik}^{\text{re}}[m] + b_{ik}^{\text{re}}[m] \right) \right.$$
$$\left. + a_i^{\text{re}}[n-m] \left(h_{ik}^{\text{im}}[m] + b_{ik}^{\text{im}}[m] \right) \right\} + \zeta_k^{\text{im}}[n] \tag{3.12}$$

According to the modulation format as described above and in Section 2.3.2.1, the real and imaginary input data symbols belong to the sets $\mathcal{S}_i^{\text{re}}$ and $\mathcal{S}_i^{\text{im}}$, respectively:

$$a_i^{\text{re}}[n] \in \mathcal{S}_i^{\text{re}} \tag{3.13}$$

$$a_i^{\text{im}}[n] \in \mathcal{S}_i^{\text{im}} \tag{3.14}$$

where $\mathcal{S}_i^{\text{re}}$ and $\mathcal{S}_i^{\text{im}}$ are defined in Equations (2.8) and (2.9).

The input signals to the decision devices $\tilde{a}_k^{\text{re}}[n]$ and $\tilde{a}_k^{\text{im}}[n]$, given by Equations (3.11) and (3.12), consist of a noise component and a signal component. The signal component of the inphase signal $\tilde{a}_k^{\text{re}}[n]$ is equal to $a_k^{\text{re}}[n]h_{kk}^{\text{re}}[0]$. Analogously, $a_k^{\text{im}}[n]h_{kk}^{\text{re}}[0]$ is the signal component of the quadrature signal $\tilde{a}_k^{\text{im}}[n]$. It can easily be shown that the optimal slicing levels of the decision element are equal to the midpoints between two adjacent signal components [34]. In the considered case, all possible signal compo-

nents of the inphase component are given by the elements of the set $\mathcal{S}_i^{\text{re}}$ multiplied by the bias coefficient $h_{kk}^{\text{re}}[0]$. Analogously, all signal components of the quadrature component are $\mathcal{S}_i^{\text{re}} h_{kk}^{\text{re}}[0]$. Thus, the optimal slicing levels of the inphase and quadrature signal of the k-th user are

$$0, \pm\kappa_k h_{kk}^{\text{re}}[0], \pm 2\kappa_k h_{kk}^{\text{re}}[0], \dots, \pm\left(\frac{L_k^{\text{re}}}{2} - 1\right)\kappa_k h_{kk}^{\text{re}}[0] \tag{3.15}$$

$$0, \pm\kappa_k h_{kk}^{\text{re}}[0], \pm 2\kappa_k h_{kk}^{\text{re}}[0], \dots, \pm\left(\frac{L_k^{\text{im}}}{2} - 1\right)\kappa_k h_{kk}^{\text{re}}[0] \tag{3.16}$$

For the inphase signal, the probability of exceeding the decision threshold in the positive direction is

$$P_{\text{ex},k}^{\text{re}} = \text{Prob}\left\{\tilde{a}_k^{\text{re}}[n] > \left(a_k^{\text{re}}[n] + \frac{1}{2}\kappa_k\right) h_{kk}^{\text{re}}[0]\right\} \tag{3.17}$$

$$= \text{Prob}\left\{\sum_{i=1}^{N}\sum_{m=-\infty}^{\infty}\left\{a_i^{\text{re}}[n-m]\left(h_{ik}^{\text{re}}[m] + b_{ik}^{\text{re}}[m]\right) - a_i^{\text{im}}[n-m]\left(h_{ik}^{\text{im}}[m] + b_{ik}^{\text{im}}[m]\right)\right\}\right.$$

$$\left. - a_k^{\text{re}}[n] h_{kk}^{\text{re}}[0] + \zeta_k^{\text{re}}[n] > \frac{1}{2}\kappa_k h_{kk}^{\text{re}}[0]\right\} \tag{3.18}$$

Analogously for the quadrature signal, we get

$$P_{\text{ex},k}^{\text{im}} = \text{Prob}\left\{\tilde{a}_k^{\text{im}}[n] > \left(a_k^{\text{im}}[n] + \frac{1}{2}\kappa_k\right) h_{kk}^{\text{re}}[0]\right\} \tag{3.19}$$

$$= \text{Prob}\left\{\sum_{i=1}^{N}\sum_{m=-\infty}^{\infty}\left\{a_i^{\text{im}}[n-m]\left(h_{ik}^{\text{re}}[m] + b_{ik}^{\text{re}}[m]\right) + a_i^{\text{re}}[n-m]\left(h_{ik}^{\text{im}}[m] + b_{ik}^{\text{im}}[m]\right)\right\}\right.$$

$$\left. - a_k^{\text{im}}[n] h_{kk}^{\text{re}}[0] + \zeta_k^{\text{im}}[n] > \frac{1}{2}\kappa_k h_{kk}^{\text{re}}[0]\right\} \tag{3.20}$$

Note that the probability density of the combined interference and noise is an even function and the distance between the ideal signal level and either of the two adjacent decision thresholds is the same. Therefore, the probabilities of exceeding the decision threshold in the negative direction are also equal to $P_{\text{ex},k}^{\text{re}}$ and $P_{\text{ex},k}^{\text{im}}$, respectively.

Let the modulation scheme for the inphase or quadrature signal of the k-th user be L_k-level PAM. There are $(L_k - 2)$ inner levels for which an error occurs when the

decision threshold is exceeded in either the positive or negative direction. Since the probability of exceeding either threshold is $P_{\text{ex},k}$, the probability of a symbol error for an inner level is $2P_{\text{ex},k}$. For the two remaining outer levels, the threshold can only be exceeded in one direction, leading to a symbol error probability of $P_{\text{ex},k}$. If we consider in addition Gray coding, i.e. adjacent symbols differ in exactly one bit, and assume that all symbols are equiprobable, the bit error rate (BER) for the inphase or quadrature signal of user k is with very high accuracy[5].

$$P_{b,k} = 2\,\frac{L_k - 1}{L_k}\,P_{\text{ex,k}}. \tag{3.21}$$

It is assumed that the data symbols are generated randomly and take on each element of the set $\mathcal{S}_k^{\text{re}}$ (or $\mathcal{S}_k^{\text{im}}$) with equal probability. The variance of the two real pulse amplitude modulated signals $a_k^{\text{re}}[n]$ and $a_k^{\text{im}}[n]$, denoted by $\mathcal{E}_{a,k}^{\text{re}}$ and $\mathcal{E}_{a,k}^{\text{im}}$, respectively, is then given by Equations (2.10) and (2.11).

The noise signals, which are Gaussian distributed with zero mean and variance $\mathcal{E}_{\zeta,k}$, and the data sequences are assumed to be independent, i.e.

$$E\left[|\zeta_k[n]|^2\right] \triangleq \mathcal{E}_{\zeta,k} \tag{3.22}$$

$$E\left[|\zeta_k^{\text{re}}[n]|^2\right] \triangleq \mathcal{E}_{\zeta,k}^{\text{re}} = \frac{1}{2}\mathcal{E}_{\zeta,k} \tag{3.23}$$

$$E\left[|\zeta_k^{\text{im}}[n]|^2\right] \triangleq \mathcal{E}_{\zeta,k}^{\text{im}} = \frac{1}{2}\mathcal{E}_{\zeta,k} \tag{3.24}$$

$$E\left[a_i^*[n]\zeta_k[m]\right] = 0, \quad \forall i,k,n,m \tag{3.25}$$

All data signals a_i^{re} and a_i^{im} are considered to be mutually and temporally independent with zero mean. This implies the following relations (Equation (A.9),

---

[5]The assumption made is that a symbol error causes exactly one bit error. Using Gray coding, symbols adjacent to each other differ in only one bit. Considering a sufficiently high SINR, the majority of errors are caused by exceeding only the closest decision threshold, resulting in exactly one bit error per symbol error. In this case, the probability for the decision variable to exceed more than the adjacent threshold is very small and may be neglected. As a result, Equation (3.21) is an excellent approximation to the BER provided that the SINR at the input to the decision device is sufficiently high. In low SINR systems, the decision variable may exceed two or more consecutive thresholds relatively often, resulting in a decision which differs by more than one bit from the correct symbol. Under this circumstance, the exact BER may be significantly larger than the value provided by Equation (3.21).

(A.10))

$$E\left[a_i^{\text{re}}[n]a_k^{\text{re}}[m]\right] = \mathcal{E}_{a,i}^{\text{re}}\,\delta_K[i-k]\delta_K[n-m] \tag{3.26}$$

$$E\left[a_i^{\text{im}}[n]a_k^{\text{im}}[m]\right] = \mathcal{E}_{a,i}^{\text{im}}\,\delta_K[i-k]\delta_K[n-m] \tag{3.27}$$

$$E\left[a_i^{\text{re}}[n]a_k^{\text{im}}[m]\right] = 0, \quad \forall i,k,n,m \tag{3.28}$$

where $\delta_K[n]$ is the Kronecker delta sequence (see Table A.3).

In order to simplify the notation, define the sequences

$$\tilde{\alpha}_n^{(p)} \triangleq \begin{cases} \tilde{a}_k^{\text{re}}[n], & p = 2k-2 \\ \tilde{a}_k^{\text{im}}[n], & p = 2k-1 \end{cases} \tag{3.29}$$

$$\alpha_n^{(l)} \triangleq \begin{cases} a_i^{\text{re}}[n], & l = 2i-2 \\ a_i^{\text{im}}[n], & l = 2i-1 \end{cases} \tag{3.30}$$

$$h_n^{(l,p)} \triangleq \begin{cases} h_{ik}^{\text{re}}[n] + b_{ik}^{\text{re}}[n], & p = 2k-2 \quad l = 2i-2 \\ -(h_{ik}^{\text{im}}[n] + b_{ik}^{\text{im}}[n]), & p = 2k-2 \quad l = 2i-1 \\ h_{ik}^{\text{im}}[n] + b_{ik}^{\text{im}}[n], & p = 2k-1 \quad l = 2i-2 \\ h_{ik}^{\text{re}}[n] + b_{ik}^{\text{re}}[n], & p = 2k-1 \quad l = 2i-1 \end{cases} \tag{3.31}$$

$$\zeta_n^{(p)} \triangleq \begin{cases} \zeta_k^{\text{re}}[n], & p = 2k-2 \\ \zeta_k^{\text{im}}[n], & p = 2k-1 \end{cases} \tag{3.32}$$

where the subscript n denotes the time index. Note that the indices l and p take on the values $l, p \in \{0, 1, 2, \dots, 2N-1\}$. With the above definitions, the expressions for the inphase (3.11) and quadrature parts (3.12) of the input signal to the decision device may be combined into a single equation:

$$\tilde{\alpha}_n^{(p)} = \sum_{l=0}^{2N-1} \sum_{m=-\infty}^{\infty} \alpha_{n-m}^{(l)} h_m^{(l,p)} + \zeta_n^{(p)} \tag{3.33}$$

Consider that the parameters n and p are fixed. In order to simplify the notation further, the substitution $i = 2Nm + l - p$ is introduced and the following variables

are defined:

$$\tilde{\alpha}_0 \triangleq \tilde{\alpha}_n^{(p)} \tag{3.34}$$

$$\alpha_i = \alpha_{2Nm+l-p} \triangleq \alpha_{n-m}^{(l)} \tag{3.35}$$

$$h_i = h_{2Nm+l-p} \triangleq h_m^{(l,p)}. \tag{3.36}$$

$$\zeta_0 \triangleq \zeta_n^{(p)} \tag{3.37}$$

The desired symbol has the indices $l = p$ and $m = 0$. This translates into $i = 0$. Hence, the desired signal information is contained in the product of $\alpha_n^{(p)} = \alpha_0$ and $h_0^{(p,p)} = h_0$. Using the above notational transformation, the decision variable of the quantizer is

$$\tilde{\alpha}_0 = \alpha_0 h_0 + \sum_{\substack{i=-\infty \\ i \neq 0}}^{\infty} \alpha_i h_i + \zeta_0. \tag{3.38}$$

The first term on the right hand side of the above equation constitutes the signal component while the summation term is the interference part comprising ACI, CCI and ISI. The third term is Gaussian noise.

Combining Definitions (3.30) and (3.32) with Equations (3.22) to (3.28) yields the following expressions for the cross-correlations of data and noise

$$E\left[\alpha_i \alpha_l\right] = \mathcal{E}_{\alpha,i}\, \delta_K[i-l], \quad \forall i, l \in \mathbb{Z} \tag{3.39}$$

$$E\left[\alpha_i \zeta_0\right] = 0, \quad \forall i \in \mathbb{Z} \tag{3.40}$$

$$E\left[|\zeta_0|^2\right] = \mathcal{E}_\zeta. \tag{3.41}$$

Using the optimal slicing levels as specified in Equation (3.15) or (3.16), the prob-

ability of exceeding the decision threshold in the positive direction is given by

$$P_{ex} = \text{Prob} \left\{ \tilde{\alpha}_0 > \left(\alpha_0 + \frac{1}{2} \kappa_0 \right) h_0 \right\} \tag{3.42}$$

$$= \text{Prob} \left\{ \sum_{\substack{i=-\infty \\ i \neq 0}}^{\infty} \alpha_i h_i + \zeta_0 > \frac{1}{2} \kappa_0 h_0 \right\} \tag{3.43}$$

where κ_0 is the distance between two adjacent modulation levels of the symbol α_0. The probability of exceeding the decision threshold in the negative direction is also equal to P_{ex}. If L is the number of PAM signal levels for the data symbol α_0 and Gray coding is applied, the bit error rate will be very well approximated by

$$P_b = 2 \frac{L-1}{L} P_{ex}. \tag{3.44}$$

Let us summarize the main results of this section. The relatively tedious expressions (3.11) and (3.12) for the input signals to the decision device have been formulated in the equivalent but significantly simpler form (3.38). This shows that ISI, CCI and interference from the quadrature signals can be described mathematically in the same fashion. In fact, the simple model (3.38) completely describes any multiuser system that includes an arbitrary linear equalizer. It may also describe a multiuser system using a decision-feedback equalizer provided that the effect of fed-back decision errors can be neglected.

3.3 Saltzberg Bound for Multiple-Input Multiple-Output Systems

The work of Saltzberg [103] is used in this section in order to find an upper bound on the error probability which depends exclusively on the signal-to-interference-and-noise ratio (SINR). Initially, rectangular QAM with possibly a different number of modulation levels for inphase and quadrature components is considered. It is shown for this case that the upper bounds are generally different for inphase and quadrature

signals. After that, the special case of square QAM is investigated, for which the number of inphase and quadrature modulation levels is the same. It turns out that, in this situation, the upper error bounds for both inphase and quadrature signals are identical. Moreover, it is shown that the error bound may be expressed in terms of the SINR of the complex baseband output signal $\tilde{a}_k$. Since this SINR and the MMSE of a linear or decision-feedback equalizer are connected through a unique relationship (Section 4.4), the upper bound on the error probability can be expressed in terms of the MMSE. This is an important result because it enables a performance evaluation of equalizers using a simple expression, which depends only on the MMSE.

Let us start with *rectangular* QAM at the transmitters. The number of modulation levels is L_k^{re} and L_k^{im} for the inphase and quadrature signal, respectively. The two real input signals to the decision device, $\tilde{a}_k^{\mathrm{re}}$ and $\tilde{a}_k^{\mathrm{im}}$, are given in Equations (3.11) and (3.12), respectively. The final decision depends on both the *signal component* and the *distortion component*, where the latter is responsible for possible errors. It is obvious that the signal components of $\tilde{a}_k^{\mathrm{re}}$ and $\tilde{a}_k^{\mathrm{im}}$ are

$$\chi_{\mathrm{S},k}^{\mathrm{re}}[n] = a_k^{\mathrm{re}}[n]h_{kk}^{\mathrm{re}}[0] \tag{3.45}$$

$$\chi_{\mathrm{S},k}^{\mathrm{im}}[n] = a_k^{\mathrm{im}}[n]h_{kk}^{\mathrm{re}}[0], \tag{3.46}$$

respectively. All other remaining terms in $\tilde{a}_k^{\mathrm{re}}$ and $\tilde{a}_k^{\mathrm{im}}$ are either interference or noise components. Together, they constitute the distortion components

$$\chi_{\mathrm{IN},k}^{\mathrm{re}}[n] = \tilde{a}_k^{\mathrm{re}}[n] - a_k^{\mathrm{re}}[n]h_{kk}^{\mathrm{re}}[0] \tag{3.47}$$

$$\chi_{\mathrm{IN},k}^{\mathrm{im}}[n] = \tilde{a}_k^{\mathrm{im}}[n] - a_k^{\mathrm{im}}[n]h_{kk}^{\mathrm{re}}[0]. \tag{3.48}$$

The energy in the signal component determines the *signal energy*

$$\mathcal{E}_{\mathrm{S},k}^{\mathrm{re}} \triangleq E\left[\left|\chi_{\mathrm{S},k}^{\mathrm{re}}[n]\right|^2\right] = \mathcal{E}_{a,k}^{\mathrm{re}}(h_{kk}^{\mathrm{re}}[0])^2 \tag{3.49}$$

$$\mathcal{E}_{\mathrm{S},k}^{\mathrm{im}} \triangleq E\left[\left|\chi_{\mathrm{S},k}^{\mathrm{re}}[n]\right|^2\right] = \mathcal{E}_{a,k}^{\mathrm{im}}(h_{kk}^{\mathrm{re}}[0])^2. \tag{3.50}$$

Analogously, the *distortion energies* are

$$
\begin{aligned}
\mathcal{E}_{\text{IN},k}^{\text{re}} &\triangleq E\left[\left|\chi_{\text{IN},k}^{\text{re}}[n]\right|^2\right] \\
&= \sum_{i=1}^{N}\sum_{m=-\infty}^{\infty}\left\{\mathcal{E}_{a,i}^{\text{re}}\left(h_{ik}^{\text{re}}[m]+b_{ik}^{\text{re}}[m]\right)^2 + \mathcal{E}_{a,i}^{\text{im}}\left(h_{ik}^{\text{im}}[m]+b_{ik}^{\text{im}}[m]\right)^2\right\} \\
&\quad - \mathcal{E}_{a,k}^{\text{re}}(h_{kk}^{\text{re}}[0])^2 + \mathcal{E}_{\zeta,k}^{\text{re}} \\[4pt]
\mathcal{E}_{\text{IN},k}^{\text{im}} &\triangleq E\left[\left|\chi_{\text{IN},k}^{\text{im}}[n]\right|^2\right] \\
&= \sum_{i=1}^{N}\sum_{m=-\infty}^{\infty}\left\{\mathcal{E}_{a,i}^{\text{re}}\left(h_{ik}^{\text{im}}[m]+b_{ik}^{\text{im}}[m]\right)^2 + \mathcal{E}_{a,i}^{\text{im}}\left(h_{ik}^{\text{re}}[m]+b_{ik}^{\text{re}}[m]\right)^2\right\} \\
&\quad - \mathcal{E}_{a,k}^{\text{im}}(h_{kk}^{\text{re}}[0])^2 + \mathcal{E}_{\zeta,k}^{\text{im}}
\end{aligned}
$$

(3.51)

(3.52)

where the final result is obtained by substituting Equations (3.11) and (3.12) for the quantities in the expectations. The signal-to-interference-and-noise ratio is defined as the ratio between signal and distortion energies. Thus, the inphase and quadrature SINR of user k are

$$
\Phi_k^{\text{re}} \triangleq \frac{\mathcal{E}_{\text{S},k}^{\text{re}}}{\mathcal{E}_{\text{IN},k}^{\text{re}}}
$$

(3.53)

$$
\Phi_k^{\text{im}} \triangleq \frac{\mathcal{E}_{\text{S},k}^{\text{im}}}{\mathcal{E}_{\text{IN},k}^{\text{im}}}.
$$

(3.54)

The error rate is determined by the probability of exceeding the decision threshold, which is formulated for inphase and quadrature signals of user k in Equations (3.18) and (3.20), respectively. This probability can be upper bounded as described by Saltzberg [103]. In particular, since the data symbols are mutually uncorrelated for

all $i \in \mathbb{Z}$, one may use the approximation [103]

$$
P_{\mathrm{ex},k}^{\mathrm{re}} \leq \exp\Bigg\{ - \left(\frac{1}{2}\kappa_k h_{kk}^{\mathrm{re}}[0]\right)^2 \Big/ \bigg[2\sum_{i=1}^{N}\sum_{m=-\infty}^{\infty} \big\{ \mathcal{E}_{a,i}^{\mathrm{re}} \left(h_{ik}^{\mathrm{re}}[m] + b_{ik}^{\mathrm{re}}[m]\right)^2
$$
$$
+ \mathcal{E}_{a,i}^{\mathrm{im}} \left(h_{ik}^{\mathrm{im}}[m] + b_{ik}^{\mathrm{im}}[m]\right)^2 \big\} - 2\mathcal{E}_{a,k}^{\mathrm{re}}(h_{kk}^{\mathrm{re}}[0])^2 + 2\mathcal{E}_{\zeta,k}^{\mathrm{re}} \bigg] \Bigg\} \tag{3.55}
$$

$$
P_{\mathrm{ex},k}^{\mathrm{im}} \leq \exp\Bigg\{ - \left(\frac{1}{2}\kappa_k h_{kk}^{\mathrm{re}}[0]\right)^2 \Big/ \bigg[2\sum_{i=1}^{N}\sum_{m=-\infty}^{\infty} \big\{ \mathcal{E}_{a,i}^{\mathrm{re}} \left(h_{ik}^{\mathrm{im}}[m] + b_{ik}^{\mathrm{im}}[m]\right)^2
$$
$$
+ \mathcal{E}_{a,i}^{\mathrm{im}} \left(h_{ik}^{\mathrm{re}}[m] + b_{ik}^{\mathrm{re}}[m]\right)^2 \big\} - 2\mathcal{E}_{a,k}^{\mathrm{im}}(h_{kk}^{\mathrm{re}}[0])^2 + 2\mathcal{E}_{\zeta,k}^{\mathrm{im}} \bigg] \Bigg\} \tag{3.56}
$$

Substituting Equations (3.49) to (3.54) into these bounds and considering (2.10), (2.11) results in

$$
P_{\mathrm{ex},k}^{\mathrm{re}} \leq \exp\left\{ -\frac{\Phi_k^{\mathrm{re}}}{2\rho(L_k^{\mathrm{re}})} \right\} \tag{3.57}
$$

$$
P_{\mathrm{ex},k}^{\mathrm{im}} \leq \exp\left\{ -\frac{\Phi_k^{\mathrm{im}}}{2\rho(L_k^{\mathrm{im}})} \right\} \tag{3.58}
$$

where the function $\rho(L)$ is defined by

$$
\rho(L) \triangleq \frac{1}{3}\left[L^2 - 1\right]. \tag{3.59}
$$

Applying Equation (3.21), the bit error rates (BER) for the inphase and quadrature signal of the k-th user are upper bounded by

$$
P_{b,k}^{\mathrm{re}} \leq 2\frac{L_k^{\mathrm{re}} - 1}{L_k^{\mathrm{re}}} \exp\left\{ -\frac{\Phi_k^{\mathrm{re}}}{2\rho(L_k^{\mathrm{re}})} \right\} \tag{3.60}
$$

$$
P_{b,k}^{\mathrm{im}} \leq 2\frac{L_k^{\mathrm{im}} - 1}{L_k^{\mathrm{im}}} \exp\left\{ -\frac{\Phi_k^{\mathrm{im}}}{2\rho(L_k^{\mathrm{im}})} \right\}. \tag{3.61}
$$

These equations are the final results for the rectangular QAM case. It can be seen that the upper bound on the error probability depends only on the number of PAM levels and on the SINR of the particular signal component at the input to the decision device. Note that the signal energies of inphase and quadrature signals are in general

not identical (Equations (3.49) and (3.50)). The same applies for the distortion energies in Equations (3.51) and (3.52). Therefore, the error probabilities for the inphase and quadrature component will be different unless the number of inphase and quadrature modulation levels are identical for all users, i.e. $L_i^{\mathrm{re}} = L_i^{\mathrm{im}} \; \forall i \in \mathcal{I}_N$.

Special Case: Square QAM Let us now consider the special case of square QAM, i.e.

$$L_i = L_i^{\mathrm{re}} = L_i^{\mathrm{im}}, \quad \forall i \in \mathcal{I}_N. \tag{3.62}$$

The number of symbols in the QAM scheme (alphabet size) is equal to L_i^2. Since the variance of the complex data symbols $a_k[n]$ is normalized to unity, we obtain for the variances of inphase and quadrature components the condition $\mathcal{E}_{a,i}^{\mathrm{re}} + \mathcal{E}_{a,i}^{\mathrm{im}} = 1$. In addition, the number of modulation levels and the distance between constellation points is identical for both inphase and quadrature signals, resulting in identical variances $\mathcal{E}_{a,i}^{\mathrm{re}} = \mathcal{E}_{a,i}^{\mathrm{im}}$. Combining the last two conditions results in

$$\mathcal{E}_{a,i}^{\mathrm{re}} = \frac{1}{2} \tag{3.63}$$

$$\mathcal{E}_{a,i}^{\mathrm{im}} = \frac{1}{2}. \tag{3.64}$$

The complex baseband signal at the input to the k-th decision device, $\tilde{a}_k$, is given by Equation (3.3). The signal and distortion components of $\tilde{a}_k$ are

$$\chi_{\mathrm{S},k}[n] = a_k[n] h_{kk}^{\mathrm{re}}[0] \tag{3.65}$$

$$\chi_{\mathrm{IN},k}[n] = \tilde{a}_k[n] - a_k[n] h_{kk}^{\mathrm{re}}[0]. \tag{3.66}$$

With this, Equation (3.5) and the fact that the symbols $a_i[n]$ are zero mean, mutually uncorrelated random variables with unit variance, the signal and distortion energies

are found to be

$$\mathcal{E}_{\mathrm{S},k} \triangleq E\left[|\chi_{\mathrm{S},k}[n]|^2\right] = (h_{kk}^{\mathrm{re}}[0])^2 \tag{3.67}$$

$$\mathcal{E}_{\mathrm{IN},k} \triangleq E\left[|\chi_{\mathrm{IN},k}[n]|^2\right]$$

$$= \sum_{i=1}^{N} \mathcal{E}_{a,i} \sum_{m=-\infty}^{\infty} |h_{ik}[m] + b_{ik}[m]|^2 - (h_{kk}^{\mathrm{re}}[0])^2 + \mathcal{E}_{\zeta,k}$$

$$= \sum_{i=1}^{N} \mathcal{E}_{a,i} \sum_{m=-\infty}^{\infty} \left\{ (h_{ik}^{\mathrm{re}}[m] + b_{ik}^{\mathrm{re}}[m])^2 + (h_{ik}^{\mathrm{im}}[m] + b_{ik}^{\mathrm{im}}[m])^2 \right\} - (h_{kk}^{\mathrm{re}}[0])^2 + \mathcal{E}_{\zeta,k}.$$

$$\tag{3.68}$$

The total SINR at the input to the decision device is defined as the ratio of signal and distortion energies, i.e.

$$\Phi_k \triangleq \frac{\mathcal{E}_{\mathrm{S},k}}{\mathcal{E}_{\mathrm{IN},k}}. \tag{3.69}$$

Substituting Equations (3.23), (3.24), (3.63), (3.64) into (3.49), (3.50), (3.51), (3.52) and comparing the result with Equations (3.67), (3.68) yields the following relationships

$$\mathcal{E}_{\mathrm{S},k} = 2\mathcal{E}_{\mathrm{S},k}^{\mathrm{re}} = 2\mathcal{E}_{\mathrm{S},k}^{\mathrm{im}} \tag{3.70}$$

$$\mathcal{E}_{\mathrm{IN},k} = 2\mathcal{E}_{\mathrm{IN},k}^{\mathrm{re}} = 2\mathcal{E}_{\mathrm{IN},k}^{\mathrm{im}} \tag{3.71}$$

$$\Phi_k = \Phi_k^{\mathrm{re}} = \Phi_k^{\mathrm{im}}. \tag{3.72}$$

Substituting the last expression together with Equation (3.62) into Equations (3.57) and (3.58), it is found that the probability of exceeding the decision threshold for the inphase as well as the quadrature signal of user k is bounded by

$$P_{\mathrm{ex},k} \leq \exp\left\{ -\frac{\Phi_k}{2\rho(L_k)} \right\}. \tag{3.73}$$

Finally, if Gray coding is used the total BER of the k-th signal will be upper bounded by

$$P_{b,k} \leq 2 \frac{L_k - 1}{L_k} \exp\left\{-\frac{\Phi_k}{2\rho(L_k)}\right\}. \tag{3.74}$$

This shows that an upper bound on the total BER can be found for square QAM schemes if the SINR of the complex baseband signal at the input to the decision device is known.

3.4 A Class of Error Probability Bounds and Approximations

A class of error probability bounds based on an approximation of the Gaussian probability distribution is presented and analyzed in this section. Given is a real signal consisting of a signal component, interference and noise, and the objective is to find the probability that the signal exceeds a certain threshold. Three crucial assumptions are made: Firstly, the noise is a random variable with Gaussian (normal) probability distribution and zero mean; secondly, the noise is independent of both signal component and interference; and finally, the data symbols of the signal and interference are mutually independent and zero mean.

The main idea is to approximate the natural logarithm of the Q-function, $\ln Q(x)$, by a truncated version of its Taylor series. As a result, the Q-function can be expressed as a finite product of exponential functions. In this form, it is possible to determine the threshold probability in an elegant and efficient manner provided that the individual components of the interference are mutually independent. This method and results have been published in a paper [109].

In Section 3.4.2, the Taylor series of $\ln Q(x)$ is truncated after the linear term. This results in an upper bound on the error probability and corresponds to a method briefly outlined by McGee [72]. The general first-order approximation requires full knowledge of the interference weights h_i and leads to a tight upper bound. In certain situations, only the energy of the total interference may be known, while the values

of the h_i are not available. For this case, a simpler albeit looser upper bound is described in Section 3.4.2.1.

A very good approximation to the error probability is obtained by taking the quadratic term of the Taylor series expansion into account (Section 3.4.3). It will be shown that this approach leads to very accurate results. The main reason for this is the fact that $\ln Q(x)$ may be approximated very well by a second order polynomial in the vicinity of a point $x_0 \geq 1$. A disadvantage is that the result is not a strict upper bound, but rather an approximation to the error probability. However, the result will almost exclusively be larger than the true error probability. Therefore, the second-order error probability approximation will be referred to as "approximate upper bound".

3.4.1 Problem Formulation

The decision variable at the input to the quantizer is according to Equation (3.38)

$$\tilde{\alpha}_0 = \alpha_0 h_0 + \sum_{\substack{i=-\infty \\ i \neq 0}}^{\infty} \alpha_i h_i + \zeta_0. \tag{3.75}$$

The data symbols α_i are zero mean random variables drawn from a pulse amplitude modulation (PAM) alphabet with L_i levels (L_i even) and distance κ_i. h_i denotes the i-th channel weight and ζ_0 is a Gaussian distributed random variable with zero mean and variance $\mathcal{E}_\zeta$.

Let us, for reasons explained later, take the interference samples h_i ($i \in \mathbb{Z} \setminus 0$), multiply them with one half of the distance of the corresponding signal alphabet ($\kappa_i/2$), normalize the result by the standard deviation $\sqrt{\mathcal{E}_\zeta}$ of the Gaussian noise ζ_0 and map them bijectively into a new sequence f_k ($k \in \mathbb{N}$) such that the magnitudes of f_k are nonincreasing. The corresponding data symbols α_i are mapped into the

sequence d_k, so that

$$\{h_i | i \in \mathbb{Z} \setminus 0\} \overset{i \mapsto k}{\longmapsto} \left\{ f_k = \frac{\kappa_i h_i}{2\sqrt{\mathcal{E}_\zeta}} \,\middle|\, f_k^2 \geq f_{k+1}^2, \forall k \in \mathbb{N} \right\} \tag{3.76}$$

$$\{\alpha_i | i \in \mathbb{Z} \setminus 0\} \overset{i \mapsto k}{\longmapsto} \left\{ d_k = \frac{2\alpha_i}{\kappa_i} \,\middle|\, k \in \mathbb{N} \right\} \tag{3.77}$$

$$f_0 = \frac{\kappa_0 h_0}{2\sqrt{\mathcal{E}_\zeta}} \tag{3.78}$$

$$d_0 = \frac{2\alpha_0}{\kappa_0}. \tag{3.79}$$

The normalized decision variable is then

$$\frac{\tilde{\alpha}_0}{\sqrt{\mathcal{E}_\zeta}} = d_0 f_0 + \sum_{k=1}^{\infty} d_k f_k + \bar{\zeta}_0$$

$$= d_0 f_0 + z + \bar{\zeta}_0 \tag{3.80}$$

where $\bar{\zeta}_0 \triangleq \zeta_0 / \sqrt{\mathcal{E}_\zeta}$ is the normalized Gaussian noise random variable with zero mean and unit variance and the *interference random variable* is defined as

$$z \triangleq \sum_{k=1}^{\infty} d_k f_k = \frac{1}{\sqrt{\mathcal{E}_\zeta}} \sum_{\substack{i=-\infty \\ i \neq 0}}^{\infty} \alpha_i h_i. \tag{3.81}$$

The individual data symbols d_k are zero mean, mutually independent random variables. As a result of the transformation (3.77), (3.79), their possible values belong to the set of odd integer numbers between $-(L_k - 1)$ and $L_k - 1$:

$$d_k \in \{\pm 1, \pm 3, \pm 5, \ldots, \pm(L_k - 1)\}. \tag{3.82}$$

It is assumed that the random variables are *uniformly distributed*, i.e. they assume each value of the above set with equal probability. Therefore, the variance of d_k is

$$E\left[|d_k|^2\right] = \rho(L_k), \quad \forall k \in \mathbb{N}_0 \tag{3.83}$$

where the function $\rho(L)$ is defined in Equation (3.59).

Using the optimal slicing levels as specified in Equation (3.15) or (3.16), the probability of exceeding the decision threshold in the positive direction is given by

$$P_{\text{ex}} = \text{Prob}\left\{\frac{\tilde{\alpha}_0}{\sqrt{\mathcal{E}_\zeta}} > (d_0 + 1)f_0\right\}$$

$$= \text{Prob}\left\{\bar{\zeta}_0 > f_0 - z\right\}$$

$$= \int_{-\infty}^{\infty} Q(f_0 - z)\, p_z(z)\, dz \tag{3.84}$$

$$= E\left[Q\left(f_0 - z\right)\right] \tag{3.85}$$

where the expectation is taken over the interference random variable z, and the Q-function as well as the expectation operator 'E' are defined in Table A.3. The problem is that Equation (3.85) cannot be solved in this form. In general, it is not possible or extremely difficult to determine the expectation taken over a nonlinear function of the interference random variable. There are, however, some special nonlinear functions for which it is feasible or for which a closed form expression exists. For example, it is possible to determine the moments $E[z^n]$ ($n \in \mathbb{N}$) with moderate computational effort. An even simpler solution can be obtained for the exponential moment $E[e^z]$. The problem might therefore be solved by replacing the Q-function in Equation (3.85) with another nonlinear function for which the expectation can be determined. The method described here approximates the Q-function by a product of exponentials in z.

It follows from Equation (3.84) that $Q(f_0 - z)$ has to be approximated accurately only in the interval in which $p_z(z)$ is supported, i.e. only for $-D \le z \le D$, where $D \triangleq \sum_{k=1}^{\infty}(L_k - 1)|f_k|$ denotes the peak distortion of the interference. One may, for example, approximate $Q(f_0 - z)$ reasonably well within the whole region of support (ROS) $|z| \le D$ (Legendre polynomial, Chebyshev polynomial, Fourier series). Another possibility is to use a locally optimal approximation around a point z_0 such that the approximation error vanishes for $z = z_0$ and grows with increasing distance from z (Taylor series). At first sight, a close approximation of $Q(f_0 - z)$ within the whole ROS seem to be preferable. However, a locally optimal approximation may yield superior results in this case since the point of development, $z = z_0$, may be

chosen favorably. Note in this context that $p_z(z)$ is even symmetrical around $z = 0$ and decreases, on average, strongly with increasing distance from the origin. On the other hand, $Q(f_0 - z)$ increases strongly between $z = 0$ and $z \lesssim f_0$. Assume that the eye is open ($D < f_0$) and that the product $Q(f_0 - z) \, p_z(z)$ is maximal at or close to $z = z_0$. It can then be shown that, with growing distance from $z = z_0$ into either direction, the decreasing function will dominate over the increasing one such that the product $Q(f_0 - z) \, p_z(z)$ vanishes eventually. This behavior suggests to perform a locally optimal approximation of $Q(f_0 - z)$ around z_0 since these values contribute by far the most towards the integral (3.84). Conversely, less accuracy is necessary with growing distance from z_0 provided that the product of the approximation of $Q(f_0 - z)$ with $p_z(z)$ tends towards zero in this case. Thus, a locally optimal approximation of $Q(f_0 - z)$ using a Taylor series approach is considered here.

Exponential Product Form of $Q(x)$. The natural logarithm of the Q-function may be expanded into a Taylor series:

$$\ln Q(x) = \sum_{n=0}^{\infty} \frac{1}{n!} \left. \frac{d^n}{dx^n} \ln Q(x) \right|_{x=x_0} (x - x_0)^n \tag{3.86}$$

where $x_0 \in \mathbb{R}$ is arbitrary and $n!$ is the factorial of n (see Table A.3). Taking the exponent of the above equation yields

$$Q(x) = Q(x_0) \prod_{n=1}^{\infty} e^{c_n (x - x_0)^n} \tag{3.87}$$

where the coefficients c_n are given by

$$c_n = \frac{1}{n!} \left. \frac{d^n}{dx^n} \ln Q(x) \right|_{x=x_0}. \tag{3.88}$$

The product form of $Q(x)$ serves as the starting point for the first- and second-order approximations in Sections 3.4.2 and 3.4.3.

Exponential Moment of the Interference. The *exponential moment* $E[e^{\Lambda z}]$ of the interference random variable needs to be determined for later use. The param-

eter Λ is in general a complex number, which can be expressed in terms of its real and imaginary components:

$$\Lambda = \lambda + j\mu. \tag{3.89}$$

Substituting Definition (3.81) into the exponential moment and using the fact that the symbols d_k are mutually independent random variables for all $k \in \mathbb{N}$, we get

$$\begin{aligned}
E\left[e^{\Lambda z}\right] &= E\left[e^{\Lambda \sum_{k=1}^{\infty} d_k f_k}\right] \\
&= E\left[\prod_{k=1}^{\infty} e^{\Lambda d_k f_k}\right] \\
&= \prod_{k=1}^{\infty} E\left[e^{\Lambda d_k f_k}\right].
\end{aligned} \tag{3.90}$$

Since the data symbols d_k are uniformly distributed over the discrete set (3.82)), the individual exponential moment becomes

$$\begin{aligned}
E\left[e^{\Lambda d_k f_k}\right] &= \frac{1}{L_k} \sum_{i=0}^{L_k-1} e^{(2i-L_k+1)\Lambda f_k} \\
&= \frac{1}{L_k} e^{-(L_k-1)\Lambda f_k} \sum_{i=0}^{L_k-1} \left(e^{2\Lambda f_k}\right)^i \\
&= \frac{1}{L_k} e^{-(L_k-1)\Lambda f_k} \frac{\left(e^{2\Lambda f_k}\right)^{L_k} - 1}{e^{2\Lambda f_k} - 1} \\
&= \frac{1}{L_k} \frac{e^{L_k\Lambda f_k} - e^{-L_k\Lambda f_k}}{e^{\Lambda f_k} - e^{-\Lambda f_k}} \\
&= \frac{1}{L_k} \frac{\sinh\left(L_k\Lambda f_k\right)}{\sinh\left(\Lambda f_k\right)}.
\end{aligned} \tag{3.91}$$

Alternatively, the individual exponential moment can be bounded from above. Saltzberg [103] has found an upper bound on the sum of hyperbolic cosines:

$$\frac{2}{L_k} \sum_{i=1}^{L_k/2} \cosh[(2i-1)\lambda f_k] < \exp\left(\frac{1}{2}\rho(L_k)\lambda^2 f_k^2\right) \tag{3.92}$$

where $\lambda \in \mathbb{R}$ and the function $\rho(L)$ is defined in Equation (3.59). Note that $\rho(L_k)$

is the variance of the random data symbol d_k. Using Saltzberg's approximation, an upper bound for the absolute value of the individual exponential moment is given by

$$
\begin{aligned}
\left| E\left[e^{\Lambda d_k f_k} \right] \right| &= \left| \frac{1}{L_k} \sum_{i=0}^{L_k-1} e^{(2i-L_k+1)\Lambda f_k} \right| \\
&= \frac{1}{L_k} \left| \sum_{i=0}^{L_k-1} e^{(2i-L_k+1)\lambda f_k}\, e^{j(2i-L_k+1)\mu f_k} \right| \\
&\leq \frac{1}{L_k} \sum_{i=0}^{L_k-1} e^{(2i-L_k+1)\lambda f_k} \\
&= \frac{2}{L_k} \sum_{i=1}^{L_k/2} \cosh[(2i-1)\lambda f_k] \\
&< \exp\left(\frac{1}{2} \rho(L_k)\lambda^2 f_k^2 \right).
\end{aligned}
\tag{3.93}
$$

3.4.2 First-Order Approximation

For the remainder of this section, only the term $n = 1$ in the product of Equation (3.87) is kept while all other terms are neglected. It can be shown, [72], that this first-order approximation is a strict upper bound for the Q-function, i.e.

$$
Q(x) \leq Q(x_0)\, e^{c_1(x-x_0)}.
\tag{3.94}
$$

Setting $x = f_0 - z$, $x_0 = f_0 - z_0$, $c_1 = -\lambda$ and substituting the above expression into Equation (3.85) yields the probability

$$
P_{\mathrm{ex}} < Q(f_0 - z_0)\, e^{-\lambda z_0}\, E\left[e^{\lambda z} \right]
\tag{3.95}
$$

where

$$
\lambda \triangleq -\frac{Q'(f_0 - z_0)}{Q(f_0 - z_0)}
\tag{3.96}
$$

and $Q'(f_0 - z_0)$ is the first derivative of $Q(x)$ evaluated at the point $x = f_0 - z_0$. z_0 is a parameter that can be chosen arbitrarily. It will be determined later such that

the tightest bound is obtained.

Equation (3.95) contains the exponential moment of the interference. It can be expressed as product of the individual exponential moments, as shown in Equation (3.90). An exact expression for the individual moments has been derived in Equation (3.91). Generally, this relationship may be used for all interference components. In some cases, however, the number of interference components is large, and the computational effort required when considering all of them may be rather high. It is often found that only a few components are large in magnitude while the remaining components f_k are very small. A popular approach is to use only the strong interference samples and neglect all weaker ones (truncated pulse train approximation). This may lead, however, to optimistic results since the neglected samples can indeed contribute considerably to the overall error probability. Even if their individual magnitude is small, the combined energy of the neglected components may be significant. This problem can be solved by upper bounding the contribution from the small interference samples. A good choice is Saltzberg's approximation (3.93), which is rather loose if the exponent $\lambda d_k f_k$ is large. However, the smaller the magnitude of the exponent becomes, the tighter the bound will be. For the required task of bounding small components f_k, it turns out to be an excellent approximation. Therefore, the set of interference samples will be divided into two groups: One with relatively large magnitudes and the other with small ones.

The reason for reorganizing the interference sequence in nonincreasing order (Transformation (3.76)) becomes now obvious. Consider that there are M large interference terms f_k ($k \in \mathcal{I}_M$). For these terms, the exact expression for the individual exponential moment (3.91) will be used. The remaining interference contributions are assumed to be sufficiently small such that their individual exponential moments are very well approximated by the bound in Equation (3.93). Following Equation (3.90), the exponential moment of the interference may be upper bounded by

$$
E\left[e^{\lambda z}\right] < \exp\left(\frac{1}{2}\mathcal{E}_{z,M}\lambda^2\right) \prod_{k=1}^{M} \frac{1}{L_k} \frac{\sinh\left(L_k\lambda f_k\right)}{\sinh\left(\lambda f_k\right)} \tag{3.97}
$$

where $\mathcal{E}_{z,M}$ is the combined energy of the small interference components:

$$\mathcal{E}_{z,M} \triangleq \sum_{k=M+1}^{\infty} \rho(L_k) f_k^2. \tag{3.98}$$

Substituting Equation (3.97) into (3.95) results in the *general first-order upper bound* $P_{\text{ex}} < F_1(z_0)$, where

$$F_1(z_0) \triangleq Q(f_0 - z_0) \exp\left(\frac{1}{2}\mathcal{E}_{z,M}\lambda^2 - \lambda z_0\right) \prod_{k=1}^{M} \frac{1}{L_k} \frac{\sinh\left(L_k \lambda f_k\right)}{\sinh\left(\lambda f_k\right)}. \tag{3.99}$$

Note that this bound is valid for all values $z_0 \in \mathbb{R}$.

Tightest Upper Bound   The tightest bound is obtained by minimizing the upper bound $F_1(z_0)$ with respect to z_0. It is shown in Appendix F that the first derivative of $F_1(z_0)$ is given by

$$\frac{dF_1(z_0)}{dz_0} = F_1(z_0) \frac{d\lambda}{dz_0} g(z_0) \tag{3.100}$$

where $g(z_0)$ is defined as

$$g(z_0) \triangleq \mathcal{E}_{z,M}\lambda - z_0 + \sum_{k=1}^{M} f_k \left[L_k \coth(L_k \lambda f_k) - \coth(\lambda f_k)\right]. \tag{3.101}$$

Lemma 3.1 (a) *The function $F_1(z_0)$ is always positive, i.e.*

$$F_1(z_0) > 0, \quad \forall z_0 \in \mathbb{R}. \tag{3.102}$$

(b) λ *is always positive, i.e.*

$$\lambda > 0, \quad \forall z_0 \in \mathbb{R}. \tag{3.103}$$

(c) *The derivative $d\lambda/dz_0$ is always negative, i.e.*

$$\frac{d\lambda}{dz_0} < 0, \qquad \forall z_0 \in \mathbb{R}. \tag{3.104}$$

(d) *$g(z_0)$ is a strictly monotonically decreasing function in z_0, i.e.*

$$g(z_0 + \delta z_0) < g(z_0), \qquad \forall \delta z_0 > 0, z_0 \in \mathbb{R}. \tag{3.105}$$

(e) *$g(z_0)$ has exactly one root $\bar{z}_0$, i.e.*

$$g(z_0) = 0, \qquad \text{if and only if } z_0 = \bar{z}_0. \tag{3.106}$$

Proof. See Appendix F.

∎

By applying the results of Lemma 3.1 to Equation (3.100), it follows that $dF_1(z_0)/dz_0 = 0$ if and only if $z_0 = \bar{z}_0$. Moreover, it is obvious that $dF_1(z_0)/dz_0 < 0$ for $z_0 < \bar{z}_0$ and $dF_1(z_0)/dz_0 > 0$ for $z_0 > \bar{z}_0$. Thus, the global minimum of the function $F_1(z_0)$ is located at the point $z_0 = \bar{z}_0$. $\bar{z}_0$ is the solution of the transcendental equation $g(\bar{z}_0) = 0$. The final result is stated in the following theorem.

Theorem 3.1 *The tightest first-order upper bound for the threshold probability is*

$$P_{ex} < Q(f_0 - \bar{z}_0) \exp\left(\frac{1}{2}\mathcal{E}_{z,M}\bar{\lambda}^2 - \bar{\lambda}\bar{z}_0\right) \prod_{k=1}^{M} \frac{1}{L_k} \frac{\sinh\left(L_k\bar{\lambda}f_k\right)}{\sinh\left(\bar{\lambda}f_k\right)} \tag{3.107}$$

where the optimal parameters $\bar{\lambda}$ and $\bar{z}_0$ satisfy the conditions

$$\bar{\lambda} = -\frac{Q'(f_0 - \bar{z}_0)}{Q(f_0 - \bar{z}_0)} \tag{3.108}$$

$$\bar{z}_0 = \mathcal{E}_{z,M}\bar{\lambda} + \sum_{k=1}^{M} f_k \left[L_k \coth(L_k\bar{\lambda}f_k) - \coth(\bar{\lambda}f_k)\right]. \tag{3.109}$$

Numerical Determination of the Optimal Parameter The solution of $g(\bar{z}_0) = 0$ determines the optimal parameter $\bar{z}_0$. A closed form solution does not

exist because it is a transcendental equation. However, this does not pose a problem in practice since effective iterative algorithms are well known in order to find the solution for such expressions. One example is "Newton algorithm". In the particular case of the above equation, however, it was found that the algorithm diverges in certain extreme situations. In order to guarantee convergence, other well known methods can be applied. These algorithms enclose the solution between two values and narrow the region successively until the desired root is found with appropriate precision. The most efficient methods are those by Dowell and Jarratt [25, 26], Anderson and Björck [8] and King [59]. A very good description and comparison of these methods is presented in the book of Engeln-Müllges and Reutter [32].

3.4.2.1 Energy Upper Bound

The general first-order bound of Theorem 3.1 becomes tighter the more individual exponential moments are calculated by the exact expression in Equation (3.91), i.e. the larger the value of M is chosen. This requires, on the other hand, explicit knowledge of the interference weights f_k for all $k \in \mathcal{I}_M$, which may not be available in some situations. If only the respective energies of interference and Gaussian noise are known, the special case $M = 0$ could be considered. Under this condition, the upper bound of Theorem 3.1 reduces to

$$P_{\text{ex}} < Q(f_0 - \bar{z}_0) \, \exp\left(-\frac{\bar{z}_0^2}{2\mathcal{E}_{z,0}}\right) \tag{3.110}$$

where the optimal parameter $\bar{z}_0$ is the solution of the transcendental equation

$$\bar{z}_0 = \mathcal{E}_{z,0} \, \frac{Q'(f_0 - \bar{z}_0)}{Q(f_0 - \bar{z}_0)}. \tag{3.111}$$

Note that $\mathcal{E}_{z,0}$ is the variance of the normalized interference, i.e.

$$
\begin{aligned}
\mathcal{E}_{z,0} &= \sum_{k=1}^{\infty} \rho(L_k) f_k^2 \\
&= E\left[|z|^2\right] \\
&= \frac{1}{\mathcal{E}_\zeta} \sum_{\substack{i=-\infty \\ i \neq 0}}^{\infty} \mathcal{E}_{\alpha,i} h_i^2.
\end{aligned}
\tag{3.112}
$$

The last expression shows that $\mathcal{E}_{z,0}$ is equal to the *interference-to-noise ratio* (INR), i.e. the ratio of interference energy to Gaussian noise energy.

The numerical algorithms described in the previous section may be used to find the solution of Equation (3.111). These methods require starting values for the iteration. One can use for example $\bar{z}_{0,0} = 0$. Alternatively, an initial value may be obtained from the following observations. For high signal to interference and noise ratios, the argument $f_0 - \bar{z}_0$ is considerably larger than 1. Under this condition, the approximation in Equation (F.19) and (F.2) may be substituted into Equation (3.111). This yields

$$
\bar{z}_0 \gtrapprox \frac{\mathcal{E}_{z,0}}{\mathcal{E}_{z,0} + 1} f_0.
\tag{3.113}
$$

The value on the right hand side of the above equation turns out to be a good choice for the iteration start value $\bar{z}_{0,0}$ provided that the SINR is high.

3.4.2.2   Special Case: Binary Modulation

In the case of binary modulation there are only two modulation levels, i.e.

$$
\begin{aligned}
d_k &\in \{-1, 1\} \\
L_k &= 2
\end{aligned}
\quad \forall k \in \mathbb{N}_0.
\tag{3.114}
$$

Using the hyperbolic trigonometric relationships [5]

$$\sinh(2x) = 2\,\sinh(x)\,\cosh(x)$$

$$\cosh(2x) = \cosh^2(x) + \sinh^2(x), \quad \forall x \in \mathbb{C},$$

it can easily be shown that

$$\frac{1}{2}\frac{\sinh(2x)}{\sinh(x)} = \cosh(x) \tag{3.115}$$

$$2\,\coth(2x) - \coth(x) = \tanh(x). \tag{3.116}$$

These two expressions can be substituted into Equations (3.107) and (3.109). Provided that binary modulation is used, the tightest first-order bound for the threshold probability is given by

$$P_{\text{ex}} < Q(f_0 - \bar{z}_0)\,\exp\left(\frac{1}{2}\mathcal{E}_{z,M}\bar{\lambda}^2 - \bar{\lambda}\bar{z}_0\right)\prod_{k=1}^{M}\cosh(\bar{\lambda}f_k) \tag{3.117}$$

where the optimal parameters $\bar{\lambda}$ and $\bar{z}_0$ satisfy the conditions (3.108) and

$$\bar{z}_0 = \mathcal{E}_{z,M}\bar{\lambda} + \sum_{k=1}^{M} f_k\,\tanh(\bar{\lambda}f_k). \tag{3.118}$$

3.4.3 Second-Order Approximation

The product form of $Q(x)$ in Equation (3.87) shall now be truncated after the second term. This yields the approximation

$$Q(x) \approx Q(x_0)\,e^{c_1(x-x_0)}\,e^{c_2(x-x_0)^2} \tag{3.119}$$

where the parameters c_1 and c_2 are determined by Equation (3.88). The major problem with this expression is that a simple closed-form solution of the exponential interference moment $E[e^{z+z^2}]$ does not exist. This difficulty may be resolved by approximating the exponential e^{-x^2} with a more convenient expression. For example, the general form of e^{-x^2} is similar to the cosine function around $x = 0$. In particular,

the exponential may be upper bounded by

$$e^{-x^2} \leq \frac{1}{3} \left[2 + \cos(\sqrt{6}x) \right]$$
$$= \frac{2}{3} + \frac{1}{6} \exp(j\sqrt{6}x) + \frac{1}{6} \exp(-j\sqrt{6}x). \tag{3.120}$$

The parameters of the cosine function have been chosen such that the best approximation around $x = 0$ is obtained. Expanding both e^{-x^2} and the cosine function into a Taylor series, it appears that the first three non-zero terms are identical. The series become different only for sixth and higher orders in x.

The second-order approximation (3.119) and bound (3.120) are now used to determine the threshold probability P_{ex}. Using Equation (3.88) and the substitution $x_0 = f_0 - z_0$, the coefficients c_1 and c_2 are given by:

$$c_1 = \frac{d}{dx} \ln Q(x) \Big|_{x=x_0}$$
$$= \frac{Q'(f_0 - z_0)}{Q(f_0 - z_0)}$$
$$\stackrel{(3.96)}{=} -\lambda \tag{3.121}$$
$$c_2 = \frac{1}{2} \frac{d^2}{dx^2} \ln Q(x) \Big|_{x=x_0}$$
$$= \frac{1}{2} \frac{Q''(f_0 - z_0)}{Q(f_0 - z_0)} - \frac{1}{2} \left[\frac{Q'(f_0 - z_0)}{Q(f_0 - z_0)} \right]^2$$
$$\stackrel{(F.16)}{=} \frac{1}{2} \lambda(f_0 - z_0 - \lambda). \tag{3.122}$$

Note that $c_2 < 0$ since $\lambda > 0$ and $\lambda - f_0 + z_0 > 0$ according to Lemma 3.1(b) and Equation (F.21), respectively. This guarantees that the second-order exponential is of the form e^{-x^2} with a negative exponent. Substituting Equations (3.119) and (3.120) as well as the relationships $x = f_0 - z$, $x_0 = f_0 - z_0$, $\lambda = -c_1$ and $\mu = \sqrt{-6c_2}$ into (3.85) results in

$$P_{\text{ex}} \approx Q(f_0 - z_0) \left\{ \frac{2}{3} e^{-\lambda z_0} E\left[e^{\lambda z}\right] + \frac{1}{6} e^{-\Lambda z_0} E\left[e^{\Lambda z}\right] + \frac{1}{6} e^{-\Lambda^* z_0} E\left[e^{\Lambda^* z}\right] \right\} \tag{3.123}$$

where $\Lambda \triangleq \lambda + j\mu$ according to Equation (3.89). The quantity λ is defined by Equation (3.96), while μ is given by

$$
\begin{aligned}
\mu &\triangleq \sqrt{-6c_2} \\
&= \sqrt{3\lambda(\lambda - f_0 + z_0)}.
\end{aligned}
\tag{3.124}
$$

The exponential moments of the interference may be expressed as product of individual exponential exponents (3.90). Analog to Section 3.4.2, the exact expression for the individual exponential moment (3.91) is used for the interference samples with large magnitudes $f_k, \forall k \in \mathcal{I}_M$, while the small interference samples $(f_k, \forall k > M)$ are bounded by Expression (3.93). This results in the second-order approximation of the threshold probability:

$$
\begin{aligned}
P_{\text{ex}} \approx Q(f_0 - \bar{z}_0) \, \exp\left(\frac{1}{2}\,\mathcal{E}_{z,M}\bar{\lambda}^2\right) \Bigg\{ &\frac{2}{3}\, e^{-\bar{\lambda}\bar{z}_0} \prod_{k=1}^{M} \frac{1}{L_k} \frac{\sinh\left(L_k\bar{\lambda}f_k\right)}{\sinh\left(\bar{\lambda}f_k\right)} \\
&+ \frac{1}{6}\, e^{-\bar{\Lambda}\bar{z}_0} \prod_{k=1}^{M} \frac{1}{L_k} \frac{\sinh\left(L_k\bar{\Lambda}f_k\right)}{\sinh\left(\bar{\Lambda}f_k\right)} \\
&+ \frac{1}{6}\, e^{-\bar{\Lambda}^*\bar{z}_0} \prod_{k=1}^{M} \frac{1}{L_k} \frac{\sinh\left(L_k\bar{\Lambda}^*f_k\right)}{\sinh\left(\bar{\Lambda}^*f_k\right)} \Bigg\}.
\end{aligned}
\tag{3.125}
$$

In order to get a good approximation, the value $z_0 = \bar{z}_0$ has to be chosen carefully. It is known from the previous section that the best first-order bound is obtained when the parameter $\bar{z}_0$ satisfies condition (3.109). Obviously, the Taylor approximation (3.94) of $Q(f_0 - z)$ around this value leads to the best estimate of the error probability when it is substituted into the expectation (3.85). It is therefore reasonable to assume that the same point of development will also provide a good result for the second-order approximation because it is based on the same Taylor series expansion. Furthermore, the second-order product representation is a better approximation of $Q(x)$ than the first-order expansion (3.94). Thus, using the same value for $\bar{z}_0$ in expression (3.125) will yield a better estimation of P_{ex} than the respective first-order formula (3.107). Consequently, the same optimization criterion is used as in the first-order case, and the parameters $\bar{\lambda}$ and $\bar{z}_0$ are chosen such that they satisfy the conditions (3.108) and

(3.109), respectively. The parameter $\bar{\Lambda}$ is then obtained through

$$\bar{\Lambda} = \bar{\lambda} + j\bar{\mu} \tag{3.126}$$

$$\bar{\mu} = \sqrt{3\bar{\lambda}(\bar{\lambda} - f_0 + \bar{z}_0)}. \tag{3.127}$$

3.4.3.1 Special Case: Binary Modulation

For binary modulation, $L_k = 2 \ \forall k \in \mathbb{N}_0$. The relation (3.115) may be substituted into Equation (3.125) and the second-order approximation turns out to be

$$
\begin{aligned}
P_{\text{ex}} \approx & Q(f_0 - \bar{z}_0) \, \exp\left(\frac{1}{2}\,\mathcal{E}_{z,M}\,\bar{\lambda}^2\right) \left\{ \frac{2}{3}\, e^{-\bar{\lambda}\bar{z}_0} \prod_{k=1}^{M} \cosh(\bar{\lambda} f_k) \right. \\
& \left. + \frac{1}{6}\, e^{-\bar{\Lambda}\bar{z}_0} \prod_{k=1}^{M} \frac{1}{L_k} \cosh(\bar{\Lambda} f_k) + \frac{1}{6}\, e^{-\bar{\Lambda}^* \bar{z}_0} \prod_{k=1}^{M} \frac{1}{L_k} \cosh(\bar{\Lambda}^* f_k) \right\}
\end{aligned} \tag{3.128}
$$

where $\bar{\Lambda} = \bar{\lambda} + j\bar{\mu}$. The parameters $\bar{\lambda}$ and $\bar{\mu}$ have to be determined by finding the solution $\bar{z}_0$ of the transcendental Equation (3.118) and substituting it into the expressions (3.108) and (3.127).

3.5 Numerical Results and Comparison

This section is dedicated to the performance evaluation of the first- and second-order error approximations derived previously. In addition, their performance is compared to that of the following standard approximations:

- Gaussian approximation,

- Saltzberg energy upper bound,

- Prabhu's upper bound [96], and

- Yue's approximation [135].

In the Gaussian approximation, the interference is replaced by Gaussian noise with the same energy. This leads readily to the following approximation of the threshold

probability P_{ex}

$$\tilde{P}_{\text{Gauss}} = Q\left(\sqrt{\frac{\Phi}{\rho(L_0)}}\right) \tag{3.129}$$

where $\rho(L_0)$ is defined in Equation (3.59) and the signal-to-interference-and-noise ratio (SINR) Φ is given by

$$\Phi = \frac{\rho(L_0) f_0^2}{\mathcal{E}_{z,0} + 1}. \tag{3.130}$$

Note that the interference samples $f_k, \forall k \in \mathbb{N}_0$ are normalized by the standard deviation of the (unnormalized) Gaussian noise ζ_0 (Equation (3.76)) and the normalized Gaussian noise $\bar{\zeta}_0$ has unit variance.

A bound is usually preferred to an approximation because it provides a best or worst case estimate. The Saltzberg upper energy bound requires, as the Gaussian approximation, only information about the SINR at the input to the decision device. According to Section 3.3, the threshold probability is upper bounded by

$$\tilde{P}_{\text{Saltz}} = \exp\left\{-\frac{\Phi}{2\rho(L_0)}\right\}. \tag{3.131}$$

It can easily be shown that the Saltzberg energy bound is always larger than the Gaussian approximation.

Compared to the above energy approximations, the estimates of Prabhu [96] and Yue [135] require considerably more information. In particular, it is necessary to explicitly know the values of the interference samples $h_i, \forall i \in \mathbb{Z}$ and the Gaussian noise variance $\mathcal{E}_\zeta$ (or, alternatively, the normalized interference samples $f_k, \forall k \in \mathbb{N}_0$). Both estimates also require a substantial higher number of computations. This is due to the two main steps in the algorithms: firstly, the solution of a one-dimensional transcendental equation has to be determined; secondly, an exponential moment or a comparable quantity needs to be computed via a series expression, involving the repeated application of logarithm and hyperbolic trigonometric functions.

In terms of necessary information and computational complexity, the first-order energy upper bound of Section 3.4.2.1 can be compared to the Gaussian and Saltzberg approximations. In addition to the SINR, knowledge of the interference-to-noise ratio (INR) $\mathcal{E}_{z,0}$ is explicitly needed, i.e. it is necessary to know how the distortion energy is distributed between interference and Gaussian noise. The first-order energy bound is also computationally more complex since the solution of the transcendental Equation (3.111) has to be determined. However, it requires significantly less computations than the algorithms of Prabhu, Yue and the exact first- and second-order bounds because the transcendental equation has a simpler form and no exponential moments have to be calculated.

As the methods of Prabhu and Yue, the exact first- and second-order approximations described in Sections 3.4.2 and 3.4.3 require the knowledge of all interference samples $h_i\,(f_k)$ as well as the variance of the Gaussian noise. They are also comparable to Prabhu's and Yue's estimates in terms of computational complexity. All of those algorithms need to calculate the solution of a transcendental equation of comparable complexity. Furthermore, the first-order bound has to calculate one exponential moment. Hence, it is computationally as complex as Prabhu's algorithm. The second-order bound requires an additional complex exponential moment, which makes it slightly less efficient than the former bounds and comparable to Yue's approximation. In practice, certain properties of the series expression in Yue's algorithm may be exploited to reduce the number of computations. This places it in terms of computational efficiency between the exact first- and second-order approximations. On a larger scale, the computational complexity of all four algorithms is approximately the same.

The performance of the above approximations is evaluated using the *relative error* between the value $\tilde{P}_{\mathrm{ex}}$ obtained from the approximation and the exact threshold probability P_{ex}:

$$\varepsilon \triangleq \frac{\tilde{P}_{\mathrm{ex}} - P_{\mathrm{ex}}}{\min\left\{\tilde{P}_{\mathrm{ex}}; P_{\mathrm{ex}}\right\}}. \tag{3.132}$$

The "minimum" normalization in this definition ensures that too large and too small approximations are weighted equally. Consider for example $P_{\mathrm{ex}} = 10^{-6}$, $\tilde{P}_{\mathrm{ex},s} = 10^{-9}$ and $\tilde{P}_{\mathrm{ex},l} = 10^{-3}$. Both approximations are inaccurate by the same factor 1000. The relative errors according to Equation (3.132) are $\varepsilon_s = -999$ and $\varepsilon_l = 999$, respectively.

Since the calculation of the exact threshold probability according to the exhaustive evaluation of all possible information sequences becomes unpractical for a moderate and large number of interference samples, a reference algorithm is used to provide a very good approximation of P_{ex}. The method of Helstrom [47] has been chosen for this purpose. This algorithm approximates a Laplace inversion integral along a contour in the complex plane via numerical quadrature. By successively extending the numerical integration limits and narrowing the step size, the exact threshold probability P_{ex} can be calculated with arbitrary accuracy. For given integration limits, an upper bound of the relative error can be determined if the noise ζ_0 is Gaussian distributed. This allows to reduce the relative error due to truncation of the integration range below a preselected accuracy. Additionally, the numerical integration step size may be reduced until the desired accuracy is achieved. For the following results, the relative error of P_{ex} obtained by Helstrom's algorithm was forced to be below 10^{-10}. Obviously, the feature of preselecting an arbitrary accuracy is highly desirable. It comes, however, at the price of significantly increased computational complexity. For each interpolation point of the integral in the upper complex plane, one exponential moment has to be calculated. Depending on the desired accuracy, the interference and Gaussian noise characteristics, the number of exponential moments to be computed may be very large. Although extremely more efficient than the exhaustive method, Helstrom's algorithm requires distinctly more numerical calculations than the approximations mentioned above.

Three Standard Pulses   The threshold probability is determined by two factors: the signal-to-(Gaussian)-noise ratio (SNR) and the amplitude distribution of the interference at the input of the decision device. The latter depends on the received pulse waveform and on the sampling instant if a simple communications system without equalizer is considered.

A good error approximation algorithm provides accurate results for all possible parameter values (SNR, sampling instant) and pulse shapes. Therefore, the proposed approximations have to be tested for a broad range of parameters and different pulses. The most commonly used test waveforms have been adopted from the literature and include three pulse shapes: the *Gaussian pulse*, the *Chebyshev pulse* and the *ideal bandlimited pulse* (*sinc pulse*). These three waveforms cover to some extent the possible characteristics of interference, such as for example peak distortion, number of significant interferers or the amount of magnitude decay between adjacent interference samples. It is interesting to note that the performance evaluation of almost all approximation algorithms described in the literature relies at most on only the three mentioned waveforms. This seems, at first sight, to be not sufficient, however, good performance of a certain approximation algorithm for all of the three pulses is a strong indicator that it will perform well for other waveforms. This section investigates the performance of the different algorithms for all three pulses mentioned and for a broad range of SNR's and sampling instants.

Consider a certain pulse waveform $h(t)$. The interference samples $h_i, \forall i \in \mathbb{Z}$ (Equation (3.75)) are then obtained by sampling the pulse at the times $t = t_0 + iT$, which yields $h_i = h(t_0 + iT)$, where T is the symbol period. It is, for practical reasons, desirable to restrict the number of non-zero interference samples to a finite number (for example, computer simulations require that the amount of data be finite). Thus, a finite set of N_h interference samples is chosen according to the rule

$$
h_i = \begin{cases} h(t_0 + iT), & -\lceil N_h/2 \rceil \leq i \leq \lceil N_h/2 \rceil \\ 0, & i < -\lceil N_h/2 \rceil \text{ or } i > \lceil N_h/2 \rceil \end{cases} \tag{3.133}
$$

where $i \in \mathbb{Z}$ and $\lceil x \rceil$ is the smallest integer larger than or equal to x (Table A.3). t_0/T is called the *sampling instant*. Ideally, one would like to realize an optimal sampling instant of $t_0/T = 0$. An increasing deviation from the ideal sampling instant causes usually an increase in the interference and a decrease in the received signal energy. Both factors lead to a deterioration of the system performance. The SNR defines in this section the ratio of the expected energy contained in the ideal reference sample

$\alpha_0 h(0)$ and the Gaussian noise energy. The SNR is then defined as [6]

$$\text{SNR} \triangleq \frac{\mathcal{E}_{\alpha,0} h^2(0)}{\mathcal{E}_\zeta} \tag{3.134}$$

where $\mathcal{E}_{\alpha,0}$ is the variance of the data symbol to be estimated (α_0).

The three pulse waveforms used for performance evaluation correspond to different characteristics of the interference. The Gaussian pulse is defined by the shape [67]

$$h(t) = \exp\left\{ -\left(\frac{8t}{5T}\right)^2 \right\}. \tag{3.135}$$

Two characteristics of this pulse shape are that the amplitude of consecutive interference samples is decaying very strongly and that interference will always be present, even if the sampling instant is ideal ($t_0/T = 0$). The first property ensures that there are only very few significant interference samples. The term 'peak distortion' defines the worst case or maximal possible amplitude value that the combined interference can assume. Generally, the peak distortion of the Gaussian pulse is relatively small even for larger sampling instant deviations.

The second waveform considered is the Chebyshev pulse [67]

$$h(t) = \sum_{i=1}^{2} A_i \cos\left(\omega_i \frac{|t|}{T} - \phi_i\right) \exp\left(-\beta_i \frac{|t|}{T}\right) \tag{3.136}$$

with

$$A_1 = 0.4032 \quad \omega_1 = 2.839 \quad \phi_1 = 0.7553 \quad \beta_1 = 0.4587$$
$$A_2 = 0.7163 \quad \omega_2 = 1.176 \quad \phi_2 = 0.1602 \quad \beta_2 = 1.107.$$

The interference samples of this pulse are decaying more slowly. Thus, there will be more interference samples with significant amplitude than for the Gaussian pulse.

---

[6]In other sections of this dissertation, the term 'SNR' refers to the received signal-to-noise ratio which is defined by the ratio of the total energy contained in the waveform $h(t)$ and power spectral density of the white Gaussian noise (N_0), i.e. $\text{SNR} \triangleq \mathcal{E}_{\alpha,0}/N_0 \int_{-\infty}^{\infty} |h(t)|^2 \, dt$. The definition of the SNR according to Equation (3.134) is used here in order to conform with the literature.

This causes a larger peak distortion for non-ideal sampling instants. Additionally, interference will be present for all sampling instants.

Finally, the ideal bandwidth limited pulse is considered. It has the shape of a sinc function:

$$h(t) = \frac{\sin(\pi t/T)}{\pi t/T}.$$ (3.137)

In this case, the interference samples decay relatively slowly since their amplitude is inversely proportional to the time t. There will be no interference if the sampling instant is ideal ($t_0/T = 0$). However, deviations from the ideal sampling instant cause a strong increase in interference. An interesting characteristic of this pulse is that the peak distortion will be infinitely large for any non-ideal sampling instant if an infinite number of interference samples is considered ($N_h \to \infty$).

Quantities Describing the Interference The above method to define interference uses three different parameters: SNR, sampling instant and pulse shape. These parameters are oriented towards practical situations occurring in basic communications systems. For more sophisticated receivers including, for example, equalizers, the sampling instant loses its significance and a more valuable parameter than the SNR at the receiver input is the SINR at the input to the decision device. Moreover, the 'parameter' signal shape is more of qualitative nature and cannot easily be quantified.

More meaningful and quantifiable parameters that are also intuitively applicable to sophisticated receivers are the *signal-to-interference-and-noise ratio* (SINR), the *interference-to-noise ratio* (INR) and the *relative peak distortion* (D). It should, however, be noted that these three parameters are not able to describe the interference completely. The SINR defines the ratio of expected signal energy available at the decision device input and the combined energy of interference and noise. For the signal defined in Equation (3.80), the SINR is given by the expression in Equation (3.130). Accordingly, the INR is defined by the ratio of interference energy to (Gaussian) noise energy at the input to the decision device. For the normalized signal[7], the INR is

---

[7]The normalized input signal to the decision device is $\tilde{\alpha}_0/\sqrt{\mathcal{E}_\zeta} = d_0 f_0 + \sum_{k=1}^{\infty} d_k f_k + \bar{\zeta}_0$, as defined
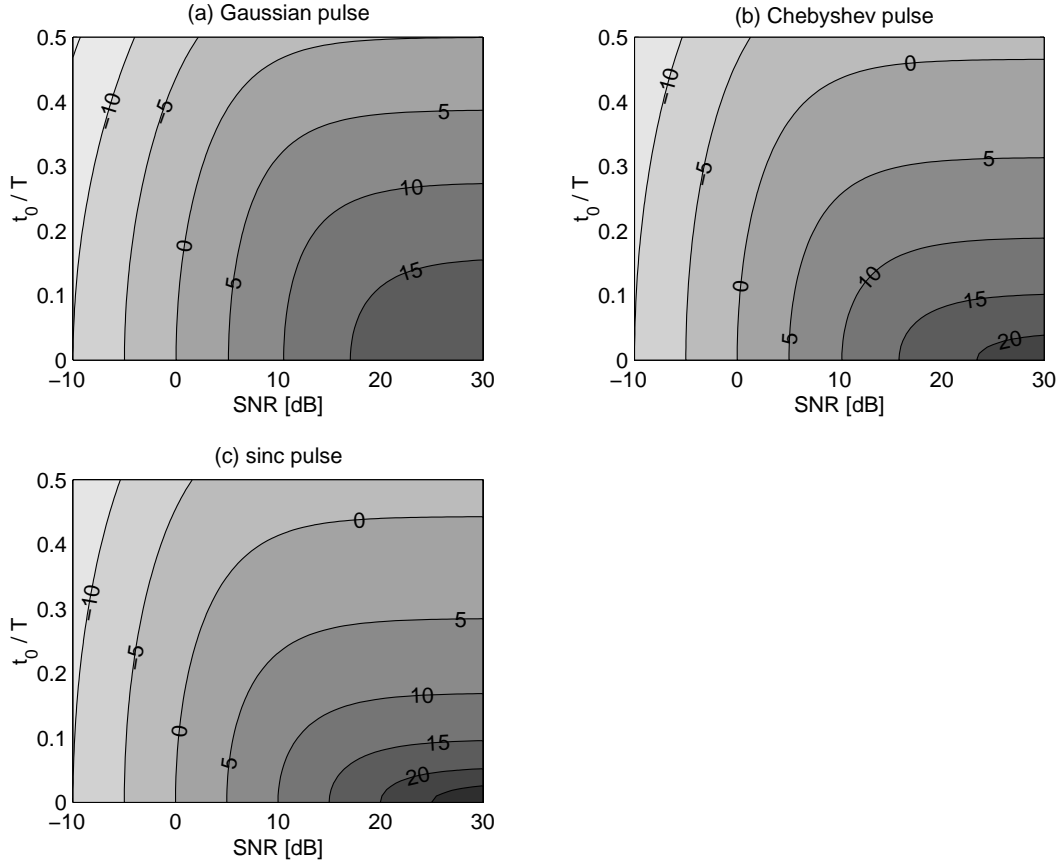
Figure 3.2: Contour plots of the SINR (in dB) versus SNR and the sampling instant t_0/T for (a) the Gaussian pulse, (b) the Chebyshev pulse, and (c) the ideal bandlimited pulse.

identical to the combined, expected energy $\mathcal{E}_{z,0}$ of all interference samples. Finally, the relative peak distortion is the peak distortion normalized by the magnitude of the signal sample, i.e. for the normalized signal

$$D = \frac{\sum_{k=1}^{\infty}(L_k - 1)|f_k|}{|f_0|}. \tag{3.138}$$

It indicates whether the 'eye' of the communications system is open $(D < 1)$ or closed $(D \geq 1)$.

The following graphs illustrate how the SINR, INR and normalized peak distortion

---

in Equation (3.80). The data symbols d_k are assumed to be amplitude modulated with an even number of L_k levels, each level being one of the odd integers $\pm 1, \pm 3, \ldots, \pm(L_k - 1)$ (Equation (3.82)). The slicing levels of the decision device are $0, \pm 2f_0, \pm 4f_0, \ldots, \pm(L_0 - 2)f_0$.

depend on the SNR and the sampling instant for the Gaussian, Chebyshev and sinc pulses for $N_h = 1000$ nonzero interference samples (Equation (3.133)). Figure 3.2 shows, for each pulse, a contour plot of the SINR. Each contour line represents a region of constant SINR, whose value in dB is printed on the line. For the Gaussian and Chebyshev pulses, it can be seen that the SINR is always lower than the SNR, even if $t_0/T = 0$. This is a direct consequence of the fact that, no matter what the sampling instant is, interference is always present. Note that the decline in SINR with increasing t_0/T is strongest for the sinc pulse, slightly less for the Chebyshev pulse, and weakest for the Gaussian pulse. Hence, the energy in the interference depends stronger on the sampling instant for the sinc and Chebyshev pulses than for the Gaussian pulse. Contour plots of INR versus SNR and t_0/T are shown in Figure 3.3.

The peak distortion is only a function of the sampling instant and independent on the SNR. The plot in Figure 3.4 shows this relationship for all three pulses. It is clear that D grows most strongly with increasing t_0/T for the sinc pulse. The dependency is in this case almost linear and the eye will become closed if t_0/T exceeds 0.07. D is least sensitive with respect to the sampling instant for the Gaussian pulse. This pulse has a closed eye for practically all values of the sampling instant.

Numerical Results The performance of the different approximation algorithms shall now be investigated. Results are obtained for the Gaussian, Chebyshev and ideal bandlimited pulses. The maximum number of non-zero interference pulses has been set to $N_h = 1000$ (Equation (3.133)). For simplicity, BPSK modulation ($L_k = 2, \forall k \in \mathbb{N}_0$) has been considered for the simulations. The SNR and sampling instant ranges have been chosen to cover a wide range including the cases of most practical interest, in particular -10 dB $\leq$ SNR ≤ 30 dB and $0 \leq t_0/T \leq 0.5$.

Helstrom's reference algorithm provides threshold probabilities P_{ex} with relative errors of less than 10^{-10}. The results of the other approximation algorithms, denoted $\tilde{P}_{\text{ex}}$ are then compared with the reference values by calculating the relative errors according to Equation (3.132). For all following contour plots, the convention is used that increasing levels of darkness correspond to larger values. The ratio between two
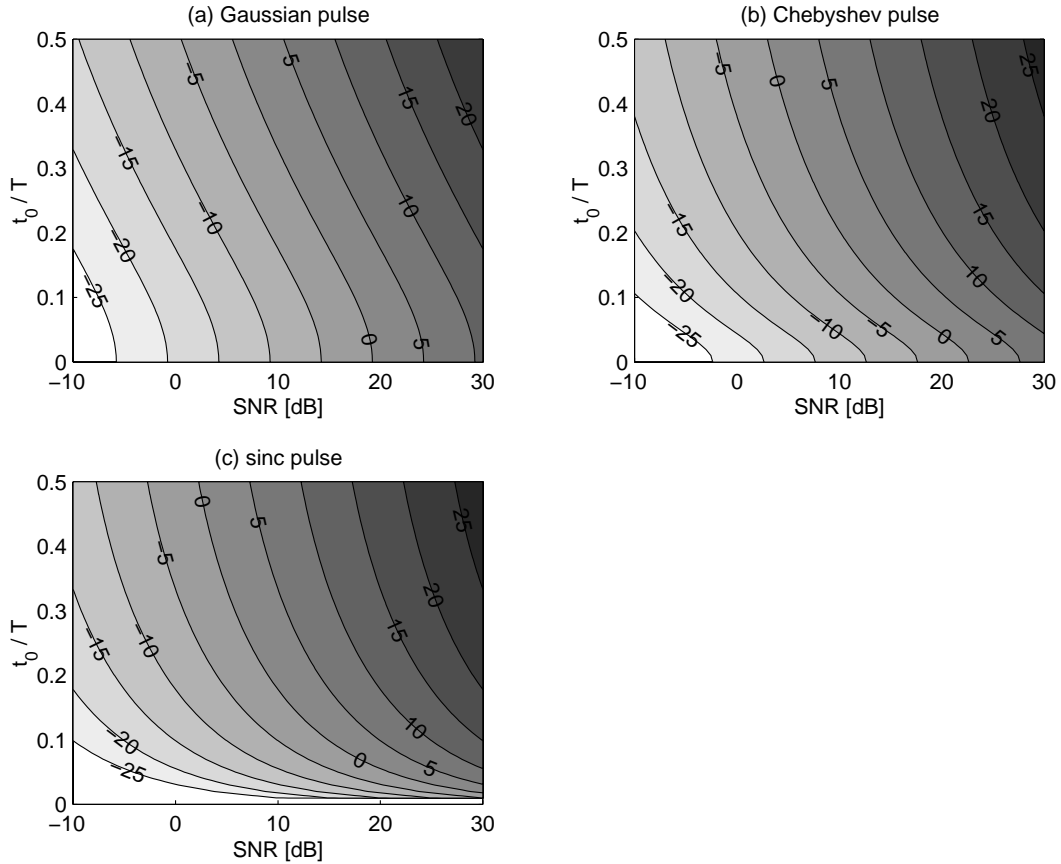
Figure 3.3: Contour plots of the INR (in dB) versus SNR and the sampling instant t_0/T for (a) the Gaussian pulse, (b) the Chebyshev pulse, and (c) the ideal bandlimited pulse.

consecutive contour lines is always a factor of ten. The values printed on the lines represent the logarithm of the respective value to the base 10, i.e. a contour line with the value '-2' shows the region of constant values $P_{\mathrm{ex}} = 10^{-2}$ or $|\varepsilon| = 10^{-2}$, respectively.

Figure 3.5 shows four contour plots for the Gaussian pulse. The first plot in the upper left corner represents the values of the exact threshold probability P_{ex}. The other three plots display, in clockwise order, the magnitude of the relative errors ($|\varepsilon|$) for the Gaussian approximation, the energy first-order bound and the Salzberg bound.

The threshold probability (Figure 3.5(a)) starts to decrease strongly when the SNR exceeds 10 dB. This is valid for a broad range of sampling instants. Only if t_0/T
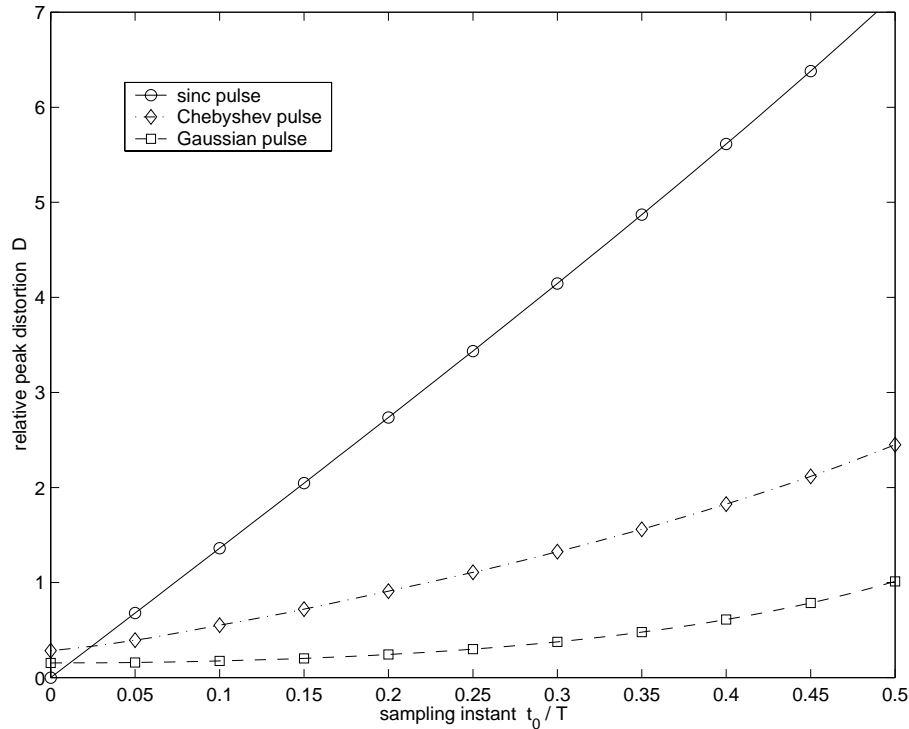
Figure 3.4: Relative peak distortion versus sampling instant for the sinc, Chebyshev and Gaussian pulses.

assumes large values greater than 0.35, the SNR needs to be increased significantly for low error probabilities.

The contour plots of the relative errors show that all three "energy" approximations perform unsatisfactorily when the exact threshold probability is very low, i.e. for high SNR's and $t_0/T < 0.45$. In this region, the estimates of the approximation algorithms are by several orders of magnitude too large, and the results are overly pessimistic.

Although providing poor results for high SNR's, the Gaussian approximation performs very well when the SNR is below 15 dB. This behavior can be anticipated since the Gaussian noise contributes more and more to the overall distortion energy when the SNR shrinks. As a result, the random variable consisting of interference and noise will have a probability distribution that increasingly resembles a Gaussian distribution.

The Saltzberg bound performs as badly as the Gaussian approximation for SNR's
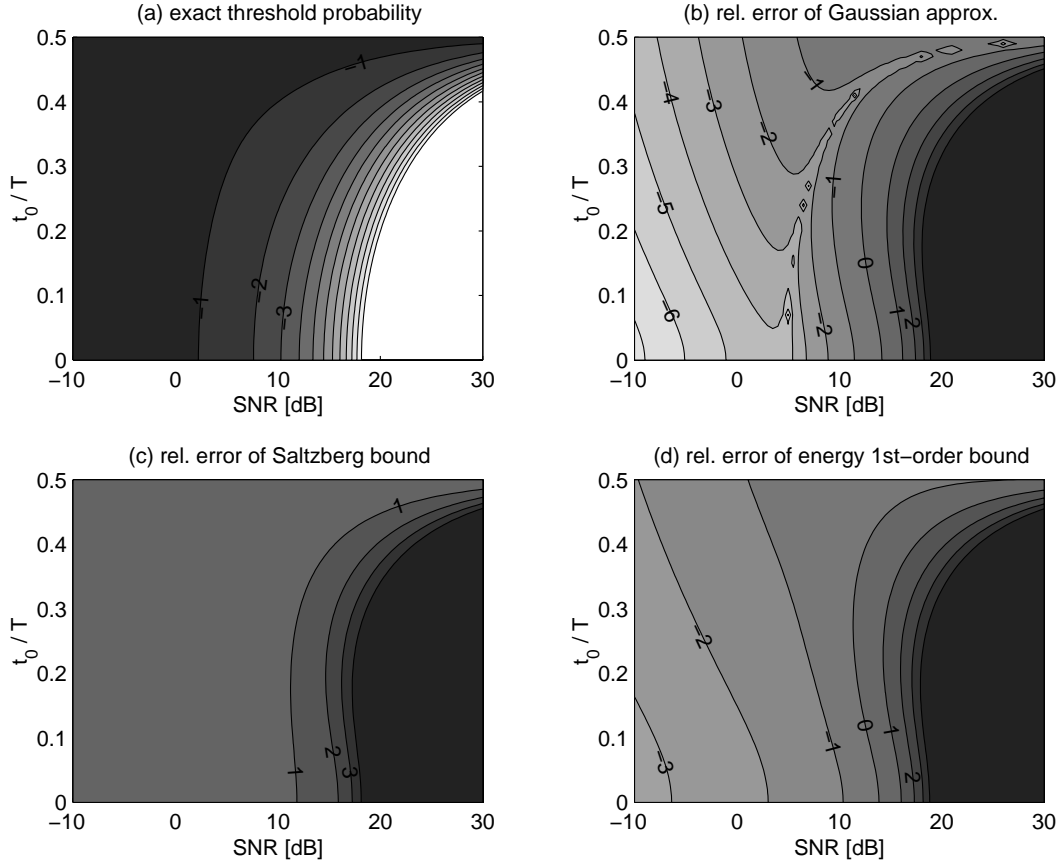
Figure 3.5: Contour plots for the Gaussian pulse showing (a) the exact threshold probability $\log_{10} P_{\text{ex}}$, and the relative errors $\log_{10} |\varepsilon|$ for (b) the Gaussian approximation, (c) the Saltzberg bound, and (d) the energy first-order bound.

larger than 18 dB. Unlike the latter, its results are also relatively poor for low SNR's. The relative error never fell below 100% for the SNR and sampling instant ranges shown in Figure 3.5(c). Depending on the individual situation, the results of the Saltzberg bound are between two times and many orders of magnitude too pessimistic.

The results of the energy first-order bound are comparable to those of the Gaussian approximation. While providing good estimates in the low SNR range, the algorithm performs poorly when the noise is low. Overall, the relative errors of the energy first-order bound are slightly larger than those of the Gaussian approximation.

Unlike the energy estimates, the algorithms of Prabhu, Yue and the exact first- and second-order approximations require explicit knowledge of all interference samples h_i (f_k). The relative errors of these methods obtained for the Gaussian pulse are shown in
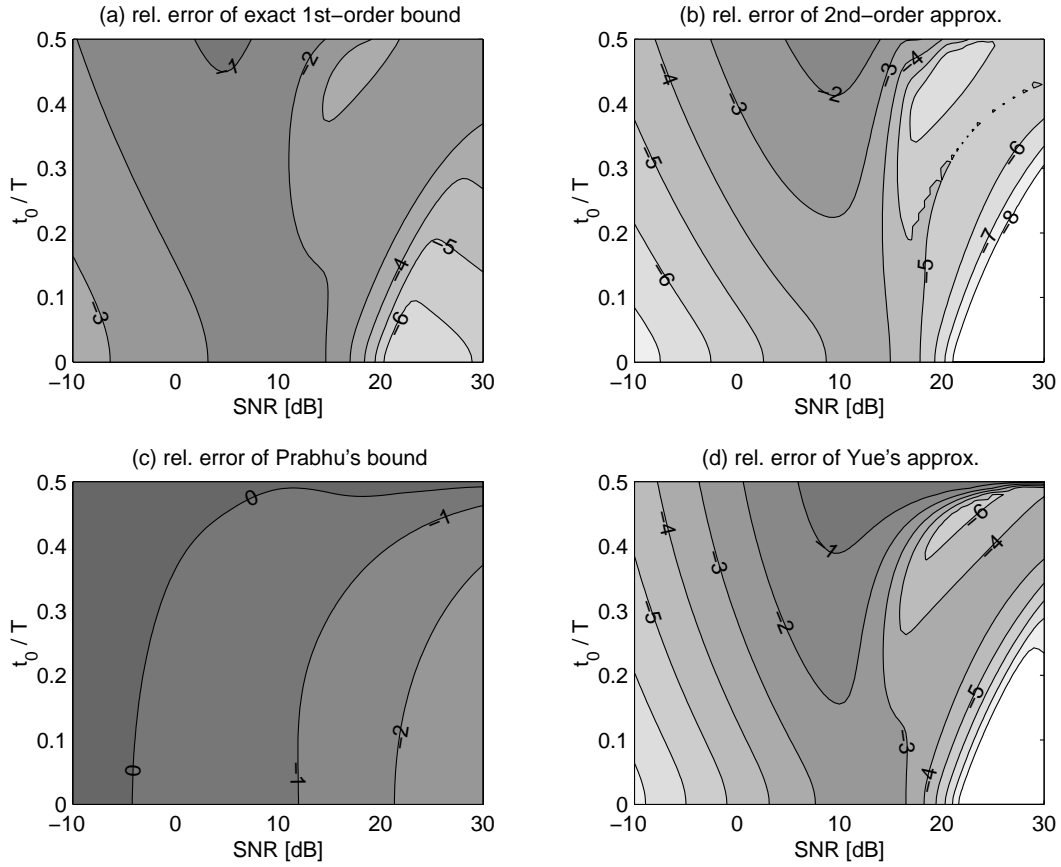
Figure 3.6: Contour plots for the Gaussian pulse showing the relative errors $\log_{10}|\varepsilon|$ for (a) the exact first-order bound, (b) the second-order approximation, (c) Prabhu's bound, and (d) Yue's approximation.

Figure 3.6. All four algorithms perform good to excellent for all values of the SNR and sampling instant considered here. Particularly for high SNR's and low to moderate sampling instants, i.e. in the region where the energy approximations completely fail, the more complex algorithms provide astonishingly small relative errors. Especially the second-order and Yue's approximation achieve practically error-free results in this area.

Of the four methods considered, Prabhu's bound performs worst. It produces comparatively high relative errors exceeding 100% in low SNR scenarios. However, the results become increasingly good for growing SNR's and smaller sampling instants. The other three algorithms provide generally very good results. The best performance is obtained with the second-order bound and Yue's method. The second-order bound
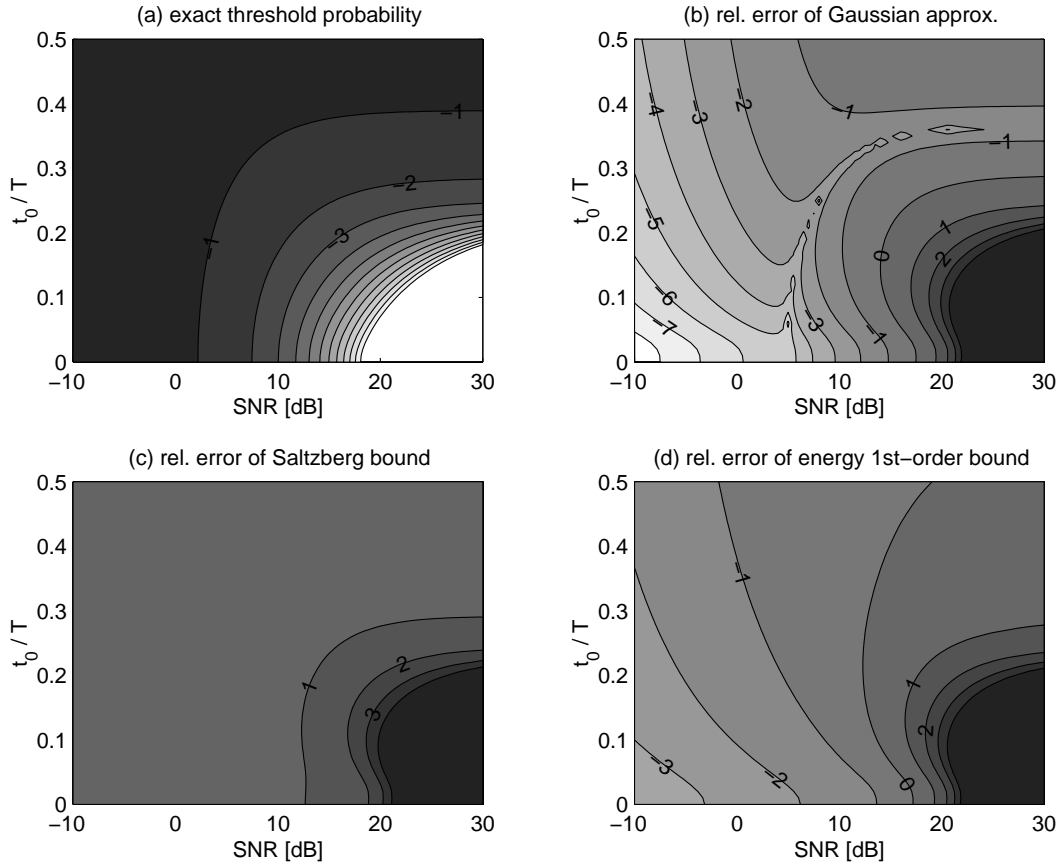
Figure 3.7: Contour plots for the Chebyshev pulse showing (a) the exact threshold probability $\log_{10} P_{\text{ex}}$, and the relative errors $\log_{10} |\varepsilon|$ for (b) the Gaussian approximation, (c) the Saltzberg bound, and (d) the energy first-order bound.

is slightly superior with relative errors always below 10%.

The next two Figures show the results for the Chebyshev pulse. Figure 3.7 displays contour plots of the exact threshold probability (a), and relative errors for the three energy bounds. The relative errors caused by the more complex methods are plotted in Figure 3.8.

An increase in the sampling instant has a stronger impact on the exact threshold probability for the Chebyshev pulse compared to the Gaussian pulse. In particular, the threshold probability becomes relatively high for sampling instants exceeding 0.25 even if the SNR is large.

The general performance of the energy approximations shows comparable behavior for both the Chebyshev and the Gaussian pulse. In the regions, where the exact
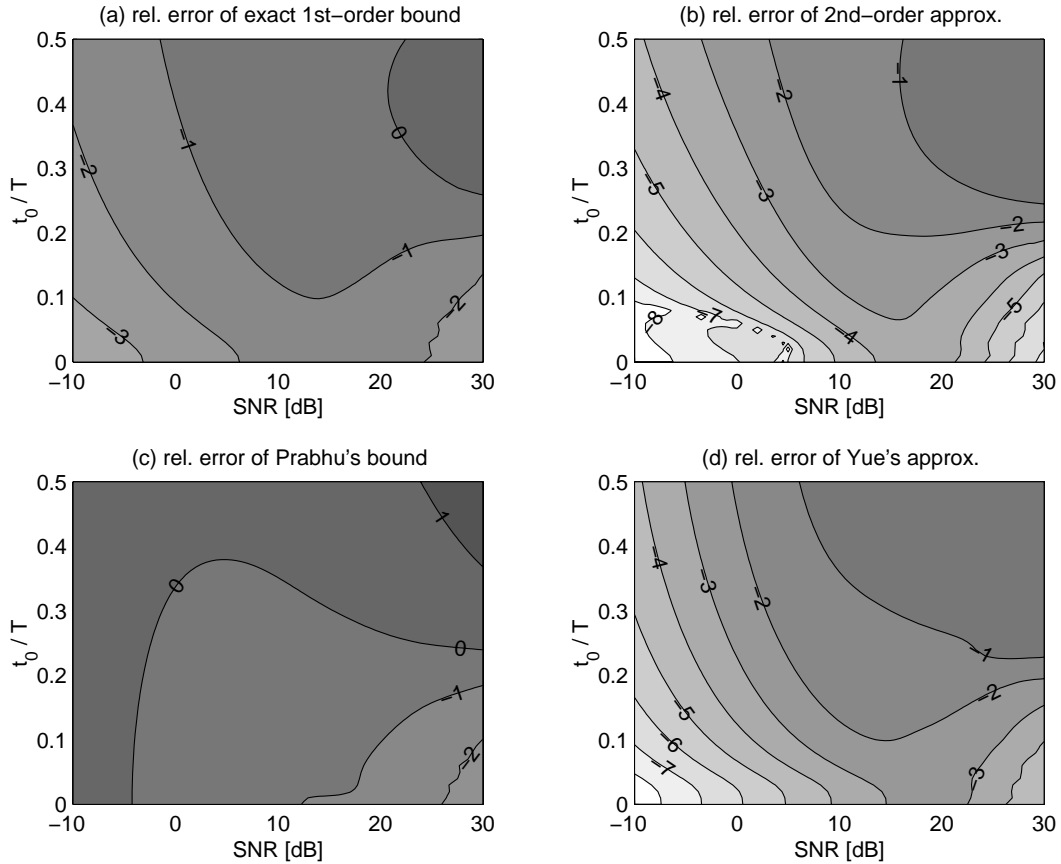
Figure 3.8: Contour plots for the Chebyshev pulse showing the relative errors $\log_{10}|\varepsilon|$ for (a) the exact first-order bound, (b) the second-order approximation, (c) Prabhu's bound, and (d) Yue's approximation.

threshold probability is low, the energy bounds fail to provide acceptable results. Depending on the required accuracy, the results of the Gaussian approximation and the energy first-order bound will be satisfactory to good if the SNR is below 15 dB. The Saltzberg energy bound may only be recommended if a 2 to 10 times too large estimate is acceptable and the SNR is moderate to small.

Although their results are worse compared the Gaussian pulse case, the more accurate methods also perform well for the Chebyshev pulse (Figure 3.8). Even in the most extreme situations of high SNR's and large sampling instants, the relative error never exceeded 100% for both the second-order and Yue's approximation. The results of the first-order and Prabhu's bound are worse, but still very good to acceptable in most regions.
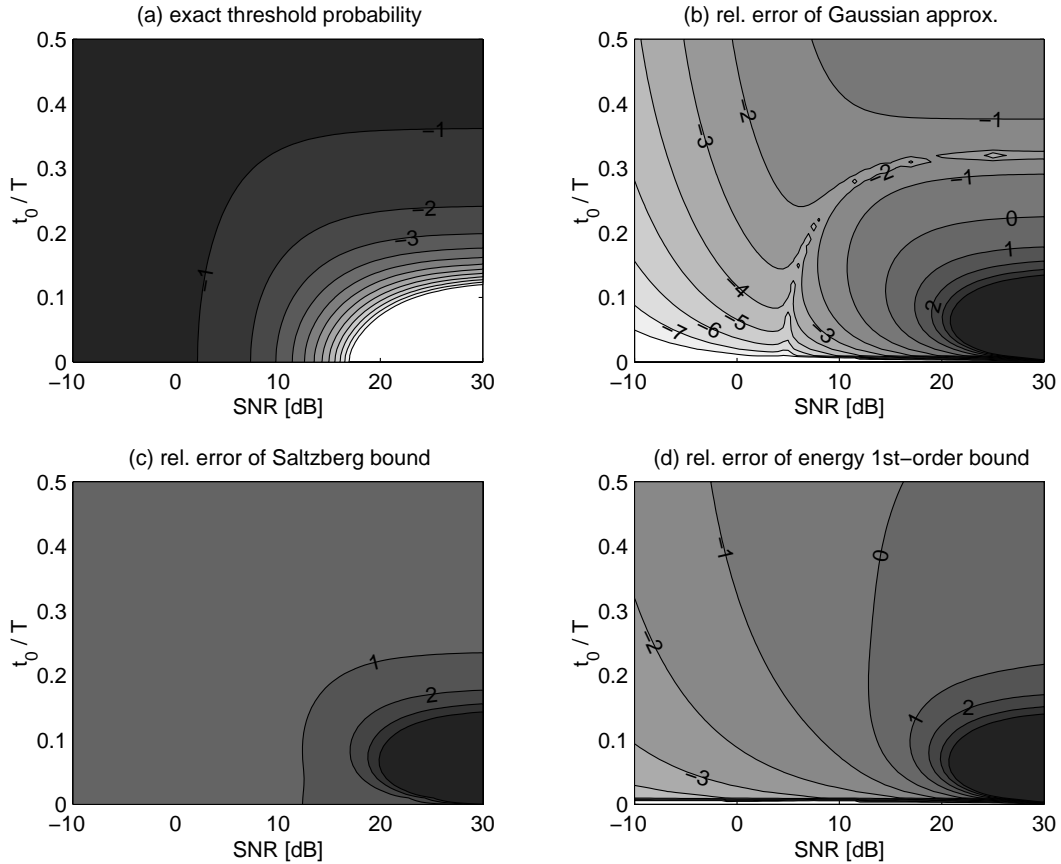
Figure 3.9: Contour plots for the sinc pulse showing (a) the exact threshold probability $\log_{10} P_{\mathrm{ex}}$, and the relative errors $\log_{10} |\varepsilon|$ for (b) the Gaussian approximation, (c) the Saltzberg bound, and (d) the energy first-order bound.

Finally, results for the ideal bandwidth limited pulse are shown in Figures 3.9 and 3.10. The sinc pulse is most sensitive to an increase in the sampling instant, resulting in a relatively large amount of interference and high peak distortion. In general, the qualitative results for the energy and more complex approximations are the same as for the Gaussian and Chebyshev pulses. The relative errors of Yue's algorithm are in this case slightly better than those of the second-order bound if the SNR's are high. These two methods outperform the other algorithms.

Summary   All three energy bounds produce large errors when the exact threshold probability is low, i.e. for high SNR's and small to moderate sampling instants. Considering the relative error, the Gaussian approximation yields the best results among
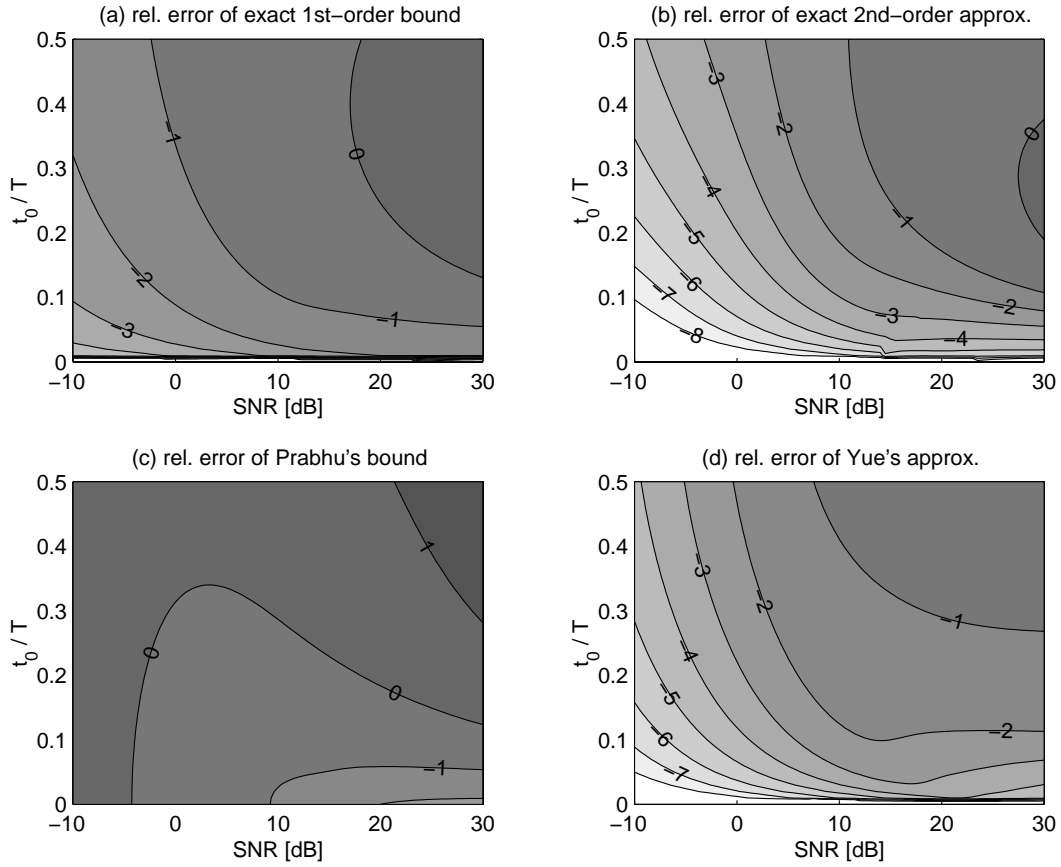
Figure 3.10: Contour plots for the sinc pulse showing the relative errors $\log_{10}|\varepsilon|$ for (a) the exact first-order bound, (b) the second-order approximation, (c) Prabhu's bound, and (d) Yue's approximation.

the energy based methods. A disadvantage is that its estimate is an approximation which can be larger or smaller than the exact threshold probability. The results of the energy first-order bound are slightly worse, however, they are always larger than the exact values (upper bound). It provides therefore a strict worst case approximation, which may be desirable for certain applications. The Saltzberg bound yielded the worst performance of the three energy approximations, deviating by at least two times from the exact value.

Despite their limited performance, there is no alternative to the energy approximations if information is available about only the energy of interference and noise. When an approximation to the threshold probability is sufficient and the SNR is below 15 dB, the Gaussian approximation can be recommended. If, on the other hand,

a worst case estimate is desirable, the energy first-order bound should be applied. In general, neither energy bound can be recommended in situations when the SNR is larger than 15 dB or when the threshold probability falls below 10^{-6}. In these cases, all investigated energy methods produce large errors. It seems that approximations solely based on the variance of noise and interference fail when the SNR becomes large. In this situation, more information about the interference appears to be necessary in order to obtain good estimates.

Whenever explicit knowledge about all interference samples is available, one of the more complex algorithms should be used. Especially the second-order and Yue's approximation provided excellent estimates for all SNR's and sampling instants. The results shown indicate that their performance should also be very good for other pulse shapes and interference distributions. If the number of computations is at a premium and accurate results are required, the first-order bound may be considered. Prabhu's algorithm is not recommended because it performed always worse then the first-order bound while requiring approximately the same amount of operations.

3.6   Conclusion

New strict and approximate upper bounds on the error probability have been introduced which are computationally efficient. The approximations include an arbitrary parameter that is optimized in order to achieve the tightest bound. The resulting exponential moments of the interference can be computed easily [96]. For the calculation of the approximations, it is simply required to find numerically the root of a transcendental equation and to evaluate exponential moments. An additional feature is that small interference components can be tightly upper bounded by an expression involving only their combined variance.

Terminating the Taylor series of $\ln Q(x)$ after the linear term results in the first-order upper bound. A special case of it, the energy upper bound, requires knowledge about only the variance (energy) of the interference and the variance of the Gaussian noise. This bound provides reasonable accuracy for low to moderate SNR's. However, its results are extremely pessimistic when the true error probability is very small

$(< 10^{-3})$.

The general first-order upper bound requires explicit knowledge about the strong interference samples. As a consequence, it provides significantly better results especially in situations where the energy bound fails. For the three pulses investigated (Gaussian, Chebyshev, sinc pulse) and an open eye, the relative errors between the first-order bound and the exact error probability did not exceed 20 %. This number increased to a maximum of 171 % when the eye was closed.

The second-order approximation considers in addition the quadratic term of the Taylor series and replaces the resulting factor e^{-x^2} with a cosine function. It is the most accurate albeit most complex of the derived algorithms. For the three pulses investigated here, the relative errors were always below 1 % (open eye) and 120 % (closed eye). Note that these values are the absolute worst case numbers that are highly pessimistic. The price to be paid for the high accuracy is an increased amount of necessary operations. Instead of none (energy bound) or one real exponential moment (first-order bound), it requires the evaluation of one real and one complex exponential moment. This is comparable to the complexity of Yue's approximation [135]. In addition, the proposed and Yue's method yield comparable accuracies. The difference is that Yue's results turn out to be below the true error probability in most cases while we derived strict and approximate upper bounds.

The presented bounds are significantly more efficient than the more accurate approximations of Helstrom [47] and Beaulieu [11]. Helstrom's algorithm, for example, performs the calculation of an inverse Laplace transformation by numerical quadrature and requires the evaluation of one complex exponential moment at each integration point. Depending on the system parameters and the desired accuracy, the number of necessary integration points can vary between ten and several hundred. Beaulieu's approximation has a similar degree of computational complexity.

Chapter 4

Equalizers for Spread Spectrum Multiuser Systems

4.1 Introduction

This chapter analyzes and discusses different multiple-input multiple-output (MIMO) equalizer structures that can be used for the joint detection of multiple signals. In addition, the effect of diversity and number of users on the performance is discussed and quantified for the considered equalizers when they are employed in a wireless multiuser system as described in Chapter 2.

The different types of MIMO equalizers analyzed include the linear equalizer (LE) and the decision-feedback equalizer (DFE), whose structure is considered in both the conventional (C-DFE) and the noise-predictive (NP-DFE) form. Considering stationary or quasi-stationary environments, the analysis, based on a MMSE or ZF criterion, may be carried out in either time- or frequency domain. Both approaches are described and compared with respect to the number of necessary operations to calculate the optimal equalizer filters[1].

A new frequency-domain formulation of the optimal MMSE LE is derived, which can be interpreted as a generalization of the *noncausal Wiener filter* [89]. This solu-

---

[1]Unless otherwise mentioned, the term "optimal" refers to "optimal with respect to the MMSE (or ZF) criterion".

tion does not require information about the communication channels or the system noise, which is necessary for the calculation of the well-known optimal LE structure in the frequency domain [57, 51, 27]. The only quantities required are relatively easy to determine or directly accessible.

Results and conclusions are obtained for the considered equalizer structures from numerous investigations concerning the dependency of the detector performance on the number of users, number of receive antennas and processing gain. Special attention is dedicated to a comparison between LE and DFE in terms of error probability, outage probability and capacity. A new lower bound on the average MMSE of the LE is derived. Finally, a formal proof is given that the direct relationship between SINR and MMSE for the single-input single-output LE and DFE also holds for both the MIMO LE and DFE. This enables the application of Foschini *et al.*'s [34] and Saltzberg's [103] upper error probability bound to MIMO equalizers.

Consider the system described in Chapter 2. The reverse link is investigated for a system with N users and a single base station. The base station receives the asynchronous signals at A different antennas. In addition to antenna diversity, frequency diversity is used by transmitting signals with larger than Nyquist bandwidth. The receiver consists of a multiple-input multiple-output (MIMO) linear (LE) or decision-feedback equalizer (DFE). The quasi-stationary, frequency selective radio channels between all users and the base station are assumed to be known at the receiver. This describes the reverse link of a spectrally efficient, high data rate multiuser system that combines the concepts of both frequency and antenna diversity in order to increase the capacity and enable the system to support several users simultaneously. Frequency diversity is introduced by spreading the bandwidth of all system users to K-times the Nyquist bandwidth. The multiple access scheme associated with this method is spread-spectrum multiple access (SSMA). Receiving the signals at A sufficiently spaced antennas provides antenna diversity.

Several different receiver types have been developed in the past to suppress the interfering signals and to allow for a reliable detection of all users. Among them are the conventional matched filter receiver, maximum likelihood (MLSE) detector [122], multistage detectors [120], successive and parallel interference cancelers [125, 50], and

equalizer/combiner structures [131, 27]. Considering the number of publications, the latter have proven to be highly attractive as they constitute an excellent compromise between low complexity, low performance detectors (conventional matched filter receiver) and high complexity, high performance receivers (MLSE detector). In addition, these receivers may offer a very high spectral efficiency, which is shown in subsequent sections.

In general, equalizers may be categorized according to the following criteria:

- Employment of past decisions. The *linear equalizer* (LE) utilizes no past decisons in the estimation process, while the *decision-feedback equalizer* (DFE) does.

- Feedback structure. This criterion applies only to DFE's and distinguishes between the *conventional DFE* and the *noise-predictive DFE* (NP-DFE).

- Optimization criterion: minimum mean-square error (MMSE) or zero-forcing (ZF).

- Optimization domain: frequency or time.

There are two main types of equalizers: the linear equalizer (LE) and the decision-feedback equalizer. The former structure performs only linear operations on the received signals *before* the decision device. In contrast, the DFE uses past decisions in order to estimate and cancel interference and possibly noise in the present data symbol. The use of former decisions, obtained through a nonlinear quantization operation, causes the input of the decision device to be a nonlinear estimate.

The conventional DFE uses former decisions directly as inputs to the feedback filter. Belfiore [13, 14] first described a feedback structure which calculates a sequence of estimation errors[2] by taking the difference between the decisions and the output of the forward filter. Some past estimation errors are used as inputs to a linear prediction filter which extrapolates and cancels the present estimation errors at the output of the forward filter.

---

[2]Under the assumption that all decisions are correct.

Most equalizers are optimized with respect to the minimum mean-square error (MMSE) criterion, which minimizes the combined energy of both interference and noise in the final, unquantized estimate. The main reason for this is two-fold: On one hand, the MMSE criterion leads to a tractable and relatively simple mathematical formulation, which may readily be solved. On the other hand, the mean-square error (MSE) is a good indicator of the system performance because it strongly influences the symbol error probability[3]. Additionally, the MMSE criterion lends itself to an adaptive implementation of the equalizer parameters (tap weights) and leads generally to a better performance than the zero-forcing (ZF) rule. The ZF criterion completely nulls out all interference components in the final, unquantized estimate. This causes, however, a more or less strong amplification of the Gaussian noise component such that the overall distortion energy in the estimate is always higher than that of an MMSE equalizer. Another disadvantage of the ZF rule is that it cannot as easily be implemented for adaptive equalizers. In terms of mathematical tractability, conceptional and computational complexity, both MMSE and ZF criteria are practically identical.

The error probability is hardly used as a criterion for equalizer optimization since it is extremely difficult, if not impossible [117], to determine the detector parameters which minimize the probability of error.

It is generally possible to describe the system and its signals in either time- or frequency-domain notation. Both approaches, which lead to different formulations of the optimal equalizers, are described in the following sections. The different equalizer formulations have advantages and disadvantages, which are discussed in more or less detail. Overall, the particular application and the system properties determine which solution is the better choice.

---

[3]In particular, it will be shown later in this chapter that a certain upper bound on the error probability (Saltzberg bound) is a strictly monotonically increasing function of the MSE. Minimizing the MSE therefore also minimizes this upper bound.
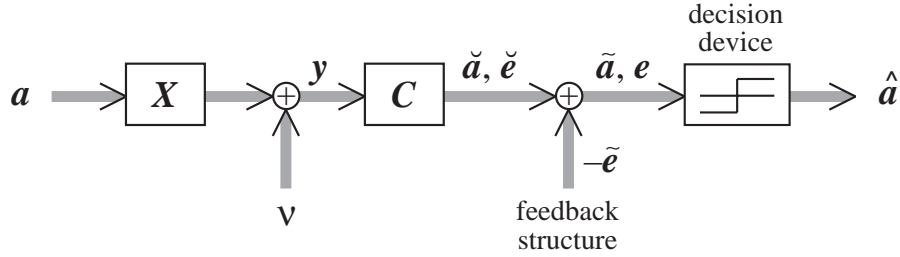
Figure 4.1: System including MIMO linear or decision-feedback equalizer.

4.1.1 General Notation and Mean-Square Error

The general notation and signal definition used throughout the current chapter will be introduced in the following paragraphs. Figure 4.1 shows the most general system structure which is suitable for both linear and decision-feedback MIMO equalizers. The signals and system blocks are described in Table 4.1.

The signals $\breve{e}$ and e describe the estimation error signals at the output of the forward filter and the input to the decision device, respectively:

$$\breve{e} \triangleq \breve{a} - a \tag{4.1}$$

$$e \triangleq \tilde{a} - a \tag{4.2}$$

where the k-th components of $\breve{e}$ and e shall be denoted by $\breve{e}_k$ and e_k, respectively:

$$e_k \triangleq [e]_k \tag{4.3}$$

$$\breve{e}_k \triangleq [\breve{e}]_k . \tag{4.4}$$

If a decision-feedback structure is used in the equalizer, the signal $\tilde{e}$ will represent an estimate of the error signal $\breve{e}$. The error estimate at time n, $\tilde{e}[n]$, is based on previous decisions $\hat{a}[m]$ for $m < n$. On the other hand, if the detector consists of a MIMO linear equalizer, there will be no error estimate from a feedback structure and therefore $\tilde{e}[n] = \mathbf{0}_N, \forall n \in \mathbb{Z}$, where $\mathbf{0}_N$ is the all zero row vector with N components (Table A.7).

The mean-square errors (MSE's) at the input to the decision device may be calculated in either the time- or the frequency-domain. Define the autocorrelation matrix

Table 4.1: Description of system blocks and signals.

Variable	Description	Form
$\boldsymbol{X}$	overall channel matrix	$N \times AK$ matrix filter
$\boldsymbol{C}$	forward filter of the MIMO equalizer	$AK \times N$ matrix filter
$\boldsymbol{a}$	transmitted data signal	$1 \times N$ row vector signal
$\boldsymbol{\nu}$	colored, correlated noise signal	$1 \times AK$ row vector signal
$\boldsymbol{y}$	input signal to the equalizer	$1 \times AK$ row vector signal
$\breve{\boldsymbol{a}}$	linear estimate at the output of the MIMO forward filter	$1 \times N$ row vector signal
$\breve{\boldsymbol{e}}$	estimation error at the output of the MIMO forward filter	$1 \times N$ row vector signal
$\tilde{\boldsymbol{e}}$	feedback estimate of the error signal $\breve{\boldsymbol{e}}$	$1 \times N$ row vector signal
$\tilde{\boldsymbol{a}}$	continuous-valued estimate at the input to the decision device	$1 \times N$ row vector signal
$\boldsymbol{e}$	estimation error at the input to the decision device	$1 \times N$ row vector signal
$\hat{\boldsymbol{a}}$	final quantized estimate of the transmitted data signal $\boldsymbol{a}$	$1 \times N$ row vector signal

of the estimation error $\boldsymbol{e}$ by

$$\boldsymbol{R}_e[m] \triangleq E\left[\boldsymbol{e}^H[n-m]\boldsymbol{e}[n]\right]. \tag{4.5}$$

Correspondingly, the power spectrum of the estimation error signal is

$$\boldsymbol{S}_e(D) \triangleq E_M\left[\boldsymbol{e}^H(D^{-*})\boldsymbol{e}(D)\right]. \tag{4.6}$$

Autocorrelation matrix and power spectrum are related through the D-transform:

$$\boldsymbol{R}_e[m] \xleftrightarrow{\mathcal{D}} \boldsymbol{S}_e(D). \tag{4.7}$$

Furthermore, the power spectrum evaluated on the unit circle $D = e^{-j2\pi\breve{f}}$, $\boldsymbol{S}_e(e^{-j2\pi\breve{f}})$, is the discrete-time Fourier transform (DTFT) of the estimation error autocorrelation:

$$\boldsymbol{S}_e(e^{-j2\pi\breve{f}}) = \mathcal{F}_{dc}\{\boldsymbol{R}_e[m]\}. \tag{4.8}$$

According to the derivation of the equivalent discrete-time model in Section 2.4, all discrete-time signals used here may be obtained by sampling the respective continuous-time signals at a period of T [s]. The *normalized frequency* $\check{f}$ can thus be interpreted as

$$\check{f} \triangleq fT \tag{4.9}$$

where f is the physical frequency in Hertz (Hz).

The k-th mean-square error J_k is defined as the expectation over the squared difference between the estimate at the input to the decision device, $\tilde{a}_k$, and the transmitted data of user k, a_k,

$$J_k \triangleq E\left[|e_k[n]|^2\right] \tag{4.10}$$

Note that J_k is equal to the k-th main diagonal element of the estimation error autocorrelation matrix $\boldsymbol{R}_e[m]$ at lag $m = 0$:

$$J_k = [\boldsymbol{R}_e[0]]_{kk}, \quad \forall k \in \mathcal{I}_N. \tag{4.11}$$

Alternatively, the MSE J_k may be calculated by integrating the power spectrum of the error estimate over the unit circle.

$$J_k = \int_0^1 \left[\boldsymbol{S}_e(e^{-j2\pi\check{f}})\right]_{kk} d\check{f}, \quad \forall k \in \mathcal{I}_N. \tag{4.12}$$

This is a direct consequence of the fact that $\boldsymbol{S}_e(e^{-j2\pi\check{f}})$ is the DTFT of $\boldsymbol{R}_e[m]$.

4.2   MIMO Linear Equalizer

The linear equalizer (LE) combines the received signals linearly. According to Section 2.3, the received analog signals have been lowpass filtered and sampled before they enter the detector. A MIMO LE with M inputs and P outputs can then be fully described by a $M \times P$ discrete-time matrix filter $\boldsymbol{C}[n]$. A block diagram of the MIMO
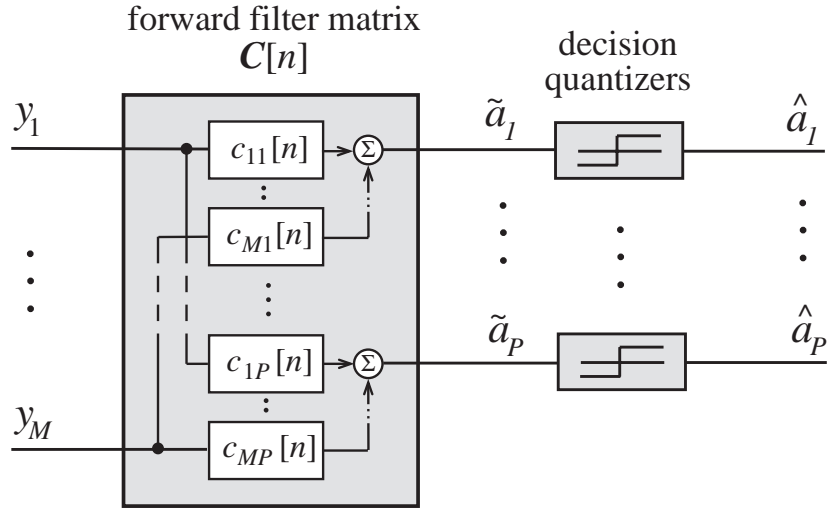
Figure 4.2: Structure of the multiple-input multiple-output (MIMO) linear equalizer (LE).

LE detector is shown in Figure 4.2. The (m, p)-th element $(m \in \mathcal{I}_M, p \in \mathcal{I}_P)$ of the matrix $\boldsymbol{C}[n]$ is a scalar sequence $c_{mp}[n]$ which represents the impulse response of a linear time-invariant discrete-time filter between the m-th input and the p-th output of the equalizer. The output signals of all M individual filters c_{mp} ($\forall m \in \mathcal{I}_M, p$ fixed) are added at the p-th matrix filter output and form the linear estimate $\tilde{a}_p$ of the input data sequence a_p of user p. Finally, the decision device performs a nonlinear quantization operation on the linear estimate which maps it to the closest number in the finite, discrete set of possible data symbols.

The system model including the receiver front end has been introduced in Chapter 2. Combining this (Figure 2.14) with the detector model for the MIMO LE (Figure 4.2) results in the complete system model shown in Figure 4.3. There are N users or system input signals. They are represented by the data vector $\boldsymbol{a}$, which has N components a_i, one for each user $i \in \mathcal{I}_N$. The transmitted signals travel through AK diversity channels, described by the $N \times AK$ overall channel matrix filter $\boldsymbol{X}$, and are additively distorted by correlated, colored Gaussian noise signals ν_l^v ($l \in \mathcal{I}_A$, $v \in \mathcal{I}_K$) before they enter the MIMO detector. The input signal to the detector is described by the vector $\boldsymbol{y}$, which consists of AK components. This determines that the matrix filter $\boldsymbol{C}$ of the MIMO LE be of size $AK \times N$, corresponding to AK detector input
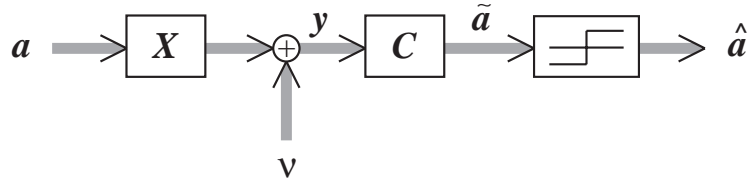
Figure 4.3: Complete multiuser system model including MIMO LE.

signals and N output signals $\tilde{a}_k$ ($k \in \mathcal{I}_N$). The final decision $\hat{a}_k$ on user k's transmitted data is a nonlinear estimate. It constitutes the k-th component of the final $1 \times N$ decision vector $\hat{\boldsymbol{a}}$.

Let us describe the signals of the system in the D-domain. It follows then immediately from Figure 4.3 that

$$\boldsymbol{y}(D) = \boldsymbol{a}(D)\boldsymbol{X}(D) + \boldsymbol{\nu}(D) \tag{4.13}$$

$$\tilde{\boldsymbol{a}}(D) = \boldsymbol{y}(D)\boldsymbol{C}(D). \tag{4.14}$$

4.2.1 Minimum Mean-Square Error Linear Equalizer

The coefficients of the MMSE MIMO LE are defined by the requirement that the mean-square errors (MSE's) $J_k \triangleq E[|e_k[n]|^2]$ be minimal for all $k \in \mathcal{I}_N$.

4.2.1.1 Frequency-Domain Approach

This section describes the MMSE MIMO LE in the frequency domain. The solution for the optimum equalizer is well known in the literature. In the following, the known results are adapted to the notation and the assumptions of the introduced system model.

To my knowledge, the first work describing the general structure of the MMSE MIMO LE was published by Kaye and George [57]. Assuming white Gaussian noise signals and a continuous-time system, it was shown that the MMSE MIMO LE consists of three parts: a bank of filters matched to the combined channels; N symbol-rate samplers[4]; and finally a $N \times N$ discrete-time matrix filter. The bank of matched filters

---

[4]N is the number of users or multiplexed signals.

can be described by a $AK \times N$ continuous-time matrix filter $\boldsymbol{X}_C^H(-t)$ matched to the overall channel matrix $\boldsymbol{X}_C(t)^5$.

It has been shown by van Etten [117] that this result can be easily extended to correlated, colored Gaussian noise signals by including a noise-whitening matrix filter at the detector front end. This linear transformation makes sure that the resulting signals include only white noise and the result of Kaye and George may be applied. Thus, an additional matrix filter matched to the noise-whitening matrix filter is required, followed by the previous structure consisting of a channel matched matrix filter, samplers and a discrete-time matrix filter. Van Etten has shown that the transfer function for the cascade of noise-whitening filter and the filter matched to it is equal to the inverse of the noise power spectral density function. The same result holds for the multidimensional matrix case, i.e. the transfer matrix for the cascade of noise-whitening matrix filter and the matrix filter matched to it is equal to the inverse of the noise power spectrum.

Under very mild conditions (Nyquist theorem), the sets of discrete-time signals and bandwidth-limited continuous-time signals are related to each other by a bijective transformation, i.e. each discrete-time signal corresponds to one and only one bandwidth-limited continuous-time signal. Thus, the above results for the optimal equalizer structure may be applied to discrete-time systems. In conclusion, the structure of the MMSE MIMO LE for the discrete-time system described in Chapter 2 may be realized with the following elements:

- cascade of noise-whitening matrix filter and matrix filter matched to it. The transfer function of these two elements is equal to $\boldsymbol{S}_\nu^{-1}(D)$, which is the inverse of the noise power spectrum defined in Equation (2.62);

- matrix filter $\boldsymbol{X}^H(D^{-*})$, which is matched to the overall channel matrix $\boldsymbol{X}(D)$;

- $N \times N$ matrix filter $\boldsymbol{L}_{\text{le,mmse}}(D)$.

---

[5]AK is the number of separately received signals.

The forward matrix filter of the MMSE MIMO LE is then given by

$$\boldsymbol{C}_{\text{le,mmse,1}}(D) = \boldsymbol{S}_{\nu}^{-1}(D)\boldsymbol{X}^{H}(D^{-*})\boldsymbol{L}_{\text{le,mmse}}(D). \tag{4.15}$$

Combining the overall channel $\boldsymbol{X}(D)$ and the detector front-end consisting of $\boldsymbol{S}_{\nu}^{-1}(D)$ and $\boldsymbol{X}^{H}(D^{-*})$ results in a discrete-time model with special properties: it can be described by a N-input N-output *equivalent channel* $\boldsymbol{S}_x$ with

$$\boldsymbol{S}_x(D) \triangleq \boldsymbol{X}(D)\boldsymbol{S}_{\nu}^{-1}(D)\boldsymbol{X}^{H}(D^{-*}), \tag{4.16}$$

where the power spectrum of the noise signals in the new model is also equal to $\boldsymbol{S}_x$. This system was the basis for a publication by Duel-Hallen, [27], in which she showed that the last element of the MMSE MIMO LE can be determined by

$$\boldsymbol{L}_{\text{le,mmse}}(D) = \boldsymbol{Q}^{-1}(D) \tag{4.17}$$

where $\boldsymbol{Q}(D)$ is defined as

$$\boldsymbol{Q}(D) \triangleq \boldsymbol{S}_x(D) + \boldsymbol{S}_a^{-1}(D) \tag{4.18}$$

and $\boldsymbol{S}_a(D)$ is the power spectrum of the input data (Equation (2.61)). $\boldsymbol{S}_a(D)$ may alternatively be calculated by taking the D-transform of the input data autocorrelation:

$$\boldsymbol{S}_a(D) = \mathcal{D}\left\{\boldsymbol{R}_a[m]\right\} \tag{4.19}$$

$$\boldsymbol{R}_a[m] \triangleq E[\boldsymbol{a}^{H}[n-m]\boldsymbol{a}[n]]. \tag{4.20}$$

Let us now determine the performance of the equalizer in terms of the *minimum mean-square error* (MMSE). This can be done by integrating the power spectrum of the estimation error, $\boldsymbol{S}_e(D)$, over the unit circle (Equation (4.12)). The estimation

error may be obtained by substituting Equations (4.14) and (4.13) into (4.2)

$$\boldsymbol{e}(D) = \boldsymbol{a}(D)\left[\boldsymbol{S}_x(D)\boldsymbol{L}_{\text{le,mmse}}(D) - \boldsymbol{I}_N\right] + \boldsymbol{\nu}(D)\boldsymbol{S}_\nu^{-1}(D)\boldsymbol{X}^H(D^{-*})\boldsymbol{L}_{\text{le,mmse}}(D).$$
(4.21)

The power spectrum of the estimation error can then be calculated by performing the following steps: at first, the above equation for $\boldsymbol{e}(D)$ is substituted into Definition (4.6); the resulting expression is expanded and the occurring expectations are replaced by the terms in Equations (2.61), (2.62) and (2.63); certain terms are replaced by $\boldsymbol{S}_x(D)$ and $\boldsymbol{L}(D)$ according to Equations (4.16) and (4.17); the expression is manipulated using the fact that $\boldsymbol{S}_x(D) = \boldsymbol{S}_x^H(D^{-*})$ and $\boldsymbol{L}_{\text{le,mmse}}(D) = \boldsymbol{L}_{\text{le,mmse}}^H(D^{-*})$; and finally, the term is expanded and simplified, which results in the simple relationship

$$\boldsymbol{S}_e(D) = \boldsymbol{L}_{\text{le,mmse}}(D).$$
(4.22)

Applying Equation (4.12), the MMSE for the k-th user of the MMSE MIMO LE is

$$J_{k,\text{le,mmse}} = \int_0^1 \left[\boldsymbol{L}_{\text{le,mmse}}(e^{-j2\pi\check{f}})\right]_{kk} d\check{f}, \quad \forall k \in \mathcal{I}_N.$$
(4.23)

The frequency-domain description of the MMSE MIMO LE according to Equations (4.15) and (4.17) is formally and mathematically correct. However, it may not be obvious how to calculate the equalizer parameters (tap weights) in practice from these formulas, especially because it may be tedious to calculate inverses and express the channel transfer function in the D-domain and perform an inverse D-transform. A practical and computationally simple method is to evaluate the D-transform equations on the unit circle, $D = e^{-j2\pi\check{f}}$, and replace the D-transform with the appropriate Fourier transform. In particular, we may calculate the transfer function of the overall channel matrix by applying the discrete-time Fourier transform (Table A.9) on the

matrix sequence $\boldsymbol{X}[n]$:

$$\boldsymbol{X}(e^{-j2\pi\check{f}}) = \sum_{n=-\infty}^{\infty} \boldsymbol{X}[n]\,e^{-j2\pi\check{f}n}. \tag{4.24}$$

Note that the result is equal to $\boldsymbol{X}(D)$ evaluated on the unit circle. The inverse of a matrix transfer function $\boldsymbol{Y}(e^{-j2\pi\check{f}})$ is calculated by determining, for each fixed frequency $\check{f}$, the inverse of the resulting matrix. Finally, the relatively simple inverse discrete-time Fourier transform replaces the more complicated inverse D-transform. The described method of calculating the equalizer by evaluating the D-transform quantities on the unit circle corresponds to approximating a pole/zero IIR filter by an all-zero transversal filter. As a positive side-effect, this averts instability problems of the resulting matrix filters.

For an implementation of the above method on a digital computer, the discrete Fourier series should be applied instead. This brings the advantage that both time and frequency signals may be described as finite discrete-domain sequences. For example, the inverse of a matrix transfer function can then be calculated by computing only a finite number of matrix inversions; in particular one matrix inversion at each discrete frequency $\check{f} = k/L$, where L is the length of the finite time- and frequency-domain sequences. L has to be chosen of appropriate length in order to allow only negligible time-domain aliasing and to minimize errors caused by this form of spectral inversion[6].

The MMSE MIMO LE has also been derived by Salz [105] for a N-input N-output continuous-time system and the case of uncorrelated data and white noise. His analysis has been based on a time-domain approach. Later, Honig *et al.* [51] derived the solution for the MMSE MIMO LE in a continuous-time system with arbitrarily correlated data and noise signals. They used an approach different from Salz', applying properties of the z-transform and using a variational method to minimize the MSE. The result is practically identical to Equations (4.15) and (4.17).

---

[6]In most cases, the inverse of a matrix filter $\boldsymbol{Y}(e^{-j2\pi\check{f}})$, $\boldsymbol{Y}^{-1}(e^{-j2\pi\check{f}})$, corresponds to a time domain matrix impulse response which is longer than the original matrix sequence $\boldsymbol{Y}[n]$. The effect is similar to the convolution operation, where the length of the output sequence is equal to the sum of the lengths of input sequence and filter impulse response. However, such a general relation for the required length is not known for the operation of frequency-domain inversion.

In the following, the optimal MMSE MIMO LE matrix filter is derived differently. This method will lead to a new expression for the optimal MMSE MIMO LE. In addition, it will demonstrate the simplicity of the D-transform notation and its suitability to the current problem. The method is somewhat similar to but simpler and more elegant than Honig *et al.*'s method [51]. It can be viewed as an application of Duel-Hallen's approach [27] to the more general system model considered here.

The new expression shows that the frequency-domain representation of the optimal MMSE MIMO LE matrix filter is equal to the inverse of the received signal's power spectrum multiplied by the cross-power spectrum of the received signal and the desired data. Note that this is an important result since the received signal is known and some information about the desired data is usually available (e.g. from a training sequence). The new expression represents an extension to the *noncausal Wiener filter* [89], a well-known result from estimation theory which expresses the optimal mean-square estimator of a scalar random process in the frequency-domain. In particular, the noncausal Wiener filter is a special case of the derived MIMO expression for the single-input single-output (SISO) scenario.

Let us start with a necessary and sufficient condition for the equalizer to attain the minimum MSE. One such condition is the *orthogonality principle*, which states that an equalizer produces the minimal achievable MSE if and only if each estimation error $e_k[n]$ ($\forall k \in \mathcal{I}_N$) is orthogonal to all samples $y_q[n-m]$ ($\forall q \in \mathcal{I}_{AK}, \forall m \in \mathbb{Z}$) of each input signal that enters the detector [46]. Mathematically, the orthogonality principle can be formulated as

$$E[\boldsymbol{y}^H[n-m]\boldsymbol{e}[n]] = \boldsymbol{O}_{AK \times N}, \quad \forall m \in \mathbb{Z} \tag{4.25}$$

where $\boldsymbol{O}_{AK \times N}$ is the $AK \times N$ null matrix (Table A.7). It may as well be expressed in the D-domain. Taking the D-transform of Equation (4.25) results, according to Lemma 1.2, in the following equivalent formulation of the orthogonality principle:

$$E_M[\boldsymbol{y}^H(D^{-*})\boldsymbol{e}(D)] = \boldsymbol{O}_{AK \times N}, \quad \forall D \in \mathbb{C}. \tag{4.26}$$

Let us define the power spectrum of the equalizer input signal, $\boldsymbol{S}_y(D)$, and the cross-

power spectrum between the equalizer input signal and the transmitted data, $\boldsymbol{S}_{ya}(D)$:

$$\boldsymbol{S}_y(D) \triangleq E_M[\boldsymbol{y}^H(D^{-*})\boldsymbol{y}(D)]$$

$$= \boldsymbol{X}^H(D^{-*})\boldsymbol{S}_a(D)\boldsymbol{X}(D) + \boldsymbol{S}_\nu(D) \tag{4.27}$$

$$\boldsymbol{S}_{ya}(D) \triangleq E_M[\boldsymbol{y}^H(D^{-*})\boldsymbol{a}(D)]$$

$$= \boldsymbol{X}^H(D^{-*})\boldsymbol{S}_a(D) \tag{4.28}$$

where the last expressions are obtained by substituting Equations (4.13), (2.61), (2.62) into the definitions. It is easy to show with the last two equations that the power spectrum $\boldsymbol{S}_y(D)$ may alternatively be expressed in the form

$$\boldsymbol{S}_y(D) = \boldsymbol{S}_{ya}(D)\boldsymbol{S}_a^{-1}(D)\boldsymbol{S}_{ya}^H(D^{-*}) + \boldsymbol{S}_\nu(D). \tag{4.29}$$

Expanding the orthogonality principle (4.26) using Equations (4.2), (4.14) and substituting Equations (2.61), (2.62) and (2.63) yields the condition

$$\boldsymbol{S}_y(D)\boldsymbol{C}(D) - \boldsymbol{S}_{ya}(D) = \boldsymbol{O}_{AK \times N}, \quad \forall D \in \mathbb{C}. \tag{4.30}$$

This equation will be fulfilled if $\boldsymbol{C}(D)$ is given by either of the two following expressions:

$$\boldsymbol{C}_{\text{le,mmse,1}}(D) = \boldsymbol{S}_\nu^{-1}(D)\boldsymbol{S}_{ya}(D)\left[\boldsymbol{S}_{ya}^H(D^{-*})\boldsymbol{S}_\nu^{-1}(D)\boldsymbol{S}_{ya}(D) + \boldsymbol{S}_a(D)\right]^{-1}\boldsymbol{S}_a(D) \tag{4.31}$$

$$\boldsymbol{C}_{\text{le,mmse,2}}(D) = \boldsymbol{S}_y^{-1}(D)\boldsymbol{S}_{ya}(D). \tag{4.32}$$

Note that the structure of both solutions is different. The second expression is obtained simply by solving Equation (4.30) directly for $\boldsymbol{C}(D)$. On the other hand, the first expression is identical with Equation (4.15), which can be shown immediately by substituting Equation (4.28) into (4.31). The first solution may be found by applying the *matrix inversion lemma* [46] to Equation (4.29), substituting this expression into Equation (4.32) and simplifying the resulting term. A simpler proof is to substitute solution (4.31) directly into Equation (4.30), which shows after some manipulation

that the condition for the MMSE MIMO LE is satisfied.

It has been chosen to express the two solutions for the MMSE MIMO LE in terms of the power spectra $\boldsymbol{S}_y$ and $\boldsymbol{S}_{ya}$ since these quantities may be directly calculated from a known training sequence and the input signal to the equalizer. Thus, both solutions are directly expressed in terms of "available" quantities[7].

A closed-form expression for the MMSE, which depends only on the directly available spectra $\boldsymbol{S}_y$ and $\boldsymbol{S}_{ya}$, shall now be derived. Considering the second form of the MMSE MIMO LE (Equation (4.32)), the estimation error at the input to the decision device is

$$\boldsymbol{e}(D) = \boldsymbol{y}(D)\boldsymbol{S}_y^{-1}(D)\boldsymbol{S}_{ya}(D) - \boldsymbol{a}(D).\qquad(4.33)$$

Substituting this expression into the definition for the error power spectrum $\boldsymbol{S}_e(D)$, Equation (4.6), expanding the resulting term and applying the definitions (2.61), (4.27), (4.28) yields

$$\boldsymbol{S}_e(D) = \boldsymbol{S}_a(D) - \boldsymbol{S}_{ya}^H(D^{-*})\boldsymbol{S}_y^{-1}(D)\boldsymbol{S}_{ya}(D).\qquad(4.34)$$

This relationship can then directly be used in Equation (4.12) in order to calculate the MMSE's $J_{k,\text{le,mmse}}$.

The above results show that the MMSE MIMO LE may be realized by two different structures. The first one, $\boldsymbol{C}_{\text{le,mmse,1}}(D)$, is identical to the well known cascade of three elements: firstly a noise-whitening matched matrix filter $\boldsymbol{S}_\nu^{-1}(D)$; secondly a channel matched matrix filter $\boldsymbol{X}^H(D^{-*})$; and finally a $N \times N$ matrix filter $\boldsymbol{L}_{\text{le,mmse}}(D)$.

The second structure is different. It may be described by an $AK \times AK$ matrix filter whose transfer function is identical to the inverse of the equalizer input signal power spectrum $\boldsymbol{S}_y(D)$. This is followed by a matrix filter whose transfer function is equal to the cross-correlation $\boldsymbol{S}_{ya}(D)$ between the equalizer input signal $\boldsymbol{y}$ and the input data $\boldsymbol{a}$.

---

[7]Equation (4.15) expresses the first solution for the MMSE MIMO LE in terms of the channel transfer function $\boldsymbol{X}(D)$. Although this quantity cannot be measured directly, it does not pose a practical problem since $\boldsymbol{X}(D)$ may be obtained from the quantity $\boldsymbol{S}_{ya}(D)$ with Equation (4.28).

The second structure may also be interpreted in a different way: The input signal to the equalizer $\boldsymbol{y}$ can be viewed as a wide sense stationary random process with spectrum $\boldsymbol{S}_y(D)$. It is possible to factor this spectrum according to

$$\boldsymbol{S}_y(D) = \boldsymbol{\Upsilon}^H(D^{-*})\boldsymbol{\Upsilon}(D). \tag{4.35}$$

There is an infinite number of factors $\boldsymbol{\Upsilon}(D)$ which satisfy the above equation, however, one of them is usually of special interest: there exists one stable and causal matrix filter $\boldsymbol{\Upsilon}(D)$, which has a causal inverse [126, 127]. In this case $\boldsymbol{\Upsilon}^{-1}(D)$ is the *whitening filter* or the *linear prediction-error filter* of the process $\boldsymbol{y}$. The MMSE MIMO LE can now be expressed in the form

$$\boldsymbol{C}_{\text{le,mmse,2}}(D) = \boldsymbol{\Upsilon}^{-1}(D)\boldsymbol{\Upsilon}^{-H}(D^{-*})\boldsymbol{X}^H(D^{-*})\boldsymbol{S}_a(D) \tag{4.36}$$

where the superscripts are defined in Table A.3. This leads to the following statement:

The MMSE MIMO LE may be realized by a cascade of three elements:

1. a matrix filter $\boldsymbol{\Upsilon}^{-1}(D)$ which whitens the input signal to the equalizer;

2. a matrix filter $\boldsymbol{\Upsilon}^{-H}(D^{-*})\boldsymbol{X}^H(D^{-*})$ matched to the transfer function between the transmitted data and the whitened equalizer input signals;

3. a matrix filter whose transfer function is equal to the power spectrum $\boldsymbol{S}_a(D)$ of the transmitted data.

4.2.1.2 Time-Domain Approach

This section briefly presents expressions, obtained from a time-domain analysis, for the optimal forward filter and the MMSE of the finite-length MMSE MIMO LE. A detailed derivation and discussion is presented in Appendix G.1.

Consider a finite-length forward matrix filter $\boldsymbol{C}[n]$, which is restricted to M_C non-zero matrix samples $\boldsymbol{C}[0], \boldsymbol{C}[1], \boldsymbol{C}[2], \dots, \boldsymbol{C}[M_C - 1]$. Let us define the *extended*

equalizer coefficient matrix

$$\bar{\boldsymbol{C}} \triangleq \begin{bmatrix} \boldsymbol{C}[M_C - 1] \\ \boldsymbol{C}[M_C - 2] \\ \boldsymbol{C}[M_C - 3] \\ \vdots \\ \boldsymbol{C}[0] \end{bmatrix}. \tag{4.37}$$

This matrix contains all parameters of the equalizer that have to be chosen such that the mean-squared error (MSE) is minimized. It is shown in Appendix G.1 that the optimal coefficients and the MMSE of the k-th signal are given by

$$\bar{\boldsymbol{C}}_{\text{le,mmse}} = \boldsymbol{R}_{\bar{y}}^{-1} \boldsymbol{R}_{\bar{y}a} \tag{4.38}$$

$$J_{k,\text{le,mmse}} = \left[\boldsymbol{R}_a[0] - \boldsymbol{R}_{\bar{y}a}^H \boldsymbol{R}_{\bar{y}}^{-1} \boldsymbol{R}_{\bar{y}a} \right]_{kk}, \quad \forall k \in \mathcal{I}_N \tag{4.39}$$

where $\boldsymbol{R}_a[0]$ is the autocorrelation matrix of the input data $\boldsymbol{a}$ at time-lag $m = 0$ (Equation (2.64)). The matrices $\boldsymbol{R}_{\bar{y}}$ and $\boldsymbol{R}_{\bar{y}a}$ are defined in Appendix G.1. $\boldsymbol{R}_{\bar{y}}$ is positive semidefinite, Hermitian and block Toeplitz. Its size is $M_C A K \times M_C A K$. $\boldsymbol{R}_{\bar{y}a}$ is of size $M_C A K \times A K$.

4.2.1.3   Comparison: Frequency- and Time-Domain Solutions

Three structurally different solutions for the MMSE MIMO LE have been obtained in the previous sections. The first two expressions (4.31) and (4.32) are the result of a frequency-domain approach while the third solution (4.38) has been found using time-domain analysis. This section will provide a brief discussion of the different equalizer expressions based on a simplified operation count and other properties.

Let us start with the assumptions being made for the operation count:

- the frequency-domain solutions are used to calculate a truncated approximation of the optimal infinite-length MMSE MIMO LE;

- the length of all truncated equalizer structures is M_C samples;

- all of the matrix sequences $\boldsymbol{S}_{ya}(e^{-j2\pi m/M_C})$, $\boldsymbol{R}_{ya}[m]$, $\boldsymbol{S}_y(e^{-j2\pi m/M_C})$, $\boldsymbol{R}_y[m]$, $\boldsymbol{S}_\nu^{-1}(e^{-j2\pi m/M_C})$ are readily available and it is assumed that the numerical effort to obtain them is the same for each one;

- possible sparsity of the matrices $\boldsymbol{S}_\nu^{-1}(e^{-j2\pi m/M_C})$, which might reduce the number of necessary operations, is *not* considered;

- the transmitted data signals are assumed to be stationary discrete-time stochastic processes which are mutually and temporally independent with zero mean and unit variance, i.e., $\boldsymbol{S}_a(D) = \boldsymbol{I}_N$;

- the computational effort needed to transform the frequency-domain solutions $\boldsymbol{C}(e^{-j2\pi m/M_C})$ back into the time domain is not considered.

Generally, the frequency-domain solutions (4.31) and (4.32) describe the infinite-length MMSE MIMO LE while the time-domain expression represents the optimal finite-length equalizer. For practical purposes, the infinite-length solutions have to be truncated. Truncated versions of the frequency-domain solutions are obtained by evaluating the expressions for the equalizer, $\boldsymbol{C}(D)$, on the unit circle $D = e^{-j2\pi \check{f}}$ and sampling the normalized frequency $\check{f}$ at M_C equidistant points $\check{f}_m = m/M_C$, where $m = 0, 1, 2, \ldots, M_C - 1$ and M_C will be the length of the resulting truncated equalizer impulse responses. In order to simplify the comparison, the lengths of all three equalizer structures are chosen to be M_C samples.

The number of operations necessary to transform discrete-domain frequency spectra into correlation functions and vice versa is determined by the number of computations that a (inverse) fast Fourier transform (IFFT/FFT) requires. The number of these operations may add to the overall computations needed to determine the equalizer. This factor is, however, not considered in the following since whether or not a IFFT/FFT is necessary depends on the implementation and technical details of the equalizer.

For simplicity, it is assumed that the determination of the inverse noise spectrum $\boldsymbol{S}_\nu^{-1}(e^{-j2\pi m/M_C})$ requires approximately the same numerical effort as the computation of $\boldsymbol{S}_{ya}(e^{-j2\pi m/M_C})$, $\boldsymbol{R}_{ya}[m]$, $\boldsymbol{S}_y(e^{-j2\pi m/M_C})$ or $\boldsymbol{R}_y[m]$. This may not be true in practice

and depends mainly on the individual situation.

The matrices $\boldsymbol{S}_\nu^{-1}(e^{-j2\pi m/M_C})$ may or may not be sparse, i.e. contain a large number of elements that are zero. If this is the case, the number of operations that an inversion or matrix multiplication requires might be significantly reduced. For example, if the noise consists only of random Gaussian processes that are mutually independent at different receiver inputs (antennas), the inverse noise spectrum will contain many zeros (Section 2.4.3). On the other hand, if the noise signals contain cyclostationary interference (originating, for example, from jammers or adjacent channel signals), there will be no or only few zeros in the noise spectrum. The latter case is considered in the following.

The transmitted data sequences a_k $(k \in \mathcal{I}_N)$ are in general mutually independent for a multiuser system in which the data signals originate from spatially separated users. Furthermore, the assumption that a certain data symbol $a_k[n]$ is independent with any other symbol $a_k[m]$ (for all $n \neq m$) is quite common for digital systems.

An equalizer is typically realized in a time-domain tapped delay-line structure. For this, the frequency-domain solutions would have to be transformed to the time-domain via IFFT. The number of operations required for this task is not considered in the following.

The number of approximate operations (op) will be determined for each of the three equalizer expressions. One operation is defined as the common execution of one complex multiplication and one complex addition. In general, the multiplication of a $N \times M$- and a $M \times K$-matrix requires NMK op (operations). The matrices to be inverted are exclusively Hermitian. Thus, the matrix multiplication $\boldsymbol{A}^{-1}\boldsymbol{B}$ is most efficiently solved by Cholesky factorization of $\boldsymbol{A}$ and backsubstitution with each column of $\boldsymbol{B}$ [97]. If the matrices $\boldsymbol{A}$ and $\boldsymbol{B}$ are of the sizes $N \times N$ and $N \times M$, respectively, the matrix multiplication $\boldsymbol{A}^{-1}\boldsymbol{B}$ will require approximately $N^3/6 + N^2M$ op (operations).

Let us start with the first solution

$$\boldsymbol{C}_{\text{le,mmse},1}(D) = \boldsymbol{S}_\nu^{-1}(D)\boldsymbol{S}_{ya}(D)\left[\boldsymbol{S}_{ya}^H(D^{-*})\boldsymbol{S}_\nu^{-1}(D)\boldsymbol{S}_{ya}(D) + \boldsymbol{I}_N\right]^{-1}$$

where $D = e^{-j2\pi m/M_C}, \forall m = 1, 2, 3, \ldots, M_C - 1$. Note that, for a fixed frequency sample m, the matrices $\boldsymbol{S}_\nu^{-1}(e^{-j2\pi m/M_C})$ and $\boldsymbol{S}_{ya}(e^{-j2\pi m/M_C})$ are of size $AK \times AK$ and $AK \times N$, respectively. Matrix multiplication or inversion has to be performed at each frequency sample separately, which means that the number of operations grows linearly with the equalizer length M_C. The calculation of the equalizer can be broken down into three steps which require the following numbers of computations:

1. $\boldsymbol{G}_1(D) = \boldsymbol{S}_\nu^{-1}(D)\boldsymbol{S}_{ya}(D)$: $\qquad\qquad M_C(AK)^2 N$ op;

2. $\boldsymbol{G}_2(D) = \boldsymbol{S}_{ya}^H(D^{-*})\boldsymbol{G}_1(D)$: $\qquad\qquad M_C AKN^2$ op;

3. $\boldsymbol{C}_{\text{le,mmse,1}}(D) = \boldsymbol{G}_1(D)\left[\boldsymbol{G}_2(D) + \boldsymbol{I}_N\right]^{-1}$: $\quad M_C[N^3/6 + AKN^2]$ op.

The second frequency-domain solution for the MMSE MIMO LE is

$$\boldsymbol{C}_{\text{le,mmse,2}}(D) = \boldsymbol{S}_y^{-1}(D)\boldsymbol{S}_{ya}(D).$$

Again, this expression has to be evaluated at M_C discrete frequencies $D = e^{-j2\pi m/M_C}$ $(m = 1, 2, 3, \ldots, M_C - 1)$. $\boldsymbol{S}_y^{-1}(e^{-j2\pi m/M_C})$ is a $AK \times AK$ matrix while $\boldsymbol{S}_{ya}(e^{-j2\pi m/M_C})$ is of size $AK \times N$ (m fixed). The combined execution of matrix inversion and multiplication, which results in $\boldsymbol{C}_{\text{le,mmse,2}}(e^{-j2\pi m/M_C}), \forall m = 1, 2, 3, \ldots, M_C - 1$, requires thus $M_C\left[(AK)^3/6 + (AK)^2 N\right]$ op.

Finally, the time-domain solution is according to Equation (4.38)

$$\bar{\boldsymbol{C}}_{\text{le,mmse}} = \boldsymbol{R}_{\bar{y}}^{-1}\boldsymbol{R}_{\bar{y}a}$$

where the matrices $\boldsymbol{R}_{\bar{y}}$ and $\boldsymbol{R}_{\bar{y}a}$ are of size $M_C AK \times M_C AK$ and $M_C AK \times N$, respectively. Hence, for the calculation of $\bar{\boldsymbol{C}}_{\text{le,mmse}}$, approximately $(M_C AK)^3/6 + (M_C AK)^2 N$ op have to be executed. This estimate does not take into account that the block-Toeplitz structure of $\boldsymbol{R}_{\bar{y}}$ (Equation (G.15)) may be exploited in order to reduce the number of computations. However, a reduction in the order of that promised by the standard Levinson-Durbin algorithm cannot be expected since it may not be applied to the inversion of $\boldsymbol{R}_{\bar{y}}$, which is merely block-Toeplitz.

Table 4.2 summarizes the approximate number of operations required for each of the three MMSE MIMO LE expressions. It can be seen that the number of operations

Table 4.2: Approximate number of operations required for the parameter calculation of different MMSE MIMO LE implementations.

LE Implementation	Eqn.	Number of Operations
$C_{\text{le,mmse,1}}(e^{-j2\pi m/M_C})$	(4.31)	$M_C\left[(AK)^2N + 2AKN^2 + \frac{1}{6}N^3\right]$
$C_{\text{le,mmse,2}}(e^{-j2\pi m/M_C})$	(4.32)	$M_C\left[(AK)^2N + \frac{1}{6}(AK)^3\right]$
$\bar{C}_{\text{le,mmse}}$	(4.38)	$M_C^2(AK)^2N + \frac{1}{6}M_C^3(AK)^3$

grows linearly with the equalizer length M_C for the two frequency-domain solutions $C_{\text{le,mmse,1}}(e^{-j2\pi m/M_C})$ and $C_{\text{le,mmse,2}}(e^{-j2\pi m/M_C})$. For long equalizers, this is significantly more efficient than the time-domain solution $\bar{C}_{\text{le,mmse}}$ whose computational load increases proportional to M_C^3. Moreover, a problem of the time-domain solution has been encountered in simulations: the matrix $R_{\bar{y}}$ has a tendency to become poorly conditioned if its size and the SNR increase. On the other hand, this problem has not occurred in the frequency-domain approach under exactly the same conditions. The matrices to be inverted in the frequency-domain turned out to be well conditioned for practically all simulations.

Another aspect for the comparison of the different solutions is the optimality of the resulting equalizer. The time-domain solution yields the optimal finite-length MMSE MIMO LE. In other words, the equalizer achieves the minimal MSE for a preselected matrix filter length M_C. On the other hand, evaluating the frequency-domain expressions (4.31) and (4.32) on the unit circle $D = e^{-j2\pi \check{f}}$ results in the optimal infinite-length MMSE MIMO LE after an inverse DTFT (discrete-time Fourier transform) has been performed. The finite-length equalizer obtained by sampling the normalized frequency $\check{f}$ at M_C points can be viewed as approximation to the optimal infinite-length equalizer. This approximation is not necessarily optimal for the given equalizer length (number of tap weights). Therefore, the finite-length equalizers obtained from the frequency-domain expressions have a theoretical performance that is worse than that of time-domain optimized equalizers. However, if the equalizer length M_C is sufficiently high, the performance difference will become negligible.

The choice about which frequency-domain solution is preferable depends mainly on the number of required operations. This, on the other hand, is strongly determined by

the individual situation. For the assumptions made at the beginning of this section, namely that the inverse noise spectrum, $\boldsymbol{S}_\nu^{-1}(D)$, is readily available and that the transmitted symbols are mutually uncorrelated $(\boldsymbol{S}_a(D) = \boldsymbol{I}_N)$, the application of the first solution $\boldsymbol{C}_{\text{le,mmse,1}}(D)$ might be more efficient if $N < AK$. However, if these conditions do not apply, the second expression $\boldsymbol{C}_{\text{le,mmse,2}}(D)$ will normally require less operations.

4.2.1.4 Lower Bound for the Average Minimum Mean-Square Error

In the following, a lower bound for the average MMSE of the linear equalizer will be derived for situations when the number of system users exceeds the number of diversity channels $(N > AK)$. Consider that the transmitted signals a_k $(k \in \mathcal{I}_N)$ of different users are mutually independent. Additionally, the samples of the sequence transmitted by user k are assumed to be independent with zero mean and unit variance. Thus,

$$E\left[a_k^*[n]a_i[m]\right] = \delta_K[k - i]\delta_K[n - m], \quad \forall k, i \in \mathcal{I}_N; \forall n, m \in \mathbb{Z} \qquad (4.40)$$

where $\delta_K[k]$ is the Kronecker delta sequence (Table A.3). In this case, the spectrum of the input signal is equal to the $N \times N$ identity matrix and does not depend on D:

$$\boldsymbol{S}_a = \boldsymbol{I}_N \qquad (4.41)$$

The MMSE of user k can be obtained by substituting Equations (4.22), (4.17) and (4.18) into (4.12)

$$J_k = \left[\int_0^1 \left[\boldsymbol{S}_x(e^{-j2\pi\check{f}}) + \boldsymbol{I}_N\right]^{-1} d\check{f}\right]_{kk}. \qquad (4.42)$$

Consider now the singular value decomposition (SVD)

$$\boldsymbol{S}_x(e^{-j2\pi\check{f}}) = \boldsymbol{\Theta}(e^{-j2\pi\check{f}})\boldsymbol{\Lambda}(e^{-j2\pi\check{f}})\boldsymbol{\Theta}^H(e^{-j2\pi\check{f}}) \qquad (4.43)$$

where $\boldsymbol{\Theta}(e^{-j2\pi\check{f}})$ is a unitary $N \times N$ matrix[8] for all $\check{f} \in [0,1)$, and $\boldsymbol{\Lambda}(e^{-j2\pi\check{f}})$ is a $N \times N$ diagonal matrix containing the eigenvalues

$$\lambda_k(e^{-j2\pi\check{f}}) \triangleq [\boldsymbol{\Lambda}(e^{-j2\pi\check{f}})]_{kk} \tag{4.44}$$

The MMSE of user k may now be written as

$$J_k = \left[\int_0^1 \boldsymbol{\Theta}(e^{-j2\pi\check{f}}) \left[\boldsymbol{\Lambda}(e^{-j2\pi\check{f}}) + \boldsymbol{I}_N \right]^{-1} \boldsymbol{\Theta}^H(e^{-j2\pi\check{f}}) \, d\check{f} \right]_{kk}. \tag{4.45}$$

$\boldsymbol{S}_x(e^{-j2\pi\check{f}})$ is positive semidefinite[9] for all $\check{f} \in [0,1)$. Hence, its eigenvalues are greater than or equal to zero. The number of "zero" eigenvalues is equal to the nullity (rank deficiency) of $\boldsymbol{S}_x(e^{-j2\pi\check{f}})$, which is defined in Equation (4.16). It has been shown in Section 2.4.3 that $\boldsymbol{S}_\nu(e^{-j2\pi\check{f}})$ and thus $\boldsymbol{S}_\nu^{-1}(e^{-j2\pi\check{f}})$ are positive definite for all frequencies. The rank of $\boldsymbol{S}_x(e^{-j2\pi\check{f}})$ depends therefore completely on the combined channel matrix $\boldsymbol{X}(e^{-j2\pi\check{f}})$, which has N rows and AK columns. If $N \leq AK$, $\boldsymbol{X}(e^{-j2\pi\check{f}})$ may be of full row rank and $\boldsymbol{S}_x$ may be regular. On the other hand, if $N > AK$ the rank of $\boldsymbol{X}(e^{-j2\pi\check{f}})$ is at most AK. In this case, the $N \times N$ matrix $\boldsymbol{S}_x(e^{-j2\pi\check{f}})$ is singular. Its rank is smaller than or equal to AK and its nullity (rank deficiency) is greater than or equal to the *overpopulation number* [136, p.164–67]

$$\xi \triangleq N - AK. \tag{4.46}$$

This means that at least ξ of the N eigenvalues $\lambda_k(e^{-j2\pi\check{f}})$ are equal to zero for all frequencies $\check{f} \in [0,1)$.

Let the average MMSE over all N users be

$$\bar{J} \triangleq \frac{1}{N} \sum_{k=1}^N J_k. \tag{4.47}$$

---

[8]This means that $\boldsymbol{\Theta}^{-1}(e^{-j2\pi\check{f}}) = \boldsymbol{\Theta}^H(e^{-j2\pi\check{f}})$.

[9]The positive semidefiniteness of $\boldsymbol{S}_x(e^{-j2\pi\check{f}})$ follows from Definition (4.16) and the fact that $\boldsymbol{S}_\nu(e^{-j2\pi\check{f}})$ is positive definite for all $\check{f} \in [0,1)$ (see Section 2.4.3).

Substituting Equation (4.45) into this expression yields

$$
\begin{aligned}
\bar{J} &= \frac{1}{N} \operatorname{tr} \left\{ \int_0^1 \mathbf{\Theta}(e^{-j2\pi\check{f}}) \left[\mathbf{\Lambda}(e^{-j2\pi\check{f}}) + \boldsymbol{I}_N \right]^{-1} \mathbf{\Theta}^H(e^{-j2\pi\check{f}}) \, d\check{f} \right\} \\
&= \frac{1}{N} \int_0^1 \operatorname{tr} \left\{ \left[\mathbf{\Lambda}(e^{-j2\pi\check{f}}) + \boldsymbol{I}_N \right]^{-1} \right\} d\check{f} \\
&= \frac{1}{N} \int_0^1 \sum_{k=1}^N \left[\lambda_k(e^{-j2\pi\check{f}}) + 1 \right]^{-1} d\check{f}
\end{aligned}
\tag{4.48}
$$

where $\operatorname{tr}\{\dots\}$ denotes the trace of the matrix enclosed by the curly brackets (see Table A.3). It is now possible to find a lower bound for the average MMSE in over-populated systems. It has been shown above that if $N > AK$, at least ξ eigenvalues $\lambda_i(\check{f})$ are equal to zero for each frequency $\check{f} \in [0, 1)$. Consider now only these singular eigenvalues for the lower bound while the other non-zero eigenvalues are neglected. It follows then from Equation (4.48) that the average MMSE is lower bounded by

$$
\bar{J} > \frac{1}{N} \int_0^1 \left[\sum_{i=1}^\xi 1 \right] d\check{f} = \frac{\xi}{N}.
\tag{4.49}
$$

Substituting Equation (4.46) into (4.49) yields the sought after lower bound for the average MMSE $\bar{J}$ in overpopulated systems

$$
\bar{J} > 1 - \frac{AK}{N}, \quad N > AK.
\tag{4.50}
$$

4.2.2 Zero-Forcing Linear Equalizer

The frequency-domain solution for the infinite-length zero-forcing multiple-input multiple-output linear equalizer (ZF MIMO LE) is described in this section. The *zero-forcing linear equalizer*, also known as *decorrelating detector* or *decorrelator*, is the linear receiver which achieves the minimal MSE under the constraint that all interference from the K intracell users (ISI and CCI) be completely eliminated. The output of the ZF MIMO LE will thus be distorted only by Gaussian noise if no external interference (intercell interference, jammers) is present. In general, the performance of the ZF detector is worse than that of the MMSE equalizer since the constraint of completely

nulling out all interference leads to a stronger amplification of the noise component such that the variance of the error signal at the input to the decision device is always larger for the ZF equalizer. This and other disadvantages discussed later make the ZF detector less attractive than the MMSE LE for an implementation in real systems. However, the fact that the error signal of the ZF LE is Gaussian distributed is one of the reasons for the considerable attention this detector received in the literature: due to this property, a compact closed-form expression for the error probability of the ZF LE can easily be found. Conversely, a closed-form expression does not exist for the MMSE LE, which leads to a significantly more complicated calculation of the error probability.

The ZF decorrelating detector has been derived and discussed extensively in the literature for a wide variety of situations, systems and assumptions. This section is limited to the assumptions of Section 2.1, i.e. most importantly the MIMO case, frequency-selective, quasi-stationary channels and a discrete-time model that implicitly contains an arbitrary continuous-time channel. It seems that the necessary and sufficient frequency-domain condition for the ZF MIMO LE has been derived and mentioned at first by van Etten [117]. He also found that the ZF MIMO LE and the MMSE MIMO LE have the same structure, i.e. they both consist of a noise-whitening matched filter followed by a channel matched filter and a $N \times N$ linear transformation. Later, several papers stated explicitly the frequency-domain expression of the ZF MIMO LE [69, 51, 119, 29, 42]. Except for partly different system assumptions and notations, all these expressions are basically identical. Considering the system and notation used in this dissertation, the matrix filter of the ZF MIMO LE is described by

$$\boldsymbol{C}_{\mathrm{le,zf}}(D) = \boldsymbol{S}_\nu^{-1}(D)\boldsymbol{X}^H(D^{-*})\boldsymbol{L}_{\mathrm{le,zf}}(D) \tag{4.51}$$

$$\boldsymbol{L}_{\mathrm{le,zf}}(D) = \boldsymbol{S}_x^{-1}(D) \tag{4.52}$$

where the equivalent channel $\boldsymbol{S}_x(D)$ is defined by Equation (4.16). Noting that the estimation error $\boldsymbol{e}$ at the input to the decision device contains only Gaussian noise,

the spectrum of the estimation error is easily found to be

$$\boldsymbol{S}_e(D) = \boldsymbol{L}_{\text{le,zf}}(D). \tag{4.53}$$

A comparison of the expressions for the ZF and MMSE MIMO LE reveals that the front-end is identical $(\boldsymbol{S}_\nu^{-1}(D)\boldsymbol{X}^H(D^{-*}))$ and that the $N \times N$ matrix filters $\boldsymbol{L}_{\text{le,zf}}(D)$ and $\boldsymbol{L}_{\text{le,mmse}}(D)$ differ only slightly: $\boldsymbol{L}_{\text{le,zf}}(D)$ is equal to the inverse of the equivalent channel $\boldsymbol{S}_x(D)$ while $\boldsymbol{L}_{\text{le,mmse}}(D)$ is equal to the inverse of the sum of $\boldsymbol{S}_x(D)$ and the transmitted data spectrum $\boldsymbol{S}_a(D)$. This small difference has some practical implications:

- the individual MSE's of the MMSE MIMO LE are always smaller than those of the ZF MIMO LE;

- the ZF MIMO LE does not exist if the system is overpopulated, i.e., when the number of users is larger than the number of diversity channels $(N > AK)$;

- the MMSE MIMO LE does always exist.

The first attribute follows from the fact that the spectrum $\boldsymbol{S}_a(D)$ is positive definite on the unit circle $D = e^{-j2\pi\check{f}}$. Hence, the main diagonal elements of the MMSE MIMO LE error spectrum $\boldsymbol{S}_e(e^{-j2\pi\check{f}})$ are smaller than that of the ZF MIMO LE, which causes smaller MSE's according to Equation (4.12).

If the number of users is larger than the number of diversity channels, the equivalent channel $\boldsymbol{S}_x(D)$ will be singular on the unit circle. The singularity is caused by the $N \times AK$ matrix $\boldsymbol{X}(D)$ which is a part of the definition of $\boldsymbol{S}_x(D)$ (4.16): If $N > AK$, $\boldsymbol{X}(D)$ has more columns than rows and the product (4.16) becomes singular.

Even if $\boldsymbol{S}_x(D)$ is singular, the sum $\boldsymbol{S}_x(D) + \boldsymbol{S}_a(D)$ will always be regular since $\boldsymbol{S}_a(D)$ is positive definite. Hence, the MMSE MIMO LE filter $\boldsymbol{L}_{\text{le,mmse}}(D)$ (Equation (4.17)) does always exist for any values of N and AK.

As in Section 4.2.1.1, the equalizer can be expressed in terms of the spectra $\boldsymbol{S}_{ya}(D)$, $\boldsymbol{S}_\nu^{-1}(D)$ and $\boldsymbol{S}_a(D)$:

$$\boldsymbol{C}_{\text{le,zf}}(D) = \boldsymbol{S}_\nu^{-1}(D)\boldsymbol{S}_{ya}(D)\left[\boldsymbol{S}_{ya}^H(D^{-*})\boldsymbol{S}_\nu^{-1}(D)\boldsymbol{S}_{ya}(D)\right]^{-1}\boldsymbol{S}_a(D). \tag{4.54}$$

This expression may be preferable if the inverse of the noise spectrum can easily be obtained.

On the other hand, an expression equivalent to Equation (4.32) does not exist for the ZF MIMO LE. Thus, the ZF detector may be more difficult to implement in practice than the MMSE MIMO LE since the latter requires knowledge only about the power and crosscorrelation spectra of the signals y and a. These signals are directly available at the receiver when an a priori known training sequence is transmitted.

The above expressions describe the infinite-length ZF MIMO LE in the frequency-domain. The optimal finite-length ZF MIMO LE has been derived by van Etten [117] using a time-domain approach. The resulting equations resemble in some respects those stated in Section 4.2.1.2 for the MMSE equalizer.

4.3 MIMO Decision-Feedback Equalizer

Historically, equalizers in general and decision-feedback equalizers (DFE) in particular have been considered initially only for single-input single-output (SISO) and single user systems. The first description of the decision-feedback principle seems to be given in an article by Aein and Hancock in 1963 [6]. Since then, a wide variety of DFE's have been analyzed. Of particular interest to this work are multiple-input multiple-output (MIMO) DFE's [55, 27], which are a multidimensional extension to the basic SISO structure.

The vast majority of articles is concerned with the *conventional* DFE structure in which the decisions are directly fed into a linear feedback filter. Belfiore and Park [14] described an alternative DFE structure, termed the *noise-predictive* DFE, which calculates at first the difference between the decisions and the output of the DFE forward filter and then uses this signal as input to the feedback filter. A multidimensional extension, the *multiple-input multiple-output noise-predictive decision-feedback equalizer* (MIMO NP-DFE) has been described in a patent by Eleftheriou and Petersen [31]. Analytically and performance-wise, both the conventional and noise-predictive DFE's are identical. There are, however, practical and implementational differences. In addition, both structures complement each other from a pedagogical point of view since

their operation can be interpreted in different ways.

The decision-feedback equalizer (DFE) may be viewed as an extension to the linear equalizer (LE). In particular, the DFE structure (Figure 4.1) is obtained by adding a linear feedback filter to the structure of the LE (Figure 4.3). The input signals to the feedback filter are a function of the nonlinear, quantized estimates $\hat{\boldsymbol{a}}$ of the transmitted symbols. Since the fed-back estimates $\hat{\boldsymbol{a}}$ are obtained by a nonlinear operation in the decision device, the continuous-valued estimate $\tilde{\boldsymbol{a}}$ depends *nonlinearly* on the transmitted data $\boldsymbol{a}$. Therefore, the DFE has been classified as a nonlinear detector.

Despite the DFE being a nonlinear detector, its mathematical analysis performed in the following sections uses a crucial assumption under which the DFE becomes a linear detector. In particular, it is assumed that all decisions fed into the linear feedback filter are correct, i.e.

$$\hat{\boldsymbol{a}} = \boldsymbol{a}. \tag{4.55}$$

Strictly speaking, this assumption is not entirely true. It is, however, justified in situations when the error probability is relatively low ($< 10^{-3}$). Under these circumstances, the error incurred by the (wrong) assumption becomes small or even negligible. The primary driving force behind this strategy is the fact that the analysis of the DFE will become mathematically intractable if the nonlinear dependency of the estimate $\tilde{\boldsymbol{a}}$ on $\boldsymbol{a}$ is taken into account.

There are two different implementations of the DFE: the *conventional DFE* (C-DFE) and the *noise-predictive DFE* (NP-DFE). For the C-DFE, the input signals to the feedback filter are identical to the previous decisions $\hat{\boldsymbol{a}}$. On the other hand, the NP-DFE approximates the negative estimation error $-\breve{\boldsymbol{e}}$ at the output of the forward filter by taking the difference $\boldsymbol{a} - \breve{\boldsymbol{a}}$, which constitutes the input to the feedback filter.

The optimization criteria considered are again the *minimum mean-square error* (MMSE) and the *zero-forcing* (ZF) conditions. For the MMSE criterion, the objective is to determine the optimal forward and feedback matrix filters $\boldsymbol{C}_{\text{mmse}}$ and $\boldsymbol{B}_{\text{mmse}}$, respectively, which minimize the mean-square errors (MSE) $J_k \triangleq E[|e_k[n]|^2]$ for all

$k \in \mathcal{I}_N$ under the assumption that all decisions are correct ($\hat{\boldsymbol{a}} = \boldsymbol{a}$):

$$J_k(\boldsymbol{C}_{\mathrm{mmse}}, \boldsymbol{B}_{\mathrm{mmse}}) = \min_{\boldsymbol{C}, \boldsymbol{B}} J_k(\boldsymbol{C}, \boldsymbol{B}), \quad \forall k \in \mathcal{I}_N. \tag{4.56}$$

For the zero-forcing (ZF) condition, it is also required to minimize all MSE's under the additional constraint that all interference components in the residual error be zero.

The following sections describe both the conventional and the noise-predictive DFE for the MMSE and ZF criteria. Description and derivation of the DFE matrix filters are done in the frequency-domain. In addition, a time-domain analysis is provided for the MMSE MIMO C-DFE. The performance of the different structures is expressed in terms of the mean-square error (MSE).

4.3.1 Minimum Mean-Square Error Conventional Decision-Feedback Equalizer

The structure of the multiple-input multiple-output conventional decision-feedback equalizer (MIMO C-DFE) consists of three main elements: a $AK \times N$ linear forward matrix filter $\boldsymbol{C}_c$; a $N \times N$ linear feedback matrix filter $\boldsymbol{B}_c$; and a nonlinear decision device. Figure 4.4 shows the block diagram of the MIMO C-DFE. The corresponding vector model including the remaining system (Chapter 2) is given in Figure 4.5.

4.3.1.1 Frequency-Domain Approach

It appears that the first frequency-domain description of the MMSE MIMO C-DFE was formulated by Duel-Hallen [27]. She implicitly assumed that the receiver structure consists of a matched matrix filter (and possibly noise-whitening matched matrix filter) front-end, without explicitly showing that this structure is optimal. The combination of channel and receiver front-end results in a $N \times N$ equivalent discrete-time channel, for which she derived the MMSE MIMO C-DFE forward and feedback matrix filters in the frequency- or D-domain. The resulting equations depend on the channel transfer function and the noise characteristics, which have to be known in
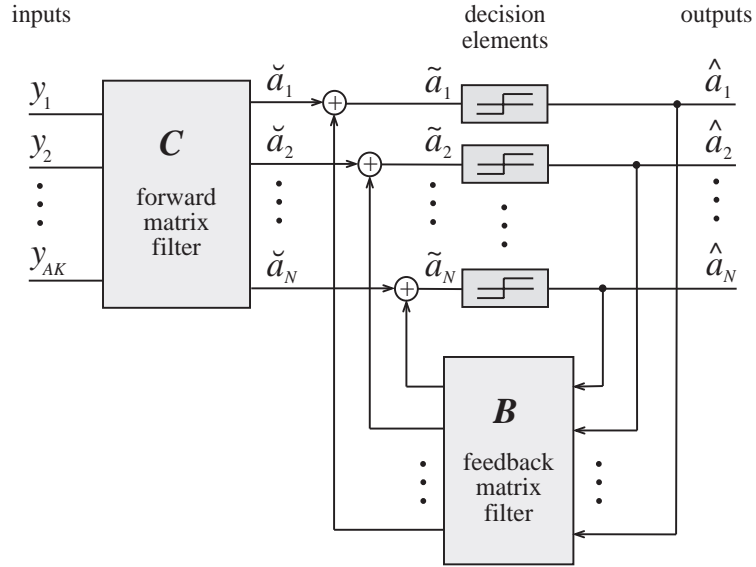
Figure 4.4: Block diagram of the MIMO C-DFE detector.

order to determine the equalizer filters.

Vandendorpe *et al.* finally proved under the assumption of white noise that the channel matched receiver front-end, $\boldsymbol{X}^H(D^{-*})$, is indeed the optimal structure [118]. They also calculated the remaining forward and feedback matrix filters of the MMSE MIMO C-DFE which are identical to those derived by Duel-Hallen [27].

For non-white, correlated noise, the final step may be made by applying van Etten's result [117] which shows that the non-white noise case can easily be transformed into the white noise case by including a noise-whitening filter as first equalizer element. The structure described by Vandendorpe *et al.* therefore has to be extended only by a noise-whitening matched filter whose transfer function is equal to the inverse of the noise power spectrum, $\boldsymbol{S}_\nu^{-1}(D)$.

Applying the results of Vandendorpe *et al.* and van Etten, the forward filter of the C-DFE may be described by a cascade of three elements

$$\boldsymbol{C}_{\text{c,mmse}}(D) = \boldsymbol{S}_\nu^{-1}(D)\boldsymbol{X}^H(D^{-*})\boldsymbol{L}_{\text{c,mmse}}(D) \tag{4.57}$$

where $\boldsymbol{S}_\nu^{-1}(D)$ is the noise-whitening matched filter, $\boldsymbol{X}^H(D^{-*})$ is the channel matched filter and $\boldsymbol{L}_{\text{c,mmse}}(D)$ is a $N \times N$ matrix filter. Considering the system block diagram
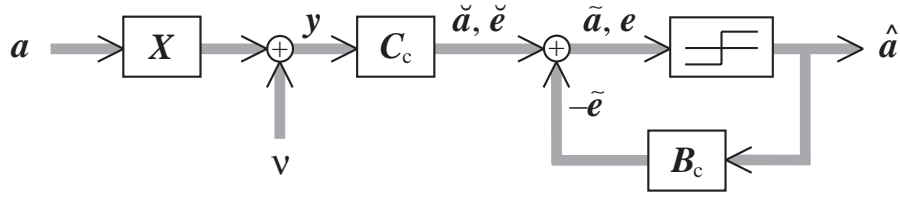
Figure 4.5: Vector block diagram of the system model followed by the MIMO C-DFE detector.

in Figure 4.5, the channel and the first two elements of the equalizer forward filter can be combined to the *equivalent channel* (Equation (4.16))

$$\boldsymbol{S}_x(D) \triangleq \boldsymbol{X}(D)\boldsymbol{S}_\nu^{-1}(D)\boldsymbol{X}^H(D^{-*}).$$

With these definitions, the system model (Figure 4.5) is represented equivalently by the block diagram shown in Figure 4.6. The signal $\boldsymbol{z}$ represents here the Gaussian noise at the output of the channel matched filter:

$$\boldsymbol{z}(D) \triangleq \boldsymbol{\nu}(D)\boldsymbol{S}_\nu^{-1}(D)\boldsymbol{X}^H(D^{-*}). \tag{4.58}$$

The power spectrum of this noise signal is

$$
\begin{aligned}
\boldsymbol{S}_z(D) \quad &\triangleq \quad E_M\left[\boldsymbol{z}^H(D^{-*})\boldsymbol{z}(D)\right] && (4.59)\\
&\overset{(4.58)}{=} \quad \boldsymbol{X}(D)\boldsymbol{S}_\nu^{-1}(D)E_M\left[\boldsymbol{\nu}^H(D^{-*})\boldsymbol{\nu}(D)\right]\boldsymbol{S}_\nu^{-1}(D)\boldsymbol{X}^H(D^{-*})\\
&\overset{(2.62)}{=} \quad \boldsymbol{S}_x(D). && (4.60)
\end{aligned}
$$

The optimal forward and feedback filters of the MMSE MIMO C-DFE have been derived by Duel-Hallen [27] for the equivalent system model shown in Figure (4.6). The results are based on the spectrum $\boldsymbol{Q}(D)$ defined in Equation (4.18). This spectrum may be factored into [126]

$$\boldsymbol{Q}(D) = \boldsymbol{\Psi}(D)\boldsymbol{G}^{-1}\boldsymbol{\Psi}^H(D^{-*}) \tag{4.61}$$

where $\boldsymbol{\Psi}(D)$ is a causal and stable matrix with $\boldsymbol{\Psi}(D) = \sum_{n=0}^{\infty} \boldsymbol{\Psi}[n]D^n$. $\boldsymbol{\Psi}[0]$ is con-
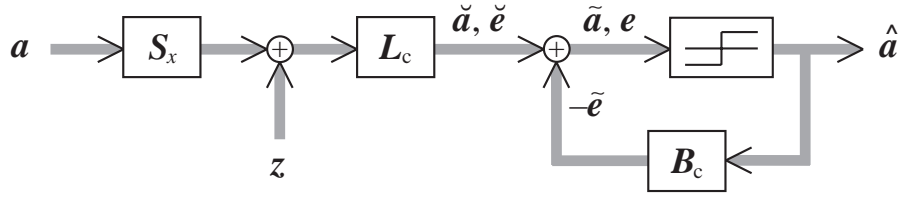
Figure 4.6: Vector block diagram of the equivalent system model including MMSE MIMO C-DFE detector.

strained to be an upper triangular matrix with ones on the main diagonal. $\boldsymbol{G}^{-1}$ is a diagonal matrix independent on D.

For the calculation of the optimal equalizer, it is necessary to perform the spectral factorization (4.61) on the given matrix function $\boldsymbol{Q}(D)$ and to determine the purely causal part $\boldsymbol{\Psi}(D)$ as well as the diagonal matrix $\boldsymbol{G}$. One algorithm is described by Wiener and Masani [127], however, their iterative method converges very slowly and cannot be recommended in practice. Harris and Davis derived a very fast converging algorithm [43] which requires usually less than 10 iterations. Nonetheless, the method is computationally very intensive. Appendix I describes the algorithm and discusses practical issues for performing a matrix spectral factorization.

The forward and feedback filters of the MMSE MIMO C-DFE are given by [27]

$$\boldsymbol{L}_{\text{c,mmse}}(D) = \boldsymbol{\Psi}^{-H}(D^{-*})\boldsymbol{G} \tag{4.62}$$

$$\boldsymbol{B}_{\text{c,mmse}}(D) = \boldsymbol{I}_N - \boldsymbol{\Psi}(D). \tag{4.63}$$

Using the above expressions it can easily be shown that the spectrum of the estimation error $\boldsymbol{e}$ is

$$\boldsymbol{S}_e(D) = \boldsymbol{G}. \tag{4.64}$$

This shows that the estimation error at the input to the decision device is completely uncorrelated and white since its spectrum is constant (it does not depend on D) and all off-diagonal elements are equal to zero. In fact, the continuous-valued estimates $\tilde{\boldsymbol{a}}$ are optimal unless additional a priori information about the transmitted data is exploited (in particular the knowledge that the transmitted data symbols belong to

a known discrete alphabet).

The individual MMSE values may now easily be determined by applying Equation (4.12). The result is simply

$$J_{k,\text{c,mmse}} = [\boldsymbol{G}]_{kk} \,. \tag{4.65}$$

In general, it is necessary to perform a matrix spectral factorization in order to determine the individual MMSE's J_k. However, a special case exists for the geometric average of the individual MMSE's

$$\bar{J}_\Pi \triangleq \sqrt[N]{\prod_{k=1}^{N} J_k}. \tag{4.66}$$

Duel-Hallen has shown [27] that $\bar{J}_\Pi$ can be calculated for the MMSE MIMO C-DFE with the closed-form expression

$$\bar{J}_\Pi = \exp\left\{-\frac{1}{N} \int_0^1 \ln\left(\det\left[\boldsymbol{Q}(e^{-j2\pi\check{f}})\right]\right) d\check{f}\right\}. \tag{4.67}$$

Note that this is the multiuser generalization of Salz' closed-form expression for the MMSE of the single-input single-output DFE [104, Eqn.(13)]. For $N = 1$, the individual MMSE and the geometrical average MMSE is identical and the matrix $\boldsymbol{Q}(D)$ reduces to a scalar function. Salz' formula results then directly from Equation (4.67).

It may be more convenient in practice to express the forward and feedback filters in terms of available or easily measurable quantities. In analogy to Section 4.2.1.1, the results are presented with respect to the power spectrum $\boldsymbol{S}_y(D)$ of the received signal $\boldsymbol{y}$ (Equation (4.27)) and the cross-power spectrum $\boldsymbol{S}_{ya}(D)$ between the received signal and the transmitted data signal $\boldsymbol{a}$. (Equation (4.28)). Let us start with the observation that $\boldsymbol{Q}^{-1}(D)$ may be expressed in the form

$$\boldsymbol{Q}^{-1}(D) = \boldsymbol{S}_a(D) - \boldsymbol{S}_{ya}^H(D^{-*})\boldsymbol{S}_y^{-1}(D)\boldsymbol{S}_{ya}(D). \tag{4.68}$$

This follows directly from substitution of Equations (4.22) and (4.34) into (4.17).

Considering Equations (4.15), (4.17) and (4.61), it occurs that the forward matrix filter of the MMSE MIMO LE may be written as

$$\boldsymbol{C}_{\text{le,mmse}}(D) = \boldsymbol{S}_\nu^{-1}(D)\boldsymbol{X}^H(D^{-*})\boldsymbol{\Psi}^{-H}(D^{-*})\boldsymbol{G}\boldsymbol{\Psi}^{-1}(D). \qquad (4.69)$$

Comparing this expression with Equations (4.57) and (4.62) describing the forward filter of the MMSE MIMO C-DFE it follows that

$$\boldsymbol{C}_{\text{le,mmse}}(D) = \boldsymbol{C}_{\text{c,mmse}}(D)\boldsymbol{\Psi}^{-1}(D). \qquad (4.70)$$

Applying this relationship to Equation (4.32) yields for the forward matrix filter of the MMSE MIMO C-DFE the final expression

$$\boldsymbol{C}_{\text{c,mmse}}(D) = \boldsymbol{S}_y^{-1}(D)\boldsymbol{S}_{ya}(D)\boldsymbol{\Psi}(D). \qquad (4.71)$$

The feedback matrix filter may still be calculated using Equation (4.63).

Consider now the practical implementation of the equalizers via approximation of the forward filters by FIR filters. It can be observed from Equation (4.70) that the forward filter (FF) of the MMSE MIMO LE is identical to the MMSE MIMO C-DFE FF $\boldsymbol{C}_{\text{c,mmse}}(D)$ followed by the purely causal matrix filter $\boldsymbol{\Psi}^{-1}(D)$. Thus, for a comparable truncation error, the FIR approximation of the LE FF requires longer delay lines (i.e. more tap weights) than that of C-DFE FF. In other words, the forward filter of the MMSE MIMO C-DFE is shorter than the forward filter of the MIMO LE.

4.3.1.2 Time-Domain Approach

Expressions for the MMSE and the optimal matrix filters of the MMSE MIMO C-DFE are provided. A detailed time-domain analysis of this equalizer is given in Appendix G.2.

The MIMO C-DFE is described by linear forward and feedback filter matrices $\boldsymbol{C}[n]$ and $\boldsymbol{B}[n]$. Let us assume that the time-lengths of these filters are given by the integer numbers M_C and M_B, respectively. Hence, the equalizer is fully de-

scribed by the matrices $\boldsymbol{C}[0], \boldsymbol{C}[1], \boldsymbol{C}[2], \ldots, \boldsymbol{C}[M_C - 1]$ for the forward part and $\boldsymbol{B}[0], \boldsymbol{B}[1], \boldsymbol{B}[2], \ldots, \boldsymbol{B}[M_B - 1]$ for the feedback part.

Let us define the *extended equalizer coefficient matrix*

$$
\boldsymbol{P} \triangleq \begin{bmatrix} \boldsymbol{C}[M_C - 1] \\ \boldsymbol{C}[M_C - 2] \\ \boldsymbol{C}[M_C - 3] \\ \vdots \\ \boldsymbol{C}[0] \\ \boldsymbol{B}[M_B - 1] \\ \boldsymbol{B}[M_B - 2] \\ \boldsymbol{B}[M_B - 3] \\ \vdots \\ \boldsymbol{B}[0] \end{bmatrix}
\tag{4.72}
$$

which contains all equalizer coefficients to be optimized.

Due to causality reasons, the zeroth feedback sample matrix $\boldsymbol{B}[0]$ is constrained to be zero on the main diagonal and half of its side-diagonal elements must be zero as well. Without loss of generality, $\boldsymbol{B}[0]$ is chosen to be an upper triangular matrix with zeros on the main diagonal. Hence, the extended equalizer coefficient matrix $\boldsymbol{P}$ may be represented in the form

$$
\boldsymbol{P} = \begin{bmatrix} \boldsymbol{p}_1^H & \boldsymbol{p}_2^H & \boldsymbol{p}_3^H & \cdots & \boldsymbol{p}_N^H \\ \boldsymbol{0}_N^H & \boldsymbol{0}_{N-1}^H & \boldsymbol{0}_{N-2}^H & \cdots & \boldsymbol{0}_1^H \end{bmatrix}
\tag{4.73}
$$

where $\boldsymbol{0}_i^H$ is an i-dimensional column vector in which each element is equal to zero (Table A.7) and the column vector $\boldsymbol{p}_k^H$ is defined by

$$
\boldsymbol{p}_k^H \triangleq [\boldsymbol{P}]_{[1(1)L_k],k} \,.
\tag{4.74}
$$

The matrix function $[\ldots]_{[f(s)l],c}$ is defined in Tables A.3, A.7 and Equation (A.8).

Consequently, the column vector $\boldsymbol{p}_k^H$ is obtained by taking the first L_k elements in the k-th column of the matrix $\boldsymbol{P}$ (or, equivalently, by taking all elements in the k-th column of $\boldsymbol{P}$ except for the last $N - k + 1$ components). L_k is a positive integer number defining the lengths of the above vectors:

$$L_k = M_C A K + M_B N - N + k - 1. \tag{4.75}$$

It is shown in Appendix G.2 that the optimal equalizer parameters with respect to the MMSE criterion can be calculated with the expression

$$\boldsymbol{p}_{k,\text{c,mmse}}^H = \boldsymbol{R}_{u,k}^{-1} \boldsymbol{r}_{au,k}^H. \tag{4.76}$$

In addition, the MMSE of the k-user is

$$J_k = 1 - \boldsymbol{r}_{au,k} \boldsymbol{R}_{u,k}^{-1} \boldsymbol{r}_{au,k}^H \tag{4.77}$$

where the $L_k \times 1$ column vector $\boldsymbol{r}_{au,k}^H$ and the $L_k \times L_k$ matrix $\boldsymbol{R}_{u,k}$ are defined in Appendix G.2.

4.3.2 Minimum Mean-Square Error Noise-Predictive Decision-Feedback Equalizer

Belfiore [13, 14] described an alternative structure to the conventional DFE. This structure is referred to as *noise-predictive decision-feedback equalizer* (NP-DFE). It differs from the conventional DFE (C-DFE) by the input signal to the feedback block. While the C-DFE puts the decisions directly into the feedback filter, the NP-DFE uses instead the difference between the decisions and the output signal of the DFE forward filter.

Eleftheriou and Petersen [31] developed a multiple-input multiple-output (MIMO) extension to the basic single-input single-output (SISO) NP-DFE of Belfiore and Park (Figure 4.7). In the MIMO case, vector-valued signals and matrix filters replace the scalar-valued signals and regular filters of the SISO NP-DFE. Figure 4.8 shows the
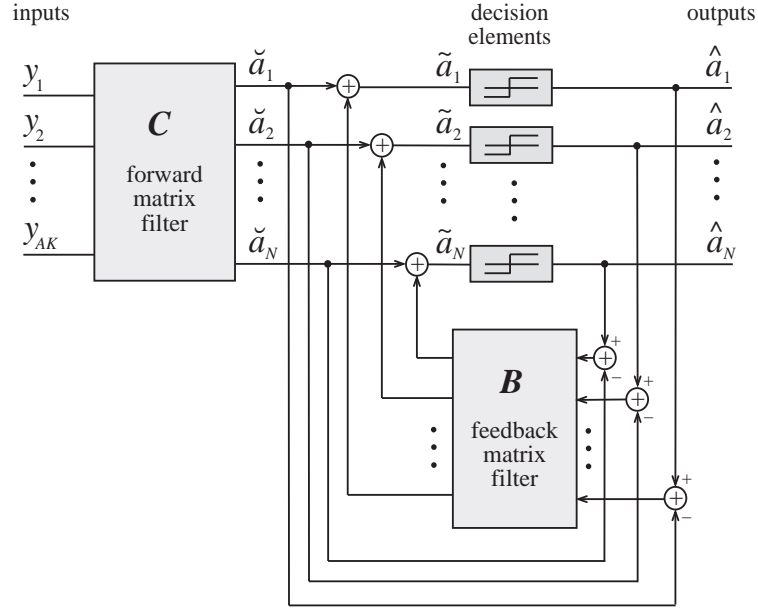
Figure 4.7: Block diagram of the MIMO MMSE NP-DFE.

multiuser system model containing implicitly the transmitters of several users, the radio channels and a multi-element receiver including a MIMO NP-DFE. It can be seen that the input signal to the feedback filter matrix is the negative approximation $-\hat{\boldsymbol{e}}$ of the estimation error $\breve{\boldsymbol{e}}$. Provided that all decisions are correct $(\hat{\boldsymbol{a}} = \boldsymbol{a})$, the estimated and real error signals at the forward filter output are identical, i.e.

$$\hat{\boldsymbol{e}} = \breve{\boldsymbol{e}}. \tag{4.78}$$

The past and some present symbols of the signal $-\hat{\boldsymbol{e}}$ are used in the purely causal feedback matrix filter in order to predict or extrapolate the current value of the negative error $-\breve{\boldsymbol{e}}$. Hence, the feedback block can be interpreted as a MIMO linear prediction filter. This opens the powerful prediction theory of multivariate stochastic processes developed by Wiener and Masani [126, 127] for the analysis of the MIMO NP-DFE.

The MMSE criterion and a frequency-domain approach is used in this section to analyze the MIMO NP-DFE. The optimal forward and feedback matrix filters are derived for the general system described in Chapter 2. It is shown that the forward matrix filters of both the MMSE MIMO NP-DFE and the MMSE MIMO C-DFE
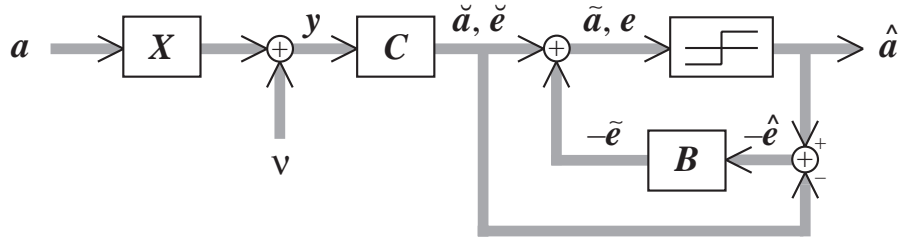
Figure 4.8: Vector block diagram including the system model and the MIMO MMSE NP-DFE detector.

consist at the front-end of a noise-whitening matched filter followed by a channel matched filter and a $N \times N$ symbol-rate filter. This is the same result as obtained by Vandendorpe *et al.* [118], except that the derivation is different. The expressions for the forward and feedback filters are identical to those derived by Eleftheriou and Petersen [31]. However, their results have been obtained for the less general case of asynchronous CDMA over flat fading (frequency non-selective) channels. Furthermore, a receiver front-end consisting of matched filters was implicitly assumed without proving the optimality of this configuration.

Let us now start with the frequency-domain analysis of the MMSE MIMO NP-DFE. Consider the system shown in Figure 4.8. The discrete-time sequences $a_i[n]$ ($i \in \mathcal{I}_N$), transmitted from N users, define the signal vector $\boldsymbol{a} = [a_1, a_2, \ldots, a_N]$. This signal is transmitted through the combined channel matrix filter $\boldsymbol{X}$, which has N inputs and AK outputs. The NP-DFE receiver consists of a forward matrix filter $\boldsymbol{C}$ with AK inputs and N outputs and a $N \times N$ feedback matrix filter $\boldsymbol{B}$. The input signal to the receiver, $\boldsymbol{y}$, is the superposition of the channel output signal and additive noise $\boldsymbol{\nu}$ (Section 2.4). Each component of the final output signal $\hat{\boldsymbol{a}} = [\hat{a}_1, \hat{a}_2, \ldots, \hat{a}_N]$ represents the quantized estimate of the corresponding transmitted sequence in $\boldsymbol{a}$.

The input and noise signals are assumed to be uncorrelated. $\boldsymbol{S}_a(D)$, $\boldsymbol{S}_\nu(D)$ and $\boldsymbol{S}_{a\nu}(D)$ are the auto- and cross-correlation spectra of these signals. Their definitions are given by Equations (2.61), (2.62) and (2.63).

Define the following internal receiver signals (Figure 4.8):

$$\breve{\boldsymbol{a}}(D) = \boldsymbol{y}(D)\boldsymbol{C}(D) \tag{4.79}$$

$$\breve{\boldsymbol{e}} = \breve{\boldsymbol{a}} - \boldsymbol{a} \tag{4.80}$$

$$\hat{\boldsymbol{e}} = \breve{\boldsymbol{a}} - \hat{\boldsymbol{a}} \tag{4.81}$$

$$\tilde{\boldsymbol{e}}(D) = \hat{\boldsymbol{e}}(D)\boldsymbol{B}(D) \tag{4.82}$$

$$\tilde{\boldsymbol{a}} = \breve{\boldsymbol{a}} - \tilde{\boldsymbol{e}} \tag{4.83}$$

$$\boldsymbol{e} = \tilde{\boldsymbol{a}} - \boldsymbol{a}$$

$$= \breve{\boldsymbol{e}} - \tilde{\boldsymbol{e}}. \tag{4.84}$$

$\breve{\boldsymbol{a}}$ is the output of the forward matrix filter. The difference between $\breve{\boldsymbol{a}}$ and the transmitted signal defines the error signal $\breve{\boldsymbol{e}}$. Assuming that all previous decisions are correct (i.e. $\hat{\boldsymbol{a}} = \boldsymbol{a}$), the input signal to the feedback filter is identical to the negative value of the error $\breve{\boldsymbol{e}}$ (Equation (4.78)). Thus, the causal feedback filter $\boldsymbol{B}$ tries to predict the negative value of the present error vector, $-\breve{\boldsymbol{e}}[n]$, from the past and some present samples of $-\hat{\boldsymbol{e}} = -\breve{\boldsymbol{e}}$. After that, the input signal to the quantizers, $\tilde{\boldsymbol{a}}$, is obtained by adding the negative predicted error $-\tilde{\boldsymbol{e}}$ to the forward filter output $\breve{\boldsymbol{a}}$. $\boldsymbol{e}$ is the error in the continuous-valued signal estimate $\tilde{\boldsymbol{a}}$ to be quantized.

Consider that the decisions in the quantizer are made in the same order as in previous sections: At time n, the first component of $\tilde{\boldsymbol{a}}[n]$, $\tilde{a}_1[n]$, is quantized first, followed by the second component $\tilde{a}_2[n]$ and so on, until finally a decision is made on $\tilde{a}_N[n]$. After that, the quantization proceeds in the same fashion for the next input vector $\tilde{\boldsymbol{a}}[n+1]$. Note that at the time when $\bar{a}_i[n]$ is to be quantized, not only all past decisions $\hat{\boldsymbol{a}}[n-m]$ $(m > 0)$ are available to the feedback filter but also some present decisions $\hat{a}_k[n]$ $(k < i)$ may be used. Other decisions have not been made yet and are not available to the causal feedback filter $\boldsymbol{B}$.

The linear filter matrices $\boldsymbol{C}$ and $\boldsymbol{B}$ which satisfy the MMSE criterion (4.56) may be obtained by applying the orthogonality principle [46]. In particular, the error in the final continuous-valued estimate $\tilde{\boldsymbol{a}}$ has to be statistically orthogonal to all input symbols of both forward and feedback filters. If e_k and $\breve{e}_i$ are the k-th and i-th

component of $\boldsymbol{e}$ and $\boldsymbol{\breve{e}}$, respectively, the orthogonality principle can be formulated for the MMSE MIMO NP-DFE in three equations:

$$E[y_l^*[n-m]e_k[n]] = 0, \quad \forall m \in \mathbb{Z}; \ l \in \mathcal{I}_{AK}, \ k \in \mathcal{I}_N \tag{4.85}$$

$$E[\breve{e}_i^*[n-m]e_k[n]] = 0, \quad \forall m > 0 \ (m \in \mathbb{N}); \ i, k \in \mathcal{I}_N \tag{4.86}$$

$$E[\breve{e}_i^*[n]e_k[n]] = 0, \quad \forall k > i; \ i, k \in \mathcal{I}_N \tag{4.87}$$

where $\mathbb{Z}$ is the set of all positive and negative integer numbers, while $\mathbb{N}$ contains only all positive integers (see Table A.7). y_l is the l-th component of $\boldsymbol{y}$.

Let us define the cross-correlation functions

$$\boldsymbol{R}_{ye}[m] \triangleq E[\boldsymbol{y}^H[n-m]\boldsymbol{e}[n]] \tag{4.88}$$

$$\boldsymbol{R}_{\breve{e}e}[m] \triangleq E[\boldsymbol{\breve{e}}^H[n-m]\boldsymbol{e}[n]]. \tag{4.89}$$

The orthogonality principle expressed in Equations (4.85) to (4.87) can then alternatively be formulated as

$$\boldsymbol{R}_{ye}[m] = \boldsymbol{O}_{AK \times N}, \quad \forall m \in \mathcal{Z} \tag{4.90}$$

$$\boldsymbol{R}_{\breve{e}e}[m] = \boldsymbol{O}_{N \times N}, \quad \forall m > 0 \tag{4.91}$$

$$\boldsymbol{R}_{\breve{e}e}[0] \text{ is a lower triangular matrix.} \tag{4.92}$$

The last two equations reflect the fact that the feedback filter can only utilize decisions already made. This ensures the causality of $\boldsymbol{B}$.

The cross spectra

$$\boldsymbol{S}_{ye}(D) \triangleq E_M\left[\boldsymbol{y}^H(D^{-*})\boldsymbol{e}(D)\right] \tag{4.93}$$

$$\boldsymbol{S}_{\breve{e}e}(D) \triangleq E_M\left[\boldsymbol{\breve{e}}^H(D^{-*})\boldsymbol{e}(D)\right] \tag{4.94}$$

are the D-transforms of the cross-correlation functions $\boldsymbol{R}_{ye}$ and $\boldsymbol{R}_{\breve{e}e}$, respectively.

Transforming the orthogonality relations (4.90) to (4.92) into the D-domain yields

$$\boldsymbol{S}_{ye}(D) = \boldsymbol{O}_{AK \times N} \tag{4.95}$$

$$\{\boldsymbol{S}_{\breve{e}e}(D)\}^{+} = \boldsymbol{O}_{N \times N} \tag{4.96}$$

where $\{\boldsymbol{F}(D)\}^{+}$ denotes the purely causal part of the matrix-valued function $\boldsymbol{F}(D) = \sum_{m=-\infty}^{\infty} \boldsymbol{F}[m]D^m$. The purely causal part contains only the positive time samples and the upper triangular part of the zeroth time sample. Thus, the purely causal part of $\boldsymbol{F}(D)$ is defined by

$$\{\boldsymbol{F}(D)\}^{+} \triangleq \boldsymbol{F}^{\blacktriangleleft}[0] + \sum_{m=1}^{\infty} \boldsymbol{F}[m]D^m \tag{4.97}$$

where $\boldsymbol{F}^{\blacktriangleleft}[0]$ is the upper triangular part of $\boldsymbol{F}[0]$ with zeros on and below the main diagonal.

An expression for $\boldsymbol{S}_{ye}(D)$ can be obtained by expanding $E_M[\boldsymbol{y}^H(D^{-*})\boldsymbol{e}(D)]$ with Equations (4.84), (4.82), (4.78), (4.80) and (4.79):

$$\boldsymbol{S}_{ye}(D) = \{\boldsymbol{S}_y(D)\boldsymbol{C}(D) - \boldsymbol{S}_{ya}(D)\}[\boldsymbol{I}_N - \boldsymbol{B}(D)] \tag{4.98}$$

where the spectra $\boldsymbol{S}_y(D) = E_M[\boldsymbol{y}^H(D^{-*})\boldsymbol{y}(D)]$ and $\boldsymbol{S}_{ya}(D) = E_M[\boldsymbol{y}^H(D^{-*})\boldsymbol{a}(D)]$ are the power spectrum of the equalizer input signal and the cross-power spectrum between the equalizer input and the transmitted data, respectively. $\boldsymbol{S}_y(D)$ and $\boldsymbol{S}_{ya}(D)$ can be calculated according to Equations (4.27) and (4.28).

Applying Equations (4.80), (4.79) to $E_M[\breve{\boldsymbol{e}}^H(D^{-*})\boldsymbol{e}(D)]$, noting that $\boldsymbol{S}_{ye}(D) = \boldsymbol{O}_{AK \times N}$, and substituting Equations (4.78) and (4.79) through (4.84) into the remaining term yields

$$\boldsymbol{S}_{\breve{e}e}(D) = [\boldsymbol{S}_a(D) - \boldsymbol{S}_{ya}^H(D^{-*})\boldsymbol{C}(D)][\boldsymbol{I}_N - \boldsymbol{B}(D)]. \tag{4.99}$$

Comparing Equations (4.95), (4.98) and (4.96), (4.99), it follows that the orthog-

onality principle may be equivalently formulated as

$$\{\boldsymbol{S}_y(D)\boldsymbol{C}(D) - \boldsymbol{S}_{ya}(D)\}[\boldsymbol{I}_N - \boldsymbol{B}(D)] = \boldsymbol{O}_{AK \times N} \tag{4.100}$$

$$\left\{[\boldsymbol{S}_a(D) - \boldsymbol{S}_{ya}^H(D^{-*})\boldsymbol{C}(D)][\boldsymbol{I}_N - \boldsymbol{B}(D)]\right\}^+ = \boldsymbol{O}_{N \times N}. \tag{4.101}$$

Equation (4.100) can be solved by requiring that the term in the curly brackets be equal to the $AK \times N$ null matrix. This leads to the same optimality condition as that for the forward filter of the MMSE MIMO linear equalizer (Equation (4.30)). Thus, the forward matrix filters of the MMSE MIMO LE and the MMSE MIMO NP-DFE are identical. In particular, we may calculate the optimal forward filter by either of the following two expressions:

$$\boldsymbol{C}_{\mathrm{np,mmse,1}}(D) = \boldsymbol{S}_\nu^{-1}(D)\boldsymbol{X}^H(D^{-*})\boldsymbol{L}_{\mathrm{np,mmse}}(D). \tag{4.102}$$

$$\boldsymbol{C}_{\mathrm{np,mmse,2}}(D) = \boldsymbol{S}_y^{-1}(D)\boldsymbol{S}_{ya}(D) \tag{4.103}$$

where

$$\boldsymbol{L}_{\mathrm{np,mmse}}(D) = \left[\boldsymbol{S}_x(D) + \boldsymbol{S}_a^{-1}(D)\right]^{-1}. \tag{4.104}$$

With knowledge of the forward filter (4.103), the feedback filter can immediately be obtained by fulfilling the second orthogonality condition (4.101). Combining both expressions yields

$$\left\{[\boldsymbol{S}_a(D) - \boldsymbol{S}_{ya}^H(D^{-*})\boldsymbol{S}_y^{-1}(D)\boldsymbol{S}_{ya}(D)][\boldsymbol{I}_N - \boldsymbol{B}(D)]\right\}^+ = \boldsymbol{O}_{N \times N}. \tag{4.105}$$

Note that the term inside the first rectangular brackets is equal to the inverse of $\boldsymbol{Q}(D)$ (Equation (4.68)), which has been defined in Equation (4.18):

$$\boldsymbol{Q}^{-1}(D) = \boldsymbol{S}_a(D) - \boldsymbol{S}_{ya}^H(D^{-*})\boldsymbol{S}_y^{-1}(D)\boldsymbol{S}_{ya}(D).$$

It is possible to factorize $\boldsymbol{Q}(D)$ spectrally according to Equation (4.61) into

$$\boldsymbol{Q}(D) = \boldsymbol{\Psi}(D)\boldsymbol{G}^{-1}\boldsymbol{\Psi}^H(D^{-*})$$

where $\boldsymbol{\Psi}(D)$ is a causal and stable matrix with $\boldsymbol{\Psi}(D) = \boldsymbol{\Psi}[0] + \boldsymbol{\Psi}[1]D + \boldsymbol{\Psi}[2]D^2 + \ldots$. The zeroth sample matrix $\boldsymbol{\Psi}[0]$ is constrained to be an upper triangular matrix with ones on the main diagonal. $\boldsymbol{G}^{-1}$ is a diagonal matrix which does not depend on D. With this it can easily be shown that the optimum feedback filter, which solves Equation (4.105), is

$$\boldsymbol{B}_{\mathrm{np,mmse}}(D) = \boldsymbol{I}_N - \boldsymbol{\Psi}(D). \tag{4.106}$$

The expression in Equation (4.102) shows that the optimal forward matrix filter of the MMSE MIMO NP-DFE may be realized by a cascade consisting of a noise-whitening matched filter $\boldsymbol{S}_\nu^{-1}(D)$ followed by a channel matched filter $\boldsymbol{X}^H(D^{-*})$ and a $N \times N$ matrix filter $\boldsymbol{L}_{\mathrm{np,mmse}}(D)$. The optimal structure of the MMSE MIMO C-DFE can also be realized in this form since NP-DFE and conventional DFE are equivalent. This can be shown most easily with the block diagrams in Figure 4.9. The first block diagram (a) represents the NP-DFE redrawn such that both the output of the forward filter, $\breve{\boldsymbol{a}}$, and the decisions $\hat{\boldsymbol{a}}$ pass separately through the same feedback filter $\boldsymbol{B}$. Figure 4.9 (b) displays the conventional DFE. Comparing both figures, it is obvious that there exists a one to one relationship between the two different DFE structures. In particular, the feedback filters of both the NP-DFE and the C-DFE are identical (see also Equations (4.63) and (4.106)). For the forward filters, the unique relationship is

$$\boldsymbol{C}_{\mathrm{c}}(D) = \boldsymbol{C}_{\mathrm{np}}(D)[\boldsymbol{I}_N - \boldsymbol{B}(D)]. \tag{4.107}$$

Note that the expressions in Equation (4.71) and (4.103), (4.106) satisfy this condition. This completes the proof for the optimal structures of the C-DFE and NP-DFE forward filter matrices.
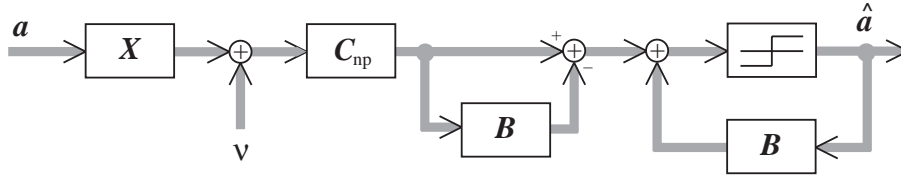
(a) equivalent block diagram for the NP-DFE
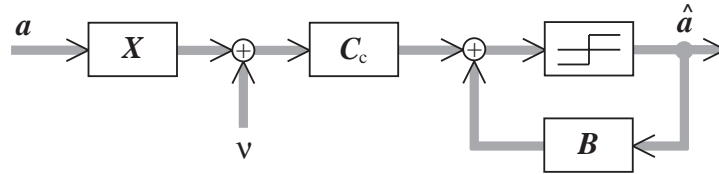
(b) conventional DFE

Figure 4.9: System block diagram for (a) the MIMO NP-DFE and (b) the conventional DFE.

4.3.3 Zero-Forcing Decision-Feedback Equalizers

The zero-forcing decision-feedback equalizers (ZF DFE) minimize the mean-square error (MSE) under the constraint that the residual interference in the input signal to the decision device be completely nulled out. The ZF DFE structure may be realized in conventional (Figure 4.5) or noise-predictive form (Figure 4.8). The following results assume explicitly a receiver front-end structure consisting of a noise-whitening matched filter, $\boldsymbol{S}_\nu^{-1}(D)$, and a channel matched filter $\boldsymbol{X}^H(D^{-*})$. The optimality of this configuration will not be proven, i.e. it is not shown that the minimum MSE under a ZF constraint can be achieved with this particular front-end structure. Given the aforementioned configuration, however, the following filters are optimal. The optimal, infinite-length matrix filters are described in the frequency domain.

The results are based on the $N \times N$ equivalent channel $\boldsymbol{S}_x$ which is defined in Equation (4.16). Since $\boldsymbol{S}_x(D)$ is non-negative definite and Hermitian on the unit circle, it may be factored into [126, Theorem 7.13]

$$\boldsymbol{S}_x(D) = \boldsymbol{\Psi}_x(D)\boldsymbol{G}_{\text{zf}}^{-1}\boldsymbol{\Psi}_x^H(D^{-*}) \qquad (4.108)$$

where $\boldsymbol{\Psi}_x(D)$ is a causal and stable matrix with $\boldsymbol{\Psi}_x(D) = \sum_{n=0}^{\infty} \boldsymbol{\Psi}_x[n]D^n$. $\boldsymbol{\Psi}_x[0]$ is

constrained to be an upper triangular matrix with ones on the main diagonal. $\boldsymbol{G}_{\mathrm{zf}}^{-1}$ is a non-negative definite diagonal matrix independent on D.

Let us start with the ZF MIMO C-DFE shown in Figure 4.5. Adapting the results of Duel-Hallen [29] to the system model of Section 2.4 results in the following expressions for the optimal forward and feedback filters:

$$\boldsymbol{C}_{\mathrm{c,zf}}(D) = \boldsymbol{S}_{\nu}^{-1}(D)\boldsymbol{X}^{H}(D^{-*})\boldsymbol{L}_{\mathrm{c,zf}}(D) \tag{4.109}$$

$$\boldsymbol{L}_{\mathrm{c,zf}}(D) = \boldsymbol{\Psi}_{x}^{-H}(D^{-*})\boldsymbol{G}_{\mathrm{zf}} \tag{4.110}$$

$$\boldsymbol{B}_{\mathrm{c,zf}}(D) = \boldsymbol{I}_{N} - \boldsymbol{\Psi}_{x}(D). \tag{4.111}$$

It has been shown before that the noise-predictive and conventional DFE structures are equivalent: the feedback filters are identical and the forward filters are related through Equation (4.107). As a result, the optimum filters of the ZF MIMO NP-DFE (Figure 4.8) are given by

$$\boldsymbol{C}_{\mathrm{np,zf}}(D) = \boldsymbol{S}_{\nu}^{-1}(D)\boldsymbol{X}^{H}(D^{-*})\boldsymbol{L}_{\mathrm{np,zf}}(D) \tag{4.112}$$

$$\boldsymbol{L}_{\mathrm{np,zf}}(D) = \boldsymbol{S}_{x}^{-1}(D) \tag{4.113}$$

$$\boldsymbol{B}_{\mathrm{np,zf}}(D) = \boldsymbol{I}_{N} - \boldsymbol{\Psi}_{x}(D). \tag{4.114}$$

Comparing Equations (4.52) and (4.113) shows that the ZF MIMO linear and noise-predictive equalizer have identical forward matrix filters. Hence, the ZF MIMO LE may be extended by a noise-predictive feedback part without changing the forward filter.

The performance of both ZF MIMO DFE structures is identical. It can easily be shown that the power spectrum of the error signal is $\boldsymbol{S}_{e}(D) = \boldsymbol{G}_{\mathrm{zf}}$. Since $\boldsymbol{G}_{\mathrm{zf}}$ is a diagonal matrix independent on D, the error signal $\boldsymbol{e}$ is white and different components of $\boldsymbol{e}$ are uncorrelated. According to Equation (4.12), the minimum mean-square errors $J_{k,\mathrm{dfe,zf}}$ $(k \in \mathcal{I}_{N})$ are

$$J_{k,\mathrm{dfe,zf}} = [\boldsymbol{G}_{\mathrm{zf}}]_{kk} \tag{4.115}$$

where the function $[\ldots]_{kk}$ is defined in Table A.3.

4.4 Relationship between SINR and MMSE

The Saltzberg upper bound (Section 3.3) may be applied in order to obtain an estimate of the error probability of a multiuser system with MIMO equalizer. The expression for the error probability bound (3.73) is expressed in terms of the signal-to-interference-and-noise ratio (SINR), Φ_k, at the equalizer output. On the other hand, the measure of performance for the equalizers has been the minimum mean-square error (MMSE) J_k (4.10) in previous sections. In the following, a relationship between SINR and MMSE is derived for the MMSE and ZF equalizers. This SINR/MMSE relationship is valid under the crucial assumption that the data signals a_i $(i \in \mathcal{I}_N)$ are wide-sense stationary stochastic processes which are mutually and temporally uncorrelated with zero mean (see Section A.6).

The availability of a SINR/MMSE expression leads to simple bounds or approximations for the error probability, which are solely based on the MMSE. The MMSE, on the other hand, can be determined for each equalizer with the equations given in previous sections.

It is well known that there exists a unique relationship between SINR and MMSE for the single-input single-output (SISO) MMSE linear and decision-feedback equalizer [99]. The following analysis provides a proof that the same relationship holds also for both the MMSE MIMO LE and DFE[10]. This includes in particular the derivation of an expression linking the MMSE and the bias coefficient for both MIMO equalizers.

The ZF equalizers cancel out all interference. Hence, the SINR is equal to the SNR at the equalizer output. In the SISO case, the SNR is simply the inverse of the MMSE [99]. It is briefly shown in the following that the same is also true for the ZF MIMO LE and DFE.

According to the multiuser system model including a MIMO LE or DFE (Fig-

---

[10]For the DFE, the SINR/MMSE expression is formally correct only under the assumption that all decisions used in the feedback filter are correct.

ure 4.1), the output signal of the equalizer is

$$\tilde{\boldsymbol{a}}(D) = \boldsymbol{a}(D)\boldsymbol{H}(D) + \hat{\boldsymbol{a}}(D)\boldsymbol{B}(D) + \boldsymbol{\zeta}(D) \tag{4.116}$$

where $\boldsymbol{B}(D)$ is an optional feedback filter and

$$\boldsymbol{H}(D) \triangleq \boldsymbol{X}(D)\boldsymbol{C}(D) \tag{4.117}$$

$$\boldsymbol{\zeta}(D) \triangleq \boldsymbol{\nu}(D)\boldsymbol{C}(D) \tag{4.118}$$

are the total transfer function from the data input to the equalizer output and the noise signal at the equalizer output, respectively. Let $\boldsymbol{H}[n]$, $\boldsymbol{B}[n]$ and $\boldsymbol{\zeta}[n]$ be the inverse D-transforms of $\boldsymbol{H}(D)$, $\boldsymbol{B}(D)$ and $\boldsymbol{\zeta}(D)$, respectively. With

$$h_{ik} \triangleq [\boldsymbol{H}]_{ik} \tag{4.119}$$

$$b_{ik} \triangleq [\boldsymbol{B}]_{ik} \tag{4.120}$$

$$\zeta_k \triangleq [\boldsymbol{\zeta}]_k, \quad i, k \in \mathcal{I}_N \tag{4.121}$$

the input to the k-th decision element may be expressed as

$$\tilde{a}_k[n] = \sum_{i=1}^{N} \sum_{m=-\infty}^{\infty} a_i[n-m]h_{ik}[m] + \sum_{i=1}^{N} \sum_{m=0}^{\infty} \hat{a}_i[n-m]b_{ik}[m] + \zeta_k[n], \quad \forall k \in \mathcal{I}_N. \tag{4.122}$$

Since the feedback filter is constrained to be purely causal, some of the zero lag feedback coefficients must be zero: $b_{ik}[0] = 0$, $\forall i \geq k$.

The signal component at the input to the decision element is identical to the part on the left hand side in the above expression which contains the desired symbol $a_k[n]$ with undistorted phase. Thus, $a_k[n]h_{kk}^{\mathrm{re}}[0]$ is the signal component, where the *bias coefficient* $h_{kk}^{\mathrm{re}}[0]$ is the real part of the sample $h_{kk}[0]$. In general, each sample $h_{ik}[n]$ of the impulse response can be expressed in terms of a real and an imaginary part

$$h_{ik}[n] = h_{ik}^{\mathrm{re}}[n] + jh_{ik}^{\mathrm{im}}[n]. \tag{4.123}$$

The average signal energy $\mathcal{E}_{\text{S},k}$ is defined as the expected energy in the signal component:

$$\mathcal{E}_{\text{S},k} \triangleq E\left[|a_k[n]h_{kk}^{\text{re}}[0]|^2\right]$$
$$= (h_{kk}^{\text{re}}[0])^2 \tag{4.124}$$

where property (2.4) was used for the last expression. Conversely, the average noise energy is the expected energy of the remaining noise and interference terms:

$$\mathcal{E}_{\text{IN},k} \triangleq E\left[|\tilde{a}_k[n] - a_k[n]h_{kk}^{\text{re}}[0]|^2\right]. \tag{4.125}$$

This equation may be expanded into

$$\mathcal{E}_{\text{IN},k} = E\left[|\tilde{a}_k[n] - a_k[n] + a_k[n](1 - h_{kk}^{\text{re}}[0])|^2\right]$$
$$= E\left[|\tilde{a}_k[n] - a_k[n]|^2\right] + (1 - h_{kk}^{\text{re}}[0])^2\, E\left[|a_k[n]|^2\right]$$
$$+ (1 - h_{kk}^{\text{re}}[0])\left\{E\left[\tilde{a}_k^*[n]a_k[n]\right] + E\left[a_k^*[n]\tilde{a}_k[n]\right] - 2\,E\left[|a_k[n]|^2\right]\right\}. \tag{4.126}$$

Assume that the data signals a_k ($k \in \mathcal{I}_N$) are mutually and temporally uncorrelated with zero mean and unit variance (Equations (A.9), (A.10)). Furthermore, the data signals are uncorrelated with the noise (Equation 2.14). Considering that only correct decisions are provided to the feedback filter ($\hat{a}_k[n] = a_k[n]$, $\forall k \in \mathcal{I}_N$, $n \in \mathbb{Z}$), it is easy to show that

$$E\left[a_k^*[n]\tilde{a}_k[n]\right] = h_{kk}[0]. \tag{4.127}$$

Furthermore, the expectation $E[|\tilde{a}_k[n] - a_k[n]|^2]$ is equal to the MMSE J_k and $E[|a_k[n]|^2] = 1$. Substituting these expression into Equation (4.126) yields

$$\mathcal{E}_{\text{IN},k} = J_k - (1 - h_{kk}^{\text{re}}[0])^2. \tag{4.128}$$

It is proven in Appendix H for both the MMSE MIMO LE and the DFE that the

MMSE $J_{k,\text{mmse}}$ and the bias coefficient $h_{kk}^{\text{re}}[0]$ are related through

$$h_{kk}^{\text{re}}[0] = 1 - J_{k,\text{mmse}}, \quad \forall k \in \mathcal{I}_N. \tag{4.129}$$

Substituting this result into Equations (4.124) and (4.128) yields for the MMSE MIMO equalizers the sought after relationship between SINR $\Phi_{k,\text{mmse}} = \mathcal{E}_{\text{S},k}/\mathcal{E}_{\text{IN},k}$ and MMSE $J_{k,\text{mmse}}$:

$$\Phi_{k,\text{mmse}} = \frac{1 - J_{k,\text{mmse}}}{J_{k,\text{mmse}}}. \tag{4.130}$$

For the ZF MIMO LE and DFE, it is shown in Appendix H.3 that the bias coefficient $h_{kk}^{\text{re}}[0]$ is equal to unity. Substituting this into Equations (4.124) and (4.128) results immediately in

$$\Phi_{k,\text{zf}} = \frac{1}{J_{k,\text{zf}}}. \tag{4.131}$$

Thus, the k-th output SNR of the ZF MIMO equalizers is equal to the inverse of the MMSE for user k.

4.5 Error Probability and Capacity

This section describes several estimates for the error probability and a derivation of a lower bound on the system capacity.

With the expressions for the channel $\boldsymbol{X}$ and the equalizer filters $\boldsymbol{C}$, $\boldsymbol{B}$, it is possible to calculate all interference terms of the MMSE equalizers. Additional knowledge of the input noise spectrum $\boldsymbol{S}_\nu(D)$ makes it possible to apply the accurate methods described in Chapter 3 in order to estimate the error probability. However, those methods require considerable computational workload. For situations in which a rough estimate is sufficient, significantly simpler expressions may be used. For example, the Saltzberg upper bound on the error probability and the Gaussian approximation depend only on the mean-square error.

Consider a multiuser system with a MMSE MIMO equalizer. All users employ

independent square QAM as modulation scheme and each modulation symbol occurs with the same probability. In addition, the transmitted data signals are assumed to be mutually and temporally independent stationary stochastic processes with zero mean and unit variance (see Section A.6). The Saltzberg bound, $\tilde{P}_{\text{ex},k}^{(\text{Saltz})}$, provides an estimate which is always larger than the probability of exceeding the decision threshold, $P_{\text{ex},k,\text{mmse}}$. Substituting Equation (4.130) into the Saltzberg bound (3.73) results in

$$\tilde{P}_{\text{ex},k}^{(\text{Saltz})} = \exp\left\{-\frac{1 - J_{k,\text{mmse}}}{2\,J_{k,\text{mmse}}\rho(L_k)}\right\} \tag{4.132}$$

where $J_{k,\text{mmse}}$ is the MMSE of user k and $\rho(L_k) = [L_k^2 - 1]/3$ (Equation (3.59)). Note that this bound will apply to decision-feedback equalizers in a strict sense only if it is assumed that all decisions used in the feedback filter are correct.

Another estimate approximates the interference component by a normal distributed random variable with the same variance. This yields the Gaussian approximation (3.129). Using Equation (4.130), the Gaussian approximation may be expressed as

$$\tilde{P}_{\text{ex},k}^{(\text{Gauss})} = Q\left(\sqrt{\frac{1 - J_{k,\text{mmse}}}{J_{k,\text{mmse}}\rho(L_k)}}\right). \tag{4.133}$$

An interesting property of the zero-forcing equalizers is that their error probability can easily be determined. The distortion in the equalizer output signal contains only normal distributed noise and no interference. Hence, the error probability can be calculated exactly with a Gaussian model. In particular, the probability of exceeding the decision threshold when using a ZF MIMO equalizer is equal to

$$P_{\text{ex},k,\text{zf}} = Q\left(\sqrt{\frac{1}{J_{k,\text{zf}}\rho(L_k)}}\right). \tag{4.134}$$

This equation is valid for decision-feedback structures under the assumption that all decisions provided to the feedback filter are correct.

The capacity of a system is another performance measure. Assuming fixed transmitter properties (transmit powers, filters) and channels, it depends only on the

receiver. An upper bound on the capacity of MMSE MIMO equalizers will be derived.

Let us start with a definition of *capacity* for the reverse link of a multiuser system:

Definition 4.1 *The* capacity *of a multiuser system is equal to the total number of bits per second conveyable by all users, normalized by the number of diversity channels, $U_{div} = AK$, with each detected bit having a bit error probability of less than a preselected value P_b.*

$$C \triangleq \frac{1}{AK} \sum_{k=1}^{N} b_k \qquad (4.135)$$

where C is the capacity in bits per diversity unit, N is the number of system users and b_k denotes the maximum number of bits that user k can transmit while still maintaining a bit error rate (BER) of less than a given value P_b.

Note that the capacity depends on the channel characteristics, the modulation scheme, the number of diversity channels (U_{div}), the number of users (N), and the desired worst case bit error probability (P_b).

Consider the same multiuser system as in the previous sections. The modulation scheme is assumed to be an independent square QAM, in which both the inphase and the quadrature component are independently pulse amplitude modulated. The PAM schemes of inphase and quadrature signal are identical and they have L_k levels each (for the k-th user). All symbols of the modulation scheme occur with the same probability. In addition, the data signals are mutually and temporally independent with zero mean and unit variance. Using Gray coding, the BER of the k-th signal, $P_{b,k}$, is smaller than the Saltzberg bound (3.74):

$$P_{b,k} \le 2 \frac{L_k - 1}{L_k} \exp\left\{ -\frac{\Phi_k}{2\rho(L_k)} \right\}.$$

Note that the signal-to-interference-and-noise ratio (SINR) Φ_k can be calculated directly from the MMSE. The relationships for the MMSE and ZF MIMO equalizers are given by Equations (4.130) and (4.131), respectively.

The above expression is simplified by further loosening the bound according to $(L_k - 1)/L_k < 1$

$$P_{b,k} < 2 \exp\left\{-\frac{\Phi_k}{2\rho(L_k)}\right\}.$$ (4.136)

Applying $\rho(L_k) = (L_k^2 - 1)/3$, one can solve for the alphabet size of the square QAM scheme, L_k^2:

$$L_k^2 > \frac{\Phi_k}{\frac{2}{3}\ln\left(\frac{2}{P_{b,k}}\right)} + 1.$$ (4.137)

If b_k denotes the number of information bits coded into each QAM symbol, it readily occurs that $2^{b_k} = L_k^2$. Substituting this relationship into the last equation and solving for b_k yields

$$b_k > \log_2\left\{\frac{\Phi_k}{\frac{2}{3}\ln\left(\frac{2}{P_{b,k}}\right)} + 1\right\}.$$ (4.138)

It has to be pointed out that, so far, no restrictions have been imposed upon L_k. In practice, the number of PAM levels for the inphase and quadrature signals has to be an even integer number. The *asymptotic capacity*, C_{as}, shall now be defined as the system capacity excluding the practical constraint for the number of PAM levels. Thus, C_{as} constitutes an upper bound on the practically achievable system capacity C. Substituting expression (4.138) into definition (4.135) and requiring that the BER for all users be less than or equal to P_b, the asymptotic capacity may be estimated with

$$C_{as} > \frac{1}{AK}\sum_{k=1}^{N}\log_2\left\{\frac{\Phi_k}{\frac{2}{3}\ln\left(\frac{2}{P_b}\right)} + 1\right\}.$$ (4.139)

Following Equation (4.137) and taking into account that L_k has to be an even

integer, one gets

$$L_k > 2 \left\lfloor \frac{1}{2} \sqrt{\frac{\Phi_k}{\frac{2}{3} \ln\left(\frac{2}{P_{b,k}}\right)} + 1} \right\rfloor \tag{4.140}$$

where $\lfloor x \rfloor$ is the largest integer smaller than or equal to x (Table A.3). This result may be converted to the number of bits transmitted using the relationship $L_k^2 = 2^{b_k}$:

$$b_k > \max\left\{0; 2\log_2\left(2\left\lfloor \frac{1}{2}\sqrt{\frac{\Phi_k}{\frac{2}{3}\ln\left(\frac{2}{P_{b,k}}\right)} + 1}\right\rfloor\right)\right\} \tag{4.141}$$

where the "maximum" expression ensures that the number of information bits is not negative. Substituting the last equation into definition (4.135) yields a lower bound for the system capacity:

$$C > \frac{1}{AK}\sum_{k=1}^{N}\max\left\{0; 2\log_2\left(2\left\lfloor \frac{1}{2}\sqrt{\frac{\Phi_k}{\frac{2}{3}\ln\left(\frac{2}{P_b}\right)} + 1}\right\rfloor\right)\right\}. \tag{4.142}$$

4.6 Summary: Performance Bounds and Expressions

The theoretical part of this chapter will be completed by summarizing the expressions for the optimal filters and the performance of different multiple-input multiple-output (MIMO) equalizers.

Results are presented only for the frequency-domain approach. While the frequency-domain analysis is in general computationally more efficient and leads to optimal infinite-length filters, the time-domain method provides the optimal filters for a specified, finite filter length.

As before, the equalizers are categorized according to the optimization criterion and the type. The optimization criteria considered were the minimum mean-square error (MMSE) and the zero-forcing (ZF) conditions. Additionally, three different MIMO

equalizer types were investigated, namely the linear equalizer (LE), the conventional decision-feedback equalizer (C-DFE) and the noise-predictive decision-feedback equalizer (NP-DFE). Block diagrams of the multiuser system and the three different equalizer types are shown in Figure 4.3 (LE), Figure 4.5 (C-DFE) and Figure 4.8 (NP-DFE).

It has been shown in Sections 4.2.1.1, 4.3.1.1 and 4.3.2 that the optimal forward filter of all MMSE equalizer types may be calculated and implemented by either a *direct realization* (DR) or a *matched filter realization* (MFR).

Using the DR method, one calculates $\boldsymbol{C}(D)$ directly and the forward filter structure consists of a single element. The initial quantities needed in the forward filter calculation are the power spectrum $\boldsymbol{S}_y(D)$ and the cross-power spectrum $\boldsymbol{S}_{ya}(D)$:

$$\boldsymbol{S}_y(D) \triangleq E_M[\boldsymbol{y}^H(D^{-*})\boldsymbol{y}(D)]$$
$$\boldsymbol{S}_{ya}(D) \triangleq E_M[\boldsymbol{y}^H(D^{-*})\boldsymbol{a}(D)]$$

where $\boldsymbol{y}$ is the input signal to the equalizer and $\boldsymbol{a}$ is the transmitted data. $\boldsymbol{y}$ is directly available at the receiver. Information about $\boldsymbol{a}$ may be obtained from training sequences transmitted by all desired users.

According to the MFR method, the forward filter is realized by a cascade of three elements: a noise-whitening matched filter $\boldsymbol{S}_\nu^{-1}(D)$, a channel matched filter $\boldsymbol{X}^H(D^{-*})$ and a $N \times N$ symbol-rate matrix filter $\boldsymbol{L}(D)$, i.e.

$$\boldsymbol{C}(D) = \boldsymbol{S}_\nu^{-1}(D)\boldsymbol{X}^H(D^{-*})\boldsymbol{L}(D).$$

The individual elements may be determined from the channel transfer matrix $\boldsymbol{X}(D)$, the noise spectrum $\boldsymbol{S}_\nu(D)$ and the input data spectrum $\boldsymbol{S}_a(D)$:

$$\boldsymbol{S}_\nu(D) \triangleq E_M[\boldsymbol{\nu}^H(D^{-*})\boldsymbol{\nu}(D)]$$
$$\boldsymbol{S}_a(D) \triangleq E_M[\boldsymbol{a}^H(D^{-*})\boldsymbol{a}(D)]$$

where $\boldsymbol{\nu}$ is the noise component in the equalizer input signal $\boldsymbol{y}$. While $\boldsymbol{S}_a(D)$ is usually known, $\boldsymbol{X}(D)$ and $\boldsymbol{S}_\nu(D)$ may be estimated based on knowledge of the equalizer input

signal and a training sequence.

Important quantities required for the calculation of the equalizer filters are the $N \times N$ equivalent channel $\boldsymbol{S}_x(D)$ and the spectrum $\boldsymbol{Q}(D)$:

$$\boldsymbol{S}_x(D) \triangleq \boldsymbol{X}(D)\boldsymbol{S}_\nu^{-1}(D)\boldsymbol{X}^H(D^{-*})$$

$$\boldsymbol{Q}(D) \triangleq \boldsymbol{S}_x(D) + \boldsymbol{S}_a^{-1}(D).$$

According to Section 4.3.1.1, the inverse of the latter spectrum may alternatively be obtained by

$$\boldsymbol{Q}^{-1}(D) = \boldsymbol{S}_a(D) - \boldsymbol{S}_{ya}^H(D^{-*})\boldsymbol{S}_y^{-1}(D)\boldsymbol{S}_{ya}(D).$$

Since $\boldsymbol{S}_x(D)$ and $\boldsymbol{Q}(D)$ are positive semidefinite and Hermitian on the unit circle, they may be factored into a purely causal and a purely anticausal part:

$$\boldsymbol{S}_x(D) = \boldsymbol{\Psi}_x(D)\boldsymbol{G}_{\mathrm{zf}}^{-1}\boldsymbol{\Psi}_x^H(D^{-*})$$

$$\boldsymbol{Q}(D) = \boldsymbol{\Psi}(D)\boldsymbol{G}^{-1}\boldsymbol{\Psi}^H(D^{-*})$$

Both $\boldsymbol{\Psi}_x(D)$ and $\boldsymbol{\Psi}(D)$ are purely causal and stable matrices, i.e. $\boldsymbol{\Psi}_x(D) = \sum_{n=0}^{\infty} \boldsymbol{\Psi}_x[n]D^n$ and $\boldsymbol{\Psi}(D) = \sum_{n=0}^{\infty} \boldsymbol{\Psi}[n]D^n$. In addition, $\boldsymbol{\Psi}_x[0]$ and $\boldsymbol{\Psi}[0]$ are constrained to be upper triangular matrices with ones on the main diagonal. $\boldsymbol{G}_{\mathrm{zf}}^{-1}$ and $\boldsymbol{G}^{-1}$ are non-negative definite diagonal matrices that are independent on D.

The optimal infinite-length forward and feedback filters of all three equalizer types are listed in Table 4.3 for both the MMSE and the ZF criterion.

Table 4.4 contains expressions of the equalizer performance in terms of the MMSE and the error probability. Note that the expressions for the MMSE are exact for the linear equalizers. They would be exact for the decision-feedback equalizers if all decisions provided to the feedback filter were correct. In practice, however, wrong decisions cause a larger MMSE than the displayed MMSE for DFE structures. The difference depends mainly on the error probability and can be neglected in many cases.

Table 4.3: Frequency-domain expressions for the optimal infinite-length forward and feedback filters of MIMO equalizers

Optimization Criterion	MIMO Equalizer	Forward Filter		Feedback Filter
		direct realization $\boldsymbol{C}(D)$	matched filter realization $\boldsymbol{L}(D)$	$\boldsymbol{B}(D)$
MMSE	LE	$\boldsymbol{S}_y^{-1}(D)\boldsymbol{S}_{ya}(D)$	$\boldsymbol{Q}^{-1}(D)$	—
	NP-DFE			$\boldsymbol{I}_N - \boldsymbol{\Psi}(D)$
	C-DFE	$\boldsymbol{S}_y^{-1}(D)\boldsymbol{S}_{ya}(D)\boldsymbol{\Psi}(D)$	$\boldsymbol{\Psi}^{-H}(D^{-*})\boldsymbol{G}$	
ZF	LE		$\boldsymbol{S}_x^{-1}(D)$	—
	NP-DFE	—		$\boldsymbol{I}_N - \boldsymbol{\Psi}_x(D)$
	C-DFE		$\boldsymbol{\Psi}_x^{-H}(D^{-*})\boldsymbol{G}_{\mathrm{zf}}$	

Table 4.4: Performance expressions of infinite-length MIMO equalizers

Optimiz. Criterion	MIMO Equal.	MMSE J_k	Error Probability	
			Saltzberg bound $\tilde{P}_{\mathrm{ex},k}^{(\mathrm{Saltz})}$	Gaussian estimate $\tilde{P}_{\mathrm{ex},k}^{(\mathrm{Gauss})}$
MMSE	LE	$\displaystyle\int_0^1 \left[\boldsymbol{Q}^{-1}(e^{-j2\pi\check{f}})\right]_{kk} d\check{f}$	$\displaystyle\exp\left\{-\frac{1-J_k}{2\,J_k\rho(L_k)}\right\}$	$\displaystyle Q\left(\sqrt{\frac{1-J_k}{J_k\rho(L_k)}}\right)$
	DFE	$[\boldsymbol{G}]_{kk}$		
ZF	LE	$\displaystyle\int_0^1 \left[\boldsymbol{S}_x^{-1}(e^{-j2\pi\check{f}})\right]_{kk} d\check{f}$	—	$\displaystyle Q\left(\sqrt{\frac{1}{J_k\rho(L_k)}}\right)$ [†]
	DFE	$[\boldsymbol{G}_{\mathrm{zf}}]_{kk}$		

[†] For the ZF LE, the Gaussian estimate is equal to the correct error probability, i.e. $P_{\mathrm{ex},k,\mathrm{zf}} = \tilde{P}_{\mathrm{ex},k,\mathrm{zf}}^{(\mathrm{Gauss})}$. This is, in a strict sense, not the case for the ZF DFE since some decisions used in the feedback filter are wrong. However, the effect of error propagation may be neglected under certain circumstances.

The error probability results are valid for mutually and temporally independent stationary data sequences whose individual symbols have zero mean and unit variance and assume all constellation points of independent square QAM with equal probabil-

ity. The function $\rho(L)$ occurring in the expressions of Table 4.4 is defined by

$$\rho(L) \triangleq \frac{1}{3} \left[L^2 - 1 \right].$$

Note that the bit error rate (BER) might be calculated from the probability of exceeding the decision threshold with Equation (3.21) if Gray coding is applied.

   While the expression for the ZF equalizers is equal to the exact error probability[11], all of the given formulas for the MMSE equalizers are approximations. The Saltzberg bound is a true upper bound for the MMSE MIMO LE, while this may not be true for the MMSE MIMO DFE because of feedback errors. It has been shown in Chapter 3 that the Gaussian approximation provides good estimates for MMSE equalizers in situations when the error probability is relatively large ($P_{\mathrm{ex}} > 10^{-3}$). However, its results are very pessimistic for low error probabilities of 10^{-6} or smaller. This is also a characteristic of the Saltzberg bound, which becomes less accurate for decreasing error probabilities (see Section 3.5).

4.7   Numerical Results

The results presented in this section were obtained under the following ideal assumptions:

- Infinite length forward and (for the DFE) feedback filters,

- the channel impulse responses are known without error,

- the equalizer signals and tap weights are of infinite precision, and

- all decisions fed back into the DFE feedback filter are correct, i.e. the results do not include error propagation.

   Two systems with a different number of diversity channels have been considered:

1. 2×2 system (low diversity): $A = 2, K = 2, U_{\mathrm{div}} = 4$,

---

[11]this is also the case for the ZF DFE if all decisions used in the feedback filter are assumed to be correct.

2. 4×4 system (high diversity): $A = 4, K = 4, U_{\text{div}} = 16$.

The low diversity system is investigated exclusively for a symbol period of $T = 50$ ns and equal energy users, i.e. it is assumed that the average energy received from all users is identical ($\Gamma_k = \Gamma, \forall k \in \mathcal{I}_N$, see Equation (D.6)). This corresponds to a system with perfect power control. For the high diversity system, symbol periods of $T = 50$ ns and $T = 200$ ns have been chosen. In addition to the case of equal energy users, a second scenario with different energy users is also considered. This involves a maximum difference in the received energy (*near-far ratio*) of 10 dB between the strongest and the weakest user. The energies of the users are randomly chosen within the 10 dB interval, the distribution of the random energies being uniform in that interval.

It is assumed for the following results that the data signals a_i are mutually and temporally independent, stationary continuous-time stochastic processes with zero mean and unit variance (Definitions A.1 and A.1). The MMSE results are valid for any linear modulation scheme. On the other hand, the error probability depends critically on the modulation format. The bit-error rate (BER) and outage probability results are obtained for 4-QAM with independently modulated inphase and quadrature signals, i.e.

$$a_i[n] \in \frac{1}{\sqrt{2}} \{1 + j, 1 - j, -1 + j, -1 - j\}, \; L_i = 2, \quad \forall i \in \mathcal{I}_N, \; n \in \mathbb{Z}. \qquad (4.143)$$

In addition, it is assumed that all symbols in the modulation alphabet occur with the same probability.

For the capacity results, independent square QAM has been considered. The number of modulation levels per user, L_i, is maximized under the constraint that a maximum BER of 10^{-4} be not exceeded.

Identical fifth-order Butterworth lowpass filters with a cut-off frequency $f_{\text{3dB}} = K/(2T)$ (i.e. $K_{\text{3dB}} = K$) have been chosen for the analog transmit and receive filters $p_C(t)$ and $b_C(t)$. More detailed information about those filters is given in Section 2.3.3.1.

The spreading filters of all users have been set to $q_i[n] = \delta_K[n]$. In other words, the filters q_i ($\forall i \in \mathcal{I}_N$) have been omitted completely. This was justified because the individual channels were strongly frequency selective (for $T = 50$ ns) and mutually uncorrelated. Thus, the use of orthogonal and other spreading filters can be expected to yield no significant improvement. However, better results may be obtained with different spreading filters in less frequency selective environments, as for example in the $T = 200$ ns system.

The results have been obtained with a semi-analytical approach. Based on the channel information and a statistical model for the input data as described above, the individual MMSE's of the infinite-length equalizers have been calculated according to the frequency-domain approach (see Sections 4.2.1.1 and 4.3.1.1). After that, bounds on the bit error rate (BER) and system capacity have been determined using expressions (4.132) and (4.142), which are based on the Saltzberg bound. Finally, the results have been averaged over several scenarios with different radio channels drawn from an ensemble of measured indoor channel impulse responses (CIR's). Details about the measurements and the characteristics of the CIR's are described in Section 2.3.3.2. The RMS delay spread distribution of the CIR's had a mean of 40.4 ns and a standard deviation of 9.2 ns [12]. These values indicate that the channels are frequency selective for the chosen symbol period of $T = 50$ ns. A considerable amount of ISI and CCI over several symbols can be expected in this case.

The reverse link of the system has been simulated by randomly selecting M out of a total of 2044 CIR sets[12] and assigning each to one of M users[13]. These users have been divided into several groups of N portables for which the theoretical MMSE's, BER bounds, outage probabilities and capacities have been calculated. This procedure has been repeated 100 times for each value of N with different CIR sets. The final results are the average over the 100 channel scenarios.

Let us start with the MMSE results for the 4×4 system. Figure 4.10 shows the absolute MMSE versus the number of system users in a scenario with $T = 50$ ns and

---

[12]Each set consists of 4 individual CIR's. The CIR's belonging to the same set have been measured between one stationary transmit antenna and one of the four wavelength-spaced receive elements on the mobile at the same location.

[13]Depending on the investigated scenario, M took on the values 8, 20 and 30.
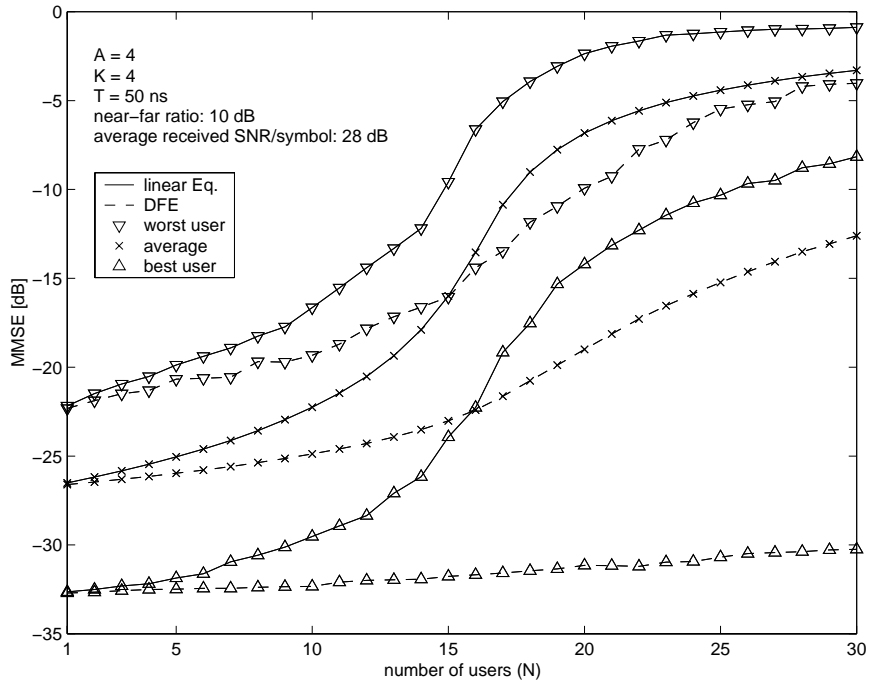
Figure 4.10: Maximal, average and minimal MMSE for 4×4, $T = 50$ ns system with an average received SNR/symbol of 28 dB and a near-far ratio of 10 dB.

an average received SNR/symbol of 28 dB. The near-far ratio, i.e. the ratio of the received SNR's between the strongest and the weakest user, was 10 dB. Thus, this system can be considered as applying no or only partial power control. The figure displays, for both MIMO LE and DFE, the mean MMSE averaged over all users and channel trials. Also shown is the largest (worst user) and smallest (best user) individual MMSE that occurred among all users and channel situations. While close to the curves of the LE for small N, the MMSE of the DFE increasingly surpasses that of the LE for larger user populations. This behavior already indicates a better performance of the DFE. At and around the point where N equals the number of diversity channels ($U_{\mathrm{div}} = 16$), a significant increase in the MMSE of the LE can be observed. The MMSE of the DFE also starts to increase at that point, however not as strongly. The results for the DFE at $N \gg 16$ must be treated with attention since error propagation effects are neglected. These tend to become increasingly pronounced when the performance of one or more users drops significantly, which is the case in strongly overpopulated systems. This can be seen in the worst user MMSE
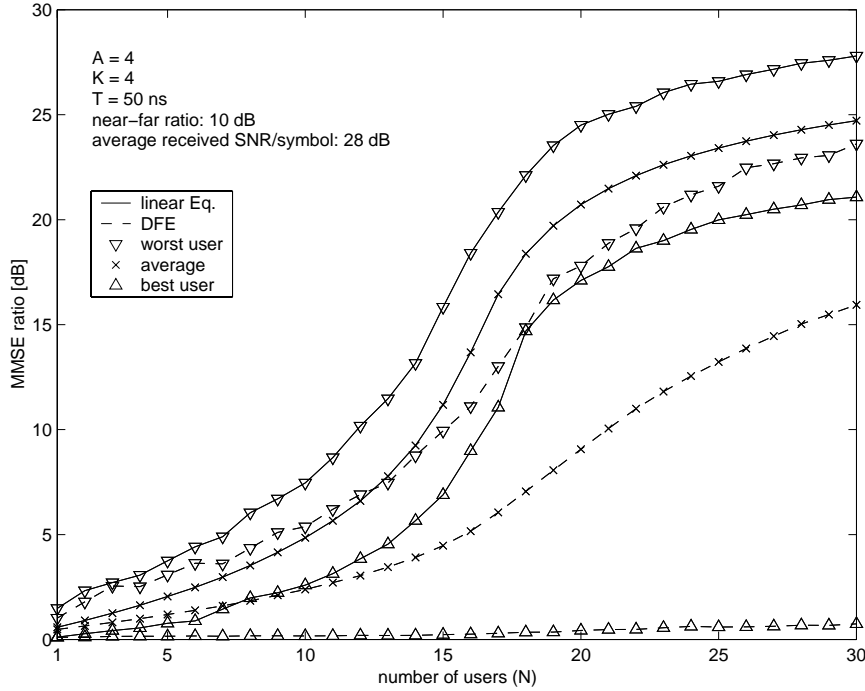
Figure 4.11: Maximal, average and minimal *relative* MMSE for 4×4, $T = 50$ ns system with an average received SNR/symbol of 28 dB and a near-far ratio of 10 dB.

of the DFE, which exceeds -10 dB for more than 20 users.

As an alternative to absolute performance measures, the relative MMSE, i.e. the ratio between the MMSE and the matched filter bound, can be used. This quantity is very instructive since it is not biased by performance differences due to different received energies per user. As a result, the relative MMSE directly measures the performance deterioration caused by an increased user population. For the aforementioned system, the relative MMSE is shown in Figure 4.11. These results shall be compared to a system with a symbol period of $T = 200$ ns but otherwise identical properties (Figure 4.12). It can be noted that, especially for the LE, the difference between the best and worst user curves is significantly larger than that for the higher symbol rate system. This leads to an inferior overall system performance. The same effect has also been observed by Monsen [78] and Clark *et al.* [20, 21]. They have attributed the better performance of systems with a longer delay spread (stronger frequency selective channels) to an increased amount of "intrinsic" or "implicit" frequency diversity, which is not related to the diversity discussed earlier (antenna diversity A,
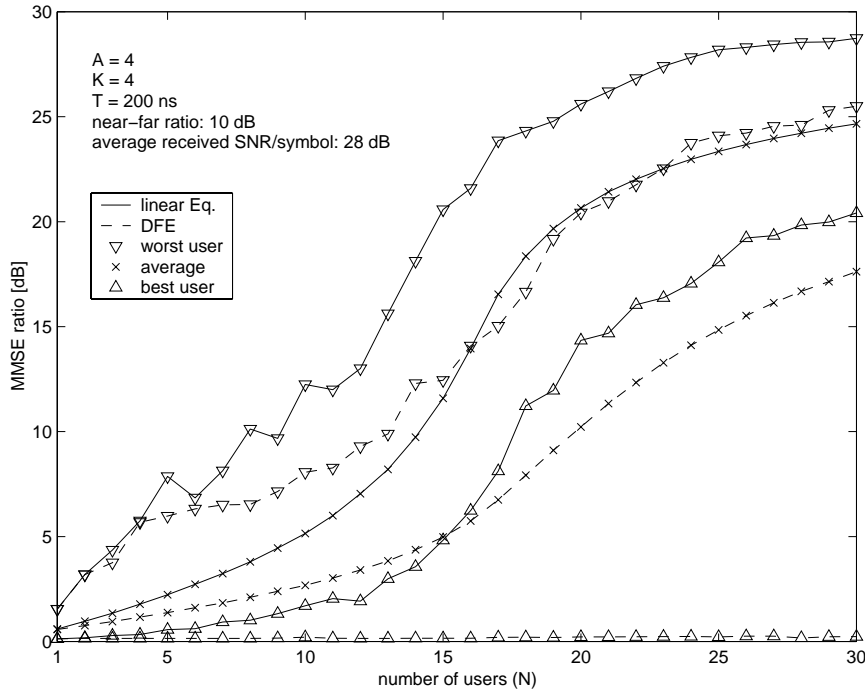
Figure 4.12: Maximal, average and minimal *relative* MMSE for 4×4, $T = 200$ ns system with an average received SNR/symbol of 28 dB and a near-far ratio of 10 dB.

frequency diversity K, number of diversity channels U_{div}). The potentially better performance of higher frequency selective channels requires however more complex receivers (i.e. longer filters with more coefficients) to take advantage of the implicit diversity because the amount of ISI and CCI is greater.

Figure 4.13 shows the average MMSE, averaged over all users and trials, in the 2×2 system for different receiver input SNR's. The corresponding results for the 4×4 system are displayed in Figure 4.14. Included is the new lower bound on the average MMSE for overpopulated systems with a linear equalizer (4.50). As can be seen, the bound is very tight. It was found that it becomes tighter the larger the received SNR. The figures show again that the average performance degradation paid for each additional user is stronger for the LE than for the DFE. While the LE yields unsatisfactory results in the overpopulated region (average MMSE > -10 dB), the DFE may allow communication with restricted quality when N exceeds U_{div}. However, error propagation effects may deteriorate the final performance such that reliable communication may not be possible in practice.
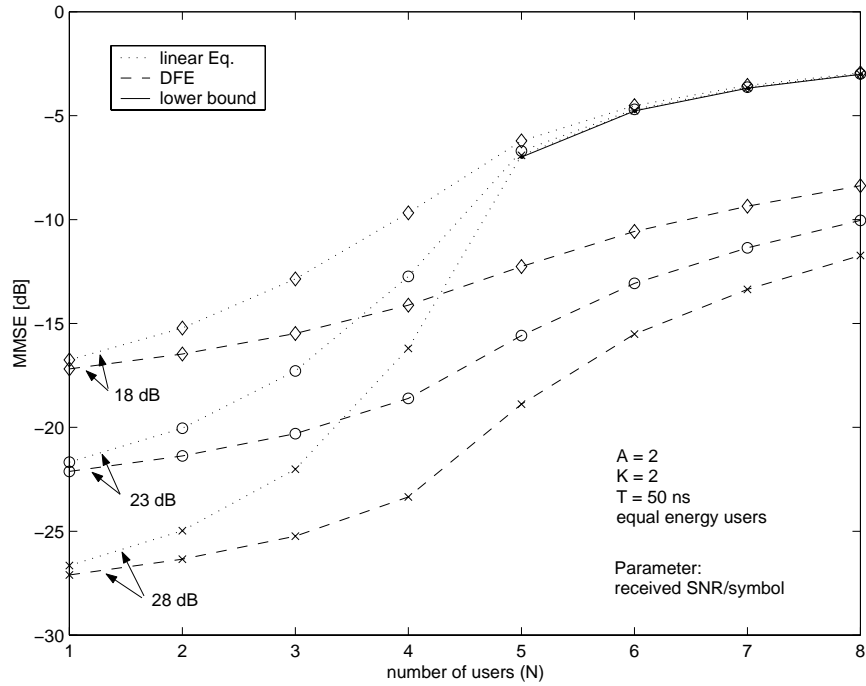
Figure 4.13: Average MMSE for identical 2×2, $T = 50$ ns systems with different average received SNR's and equal energy users.
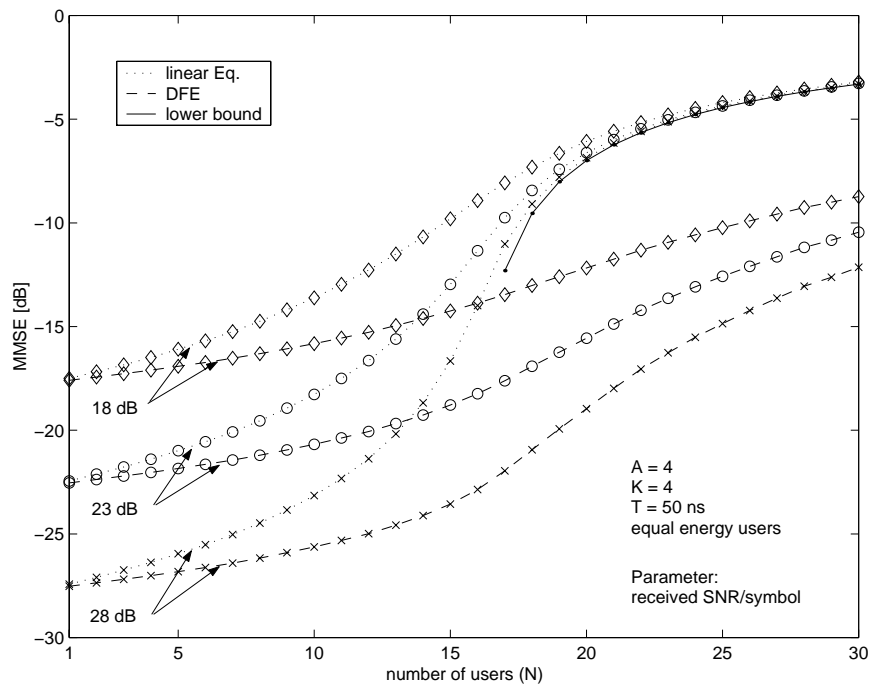
Figure 4.14: Average MMSE for identical 4×4, $T = 50$ ns systems with different average received SNR's and equal energy users.
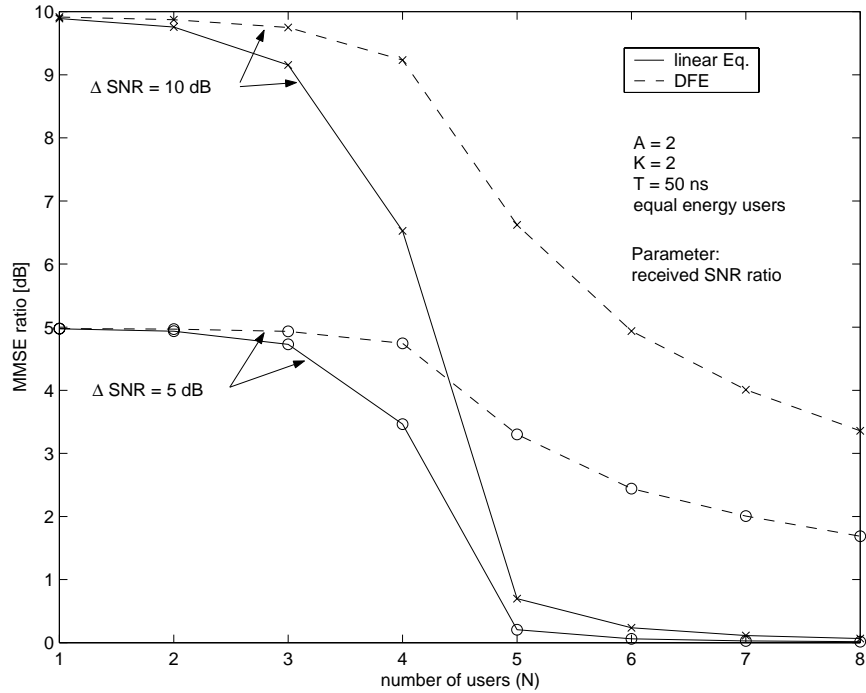
Figure 4.15: MMSE ratio between identical 2×2, $T = 50$ ns systems with different average received SNR's and equal energy users.

The average MMSE ratio for identical 2×2 systems[14] with different received SNR's is shown in Figure 4.15. The circles correspond to the MMSE ratio between the 28 and 23 dB SNR curves of Figure 4.13. Analogously, the crosses represent the ratio between the 28 and 18 dB SNR curves. Consequently, the difference in received SNR between the two compared systems is 5 dB and 10 dB, respectively. The results for the 4×4 system are shown in Figure 4.16. Considering the linear equalizer (LE), it can clearly be seen that there are large MMSE advantages for systems with higher SNR levels if the number of users is smaller than or equal to the number of diversity channels. For overpopulated systems, larger SNR's have negligible effects on the MMSE performance. This is in agreement with the lower bound on the average MMSE for overpopulated systems, Equation (4.50), which depends only on the number of users and the number of diversity channels but not on the received SNR. In particular, an overpopulated system with LE can be considered as completely

---

[14]The systems compared differed only in the received SNR, i.e. only the noise level was different. All other system characteristics, especially the channels, were identical.
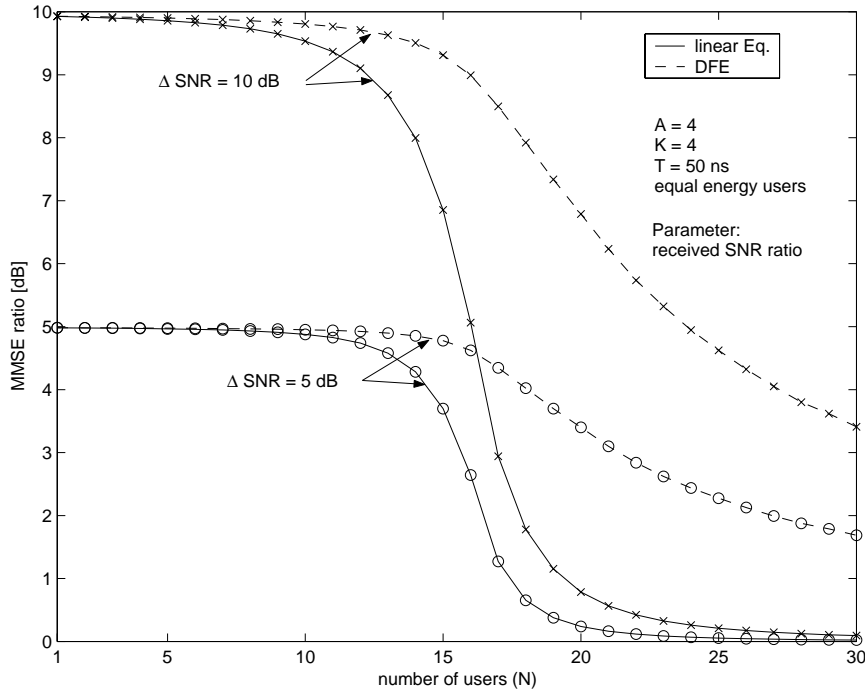
Figure 4.16: MMSE ratio between identical 4×4, $T = 50$ ns systems with different average received SNR's and equal energy users.

interference limited since the received SNR does not or only marginally influence its performance. However, the ratio of the average MMSE for small N is practically identical to the SNR difference between the two systems. Thus, if $N \ll U_{\mathrm{div}}$, an increase of the SNR will result in an almost identical decrease of the MMSE (in dB).

The transition of the MMSE ratio at $N = U_{\mathrm{div}}$ to overpopulated systems is steep but continuous. More detailed simulations have shown that it is influenced by the SNR level. If high SNR systems are compared, the transition will become more abrupt, changing almost step like from the SNR difference ($N \leq U_{\mathrm{div}}$) to zero (overpopulated systems). On the other hand, the transition around $N = U_{\mathrm{div}}$ becomes more and more continuous the lower the SNR's of the compared systems are.

The MMSE ratio for identical systems with different SNR's decreases not as strongly around $N = U_{\mathrm{div}}$ for a DFE. In contrast to the LE, the performance of even strongly overpopulated systems will improve noticeably if the SNR is increased and error propagation effects are neglected. The performance loss due to overpopulation is visible but more moderate. Thus, an overpopulated system with DFE does
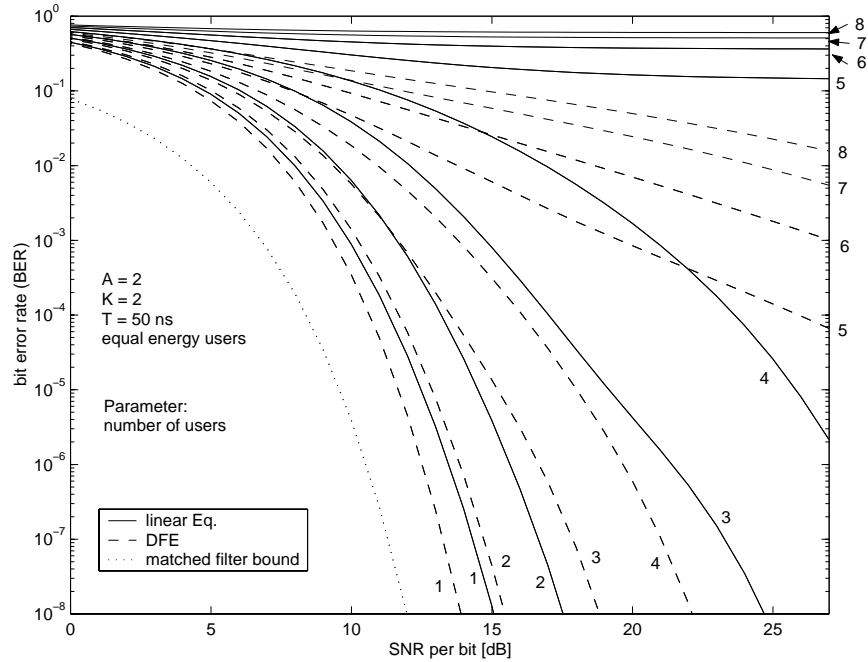
Figure 4.17: Upper BER bound versus average received SNR for 2×2, $T = 50$ ns systems with a different number of equal energy users.

not seem to be completely interference limited.

Let us now investigate the upper BER bounds, averaged over all users and trials, for the MIMO MMSE LE and DFE. Figure 4.17 displays the BER versus the received SNR for the 2×2 system. There are 8 curves for both equalizers, each one for a different system population ($N = 1, 2, \ldots, 8$). It can be seen that the DFE performs in all cases considerably better than the linear equalizer. The LE displays the characteristic waterfall-like shape of the BER for $N = 1, 2, 3$ users. For 4 users the BER also seems to decrease, however, a much higher input SNR is required for low BER values. For more than 4 users, the curves of the LE show an irreducible BER floor. This is explained by the fact that the number of diversity channels in this system is $U_{\text{div}} = 4$, allowing up to 4 users with reliable performance if a LE is employed. Figure 4.18 shows the corresponding results for the 4×4 system. Remarkable is the performance of the DFE with 20 users, i.e. 4 more users than diversity channels. Average BER's of less than 10^{-6} can be achieved for received SNR's per bit greater than 27 dB. This means that the DFE performs well even in overpopulated systems. Error propagation effects have most probably no qualitative influence on
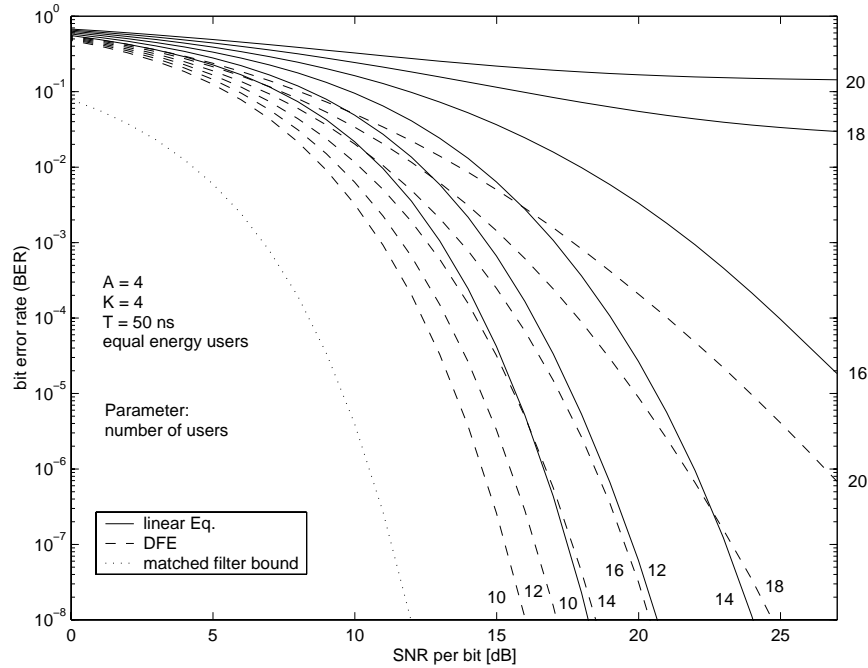
Figure 4.18: Upper BER bound versus average received SNR for 4×4, $T = 50$ ns systems with a different number of equal energy users.

this result since the variation of all calculated BER's, including the ones from the worst users, is relatively small around the average values shown in the figures. Hence, the performance of all system users is good, which makes the occurrence of errors relatively rare. Under this circumstance, it has been shown that error propagation does not lead to pathological situations but only to an overall performance loss of approximately 2 dB [99].

Results for an identical 4×4 system except a longer symbol period of $T = 200$ ns are given in Figure 4.19. The lower amount of "implicit" diversity [21, 78] leads to a worse performance of the LE compared to the $T = 50$ ns case for all user populations shown while the results of the DFE seem to be degraded only in overpopulated scenarios.

The next two Figures 4.20 and 4.21 show the average BER versus the number of users with the received SNR/bit as parameter. It can be observed that the DFE is able to support consistently a larger number of users for the same error probability than the LE. These figures also confirm that a larger received SNR does not have
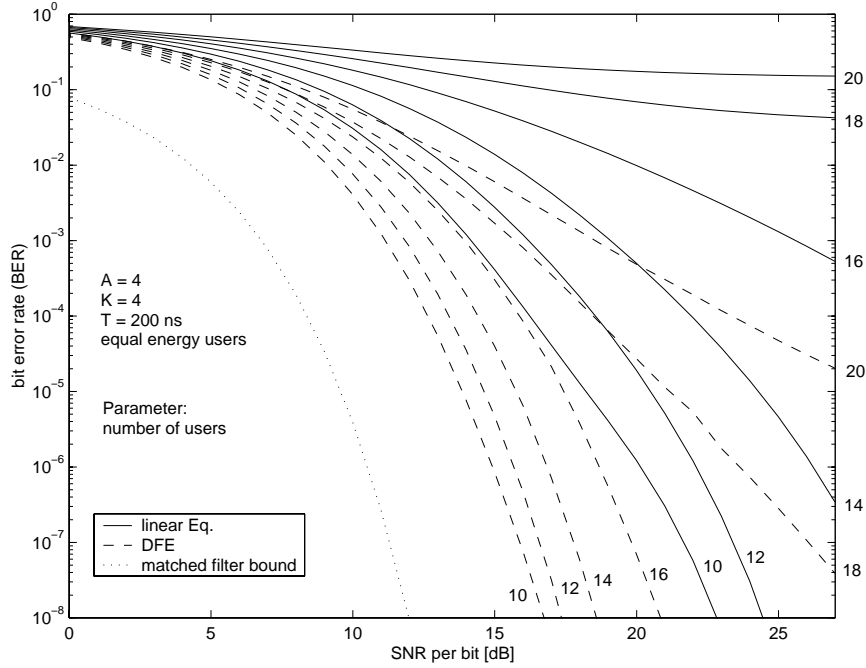
Figure 4.19: Upper BER bound versus average received SNR for 4×4, $T = 200$ ns systems with a different number of equal energy users.

much effect on the performance of the LE when the system is overpopulated. On the other hand, the DFE has the potential to achieve a distinctly better performance gain by increasing the SNR in situations with many users.

The next results measure the system performance in terms of the outage probability. An outage condition is assumed when the Saltzberg upper bound BER of an individual user is larger than 10^{-4}. The outage probability is then

$$P_{\text{out}} = \text{Prob} \left\{ P_{b,k} > 10^{-4} \right\} \tag{4.144}$$

where $P_{b,k}$ is the upper bound of the BER. For the transfer of data, a raw BER of 10^{-4} before coding is generally considered appropriate. An estimate of the outage probability is calculated with

$$\hat{P}_{\text{out}} = \frac{N_{\text{out}}}{N_{\text{tot}}} \tag{4.145}$$
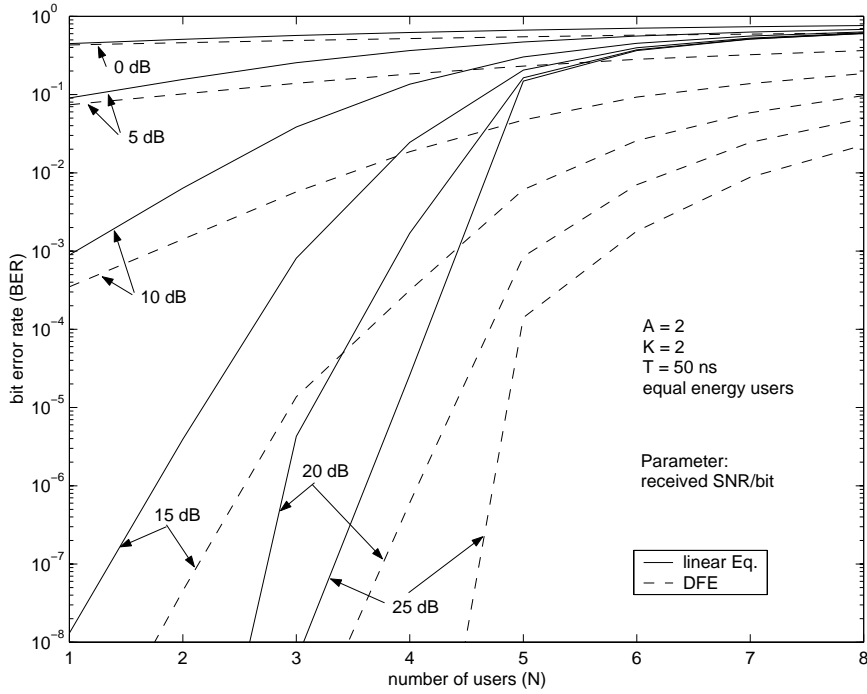
Figure 4.20: Upper BER bound versus number of users for 2×2, $T = 50$ ns systems with different average received SNR's and equal energy users.
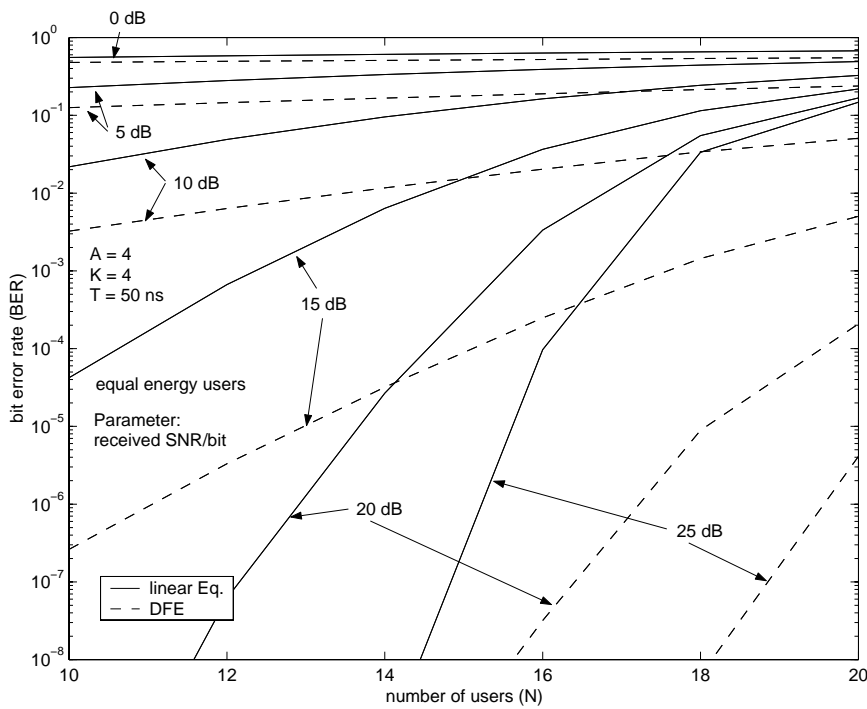
Figure 4.21: Upper BER bound versus number of users for 4×4, $T = 50$ ns systems with different average received SNR's and equal energy users.
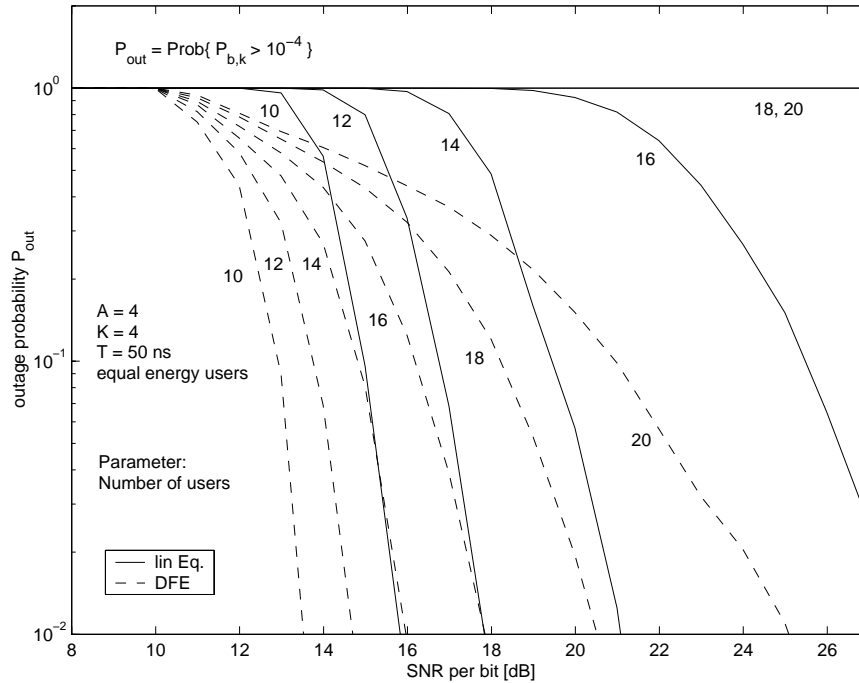
Figure 4.22: Estimated outage probability versus average received SNR for 4×4, $T = 50$ ns systems with a different number of equal energy users.

where N_{out} is the number of users whose upper bound BER exceeded 10^{-4} and $N_{\text{tot}} = 2000$ is the total number of users for which the BER bound was computed.

The estimated outage probability versus the received SNR/bit for the 4×4 system with $T = 50$ ns is shown in Figure 4.22. As can be seen, the LE may achieve outage probabilities of less than 1% for 10, 12 and 14 users. For $N = 16$, a considerably higher SNR is necessary in order to obtain low outage values. When the number of users is larger than the number of diversity channels, the outage probability does not decrease considerably below 100% over the whole SNR range displayed. The DFE may achieve low outage probabilities for $N < 16$. Even if the number of users becomes larger than 16, small outage probabilities can be obtained in low noise environments. This example provides further evidence for the superiority of the DFE especially in highly populated and overpopulated systems.

The next two figures plot the outage probability over the number of system users. In the equal energy user case (Figure 4.23), between 4 and 5 more users can be supported for the same outage probability if a DFE receiver is employed instead of a

LE. This result was found to be independent of the received SNR/bit. It also seems as if the DFE may allow a significant portion of the users (about 40% for 25 dB SNR/bit) to communicate reliably even if the number of users is almost twice the number of diversity channels. In this case, however, the effect of incorrect decisions must be taken into account. The users which are in an outage condition may cause a considerable amount of errors. This affects, in turn, also the better users through the decision-feedback loop. Since the number of users which perform poorly is large and since their error probability might be high, the negligence of error propagation leads in Figures 4.23 and 4.24 to overly optimistic results for $N \gg U_{\text{div}}$. Figure 4.24 considers users whose signals are received at different SNR's (near-far effect). The near-far ratio (maximal possible SNR ratio between signals received from different users) was set to 10 dB. Compared to the equal energy case, the performance suffers between dramatically for low SNR's of 15 dB to mildly at higher SNR's. The advantage of a DFE over a LE seems to be hardly affected. Overall, all equalizers proved to be *near-far resistant*[15].

The final investigation considers the system capacity. The average asymptotic capacity (Equation (4.139)) of the 4×4, 50 ns system with equal energy users is shown in Figure 4.25 for a desired minimum BER probability of $P_b = 10^{-4}$. A clear difference in the behavior of LE and DFE can be noticed. The asymptotic capacity of the LE has a distinct maximum for 12 users and decreases for increasing N. In largely overpopulated systems, the asymptotic capacity is not dependent on the received SNR. On the other hand, the asymptotic capacity of the DFE increases almost linearly for small N. After the maximum is reached for approximately 19 users,

---

[15]Near-far resistance is a measure of how well a multiuser detector is able to suppress multiple access interference (CCI and ISI). It is defined as the worst case *asymptotic efficiency* for a certain bit of a specified user over all possible energies of the other (interfering and noninterfering) bits [69]. The asymptotic efficiency describes the performance degradation due to interference from other users and ISI in the limit of no Gaussian noise [69, 122, 123].

If the multiple access interference (MAI) causes an irreducible error floor even in the absence of Gaussian noise, the near-far resistance of the detector will be zero. In other words, the detector will not be near-far resistant. On the other hand, a near-far resistant detector does not have an irreducible error floor in the presence of MAI, and its error probability decreases monotonically towards zero for increasing SNR. For example, the conventional matched filter detector is not near-far resistant. Conversely, the ZF and MMSE MIMO LE as well as DFE have been found to be near-far resistant for linearly independent channels [69, 79].
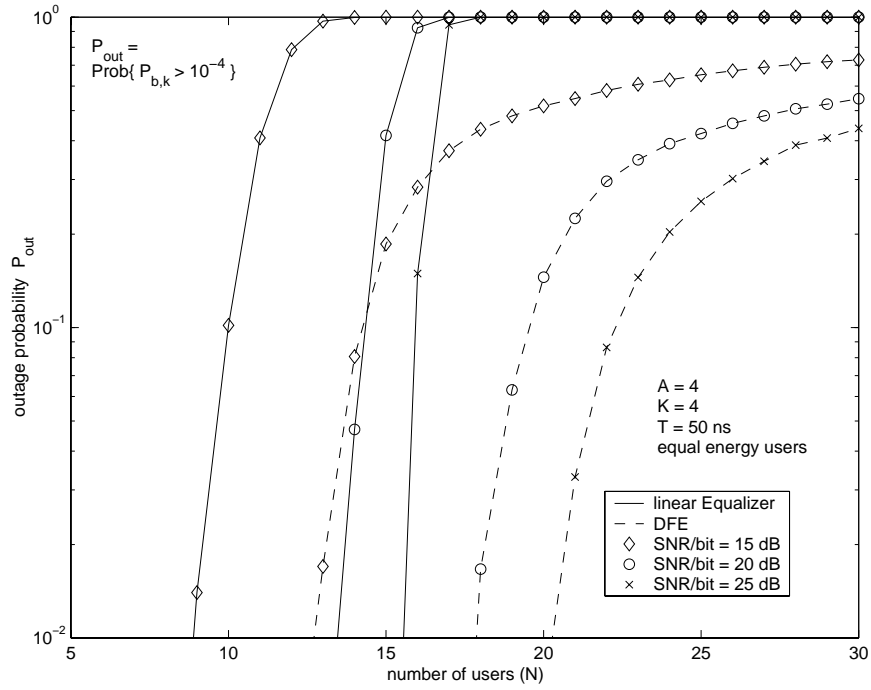
Figure 4.23: Estimated outage probability versus number of users for 4×4, $T = 50$ ns systems with different average received SNR's and equal energy users.
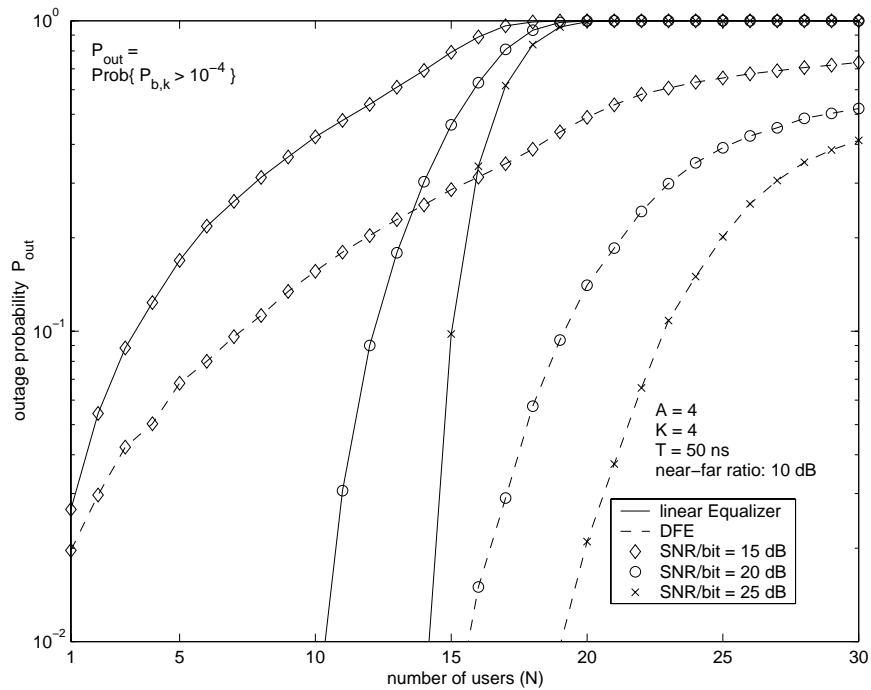
Figure 4.24: Estimated outage probability versus number of users for 4×4, $T = 50$ ns systems with different average received SNR's a near-far ratio of 10 dB.
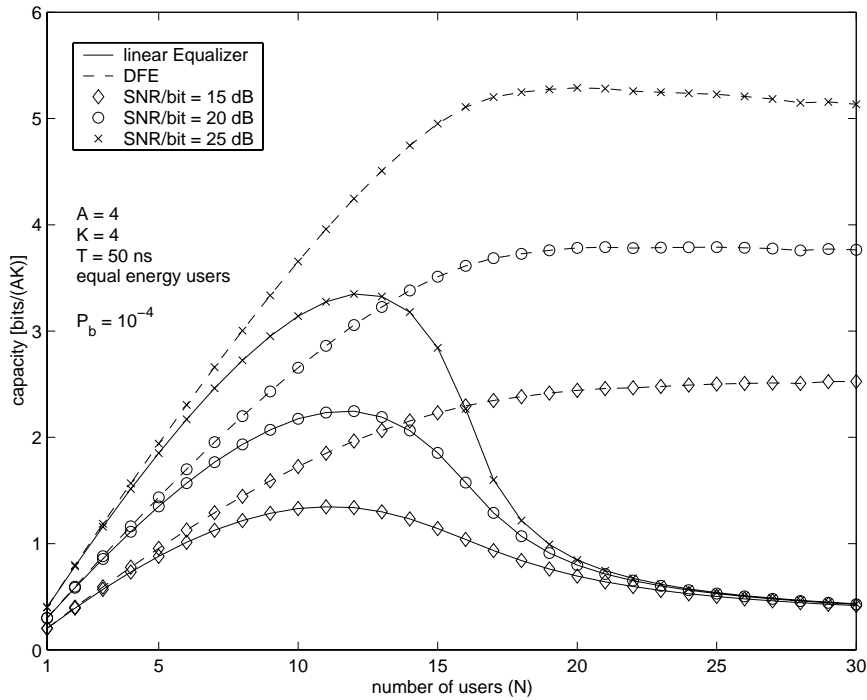
Figure 4.25: Asymptotic capacity versus number of users for 4×4, $T = 50$ ns systems with different average received SNR's and equal energy users.

the capacity decreases only marginally. The asymptotic capacity of the DFE for large N still depends on the received SNR. Almost identical results for the asymptotic capacity were found for users received with unequal energies (near-far scenario).

A more realistic performance measure is the practically achievable capacity (Equation 4.142). Figure 4.26 shows this quantity for the same system as above. The differences are obvious. For small values of N, the capacity curves increase linearly with three different slopes, each corresponding to a modulation scheme with a different number of constellation points. Some curves have local maxima. Independent of the received SNR, the capacity of the LE is zero in overpopulated scenarios. The curves of the DFE have to be treated with caution for large N because error propagation is neglected. In all cases, the DFE achieves its capacity maximum at larger N than the LE.

Interestingly, in contrast to the asymptotic capacity, the practically achievable capacity results are quite different for the equal and unequal energy user cases. An example with a near-far ratio of 10 dB is displayed in Figure 4.27. The curves resemble
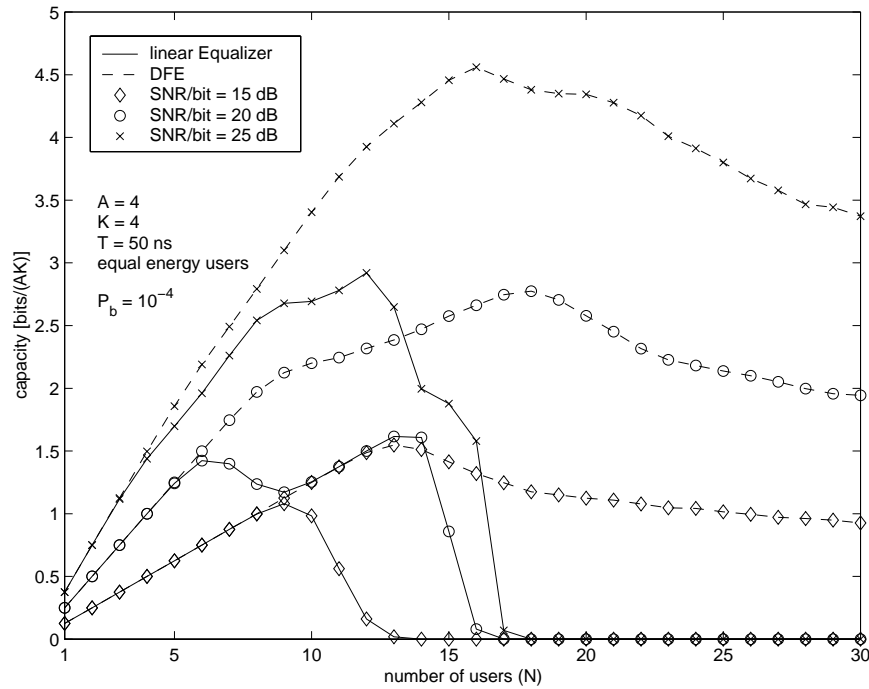
Figure 4.26: Practical capacity versus number of users for 4×4, $T = 50$ ns systems with different average received SNR's and equal energy users.

more those of the asymptotic capacity and have only one maximum. For the DFE, the capacity values at the maxima are approximately the same for both equal and unequal energy scenarios. The practically achievable capacity of the LE decreases slightly for increasing near-far ratios. Overall, both DFE and LE suffer only small capacity losses due to near-far situations.

4.8 Conclusion

Different multiple-input multiple-output (MIMO) equalizer structures used for joint detection of multiple signals have been described and analyzed. In addition, the effect of diversity and the number of system users on the performance of these detectors is quantified and discussed.

The MIMO equalizers analyzed include the linear equalizer (LE) and two different structures of the decision-feedback equalizer (C-DFE, NP-DFE). Both minimum mean-square error (MMSE) and zero-forcing (ZF) criteria have been considered as
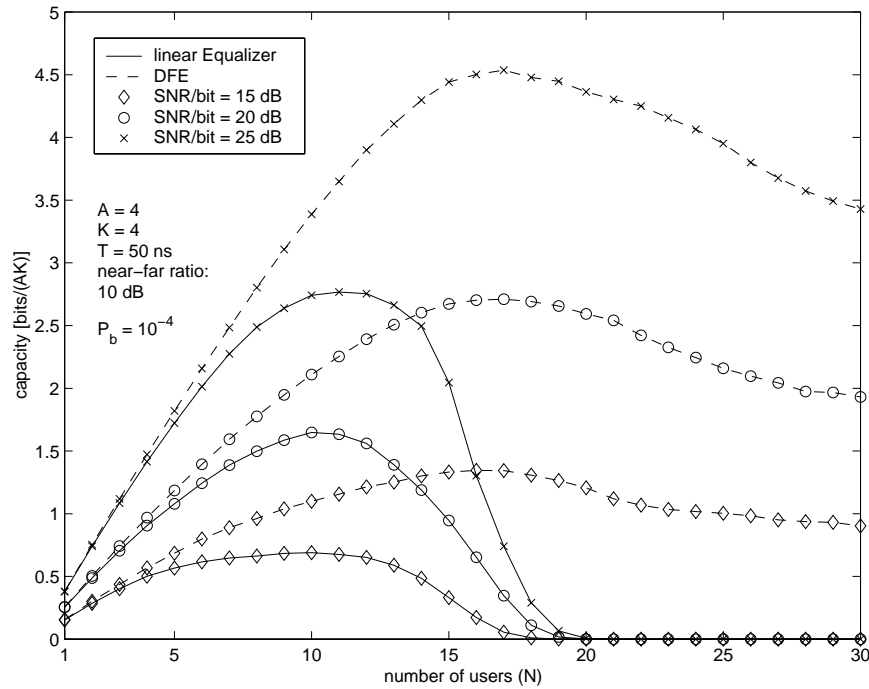
Figure 4.27: Practical capacity versus number of users for 4×4, $T = 50$ ns systems with different average received SNR's and a near-far ratio of 10 dB.

optimization criteria.

Considering stationary environments, the analysis may be carried out in either time- or frequency-domain. It has been shown that the frequency-domain approach is generally more efficient and leads to the optimal infinite-length MMSE (ZF) equalizer. On the other hand, the time-domain analysis is conceptually simpler (especially for the DFE) and yields the optimal finite-length equalizer.

Despite the potential advantages of the frequency-domain analysis, it has not received nearly as much attention in the literature as the time-domain approach. One reason is that the latter is definitively more appropriate for systems with non-stationary channels or when adaptive solutions are desired. As for stationary environments, the frequency-domain analysis may be conceptually more complicated and requires apparently a more complex implementation of the equalizer structure. On the positive side are potentially significant efficiency gains for the calculation of the equalizer filters and a better numerical stability. The issue of a more complex implementation is mainly a result of the well-known frequency-domain structure. This

form consists of a noise-whitening matched filter and a channel matched filter followed by the actual equalizer [27, 51, 118]. The determination and implementation of this structure seems to be less attractive. However, it has been shown here that a simpler structure of the linear equalizer exists which does not require knowledge about the noise characteristics and the channels. Rather, it is based on the characteristics of directly measurable (received signal) and known (training symbols provided) quantities. This and the other advantages mentioned above may make the frequency-domain based approach attractive for the determination of the MMSE MIMO LE.

The calculation of the DFE filters in the frequency-domain is complicated by the need for a matrix spectral factorization. This procedure is complex and requires a relatively large amount of operations [43]. However, the number of necessary operations increases still only linearly with the equalizer (time-) length versus cubically for the time-domain approach. Hence, the frequency-domain analysis may still be more efficient, especially when the channels are strongly frequency selective.

A new lower bound of the average MMSE has been derived for the MIMO LE in overpopulated systems[16]. This bound shows the basic limitation of the LE when the number of users is larger than the number of diversity channels in the system.

It has been proved that the general relationship between equalizer output SINR and MMSE for single-input single-output (SISO) equalizers is also valid for their MIMO counterparts. This enabled a formal application of error probability bounds for MIMO equalizers.

The performance of the equalizers considered here has been investigated in terms of the MMSE, BER, outage probability and capacity. It has been found that the decision-feedback equalizer (DFE) may achieve sufficiently good results in systems where the number of users exceeds the number of diversity channels, while a linear equalizer (LE) always performed unsatisfactorily under these circumstances. In situations when the number of users was distinctly smaller than the number of diversity channels, the LE achieved almost as good results as the DFE. With growing user populations, the performance advantage of the DFE was increasing. Therefore,

---

[16]A system is defined as *overpopulated* when the number of users (N) is larger than the number of diversity channels (U_{div}).

the LE may be a good choice for systems with low user populations with respect to the number of diversity channels (U_{div}) since it is less complex than the DFE. For densely populated and especially overpopulated systems, only a DFE may offer reliable communication quality. Both equalizer types proved to be robust in near-far scenarios.

Chapter 5

Delayed-Decision-Feedback Equalization

5.1 Introduction

This chapter describes a method to improve the overall performance of multiple-input multiple-output (MIMO) decision-feedback equalizers used in the reverse link of multiuser systems. The method is effective if the channels between users and receiver are frequency selective and if the signal power received from different users varies significantly.

The MIMO DFE detectors described in Chapter 4 improve the performance by means of a feedback filter which uses previously detected symbols in order to estimate and cancel interference and noise in the input signal to the decision device. Since almost the same decisions are available to the feedback filters of all users, their performance benefits more or less equally.

Consider now that the base station receives the signals of different users with significantly varying average powers. This may lead to large performance differences for the detected signals of different users. Signals of users received at a high SNR may perform well while the detection of weak users may show an unsatisfactory error probability. In addition, the unreliable decisions of the weak users are used in the feedback filter to cancel interference in the strong users' symbol estimates, which may

eventually cause a worse performance than without a feedback section. A possible solution to this problem is to use more of the (reliable) decisions of the strong users' signals in order to further improve the quality of the weak users' estimates, while employing less or no (unreliable) decisions of the weak users' signals in the feedback process for the strong users. This is practically achieved by delaying the decisions for weaker users relatively to those of the stronger users. It ensures that more reliable signals are processed at first, making more decisions available to improve the weaker signals. In return, the weaker signals are processed later and they have, thus, less malicious influence on the detection of the earlier processed strong signals.

Let us consider the reverse link of a multiuser system in a frequency-selective environment as described in Chapter 2. A common characteristic of such systems is that the received signal powers from different users may vary significantly due to their spatial location with respect to the base station and the structure of the environment. In general, signals of users close to the base station are received at a higher power than signals transmitted by more remote users unless power control techniques are applied. This situation of relatively strongly differing received signal powers is termed *near-far effect*.

It is shown in Chapter 4 that the structure of the optimal MMSE equalizers may be described by a cascade consisting of a noise-whitening matched filter, followed by a channel matched filter and finally a $N \times N$ matrix filter, where N is the number of users in the system. As a result of the combination of time dispersive (frequency selective) channels and a channel matched matrix filter in the base station, each received sample will consist of several successively transmitted symbols from each user. Consider now the output signal of the forward filter, $\breve{a}_k[n]$, which is a linear estimate of $a_k[n]$, the n-th symbol transmitted by user k. This estimate contains, due to the time-dispersive channel plus channel matched filter structure, interference components from "previously" transmitted symbols $a_i[n-m]$ ($m > 0$, $i \in \mathcal{I}_N$), "presently" transmitted symbols $a_i[n]$ ($i \neq k$, $i \in \mathcal{I}_N$) and "subsequently" transmitted symbols $a_i[n+m]$ ($m > 0$, $i \in \mathcal{I}_N$).

Recall the MIMO DFE's analyzed in Chapter 4. The feedback part of these equalizers makes use of decisions for the previously and some of the presently trans-

mitted symbols in order to estimate and cancel interference. However, subsequently transmitted symbols cannot be employed because the detector must be causal. As a result, it is possible to cancel interference (ISI and CCI) caused by previously and some presently transmitted symbols in the linear data estimate for each user. On the other hand, the feedback part is not able to reduce interference caused by subsequently transmitted symbols. Another characteristic of these DFE's is that all users benefit, correct decisions provided, almost equally from the feedback structure since approximately the same number of decisions is available for interference cancellation in each of the N estimated data streams.

Due to the near-far effect of the multiuser system considered, the performance of the strong users' data estimates may already be sufficient after the forward filter. Thus further improvement by the feedback process may not be necessary. On the other hand, the weak users' data estimates after forward filtering are generally significantly worse and require more improvement by the feedback filter. In addition, it may not be desirable to employ less reliable decisions of the weaker users in the feedback process for the strong users since frequent decision errors may impair the overall quality of the data estimates. In return, employing more decisions of the stronger users decreases the probability that erroneous decisions enter the feedback loop.

The strategy of putting more weight on the improvement of the weak users leads to a lower performance spread between the best and the worst data estimates. Hence, the quality difference of the decisions for different users will become smaller, which is generally desired. In addition, the weak users' error rates may limit the overall performance of the entire system. Thus, by enhancing the weak users' estimates, the overall system performance may be significantly improved.

5.1.1 Decision Path

Decision-feedback equalizers (DFE) use already detected symbols in a feedback procedure in order to improve the quality of the signals at the input to the quantizers. Due to causality constraints, only previously detected symbols may be used in the feedback process . Note that, in general, previously detected symbols are not neces-

sarily identical to previously transmitted or received symbols. Therefore, the order in which the decisions are made may affect the performance of the DFE significantly.

Let us define the *decision path* as the order in which the final decisions on the symbols are made. Consider at first the single user case. The input to the decision quantizer is the scalar signal $\tilde{a}[n]$. The natural way to perform the symbol-by-symbol decisions is in chronological order, i.e. quantizing at first the symbol $\tilde{a}[n]$, then $\tilde{a}[n+1]$, after that $\tilde{a}[n+2]$, and so on. The decision path proceeds in this case successively from $n = -\infty$ to $n = \infty$. In general, the decision path may be chosen arbitrarily. For example, one could, by modifying the equalizer structure appropriately, perform the decisions in the following order: $\tilde{a}[0], \tilde{a}[2], \tilde{a}[1], \tilde{a}[3], \ldots$. Let us quantify the decision path with the *decision order function* $d[n]$. This function maps the symbol index n into an integer number. The value of d shall be interpreted as the decision index, i.e. the $d[n_0]$-th decision is made on the symbol $\tilde{a}[n_0]$. For the chronological decision order, d can be expressed as $d[n] = n$.

Consider now a multiuser system with N users. Let us express the signal to be quantized as two-dimensional scalar function $\tilde{a}[k, n] \triangleq \tilde{a}_k[n]$, where k is the user number and n is the time index. The decision path can now be chosen arbitrarily in the $[k, n]$-plane. This is described by a two-dimensional decision order function $d[k, n]$.

As a special case, one might choose to perform the decisions at first with respect to the users and afterwards with respect to time. Figure 5.1 shows the decision path for a system with 4 users and sequences of length 4. The horizontal direction represents the time dimension and the different users are ordered vertically. Each circle represents a symbol at the input to the decision element. The values of the decision order function d are printed inside the circles. The detection of the different sequences is performed almost parallel with respect to the time dimension. Therefore, this decision order is referred to as *parallel*. Note that the DFE structures described in Chapter 4 perform the decisions in this order.

When the whole data sequences of each user are detected subsequently, the decision order is called *successive*. In this case the decision path is chosen as shown in Figure 5.2. For infinite-length sequences, at first the symbols of user 1 are detected
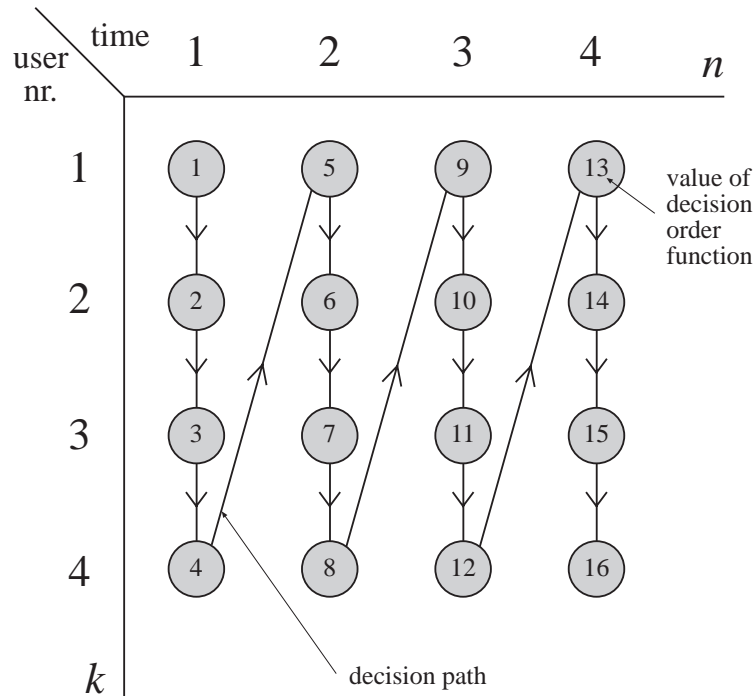
Figure 5.1: Decision path for parallel decision order in a system with 4 users and 4 symbols per user.

for all times $n \in \mathbb{Z}$. After that all symbols of user 2 are detected, and so on, until all sequences are quantized. Note that for the decision of symbol $\tilde{a}[k_0, n_0]$ *all* symbols of the sequences $1, 2, \ldots, k_0 - 1$ are available and may be used in the feedback loop. Also available are all temporally preceding symbols of the same sequence, i.e. the symbols $\tilde{a}[k_0, n]$ for $n < n_0$.

5.1.2 MIMO Delayed DFE Structures

The well-known DFE structures for multiuser systems are parallel detectors [55, 27, 31]. Their decision order is strictly defined and cannot be changed. A more flexible detection order can be achieved by including delay elements after the linear forward filter matrix [107]. The MIMO conventional delayed-decision-feedback equalizer (C-DDFE) is an extension of the MIMO C-DFE (Section 4.3.1, Figure 4.4). It is obtained by inserting a delay element after each output of the forward filter matrix $\boldsymbol{C}$. Figure 5.3 shows the block diagram of the MIMO C-DDFE. The delay elements D^{Δ_k}
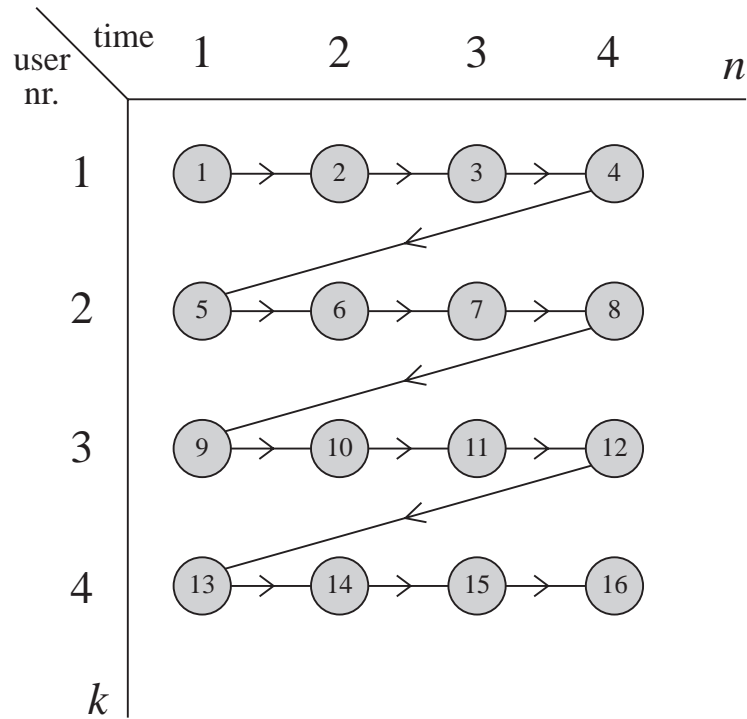
Figure 5.2: Decision path for successive decision order in a system with 4 users and 4 symbols per user.

$(k \in \mathcal{I}_N)$ delay the input sequence $\breve{a}_k$ by Δ_k symbols, where Δ_k may be an arbitrary nonnegative integer number.

Consider the following example in order to understand the effect of the delay elements on the decision path. Let the first branch be without delay ($\Delta_1 = 0$). The remaining branches are delayed by one symbol with respect to the previous branch, i.e. $\Delta_k = \Delta_{k-1} + 1$, $\forall k = 2, 3, \ldots, N$. The decisions are then made in the order shown in Figure 5.4 for a 4 user system with 4 received symbol per user. Each circle represents a symbol $\breve{a}_k[n]$ at the output of the forward filter. The decision path visualizes the order in which the decisions are made.

Figure 5.5 shows how a delay in its data sequence benefits a higher indexed user (user 2) with respect to the less delayed lower indexed user (user 1). This diagram contains for clarity only two users. The first user's signal is undelayed while the sequence of user 2 is delayed by one symbol. The lower left part of the figure shows the sequences of both users before the delay. As a result of the frequency selective
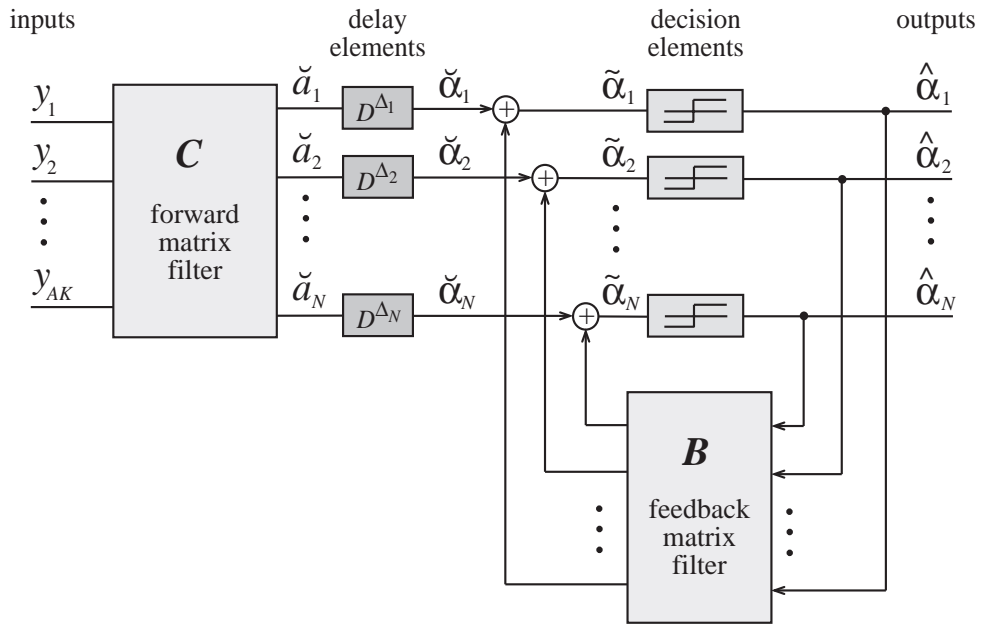
Figure 5.3: Block diagram of the MIMO conventional delayed-decision-feedback equalizer (C-DDFE).
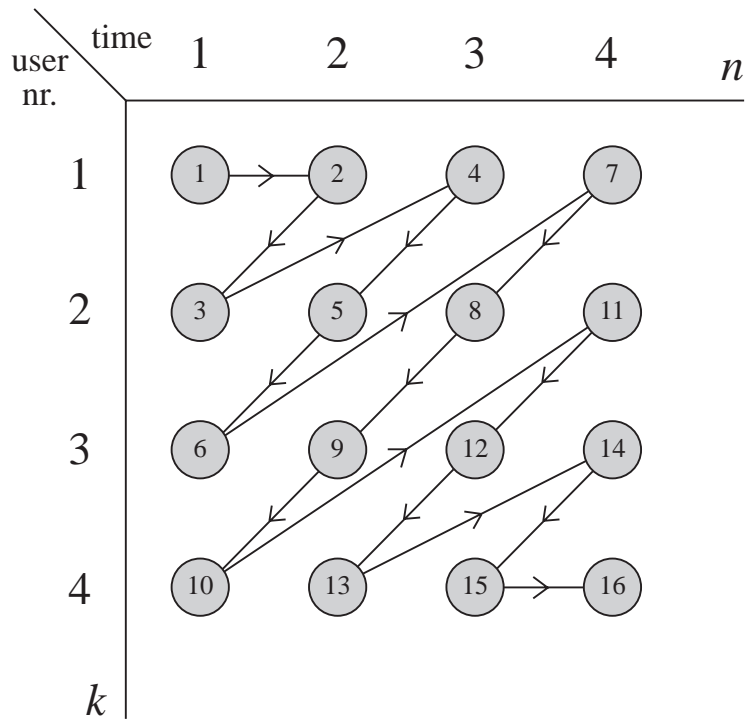
Figure 5.4: Decision path for the delayed DFE with a relative delay of one symbol between two adjacent data sequences for a system with 4 users and 4 symbols per user.

channels and the noise-whitening/channel matched filter structure at the receiver front-end, the symbol denoted x of user 2 contains cochannel interference (CCI) from the previous (a), present (b) and subsequent (c) symbols of the first user. If the sequence of user 2 were not delayed, the decision on symbol x would be made before the decision on c. Thus, only the symbols a and b would be available to the feedback filter in order to reduce interference caused by them in symbol x. However, after delaying the second users sequence, the decision on symbols a, b and c is made *before* that on x and the knowledge of all three CCI causing symbols can be used in the feedback filter to reduce the interference in x before the decision. In conclusion, the continuous-valued estimate of x before quantization becomes more reliable since more information of CCI causing symbols is available to the feedback filter, which is then able to produce a better estimate of the noise component in x. Conversely, less information can be used in the feedback process in order to reduce the interference in the symbols of user 1. Therefore, while user 2 will benefit from the delay of its sequence, the estimate of user 1 will become less reliable (provided that the decisions used in the feedback filter are correct).

The delayed version of the MIMO noise-predictive DFE (Section 4.3.2, Figure 4.7) is obtained by including a delay element after each forward filter output. The block diagram of the resulting MIMO NP-DDFE is shown in Figure 5.6.

5.2   Optimal Parameters and Ideal Performance

Expressions for the optimal forward and feedback matrix filters, based on the MMSE criterion, are given in the following subsections. It is assumed that all decisions used in the feedback filter are correct. At first, the conventional DDFE structure is considered and the optimal filters are derived in the frequency domain. The same approach is used for the noise-predictive DDFE. In addition, the feedback filter of the NP-DDFE can be calculated in the time-domain, while the forward filter may be determined in the frequency-domain. With this hybrid approach, a matrix spectral factorization is avoided and only matrix inversions are required for the calculation of the NP-DDFE filters.
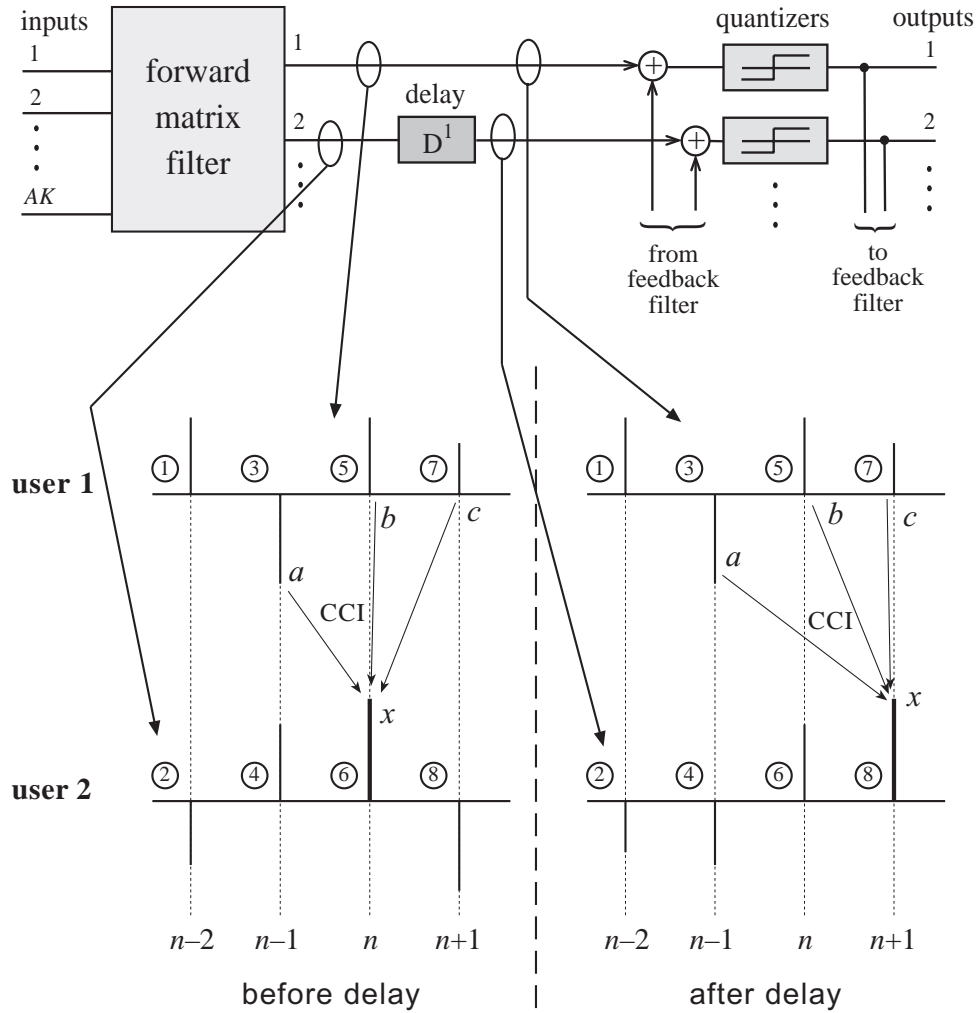
Figure 5.5: Example showing the first two users' signals in a MIMO DDFE. The second user's sequence is delayed by one symbol while user 1's signal is not delayed.

5.2.1 Conventional DDFE

It is well known (Section 4.3) that the optimal MMSE MIMO DFE forward filter can be expressed by a cascade of three elements: firstly a noise-whitening matched filter $\boldsymbol{S}_\nu^{-1}(D)$; secondly a channel matched filter $\boldsymbol{X}^H(D^{-*})$; and lastly a $N \times N$ matrix filter $\boldsymbol{L}$. This matched filter structure is the starting point for the system model. As in Section 4.3.1.1, the first two elements of the forward filter can be combined with
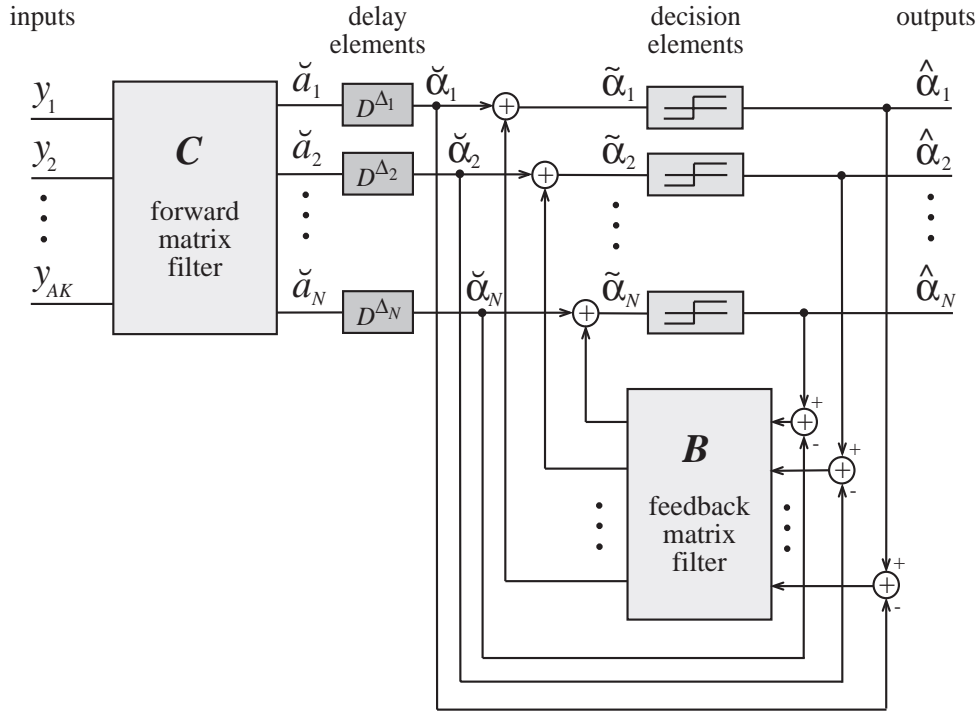
Figure 5.6: Block diagram of the MIMO noise-predictive delayed-decision-feedback equalizer (NP-DDFE).

the channel $\boldsymbol{X}(D)$ to form the equivalent channel

$$\boldsymbol{S}_x(D) \triangleq \boldsymbol{X}(D)\boldsymbol{S}_\nu^{-1}(D)\boldsymbol{X}^H(D^{-*}). \tag{5.1}$$

The resulting Gaussian noise at the output of the channel matched filter, $\boldsymbol{z}$, is a correlated vector signal with N components. Its power spectrum is (Equation (4.60))

$$\boldsymbol{S}_z(D) \triangleq E_M\left[\boldsymbol{z}^H(D^{-*})\boldsymbol{z}(D)\right] = \boldsymbol{S}_x(D). \tag{5.2}$$

In order to define a vector model, the delay elements after the forward filter of the C-DDFE (Figure 5.3) are described by the *delay matrix*

$$\boldsymbol{\Delta}(D) = \mathbf{Diag}\langle D^{\Delta_k}\rangle, \quad k = 1, 2, \dots, N \tag{5.3}$$

where $\mathbf{Diag}\langle D^{\Delta_k}\rangle$ is a $N \times N$ diagonal matrix with diagonal elements D^{Δ_k} for $k = 1, 2, \dots, N$ (Table A.3) and $\Delta_k \in \mathbb{N}_0$. With this, the vector model of the system
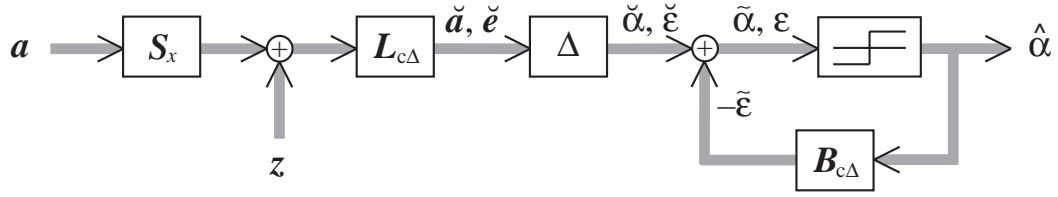
Figure 5.7: Vector block diagram of the equivalent system model including MMSE MIMO C-DDFE detector.

including MMSE MIMO C-DDFE is shown in Figure 5.7.

Define the *delayed data signal*, $\boldsymbol{\alpha}$, and the *delayed quantized estimate*, $\hat{\boldsymbol{\alpha}}$, according to

$$\boldsymbol{\alpha}(D) \triangleq \boldsymbol{a}(D)\boldsymbol{\Delta}(D) \tag{5.4}$$

$$\hat{\boldsymbol{\alpha}}(D) \triangleq \hat{\boldsymbol{a}}(D)\boldsymbol{\Delta}(D). \tag{5.5}$$

The power spectrum of the delayed data signal is easily found to be

$$\boldsymbol{S}_\alpha(D) \triangleq E_M\left[\boldsymbol{\alpha}^H(D^{-*})\boldsymbol{\alpha}(D)\right] = \boldsymbol{\Delta}^{-1}(D)\boldsymbol{S}_a(D)\boldsymbol{\Delta}(D) \tag{5.6}$$

where $\boldsymbol{S}_a(D)$ is the power spectrum of the data signal $\boldsymbol{a}$ (Equation (2.61)) and $\boldsymbol{\Delta}^{-1}(D)$ is the anticausal inverse of the delay matrix. Note that

$$\boldsymbol{\Delta}^H(D^{-*}) = \boldsymbol{\Delta}^{-1}(D) \tag{5.7}$$

since for each diagonal element $[(D^{-*})^{\Delta_k}]^* = D^{-\Delta_k}$.

The signal $\breve{\boldsymbol{a}}$ is the linear estimate of the data signal $\boldsymbol{a}$ at the output of the forward filter $\boldsymbol{L}_{c\Delta}$. The difference between this estimate and the data signal is $\breve{\boldsymbol{e}} \triangleq \breve{\boldsymbol{a}} - \boldsymbol{a}$ (Equation (4.1)).

The output of the delay matrix is given by

$$\breve{\boldsymbol{\alpha}}(D) \triangleq \breve{\boldsymbol{a}}(D)\boldsymbol{\Delta}(D) \tag{5.8}$$

which represents a linear estimate of the delayed data $\boldsymbol{\alpha}(D)$. The error in this estimate

is

$$\breve{\varepsilon}(D) \triangleq \breve{\alpha}(D) - \alpha(D) = \breve{e}(D)\Delta(D). \tag{5.9}$$

The decisions $\hat{\alpha}$ are used as inputs to the purely causal feedback filter $\boldsymbol{B}_{c\Delta}$, which produces an estimate of the negative error signal $-\breve{\varepsilon}$. Assuming that all decisions are correct, $\hat{\alpha} = \alpha$, the error estimate is

$$-\tilde{\varepsilon}(D) = \alpha(D)\boldsymbol{B}_{c\Delta}(D). \tag{5.10}$$

Finally, the input to the decision device is the continuous-valued estimate

$$\tilde{\alpha} = \breve{\alpha} - \tilde{\varepsilon}. \tag{5.11}$$

Thus, the error signal before quantization is

$$\varepsilon \triangleq \tilde{\alpha} - \alpha \tag{5.12}$$

$$= \breve{\varepsilon} - \tilde{\varepsilon}. \tag{5.13}$$

Let us now define the quantities

$$\boldsymbol{\zeta}(D) \triangleq \boldsymbol{z}(D)\Delta(D) \tag{5.14}$$

$$\boldsymbol{\Sigma}_x(D) \triangleq \Delta^{-1}(D)\boldsymbol{S}_x(D)\Delta(D) \tag{5.15}$$

$$\boldsymbol{\Lambda}_c(D) \triangleq \Delta^{-1}(D)\boldsymbol{L}_{c\Delta}(D)\Delta(D). \tag{5.16}$$

Applying these definitions to the system model as shown in Figure 5.7, the system may be described alternatively by the model in Figure 5.8.

It is easily shown that the power spectrum of the *delayed noise signal* $\boldsymbol{\zeta}$ is equal
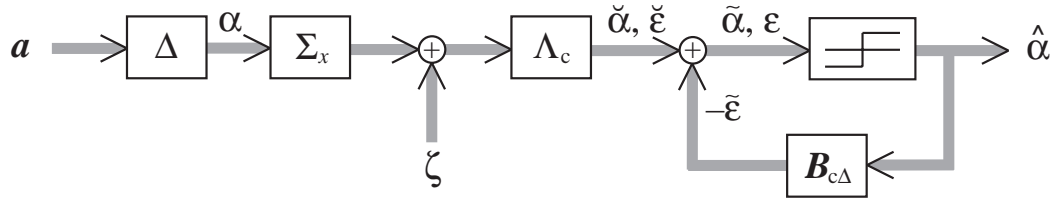
Figure 5.8: Alternative vector block diagram of the equivalent system model including MMSE MIMO C-DDFE detector.

to the transfer function of the *equivalent delay channel*

$$
\begin{aligned}
\boldsymbol{S}_\zeta(D) &\triangleq E_M\left[\boldsymbol{\zeta}^H(D^{-*})\boldsymbol{\zeta}(D)\right] \\
&\overset{(5.14)}{=} \boldsymbol{\Delta}^{-1}(D)E_M\left[\boldsymbol{z}^H(D^{-*})\boldsymbol{z}(D)\right]\boldsymbol{\Delta}(D) \\
&\overset{(5.2)}{=} \boldsymbol{\Sigma}_x(D).
\end{aligned}
\tag{5.17}
$$

Note that the model shown in Figure 5.8 is identical to the model for the parallel (undelayed) version of the MMSE MIMO C-DFE (Figure 4.6), which is analyzed in Section 4.3.1.1. In fact, the quantities $\boldsymbol{\alpha}$, $\hat{\boldsymbol{\alpha}}$, $\boldsymbol{\zeta}$, $\boldsymbol{\Sigma}_x$, $\boldsymbol{\Lambda}_c$, $\boldsymbol{B}_{c\Delta}$ replace in Figure 4.6 $\boldsymbol{a}$, $\hat{\boldsymbol{a}}$, $\boldsymbol{z}$, $\boldsymbol{S}_x$, $\boldsymbol{L}_c$, $\boldsymbol{B}_c$, respectively. Hence, the results of Section 4.3.1.1 may be applied directly in order to derive the optimal filters of the MMSE MIMO C-DDFE.

In particular, let us define the spectrum

$$
\boldsymbol{Q}_\Delta(D) \triangleq \boldsymbol{\Sigma}_x(D) + \boldsymbol{S}_\alpha^{-1}(D)
\tag{5.18}
$$

$$
= \boldsymbol{\Delta}^{-1}(D)\boldsymbol{Q}(D)\boldsymbol{\Delta}(D)
\tag{5.19}
$$

where $\boldsymbol{Q}(D) \triangleq \boldsymbol{S}_x(D) + \boldsymbol{S}_a^{-1}(D)$ (Equation (4.18)). This spectrum may be factored into [126]

$$
\boldsymbol{Q}_\Delta(D) = \boldsymbol{\Psi}_\Delta(D)\boldsymbol{G}_\Delta^{-1}\boldsymbol{\Psi}_\Delta^H(D^{-*})
\tag{5.20}
$$

where $\boldsymbol{\Psi}_\Delta(D)$ is a causal and stable matrix with $\boldsymbol{\Psi}_\Delta(D) = \sum_{n=0}^\infty \boldsymbol{\Psi}_\Delta[n]D^n$. $\boldsymbol{\Psi}_\Delta[0]$ is constrained to be an upper triangular matrix with ones on the main diagonal and $\boldsymbol{G}_\Delta^{-1}$ is a diagonal matrix independent of D. Applying the result of Equation (4.62),

the forward filter for the model in Figure 5.8 is

$$\boldsymbol{\Lambda}_{\mathrm{c}}(D) = \boldsymbol{\Psi}_{\Delta}^{-H}(D^{-*})\boldsymbol{G}_{\Delta}. \tag{5.21}$$

Considering definition (5.16) and using the result (4.63), the forward and feedback filters of the MMSE MIMO C-DDFE as shown in Figure 5.7 are given by

$$\boldsymbol{L}_{\mathrm{c}\Delta}(D) = \boldsymbol{\Delta}(D)\boldsymbol{\Psi}_{\Delta}^{-H}(D^{-*})\boldsymbol{G}_{\Delta}\boldsymbol{\Delta}^{-1}(D) \tag{5.22}$$

$$\boldsymbol{B}_{\mathrm{c}\Delta}(D) = \boldsymbol{I}_N - \boldsymbol{\Psi}_{\Delta}(D). \tag{5.23}$$

The equalizer performance in terms of the individual MMSE is

$$J_{k,\mathrm{c}\Delta} = [\boldsymbol{G}_{\Delta}]_{kk}, \quad \forall k \in \mathcal{I}_N. \tag{5.24}$$

While the determination of the individual MMSE's $J_{k,\mathrm{c}\Delta}$ requires the matrix spectral factorization (5.20), their geometric average $\bar{J}_{\Pi}$ (Equation (4.66)) may be calculated with a closed-form expression. In general, $\boldsymbol{Q}(D)$ would have to be replaced with $\boldsymbol{Q}_{\Delta}(D)$ in Equation (4.67) in order to determine $\bar{J}_{\Pi}$ for the MMSE MIMO C-DDFE. However, note that the determinants of $\boldsymbol{Q}_{\Delta}(D)$ and $\boldsymbol{Q}(D)$ are equal since

$$\begin{aligned}
\det\left[\boldsymbol{Q}_{\Delta}(D)\right] &= \det\left[\boldsymbol{\Delta}^{-1}(D)\boldsymbol{Q}(D)\boldsymbol{\Delta}(D)\right] \\
&= \det\left[\boldsymbol{\Delta}^{-1}(D)\right]\det\left[\boldsymbol{Q}(D)\right]\det\left[\boldsymbol{\Delta}(D)\right] \\
&= \det\left[\boldsymbol{Q}(D)\right]. \tag{5.25}
\end{aligned}$$

Therefore, the geometric average MMSE $\bar{J}_{\Pi}$ of the MMSE MIMO C-DDFE is exactly given by Equation (4.67). It is remarkable that $\bar{J}_{\Pi}$ does not depend on the delays D^{Δ_k}. In fact, the introduction of delays after the forward filter changes the individual MMSE's, however, their geometric average remains constant.
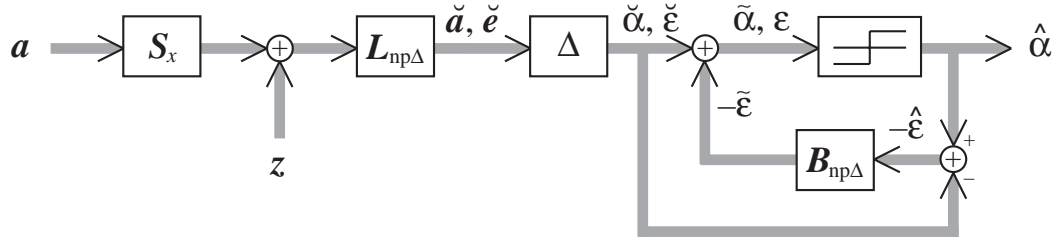
(a) equivalent system model
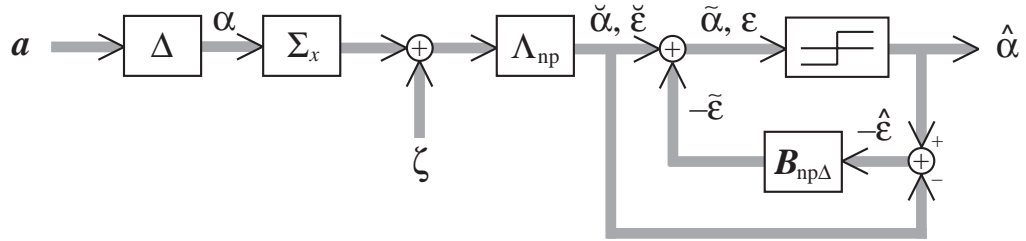
(b) alternative representation of the equivalent system model

Figure 5.9: Equivalent system models including MMSE MIMO NP-DDFE detector.

5.2.2 Noise-Predictive DDFE

5.2.2.1 Frequency-Domain Approach

Let us again assume the matched filter front-end structure of the receiver in the form

$$\boldsymbol{C}_{\mathrm{np}\Delta}(D) = \boldsymbol{S}_\nu^{-1}(D)\boldsymbol{X}^H(D^{-*})\boldsymbol{L}_{\mathrm{np}\Delta}(D). \tag{5.26}$$

With this, the vector model of the system including MIMO NP-DDFE results in the structure shown in Figure 5.9(a). The equivalent channel $\boldsymbol{S}_x(D)$ (Equation (5.1)) includes the "real" channel as well as the receiver front-end structure. The equalizer elements $\boldsymbol{L}_{\mathrm{np}\Delta}(D)$, $\boldsymbol{B}_{\mathrm{np}\Delta}(D)$, $\boldsymbol{\Delta}(D)$ are the forward filter, feedback filter and delay matrix (Equation (5.3)), respectively. Expressions for the optimal filters $\boldsymbol{L}_{\mathrm{np}\Delta}(D)$ and $\boldsymbol{B}_{\mathrm{np}\Delta}(D)$ with respect to the MMSE criterion are derived in the following.

Note that most of the signals in the NP-DDFE are described by the same expressions as those in the C-DDFE. Equations (5.1) to (5.9) and (5.11) to (5.13) apply also

to the MIMO NP-DDFE and are not repeated here for the sake of brevity. However, the input to the feedback filter is different for the NP-DDFE and it is equal to

$$-\hat{\boldsymbol{\varepsilon}} \triangleq \hat{\boldsymbol{\alpha}} - \breve{\boldsymbol{\alpha}}. \qquad (5.27)$$

Combining the assumption that all decisions provided to the feedback loop are correct, $\hat{\boldsymbol{\alpha}} = \boldsymbol{\alpha}$, with Equations (5.27) and (5.9) results in $\hat{\boldsymbol{\varepsilon}} = \breve{\boldsymbol{\varepsilon}}$. Thus, the output signal of the feedback filter is

$$-\tilde{\boldsymbol{\varepsilon}}(D) = -\breve{\boldsymbol{\varepsilon}}(D)\boldsymbol{B}_{\mathrm{np}\Delta}(D). \qquad (5.28)$$

Note that the purely causal feedback filter acts as a linear prediction filter that extrapolates the value of the present noise vector sample $\breve{\boldsymbol{\varepsilon}}[n]$ based on past noise samples $\breve{\boldsymbol{\varepsilon}}[n-m]$ ($m > 0$) and some components of the present noise sample. The final error of the continuous-valued estimate at the input to the decision device is therefore identical to the prediction error $\boldsymbol{\varepsilon} = \breve{\boldsymbol{\varepsilon}} - \tilde{\boldsymbol{\varepsilon}}$.

Define, in analogy to the previous section, the delayed noise signal $\boldsymbol{\zeta}(D)$ (Equation (5.14)), the equivalent delay channel $\boldsymbol{\Sigma}_x(D)$ (Equation (5.15) and the equivalent delay forward filter

$$\boldsymbol{\Lambda}_{\mathrm{np}}(D) \triangleq \boldsymbol{\Delta}^{-1}(D)\boldsymbol{L}_{\mathrm{np}\Delta}(D)\boldsymbol{\Delta}(D). \qquad (5.29)$$

Note that the power spectrum of the delayed noise is equal to the transfer function of the equivalent delay channel (Equation (5.17)).

With these definitions, an equivalent system model results, which is shown in Figure 5.9(b). This model does not have explicit delay elements in the equalizer structure and is identical to the parallel (undelayed) structure of the MIMO NP-DFE, which is analyzed in Section 4.3.2. Thus, the results of Section 4.3.2 may be applied here simply by replacing the quantities $\boldsymbol{a}$, $\hat{\boldsymbol{a}}$, $\boldsymbol{z}$, $\boldsymbol{S}_x$, $\boldsymbol{L}_{\mathrm{np}}$, $\boldsymbol{B}_{\mathrm{np}}$ with $\boldsymbol{\alpha}$, $\hat{\boldsymbol{\alpha}}$, $\boldsymbol{\zeta}$, $\boldsymbol{\Sigma}_x$, $\boldsymbol{\Lambda}_{\mathrm{np}}$ and $\boldsymbol{B}_{\mathrm{np}\Delta}$, respectively. In particular, applying this substitution to

Equation (4.104) yields the forward filter

$$
\begin{aligned}
\mathbf{\Lambda}_{\mathrm{np}}(D) &= \left[\mathbf{\Sigma}_x(D) + \mathbf{S}_\alpha^{-1}(D)\right]^{-1} \\
&\overset{(5.18)}{=} \mathbf{Q}_\Delta^{-1}(D).
\end{aligned}
\tag{5.30}
$$

Combining Equations (5.30), (5.29), (5.19) and applying the result in Equation (4.106) to the current model yields the final expressions for the forward and feedback filters of the MMSE MIMO NP-DDFE

$$
\mathbf{L}_{\mathrm{np}\Delta}(D) = \mathbf{Q}^{-1}(D)
\tag{5.31}
$$

$$
\mathbf{B}_{\mathrm{np}\Delta}(D) = \mathbf{I}_N - \mathbf{\Psi}_\Delta(D)
\tag{5.32}
$$

where $\mathbf{Q}(D) \triangleq \mathbf{S}_x(D) + \mathbf{S}_a^{-1}(D)$ (Equation (4.18)) and $\mathbf{\Psi}_\Delta(D)$ is the causal factor of $\mathbf{Q}_\Delta(D)$ (Equation (5.18)) obtained by matrix spectral factorization (Equation (5.20)).

Note that the forward filter of the delayed equalizer is identical to that of the (undelayed) MMSE MIMO NP-DFE and that of the MMSE MIMO linear equalizer (LE). Hence, the MMSE MIMO LE can be extended by a feedback structure with delays to become the MMSE MIMO NP-DDFE without changing the parameters of the forward filter. This enables relatively simple upgrading of linear equalizer structures to higher performance DFE detectors.

All comments and results of Section 5.2.1 with respect to the performance apply to the MMSE MIMO NP-DDFE as well. In particular, the individual MMSE's of the equalizer are given by Equation (5.24).

5.2.2.2 Hybrid Approach

In general, a determination of forward and feedback filters of the MMSE MIMO DDFE's will require the spectral factorization of a matrix function if a frequency-domain approach is used. Although not described here, the optimal parameters of the MMSE MIMO C-DDFE may also be calculated in the time-domain. Despite rendering the optimal finite-length solution for the filters, the matrix to be inverted may be of a very large dimension and it may be ill conditioned. For situations in

which it is desired to avoid a matrix spectral factorization as well as the inversion of a large matrix, a hybrid approach may be considered that uses both frequency- and time-domain techniques.

The initial idea for the hybrid approach is based on the following observations for the MMSE MIMO NP-DDFE: Firstly, the forward filter is equal to that of the MMSE MIMO LE and thus independent of the delays; and secondly, the feedback filter can be interpreted as a linear prediction filter. Hence, one may determine the forward filter in the frequency domain and the feedback filter in the time-domain. The forward filter is calculated as described for the linear equalizer in Section 4.2.1.1, for which only simple inversions of lower-dimensional matrices are required. The feedback filter can be determined independently by applying the time-domain linear prediction theory.

According to Equation (5.31), the forward filter of the MMSE MIMO NP-DDFE can be calculated in the frequency-domain with

$$\boldsymbol{L}_{\mathrm{np}\Delta}(D) = \boldsymbol{Q}^{-1}(D). \tag{5.33}$$

Provided that all decisions used in the feedback process are correct, the input to the decision device becomes $-\hat{\boldsymbol{\varepsilon}} = -\breve{\boldsymbol{\varepsilon}}$. In this case, $\boldsymbol{B}_{\mathrm{np}\Delta}$ is a linear prediction filter for the noise component $\breve{\boldsymbol{\varepsilon}}$ in the output signal of the forward filter, i.e. it extrapolates the value of $\breve{\varepsilon}_k[n]$ based on all previous samples $\breve{\varepsilon}_k[n-m]$ ($m > 0$, $\forall k \in \mathcal{I}_N$) and the present samples $\breve{\varepsilon}_i[n]$ ($\forall i < k$). Assuming that the length of the linear prediction filter is M_B (matrix) samples, the predicted value may be expressed as

$$\tilde{\boldsymbol{\varepsilon}}[n] = \sum_{m=0}^{M_B-1} \breve{\boldsymbol{\varepsilon}}[n-m]\boldsymbol{B}_{\mathrm{np}\Delta}[m] \tag{5.34}$$

where $\tilde{\boldsymbol{\varepsilon}}[n]$ is the prediction of $\breve{\boldsymbol{\varepsilon}}[n]$ and the $B_{\mathrm{np}\Delta}[m]$ are $N \times N$ matrices for all $m \in \{0, 1, 2, \dots, M_B - 1\}$. Since the feedback filter is causal, the zeroth feedback coefficient matrix $\boldsymbol{B}_{\mathrm{np}\Delta}[0]$ is constrained to be an upper triangular matrix with zeros on and below the main diagonal. Note that the prediction error $\boldsymbol{\varepsilon}[n] = \breve{\boldsymbol{\varepsilon}}[n] - \tilde{\boldsymbol{\varepsilon}}[n]$ is identical to the error in the continuous-valued data estimate $\tilde{\boldsymbol{\alpha}}[n]$ at the input to the

decision device (Equation (5.13)).

Define the *extended noise vector*

$$\epsilon[n] \triangleq [\breve{\varepsilon}[n - M_B + 1], \breve{\varepsilon}[n - M_B + 2], \breve{\varepsilon}[n - M_B + 3], \ldots, \breve{\varepsilon}[n]] \tag{5.35}$$

which contains all input symbols to the feedback filter. Furthermore, define the *extended feedback filter matrix*

$$\bar{\boldsymbol{B}}_{\text{np}\Delta} \triangleq \begin{bmatrix} \boldsymbol{B}_{\text{np}\Delta}[M_B - 1] \\ \boldsymbol{B}_{\text{np}\Delta}[M_B - 2] \\ \boldsymbol{B}_{\text{np}\Delta}[M_B - 3] \\ \vdots \\ \boldsymbol{B}_{\text{np}\Delta}[0] \end{bmatrix}. \tag{5.36}$$

Note that the dimension of this matrix is $NM_B \times N$.

As mentioned before, the matrix $\boldsymbol{B}_{\text{np}\Delta}[0]$ has zeros on and below the main diagonal. In order to avoid inconvenient constraints in the following mathematical formulation, shortened versions of the extended noise vector and the columns of $\bar{\boldsymbol{B}}_{\text{np}\Delta}$ are defined by

$$\epsilon_k[n] \triangleq [\epsilon[n]]_{[1(1)L_k]} \tag{5.37}$$

$$\boldsymbol{b}_k^H \triangleq [\bar{\boldsymbol{B}}_{\text{np}\Delta}]_{[1(1)L_k],k} \tag{5.38}$$

where the vector and matrix functions $[\ldots]_{[f(s)l]}$ and $[\ldots]_{[f(s)l],c}$ are defined in Tables A.3, A.7 and Equation (A.8). L_k is a positive integer number defining the lengths of the above vectors:

$$L_k = M_B N - N + k - 1. \tag{5.39}$$

In other words, the row vector $\epsilon_k[n]$ is formed by taking the first L_k elements of $\epsilon[n]$ and the column vector $\boldsymbol{b}_k^H$ is obtained by taking the first L_k elements in the k-th column of the matrix $\bar{\boldsymbol{B}}_{\text{np}\Delta}$.

Combining Equations (5.13), (5.34) and the above definitions yields the error signal ε_k

$$\varepsilon_k[n] = \breve{\varepsilon}_k[n] - \tilde{\varepsilon}_k[n]$$
$$= \breve{\varepsilon}_k[n] - \boldsymbol{\epsilon}_k[n]\boldsymbol{b}_k^H \quad (5.40)$$

The second moment of the signal ε_k is identical to the MMSE of the k-th user's estimate

$$J_{k,\mathrm{np}\Delta} \triangleq E\left[\varepsilon_k^*[n]\varepsilon_k[n]\right]$$
$$= J_{k,\mathrm{le,mmse}} - \boldsymbol{r}_{\breve{\varepsilon}\epsilon,k}\boldsymbol{b}_k^H - \boldsymbol{b}_k\boldsymbol{r}_{\breve{\varepsilon}\epsilon,k}^H + \boldsymbol{b}_k\boldsymbol{R}_{\epsilon,k}\boldsymbol{b}_k^H \quad (5.41)$$

where $J_{k,\mathrm{le,mmse}}$ is the k-th user's MMSE obtained with a MMSE MIMO LE (Equation (4.23)) and

$$\boldsymbol{r}_{\breve{\varepsilon}\epsilon,k}^H \triangleq E\left[\boldsymbol{\epsilon}_k^H[n]\breve{\varepsilon}_k[n]\right] \quad (5.42)$$
$$\boldsymbol{R}_{\epsilon,k} \triangleq E\left[\boldsymbol{\epsilon}_k^H[n]\boldsymbol{\epsilon}_k[n]\right]. \quad (5.43)$$

Using standard methods, the expression on the left hand side of Equation (5.41) can easily be minimized [46]. As a result, the optimal parameters of the feedback filter are given by

$$\boldsymbol{b}_{k,\mathrm{mmse}}^H = \boldsymbol{R}_{\epsilon,k}^{-1}\boldsymbol{r}_{\breve{\varepsilon}\epsilon,k}^H \quad (5.44)$$

$$\bar{\boldsymbol{B}}_{\mathrm{np}\Delta,\mathrm{mmse}} = \begin{bmatrix} \boldsymbol{b}_{1,\mathrm{mmse}}^H & \boldsymbol{b}_{2,\mathrm{mmse}}^H & \boldsymbol{b}_{3,\mathrm{mmse}}^H & \cdots & \boldsymbol{b}_{N,\mathrm{mmse}}^H \\ \boldsymbol{0}_N^H & \boldsymbol{0}_{N-1}^H & \boldsymbol{0}_{N-2}^H & \cdots & \boldsymbol{0}_1^H \end{bmatrix} \quad (5.45)$$

where $\boldsymbol{0}_i^H$ is an i-dimensional column vector in which each element is equal to zero (Table A.7). The optimal feedback filter matrices $\boldsymbol{B}_{\mathrm{np}\Delta}[m]$ are finally determined by comparing Equations (5.45) and (5.36).

Substituting the expressions for the optimal feedback filter into Equation (5.41)

yields the MMSE of user k

$$J_{k,\text{np}\Delta} = J_{k,\text{le,mmse}} - \boldsymbol{r}_{\breve{\varepsilon}\epsilon,k} \boldsymbol{R}_{\epsilon,k}^{-1} \boldsymbol{r}_{\breve{\varepsilon}\epsilon,k}^H. \tag{5.46}$$

The matrix-vector product $\boldsymbol{R}_{\epsilon,k}^{-1} \boldsymbol{r}_{\breve{\varepsilon}\epsilon,k}^H$ required for the solutions in Equations (5.44) and (5.46) is efficiently performed by applying a Cholesky factorization to the Hermitian $L_k \times L_k$-matrix $\boldsymbol{R}_{\epsilon,k}$ and backsubstitution with the elements of $\boldsymbol{r}_{\breve{\varepsilon}\epsilon,k}^H$. Note that the determination of the feedback filter coefficients can be done very efficiently: since the matrices $\boldsymbol{R}_{\epsilon,k}$ ($k = 1, 2, \ldots, N-1$) are all upper left submatrices of $\boldsymbol{R}_{\epsilon,N}$, only the latter matrix has to be Cholesky factorized. For all other submatrices, the Cholesky factors are directly obtained by partitioning the Cholesky factors of $\boldsymbol{R}_{\epsilon,N}$. Refer to Section 4.3.1.2 for more details.

Let us now find expressions for the vectors $\boldsymbol{r}_{\breve{\varepsilon}\epsilon,k}^H$ and the matrices $\boldsymbol{R}_{\epsilon,k}$, which are required to find the optimal feedback filter and the MMSE. In particular, it can be shown that

$$\boldsymbol{r}_{\breve{\varepsilon}\epsilon,k}^H = [\boldsymbol{R}_\epsilon]_{[1(1)L_k], L_k} \tag{5.47}$$

$$\boldsymbol{R}_{\epsilon,k} = [\boldsymbol{R}_\epsilon]_{[1(1)L_k], [1(1)L_k]}, \tag{5.48}$$

i.e. $\boldsymbol{r}_{\breve{\varepsilon}\epsilon,k}^H$ contains the first L_k components in the L_k-th column of the matrix $\boldsymbol{R}_\epsilon$; $\boldsymbol{R}_{\epsilon,k}$ is a submatrix consisting of the first L_k rows and columns of $\boldsymbol{R}_\epsilon$, which is defined by

$$
\begin{aligned}
\boldsymbol{R}_\epsilon \quad &\triangleq \quad E\left[\boldsymbol{\epsilon}^H[n]\boldsymbol{\epsilon}[n]\right] \\
&\overset{(5.35)}{=} \begin{bmatrix}
\boldsymbol{R}_{\breve{\varepsilon}}[0] & \boldsymbol{R}_{\breve{\varepsilon}}[1] & \ldots & \boldsymbol{R}_{\breve{\varepsilon}}[M_B - 1] \\
\boldsymbol{R}_{\breve{\varepsilon}}[-1] & \boldsymbol{R}_{\breve{\varepsilon}}[0] & \ldots & \boldsymbol{R}_{\breve{\varepsilon}}[M_B - 2] \\
\vdots & \vdots & \ddots & \vdots \\
\boldsymbol{R}_{\breve{\varepsilon}}[-M_B + 1] & \boldsymbol{R}_{\breve{\varepsilon}}[-M_B + 2] & \ldots & \boldsymbol{R}_{\breve{\varepsilon}}[0]
\end{bmatrix}
\end{aligned} \tag{5.49}
$$

where the autocorrelation sequence $\boldsymbol{R}_{\breve{\varepsilon}}[m]$ is defined by

$$\boldsymbol{R}_{\breve{\varepsilon}}[m] \triangleq E\left[\breve{\boldsymbol{\varepsilon}}^H[n - m]\breve{\boldsymbol{\varepsilon}}[n]\right]. \tag{5.50}$$

It may be calculated from the corresponding power spectrum

$$\boldsymbol{S}_{\breve{\varepsilon}}(D) \quad \triangleq \quad E_M \left[\breve{\boldsymbol{\varepsilon}}^H (D^{-*}) \breve{\boldsymbol{\varepsilon}}(D) \right] \tag{5.51}$$

$$\overset{(5.9)}{=} \quad \boldsymbol{\Delta}^{-1}(D) \, E_M \left[\breve{\boldsymbol{e}}^H (D^{-*}) \breve{\boldsymbol{e}}(D) \right] \, \boldsymbol{\Delta}(D)$$

$$= \quad \boldsymbol{\Delta}^{-1}(D) \, \boldsymbol{S}_{\breve{e}}(D) \, \boldsymbol{\Delta}(D). \tag{5.52}$$

Using the notational convention (1.24) and the D-transformation rule (1.25), one gets

$$\boldsymbol{R}_{\breve{\varepsilon}}[m] = \mathcal{D}^{-1} \left\{ \boldsymbol{S}_{\breve{\varepsilon}}(D) \right\}$$

$$= \boldsymbol{\Delta}^{-1}(D) \, \mathcal{D}^{-1} \left\{ \boldsymbol{S}_{\breve{e}}(D) \right\} \, \boldsymbol{\Delta}(D)$$

$$= \boldsymbol{\Delta}^{-1}(D) \, \boldsymbol{R}_{\breve{e}}[m] \boldsymbol{\Delta}(D)$$

$$= \begin{bmatrix} r_{\breve{e},11}[m] & r_{\breve{e},12}[m - (\Delta_2 - \Delta_1)] & \dots & r_{\breve{e},1N}[m - (\Delta_N - \Delta_1)] \\ r_{\breve{e},21}[m - (\Delta_1 - \Delta_2)] & r_{\breve{e},22}[m] & \dots & r_{\breve{e},2N}[m - (\Delta_N - \Delta_2)] \\ \vdots & \vdots & \ddots & \vdots \\ r_{\breve{e},N1}[m - (\Delta_1 - \Delta_N)] & r_{\breve{e},N2}[m - (\Delta_2 - \Delta_N)] & \dots & r_{\breve{e},NN}[m] \end{bmatrix}$$

$$\tag{5.53}$$

where $r_{\breve{e},ik}[m]$ is the (i,k)-th element of the matrix $\boldsymbol{R}_{\breve{e}}[m]$

$$r_{\breve{e},ik}[m] \triangleq \left[\boldsymbol{R}_{\breve{e}}[m] \right]_{ik}. \tag{5.54}$$

The forward filters of the MMSE MIMO NP-DDFE and the MMSE MIMO LE are identical. Thus, the error signal $\breve{\boldsymbol{e}}$ of the NP-DDFE is equal to the final error signal $\boldsymbol{e}$ of the LE before the decision. Recalling the expressions for the power spectrum of the latter signal, Equations (4.22) and (4.17), one finds for the MMSE MIMO NP-DDFE

$$\boldsymbol{S}_{\breve{e}}(D) = \boldsymbol{Q}^{-1}(D). \tag{5.55}$$

With this, the corresponding autocorrelation $\boldsymbol{R}_{\breve{e}}[m]$ may be calculated by performing

the inverse discrete-time Fourier transform (DTFT) on $\boldsymbol{S}_{\breve{e}}(e^{-j2\pi\breve{f}})$

$$\boldsymbol{R}_{\breve{e}}[m] = \int_0^1 \boldsymbol{Q}^{-1}(e^{-j2\pi\breve{f}})\, e^{j2\pi\breve{f}m}\, d\breve{f}. \tag{5.56}$$

5.3 Successive Detector

The successive DFE processes one data sequence after another. It is a special case of the delayed DFE for which the relative delays between two consecutive data sequences approach infinity.

In particular, for the interference reduction in symbol $\breve{a}_k[n]$ of user k, all decisions on previously, presently and subsequently transmitted symbols $\hat{a}_i[n-m]$ ($\forall m \in \mathbb{Z}$) of the lower indexed users $i < k$ are available to the feedback filter. Additionally, all decisions $\hat{a}_k[n-m]$ ($\forall m > 0$) on previously transmitted symbols of the same user may be employed in the feedback process. All other symbols have not been processed yet and are not available. As a result, the feedback filter $\boldsymbol{B}$ is constrained to be an upper triangular matrix function whose main diagonal elements must be causal, scalar functions.

The optimal forward and feedback filters with respect to the MMSE criterion can be determined by applying the orthogonality principle [46]. It states that all available detector input signals must be statistically orthogonal to the error in the final continuous-valued symbol estimate. Assuming that all decisions used in the feedback filter are correct, two necessary conditions to satisfy the orthogonality principle for the successive conventional decision-feedback equalizer (SC-DFE), Figure 4.6, are

$$E[u_i^*[n-m]e_k[n]] = 0, \quad \forall m \in \mathbb{Z};\ i \in \mathcal{I}_N \tag{5.57}$$

$$E[a_i^*[n-m]e_k[n]] = 0, \quad \forall m \in \mathbb{Z};\ i < k \tag{5.58}$$

where $k \in \mathcal{I}_N$. The $u_i[n]$, $a_i[n]$ and $e_i[n]$ ($i \in \mathcal{I}_N$) are the input signals to the forward filter, feedback filter and the error component in the data estimate before the decision element, respectively. $\mathbb{Z}$ is the set of all positive and negative integer numbers (see Table A.7). Note that the above equations will only be sufficient if previous decisions

of the currently decoded sequence are not used in the feedback process, i.e. if the decisions $\hat{a}_k[n-m]$ ($\forall m > 0$) are not available to the feedback filter for the detection of the symbol $a_k[n]$. This case is investigated in Section 5.3.1. However, if the previously detected symbols of the same sequence are used in the feedback filter, an additional equation is necessary in order to satisfy the orthogonality principle (Section 5.3.2).

Define the following cross-correlation functions and cross-power spectra

$$\boldsymbol{R}_{ue}[m] \triangleq E[\boldsymbol{u}^H[n-m]\boldsymbol{e}[n]] \tag{5.59}$$

$$\boldsymbol{R}_{ae}[m] \triangleq E[\boldsymbol{a}^H[n-m]\boldsymbol{e}[n]] \tag{5.60}$$

$$\boldsymbol{S}_{ue}(D) \triangleq E_M \left[\boldsymbol{u}^H(D^{-*})\boldsymbol{e}(D) \right] \tag{5.61}$$

$$\boldsymbol{S}_{ae}(D) \triangleq E_M \left[\boldsymbol{a}^H(D^{-*})\boldsymbol{e}(D) \right] \tag{5.62}$$

where $\boldsymbol{u} \triangleq [u_1, u_2, \ldots, u_N]$, $\boldsymbol{a} \triangleq [a_1, a_2, \ldots, a_N]$ and $\boldsymbol{e} \triangleq [e_1, e_2, \ldots, e_N]$. The corresponding cross-correlations and cross spectra are connected through the D-transform:

$$\boldsymbol{R}_{ue}[m] \xleftrightarrow{\mathcal{D}} \boldsymbol{S}_{ue}(D) \tag{5.63}$$

$$\boldsymbol{R}_{ae}[m] \xleftrightarrow{\mathcal{D}} \boldsymbol{S}_{ae}(D). \tag{5.64}$$

Considering the above definitions, the necessary conditions of the orthogonality principle (5.57) and (5.58) can alternatively be formulated in matrix form as

$$\boldsymbol{R}_{ue}[m] = \boldsymbol{O}_{N \times N}, \quad \forall m \in \mathcal{Z} \tag{5.65}$$

$$\{\boldsymbol{R}_{ae}[m]\}^{\blacktriangleleft} = \boldsymbol{O}_{N \times N}, \quad \forall m \in \mathcal{Z} \tag{5.66}$$

where $\{\boldsymbol{A}\}^{\blacktriangleleft}$ is a matrix whose upper triangular part is equal to that of $\boldsymbol{A}$ and which has zeros on and below the main diagonal (see Table A.3).

The necessary conditions of the orthogonality principle can also be formulated in the frequency-domain by applying the D-transform to Equations (5.65) and (5.66),

which yields

$$\boldsymbol{S}_{ue}(D) = \boldsymbol{O}_{N \times N}, \quad \forall D \in \mathcal{C} \tag{5.67}$$

$$\{\boldsymbol{S}_{ae}(D)\}^{\blacktriangleleft} = \boldsymbol{O}_{N \times N}, \quad \forall D \in \mathcal{C}. \tag{5.68}$$

The frequency-domain conditions of the orthogonality principle serve as starting point for the determination of the optimal forward and feedback filters. Consider now the vector block diagram of the system including MMSE MIMO SC-DFE with noise-whitening/channel matched filter front-end (Figure 4.6). The vector input signal to the forward filter is

$$\boldsymbol{u}(D) = \boldsymbol{a}(D)\boldsymbol{S}_x(D) + \boldsymbol{z}(D). \tag{5.69}$$

Assuming that all decisions provided to the feedback filter are correct, $\hat{\boldsymbol{a}} = \boldsymbol{a}$, the input signal to the decision element becomes

$$\tilde{\boldsymbol{a}}(D) = \boldsymbol{u}(D)\boldsymbol{L}(D) + \boldsymbol{a}(D)\boldsymbol{B}(D). \tag{5.70}$$

The error component in the final continuous-valued data estimate before quantization is then

$$\boldsymbol{e}(D) \triangleq \tilde{\boldsymbol{a}}(D) - \boldsymbol{a}(D)$$
$$= \boldsymbol{u}(D)\boldsymbol{L}(D) + \boldsymbol{a}(D)\left[\boldsymbol{B}(D) - \boldsymbol{I}_N\right]. \tag{5.71}$$

Consider the power spectra

$$\boldsymbol{S}_{az}(D) \triangleq E_M\left[\boldsymbol{a}^H(D^{-*})\boldsymbol{z}(D)\right] \tag{5.72}$$

$$\boldsymbol{S}_u(D) \triangleq E_M\left[\boldsymbol{u}^H(D^{-*})\boldsymbol{u}(D)\right] \tag{5.73}$$

$$\boldsymbol{S}_{ua}(D) \triangleq E_M\left[\boldsymbol{u}^H(D^{-*})\boldsymbol{a}(D)\right]. \tag{5.74}$$

Since $\boldsymbol{z}(D) = \boldsymbol{\nu}(D)\boldsymbol{S}_\nu^{-1}(D)\boldsymbol{X}^H(D^{-*})$ and $\boldsymbol{S}_{a\nu}(D) = \boldsymbol{O}_{N \times AK}$, $\forall D \in \mathbb{C}$ (Equa-

tion (2.63)), we get

$$\boldsymbol{S}_{az}(D) = \boldsymbol{O}_{N \times N}. \tag{5.75}$$

Substituting Equation (5.69) into (5.73) and applying the relationships (5.75), (4.60), (4.18) yields

$$\boldsymbol{S}_u(D) = \boldsymbol{S}_x(D)\boldsymbol{S}_a(D)\boldsymbol{Q}(D). \tag{5.76}$$

In the same manner, $\boldsymbol{S}_{ua}(D)$ is easily found to be

$$\boldsymbol{S}_{ua}(D) = \boldsymbol{S}_x(D)\boldsymbol{S}_a(D). \tag{5.77}$$

The cross-power spectrum $\boldsymbol{S}_{ue}(D)$ is calculated by substituting Equation (5.71) into (5.61)

$$
\boldsymbol{S}_{ue}(D) \overset{\overset{(5.71)}{(5.61)}}{=} E_M \left[\boldsymbol{u}^H(D^{-*}) \left\{ \boldsymbol{u}(D)\boldsymbol{L}(D) + \boldsymbol{a}(D)\left[\boldsymbol{B}(D) - \boldsymbol{I}_N\right] \right\} \right]
$$

$$
\overset{\overset{(5.74)}{(5.73)}}{=} \boldsymbol{S}_u(D)\boldsymbol{L}(D) + \boldsymbol{S}_{ua}(D)\left[\boldsymbol{B}(D) - \boldsymbol{I}_N\right]
$$

$$
\overset{\overset{(5.77)}{(5.76)}}{=} \boldsymbol{S}_x(D)\boldsymbol{S}_a(D)\left[\boldsymbol{Q}(D)\boldsymbol{L}(D) + \boldsymbol{B}(D) - \boldsymbol{I}_N\right]. \tag{5.78}
$$

Accordingly, the cross spectrum $\boldsymbol{S}_{ae}(D)$ is determined to be

$$
\boldsymbol{S}_{ae}(D) \overset{\overset{(5.71)}{(5.62)}}{=} E_M \left[\boldsymbol{a}^H(D^{-*}) \left\{ \boldsymbol{u}(D)\boldsymbol{L}(D) + \boldsymbol{a}(D)\left[\boldsymbol{B}(D) - \boldsymbol{I}_N\right] \right\} \right]
$$

$$
\overset{\overset{(5.74)}{(2.61)}}{=} \boldsymbol{S}_{ua}^H(D^{-*})\boldsymbol{L}(D) + \boldsymbol{S}_a(D)\left[\boldsymbol{B}(D) - \boldsymbol{I}_N\right]
$$

$$
\overset{(5.77)}{=} \boldsymbol{S}_a(D)\left[\boldsymbol{S}_x(D)\boldsymbol{L}(D) + \boldsymbol{B}(D) - \boldsymbol{I}_N\right]. \tag{5.79}
$$

The necessary conditions of the orthogonality principle as formulated above may

now be applied. Let us start with the first part (5.67). Combining this requirement with expression (5.78) and solving for the forward filter $\boldsymbol{L}(D)$ results in

$$\boldsymbol{L}(D) = \boldsymbol{Q}^{-1}(D)\left[\boldsymbol{I}_N - \boldsymbol{B}(D)\right]. \tag{5.80}$$

Substituting this equation into (5.79) yields after a few mathematical manipulations

$$\boldsymbol{S}_{ae}(D) = -\boldsymbol{L}(D) \tag{5.81}$$

$$= -\boldsymbol{Q}^{-1}(D)\left[\boldsymbol{I}_N - \boldsymbol{B}(D)\right]. \tag{5.82}$$

Comparing expression (5.81) with the orthogonality principle requirement (5.68) shows that the forward filter is a lower triangular matrix filter. Note that, in the right hand side of Equation (5.82), the notation with the factor $[\boldsymbol{I}_N - \boldsymbol{B}(D)]$ is used rather than the negative term $[\boldsymbol{B}(D) - \boldsymbol{I}_N]$. This might seem to be not significant, but it will prove very useful since the DC-coefficient of the former term, $[\boldsymbol{I}_N - \boldsymbol{B}[0]]$, is a normalized upper triangular matrix (it has ones on the main diagonal) due to the causality constraints imposed on the feedback filter.

Let us now apply the expression in Equation (5.82) to the second necessary condition of the orthogonality principle (5.68). This results in the following requirement for the feedback filter

$$\left\{-\boldsymbol{Q}^{-1}(D)\left[\boldsymbol{I}_N - \boldsymbol{B}(D)\right]\right\}^{\blacktriangleleft} = \boldsymbol{O}_{N \times N}. \tag{5.83}$$

5.3.1 Decision-Feedback Excluding the Currently Decoded Sequence

Consider that we want to ignore previous decisions $\hat{a}_k[n-m]$ of the sequence to be decoded, i.e. the sequence of user k. Thus, only the decisions $\hat{a}_i[n]$ ($\forall n \in \mathbb{Z}$) of the lower indexed data streams $i < k$ are used for interference reduction in the current estimate $\breve{a}_k[n]$. This simplifies the determination of the optimal forward and feedback filters and reduces a sufficient formulation of the orthogonality principle to the two Equations (5.57) and (5.58) (time domain) or Equations (5.67) and (5.68) (frequency

domain), respectively. Since no previous decisions of the currently decoded sequence are used in the feedback process, the feedback filter does not relate the k-th input signal to the k-th output. In other words, the main diagonal elements of $\boldsymbol{B}(D)$ are constrained to be zero, in the same manner as all elements of $\boldsymbol{B}(D)$ below the main diagonal must be zero.

The first part of the orthogonality principle is satisfied with the relationship (5.80). The second part requires to find a feedback filter which fulfills Equation (5.83).

Consider the decomposition of the matrix spectrum $\boldsymbol{Q}(D)$ by means of a Cholesky factorization

$$\boldsymbol{Q}(D) = \boldsymbol{\Gamma}(D)\boldsymbol{V}^{-1}(D)\boldsymbol{\Gamma}^H(D^{-*}) \tag{5.84}$$

where $\boldsymbol{\Gamma}(D)$ is a normalized upper triangular matrix, i.e. the elements below the main diagonal are equal to zero and the elements on the main diagonal are equal to one for all $D \in \mathbb{C}$. $\boldsymbol{\Gamma}^H(D^{-*})$ is a normalized lower triangular matrix function and $\boldsymbol{V}^{-1}(D)$ is a diagonal matrix.

Note that the Cholesky factorization (5.84) has to be interpreted as a procedure for a fixed variable D. The Cholesky factorization is, fundamentally, an operation on matrices and it is not defined for matrix functions. In practice, one may apply an approach identical to that described in Section 4.2.1.3, page 151: At first, the matrix spectrum $\boldsymbol{Q}(D)$ is frequency sampled on the unit circle $D = e^{-j2\pi\breve{f}}$ at a finite number of equidistant, discrete frequencies $\breve{f}_m = m/M_C$, where $m = 0, 1, 2, \ldots, M_C - 1$ and the number of sampling points M_C is an odd integer number. This results in M_C different points $D_m = e^{-j2\pi\breve{f}_m}$ located on the unit circle. A separate Cholesky factorization (5.84) is performed for every sample $D = D_m$, i.e. $\boldsymbol{Q}(D_m) = \boldsymbol{\Gamma}(D_m)\boldsymbol{V}^{-1}(D_m)\boldsymbol{\Gamma}^H(D_m^{-*})$, $\forall m = 0, 1, 2, \ldots, M_C - 1$.

Substituting Equation (5.84) into (5.83) yields

$$\left\{ \boldsymbol{\Gamma}^{-H}(D^{-*})\boldsymbol{V}(D)\boldsymbol{\Gamma}^{-1}(D)\left[\boldsymbol{I}_N - \boldsymbol{B}(D)\right] \right\}^{\blacktriangleleft} = \boldsymbol{O}_{N \times N}. \tag{5.85}$$

The inverse of a normalized upper (lower) triangular matrix is again a normalized upper (lower) triangular matrix [136, p.69]. Therefore, $\boldsymbol{\Gamma}^{-1}(D)$ is a normalized upper

triangular matrix, $\boldsymbol{\Gamma}^{-H}(D^{-*})$ is a normalized lower triangular matrix and $\boldsymbol{V}(D)$ is a diagonal matrix. It can now immediately be seen that the solution of Equation (5.85) is

$$\boldsymbol{\Gamma}^{-1}(D)\left[\boldsymbol{I}_N - \boldsymbol{B}(D)\right] = \boldsymbol{I}_N \tag{5.86}$$

since $\boldsymbol{\Gamma}^{-H}(D^{-*})\boldsymbol{V}(D)$ is a lower triangular matrix and, therefore, $\{\boldsymbol{\Gamma}^{-H}(D^{-*})\boldsymbol{V}(D)\}^{\blacktriangleleft} = \boldsymbol{O}_{N\times N}$ is satisfied. Solving Equation (5.86) for $\boldsymbol{B}(D)$ yields the optimal feedback filter of the MMSE MIMO SC-DFE

$$\boldsymbol{B}_{\text{sc0}}(D) = \boldsymbol{I}_N - \boldsymbol{\Gamma}(D). \tag{5.87}$$

The expression of the optimal forward filter is found by substituting the last relationship into Equation (5.80)

$$\boldsymbol{L}_{\text{sc0}}(D) = \boldsymbol{\Gamma}^{-H}(D^{-*})\boldsymbol{V}(D). \tag{5.88}$$

The power spectrum of the error signal at the input to the decision element can be found by substituting Equation (5.71) into definition (4.6) and applying the results for the optimal filters (5.87) and (5.88)

$$\boldsymbol{S}_e(D) = \boldsymbol{V}(D). \tag{5.89}$$

The individual MMSE of user k's signal can be found with Equation (4.12)

$$J_{k,\text{sc0}} = \int_0^1 \left[\boldsymbol{V}(e^{-j2\pi\check{f}})\right]_{kk} d\check{f}, \quad \forall k \in \mathcal{I}_N. \tag{5.90}$$

5.3.2 Decision-Feedback Including the Currently Decoded Sequence

The objective is now to estimate the symbol $a_k[n]$ based on the inputs to the forward filter $u_i[n-m]$ ($i \in \mathcal{I}_N$, $m \in \mathbb{Z}$), the decisions on the symbols of all lower indexed data streams $\hat{a}_i[n-m]$ ($i < k$, $m \in \mathbb{Z}$) *and* the decisions on previously detected

symbols of the same data stream $\hat{a}_k[n-m]$ ($m > 0$). The orthogonality principle for the former two information sets is formulated in Equations (5.57) and (5.58). This has to be extended by a third equation which reflects the orthogonality principle for the previous decisions of the currently decoded sequence k:

$$E[a_k^*[n-m]e_k[n]] = 0, \quad \forall m > 0, \ k \in \mathcal{I}_N. \tag{5.91}$$

Formulated in matrix form, this equation is equivalent to

$$\{\boldsymbol{R}_{ae}[m]\}^{\triangleleft} = \boldsymbol{O}_{N \times N}, \quad \forall m > 0 \tag{5.92}$$

where $\{\boldsymbol{A}\}^{\triangleleft}$ is a diagonal matrix whose diagonal elements are equal to those of $\boldsymbol{A}$ and which has zeros above and below the main diagonal (see Table A.3). Transforming the last expression into the D-domain results in

$$\left\{\{\boldsymbol{S}_{ae}(D)\}^{\triangleleft}\right\}^{+} = \boldsymbol{O}_{N \times N}, \quad \forall D \in \mathcal{C} \tag{5.93}$$

where $\{\boldsymbol{F}(D)\}^{+} \triangleq \boldsymbol{F}^{\blacktriangleleft}[0] + \sum_{m=1}^{\infty} \boldsymbol{F}[m]D^m$ denotes the purely causal part of the matrix-valued function $\boldsymbol{F}(D) \triangleq \sum_{m=-\infty}^{\infty} \boldsymbol{F}[m]D^m$ (see Table A.3). Substituting Equation (5.82) into the last expression yields

$$\left\{\{-\boldsymbol{Q}^{-1}(D)\left[\boldsymbol{I}_N - \boldsymbol{B}(D)\right]\}^{\triangleleft}\right\}^{+} = \boldsymbol{O}_{N \times N}. \tag{5.94}$$

This equation has to be used in conjunction with the conditions (5.80) and (5.83) in order to satisfy the orthogonality principle.

Consider the triangular Cholesky factorization of $\boldsymbol{Q}(D)$ in Equation (5.84) and in addition the spectral factorization of the diagonal matrix $\boldsymbol{V}^{-1}(D)$

$$\boldsymbol{V}^{-1}(D) = \boldsymbol{\Theta}(D)\boldsymbol{P}^{-1}\boldsymbol{\Theta}^{H}(D^{-*}) \tag{5.95}$$

where $\boldsymbol{P}^{-1}$ is a diagonal matrix independent of D and $\boldsymbol{\Theta}(D)$ is a causal and diagonal

matrix function as defined by

$$\mathbf{\Theta}(D) = \mathbf{I}_N + \sum_{n=1}^{\infty} \mathbf{\Theta}[n]\, D^n \tag{5.96}$$

$$\mathbf{\Theta}(D) = \{\mathbf{\Theta}(D)\}^{\triangleleft}. \tag{5.97}$$

Conversely, $\mathbf{\Theta}^H(D^{-*})$ is diagonal and anticausal.

Combining Equations (5.84) and (5.95) with the conditions (5.83) and (5.94) results in the two equations

$$\left\{\mathbf{\Gamma}^{-H}(D^{-*})\mathbf{\Theta}^{-H}(D^{-*})\mathbf{P}\mathbf{\Theta}^{-1}(D)\mathbf{\Gamma}^{-1}(D)\left[\mathbf{I}_N - \mathbf{B}(D)\right]\right\}^{\blacktriangleleft} = \mathbf{O}_{N \times N} \tag{5.98}$$

$$\left\{\left\{\mathbf{\Gamma}^{-H}(D^{-*})\mathbf{\Theta}^{-H}(D^{-*})\mathbf{P}\mathbf{\Theta}^{-1}(D)\mathbf{\Gamma}^{-1}(D)\left[\mathbf{I}_N - \mathbf{B}(D)\right]\right\}^{\triangleleft}\right\}^+ = \mathbf{O}_{N \times N}. \tag{5.99}$$

Examining Equations (5.98) and (5.99), it is clear that they are satisfied if

$$\mathbf{\Theta}^{-1}(D)\mathbf{\Gamma}^{-1}(D)\left[\mathbf{I}_N - \mathbf{B}(D)\right] = \mathbf{I}_N \tag{5.100}$$

since the term $\mathbf{\Gamma}^{-H}(D^{-*})\mathbf{\Theta}^{-H}(D^{-*})\mathbf{P}$ is a lower triangular matrix function whose main diagonal elements are anticausal functions.

Finally, the optimal feedback and forward filters of the MMSE MIMO SC-DFE are found by solving Equation (5.100) for $\mathbf{B}(D)$ and substituting the result into Equation (5.80)

$$\mathbf{B}_{\mathrm{sc}+}(D) = \mathbf{I}_N - \mathbf{\Gamma}(D)\mathbf{\Theta}(D) \tag{5.101}$$

$$\mathbf{L}_{\mathrm{sc}+}(D) = \mathbf{\Gamma}^{-H}(D^{-*})\mathbf{\Theta}^{-H}(D^{-*})\mathbf{P}. \tag{5.102}$$

The individual MMSE of user k can be determined in analogy to the previous section. It turns out that it is equal to the k-th diagonal element of the matrix $\mathbf{P}$, i.e.

$$J_{k,\mathrm{sc}+} = [\mathbf{P}]_{kk}, \quad \forall k \in \mathcal{I}_N. \tag{5.103}$$

For the determination of the forward and feedback filters, both the Cholesky factorization (5.84) and the spectral factorization (5.95) have to be performed. In practice, the spectrum is evaluated at discrete points on the unit circle $D = e^{-j2\pi m/M}$, where M is the length of the filters and $m = 0, 1, 2, \ldots, M - 1$. At first, a separate Cholesky factorization (5.84) is performed for each value of m. After that, the (matrix) spectral factorization can be efficiently evaluated by performing N separate (scalar) spectral factorizations (one for each of the scalar diagonal elements of $\boldsymbol{V}^{-1}(D)$) since $\boldsymbol{V}^{-1}(D)$ is a diagonal matrix. This significantly simplifies the complexity and the numerical requirements of the spectral factorization procedure. For example, while a matrix spectral factorization according to the algorithm of Harris and Davis [43] is computationally quite involving, a much simpler standard algorithm for the spectral factorization of scalar functions may be applied for diagonal matrices. As a result, the total number of operations required for the spectral factorization (5.95) increases only linearly with the number of users. In particular, the factorization is done by taking the i-th diagonal element of $\boldsymbol{V}^{-1}(D)$, $v_i^{-1}(D) = [\boldsymbol{V}^{-1}(D)]_{ii}$, and decomposing it into

$$v_i^{-1}(D) = p_i^{-1}\theta_i(D)\theta_i^*(D^{-*}) \tag{5.104}$$

where p_i is a scalar constant and $\theta_i(D)$ is a causal, scalar function with $\theta_k(D) = 1 + \sum_{n=1}^{\infty} \theta_k[n]\, D^n$. After this has been done for all $i \in \mathcal{I}_N$, the matrices $\boldsymbol{P}$ and $\boldsymbol{\Theta}(D)$ are given by

$$\boldsymbol{P} = \mathbf{D}\mathrm{iag}\langle p_i\rangle, \quad i = 1, 2, \ldots, N \tag{5.105}$$

$$\boldsymbol{\Theta}(D) = \mathbf{D}\mathrm{iag}\langle\theta_i(D)\rangle, \quad i = 1, 2, \ldots, N \tag{5.106}$$

where $\mathbf{D}\mathrm{iag}\langle\ldots\rangle$ is defined in Table A.3.

5.4   Numerical Results

The theoretical expressions derived in previous sections are now used in order to investigate the performance of the MIMO delayed DFE (DDFE) and the successive DFE (S-DFE) and compare it to the results obtained with the MIMO linear equalizer (LE) and the parallel, undelayed DFE.

In all cases, the equalizers have been optimized with respect to the MMSE criterion. For the sake of brevity, the abbreviations "MMSE" and "MIMO" are omitted. For example, the notation "DDFE" implies "MMSE MIMO DDFE" in this section. Note that the results do not distinguish between the noise-predictive and the conventional DFE structures because their theoretical performance is identical. Therefore, the abbreviation "DFE" refers to both C-DFE and NP-DFE. Accordingly, "DDFE" includes the C-DDFE and the NP-DDFE. "S-DFE" stands for the successive noise-predictive DFE which excludes previous decisions of the currently decoded sequence [106]. Its results are theoretically identical to the successive conventional DFE structure (SC-DFE) described in Section 5.3.1.

The following assumptions are made throughout this section:

- All equalizers use infinite-length forward filters,

- the feedback filters of the DFE and DDFE are of finite length. In particular, a constant filter length of $M_B = 7$ has been chosen,

- the feedback filter of the S-DFE is of infinite length,

- the decision-feedback of the S-DFE *excludes* previous decisions of the currently decoded sequence (see Section 5.3.1),

- the channel impulse responses are known without error,

- the equalizer signals and tap weights are of infinite precision, and

- all decisions fed back into the DFE feedback filter are correct, i.e. the results do not include error propagation.

The parameters of the system have been set to $A = 4$ antennas, a processing gain of $K = 4$ and a symbol period of $T = 50$ ns. This results in a number of diversity channels of $U_{\text{div}} = 16$ and frequency selective channels. Two different cases with respect to the distribution of the received signal energies have been investigated: The first situation considers a maximal difference in the received signal energy (*near-far ratio*) of 10 dB among all users, while the statistical distribution of the signal energies is uniform within this interval. In the second case, the near-far ratio has been set to 1 dB. Therefore, the former case refers to a situation with no or less stringent power control, while the latter describes a system with relatively tight power control.

As in Section 4.7, it is assumed that the data signals a_i are mutually and temporally independent, stationary continuous-time stochastic processes with zero mean and unit variance (Definitions A.1 and A.2). While the MMSE performance applies to any linear modulation format, this is not true for the error probability. For the bit-error rate (BER) and outage probability, 4-QAM with independently modulated inphase and quadrature signals is considered (Equation (4.143)). The symbols in the modulation alphabet are assumed to occur with equal probability.

Independent square QAM is considered for the capacity results. The number of modulation levels per user, L_i, is maximized under the constraint that a maximum BER of 10^{-4} be not exceeded.

The analog transmit and receive filters $p_C(t)$ and $b_C(t)$ are fifth-order Butterworth lowpass filters with a cut-off frequency $f_{3\text{dB}} = K/(2T)$. This implies that $K_{3\text{dB}} = K$. For more information, refer to Section 2.3.3.1. The spreading filters in the transmitters have been omitted (i.e. $q_i[n] = \delta_K[n]$, $\forall i \in \mathcal{I}_N$) for the same reason as in Section 4.7.

The same semi-analytical approach as in Section 4.7 has been used in order to determine the results. In particular, given the channel impulse responses, the MMSE's have been calculated according to Section 4.2.1.1 for the LE and Section 5.2.2.2 for both the DFE and the DDFE. In order to calculate the MMSE of the S-DFE, the method described in publication [106] has been adopted. This approach excludes previous decisions of the currently decoded sequence and leads, therefore, to the same results as the detector described in Section 5.3.1.
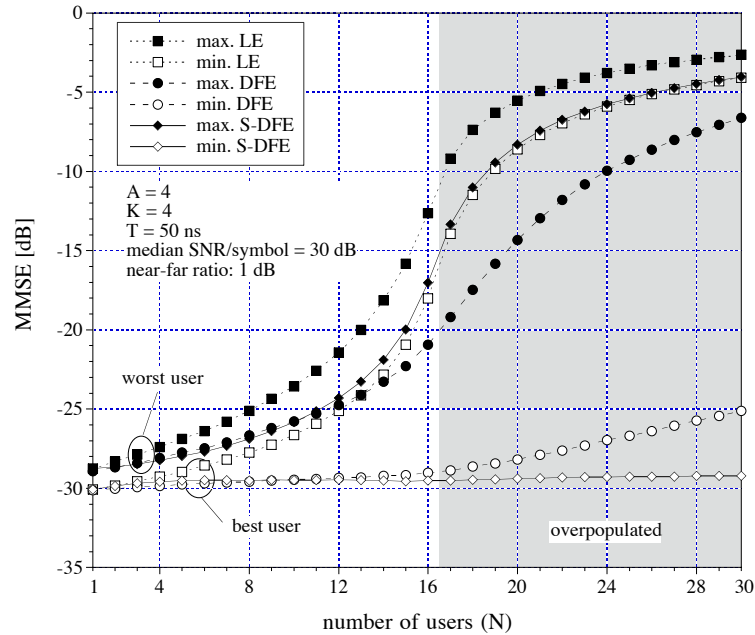
Figure 5.10: Best and worst user MMSE averaged over different channels for the LE, (parallel) DFE and S-DFE in identical 4×4, $T = 50$ ns systems with a median received SNR/symbol of 30 dB and a near-far ratio of 1 dB.

Bounds on the bit error rate (BER) and system capacity have been determined using expressions (4.132) and (4.142). All results represent the average over 100 scenarios with different radio channels, which belong to an ensemble of measured indoor channel impulse responses (Section 2.3.3.2). The radio channels are frequency selective for the chosen symbol rate of 50 ns and cause significant ISI and CCI over several symbols. Details about the channel impulse response (CIR) delay spread and other characteristics are given in Section 4.7 or in Behin's report [12]. The method for selecting the particular CIR's is identical to that described in Section 4.7.

The following performance measures are evaluated as a function of the number of system users (N). Figure 5.10 shows the MMSE of the best and the worst of all 30 users, averaged over 100 trials with different channel impulse responses. In this case, all users are received with similar average powers (maximal variation of 1 dB). The median received SNR/symbol[1] (received signal to Gaussian noise power ratio per

---

[1]The received SNR/symbol of user k, Γ_k, is the expectation over the output SNR of a maximal ratio combiner when only user k is in the system and all interference (CCI and ISI) is zero, i.e. the ideal single user, one shot case. Γ_k is defined in Section D.1, Equation (D.6). It may be calculated

user and symbol) among all system users is 30 dB. The best and worst user curves are shown for the LE, the (parallel) DFE and the S-DFE. Let us at first consider the worst user performance. It can be seen that the results for the DFE and the S-DFE are almost identical for low to medium populations of up to 12 users. In higher loaded systems, the DFE achieves a lower MMSE than the S-DFE. Note that the S-DFE worst user MMSE is lower bounded by the best user MMSE of the LE because the users are ordered according to their MSE performance after the forward filter, which is identical to the forward filter of the LE (considering a noise-predictive DFE structure). Hence, the best user of the S-DFE after the forward filter, user 1, does not benefit from the decision-feedback structure and its performance is identical to that achievable with a LE detector. The best user's MMSE curves of the S-DFE and the DFE are very close for up to 16 users. In the overpopulated region, the S-DFE seems to perform increasingly better. However, the results for large N have to be treated with care since fed-back decision errors are neglected. For example, once the worst user MMSE exceeds -10 dB, the error probability becomes relatively large and the displayed results may not be reliable. In conclusion, both decision-feedback equalizers perform almost equally for low to medium N. For highly populated and overpopulated systems, the parallel DFE is preferable since it offers a better worst user performance.

Figure 5.11 shows the same situation as before except that the maximal spread in the received power per user is increased to 10 dB. The received SNR/symbol varies between -25 dB and -35 dB with a median value of -30 dB. Firstly, we note that the LE performs consistently worse than both decision-feedback equalizers. Secondly, the results for DFE and S-DFE are now reversed as compared to the case with similar received powers (Figure 5.10). The worst user MMSE of the DFE increases continuously with each additional system user. On the other hand, the worst user MMSE of the S-DFE seems to be almost constant between 1 and 13 users. Adding more users leads to a strong increase in the MMSE since the curve follows the best user MMSE of the LE. For less than 16 users, the worst user MMSE of the S-DFE is lower than

---

from the channel impulse responses and the power spectral density of the additive white Gaussian noise with Equation (D.7).
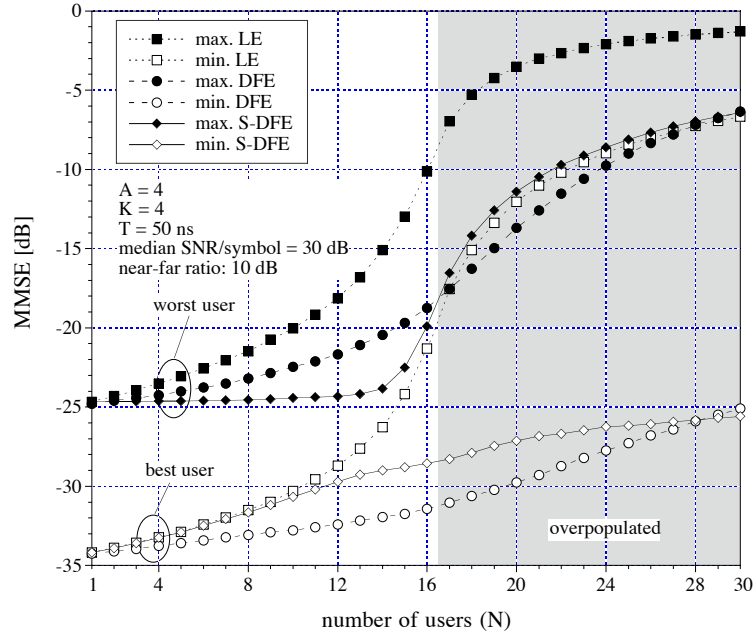
Figure 5.11: Best and worst user MMSE averaged over different channels for the LE, (parallel) DFE and S-DFE in identical 4×4, $T = 50$ ns systems with a median received SNR/symbol of 30 dB and a near-far ratio of 10 dB.

that of the DFE. This indicates overall a superior performance of the S-DFE because the worst user limits the system performance. In exchange, a higher MMSE of the best user can be tolerated since its performance is already very good and does not need further improvement. Thus, the larger best user MMSE of the S-DFE compared to that of the DFE may be considered less significant. The results prove that the S-DFE is able to achieve larger improvements for the bad users while doing less for the better ones. In particular, the performance spread between the best and the worst user narrows from 10 dB for the single user case to approximately 5 dB for 13 users. As a result, the S-DFE is able to mitigate the harmful consequences of the near-far effect.

Let us now compare the S-DFE and a DDFE with relatively long delays[2] between consecutive users. In particular, the individual delays are chosen according to $\Delta_{k+1} = \Delta_k + 3$ ($\Delta_1 = 0$). Note that the S-DFE can be viewed as a special case of the DDFE for which the individual delays between consecutive users approach infinity. Additional

---

[2] "Relatively long delays" describe delays that are longer then the rms delay spread of the channel.
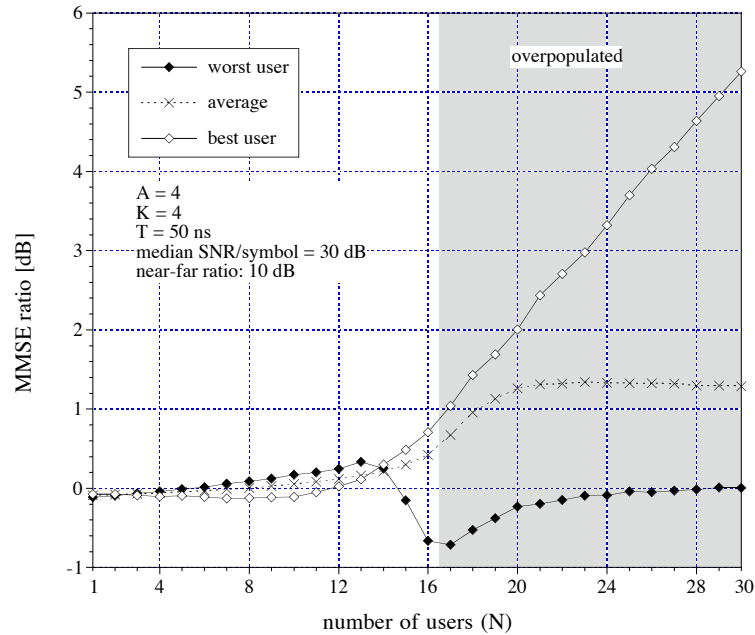
Figure 5.12: MMSE ratio between the DDFE ($\Delta_{k+1} = \Delta_k + 3$) and the S-DFE for the best, worst and mean MMSE of all N system users, averaged over different channels for identical 4×4, $T = 50$ ns systems with a median received SNR/symbol of 30 dB and a near-far ratio of 10 dB.

differences between both detectors are that the feedback filter of the DDFE is of finite length ($M_B = 7$) and that it includes previous decisions of the same data sequence in the feedback process. On the other hand, the feedback filter of the S-DFE is assumed to be infinitely long, using all decisions of the lower indexed users, but excluding previous decisions of the currently decoded sequence. Figure 5.12 plots the ratio between the MMSE of the DDFE and the MMSE of the S-DFE (in dB) versus the number of system users. Note that values larger than zero indicate that the S-DFE performs better than the DDFE and vice versa. The system parameters are identical to those in Figure 5.11, i.e. a near-far ratio of 10 dB with a median received SNR/symbol of 30 dB. Figure 5.12 shows three curves: one for the best user averaged over all trials, one for the worst user and one for the average over all users and trials. It can be seen that there is hardly any difference between the S-DFE and the DDFE for up to 14 users. For larger N, the S-DFE is able to achieve an increasingly lower MMSE for the best system user. This behavior may be attributed to the infinite length of the S-DFE compared to the truncated feedback filter of the DDFE. For the
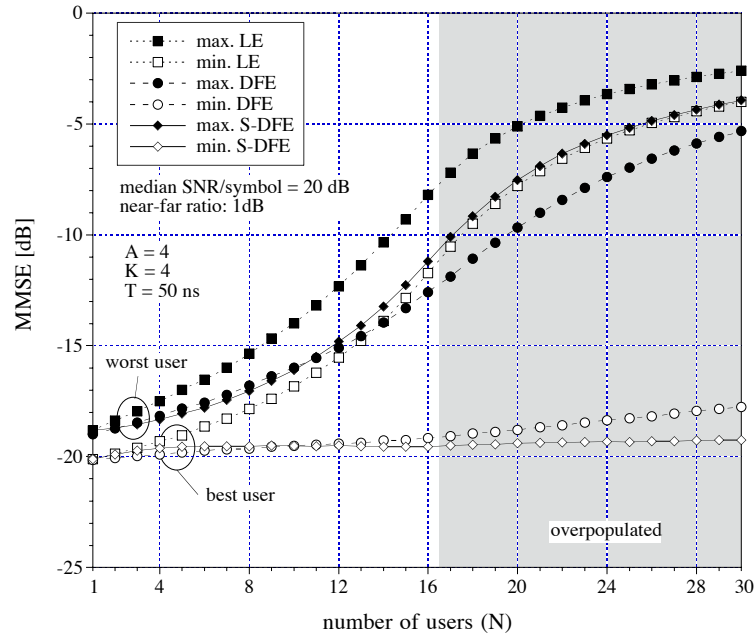
Figure 5.13: Best and worst user MMSE averaged over different channels for the LE, (parallel) DFE and S-DFE in identical 4×4, $T = 50$ ns systems with a median received SNR/symbol of 20 dB and a near-far ratio of 1 dB.

worst user, the DDFE performs better in the region $N > 14$, reaching the maximal advantage for 17 users and approaching the S-DFE for increasing N. In occurs that previous decisions of the same sequence are most useful when the system is critically loaded ($N \approx U_{\mathrm{div}}$) and all diversity paths are occupied with approximately one signal. Most importantly, however, this figure shows that the S-DFE performs indeed like a DDFE whose individual delays exceed significantly the delay spread of the channels.

The following three figures 5.13, 5.14 and 5.15 are identical to figures 5.10, 5.11 and 5.12, respectively, except that they are obtained for a lower median received SNR/symbol of 20 dB. This particular SNR/symbol will also be used for the following error probability investigations. It can be observed that the different detectors behave essentially the same for a lower received SNR/symbol. The MMSE curves are generally flatter and increase less with growing N since they start already at a higher MMSE in the single user case. For a near-far ratio of 1 dB (Figure 5.13), the difference in performance between the S-DFE and the DFE is smaller and the DFE provides slightly better worst user results in highly populated and overpopulated systems. If
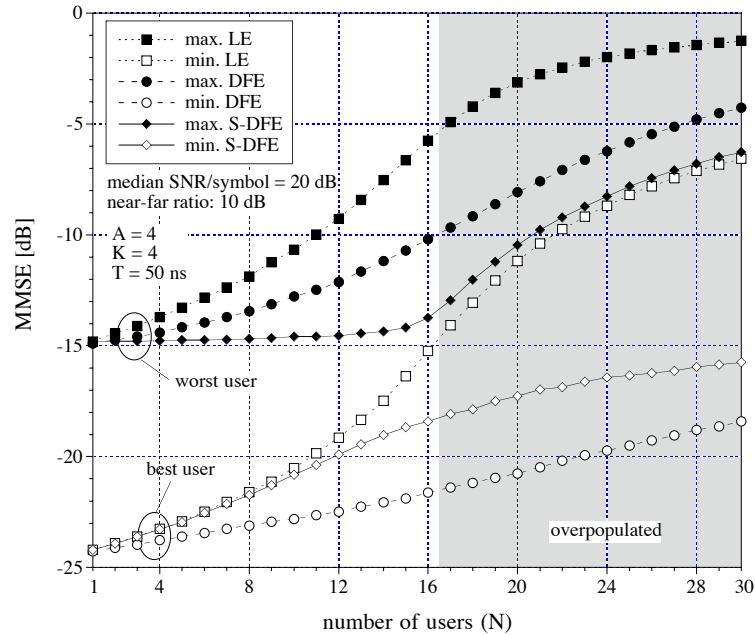
Figure 5.14: Best and worst user MMSE averaged over different channels for the LE, (parallel) DFE and S-DFE in identical 4×4, $T = 50$ ns systems with a median received SNR/symbol of 20 dB and a near-far ratio of 10 dB.

there is no or only partial power control (Figure 5.14), the S-DFE will achieve a considerable advantage over the DDFE for the worst user. The performance difference between S-DFE and DDFE, shown in Figure 5.15, becomes generally smaller for a lower received SNR and both detectors obtain very similar results especially in well populated systems ($N \leq 16$).

The Saltzberg upper bound of the *bit-error rate* (BER) for the LE, DFE and S-DFE detectors versus the number of users is shown in the next two pictures. The median received SNR/symbol is set to 20 dB as in the last examples (since 4-QAM with 2 bits/symbol is used, the median received SNR/bit is 17 dB). There are two types of curves: the black symbols ("max.") show the BER for the worst user within a set of 30 users averaged over 100 trials with different channels; the grey curves ("avg.") represent the (arithmetic) average over all users and trials.

Figure 5.16 shows the results for a situation in which the received SNR's of all users differ by at most 1 dB. Note that the S-DFE will produce less errors if the number of users is smaller than 12. For more densely populated systems, the parallel
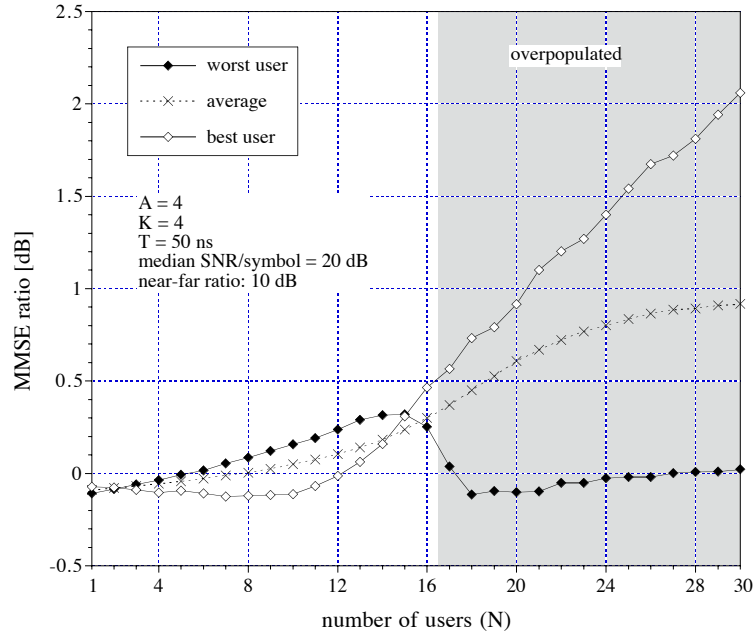
Figure 5.15: MMSE ratio between the DDFE ($\Delta_{k+1} = \Delta_k + 3$) and the S-DFE for the best, worst and mean MMSE of all N system users, averaged over different channels for identical 4×4, $T = 50$ ns systems with a median received SNR/symbol of 20 dB and a near-far ratio of 10 dB.
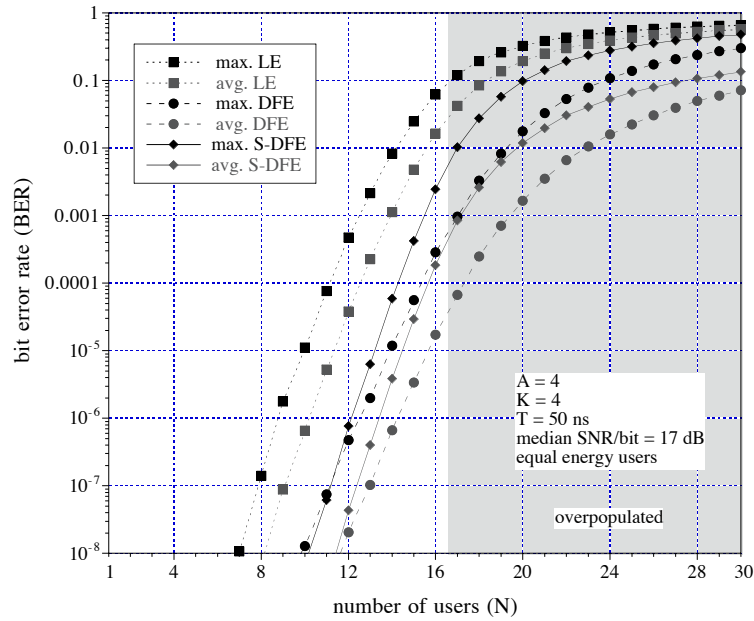
Figure 5.16: Average and worst user BER averaged over different channels for the LE, (parallel) DFE and S-DFE in identical 4×4, $T = 50$ ns systems with a median received SNR/bit of 17 dB and a near-far ratio of 1 dB.
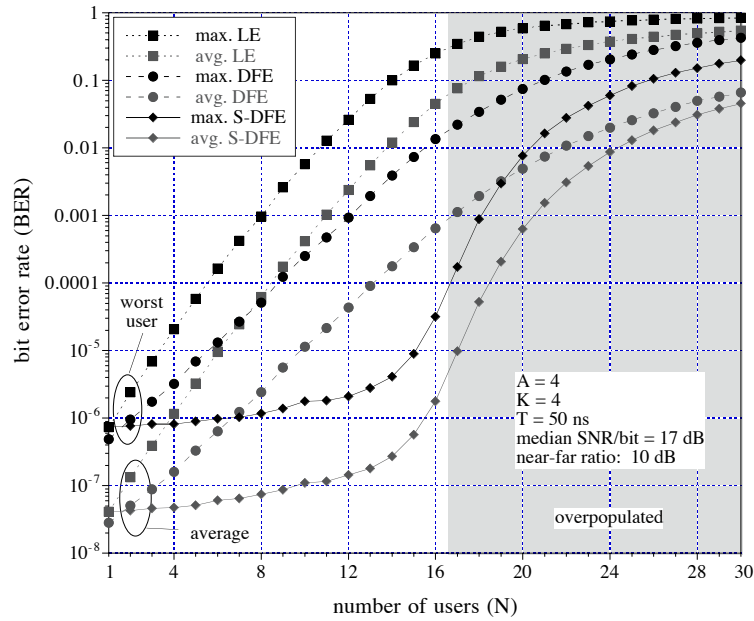
Figure 5.17: Average and worst user BER averaged over different channels for the LE, (parallel) DFE and S-DFE in identical 4×4, $T = 50$ ns systems with a median received SNR/bit of 17 dB and a near-far ratio of 10 dB.

symbol feedback of the DFE performs better than the successive method. Due to the negligence of feedback errors, the accuracy of the results is decreasing for growing BER's. However, the values shown should be reliable for worst user BER's less than 10^{-3}.

Results for the same system except for a more relaxed power control, allowing received SNR's per users to vary by up to 10 dB, are displayed in Figure 5.17. In this case, the S-DFE will perform significantly better than the DFE if there is more than one user in the system[3]. It is very interesting to compare the increase in the error probability for growing user populations. For example, if N grows from 1 to 14 users, the worst user's error probability will increase dramatically by a factor of 100,000 for the LE and a factor of 10,000 for the DFE. However, the worst user's BER of the S-DFE will increase by only 5 times. Comparable results are obtained

---

[3]In the single user case, the MIMO DFE degenerates to a single-input single-output DFE. On the other hand, the S-DFE becomes a single-input single-output linear equalizer because it does not use previous decisions in the feedback filter. Hence, for systems with only one user, the DFE performs better than the S-DFE.
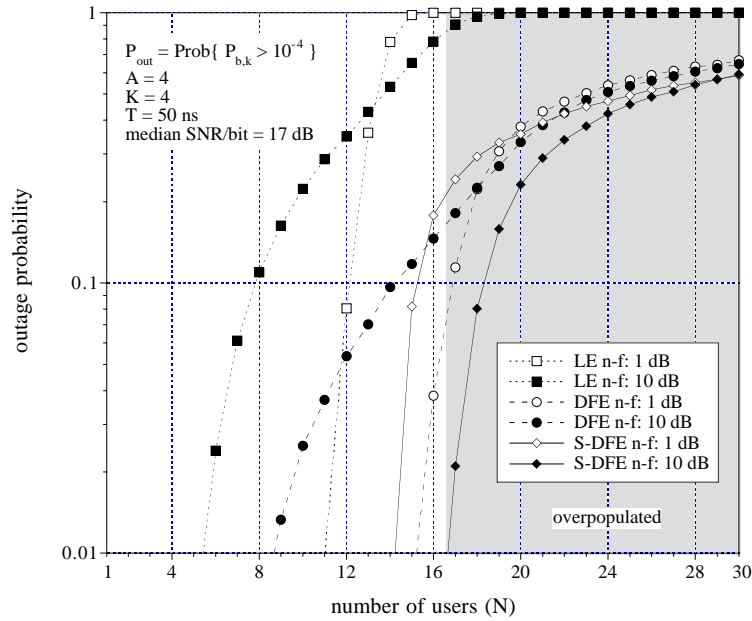
Figure 5.18: Estimated outage probability $\hat{P}_{\text{out}}$ for the LE, (parallel) DFE and S-DFE in identical 4×4, $T = 50$ ns systems with a median received SNR/bit of 17 dB and near-far ratios of 1 and 10 dB.

for the average BER[4]. Hence, the most vulnerable user with the worst performance is only very mildly affected by a growing user population as long as N is lower than the number of diversity channels. This is a very desirable property for a multiuser system because all users are in general equally important.

Let us now consider the *outage probability*, P_{out}, of the described system for the three detector types. As in Section 4.7, an outage condition is assumed when the BER exceeds 10^{-4} (Equation (4.144)). All users whose Saltzberg upper bound BER is larger than 10^{-4} are counted. This number is then divided by the total number of users considered (3000 users) in order to determine an estimate of the outage probability ($\hat{P}_{\text{out}}$, Equation (4.145)). Figure 5.18 is a plot of the estimated outage probabilities versus the number of system users for the LE, DFE and S-DFE. The white symbols represent the results for a system with relatively tight power control (near-far ratio of 1 dB) and the black symbols are obtained for identical system parameters except for more relaxed power control requirements (near-far ratio of 10 dB).

---

[4]Note that the average BER is dominated by the users whose performance is relatively bad. Therefore, the behavior of the worst user's BER and the average BER is very similar.

The outage probability results for the decision-feedback detectors are unreliable in highly overpopulated systems since erroneous decisions used in the feedback loop are neglected. In contrast to the curves for the DFE and the S-DFE shown in the figure, it can be expected that the outage probability approaches in practice 100% for large N. For a comparison of the different detectors, let us assume that a maximal outage probability of 1% is tolerated. Keeping the median received SNR/symbol constant at 20 dB and increasing the near-far ratio from 1 to 10 dB, the number of supportable users drops for the LE by 6 (from 11 to 5 users) and for the DFE by 7 (from 15 to 8 users). The S-DFE is significantly less sensitive to a change in the near-far ratio since the number of supportable users changes by only 2 (maximal 14 and 16 users, respectively). Note also that for close to equal received powers (1 dB near-far ratio), the outage probability seems to change threshold-like if a certain number of users is exceeded. This qualitative behavior will be preserved only for the S-DFE if the near-far ratio increases to 10 dB. In contrast, the outage probability of the LE and DFE grows continuously at a smaller slope for increasing N, already having significant outage probabilities for a relatively small number of users.

Lower bounds for the *system capacity* (Definition 4.1) have been derived in Section 4.5. The asymptotic capacity C_{as} (Equation (4.139)) neglects the fact that the number of symbols being transmitted must be an integer number. On the other hand, the system capacity C takes this practical constraint into account.

Figure 5.19 shows lower bounds for the asymptotic capacity of the system in bits per number of diversity channels versus the number of users for the three detector types. The received SNR's per user are varying by up to 10 dB. Two sets of curves are plotted: one for a median SNR/symbol of 20 dB (black) and the other for a median SNR/symbol of 30 dB (white). If the number of users is relatively small, the asymptotic capacity of all three equalizers increases at approximately the same rate for growing N. Using a LE, the system reaches the maximal capacity when the number of users is approximately three quarters the number of diversity channels and decreases if N grows further. The capacity for the DFE and the S-DFE increases for growing N until the number of users exceeds the number of diversity channels. After that it stays approximately constant for further increasing N. In the case of
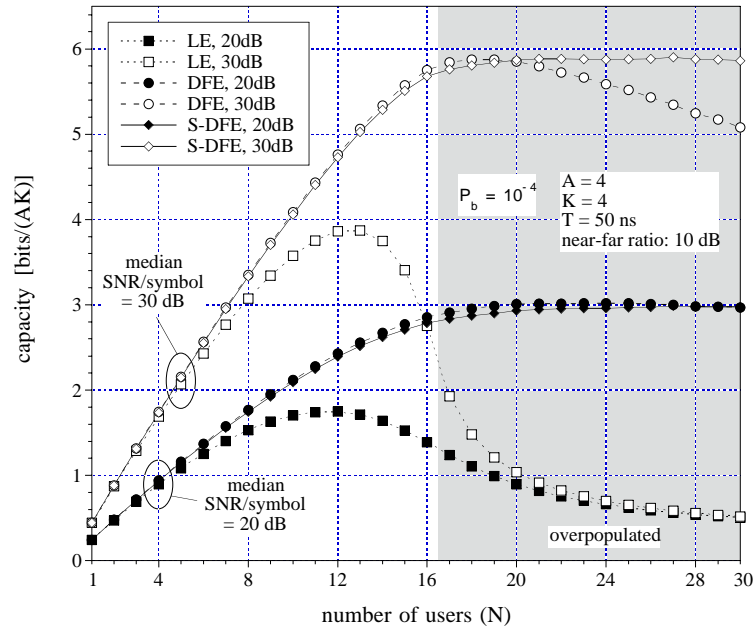
Figure 5.19: Lower bounds on the asymptotic capacity C_{as} for the LE, (parallel) DFE and S-DFE in identical 4×4, $T = 50$ ns systems with a near-far ratio of 10 dB and median received SNR/symbol of 20 and 30 dB.

higher received signal powers, the capacity of the DFE decreases to some extent in the overpopulated region for growing N. Note that the capacity of the DFE and the S-DFE is almost identical for reasonable populations between 1 and 20 users.

Lower bounds on the practically achievable capacity C are plotted in the diagram of Figure 5.20 for the same system parameters as in the previous figure. It can be observed that the capacity of the LE approaches zero very fast in the overpopulated region. The capacity curves of the DFE and C-DFE are very close. Both decision-feedback types approach their maximal system capacity when the number of users is approximately equal to the number of diversity channels.

It is interesting to compare this situation with one in which the received signal energies differ only slightly. Figure 5.21 shows lower bounds on the practically achievable capacity for a near-far ratio of only 1 dB. Note that the capacity curves of the decision-feedback equalizers change very little compared to the last figure. It seems that varying the spread of the individually received SNR's per user does not or only marginally affect the overall system capacity for the S-DFE and the DFE. In addition, both decision-feedback detectors achieve very similar capacities for all reasonable val-
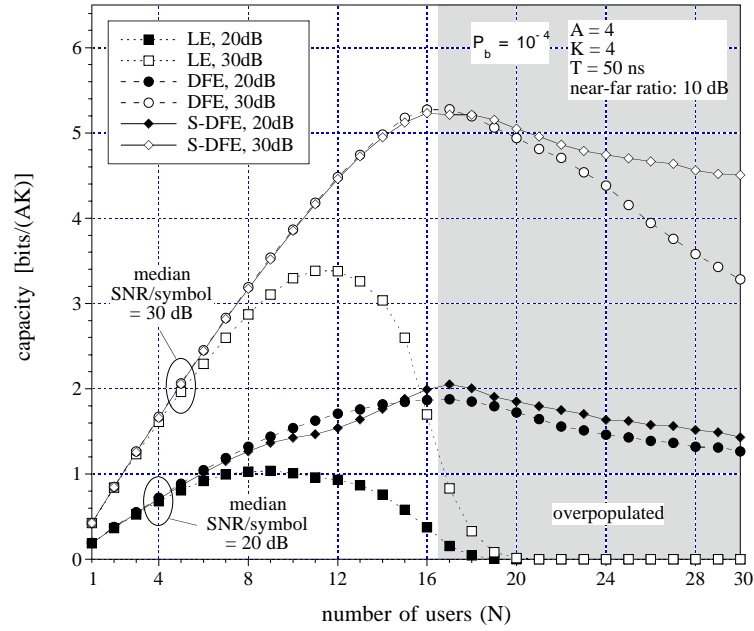
Figure 5.20: Lower bounds on the practically achievable capacity C for the LE, (parallel) DFE and S-DFE in identical 4×4, $T = 50$ ns systems with a near-far ratio of 10 dB and median received SNR/symbol of 20 and 30 dB.
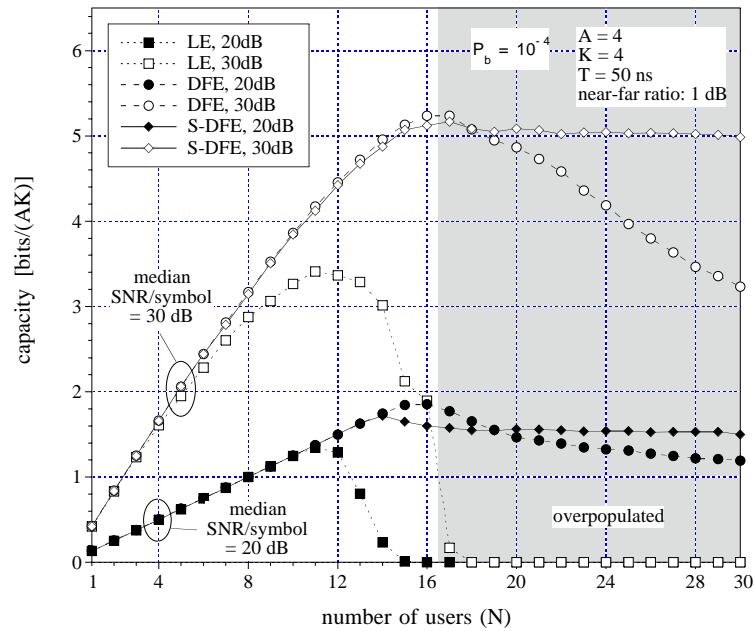
Figure 5.21: Lower bounds on the practically achievable capacity C for the LE, (parallel) DFE and S-DFE in identical 4×4, $T = 50$ ns systems with a near-far ratio of 1 dB and median received SNR/symbol of 20 and 30 dB.

ues of N. This suggests that the system capacity is more or less independent of both the near-far ratio and the delays between individual users data sequences before the decision element. In other words, the delayed MIMO DFE is not able to achieve a larger system capacity than the regular, undelayed MIMO DFE.

5.5   Conclusion

Delayed-decision-feedback equalization (DDFE) is the topic of this chapter. Based on a general idea mentioned by Duel-Hallen [29] and Fulghum [35, 36], the decisions on more reliable symbols of data streams with a better performance are made at first. This information is then used in the feedback filter in order to increase the quality of the interference estimate in the signals of lower performance users. In essence, the achievable performance improvement gained with decision-feedback is redistributed in order to improve the worse signals more and the better signals less.

The main contributions of this work are the description of a simple structure which changes the decision order of the different data sequences (delayed-decision-feedback equalizer, DDFE) and its mathematical analysis. In particular, expressions for the optimal forward and feedback equalizer as well as for the performance are derived in Section 5.2.1 for the conventional structure and in Section 5.2.2 for the noise-predictive type. Most of the analysis is done in the frequency domain, however, Section 5.2.2.2 describes a method for the calculation of the NP-DDFE feedback filter in the time-domain. A simpler solution with respect to the number of required operations is obtained by conceptually increasing the individual delays between consecutive data sequences to infinity. This results in the successive decision-feedback equalizer (S-DFE), which is described and analyzed in Section 5.3.

The numerical results in this chapter show that the absolute performance of a linear equalizer can be improved by adding a feedback filter that utilizes previous symbol decisions. The decision-feedback type equalizers achieve better results than the linear equalizer with respect to all investigated performance quantities including the MMSE, BER, outage probability and system capacity. Furthermore, the results show that a change in the relative individual delays of the DDFE affects the system

capacity only little, if at all. Hence, a DDFE may apparently not be able to improve the absolute system performance. However, the individual delays can be chosen in order to distribute, within certain limits, the amount of performance improvement individually for different data sequences. For example, it is possible to improve the weaker signals relatively more and the stronger signals relatively less while achieving the same overall improvement for all users. Hence, the DDFE narrows the performance gap between the strongest and the weakest signal. This is in practice a very desirable property since all users are in general equally important and deserve the same or at least a comparable signal quality.

A possible solution for the near-far effect, i.e. a situation in which the signals of the system users are received with significantly different energies, is a feedback path to the users which provides them with information about the channel and system properties. This information may be used in order to adjust the transmit powers of the individual portables such that the base station receives all signal with equal energy (power control). Alternatively, the transmitters may use the channel information in order to adjust their information rate (send as much bits per data symbol as possible while meeting a certain error rate). However, it has been shown in this chapter that the same or comparable improvements may be achieved with delayed-decision-feedback equalization (DDFE) at a reduced system complexity[5]. A feedback path to the users is not required because DDFE is performed exclusively at the receiver. In addition, DDFE is implemented with simple delay elements, adding practically no additional hardware complexity to the system.

---

[5]It may also be possible to replace a complex, fast and tight power control technique by a combination of DDFE with a less stringent and complex power control method.

Chapter 6

Conclusions

The central topic of this dissertation is a wireless spread spectrum based multiuser system consisting of several portables and one central base station. Considered is only the reverse link (uplink) communication from the portables to the base. The base station may receive the signals at multiple antennas.

Multiple-input multiple-output (MIMO) equalizers have been considered as detectors in order to recover the transmitted data of all users. These detectors have been designed for frequency selective and quasi-stationary systems.

Frequency-selective or time-dispersive channels cause intersymbol and cochannel interference from temporally preceding and subsequent symbols. A quasi-stationary system may be treated as completely stationary for analysis purposes if we are concerned about the detection of symbols for a certain data block only. The general assumption is that the system behavior does not change during the transmission of one data block, but may change in the long term from one block to another.

6.1 System Model

An equivalent discrete-time model is developed for the multiuser system. The model requires no pulse generators, sampling devices, up- or downsamplers. It consists simply of linear discrete-time filters and operates at the symbol rate only. These properties make it easy to handle and analyze. Despite its simple structure, the

discrete-time model is an exact representation of the initial system model.

Important information can be gained from the structure of the model. It has been shown that the number of parallel diversity channels is equal to the product of processing gain K (bandwidth spreading factor) and the number of receive antennas A. In other words, the system may be represented by a set of $U_{\mathrm{div}} = AK$ linear equations. This gives an immediate idea about the number of portables (N) that may be supported by the system: for $N < AK$, there is more information available at the receiver than signals to recover and the remaining diversity may be used to enhance the performance; for $N > AK$, not enough information is available to estimate the signals with a *linear* detector.

6.2   Calculation of the Error Probability

The Saltzberg bound is a simple and popular approximation for the error probability of linear systems. It has been adapted in this work to multiuser systems using rectangular quadrature amplitude modulation (QAM) with independent inphase and quadrature signal components. In this case, both the inphase and the quadrature signals are pulse amplitude modulated (PAM). The final expressions for the Saltzberg bound depend only on the signal-to-interference-and-noise ratio (SINR) and the number of modulation levels. For square QAM, the number of PAM levels is the same for both inphase and quadrature signals. In this case, the Saltzberg bound is identical for both components and depends on the overall SINR (i.e. the SINR of the complex baseband signal). The total SINR can be calculated from the minimum mean-square error (MMSE) of an optimal equalizer. This fact is important in Chapter 4, where the Saltzberg bound is formulated in terms of the MMSE and the number of modulation levels.

Sometimes, more accurate approximations of the error probability than the Saltzberg bound are required. A new class of strict and approximate upper bounds has been derived for systems with Gaussian noise and interference. The bounds are valid for systems with the following three properties: data symbols sent at different times are statistically independent and zero mean; the noise and data signals are indepen-

dent; and the noise is Gaussian distributed with zero mean. At first, the unique root of a transcendental expression has to be determined. After that, the root value is substituted into a given formula, which yields the approximation of the error probability. The simplest approximation is the *energy upper bound*, for which only the variance of the interference and the variance of the noise are required. However, it fails to provide accurate results in situations of high signal-to-noise ratio (SNR) and small to moderate interference. Significantly better results are achieved with the first- and second-order approximations, which require explicit knowledge of all interference samples. The second-order approximation needs approximately three times as many operations as the first-order bound, but the overall amount grows in both cases linearly with the number of interfering symbols. In exchange for the higher numerical complexity, the second-order approximation achieves a better accuracy. It has been shown that both approximations perform reliably in most situations. The worst results are obtained for a large peak distortion (maximal possible value of the interference) *and* high SNR. However, the approximation and the true error probability differed even in these cases by less than a factor of 2. Considering its accuracy, conceptual and numerical complexity, the developed method compares very well with already existing high-performance approximations.

6.3 Equalizers for Spread Spectrum Multiuser Systems

The signals transmitted by different users of spread spectrum systems are, in practice, usually not orthogonal and interfere with each other. Only true multiuser detectors, taking the special characteristics of all signals into account, are able to suppress interference effectively. The maximum likelihood sequence estimator (MLSE) achieves excellent performance. However, it is not suited for systems which have a fair amount of users as well as frequency selective channels since its numerical complexity grows exponentially in both those quantities. Multiple-input multiple-output (MIMO) equalizers perform in many situations not very much worse, are near-far resistant and the

required number of operations grows only linearly in the number of users, while it may be even independent of the frequency selectivity (memory) of the channel. Thus, these detectors are very well suited for the system considered in this work.

Two types of MIMO equalizers have been considered: The linear equalizer (LE) and the nonlinear decision-feedback equalizer (DFE). Both types are analyzed with frequency- and time-domain techniques. In addition, the equalizer coefficients have been optimized based on the minimum mean-square error (MMSE) and zero-forcing (ZF) criteria. Although all these issues are discussed, the main emphasis is laid on the frequency-domain analysis with respect to the MMSE criterion.

A comparison of both methods has been conducted. It shows that the frequency-domain determination of the equalizer coefficients is significantly more efficient than the time-domain approach provided that the system can be considered stationary.

The optimal MIMO equalizer structure may be realized by a cascade of three blocks: The first is a noise-whitening matched matrix filter which is required for correlated or colored noise signals; it is followed by a channel matched matrix filter that is matched to the received signal waveforms; finally a symbol-rate space-time matrix filter is applied. This optimal structure may be used for both time- and frequency-domain equalizers. However, it requires exact knowledge of the noise characteristics and channel impulse responses. Since this is in practice not easily available, time-domain equalizers are usually implemented directly without a matched filter front-end structure. In fact, the time-domain equalizers require for the determination of the optimal coefficients only the desired, transmitted data and the received signals. An analogous direct implementation for frequency-domain based linear equalizers has been derived here. This method needs merely information about the spectra of the former two signals. A similar structure has, to my knowledge, not yet been described in the relevant literature. Other publications applying a frequency-domain description of the linear equalizer assume, either explicitly or implicitly, a noise-whitening/channel matched filter receiver front-end.

It is well known that a ZF MIMO LE may exist only if the number of users is smaller than or equal to the number of diversity channels in the system ($N \leq AK$). In contrast, a MMSE MIMO LE exists for all user populations. However, its performance

should be strongly limited in overpopulated systems ($N > AK$). This fact is proved by deriving a new lower bound on the average MMSE for the MMSE MIMO LE. The bound is equal to zero for $N \leq AK$ and produces positive values for overpopulated situations.

Foschini *et al.* have derived an extremely useful upper bound on the error probability, which is solely a function of the MMSE [34]. The expression is valid for single-input single-output (SISO) equalizers and can be interpreted as a special case of the Saltzberg bound. A crucial result used in the derivation is the relationship between the MMSE and the bias coefficient, which was found by Mueller *et al.* for SISO equalizers [83]. However, since Foschini and Mueller considered explicitly a SISO equalizer for a single-user system, the application of the bound [34] to multiuser systems and MIMO equalizers is not straightforwardly justified. The analysis in this work proves formally that the relationship between the bias coefficient and the MMSE is the same for both single-user, SISO equalizers and multiuser MIMO equalizers. Hence, it is shown that Foschini *et al.*'s [34] very useful bound for the error probability can also be applied for MIMO equalizers in multiuser systems.

The MIMO DFE has been analyzed in the frequency domain. Both the conventional and the noise-predictive structure have been considered. Expressions for the optimal filters and the performance in terms of the MMSE are given.

A lower bound of the system capacity, based on the Saltzberg bound, has been derived for MIMO equalizers. This bound can be expressed in terms of the individual MMSE's and the desired error probability.

Numerical results for the performance of the MMSE MIMO LE and DFE have been presented in terms of the MMSE, bit error rate, outage probability and capacity. The diagrams show the performance quantities depending on either the number of system users or the SNR. It was found that the DFE performed always superior to the LE. The performance difference is moderate in systems with significantly less users than diversity channels. However, the more users are in the system, the larger is the possible performance advantage of a DFE. In particular, only the DFE may achieve satisfactory results in overpopulated systems, i.e. systems with more users than diversity channels.

6.4 Delayed-Decision-Feedback Equalization

The delayed-decision-feedback equalizer (DDFE), an extension to the MIMO DFE structure, is introduced. The idea is to include delay elements after the forward filters and delay the decision of weaker signals with respect to stronger ones. This strategy is particularly beneficial in near-far situations, i.e. when the signals of different users are received at considerably different strengths.

Very strong users can swamp weaker signals such that they may be indistinguishable by the receiver. A popular technique to overcome the harmful impacts of the near-far effect is *power control*. In this case, feedback information about the individual signal strengths is sent to the users such that they adjust their transmit power level and avoid a near-far situation. However, it is clear that power control adds considerable complexity to the system.

Since the DDFE performs best in near-far situations, it reduces the requirements for power control or may even work completely without it. In any case, the DDFE detector has the potential to improve the system performance and reduce the complexity of power control.

A model for the DDFE is introduced and mathematically analyzed. Frequency-domain expressions for the optimal filters and the detector performance are derived.

The calculation of the optimal DDFE filters requires in general a matrix spectral factorization. This procedure is numerically complex and one may want to avoid it. A method is described, which requires only matrix inversions for the determination of all equalizer coefficients. However, it has the disadvantage that it may involve the inversion of a large matrix.

Alternatively, successive detectors may be considered. These equalizers increase the delay between two consecutive signals hypothetically to infinity. This simplifies the determination of the equalizer coefficients and avoids a matrix spectral factorization. Successive detectors with or without feedback from the currently decoded signal are introduced and analyzed. Numerical results have been presented which show that the performance of the successive detector is similar to the DDFE. It achieves the largest improvement in systems with a strong near-far effect. Conversely, both the

DDFE and the successive detector will perform worse than the MIMO DFE if the received powers of all signals are similar.

6.5   Open Issues

The method of approximating the error probability described in this work starts with the error integral (1.10) and approximates the noise cdf by an exponential expression. This results finally in a second-order expression which is an approximate rather than a strict upper bound. In other words, the value of the approximation is almost exclusively larger than the true error probability, but it may occasionally be slightly lower. In addition, a slightly less accurate upper bound has been obtained, but no lower bounds have been found.

It might be promising to start with the integral error expression (1.9) and approximate the bell shaped noise pdf instead of the noise cdf. The remaining analysis would be very similar to the method described in Section 3.4. This may yield a second-order approximation which is a strict upper bound on the error probability. In addition, an approximate lower bound may be obtained. The availability of an upper and lower bound would also provide a good estimate for the achieved accuracy.

A direct structure of the MMSE MIMO LE has been derived in Section 4.2.1.1 (Equation 4.32). The optimal equalizer can be calculated from the power spectrum of the received signal and the cross-power spectrum of the received signal and the desired data. Thus, the quality of the equalizer coefficients depends in practice strongly on the quality of spectral estimates. This suggests to consider sophisticated methods for spectrum analysis, which may either provide a better estimate for a given set of samples or require less samples for a reasonable estimate. Two attractive techniques that could be considered are the *maximum entropy method* (MEM) and the *maximum likelihood method* (MLM) [18].

Simulation results have been provided which show that the DDFE or successive detector perform excellent under near-far conditions. It should be investigated how efficient these detector types work in practical situations considering quantization effects, finite word length and non-ideal channel knowledge.

Bibliography

[1] M. Abdulrahman. *DFE for Interference and Multipath Suppression in a CDMA System.* PhD thesis, Dept. of Syst. and Comp. Eng., Carleton University, Ottawa, ON, Canada, 1993.

[2] M. Abdulrahman and D. D. Falconer. Cyclostationary crosstalk suppression by decision feedback equalization on digital subscriber loops. *IEEE J. Select. Areas Commun.*, 10(3):640–649, April 1992.

[3] M. Abdulrahman, D. D. Falconer, and A. U. H. Sheikh. Equalization for interference cancellation in spread spectrum multiple access systems. In *Conf. Rec. IEEE VTC 92*, volume 1, pages 71–74, Denver, Colorado, May 1992.

[4] M. Abdulrahman, A. U. H. Sheikh, and D. D. Falconer. DFE convergence for interference cancellation in spread spectrum multiple access systems. In *Conf. Rec. IEEE VTC 93*, volume 1, pages 807–810, Secaucus, New Jersey, May 1993.

[5] M. Abramowitz and I. A. Stegun. *Handbook of Mathematical Functions with Formulas, Graphs, and Mathematical Tables.* Dover, New York, 1970. National Bureau of Standards, U.S. Department of Commerce, ninth printing, originally issued June 1964.

[6] J. M. Aein and J. C. Hancock. Reducing the effects of intersymbol interference with correlation receivers. *IEEE Trans. Inform. Theory*, IT-9(3):167–175, July 1963.

[7] P. Amadesi. A fast evaluation of the error rate of CPSK system by means of local

approximations of the error function. *CSELT Rapporti tecnici*, VIII(3):199–206, June 1981.

[8] N. Anderson and Å. Björck. A new high order method of regula falsi type for computing a root of an equation. *BIT*, 13:253–264, 1973.

[9] M. E. Austin. Equalization of dispersive channels using decision feedback. Quart. Progr. Report 84, M.I.T. Research Lab. Electr., Cambridge, MA, USA, April 1967.

[10] P. Balaban and J. Salz. Dual diversity combining and equalization in digital cellular mobile radio. *IEEE Trans. Veh. Technol.*, 40(2):342–354, May 1991.

[11] N. C. Beaulieu. The evaluation of error probabilities for intersymbol and cochannel interference. *IEEE Trans. Commun.*, 39(12):1740–1749, December 1991.

[12] R. Behin. Multi-antenna indoor radio channel measurement and analysis. Technical report, TR*Labs*, Calgary, AB, Canada, May 1998.

[13] C. Belfiore. *Decision Feedback Equalization – A Unified Approach*. PhD thesis, University of Minnesota, Minneapolis, U.S.A., March 1976.

[14] C. A. Belfiore and J. H. Park, Jr. Decision feedback equalization. *Proc. of the IEEE*, 67(8):1143–1156, August 1979.

[15] S. Benedetto, G. de Vincentiis, and A. Luvison. Error probability in the presence of intersymbol interference and additive noise for multilevel digital signals. *IEEE Trans. Commun.*, COM-21(3):181–190, March 1973.

[16] E. Biglieri, M. Elia, and L. Lopresti. The optimal linear receiving filter for digital transmission over nonlinear channels. *IEEE Trans. Inform. Theory*, 35(3):620–625, May 1989.

[17] I. N. Bronštejn, K. A. Semendjajew, G. Grosche, V. Ziegler, and D. Ziegler. *Teubner-Taschenbuch der Mathematik*. B. G. Teubner Verlagsgesellschaft, Leipzig, Germany, 1996. in German.

[18] D. G. Childers, editor. *Modern Spectrum Analysis*. IEEE Press Selected Reprint Series. IEEE Press, New York, NY, 1978.

[19] J. Chuang. High-speed wireless data for internet applications. Tutorial Manual of IEEE VTC 2000, Boston, M.A., September 2000.

[20] M. V. Clark, L. J. Greenstein, W. K. Kennedy, and M. Shafi. Matched filter performance bounds for diversity combining receivers in digital mobile radio. *IEEE Trans. Veh. Technol.*, 41(4):356–362, November 1992.

[21] M. V. Clark, L. J. Greenstein, W. K. Kennedy, and M. Shafi. Optimum linear diversity receivers for mobile communications. *IEEE Trans. Veh. Technol.*, 43(1):47–56, February 1994.

[22] S. N. Crozier, D. D. Falconer, and S. A. Mahmoud. Least sum of squared errors (LSSE) channel estimation. *IEE Proceedings-F*, 138(4):371–378, August 1991.

[23] W. Didzoleit, F. Dohmen, C. Reiermann, and M Sauga. Mobilfunk: UMTS Lizenzen mit unkalkulierbaren Risiken – das 100-milliarden ding. *Der Spiegel*, (34):82–83, August 2000. in German.

[24] D. Divsalar, M. K. Simon, and D. Raphaeli. Improved parallel interference cancellation for CDMA. *IEEE Trans. Commun.*, 46(2):258–268, February 1998.

[25] M. Dowell and P. Jarratt. A modified regula falsi method for computing the root of an equation. *BIT*, 11:168–174, 1971.

[26] M. Dowell and P. Jarratt. The "Pegasus" method for computing the root of an equation. *BIT*, 12:503–508, 1972.

[27] A. Duel-Hallen. Equalizers for multiple input/multiple output channels and PAM systems with cyclostationary input sequences. *IEEE J. Select. Areas Commun.*, 10(3):630–639, April 1992.

[28] A. Duel-Hallen. Decorrelating decision-feedback multiuser detector for synchronous code-division multiple-access channel. *IEEE Trans. Commun.*, 41(2):285–290, February 1993.

[29] A. Duel-Hallen. A family of multiuser decision-feedback detectors for asynchronous code-division multiple access channels. *IEEE Trans. Commun.*, 43(2/3/4):421–434, February/March/April 1995.

[30] A. Duel-Hallen, J. Holtzman, and Z. Zvonar. Multiuser detection for CDMA systems. *IEEE Personal Communications*, 2(2):46–58, April 1995.

[31] E. Eleftheriou and B. R. Petersen. Method and apparatus for multiuser-interference reduction. World Intellectual Property Organization, August 1995. International Patent No. WO 95/22209.

[32] G. Engeln-Müllges and F. Reutter. *Numerik-Algorithmen: Entscheidungshilfe zur Auswahl und Nutzung*. VDI Verlag, Düsseldorf, Germany, eighth edition, 1996. in German.

[33] D. D. Falconer, M. Abdulrahman, N. W. K. Lo, B. R. Petersen, and A. U. H. Sheikh. Advances in equalization and diversity for portable wireless systems. *Digital Signal Processing: A Review Journal*, 3(3):148–162, July 1993.

[34] G. J. Foschini and J. Salz. Digital communications over fading radio channels. *The Bell System Techn. J.*, 62(2):429–456, February 1983.

[35] T. L. Fulghum. *Adaptive Multielement Decision Feedback Receiver Structures for Narrowband Multiuser Detection in a Frequency Selective Channel*. PhD thesis, North Carolina State University, North Carolina, U.S.A., 1998.

[36] T. L. Fulghum and A. Duel-Hallen. Adaptive multielement DFE receivers for narrowband multiuser detection. In *Conf. Rec. IEEE VTC 98*, volume 1, pages 41–45, Ottawa, Ontario, Canada, May 1998.

[37] W. A. Gardner. Cyclic Wiener filtering: Theory and method. *IEEE Trans. Commun.*, 41(1):151–163, January 1993.

[38] W. A. Gardner, editor. *Cyclostationarity in Communications and Signal Processing*, chapter Gardner, W. A.: "An Introduction to Cyclostationary Signals", pages 1–90. IEEE Press, Piscataway, NJ, 1994.

[39] D. A. George, D. C. Coll, A. R. Kaye, and R. R. Bowen. Channel equalization for data transmission. *The Engineering Journal (Canada)*, 53, May 1970.

[40] R. D. Gitlin, J. F. Hayes, and S. B. Weinstein. *Data Communications Principles*. Plenum Press, New York, NY, 1992.

[41] F. E. Glave. An upper bound on the probability of error due to intersymbol interference for correlated digital signals. *IEEE Trans. Inform. Theory*, IT-18(3):356–363, May 1972.

[42] G. D. Golden, J. E. Mazo, and J. Salz. Transmitter design for data transmission in the presence of a data-like interferer. *IEEE Trans. Commun.*, 43(2/3/4):837–850, Feb./Mar./Apr. 1995.

[43] T. J. Harris and J. H. Davis. An iterative method for matrix spectral factorization. *SIAM J. Sci. Stat. Comput.*, 13(2):531–540, March 1992.

[44] D. J. Harrison. Adaptive equalization for channels with crosstalk. Master's thesis, Carleton University, September 1969.

[45] S. Haykin. *Communication Systems*. Wiley, New York, NY, third edition, 1994.

[46] S. Haykin. *Adaptive Filter Theory*. Prentice-Hall, Upper Saddle River, NJ, third edition, 1996.

[47] C. W. Helstrom. Calculating error probabilities for intersymbol and cochannel interference. *IEEE Trans. Commun.*, COM-34(5):430–435, May 1986.

[48] E. Y. Ho and Y. S. Yeh. A new approach for evaluating the error probability in the presence of intersymbol interference and additive Gaussian noise. *The Bell System Techn. J.*, 49:2249–2265, November 1970.

[49] E. Y. Ho and Y. S. Yeh. Error probability of a multilevel digital system with intersymbol interference and Gaussian noise. *The Bell System Techn. J.*, 50(3):1017–1023, March 1971.

[50] J. Holtzman. DS/CDMA successive interference cancellation. In *Proc. of ISSSTA'94*, pages 69–78, Oulu, Finland, July 1994.

[51] M. L. Honig, P. Crespo, and K. Steiglitz. Suppression of near- and far-end crosstalk by linear pre- and post-filtering. *IEEE J. Select. Areas Commun.*, 10(3):614–629, April 1992.

[52] Y.-C. Jenq. Does a larger intersymbol interference result in a higher probability of error? *IEEE Trans. Commun.*, COM-28(9):1771–1773, September 1980.

[53] Y.-C. Jenq, B. Liu, and J. B. Thomas. Probability of error in PAM systems with intersymbol interference and additive noise. *IEEE Trans. Inform. Theory*, IT-23(5):575–582, September 1977.

[54] M. J. Juntti and B. Aazhang. Finite memory-length linear multiuser detection for asynchronous CDMA communications. *IEEE Trans. Commun.*, 45(5):611–622, May 1997.

[55] M. Kavehrad and J. Salz. Cross-polarization cancellation and equalization in digital transmission over dually polarized multipath fading channels. *AT&T Techn. J.*, 64(10):2211–2245, December 1985.

[56] M. Kawabe, T. Kato, A. Kawahashi, T. Sato, and A. Fukasawa. Advanced CDMA scheme based on interference cancellation. In *Conf. Rec. IEEE VTC 93*, pages 448–451, Secaucus, New Jersey, May 1993.

[57] A. R. Kaye and D. A. George. Transmission of multiplexed PAM signals over multiple channel and diversity systems. *IEEE Trans. Commun. Techn.*, 18(5):520–526, October 1970.

[58] R. J. Keeler. Construction and evaluation of a decision feedback equalizer. In *Conf. Rec. IEEE ICC 71*, Montreal, Quebec, Canada, June 1971.

[59] R. F. King. An improved Pegasus-method for root finding. *BIT*, 13:423–427, 1973.

[60] A. Klein and P. W. Baier. Linear unbiased data estimation in mobile radio systems applying CDMA. *IEEE J. Select. Areas Commun.*, 11(7):1058–1066, September 1993.

[61] A. Klein, G. K. Kaleh, and P. W. Baier. Zero forcing and minimum mean-square-error equalization for multiuser detection in code-division multiple-access channels. *IEEE Trans. Veh. Technol.*, 45(2):276–287, May 1996.

[62] A. M. Legnain, D. D. Falconer, and A. U. H. Sheikh. Decision-feedback adaptive combined space-time receiver for multi-user interference rejection in CDMA systems. In *Conf. Rec. Wireless 98*, volume 1, pages 164–170, Calgary, AB, Canada, July 1998.

[63] A. M. Legnain, D. D. Falconer, and A. U. H. Sheikh. New adaptive combined space-time receiver for multiuser interference rejection in synchronous CDMA systems. In *Conf. Rec. IEEE CCECE 98*, volume 1, pages 421–424, Waterloo, ON, Canada, May 1998.

[64] A. M. Legnain, D. D. Falconer, and A. U. H. Sheikh. Centralized decision feedback adaptive combined space-time detector for CDMA systems. In *Conf. Rec. IEEE VTC 99*, volume 2, pages 932–936, Vancouver, BC, Canada, June 1999.

[65] A. J. Levy. Fast error rate evaluation in the presence of intersymbol interference. *IEEE Trans. Commun.*, COM-33(5):479–481, May 1985.

[66] R. W. Lucky, J. Salz, and E. R. Weldon, Jr. *Principles of Data Communication*. McGraw-Hill, New York, 1968.

[67] R. Lugannani. Intersymbol interference and probability of error in digital systems. *IEEE Trans. Inform. Theory*, IT-15(6):682–688, November 1969.

[68] R. Lupas and S. Verdú. Linear multiuser detectors for synchronous code-division multiple-access channels. *IEEE Trans. Inform. Theory*, 35(1):123–136, January 1989.

[69] R. Lupas and S. Verdú. Near-far resistance of multiuser detectors in asynchronous channels. *IEEE Trans. Commun.*, 38(4):496–508, April 1990.

[70] U. Madhow and M. L. Honig. MMSE interference suppression for direct-sequence spread-spectrum CDMA. *IEEE Trans. Commun.*, 42(12):3178–3188, December 1994.

[71] J. W. Matthews. Sharp error bounds for intersymbol interference. *IEEE Trans. Inform. Theory*, IT-19:440–447, July 1973.

[72] W. F. McGee. A modified intersymbol interference error bound. *IEEE Trans. Commun.*, COM-21(7):862, July 1973.

[73] P. J. McLane. Lower bounds for finite intersymbol interference error rates. *IEEE Trans. Commun.*, COM-22(6):853–857, June 1974.

[74] G. G. Messier, R. J. C. Bultitude, R. J. Davies, and B. R. Petersen. Indoor radio channel measurements. Technical report, TR*Labs*, Calgary, AB, Canada, September 1996.

[75] K. Metzger. On the probability density of intersymbol interference. *IEEE Trans. Commun.*, COM-35(4):396–402, April 1987.

[76] A. Milewski. New simple and efficient bounds on the probability of error in the presence of intersymbol interference and Gaussian noise. *IEEE Trans. Commun.*, COM-25(10):1218–1222, October 1977.

[77] S. L. Miller. An adaptive direct-sequence code-division multiple-access receiver for multiuser interference rejection. *IEEE Trans. Commun.*, 43(2/3/4):1746–1755, Feb./Mar./Apr. 1995.

[78] P. Monsen. MMSE equalization of interference on fading diversity channels. *IEEE Trans. Commun.*, COM-32(1):5–12, January 1984.

[79] S. Moshavi. Multi-user detection for DS-CDMA communications. *IEEE Communications Magazine*, 34(10):124–136, October 1996.

[80] S. Moshavi. *Multistage Linear Detectors for DS-CDMA Communications*. PhD thesis, Dept. Elec. Eng., City University New York, NY, U.S.A., 1996.

[81] S. Moshavi, E. G. Kanterakis, and D. L. Schilling. Multistage linear receivers for DS-CDMA systems. *Int. J. Wireless Info. Networks*, 3(1), January 1996.

[82] R. S. Mowbray, R. D. Pringle, and P. M. Grant. Increased CDMA system capacity through adaptive cochannel interference regeneration and cancellation. *IEE Proceedings-I*, 139(5):515–524, October 1993.

[83] M. S. Mueller and J. Salz. A unified theory of data-aided equalization. *The Bell System Techn. J.*, 60(9):2023–2038, November 1981.

[84] J. V. Murphy. Binary error rate caused by intersymbol interference and Gaussian noise. *IEEE Trans. Commun.*, COM-21:1039–1046, September 1973.

[85] M. S. Nakhla. Performance evaluation of optical fiber transmission systems. *IEEE J. Select. Areas Commun.*, 8(8):1617–1623, October 1990.

[86] M. S. Nakhla. Error probability for multilevel digital systems in presence of intersymbol interference and additive noise. *IEEE Trans. Commun.*, 42(7):2380–2383, July 1994.

[87] H. Nyquist. Certain topics in telegraph transmission theory. *AIEE Trans.*, 47:617–644, February 1928.

[88] A. V. Oppenheim and R. W. Schafer. *Discrete-Time Signal Processing*. Prentice-Hall, Englewood Cliffs, NJ, 1989.

[89] A. Papoulis. *Probability, Random Variables, and Stochastic Processes*. McGraw-Hill, New York, NY, third edition, 1991.

[90] P. Patel and J. Holtzman. Performance comparison of a DS/CDMA system using a successive interference cancellation (IC) scheme and a parallel IC scheme under fading. In *Conf. Rec. IEEE ICC 94*, pages 510–515, New Orleans, LA, May 1994.

[91] B. R. Petersen. *Equalization in Cyclostationary Interference.* PhD thesis, Carleton University, ON, Canada, 1992.

[92] B. R. Petersen and D. D. Falconer. Minimum mean-square equalization in cyclostationary and stationary interference – analysis and subscriber-line calculations. *IEEE J. Select. Areas Commun.*, 9(6):931–940, August 1991.

[93] B. R. Petersen and D. D. Falconer. Suppression of adjacent-channel, cochannel and intersymbol interference by equalizers and linear combiners. *IEEE Trans. Commun.*, 42(12):3109–3118, December 1994.

[94] H. V. Poor and S. Verdú. Probability of error in MMSE multiuser detection. *IEEE Trans. Inform. Theory*, 43(3):858–871, May 1997.

[95] V. K. Prabhu. Some considerations of error bounds in digital systems. *The Bell System Techn. J.*, 50(10):3127–3151, December 1971.

[96] V. K. Prabhu. Modified Chernoff bounds for PAM systems with noise and interference. *IEEE Trans. Inform. Theory*, IT-28(1):95–100, January 1982.

[97] W. H. Press et al. *Numerical Recipes in C: The Art of Scientific Computing.* Cambridge University Press, Cambridge, NY, second edition, 1992.

[98] R. Price. Nonlinearly feedback-equalized PAM vs. capacity for noisy linear channels. In *Conf. Rec. IEEE ICC 72*, Philadelphia, Pa., June 1972.

[99] J. G. Proakis. *Digital Communications.* McGraw-Hill, New York, NY, third edition, 1995.

[100] R. Ramésh and K. C. Zangi. Enhanced data rates for global evolution: A tutorial. Tutorial Manual of IEEE VTC 2000, Boston, M.A., September 2000.

[101] T. S. Rappaport. *Wireless Communications.* Prentice-Hall, Upper Saddle River, NJ, 1996.

[102] M. Reuter. Numerically efficient fourier-based technique for calculating error probabilities with intersymbol interference. *IEEE Trans. Commun.*, 45(6):629–632, June 1997.

[103] B. R. Saltzberg. Intersymbol interference error bounds with application to ideal bandlimited signaling. *IEEE Trans. Inform. Theory*, IT-14(4):563–568, July 1968.

[104] J. Salz. Optimum mean-square decision feedback equalization. *The Bell System Techn. J.*, 52(8):1341–1373, October 1973.

[105] J. Salz. Digital transmission over cross-coupled linear channels. *AT&T Techn. J.*, 64(6):1147–1159, July-August 1985.

[106] R. Schlagenhaufer, B. R. Petersen, and A. B. Sesay. Delayed-decision-feedback equalization for multiuser systems. In *Conf. Rec. Wireless 99*, pages 71–84, Calgary, AB, Canada, July 1999.

[107] R. Schlagenhaufer, B. R. Petersen, and A. B. Sesay. The multivariate noise-predictive delayed-decision-feedback equalizer/combiner for multiuser systems with diversity. In *Conf. Rec. IEEE CCECE 99*, pages 39–44, Edmonton, AB, Canada, May 1999.

[108] R. Schlagenhaufer, A. B. Sesay, and B. R. Petersen. A wireless multiuser system using diversity. In *Conf. Rec. IEEE VTC 99*, pages 2024–2028, Houston, Texas, May 1999.

[109] R. Schlagenhaufer, A. B. Sesay, and B. R. Petersen. Efficient evaluation of error probabilities for systems with interference and Gaussian noise. In *Conf. Rec. IEEE VTC 2000 (Fall)*, volume 1, pages 336–343, Boston, MA, September 2000.

[110] K. S. Schneider. Optimum detection of code division multiplexed signals. *IEEE Trans. Aerosp. Electr. Syst.*, AES-15(1):181–185, January 1979.

[111] K. E. Scott and S. T. Nichols. Antenna diversity with multichannel adaptive equalization in digital radio. In *Conf. Rec. IEEE ICC 91*, volume 3, pages 1463–1468, Denver, Colorado, June 1991.

[112] O. Shimbo and M. I. Celebiler. The probability of error due to intersymbol interference and Gaussian noise in digital communication systems. *IEEE Trans. Commun. Techn.*, COM-19(2):113–119, April 1971.

[113] D. A. Shnidman. A generalized Nyquist criterion and an optimum linear receiver for a pulse modulation system. *The Bell System Techn. J.*, 46(9):2163–2177, November 1967.

[114] S. Subramanian. *A Multiple-Antenna-Multiple-Equalizer System for CDMA Indoor Wireless Systems*. PhD thesis, University of Victoria, B.C., Canada, 1997.

[115] C. Tidestav, M. Sternad, and A. Ahlén. Reuse within a cell — interference rejection or multiuser detection? *IEEE Trans. Commun.*, 47(10):1511–1522, October 1999.

[116] U. Tietze and C. Schenk. *Halbleiter-Schaltungstechnik*. Springer, Berlin Heidelberg New York, tenth edition, 1993. in German.

[117] W. van Etten. An optimum linear receiver for multiple channel digital transmission systems. *IEEE Trans. Commun.*, 23(8):828–834, August 1975.

[118] L. Vandendorpe, J. Louveaux, B. Maison, and A. Chevreuil. About the asymptotic performance of MMSE MIMO DFE for filter-bank based multicarrier transmission. *IEEE Trans. Commun.*, 47(10):1472–1475, October 1999.

[119] M. K. Varanasi. Noncoherent detection in asynchronous multiuser channels. *IEEE Trans. Inform. Theory*, 39(1):157–176, January 1993.

[120] M. K. Varanasi and B. Aazhang. Multistage detection in asynchronous code division multiple-access communications. *IEEE Trans. Commun.*, COM-38(4):509–519, April 1990.

[121] M. K. Varanasi and B. Aazhang. Near-optimum detection in synchronous code-division multiple access systems. *IEEE Trans. Commun.*, COM-39(5):725–736, May 1991.

[122] S. Verdú. Minimum probability of error for asynchronous Gaussian multiple-access channels. *IEEE Trans. Inform. Theory*, IT-32(1):85–96, January 1986.

[123] S. Verdú. Optimum multiuser asymptotic efficiency. *IEEE Trans. Commun.*, COM-34(9):890–897, September 1986.

[124] S. Verdú. Multiuser detection. *Advances in Statistical Signal Processing*, 2:369–409, 1993. JAI Press.

[125] A. J. Viterbi. Very low rate convolutional codes for maximum theoretical performance of spread spectrum multiple access channels. *IEEE J. Select. Areas Commun.*, 8(4):641–649, May 1990.

[126] N. Wiener and P. Masani. The prediction theory of multivariate stochastic processes: I. the regularity condition. *Acta Mathematica*, 98, 9-573805:111–150, November 1957.

[127] N. Wiener and P. Masani. The prediction theory of multivariate stochastic processes, II: The linear predictor. *Acta Mathematica*, 99, 9-573806:93–137, April 1958.

[128] J. H. Winters. Optimum combining in digital mobile radio with cochannel interference. *IEEE J. Select. Areas Commun.*, SAC-2(4):528–539, July 1984.

[129] J. H. Winters. Optimum combining for indoor radio systems with multiple users. *IEEE Trans. Commun.*, COM-35(11):1222–1230, November 1987.

[130] J. H. Winters, J. Salz, and R. D. Gitlin. The impact of antenna diversity on the capacity of wireless communication systems. *IEEE Trans. Commun.*, 42(2/3/4):1740–1751, February/March/April 1994.

[131] Z. Xie, R. T. Short, and C. K. Rushforth. A family of suboptimum detectors for coherent multiuser communications. *IEEE J. Select. Areas Commun.*, 8(4):683–690, May 1990.

[132] K. Yao. Error probability of asynchronous spread spectrum multiple access communication systems. *IEEE Trans. Commun.*, COM-25(8):803–809, August 1977.

[133] K. Yao and E. M. Biglieri. Multidimensional moment error bounds for digital communication systems. *IEEE Trans. Inform. Theory*, IT-26(4):454–464, July 1980.

[134] K. Yao and R. M. Tobin. Moment space upper and lower error bounds for digital systems with intersymbol interference. *IEEE Trans. Inform. Theory*, IT-22(1):65–74, January 1976.

[135] O. Yue. Saddle point approximation for the error probability in PAM systems with intersymbol interference. *IEEE Trans. Commun.*, COM-27(10):1604–1609, October 1979.

[136] R. Zurmühl and S. Falk. *Matrizen und ihre Anwendungen 1*, volume 1. Springer, Berlin Heidelberg New York, seventh edition, 1997. in German.

[137] Z. Zvonar. Suboptimal multiuser detector for frequency-selective rayleigh fading synchronous CDMA channels. *IEEE Trans. Commun.*, 43(2/3/4):154–157, February/March/April 1995.

[138] Z. Zvonar. Combined multiuser detection and diversity reception for wireless CDMA systems. *IEEE Trans. Veh. Technol.*, 45(1):205–211, February 1996.

Appendix A

Notation

A.1 Symbol Notation

Throughout this thesis, the notation described in Table A.1 will be used. Various mathematical symbols are defined in Table A.2.

Functions and stochastic processes are generally denoted by a variable without argument, e.g. y_C. Sometimes, the notation $y_C(t)$ may also refer to a continuous-time function or stochastic process. In this context, both notations with and without argument, y_C and $y_C(t)$, refer to continuous-time functions (stochastic processes) and are interchangeable. However, $y_C(t)$ may also denote the particular value obtained by mapping the value t according to the rule defined by the function y_C. In case of a continuous-time stochastic process y_C, $y_C(t)$ may refer to a random variable which represents the outcome of the stochastic process at the particular time t. Note that the function (stochastic process) $y_C(t)$ and the value (random variable) $y_C(t)$ refer to fundamentally different concepts. This notational ambiguity is a result of an effort to simplify the readability and presentation in this document and to conform with the general notation used in the common literature. Confusion of the different concepts may be avoided in most cases by referring to the context.

Consequently, in the context of discrete-time functions or stochastic processes, a variable without argument (e.g. x), always denotes the function or process. On the other hand, a variable with argument (e.g. $x[n]$) may refer either to a function

Table A.1: Symbol notation.

Letter attribute	Explanation	Examples
normal type	scalar number or scalar function	a, b, $x[n]$, $X_C(f)$
lowercase normal type	time-domain function	$x[n]$, $y_C(t)$
uppercase normal type	frequency-domain function	$X[k]$, $Y_C(f)$, $Z(D)$
lowercase **bold type**	row vector or row vector function	$\boldsymbol{v}$, $\boldsymbol{a}[n]$, $\boldsymbol{a}(D)$
uppercase **bold type**	matrix or matrix function	$\boldsymbol{Q}$, $\boldsymbol{L}[n]$, $\boldsymbol{L}(D)$
subscript '$_C$'	function of a continuous-valued variable	$y_C(t)$, $X_C(f)$
round brackets '(', ')'	function of a continuous-valued variable	$y_C(t)$, $X_C(f)$, $\boldsymbol{L}(D)$
square brackets '[', ']'	function of a discrete-valued variable	$y[n]$, $X[k]$, $\boldsymbol{L}[k]$

(stochastic process) *or* to the particular value of the function x at time n (random variable described by the statistical properties of the stochastic process x at the specific time n).

A.2   Vector Notation

This document uses a *row vector* notation. In contrast, most of the literature applies a *column vector* notation. The reason for this choice is that the former has, in my opinion, a more intuitive relationship with graphical block diagrams and conforms to the common mathematical notation for matrices.

Consider, for example, a two-dimensional vector input signal $\boldsymbol{a}$, consisting of two scalar values (symbols). A system performs at first a linear transformation $\boldsymbol{X}$ on the input. This result, denoted $\boldsymbol{b}$, is then further processed by a second linear transformation $\boldsymbol{Y}$, producing the final result $\boldsymbol{r}$. For simplicity, both transformations shall be represented by 2×2 matrices. Hence, $\boldsymbol{a}$, $\boldsymbol{b}$ and $\boldsymbol{r}$ are also two-dimensional.

The system behavior can be fully described by the block diagram in Figure A.1. Note that the signal flow starts, similar to writing, at the left side and passes each system element by moving consecutively to the right until the output, $\boldsymbol{r}$, is reached.

Using the *row vector* notation $\boldsymbol{a} = [a_1, a_2]$, the system equation is obtained from the block diagram by starting with the left-most signal and proceeding to the right,

Table A.2: Mathematical symbols.

Symbol	Meaning
$=$	... is equal to ...
$\neq$	... is not equal to ...
$\triangleq$	... is defined by ...
$\equiv$	... is equivalent to ...
$>$	... is greater than ...
$<$	... is smaller than ...
$\gg$	... is much greater than ...
$\ll$	... is much smaller than ...
$\geq$	... is greater than or equal to ...
$\leq$	... is smaller than or equal to ...
$\approx$	... is approximately the same as ...
$\in$	... is an element of the set ...
$\notin$	... is not an element of the set ...
$\|$	... such that ...
$\forall$	for all ...
∞	infinity
$\mapsto$	... is mapped into ...

Comment: The dots "..." indicate that the mathematical symbol requires a variable or an expression where the dots occur.

i.e.

$$\boldsymbol{aXY} = \boldsymbol{r}. \tag{A.1}$$

Note that the linear transformations in the above equation are not commutative, i.e. the order of $\boldsymbol{X}$ and $\boldsymbol{Y}$ cannot be exchanged, because they represent matrix transformations rather than scalar transformations.

If the *column vector* notation were used, we would have to start instead at the right end of the block diagram and proceed to the left, which results in the system equation

$$\boldsymbol{r} = \boldsymbol{YXa}. \tag{A.2}$$
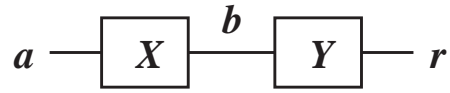
Figure A.1: Block diagram of a simple vector system.

In this case, all vectors are written in column form, i.e.

$$\boldsymbol{a} = \begin{bmatrix} a_1 \\ a_2 \end{bmatrix}. \tag{A.3}$$

Therefore, the row vector notation conforms to the intuitive "left to right" signal flow of the block diagram representation.

Consider now the 2×2 matrix $\boldsymbol{X}$. Its mathematically correct index notation is

$$\boldsymbol{X} = \begin{bmatrix} x_{11} & x_{12} \\ x_{21} & x_{22} \end{bmatrix} \tag{A.4}$$

where the first index of each element denotes the row and the second index denotes the column of the matrix. It can easily be verified that in row vector notation, the element x_{ik} represents the transformation coefficient connecting the i-th input element (a_i) with the k-th output element (b_k), which is intuitive and easy to remember. However, in column vector notation, x_{ik} represents the coefficient connecting the i-th output with the k-th input, suggesting "right to left" or "output to input" signal processing.

A.3   Functions

Several scalar and matrix functions are defined in Table A.3. The following notation has been used in the table: r and v are a real numbers, a is a complex number and X is a random variable. $\mathcal{A}$ and $\mathcal{R}$ are arbitrary sets, where the elements of the latter are real numbers. q is an arbitrary domain, real valued function. The range and probability density function (pdf) of the random variable X are the set $\mathbb{S}_X$ and $f_X(x)$, respectively. $\boldsymbol{a}$ is a vector, $\boldsymbol{A}$ and $\boldsymbol{A}_{ll}$ are $N \times M$ matrices with complex elements. $\boldsymbol{A}_{\mathrm{re}}$ and $\boldsymbol{A}_{\mathrm{im}}$ are the real and imaginary parts of $\boldsymbol{A}$, respectively. $\boldsymbol{A}$ is a

vector for either $N = 1$ or $M = 1$, and it is a scalar for $N = 1$ and $M = 1$. $\boldsymbol{B}$ is a square $N \times N$-matrix. $\boldsymbol{F}[m]$ ($m \in \mathbb{Z}$) is a discrete-domain matrix sequence whose range is the set of $N \times N$ matrices with complex elements. The D-transform of $\boldsymbol{F}[m]$ is defined as $\boldsymbol{F}(D) \triangleq \sum_{m=-\infty}^{\infty} \boldsymbol{F}[m] D^m$. $\boldsymbol{\imath}_1$ and $\boldsymbol{\imath}_2$ are vectors whose elements are positive integer numbers ($[\boldsymbol{\imath}_1]_i, [\boldsymbol{\imath}_2]_k \in \mathbb{N}$).

Table A.3: Functions

Function	Description	Definition
$\Re\{\ldots\}$	real part	$\Re\{a\} \triangleq r$, for $a = r + jv$
$\Im\{\ldots\}$	imaginary part	$\Im\{a\} \triangleq v$, for $a = r + jv$
$\max\{\ldots\}$	maximum	$\max\{\mathcal{R}\} \triangleq$ largest value in the set $\mathcal{R}$
$\max_{\mathcal{A}}\{\ldots\}$	maximum	$\max_{\mathcal{A}}\{q(a)\} \triangleq$ largest value of the function $q(a) \; \forall a \in \mathcal{A}$
$\min\{\ldots\}$	minimum	$\min\{\mathcal{R}\} \triangleq$ smallest value in the set $\mathcal{R}$
$\min_{\mathcal{A}}\{\ldots\}$	minimum	$\min_{\mathcal{A}}\{q(a)\} \triangleq$ smallest value of the function $q(a) \; \forall a \in \mathcal{A}$
$\exp\{\ldots\}$	exponent with base e	$\exp\{a\} \triangleq e^a$
$\ln\{\ldots\}$	natural logarithm	
$\log_r\{\ldots\}$	logarithm to the base r	
$\sin(\ldots)$	sine function	$\sin(a) \triangleq \dfrac{e^{ja} - e^{-ja}}{2j}$
$\cos(\ldots)$	cosine function	$\cos(a) \triangleq \dfrac{e^{ja} + e^{-ja}}{2}$
$\tan(\ldots)$	tangent	$\tan(a) \triangleq \dfrac{\sin(a)}{\cos(a)}$
$\cot(\ldots)$	cotangent	$\cot(a) \triangleq \dfrac{1}{\tan(a)}$
$\sinh(\ldots)$	hyperbolic sine	$\sinh(a) \triangleq \dfrac{e^a - e^{-a}}{2}$
$\cosh(\ldots)$	hyperbolic cosine	$\cosh(a) \triangleq \dfrac{e^a + e^{-a}}{2}$
$\tanh(\ldots)$	hyperbolic tangent	$\tanh(a) \triangleq \dfrac{\sinh(a)}{\cosh(a)}$

<div align="center">**Table A.3**: Functions (continued)</div>

Function	Description	Definition
$\coth(\dots)$	hyperbolic cotangent	$\coth(a) \triangleq \dfrac{1}{\tanh(a)}$
$\lvert\dots\rvert$	absolute value	$\lvert a \rvert \triangleq \sqrt{\Re\{a\}^2 + \Im\{a\}^2}$
$\lfloor\dots\rfloor$	largest integer number smaller or equal to the argument	$\lfloor r \rfloor \triangleq \max\{n \le r \mid n \in \mathbb{Z}\}$
$\lceil\dots\rceil$	smallest integer number greater or equal to the argument	$\lceil r \rceil \triangleq \min\{n \ge r \mid n \in \mathbb{Z}\}$
$\dots!$	factorial	$n! \triangleq \displaystyle\prod_{i=1}^{n} i$
$\dfrac{d^n}{dx^n}\dots$	n-th derivative with respect to the variable x	
$\dots'$	first derivative	$g'(x_0) \triangleq \dfrac{d}{dx}g(x)\Big|_{x=x_0}$
$\dots''$	second derivative	$g''(x_0) \triangleq \dfrac{d^2}{dx^2}g(x)\Big|_{x=x_0}$
$\dots'''$	third derivative	$g'''(x_0) \triangleq \dfrac{d^3}{dx^3}g(x)\Big|_{x=x_0}$
$Q(\dots)$	Q-function	$Q(r) \triangleq \dfrac{1}{\sqrt{2\pi}}\displaystyle\int_r^\infty e^{-\frac{x^2}{2}}\,dx$
$\delta(\dots)$	Dirac delta distribution	$g(t_0) = \displaystyle\int_{-\infty}^\infty g(t)\delta(t-t_0)\,dt$
$\delta_K[\dots]$	Kronecker delta sequence	$\delta_K[n] \triangleq \begin{cases} 1 & \text{for } n=0 \\ 0 & \text{for } n\neq 0 \end{cases},\ n \in \mathbb{Z}$
$\mathrm{Prob}\{\dots\}$	probability that the expression $\dots$ in the brackets is satisfied $(0 \le \mathrm{Prob}\{\dots\} \le 1)$	
$E[\dots]$	statistical expectation	$E[X] \triangleq \displaystyle\int_{\mathbb{S}_X} x f_X(x)\,dx$

Table A.3: Functions (continued)

Function	Description	Definition
$[\ldots]_i$	i-th element of vector	$[\boldsymbol{a}]_i \triangleq i$-th element of the vector $\boldsymbol{a}$
$[\ldots]_{i,k}$ $[\ldots]_{ik}$	(i,k)-th element of matrix	$[\boldsymbol{A}]_{i,k} \equiv [\boldsymbol{A}]_{ik} \triangleq$ element on the i-th row and k-th column of $\boldsymbol{A}$
$[\ldots]_{\boldsymbol{\imath}_1,\boldsymbol{\imath}_2}$	submatrix of a matrix	$[\boldsymbol{A}]_{\boldsymbol{\imath}_1,\boldsymbol{\imath}_2} \triangleq$ submatrix comprising elements of $\boldsymbol{A}$ defined by the vectors $\boldsymbol{\imath}_1$ and $\boldsymbol{\imath}_2$
$\|\ldots\|_\infty$	H_∞-norm	$\|\boldsymbol{A}\|_\infty \triangleq \max_{i\in\{1,2,\ldots,N\},k\in\{1,2,\ldots,M\}} |[\boldsymbol{A}]_{ik}|$
$\ldots^*$	complex conjugation	$(\boldsymbol{A}_{\mathrm{re}} + j\boldsymbol{A}_{\mathrm{im}})^* \triangleq \boldsymbol{A}_{\mathrm{re}} - j\boldsymbol{A}_{\mathrm{im}}$
$\ldots^{-1}$	inverse	$\boldsymbol{A}\boldsymbol{A}^{-1} = \boldsymbol{I}_N$
$\ldots^T$	transpose	$[\boldsymbol{A}^T]_{ik} \triangleq [\boldsymbol{A}]_{ki}, \quad i \in \{1,2,\ldots,N\}, k \in \{1,2,\ldots,M\}$
$\ldots^H$	conjugate transpose	$[\boldsymbol{A}^H]_{ik} \triangleq ([\boldsymbol{A}]_{ki})^*, \quad i \in \{1,2,\ldots,N\}, k \in \{1,2,\ldots,M\}$
$\ldots^{-*}$	complex conjugated inverse	$\boldsymbol{A}^{-*} \triangleq (\boldsymbol{A}^{-1})^*$
$\ldots^{-T}$	inverse transpose	$\boldsymbol{A}^{-T} \triangleq (\boldsymbol{A}^{-1})^T$
$\ldots^{-H}$	inverse conjugate transpose	$\boldsymbol{A}^{-H} \triangleq (\boldsymbol{A}^{-1})^H$
$\ldots^{\blacktriangleleft}$	upper triangular part	$[\{\boldsymbol{A}\}^{\blacktriangleleft}]_{ik} \triangleq \begin{cases} [\boldsymbol{A}]_{ik}, & \text{for } i < k \\ 0, & \text{for } i \geq k \end{cases}$
$\ldots^{\blacktriangleright}$	lower triangular part	$[\{\boldsymbol{A}\}^{\blacktriangleright}]_{ik} \triangleq \begin{cases} 0, & \text{for } i \leq k \\ [\boldsymbol{A}]_{ik}, & \text{for } i > k \end{cases}$
$\ldots^{\triangleleft}$	diagonal part	$[\{\boldsymbol{A}\}^{\triangleleft}]_{ik} \triangleq \begin{cases} [\boldsymbol{A}]_{ik}, & \text{for } i = k \\ 0, & \text{for } i \neq k \end{cases}$
$\ldots^+$	purely causal part	$\{\boldsymbol{F}(D)\}^+ \triangleq \boldsymbol{F}^{\blacktriangleleft}[0] + \sum_{m=1}^{\infty} \boldsymbol{F}[m]D^m$
$\ldots^-$	purely anticausal part	$\{\boldsymbol{F}(D)\}^- \triangleq \boldsymbol{F}^{\blacktriangleright}[0] + \sum_{m=-\infty}^{-1} \boldsymbol{F}[m]D^m$

Table A.3: Functions (continued)

Function	Description	Definition
$\det\{\ldots\}$	determinant of a matrix	see Zurmühl and Falk [136]
$\mathrm{tr}\{\ldots\}$	trace of a square matrix	$\mathrm{tr}\{\boldsymbol{B}\} \triangleq \sum_{i=1}^{N}[\boldsymbol{B}]_{kk}$
$\mathbf{D}\mathrm{iag}\langle\ldots\rangle$	diagonal hypermatrix	$\mathbf{D}\mathrm{iag}\langle\boldsymbol{A}_{ll}\rangle \triangleq$ $$\begin{bmatrix} \boldsymbol{A}_{11} & \boldsymbol{O}_{N\times M} & \ldots & \boldsymbol{O}_{N\times M} \\ \boldsymbol{O}_{N\times M} & \boldsymbol{A}_{22} & \ldots & \boldsymbol{O}_{N\times M} \\ \vdots & \vdots & \ddots & \vdots \\ \boldsymbol{O}_{N\times M} & \boldsymbol{O}_{N\times M} & \ldots & \boldsymbol{A}_{KK} \end{bmatrix},$$ $l \in \{1, 2, \ldots, K\}$

In addition to the descriptions in Table A.3, a few comments and examples shall be provided:

It can easily be shown that inversion and transposition are commutative, as are inversion and conjugate transposition. Thus,

$$\boldsymbol{A}^{-T} \triangleq (\boldsymbol{A}^{-1})^{T} = (\boldsymbol{A}^{T})^{-1} \tag{A.5}$$

$$\boldsymbol{A}^{-H} \triangleq (\boldsymbol{A}^{-1})^{H} = (\boldsymbol{A}^{H})^{-1}. \tag{A.6}$$

Provided that the argument is a scalar, inversion and complex conjugation are commutative:

$$a^{-*} \triangleq \left(\frac{1}{a}\right)^{*} = \frac{1}{a^{*}}. \tag{A.7}$$

A submatrix may be created from a matrix $\boldsymbol{A}$ by applying the function $[\boldsymbol{A}]_{\boldsymbol{\imath_1},\boldsymbol{\imath_2}}$. The positive integer elements in the vectors $\boldsymbol{\imath_1}$ and $\boldsymbol{\imath_2}$ define the submatrix. This function is most easily explained by an example:

$$[\boldsymbol{A}]_{[1,7],[4,2,3]} \triangleq \begin{bmatrix} [\boldsymbol{A}]_{1,4} & [\boldsymbol{A}]_{1,2} & [\boldsymbol{A}]_{1,3} \\ [\boldsymbol{A}]_{7,4} & [\boldsymbol{A}]_{7,2} & [\boldsymbol{A}]_{7,3} \end{bmatrix}. \tag{A.8}$$

Table A.4: Scalar operators.

Operator	Description	Comments
$+$	addition	
$-$	subtraction	
$\cdot$	multiplication	may be omitted, i.e. $xy \triangleq x \cdot y$
$/$	division	
$\star$	convolution	$x_C(t) \star y_C(t) \triangleq \displaystyle\int_{-\infty}^{\infty} x(\tau)y(t-\tau)\, d\tau$ $x[n] \star y[n] \triangleq \displaystyle\sum_{m=-\infty}^{\infty} x[m]y[n-m]$
$\oslash$	modulus	$n \oslash k \triangleq n - k \cdot \left\lfloor \dfrac{n}{k} \right\rfloor ,\ n, k \in \mathbb{Z}$

A.4   Operators

Table A.4 lists commonly used scalar operators and their definitions. Matrix operators are described in Table A.5 and set operators are defined in Table A.6.

A.5   Constants and Sets

Symbols denoting particular constants and sets are defined in Table A.7.

A.6   Statistical Definitions

Let us define the terms *mutually independent* and *temporally independent*. They describe certain properties of stochastic processes which turn out to be useful in the following chapters.

Definition A.1 *Consider the discrete-time stochastic processes* a_i, $i \in \mathcal{I}_N$. *The set of these stochastic processes will be called* mutually independent *if, for all* $i \in \mathcal{I}_N$, *the particular process* a_i *does, at all times* $n \in \mathbb{Z}$, *not depend on the remaining processes* $a_k \ \forall k \in \mathcal{I}_N \setminus i$.

<p align="center">**Table A.5**: Vector and matrix operators.</p>

Operator	Description	Definition
$+$	matrix addition	$[\boldsymbol{A} + \boldsymbol{B}]_{ik} \triangleq [\boldsymbol{A}]_{ik} + [\boldsymbol{B}]_{ik}$
$-$	matrix subtraction	$[\boldsymbol{A} - \boldsymbol{B}]_{ik} \triangleq [\boldsymbol{A}]_{ik} - [\boldsymbol{B}]_{ik}$
$\cdot$	matrix multiplication	$[\boldsymbol{AB}]_{ik} \triangleq [\boldsymbol{A} \cdot \boldsymbol{B}]_{ik} \triangleq \sum_{l=1}^{M}[\boldsymbol{A}]_{il} \cdot [\boldsymbol{B}]_{lk}$
$\star$	matrix convolution	$[\boldsymbol{A} \star \boldsymbol{B}]_{ik} \triangleq \sum_{l=1}^{M}[\boldsymbol{A}]_{il} \star [\boldsymbol{B}]_{lk}$

Comment: $\boldsymbol{A}$ and $\boldsymbol{B}$ are $N \times M$ and $M \times K$ matrices, respectively. They are vectors if $N = 1$ or $K = 1$, respectively. The above definitions are for all matrix elements, i.e. $\forall i \in \{1, 2, \dots, N\}, k \in \{1, 2, \dots, K\}$.

If a set of stochastic processes is mutually independent, it will also be *mutually uncorrelated*[1]. In particular, if the discrete-time stochastic processes a_i, $i \in \mathcal{I}_N$, are mutually uncorrelated and wide-sense stationary with zero mean, their cross-covariance will be zero at all time lags:

$$E[a_i^*[n-m]a_k[n]] = 0, \quad i \neq k, \ \forall i, k \in \mathcal{I}_N, \ n, m \in \mathbb{Z}. \tag{A.9}$$

Definition A.2 *Consider the discrete-time stochastic process a_i. a_i will called* temporally independent *if the outcome of the process at time n, $a_i[n]$, does not depend on the outcomes of the process at other times $m \neq n$ for all $n, m \in \mathbb{Z}$.*

Temporal independence causes directly *temporal uncorrelation*. Consider that the stochastic process a_i is temporally uncorrelated and wide-sense stationary with zero mean and variance $\mathcal{E}_{a,i}$. The autocovariance of a_i is then zero at all time lags except for lag zero:

$$E[a_i^*[n-m]a_i[n]] = \mathcal{E}_{a,i}\,\delta_K[m] \tag{A.10}$$

where $\delta_K[m]$ is the Kronecker delta sequence (Table A.3).

---

[1]However, mutually uncorrelated stochastic processes are not necessarily mutually independent.

Table A.6: Set operators.

Operator	Description	Example
$\cup$	union	$\mathcal{A} = \mathcal{B} \cup \mathcal{C}$. The set $\mathcal{A}$ contains all elements which are either in $\mathcal{B}$ or in $\mathcal{C}$ or in both.
$\cap$	intersection	$\mathcal{A} = \mathcal{B} \cap \mathcal{C}$. The set $\mathcal{A}$ contains all elements which belong to both $\mathcal{B}$ and $\mathcal{C}$.
$\setminus$	set minus	$\mathcal{A} = \mathcal{B} \setminus \mathcal{C}$. $\mathcal{A}$ consists of all elements of $\mathcal{B}$ except for those which belong to $\mathcal{C}$.

<u>Comment:</u> $\mathcal{B}$ and $\mathcal{C}$ are arbitrary sets.

A.7   Orthogonal Basis Functions

Much alike vectors of a particular vector space, functions belong to a "function space". In analogy, an orthogonal basis may be found consisting of a set of basis functions. Consider complex-valued scalar functions. A specific set of basis functions for the set of all continuous-domain and discrete-domain functions is listed in Table A.8. Additionally, basis functions for the subsets of periodic continuous- and discrete-domain functions are also included. The corresponding orthogonality relations are:

$$\int_{-\infty}^{\infty} e^{-j2\pi f_1 t} e^{j2\pi f_2 t}\, dt = \delta(f_1 - f_2) \tag{A.11}$$

$$\sum_{n=-\infty}^{\infty} e^{-j2\pi \check{f}_1 n} e^{j2\pi \check{f}_2 n} = \sum_{l=-\infty}^{\infty} \delta(\check{f}_1 - \check{f}_2 + l) \tag{A.12}$$

$$\int_{-\infty}^{\infty} e^{-j2\pi k_1 \frac{t}{T_0}} e^{j2\pi k_2 \frac{t}{T_0}}\, d\left(\frac{t}{T_0}\right) = \delta_K[k_1 - k_2] \tag{A.13}$$

$$\frac{1}{L} \sum_{n=0}^{L-1} e^{-j\frac{2\pi}{L} n k_1} e^{j\frac{2\pi}{L} n k_2} = \sum_{l=-\infty}^{\infty} \delta_K[k_1 - k_2 + lL]. \tag{A.14}$$

A.8   Fourier Transforms

Four different kinds of Fourier transforms can be defined, since the domains of the transform signal pair may be continuous or discrete. Table A.9 describes the Fourier transforms. The notational convention for the different signal types is shown in

Table A.7: Constant scalars, matrices and sets.

Constant	Definition	Description
j	$j \triangleq \sqrt{-1}$	imaginary unit, square root of "-1"
π	$\pi \triangleq 3.141592\ldots$	Ludolphian number
e	$\frac{d}{dx}e^x = e^x \ (e \triangleq 2.7182\ldots)$	constant
$\mathbb{N}$	$\mathbb{N} \triangleq \{1, 2, 3, \ldots\}$	set of positive integer numbers
$\mathbb{N}_0$	$\mathbb{N}_0 \triangleq \mathbb{N} \cup 0$	set of nonnegative integer numbers
$\mathbb{Z}$	$\mathbb{Z} \triangleq \{0, \pm 1, \pm 2, \ldots\}$	set of all integer numbers
$\mathbb{Q}$	$\mathbb{Q} \triangleq \{n/k \,|\, n, k \in \mathbb{Z}\}$	set of rational numbers
$\mathbb{R}$		set of real numbers
$\mathbb{R}^+$	$\mathbb{R}^+ \triangleq \{r | r \in \mathbb{R}, r > 0\}$	set of positive real numbers
$\mathbb{C}$	$\mathbb{C} \triangleq \{a + jb \,|\, a, b \in \mathbb{R}\}$	set of complex numbers
$\mathcal{I}_N$	$\mathcal{I}_N \triangleq \{1, 2, \ldots, N\}$	set of integer numbers between 1 and N
w_K	$w_K \triangleq e^{-j2\pi/K}, \ K \in \mathbb{Z}$	discrete basis function
$\mathbf{0}_N$	$[\mathbf{0}_N]_i \triangleq 0, \forall i \in \mathcal{I}_N$	all zero row vector with N components
$\mathbf{1}_N$	$[\mathbf{1}_N]_i \triangleq 1, \forall i \in \mathcal{I}_N$	all ones row vector with N components
$\boldsymbol{O}_{N \times M}$	$[\boldsymbol{O}_{N \times M}]_{ik} \triangleq 0, \forall i \in \mathcal{I}_N, k \in \mathcal{I}_M$	$N \times M$ null matrix
$\boldsymbol{I}_N$	$[\boldsymbol{I}_N]_{ik} \triangleq \begin{cases} 1 & \text{for } i = k \\ 0 & \text{for } i \neq k \end{cases}$, $i, k \in \mathcal{I}_N$	$N \times N$ identity matrix
$[f(s)l]$	$[f(s)l] \triangleq$ $[f, f + s, f + 2s, \ldots, l - s, l]$	row vector whose elements are defined by: $f \ldots$ start value, $s \ldots$ step size, $l \ldots$ end value,

Table A.10.

Depending on certain conditions, the appropriate Fourier transform can be chosen. Consider the arbitrary continuous-time signal $x_C(t)$. If this signal contains infinite frequency components and if it is of infinite duration, the spectrum may only be obtained with the Fourier transform (FT).

If $x_C(t)$ contains no frequency greater than f_0, no information will be lost by

Table A.8: Orthogonal basis functions.

Function Space	Basis Functions
all scalar continuous-domain functions $\{x_C \mid x_C(t) \in \mathbb{C}, \forall t \in \mathbb{R}\}$	$e^{-j2\pi ft}; f \in \mathbb{R}$
all scalar discrete-domain functions $\{x \mid x[n] \in \mathbb{C}, \forall n \in \mathbb{Z}\}$	$e^{-j2\pi \check{f}n}; \check{f} \in [0,1)$
all periodic, scalar continuous-domain functions $\{x_C \mid x_C(t + T_0) = x_C(t) \in \mathbb{C}, \forall t \in \mathbb{R}, T_0 \in \mathbb{R}\}$	$e^{-j2\pi kt/T_0}; k \in \mathbb{Z}$
all periodic, scalar discrete-domain functions $\{x \mid x[n + L] = x[n] \in \mathbb{C}, \forall n \in \mathbb{Z}, L \in \mathbb{N}\}$	$e^{-j2\pi k/L}; k \in \{0, 1, 2, \ldots, L-1\}$

sampling it at a rate $1/T_s \geq 2f_0$:

$$x[n] = x_C(nT_s). \tag{A.15}$$

We may then employ the discrete-time Fourier transform (DTFT). The spectrum of the bandlimited signal $x_C(t)$ is, except for a constant, equal to $\check{X}_C(e^{-j2\pi \check{f}_s})$ for the low frequencies $|f| \leq f_0$ and zero for $|f| > f_0$, where the normalized frequency is defined as

$$\check{f}_s \triangleq fT_s. \tag{A.16}$$

If $x_C(t)$ is not bandlimited, but of finite time duration, the nonzero portion of the signal may be taken and repeated periodically. Considering that $x_C(t)$ is nonzero only between $t_{\min}$ and $t_{\max}$, we define the resulting periodic time signal $\check{x}_C(e^{j2\pi t/T_0})$ with

$$\check{x}_C\left(e^{j2\pi \frac{t}{T_0}}\right) = x_C(t), \quad \text{for } t_{\min} \leq t < t_{\max} \tag{A.17}$$

where $T_0 = t_{\max} - t_{\min}$ is the period of the signal. Introducing the normalized time

$$\check{t}_0 \triangleq \frac{t}{T_0} \tag{A.18}$$

Table A.9: Fourier transforms.

| Transform | Domain | | Transform Pair |
	Time	Frequ.	and Notation
Fourier Transform (FT)	cont.	cont.	$X_C(f) = \mathcal{F}_{cc}\{x_C\} \triangleq \int_{-\infty}^{\infty} x_C(t)e^{-j2\pi ft}\,dt$ $x_C(t) = \mathcal{F}_{cc}^{-1}\{X_C\} \triangleq \int_{-\infty}^{\infty} X_C(f)e^{j2\pi ft}\,df$
Discrete-Time Fourier Transform (DTFT)	discr.	cont.	$\check{X}_C(e^{-j2\pi \check{f}_s}) = \mathcal{F}_{dc}\{x\} \triangleq \sum_{n=-\infty}^{\infty} x[n]e^{-j2\pi \check{f}_s n}$ $x[n] = \mathcal{F}_{dc}^{-1}\{\check{X}_C\} \triangleq \int_{0}^{1} \check{X}_C(e^{-j2\pi \check{f}_s})e^{j2\pi \check{f}_s n}\,d\check{f}_s$
Fourier Series (FS)	cont.	discr.	$\check{X}[k] = \mathcal{F}_{cd}\{\check{x}_C\} \triangleq \int_{0}^{1} \check{x}_C(e^{j2\pi \check{t}_0})e^{-j2\pi \check{t}_0 k}\,d\check{t}_0$ $\check{x}_C(e^{j2\pi \check{t}_0}) = \mathcal{F}_{cd}^{-1}\{\check{X}\} \triangleq \sum_{n=-\infty}^{\infty} \check{X}[k]e^{j2\pi \check{t}_0 k}$
Discrete Fourier Series (DFS)	discr.	discr.	$X[k] = \mathcal{F}_{dd}\{x\} \triangleq \sum_{n=0}^{L-1} x[n]e^{-j\frac{2\pi}{L}nk}$ $x[n] = \mathcal{F}_{dd}^{-1}\{X\} \triangleq \frac{1}{L}\sum_{k=0}^{L-1} X[k]e^{j\frac{2\pi}{L}nk}$

the Fourier series (FS) may be applied. The original signal $x_C(t)$ can thus alternatively be described by the discrete frequency spectrum $\check{X}[k]$.

If $x_C(t)$ is both bandwidth- and time-limited, we may represent the signal by a finite number of L samples $x[n] = x_C(nT_s)$, $n \in \{0, 1, 2, \ldots, L-1\}$. The minimum number of required samples is

$$L = \left\lceil \frac{T_0}{T_s} \right\rceil. \tag{A.19}$$

In this case, the discrete Fourier series (DFS) can be used in order to obtain the spectrum of the signal economically. Note that there exists a definite relationship between the DTFT and the DFS if the sequence $x[n]$ consists of only L non-zero samples. By comparing the transform equations for the DTFT and the DFS, it can

<div align="center">

Table A.10: Signal definition.

Signal	Description
$x_C(t)$	continuous-time signal
$\check{x}_C(e^{j2\pi \check{t}_0})$	periodic continuous-time function
$x[n]$	discrete-time signal
$X_C(f)$	Fourier transform of $x_C(t)$
$\check{X}_C(e^{-j2\pi \check{f}_s})$	discrete Fourier transform of $x[n]$
$\check{X}[k]$	Fourier series of $\check{x}_C(e^{j2\pi \check{t}_0})$
$X[k]$	discrete Fourier series of $x[n]$

</div>

immediately be verified that

$$X[k] \;=\; \check{X}_C(e^{-j2\pi \frac{k}{L}}) \tag{A.20}$$

$$\check{X}_C(e^{-j2\pi \check{f}_s})\Big|_{\check{f}_s = \frac{k}{L}} \;=\; X[k]. \tag{A.21}$$

Therefore, if $x[n]$ is restricted to a finite number of non-zero samples, the sequence $X[k]$ represents the values of the DTFT $\check{X}_C(e^{j2\pi \check{f}_s})$ at the discrete frequencies $\check{f}_s = k/L$. In other words, $X[k]$ is the frequency-sampled spectrum of the signal $x[n]$.

Appendix B

Signal Processing Elements

B.1 Up- and Downsampler

Up- and downsamplers are used in order to change the sampling rate in the discrete-time system part. The upsampler increases the sampling rate while the downsampler decreases it.

Upsampler The symbol for an upsampler is shown in Figure B.1(a). In this case, the sampling rate increases by an integer factor K. Let $a[n] \overset{\mathcal{D}}{\longleftrightarrow} a(D)$ and $s[n] \overset{\mathcal{D}}{\longleftrightarrow} s(D)$ be the input and output signal, respectively. The time-domain relationship between these signals is

$$s[Kn + m] = \begin{cases} a[n], & \text{for } m = m_0 \\ 0, & \text{for } m \in \{0, 1, 2, \dots, K-1\} \setminus m_0 \end{cases} \tag{B.1}$$

where the *sampling phase* m_0 is an integer number between 0 and $K-1$ and "$\setminus$" is the *set minus* operator (Table A.6).

Lemma B.1 *The D-domain relationship between the input and output signals of an upsampler is given by*

$$s(D) = D^{m_0} a(D^K). \tag{B.2}$$

$$a[n] \quad \boxed{\uparrow\mathrm{K}} \quad s[n] \qquad x[n] \quad \boxed{\downarrow\mathrm{K}} \quad y[n]$$

(a) upsampler (b) downsampler

Figure B.1: Upsampler and downsampler symbol blocks.

Proof. Let us start with the definition of the D-transform for the pair $s[n] \overset{\mathcal{D}}{\longleftrightarrow} s(D)$. After changing the summation variable with $l = Kn + m$, Equation (B.1) may be substituted, and we obtain after some simple calculations

$$
\begin{aligned}
s(D) &= \sum_{l=-\infty}^{\infty} s[l]D^l \\
&= \sum_{n=-\infty}^{\infty} \sum_{m=0}^{K-1} s[Kn + m]D^{Kn+m} \\
&= D^{m_0} \sum_{n=-\infty}^{\infty} a[n](D^K)^n \\
&= D^{m_0} a(D^K).
\end{aligned}
$$

∎

Frequency and time-domain signals are connected through the discrete-time Fourier transform (DTFT). The relationship between the input $\check{A}_C(e^{-j2\pi\check{f}}) = \mathcal{F}_{dc}\{a[n]\}$ and the output $\check{S}_C(e^{-j2\pi\check{f}}) = \mathcal{F}_{dc}\{s[n]\}$ is most easily obtained by evaluating the D-transform on the unit circle $D = e^{-j2\pi\check{f}}$

$$\check{S}_C(e^{-j2\pi\check{f}}) = e^{-j2\pi\check{f}m_0} \check{A}_C(e^{-j2\pi\check{f}K}). \tag{B.3}$$

For $m_0 = 0$, this relationship is identical to the one derived by Oppenheim and Schafer [88].

Downsampler A downsampler, with input $x[n]$ and output $y[n]$, is shown in Figure B.1(b). The most general relationship between output and input signal is de-

scribed by

$$y[n] = x[Kn + m_0], \quad m_0 \in \{0, 1, 2, \dots, K-1\} \tag{B.4}$$

Lemma B.2 *The D-domain relationship between the input and output signals of a downsampler is given by*

$$y(D) = \frac{1}{K} \sum_{l=0}^{K-1} x\left(D^{\frac{1}{K}} w_K^l\right) \left(D^{\frac{1}{K}} w_K^l\right)^{-m_0} \tag{B.5}$$

where $w_K \triangleq e^{-j2\pi/K}$.

Proof. Define the intermediary signal u as

$$u[n] = x[n + m_0] \tag{B.6}$$

$$y[n] = u[Kn]. \tag{B.7}$$

From the definition of the D-transform $u(D) = \sum_{n=-\infty}^{\infty} u[n]D^n$, we get

$$u\left(D^{\frac{1}{K}} w_K^l\right) = \sum_{n=-\infty}^{\infty} u[n]D^{\frac{n}{K}} w_K^{ln}. \tag{B.8}$$

With this equation, we find

$$\sum_{l=0}^{K-1} u\left(D^{\frac{1}{K}} w_K^l\right) = \sum_{n=-\infty}^{\infty} u[n]D^{\frac{n}{K}} \sum_{l=0}^{K-1} w_K^{ln} \tag{B.9}$$

$$= K \sum_{v=-\infty}^{\infty} u[Kv]D^v \tag{B.10}$$

where the orthogonality relation $\sum_{l=0}^{K-1} w_K^{ln} = K \sum_{v=-\infty}^{\infty} \delta_K[n - Kv]$ is used (Equation A.14) and $\delta_K[n]$ is the Kronecker delta sequence (Table A.3). It follows from Equation (B.7) that $y(D) = \sum_{v=-\infty}^{\infty} u[Kv]D^v$. Substituting Equation (B.10) into this

relationship yields

$$y(D) = \frac{1}{K} \sum_{l=0}^{K-1} u\left(D^{\frac{1}{K}} w_K^l\right). \tag{B.11}$$

Applying the time-shift property (Equation (1.22)) to Equation (B.6) gives $u(D) = x(D)D^{-m_0}$ and substituting this into Equation (B.11) results finally in Lemma B.2.

$\blacksquare$

The DTFT relationship is obtained by evaluating Equation (B.5) on the unit circle $D = e^{-j2\pi \check{f}}$:

$$\check{Y}_C(e^{-j2\pi\check{f}}) = \frac{1}{K} \sum_{l=0}^{K-1} \check{X}_C\left(e^{-j\frac{2\pi}{K}(\check{f}+l)}\right) e^{j\frac{2\pi}{K}(\check{f}+l)m_0} \tag{B.12}$$

where $\check{Y}_C(e^{-j2\pi\check{f}}) = \mathcal{F}_{dc}\{y[n]\}$ and $\check{X}_C(e^{-j2\pi\check{f}}) = \mathcal{F}_{dc}\{x[n]\}$.

B.2 Interfaces between Continuous-Time and Discrete-Time Systems

B.2.1 Pulse Generator

The pulse generator is an interface between a discrete-time and a continuous-time system part. The input to the impulse generator is a discrete-time signal and the output is a continuous-time signal consisting of identical time-shifted pulses. Figure B.2(a) shows the symbol of an impulse generator. Let $s[n]$ and $v_C(t)$ be the input sequence and output signal of the pulse generator, respectively. The relationship between these signals is given by

$$v_C(t) = \sum_{n=-\infty}^{\infty} s[n]\, p_C(t - nT_s) \tag{B.13}$$

where $p_C(t)$ is the pulse shape and T_s is the pulse period.

(a)

(b)
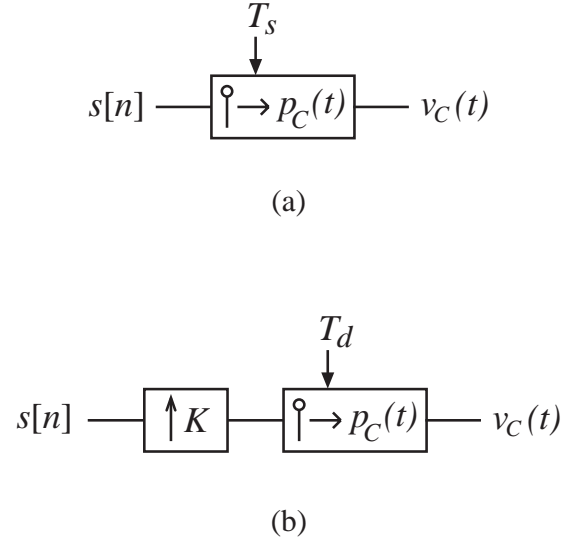
Figure B.2: (a) symbol block of the pulse generator and (b) equivalent realization.

Lemma B.3 *For the pulse generator, the Fourier transform of the output signal* $V_C(f) = \mathcal{F}_{cc}\{v_C(t)\}$ *is given by*

$$V_C(f) = \check{S}_C(e^{-j2\pi fT_s})P_C(f) \tag{B.14}$$

where $\check{S}_C(e^{-j2\pi \check{f}}) = \mathcal{F}_{dc}\{s[n]\}$ *is the discrete-time Fourier transform of the input signal* $s[n]$, $P_C(f) = \mathcal{F}_{cc}\{p_C(t)\}$ *is the Fourier transform of the pulse shape and* T_s *is the pulse period.*

Proof. This relationship is directly obtained by taking the Fourier transform (FT) of Equation (B.13) recognizing the linearity property of the FT and applying the discrete-time Fourier transform definition (Table A.9).

∎

The impulse generator in Figure B.2(a) can be replaced by the equivalent configuration shown in Figure B.2(b). This configuration consists of a K-times upsampler followed by a pulse generator with sampling period T_d, where

$$T_d = \frac{T_s}{K}, \quad K \in \mathbb{N} \tag{B.15}$$

It has the same input/output relationship given by Equations (B.13) and (B.14).

(a)

(b)
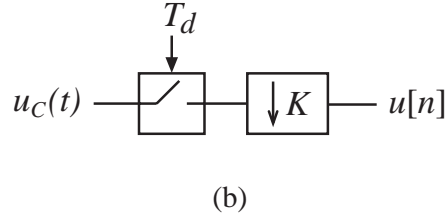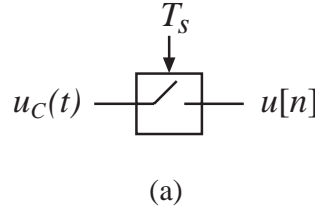
Figure B.3: (a) symbol block of the sampler and (b) equivalent realization.

B.2.2   Sampler

A sampler is used to transform a continuous-time signal into a discrete-time sequence. Figure B.3(a) shows the symbol of a sampler operating at a sampling period T_s. The most general relationship between the continuous-time input $U_C(f) = \mathcal{F}_{cc}\{u_C(t)\}$ and the discrete-time output $\check{U}_C(e^{-j2\pi \check{f}}) = \mathcal{F}_{dc}\{u[n]\}$ is given by

$$u[n] = u_C(nT_s + \tau) \tag{B.16}$$

$$\check{U}_C(e^{-j2\pi f T_s}) = \frac{1}{T_s} \sum_{l=-\infty}^{\infty} U_C\left(f - \frac{l}{T_s}\right) e^{j2\pi\left(f - \frac{l}{T_s}\right)\tau}, \quad \tau \in \mathbb{R} \tag{B.17}$$

where the time instant τ determines the sampling phase.

Proof.   Let us start with the sampler input signal $u_C(t) = \mathcal{F}_{cc}^{-1}\{U_C(f)\}$. Sampling it at the time instants $t = nT_s$ yields the discrete-time sequence $u_C(nT_s)$. According to Oppenheim and Schafer [88], the DTFT of this sequence may be expressed as

$$\mathcal{F}_{dc}\{u_C(nT_s)\} = \frac{1}{T_s} \sum_{l=-\infty}^{\infty} U_C\left(f - \frac{l}{T_s}\right). \tag{B.18}$$

Consider now the signal $u_C(t + \tau) = \mathcal{F}_{cc}^{-1}\{U_C^\tau(f)\}$, where $U_C^\tau(f)$ can be found by

applying the *time shifting* property of the Fourier transform [45]:

$$U_C^\tau(f) = U_C(f)\, e^{j2\pi f\tau}. \tag{B.19}$$

Applying Equations (B.18) and (B.19) to $\check{U}_C(e^{-j2\pi \check{f}})$ yields the final result

$$
\begin{aligned}
\check{U}_C(e^{-j2\pi \check{f}}) \quad &\triangleq \quad \mathcal{F}_{dc}\{u_C(nT_s + \tau)\} \\
&\overset{(B.18)}{=} \quad \frac{1}{T_s} \sum_{l=-\infty}^{\infty} U_C^\tau\left(f - \frac{l}{T_s}\right) \\
&\overset{(B.19)}{=} \quad \frac{1}{T_s} \sum_{l=-\infty}^{\infty} U_C\left(f - \frac{l}{T_s}\right) e^{j2\pi\left(f - \frac{l}{T_s}\right)\tau}.
\end{aligned}
$$

∎

The sampler in Figure B.3(a) can be replaced by an equivalent configuration consisting of a sampler operating at a higher sampling rate followed by a downsampler. This configuration is shown in Figure B.3(b). Both systems are equivalent if the relationship between the two sampling periods is given by Equation (B.15).

Appendix C

Details about System Components

Section 2.3.3 describes the general function and behavior of different system compo-
nents. For the simulations performed in Chapters 4 and 5, specific impulse responses
have been chosen for the radio channel, transmit and receive filters. The transmit
and receive blocks have been modeled by identical fifth-order Butterworth lowpass
filters. In order to obtain realistic results, measured indoor channel impulse responses
have been used to simulate the radio channel. Practical details and characteristics
are provided in the following sections.

C.1   Transmit and Receive Filters

For the system simulations, all transmitter pulses and receive filters have been cho-
sen to be real ($p_C(t) = b_C(t) \in \mathbb{R}$) with a Butterworth lowpass signal shape. The
frequency-domain representation $P_C(f) = \mathcal{F}_{cc}\{p_C(t)\}$ of a lowpass signal is given
by [116]

$$P_C(f) = \frac{P_0}{\prod_k (1 + j\beta_k \Omega - \gamma_k \Omega^2)} \tag{C.1}$$

where P_0 is the gain at zero frequency, $\Omega \triangleq f/f_{3\text{dB}}$ is the normalized frequency, $f_{3\text{dB}}$
is the 3 dB cut-off frequency and β_k, γ_k are the filter coefficients. The highest order
of the denominator polynomial in Ω determines the order of the pulse (n_b). For a

butterworth lowpass pulse and *even* order n_b, the coefficients are [116]

$$\beta_k = 2 \cos \frac{(2k-1)\pi}{2n_b}, \quad \text{for } k \in \left\{1, 2, 3, \dots, \frac{n_b}{2}\right\} \tag{C.2}$$

$$\gamma_k = 1 \tag{C.3}$$

while for *odd* order

$$\beta_k = \begin{cases} 1, & \text{for } k = 1 \\ \cos \frac{(k-1)\pi}{n_b}, & \text{for } k \in \left\{2, 3, 4, \dots, \frac{n_b+1}{2}\right\} \end{cases} \tag{C.4}$$

$$\gamma_k = \begin{cases} 0, & \text{for } k = 1 \\ 1, & \text{for } k \in \left\{2, 3, 4, \dots, \frac{n_b+1}{2}\right\} \end{cases}. \tag{C.5}$$

In addition, the squared frequency magnitude of the lowpass butterworth signal is

$$|P_C(f)|^2 = \frac{P_0^2}{1 + \Omega^{2n_b}}. \tag{C.6}$$

A fifth-order butterworth lowpass pulse ($n_b = 5$) has been used in the system simulations. Using Equation (C.6), it can be found that the magnitude of the signal component for $f \geq 2f_{3\text{dB}}$ is more than 30 dB below that at zero frequency. The high frequency magnitudes may be set to zero altogether with negligible error. This fact becomes important because the implementation of a simulation with discrete-time arithmetic requires that the bandwidth of all signals be strictly limited, i.e. all signal components above the maximum frequency $f_{\max}$ vanish. $f_{\max}$ has been chosen to be twice the single-sided spreading frequency $K/(2T)$:

$$f_{\max} = \frac{K}{T}. \tag{C.7}$$

Since for practical purposes $K \geq K_{3\text{dB}}$, the maximum frequency is at least twice as high as the 3 dB cut-off frequency. This guarantees that the approximation by setting $P_C(f) = 0, \forall f \geq f_{\max}$ does practically not influence the final result.

Figure C.1 shows the frequency-domain phase and magnitude of the strictly bandwidth limited pulse versus the normalized frequency $\bar{f} = 2Tf$ for $K_{3\text{dB}} = K = 4$.
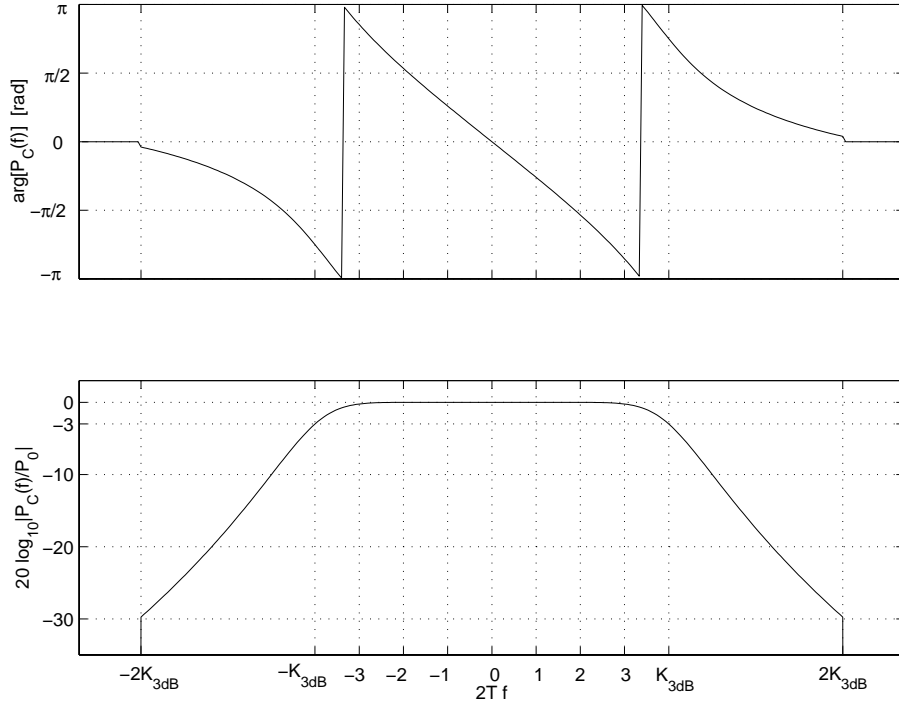
Figure C.1: Phase and magnitude of fifth-order Butterworth lowpass pulse versus the normalized frequency $\bar{f} = 2Tf$ for $K_{3\mathrm{dB}} = K = 4$.

The corresponding time-domain signal $p_C(t)/p_0$ is displayed in Figure C.2, where p_0 is the maximum of $p_C(t)$, $\forall t \in \mathbb{R}$.

C.2   Channel Impulse Response Measurements

Measurement System   The measurement system and some properties of the obtained channel impulse responses (CIR's) are described in the TR*Labs* internal technical reports by Behin [12] and Messier [74]. These documents provide also more details about the measurement hardware.

The CIR's have been measured in an indoor office environment at TR*Labs* Calgary [12]. The measurement system included four stationary transmit antennas and a mobile with four receive antennas. All four transmit antennas have been of a discone type which radiate more strongly below the horizon. They were set a height of 2.35 m. On the mobile, four quarter-wave monopoles with a circular 6 inch diameter groundplane each have been used as receive antennas. The distance between two ad-
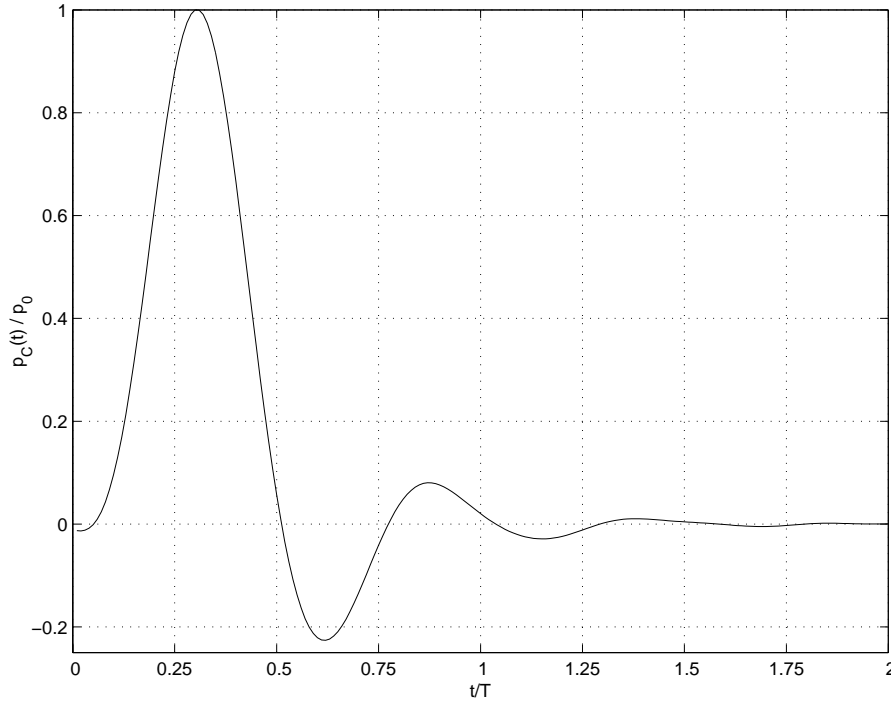
Figure C.2: Fifth-order Butterworth lowpass pulse $p_C(t)$ versus normalized time t/T for $K_{3\mathrm{dB}} = K = 4$.

jacent receive antennas was one wavelength of the carrier frequency $f_{\mathrm{car}} = 1.8$ GHz. The stationary antennas were placed in different corners of the office environment. Different impulse responses were obtained by changing the location of the mobile. Each measurement at a certain mobile location yielded four sets of four CIR's between the adjacent mobile antennas and one of the stationary antennas. The four CIR's belonging to one set had the same large scale propagation characteristics because the distances between a certain stationary antenna and each of the four mobile antennas were practically the same. The mobile was moved to 511 different locations. Therefore, a total of 2044 sets or 8176 CIR's had been obtained. The bandwidth of the measured CIR's was approximately 120 MHz. It was found that the CIR's had an RMS delay spread distribution with a mean of 40.4 ns and a standard deviation of 9.2 ns [12].

A sequence of *binary symbols* was generated in the first step of the measurement. This sequence consisted of one subsequence which was repeated three times. The subsequence was a PN sequence with 1023 symbols. Thus, the total sequence length was

3069. The modulator assigned to each symbol one impulse chosen from a set of two bipolar waveforms. These signals were transmitted at a symbol rate of 200 Msymbols/s (symbol period: 5 ns). The carrier frequency of the transmitted signal was 1.8 GHz. At the receiver, the signal was sampled at period of 1 ns (five times oversampling). Both the transmitted and the received sequences were used to estimate the discrete-time CIR (2.25).

Characteristics of the Measured Channel Impulse Responses Different algorithms can be employed to calculate the CIR. One of them is the correlation method, which correlates the transmitted PN sequence with a part of the received sequence [12]. The result of the correlation is an estimate of the discrete-time CIR. The magnitude of one of the channel transfer functions (CTF's) obtained with the correlation method is shown in Figure C.3. It can be seen that the CTF is only reliable in a short band around zero frequency. The strong attenuation for frequencies $|f| > 100$ MHz is caused by

- the sinc-function roll-off due to the PN sequence,

- bandpass and lowpass filters which limit the transmitted signal to approximately 200 MHz, and

- receive antennas that have a bandpass characteristic. Their 3 dB bandwidth is approximately 160 MHz centered around the carrier frequency.

Let us investigate the *back-to-back* system impulse response in order to obtain more insight into the attenuation characteristics of the measurement system. In the back-to-back system, transmitter and receiver are connected directly through a broadband cable. The system contains neither the antennas nor the radio channel. Thus, the back-to-back system provides information about how the measurement instruments limit the estimated CIR's. Figure C.4 shows the magnitude of the measured back-to-back transfer function $H_{\mathrm{b2b}}(f)$. The transfer function is normalized by a constant H_0 such that the values around 0 Hz are approximately equal to 0 dB. This makes it easier to determine the attenuation at different frequencies. It can be seen
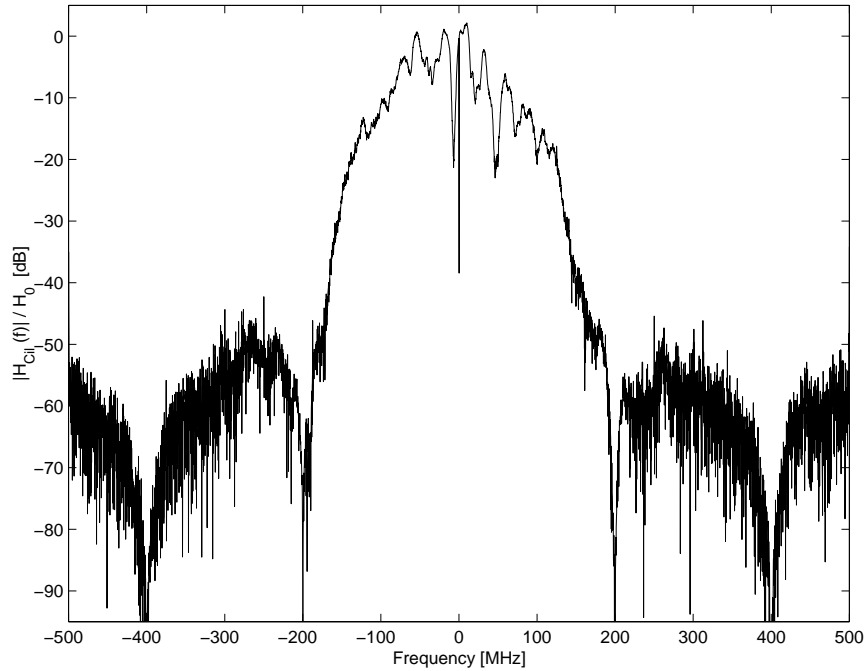
Figure C.3: Normalized magnitude of a measured radio channel transfer function — calculated with the correlation method.

that the measurement system already causes an attenuation of more than 10 dB to frequencies $|f| > 100$ MHz. Figure C.5 magnifies the frequency band $|f| < 100$ MHz from Figure C.4. It shows that the double-sided 3 dB bandwidth of the measurement system is approximately 120 MHz.

The CIR's used in the semi-analytical simulations of Chapters 4 and 5 have been obtained with the *least sum of squared errors* (LSSE) channel estimation method [22] instead of the correlation method. The reason was that the LSSE method achieved better results in terms of a higher signal-to-noise ratio (SNR) for the CIR's. In order to align the transmitted and received sequences[1], the received signal is downsampled by a factor of five. Both sequences have then a sampling period of $T_c = 5$ ns. This means that the spectrum of the estimated discrete-time CTF will be periodic with a period of $B_c = 1/T_c = 200$ MHz.

---

[1]The received signal is five times oversampled. Thus, its symbol period does not match that of the transmitted PN sequence.
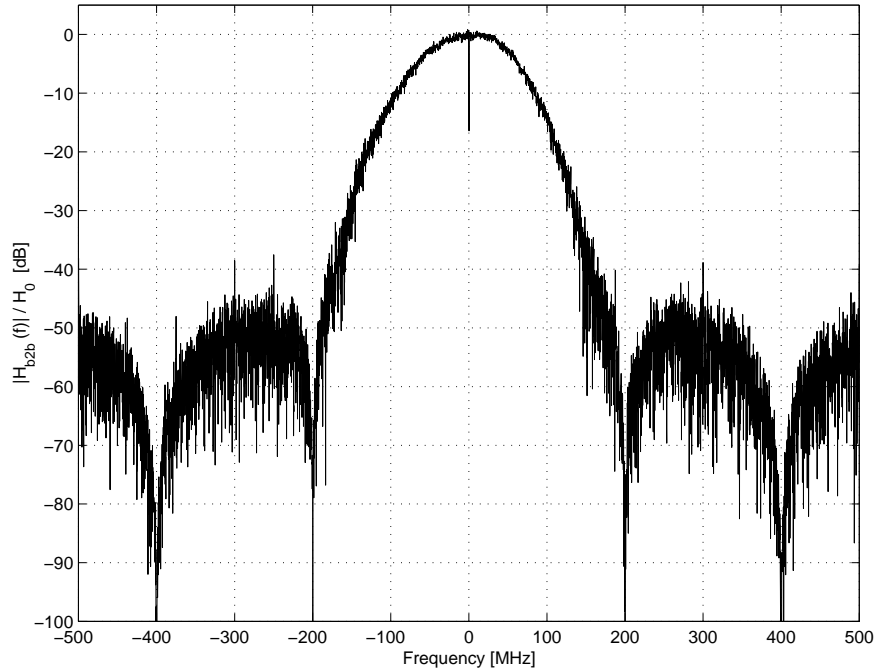
Figure C.4: Normalized magnitude of the back-to-back system transfer function for $|f| < 500$ MHz.
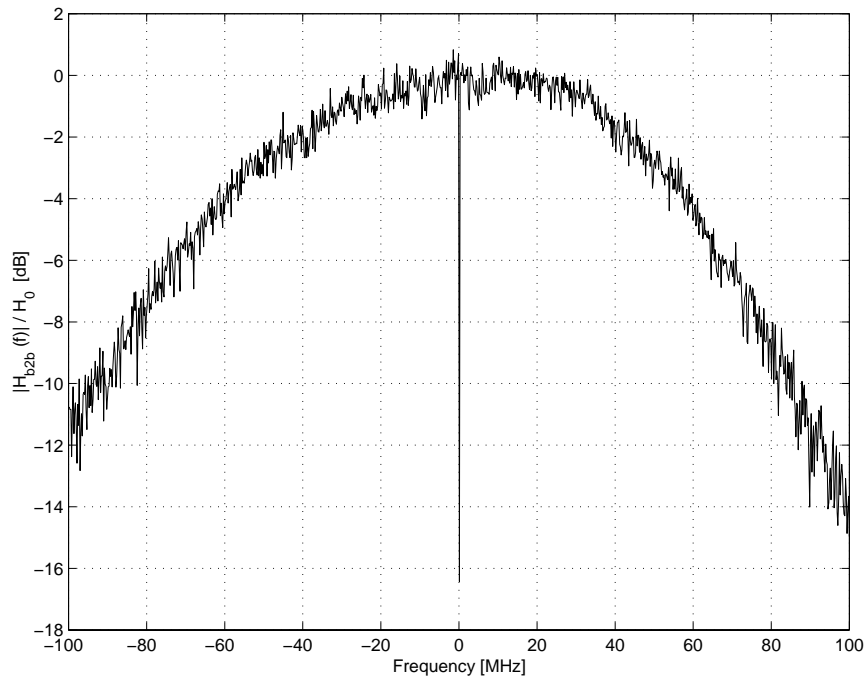
Figure C.5: Normalized magnitude of the back-to-back system transfer function for $|f| < 100$ MHz.

Prior to downsampling, the signal must be lowpass filtered in order to reduce aliasing. A frequency-domain raised cosine filter is applied to the received signal for this purpose. It has to be chosen such that an acceptable compromise among the following demands is obtained:

- the distortion of the signal in the information band ($|f| < 100$ MHz) should be as small as possible,

- aliasing should be reduced as much as possible, and

- the output sequence of the lowpass filter must have an acceptable duration.

The first two points suggest an ideal rectangular filter with a constant passband gain for $|f| < 100$ MHz and zero gain for $|f| > 100$ MHz. However, it is well known that such a filter possesses a very long impulse response. This is not acceptable for the estimated CIR's because it is intended to truncate them without causing a large error. Shorter impulse response lengths can be obtained by allowing a continuous transition between passband and the zero gain range. Generally, the longer and smoother the transition band is, the shorter is the impulse response. For the raised cosine filter, the impulse response length is controlled by the excess bandwidth.

Figure C.5 shows that the attenuation from the measuring system alone is more than 5 dB for frequencies greater than 80 MHz. Moreover, the receive antennas, whose effects are not included in the back-to-back transfer function, cause an additional attenuation at higher frequencies since their 3 dB bandwidth is approximately 120 MHz. Thus, the measurements contain less reliable channel information for frequencies $|f| > 80$ MHz. It is therefore reasonable to sacrifice the channel characteristics beyond 80 MHz.

The frequency response of the raised-cosine lowpass filter is shown in Figure C.6. The constant passband extends from -80 to 80 MHz. The transition range lies between 80 and 120 MHz. Hence, the raised-cosine filter has an excess bandwidth of 20%. After downsampling, identical copies of the low frequency signal will be present at every harmonic of 200 MHz. Thus, aliasing will appear for the frequency range 80 MHz $< |f| < 120$ MHz. However, there is no aliasing for frequencies between -80 and 80 MHz. Furthermore, the lowpass filter does not distort the CTF in this range.
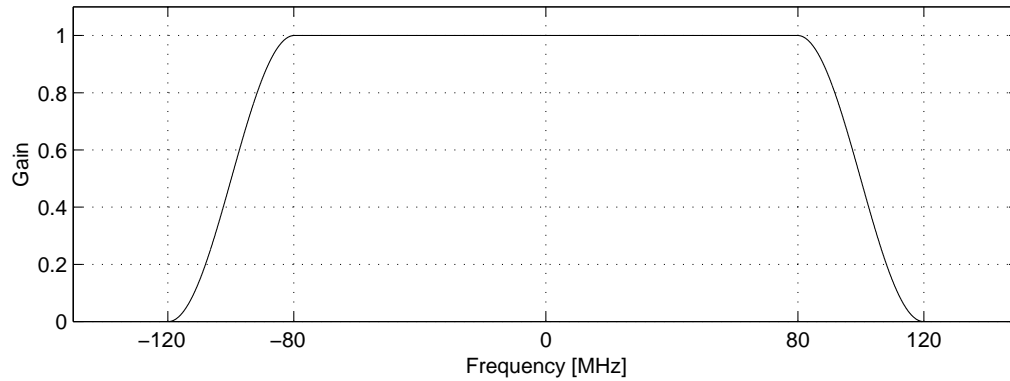
Figure C.6: Gain of the raised cosine lowpass filter.

The characteristics of the lowpass filter in Figure C.6 imply that the measured CTF's should only be used in the frequency range $|f| < 80$ MHz. Figure C.7 shows a back-to-back transfer function calculated with the LSSE method in order to obtain an idea of the error caused by using the CTF's for wideband simulations. If we assume that a signal distortion of at most 3 dB is tolerable, the signals of the simulated system must not exceed a double-sided bandwidth of 120 MHz.
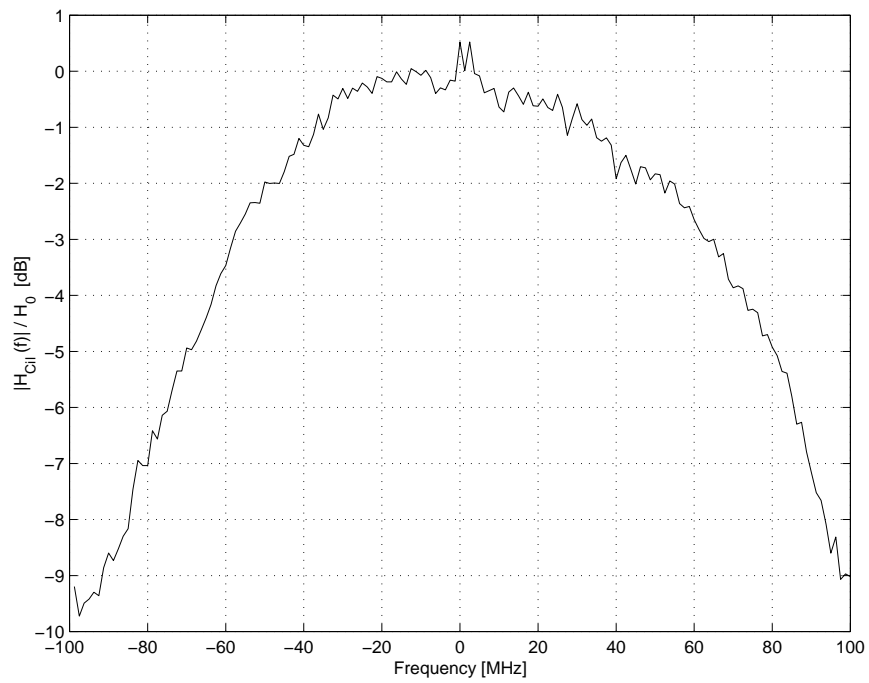
Figure C.7: Normalized Magnitude of a back-to-back transfer function obtained with the LSSE estimation method.

Appendix D

Ideal System: The Matched Filter Bound

D.1 SNR and MMSE

It is very helpful to evaluate the performance of suboptimal detectors in comparison to the results that the optimal receiver achieves under ideal conditions. The optimal performance, also referred to as the *matched filter bound* (MFB), shall be derived here. For this purpose, the system described in Section 2.3 has to be slightly modified. In particular, given the transmitters of the users and the channel characteristics, it is clear that a receiver with arbitrarily chosen lowpass filters $b_C(t)$ will not achieve the optimal performance. Therefore, the matched filter bound (MFB) will be determined based on the signals $r_{Cl}(t)$, $l \in \mathcal{I}_A$, available directly at each antenna element.

Consider a multiuser system defined by the transmitters of the users, the channels, the number of receive antennas, the characteristics of the transmitted data and the noise signals. According to the system model of Section 2.3, the signal received at antenna l can be obtained with Equation (2.34). The block diagram corresponding to these expressions is shown in Figure D.1. The objective is to find the best performance achievable for this system assuming that it is operating under ideal conditions.

A system can be considered "ideal" when it operates in an environment without interference, i.e. in the absence of ISI and CCI. It achieves under these conditions
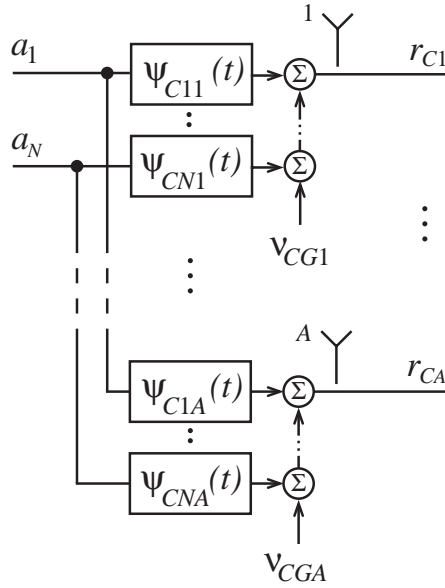
Figure D.1: System block diagram based on the overall channels ψ_{Ckl} which are including transmitters and channels.

the maximal signal-to-noise ratio (SNR)[1] and the minimal error probability of all possible systems with identical channels, transmit and noise signals. The performance of this system expressed in either receiver output SNR or error probability is generally referred to as *matched filter bound*.

The single user, one shot case fulfills the requirement that no interference be present and it has therefore the same performance as the ideal system. Consider that only user k transmits the "one-sample" sequence $a_k[n] = a_{k0}\delta_K[n]$, where $k \in \mathcal{I}_N$. a_{k0} is a random variable that can assume discrete values from the set $\mathcal{A}_k$. It has zero mean and unit variance $E[|a_{k0}|^2] = 1$. It can be shown that the largest SNR is achieved with maximal ratio combining. For that, the signal $r_{Cl}(t)$ received at antenna l ($l \in \mathcal{I}_A$) is applied to a filter $\psi_{Ckl}^*(-t)$ matched to the overall channel waveform (2.33). The output signals of all A matched filters are then summed, sampled at the ideal time $t = 0$ and finally multiplied with a constant gain[2] (see Figure D.2), such that the

---

[1]The SNR is in this case identical to the signal-to-interference-and-noise ratio (SINR) since there is no interference in the system.

[2]The last step of multiplying the combined signal with a constant gain is optional and does not change the output SNR. It is considered here merely to ensure that the signal part of $\tilde{a}_{k0}$ be equal to a_{k0}.

receiver output signal is given by

$$\tilde{a}_{k0} = a_{k0} + \eta \tag{D.1}$$

where η represents the Gaussian noise component. It can immediately be seen from this expression that the output SNR is

$$\text{SNR}_k \triangleq \frac{|a_{k0}|^2}{\sigma_\eta^2} \tag{D.2}$$

where σ_η^2 is the variance of η. On the other hand, the SNR at the output of the k-th matched filter is

$$\text{SNR}_{k,l} = \frac{|a_{k0}|^2}{N_{0,l}} \int_{-\infty}^{\infty} |\psi_{Ckl}(t)|^2 \, dt \tag{D.3}$$

where $N_{0,l}$ is the double-sided power spectral density of the white, complex Gaussian noise signal added to receive antenna l. After combining all A signals, the total SNR is

$$\text{SNR}_k = \sum_{l=1}^{A} \text{SNR}_{k,l}. \tag{D.4}$$

Using the last two expressions for SNR_k and Equation (D.3), one can solve for the Gaussian noise variance and obtain

$$\sigma_\eta^2 = \frac{1}{\sum_{l=1}^{A} \frac{1}{N_{0,l}} \int_{-\infty}^{\infty} |\psi_{Ckl}(t)|^2 \, dt}. \tag{D.5}$$

Let us finally determine the ensemble average of the output SNR for the ideal system. This value is obtained by taking the expectation of the total SNR

$$\Gamma_k \triangleq E\left[\text{SNR}_k\right]. \tag{D.6}$$
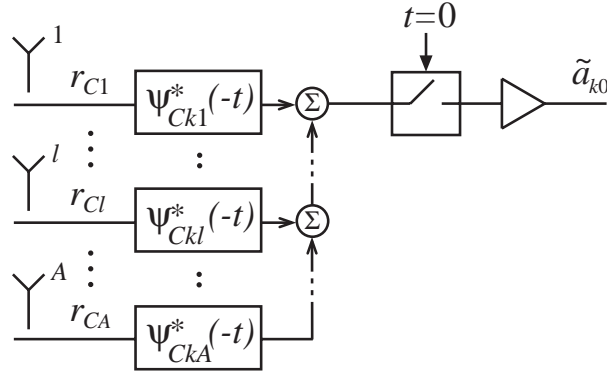
Figure D.2: Maximal ratio combiner.

Using the fact that the variance of the random variable a_{k0} is equal to unity, one gets

$$\Gamma_k = \sum_{l=1}^{A} \frac{1}{N_{0,l}} \int_{-\infty}^{\infty} |\psi_{Ckl}(t)|^2 \ dt. \tag{D.7}$$

Kavehrad and Salz have stated that output SNR and minimal achievable mean-square error of the ideal system are related through a simple expression for the single input case [55]. It can be shown that the same expression is also valid for multiple input receivers (see Section 4.4). In essence, the matched filter bound minimum mean-square error (MFB-MMSE) for user k, $J_{k,\mathrm{mfb}} \triangleq E\left[|\tilde{a}_{k0} - a_{k0}|^2\right]$, is given by

$$J_{k,\mathrm{mfb}} = \frac{1}{1 + \Gamma_k}. \tag{D.8}$$

The quantities Γ_k and $J_{k,\mathrm{mfb}}$ are useful for a comparison to real systems with interference whose measures of performance are the average receiver output signal-to-interference-and-noise ratio (SINR) or the MMSE.

D.2   Error Probability

Consider, as before, a multiuser system with fixed and given transmitters, channels, transmit and noise signals (Figure D.1). The results of this section provide the lowest error probability achievable for this system with an optimal detector under ideal conditions. Ideal conditions mean in this context that there is no interference (ISI or

CCI) present at the receiver input, i.e. only one user transmits a single symbol (one shot case). The received signal is distorted only by Gaussian noise. It is clear that the result obtained for this scenario poses a lower bound on the error probability, called the *matched filter bound*, for any system under practical conditions since interference, if uncorrelated with the signal of interest, can only increase the probability of error.

The ideal system is described in the previous section. An expression for the matched filter bound SNR has been obtained. With that and the fact that the error in the output signal of the ideal detector is Gaussian distributed (no interference present), the error probability can easily be determined. Consider as modulation format *square QAM*, i.e. both the inphase and the quadrature component are pulse amplitude modulated (PAM) with L_k symbols each ($L_k = L_k^{\mathrm{re}} = L_k^{\mathrm{im}}$). The receiver output signal of the ideal system (Equation (D.1))

$$\tilde{a}_{k0} = a_{k0} + \eta$$

consists of the the symbol transmitted, a_{k0}, and a noise component η. It can be divided into a real (inphase) and an imaginary (quadrature) part. For the remainder, only the inphase component will be considered since the error probability of the quadrature signal is, due to the symmetry caused by the square QAM scheme, identical. Let α_{k0}, $\tilde{\alpha}_{k0}$ and η^{re} denote the real parts of a_{k0}, $\tilde{a}_{k0}$ and η, respectively. The inphase output signal of the maximal ratio combiner (Figure D.2), which is the optimal detector for the given scenario, is then

$$\tilde{\alpha}_{k0} = \alpha_{k0} + \eta^{\mathrm{re}}. \tag{D.9}$$

The variance of the inphase Gaussian noise is equal to one half of the variance of the complex Gaussian noise (D.5):

$$E[|\eta^{\mathrm{re}}|^2] = \frac{1}{2}\sigma_\eta^2. \tag{D.10}$$

With the modulation levels chosen as in Equations (2.6), (2.8), the probability of

exceeding the decision threshold in the positive direction becomes

$$
\begin{aligned}
P_{\text{ex},k}^{(\text{mfb})} &= \text{Prob}\left\{ \tilde{\alpha}_{k0} > \alpha_{k0} + \frac{1}{2}\kappa_k \right\} \\
&= \text{Prob}\left\{ \eta^{\text{re}} > \frac{1}{2}\kappa_k \right\} \\
&= Q\left(\sqrt{\frac{\kappa_k^2}{2\sigma_\eta^2}} \right).
\end{aligned}
\tag{D.11}
$$

With $L_k = L_k^{\text{re}} = L_k^{\text{im}}$ and Definition (3.59), Equation (2.12) yields $\kappa_k^2 = 6/(L_k^2 - 1) = 2/\rho(L_k)$. Combining Equations (D.7) and (D.5) results in $\sigma_\eta^2 = 1/\Gamma_k$. After substituting the last two expressions into Equation (D.11), $P_{\text{ex},k}^{(\text{mfb})}$ can be expressed as

$$
P_{\text{ex},k}^{(\text{mfb})} = Q\left(\sqrt{\frac{\Gamma_k}{\rho(L_k)}} \right)
\tag{D.12}
$$

where Γ_k is the signal-to-noise ratio (SNR) at the output of the optimal detector (Equation (D.7)).

Finally, using Gray coding and similar arguments about the error probability for outer and inner modulation levels as in Section 3.2, the matched filter bound bit error rate (BER) is very well approximated by (3.44)

$$
P_{b,k}^{(\text{mfb})} = 2\frac{L_k - 1}{L_k} Q\left(\sqrt{\frac{\Gamma_k}{\rho(L_k)}} \right).
\tag{D.13}
$$

Appendix E

Spectral Correlation of Partitioned Noise Signals

Equation (2.72) is derived in this section.

Per definition, the cross-power spectra of the partitioned noise signals ν_l^m and the sampled noise sequences ν_l are

$$\sigma_{\nu,l}^{uv}(D) \triangleq [\boldsymbol{S}_{\nu,ll}(D)]_{uv} \triangleq E_M \left[\{\nu_l^u(D^{-*})\}^* \nu_l^v(D) \right] \tag{E.1}$$

$$\sigma_{\nu,l}(D) \triangleq E_M \left[\nu_l^*(D^{-*}) \nu_l(D) \right] . \tag{E.2}$$

The corresponding cross-correlation functions are defined by

$$\varrho_{\nu,l}^{uv}[k] \triangleq E \left[\{\nu_l^u[n-k]\}^* \nu_l^v[n] \right] \tag{E.3}$$

$$\varrho_{\nu,l}[k] \triangleq E \left[\nu_l^*[n-k] \nu_l[n] \right] . \tag{E.4}$$

According to Lemma 1.2, cross-correlation functions and cross-power spectra form D-transform pairs, i.e.

$$\varrho_{\nu,l}^{uv}[k] \xleftrightarrow{\mathcal{D}} \sigma_{\nu,l}^{uv}(D) \tag{E.5}$$

$$\varrho_{\nu,l}[k] \xleftrightarrow{\mathcal{D}} \sigma_{\nu,l}(D). \tag{E.6}$$

Evaluating the D-transform on the unit circle, it is easy to show that $\sigma_{\nu,l}^{uv}(e^{-j2\pi\breve{f}})$

and $\sigma_{\nu,l}(e^{-j2\pi \check{f}_s})$ form a discrete-time Fourier transform (DTFT) pair with $\varrho_{\nu,l}^{uv}[k]$ and $\varrho_{\nu,l}[k]$, respectively:

$$\sigma_{\nu,l}^{uv}(e^{-j2\pi \check{f}}) = \mathcal{F}_{dc}\{\varrho_{\nu,l}^{uv}[k]\} \tag{E.7}$$

$$\sigma_{\nu,l}(e^{-j2\pi \check{f}_s}) = \mathcal{F}_{dc}\{\varrho_{\nu,l}[k]\} \tag{E.8}$$

where $\check{f} \triangleq fT$ and $\check{f}_s \triangleq fT_s$ are the normalized frequencies[1].

It can be shown that the cross-power spectrum of the sampled noise is given by

$$\sigma_{\nu,l}(e^{-j2\pi fT_s}) = \frac{N_0}{T_s} \sum_{l=-\infty}^{\infty} \left| B_C\left(f - \frac{l}{T_s}\right) \right|^2. \tag{E.9}$$

Proof. At first, the autocorrelation of ν_l shall be expressed in terms of the receive filter impulse response $b_C(t)$ and the noise power spectral density N_0:

$$
\begin{aligned}
\varrho_{\nu,l}[k] \quad &\triangleq \quad E\left[\nu_l^*[n-k]\nu_l[n]\right] \\
&\overset{\substack{(2.41) \\ (2.38)}}{=} \quad E\left[\int_{-\infty}^{\infty} b_C^*(\tau_1)\nu_{CGl}^*((n-k)T_s - \tau_1)\,d\tau_1 \int_{-\infty}^{\infty} b_C(\tau_2)\nu_{CGl}(nT_s - \tau_2)\,d\tau_2\right] \\
&= \quad \int_{-\infty}^{\infty}\int_{-\infty}^{\infty} b_C^*(\tau_1)b_C(\tau_2)E\left[\nu_{CGl}^*((n-k)T_s - \tau_1)\nu_{CGl}(nT_s - \tau_2)\right]\,d\tau_2\,d\tau_1 \\
&\overset{(2.13)}{=} \quad N_0 \int_{-\infty}^{\infty} b_C^*(\tau_1)b_C(kT_s + \tau_1)\,d\tau_1. \tag{E.10}
\end{aligned}
$$

The cross-power spectrum $\sigma_{\nu,l}(e^{-j2\pi \check{f}_s})$ may be obtained by taking the DTFT of $\varrho_{\nu,l}[k]$:

$$
\begin{aligned}
\sigma_{\nu,l}(e^{-j2\pi \check{f}_s}) \quad &= \quad \sum_{k=-\infty}^{\infty} \varrho_{\nu,l}[k]e^{-j2\pi fT_s k} \\
&\overset{(E.10)}{=} \quad N_0 \int_{-\infty}^{\infty} b_C^*(\tau_1) \sum_{k=-\infty}^{\infty} b_C(kT_s + \tau_1)e^{-j2\pi fT_s k}\,d\tau_1. \tag{E.11}
\end{aligned}
$$

The sequence $b_C(kT_s + \tau_1)$ can be viewed as the sampled lowpass filter impulse response

---

[1]The normalized frequency $\check{f} \triangleq fT$ is used in conjunction with the demultiplexer output signal $\sigma_{\nu,l}^{uv}$ since its sample period is T provided that the data is processed in real time. Accordingly, $\check{f}_s \triangleq fT_s$ is used with the signal $\sigma_{\nu,l}$ because its sample period is T_s.

$b_C(t)$ at the time instants $t = kT_s + \tau_1$. The right hand side of Equation (E.11) contains the DTFT transformation equation for $b_C(kT_s + \tau_1)$. It was found in Section B.2.2 that the DTFT of the sampled sequence is given by (Equation (B.17))

$$\mathcal{F}_{dc}\{b_C(kT_s + \tau_1)\} = \frac{1}{T_s} \sum_{l=-\infty}^{\infty} B_C\left(f - \frac{l}{T_s}\right) e^{j2\pi\left(f - \frac{l}{T_s}\right)\tau_1}.$$

Substituting this relation into Equation (E.11) yields

$$\sigma_{\nu,l}(e^{-j2\pi\check{f}_s}) = \frac{N_0}{T_s} \sum_{l=-\infty}^{\infty} B_C\left(f - \frac{l}{T_s}\right) \int_{-\infty}^{\infty} b_C^*(\tau_1)\, e^{j2\pi\left(f - \frac{l}{T_s}\right)\tau_1}\, d\tau_1$$

$$= \frac{N_0}{T_s} \sum_{l=-\infty}^{\infty} \left| B_C\left(f - \frac{l}{T_s}\right) \right|^2.$$

∎

Consider now the cross-correlation of the partitioned noise signals

$$
\begin{aligned}
\varrho_{\nu,l}^{uv}[k] &\overset{(E.3)}{=} E\left[\{\nu_l^u[n-k]\}^*\nu_l^v[n]\right] \\
&\overset{(2.48)}{=} E\left[\nu_l^*[Kn - Kk + u - 1]\nu_l[Kn + v - 1]\right] \\
&= E\left[\nu_l^*[Kn - Kk + u - v]\nu_l[Kn]\right] \\
&\overset{(E.4)}{=} \varrho_{\nu,l}[Kk + v - u]
\end{aligned}
\tag{E.12}
$$

where the relation $\varrho_{\nu,l}[k] \triangleq E\left[\nu_l^*[n-k]\nu_l[n]\right] = E\left[\nu_l^*[Kn - k]\nu_l[Kn]\right]$ was used. Equation (E.12) shows that the signal $\varrho_{\nu,l}^{uv}[k]$ can be viewed as the output of a K-times downsampler with $\varrho_{\nu,l}[k]$ at the input. Lemma B.2 in Section B.1 shows the D-domain relationship between the input and output signals of the downsampler. This relation may be used to obtain the connection between the noise cross-power spectra $\sigma_{\nu,l}^{uv}(D)$ and $\sigma_{\nu,l}(D)$. According to Lemma B.2 we get

$$\sigma_{\nu,l}^{uv}(D) = \frac{1}{K} \sum_{i=0}^{K-1} \sigma_{\nu,l}\left(D^{\frac{1}{K}} w_K^i\right) \left(D^{\frac{1}{K}} w_K^i\right)^{u-v} \tag{E.13}$$

where $w_K \triangleq e^{-j2\pi/K}$. After evaluating this expression on the unit circle $D = e^{-j2\pi fT}$,

using $T = KT_s$ and applying several substitutions, the final result is

$$\sigma_{\nu,l}^{uv}\left(e^{-j2\pi fT}\right) \quad = \quad \frac{1}{K}\sum_{i=0}^{K-1}\sigma_{\nu,l}\left(e^{-j\frac{2\pi}{K}fT}e^{-j\frac{2\pi}{K}i}\right)\,e^{-j\frac{2\pi}{K}fT(u-v)}e^{-j\frac{2\pi}{K}i(u-v)}$$

$$= \quad \frac{1}{K}\sum_{i=0}^{K-1}\sigma_{\nu,l}\left(e^{-j2\pi\left(f+\frac{i}{T}\right)T_s}\right)\,e^{-j2\pi\left(f+\frac{i}{T}\right)T_s(u-v)}$$

$$\overset{(E.9)}{=} \quad \frac{N_0}{KT_s}\sum_{i=0}^{K-1}\sum_{l=-\infty}^{\infty}\left|B_C\left(f-\frac{Kl-i}{T}\right)\right|^2\,e^{-j2\pi\left(f+\frac{i}{T}\right)T_s(u-v)}$$

$$\overset{m=Kl-i}{=} \quad \frac{N_0}{T}\sum_{m=-\infty}^{\infty}\left|B_C\left(f-\frac{m}{T}\right)\right|^2\,e^{-j\frac{2\pi}{K}(fT-m)(u-v)}$$

where the relationship $e^{-j2\pi(u-v)l} = 1$ (u, v and l are integers) was used. This con-
cludes the proof.

Appendix F

Proof of Lemma 3.1

Let us at first collect some relationships. The Q-function and its first two derivatives are

$$Q(x) \triangleq \frac{1}{\sqrt{2\pi}} \int_x^\infty \exp\left(-\frac{u^2}{2}\right) du \tag{F.1}$$

$$Q'(x) = -\frac{1}{\sqrt{2\pi}} \exp\left(-\frac{x^2}{2}\right) \tag{F.2}$$

$$Q''(x) = \frac{x}{\sqrt{2\pi}} \exp\left(-\frac{x^2}{2}\right). \tag{F.3}$$

Define for convenience

$$e^{\{\}} \triangleq \exp\left\{\frac{1}{2}\mathcal{E}_{z,M}\lambda^2 - \lambda z_0\right\} \tag{F.4}$$

$$\Pi\{\} \triangleq \prod_{k=1}^M \frac{1}{L_k} \frac{\sinh\left(L_k\lambda f_k\right)}{\sinh\left(\lambda f_k\right)}. \tag{F.5}$$

Consider the following relationship

$$\frac{d}{d\lambda} \frac{\sinh\left(L_k\lambda f_k\right)}{\sinh\left(\lambda f_k\right)} = \frac{\sinh(\lambda f_k) L_k f_k \cosh(L_k\lambda f_k) - f_k \cosh(\lambda f_k) \sinh(L_k\lambda f_k)}{\sinh^2(\lambda f_k)}$$

$$= f_k \frac{\sinh(L_k\lambda f_k)}{\sinh(\lambda f_k)} \left[L_k \coth(L_k\lambda f_k) - \coth(\lambda f_k)\right]. \tag{F.6}$$

The derivatives of $e^{\{\}}$ and $\Pi\{\}$ with respect to z_0 are then given by

$$\frac{de^{\{\}}}{dz_0} \overset{(F.4)}{=} e^{\{\}} \left[\frac{d\lambda}{dz_0}(\mathcal{E}_{z,M}\lambda - z_0) - \lambda\right]. \tag{F.7}$$

$$\frac{d\Pi\{\}}{dz_0} \overset{(F.5)}{=} \frac{d\Pi\{\}}{d\lambda}\frac{d\lambda}{dz_0}$$

$$\overset{(F.5)}{=} \sum_{k=1}^{M}\frac{1}{L_k}\frac{d}{d\lambda}\left\{\frac{\sinh(L_k\lambda f_k)}{\sinh(\lambda f_k)}\right\}\prod_{\substack{l=1\\l\neq k}}^{M}\frac{1}{L_k}\frac{\sinh(L_k\lambda f_k)}{\sinh(\lambda f_k)}\frac{d\lambda}{dz_0}$$

$$\overset{(F.6)}{=} \frac{d\lambda}{dz_0}\Pi\{\}\sum_{k=1}^{M}f_k\left[L_k\coth(L_k\lambda f_k) - \coth(\lambda f_k)\right]. \tag{F.8}$$

Using the above quantities, the first derivative of the upper bound $F_1(z_0)$ (Equation (3.99)) with respect to z_0 is expressed by

$$\frac{dF_1(z_0)}{dz_0} \overset{(3.99)}{=} -Q'(f_0 - z_0)e^{\{\}}\Pi\{\} + Q(f_0 - z_0)\frac{de^{\{\}}}{dz_0}\Pi\{\} + Q(f_0 - z_0)e^{\{\}}\frac{d\Pi\{\}}{dz_0}$$

$$\overset{(F.7)}{=} Q(f_0 - z_0)e^{\{\}}\Pi\{\}\left\{-\frac{Q'(f_0 - z_0)}{Q(f_0 - z_0)} + \frac{d\lambda}{dz_0}(\mathcal{E}_{z,M}\lambda - z_0) - \lambda\right.$$

$$\left. + \frac{d\lambda}{dz_0}\sum_{k=1}^{M}f_k\left[L_k\coth(L_k\lambda f_k) - \coth(\lambda f_k)\right]\right\}$$

$$\overset{(3.99)}{=} F_1(z_0)\frac{d\lambda}{dz_0}g(z_0) \tag{F.9}$$

where $g(z_0)$ is defined as

$$g(z_0) \triangleq \mathcal{E}_{z,M}\lambda - z_0 + \sum_{k=1}^{M}f_k\left[L_k\coth(L_k\lambda f_k) - \coth(\lambda f_k)\right]. \tag{F.10}$$

Lemma F.1 (a) *The function $F_1(z_0)$ is always positive, i.e.*

$$F_1(z_0) > 0, \quad \forall z_0 \in \mathbb{R}. \tag{F.11}$$

(b) λ *is always positive, i.e.*

$$\lambda > 0, \quad \forall z_0 \in \mathbb{R}. \tag{F.12}$$

(c) *The derivative $d\lambda/dz_0$ is always negative, i.e.*

$$\frac{d\lambda}{dz_0} < 0, \qquad \forall z_0 \in \mathbb{R}. \tag{F.13}$$

(d) *$g(z_0)$ is a strictly monotonically decreasing function in z_0, i.e.*

$$g(z_0 + \delta z_0) < g(z_0), \qquad \forall \delta z_0 > 0, z_0 \in \mathbb{R}. \tag{F.14}$$

(e) *$g(z_0)$ has exactly one root $\bar{z}_0$, i.e.*

$$g(z_0) = 0, \qquad \text{if and only if } z_0 = \bar{z}_0. \tag{F.15}$$

Proof. (a) The first two terms in the definition of $F_1(z_0)$ in Equation (3.99) are greater than zero since $Q(x)$ and e^x are positive for all $x \in \mathbb{R}$. Additionally, each product term $\sinh(L_k \lambda f_k)/\sinh(\lambda f_k)$ is greater than zero since the hyperbolic sine is an odd function and the arguments of both hyperbolic sines in the above ratio have the same sign. Thus, $F_1(z_0) > 0, \forall z_0 \in \mathbb{R}$, q.e.d.

(b) Note that $Q'(x) = -1/\sqrt{2\pi} \exp\left(-x^2/2\right) < 0, \forall x \in \mathbb{R}$. In addition, $Q(x) > 0, \forall x \in \mathbb{R}$, and it follows that

$$\lambda = -\frac{Q'(f_0 - z_0)}{Q(f_0 - z_0)} > 0, \quad \forall z_0 \in \mathbb{R}, \text{q.e.d.}$$

(c) Comparing Equations (F.2) and (F.3) yields $Q''(x) = -xQ'(x)$ and the ratio of $Q''(f_0 - z_0)$ and $Q(f_0 - z_0)$ may be written as

$$\frac{Q''(f_0 - z_0)}{Q(f_0 - z_0)} = (f_0 - z_0)\lambda \tag{F.16}$$

where λ is defined in Equation (3.96). The first derivative of λ is then

$$\frac{d\lambda}{dz_0} \overset{(3.96)}{=} \frac{Q(f_0 - z_0)Q''(f_0 - z_0) - [Q'(f_0 - z_0)]^2}{[Q(f_0 - z_0)]^2}$$
$$\overset{(F.16)}{=} (f_0 - z_0)\lambda - \lambda^2. \tag{F.17}$$

Proof (b) showed that $Q(x) > 0$ and $Q'(x) < 0$ for all $x \in \mathbb{R}$. Therefore,

$$\frac{-Q'(x)}{Q(x)} > 0 \geq x, \quad \forall x \leq 0. \tag{F.18}$$

For the case $x > 0$, $Q(x)$ may be upper bounded by [45]

$$Q(x) = \frac{1}{2} \operatorname{erfc}\left(\frac{x}{\sqrt{2}}\right) < \frac{1}{\sqrt{2\pi}x} \exp\left(-\frac{x^2}{2}\right), \quad \forall x > 0. \tag{F.19}$$

Using this bound and the expression for $Q'(x)$ in Equation (F.2), it follows that

$$\frac{-Q'(x)}{Q(x)} > \frac{\frac{1}{\sqrt{2\pi}} \exp\left(-\frac{x^2}{2}\right)}{\frac{1}{\sqrt{2\pi}x} \exp\left(-\frac{x^2}{2}\right)} = x, \quad \forall x > 0. \tag{F.20}$$

Combining Equations (F.18) and (F.20) yields

$$-\frac{Q'(x)}{Q(x)} > x, \quad \forall x \in \mathbb{R}. \tag{F.21}$$

Thus, one can obtain

$$\frac{d\lambda}{dz_0} \overset{(F.17)}{=} \lambda\left[(f_0 - z_0) - \lambda\right] \overset{(F.21)}{<} \lambda\left[-\frac{Q'(f_0 - z_0)}{Q(f_0 - z_0)} - \lambda\right] \overset{(3.96)}{=} 0, \quad \forall z_0 \in \mathbb{R}, \text{q.e.d.} \tag{F.22}$$

(d) Taking the first derivative of $g(z_0)$ yields

$$\frac{dg(z_0)}{dz_0} = \frac{d\lambda}{dz_0}\left\{\mathcal{E}_{z,M} + \sum_{k=1}^{M} f_k^2 \left[\frac{1}{\sinh^2(\lambda f_k)} - \frac{L_k^2}{\sinh^2(L_k\lambda f_k)}\right]\right\} - 1. \tag{F.23}$$

It is shown below that (Equation (F.25))

$$\sinh^2(Lx) \geq L^2 \sinh^2(x), \quad \forall L \geq 1 \text{ and } x \in \mathbb{R}.$$

Using this expression, it can easily be shown that each summation term in the rectangular brackets of Equation (F.23) is nonnegative. Since the energy $\mathcal{E}_{z,M}$ (Equation (3.98)) is always positive, the term in the curly brackets is also positive for all

$z_0 \in \mathbb{R}$. According to Lemma 3.1(c), $d\lambda/dz_0 < 0, \forall z_0 \in \mathbb{R}$. Therefore, it follows from Equation (F.23) that

$$\frac{dg(z_0)}{dz_0} < -1, \quad \forall z_0 \in \mathbb{R}. \tag{F.24}$$

In other words, $g(z_0)$ is a strictly monotonically decreasing function, q.e.d.

(e) It is a direct consequence of (d) that $g(z_0)$ has one and only one root $\bar{z}_0$ for which $g(\bar{z}_0) = 0$.

∎

Proposition:

$$\sinh^2(Lx) \geq L^2 \sinh^2(x), \quad \forall L \geq 1 \text{ and } x \in \mathbb{R}. \tag{F.25}$$

Proof. The Taylor series expansion of $\sinh(x)$ is [17]

$$\sinh(x) = \sum_{i=1}^{\infty} \frac{x^{2i-1}}{(2i-1)!}. \tag{F.26}$$

Since the hyperbolic sine is an odd function, it follows that $|\sinh(x)| = \sinh|x|$. With this and the fact that $L \geq 1$, we get

$$|L \sinh(x)| = \sum_{i=1}^{\infty} \frac{L |x|^{2i-1}}{(2i-1)!} \tag{F.27}$$

$$|\sinh(Lx)| = \sum_{i=1}^{\infty} \frac{L^{2i-1} |x|^{2i-1}}{(2i-1)!}. \tag{F.28}$$

From the last two equations follows directly that $|\sinh(Lx)| \geq |L \sinh(x)|$ if $L \geq 1$ and $x \in \mathbb{R}$. Squaring both sides of the inequality yields $\sinh^2(Lx) \geq L^2 \sinh^2(x)$.

∎

Appendix G

Time-Domain Determination of the Optimal MMSE Equalizers

G.1 MIMO Linear Equalizer

The MMSE MIMO LE, $\boldsymbol{C}_{\text{le,mmse}}[n]$, is determined using time-domain analysis and optimization methods. In the first step, the number of non-zero impulse response samples has to be restricted to a finite number M_C. The matrix impulse response can then be written as

$$\boldsymbol{C}[n] = \sum_{m=0}^{M_C-1} \boldsymbol{C}[m]\,\delta_K[n-m] \tag{G.1}$$

where $\delta_K[n]$ is the Kronecker delta sequence (Table A.3). The linear estimate of the equalizer, $\tilde{\boldsymbol{a}}$, is a linear combination of the equalizer coefficients and the input signal samples:

$$\tilde{\boldsymbol{a}}[n] = \sum_{m=0}^{M_C-1} \boldsymbol{y}[n-m]\boldsymbol{C}[m]. \tag{G.2}$$

Let us define the *extended equalizer input vector* and the *extended equalizer coefficient matrix* as

$$\bar{\boldsymbol{y}}[n] \triangleq [\boldsymbol{y}[n - M_C + 1], \boldsymbol{y}[n - M_C + 2], \boldsymbol{y}[n - M_C + 3], \ldots, \boldsymbol{y}[n]] \qquad (G.3)$$

$$\bar{\boldsymbol{C}} \triangleq \begin{bmatrix} \boldsymbol{C}[M_C - 1] \\ \boldsymbol{C}[M_C - 2] \\ \boldsymbol{C}[M_C - 3] \\ \vdots \\ \boldsymbol{C}[0] \end{bmatrix}, \qquad (G.4)$$

respectively. The linear estimate of the equalizer may then be expressed simply in the form

$$\tilde{\boldsymbol{a}}[n] = \bar{\boldsymbol{y}}[n]\bar{\boldsymbol{C}}. \qquad (G.5)$$

In a slight modification of Equation (4.2), define the *linear estimation error*

$$\boldsymbol{e}[n] \triangleq \tilde{\boldsymbol{a}}[n] - \boldsymbol{a}[n - \Delta]. \qquad (G.6)$$

This definition takes the time-delay of the system into account and adjusts the equalizer by comparing the estimate to the symbol transmitted Δ samples before. Δ is a positive integer that has to be chosen such that the equalizer gives the best performance (smallest MMSE) for the preselected number of equalizer coefficients.

The quantities to be minimized are the MSE's J_k defined in Equation (4.10) ($\forall k \in \mathcal{I}_N$). Note that these quantities are equal to the main diagonal elements of the matrix

$$\boldsymbol{R}_e[0] = E\left[\boldsymbol{e}^H[n]\boldsymbol{e}[n]\right] \qquad (G.7)$$

where $\boldsymbol{R}_e[m] \triangleq E\left[\boldsymbol{e}^H[n - m]\boldsymbol{e}[n]\right]$ is the autocorrelation matrix of the linear estimation error. Substituting Equations (G.6) and (G.5) into (G.7) and expanding the

resulting expression yields

$$\boldsymbol{R}_e[0] = \boldsymbol{R}_a[0] - \bar{\boldsymbol{C}}^H \boldsymbol{R}_{\bar{y}a} - \boldsymbol{R}_{\bar{y}a}^H \bar{\boldsymbol{C}} + \bar{\boldsymbol{C}}^H \boldsymbol{R}_{\bar{y}} \bar{\boldsymbol{C}} \qquad \text{(G.8)}$$

where $\boldsymbol{R}_a[0]$ is the autocorrelation of the transmitted data $\boldsymbol{a}$ at time $m = 0$ (Equation (2.64)) and

$$\boldsymbol{R}_{\bar{y}} \triangleq E\left[\bar{\boldsymbol{y}}^H[n]\bar{\boldsymbol{y}}[n]\right] \qquad \text{(G.9)}$$

$$\boldsymbol{R}_{\bar{y}a} \triangleq E\left[\bar{\boldsymbol{y}}^H[n]\boldsymbol{a}[n - \Delta]\right]. \qquad \text{(G.10)}$$

Consider the autocorrelation of the equalizer input signal, $\boldsymbol{R}_y[m]$, and the cross-correlation of the equalizer input signal and the transmitted data, $\boldsymbol{R}_{ya}[m]$, (Equation (2.65))

$$\boldsymbol{R}_y[m] \triangleq E\left[\boldsymbol{y}^H[n - m]\boldsymbol{y}[n]\right] \qquad \text{(G.11)}$$

$$\boldsymbol{R}_{ya}[m] \triangleq E\left[\boldsymbol{y}^H[n - m]\boldsymbol{a}[n]\right]. \qquad \text{(G.12)}$$

These quantities are related to the power and cross-power spectra of Equations (4.27) and (4.28) by the D-transform:

$$\boldsymbol{R}_y[m] \xleftrightarrow{\mathcal{D}} \boldsymbol{S}_y(D) \qquad \text{(G.13)}$$

$$\boldsymbol{R}_{ya}[m] \xleftrightarrow{\mathcal{D}} \boldsymbol{S}_{ya}(D). \qquad \text{(G.14)}$$

Substituting Equation (G.3) into the definitions (G.9) and (G.10), expanding the resulting terms and using expressions (G.11) and (G.12), the matrices $\boldsymbol{R}_{\bar{y}}$ and $\boldsymbol{R}_{\bar{y}a}$

may be expressed in the form

$$
\boldsymbol{R}_{\bar{y}} =
\begin{bmatrix}
\boldsymbol{R}_y[0] & \boldsymbol{R}_y[1] & \boldsymbol{R}_y[2] & \dots & \boldsymbol{R}_y[M_C - 1] \\
\boldsymbol{R}_y[-1] & \boldsymbol{R}_y[0] & \boldsymbol{R}_y[1] & \dots & \boldsymbol{R}_y[M_C - 2] \\
\boldsymbol{R}_y[-2] & \boldsymbol{R}_y[-1] & \boldsymbol{R}_y[0] & \dots & \boldsymbol{R}_y[M_C - 3] \\
\vdots & \vdots & \vdots & \ddots & \vdots \\
\boldsymbol{R}_y[-M_C + 1] & \boldsymbol{R}_y[-M_C + 2] & \boldsymbol{R}_y[-M_C + 3] & \dots & \boldsymbol{R}_y[0]
\end{bmatrix}
\tag{G.15}
$$

$$
\boldsymbol{R}_{\bar{y}a} =
\begin{bmatrix}
\boldsymbol{R}_{ya}[M_C - 1 - \Delta] \\
\boldsymbol{R}_{ya}[M_C - 2 - \Delta] \\
\boldsymbol{R}_{ya}[M_C - 3 - \Delta] \\
\vdots \\
\boldsymbol{R}_{ya}[-\Delta]
\end{bmatrix}.
\tag{G.16}
$$

The correlation matrix $\boldsymbol{R}_{\bar{y}}$ is of size $M_C A K \times M_C A K$. It has a block Toeplitz structure, is Hermitian ($\boldsymbol{R}_{\bar{y}}^H = \boldsymbol{R}_{\bar{y}}$) and is positive semidefinite, which follows directly from Definition (G.9). Moreover, the correlation matrix $\boldsymbol{R}_{\bar{y}}$ is almost always positive definite and therefore regular [46, pp. 102–103].

As mentioned before, the MSE's to be minimized with respect to the equalizer coefficients $\bar{\boldsymbol{C}}$ are the main diagonal elements of the matrix $\boldsymbol{R}_e[0]$. Let us express Equation (G.8) in the equivalent quadratic form

$$
\boldsymbol{R}_e[0] = \boldsymbol{R}_a[0] - \boldsymbol{R}_{\bar{y}a}^H \boldsymbol{R}_{\bar{y}}^{-1} \boldsymbol{R}_{\bar{y}a} + \left[\bar{\boldsymbol{C}} - \boldsymbol{R}_{\bar{y}}^{-1} \boldsymbol{R}_{\bar{y}a} \right]^H \boldsymbol{R}_{\bar{y}} \left[\bar{\boldsymbol{C}} - \boldsymbol{R}_{\bar{y}}^{-1} \boldsymbol{R}_{\bar{y}a} \right]
\tag{G.17}
$$

where it is assumed that $\boldsymbol{R}_{\bar{y}}$ is regular. $\boldsymbol{R}_{\bar{y}}^{-H} = \boldsymbol{R}_{\bar{y}}^{-1}$ is Hermitian because the inverse of a regular Hermitian matrix is also Hermitian [136, pp. 49–50].

As observed before, the matrix $\boldsymbol{R}_{\bar{y}}$ is positive semidefinite and almost always positive definite. Per definition, $\boldsymbol{R}_{\bar{y}}$ will be positive definite if and only if [46, p. 102]

$$
\boldsymbol{\xi}_k \boldsymbol{R}_{\bar{y}} \boldsymbol{\xi}_k^H > 0
\tag{G.18}
$$

for every nonzero row vector $\boldsymbol{\xi}_k$. Let $\boldsymbol{\xi}_k$ be the k-th row of the matrix $\boldsymbol{\Xi}^H$. The quadratic form

$$\boldsymbol{\Xi}^H \bar{\boldsymbol{R}}_y \boldsymbol{\Xi} \tag{G.19}$$

has, for each arbitrary matrix $\boldsymbol{\Xi}$, which is not the null matrix, main diagonal elements greater than zero. Hence, the last term on the right hand side of Equation (G.17),

$$\left[\bar{\boldsymbol{C}} - \boldsymbol{R}_{\bar{y}}^{-1} \boldsymbol{R}_{\bar{y}a}\right]^H \boldsymbol{R}_{\bar{y}} \left[\bar{\boldsymbol{C}} - \boldsymbol{R}_{\bar{y}}^{-1} \boldsymbol{R}_{\bar{y}a}\right],$$

also has main diagonal elements greater than zero unless $[\bar{\boldsymbol{C}} - \boldsymbol{R}_{\bar{y}}^{-1} \boldsymbol{R}_{\bar{y}a}]$ is equal to the null matrix $\boldsymbol{O}_{M_C AK \times N}$. Since all other terms on the right hand side of this equation are constant and do not depend on the equalizer coefficients $\bar{\boldsymbol{C}}$, the main diagonal elements of $\boldsymbol{R}_e[0]$ are minimized for

$$\bar{\boldsymbol{C}}_{\text{le,mmse}} = \boldsymbol{R}_{\bar{y}}^{-1} \boldsymbol{R}_{\bar{y}a} \tag{G.20}$$

in which case the main diagonal elements of the last term are zero and thus minimal. In conjunction with Equation (G.4), the last expression defines the MMSE MIMO LE.

The *minimum mean-square error* (MMSE) performance of the MMSE MIMO LE follows immediately from Equations (4.11), (G.17) and (G.20):

$$J_{k,\text{le,mmse}} = \left[\boldsymbol{R}_a[0] - \boldsymbol{R}_{\bar{y}a}^H \boldsymbol{R}_{\bar{y}}^{-1} \boldsymbol{R}_{\bar{y}a}\right]_{kk}, \quad \forall k \in \mathcal{I}_N. \tag{G.21}$$

G.2 MIMO Decision-Feedback Equalizer

This section describes a time-domain approach to determine the MMSE MIMO C-DFE with optimal finite-length forward and feedback matrix filters. In addition, an expression for the individual MMSE $J_{k,\text{c,mmse}}$ will be given. It is assumed that the lengths of the forward and feedback matrix filters are M_C and M_B ($M_C, M_B \in \mathbb{N}_0$), respectively. According to this and Figure 4.3.1, the continuous-valued estimate $\tilde{\boldsymbol{a}}$

may be expressed as

$$\tilde{\boldsymbol{a}}[n] = \sum_{m=0}^{M_C-1} \boldsymbol{y}[n-m]\boldsymbol{C}[m] + \sum_{m=0}^{M_B-1} \hat{\boldsymbol{a}}[n-m]\boldsymbol{B}[m] \qquad \text{(G.22)}$$

where $\boldsymbol{y}$ is the input signal to the forward matrix filter and $\hat{\boldsymbol{a}}$ are the decisions supplied to the feedback matrix filter. Note that the feedback matrix filter has to be causal, i.e. only previous decisions are available in the feedback loop. However, also a part of the "present" decisions could be used if the decisions for different users are slightly delayed in time [27]. Without loss of generality, we may assume that the decisions are made in the user order, i.e. considering $\tilde{\boldsymbol{a}}[n]$ is the present symbol, the symbol estimate for user 1 ($\tilde{a}_1[n]$) is quantized at first, followed by that of user 2 ($\tilde{a}_2[n]$) and so on until finally the decision element processes $\tilde{a}_N[n]$. By following this procedure, $k-1$ "present" decisions, namely $\hat{a}_1[n], \hat{a}_2[n], \ldots, \hat{a}_{k-1}[n]$, are available to the feedback filter *before* the estimate $\tilde{a}_k[n]$ is quantized by the decision element. However, the decisions $\hat{a}_k[n], \hat{a}_{k+1}[n], \ldots, \hat{a}_N[n]$ cannot be used at this time. This constrains the zeroth feedback coefficient matrix $\boldsymbol{B}[0]$ to be an upper triangular matrix with zeros on the main diagonal.

In order to simplify the analysis, it is desirable to express Equation (G.22) in vector notation. Define the *extended forward input signal* and the *extended feedback input signal*

$$\bar{\boldsymbol{y}}[n] \triangleq [\boldsymbol{y}[n-M_C+1], \boldsymbol{y}[n-M_C+2], \boldsymbol{y}[n-M_C+3], \ldots, \boldsymbol{y}[n]] \qquad \text{(G.23)}$$

$$\bar{\boldsymbol{a}}[n] \triangleq [\hat{\boldsymbol{a}}[n-M_B+1], \hat{\boldsymbol{a}}[n-M_B+2], \hat{\boldsymbol{a}}[n-M_B+3], \ldots, \hat{\boldsymbol{a}}[n]], \qquad \text{(G.24)}$$

respectively. The *total equalizer input signal* is then

$$\boldsymbol{u}[n] \triangleq [\bar{\boldsymbol{y}}[n], \bar{\boldsymbol{a}}[n]]. \qquad \text{(G.25)}$$

Furthermore, the forward and feedback filters are represented by defining

$$\bar{\boldsymbol{C}} \triangleq \begin{bmatrix} \boldsymbol{C}[M_C - 1] \\ \boldsymbol{C}[M_C - 2] \\ \boldsymbol{C}[M_C - 3] \\ \vdots \\ \boldsymbol{C}[0] \end{bmatrix} \tag{G.26}$$

$$\bar{\boldsymbol{B}} \triangleq \begin{bmatrix} \boldsymbol{B}[M_B - 1] \\ \boldsymbol{B}[M_B - 2] \\ \boldsymbol{B}[M_B - 3] \\ \vdots \\ \boldsymbol{B}[0] \end{bmatrix} \tag{G.27}$$

$$\boldsymbol{P} \triangleq \begin{bmatrix} \bar{\boldsymbol{C}} \\ \bar{\boldsymbol{B}} \end{bmatrix} \tag{G.28}$$

where the latter matrix contains all equalizer coefficients (tap weights). It has already been mentioned that $\boldsymbol{B}[0]$ must have zeros on and below the main diagonal. In order to avoid inconvenient constraints in the following vector formulation, one needs to define shortened versions of the input signal and equalizer coefficient vectors:

$$\boldsymbol{u}_k[n] \triangleq [\boldsymbol{u}[n]]_{[1(1)L_k]} \tag{G.29}$$

$$\boldsymbol{p}_k^H \triangleq [\boldsymbol{P}]_{[1(1)L_k],k} \tag{G.30}$$

where L_k is a positive integer number defining the lengths of the above vectors:

$$L_k = M_C AK + M_B N - N + k - 1. \tag{G.31}$$

The vector and matrix functions $[\ldots]_{[f(s)l]}$ and $[\ldots]_{[f(s)l],c}$ are defined in Tables A.3, A.7 and Equation (A.8). Described in words, the row vector $\boldsymbol{u}_k[n]$ is formed by taking the first L_k elements of $\boldsymbol{u}[n]$ (or, equivalently, by taking all elements of $\boldsymbol{u}[n]$ except for the last $N - k + 1$ components). The column vector $\boldsymbol{p}_k^H$ is obtained by taking the

first L_k elements in the k-th column of the matrix $\boldsymbol{P}$ (taking all elements of the k-th column of $\boldsymbol{P}$ except for the last $N - k + 1$ components).

Using the above definitions, the k-th error signal at the input to the decision element can be written as

$$e_k[n] \triangleq \tilde{a}_k[n] - a_k[n - \Delta]$$
$$= \boldsymbol{u}_k[n]\boldsymbol{p}_k^H - a_k[n - \Delta]. \tag{G.32}$$

$\Delta \in \mathbb{N}$ is a constant which takes into account the time-delay introduced by the radio channel and other system elements. The variance of this error signal is identical to the mean-square error (MSE) of the k-th user[1]

$$[\boldsymbol{R}_e[0]]_{kk} \triangleq E\left[e_k^*[n]e_k[n]\right]$$
$$= 1 - \boldsymbol{r}_{au,k}\boldsymbol{p}_k^H - \boldsymbol{p}_k\boldsymbol{r}_{au,k}^H + \boldsymbol{p}_k\boldsymbol{R}_{u,k}\boldsymbol{p}_k^H \tag{G.33}$$

where

$$\boldsymbol{r}_{au,k}^H \triangleq E\left[\boldsymbol{u}_k^H[n]a_k[n - \Delta]\right] \tag{G.34}$$
$$\boldsymbol{R}_{u,k} \triangleq E\left[\boldsymbol{u}_k^H[n]\boldsymbol{u}_k[n]\right]. \tag{G.35}$$

It can easily be shown, [46], that the parameter coefficients which minimize the MSE (G.33) are

$$\boldsymbol{p}_{k,\text{c,mmse}}^H = \boldsymbol{R}_{u,k}^{-1}\boldsymbol{r}_{au,k}^H \tag{G.36}$$

$$\boldsymbol{P}_{\text{c,mmse}} = \begin{bmatrix} \boldsymbol{p}_{1,\text{c,mmse}}^H & \boldsymbol{p}_{2,\text{c,mmse}}^H & \boldsymbol{p}_{3,\text{c,mmse}}^H & \cdots & \boldsymbol{p}_{N,\text{c,mmse}}^H \\ \boldsymbol{0}_N^H & \boldsymbol{0}_{N-1}^H & \boldsymbol{0}_{N-2}^H & \cdots & \boldsymbol{0}_1^H \end{bmatrix} \tag{G.37}$$

where $\boldsymbol{0}_i^H$ is an i-dimensional column vector in which each element is equal to zero (Table A.7). All parameters of the MMSE MIMO C-DFE are contained in the matrix $\boldsymbol{P}_{\text{c,mmse}}$. The optimal forward and feedback filter matrices $\boldsymbol{C}_{\text{c,mmse}}$ and $\boldsymbol{B}_{\text{c,mmse}}$ are

---

[1]The fact that the variance of the data symbols $a_k[n]$ is unity is used in the calculation of Equation (G.33).

found by comparing Equations (G.26), (G.27), (G.28), and (G.37).

The minimum mean-square error (MMSE) can be determined by substituting the optimal values for the equalizer coefficients (G.36) into Equation (G.33). The MMSE of the k-th user is then

$$J_k = 1 - \boldsymbol{r}_{au,k} \boldsymbol{R}_{u,k}^{-1} \boldsymbol{r}_{au,k}^H. \tag{G.38}$$

It is possible to obtain the column vector $\boldsymbol{r}_{au,k}^H$ and the matrix $\boldsymbol{R}_{u,k}$ according to the following relationships:

$$\boldsymbol{r}_{au,k}^H = [\boldsymbol{R}_{ua}]_{[1(1)L_k],k} \tag{G.39}$$

$$\boldsymbol{R}_{u,k} = [\boldsymbol{R}_u]_{[1(1)L_k],[1(1)L_k]}, \tag{G.40}$$

i.e. $\boldsymbol{r}_{au,k}^H$ consists of the first L_k components in the k-th column of the matrix generated by cross-correlating the vectors $\boldsymbol{u}[n]$ and $\boldsymbol{a}[n-\Delta]$; $\boldsymbol{R}_{u,k}$ is a submatrix which comprises the first L_k rows and columns of the autocorrelation matrix $\boldsymbol{R}_u$:

$$\boldsymbol{R}_{ua} \triangleq E\left[\boldsymbol{u}^H[n]\boldsymbol{a}[n-\Delta]\right]$$
$$= \begin{bmatrix} \boldsymbol{R}_{\bar{y}a} \\ \boldsymbol{R}_{\bar{a}a} \end{bmatrix} \tag{G.41}$$

$$\boldsymbol{R}_u \triangleq E\left[\boldsymbol{u}^H[n]\boldsymbol{u}[n]\right]$$
$$= \begin{bmatrix} \boldsymbol{R}_{\bar{y}} & \boldsymbol{R}_{\bar{y}\bar{a}} \\ \boldsymbol{R}_{\bar{y}\bar{a}}^H & \boldsymbol{R}_{\bar{a}} \end{bmatrix}. \tag{G.42}$$

The submatrices used in the above equations are defined by

$$
\boldsymbol{R}_{\bar{y}a} \triangleq E\left[\bar{\boldsymbol{y}}^H[n]\boldsymbol{a}[n-\Delta]\right]
$$

$$
= \begin{bmatrix} \boldsymbol{R}_{ya}[M_C - 1 - \Delta] \\ \boldsymbol{R}_{ya}[M_C - 2 - \Delta] \\ \boldsymbol{R}_{ya}[M_C - 3 - \Delta] \\ \vdots \\ \boldsymbol{R}_{ya}[-\Delta] \end{bmatrix} \tag{G.43}
$$

$$
\boldsymbol{R}_{\bar{a}a} \triangleq E\left[\bar{\boldsymbol{a}}^H[n]\boldsymbol{a}[n-\Delta]\right]
$$

$$
= \begin{bmatrix} \boldsymbol{R}_{\hat{a}a}[M_B - 1 - \Delta] \\ \boldsymbol{R}_{\hat{a}a}[M_B - 2 - \Delta] \\ \boldsymbol{R}_{\hat{a}a}[M_B - 3 - \Delta] \\ \vdots \\ \boldsymbol{R}_{\hat{a}a}[-\Delta] \end{bmatrix} \tag{G.44}
$$

$$
\boldsymbol{R}_{\bar{y}} \triangleq E\left[\bar{\boldsymbol{y}}^H[n]\bar{\boldsymbol{y}}[n]\right]
$$

$$
= \begin{bmatrix} \boldsymbol{R}_y[0] & \boldsymbol{R}_y[1] & \boldsymbol{R}_y[2] & \dots & \boldsymbol{R}_y[M_C - 1] \\ \boldsymbol{R}_y[-1] & \boldsymbol{R}_y[0] & \boldsymbol{R}_y[1] & \dots & \boldsymbol{R}_y[M_C - 2] \\ \boldsymbol{R}_y[-2] & \boldsymbol{R}_y[-1] & \boldsymbol{R}_y[0] & \dots & \boldsymbol{R}_y[M_C - 3] \\ \vdots & \vdots & \vdots & \ddots & \vdots \\ \boldsymbol{R}_y[-M_C + 1] & \boldsymbol{R}_y[-M_C + 2] & \boldsymbol{R}_y[-M_C + 3] & \dots & \boldsymbol{R}_y[0] \end{bmatrix}
$$

$$
\tag{G.45}
$$

$$
\boldsymbol{R}_{\bar{a}} \triangleq E\left[\bar{\boldsymbol{a}}^H[n]\bar{\boldsymbol{a}}[n]\right]
$$

$$
= \begin{bmatrix} \boldsymbol{R}_{\hat{a}}[0] & \boldsymbol{R}_{\hat{a}}[1] & \boldsymbol{R}_{\hat{a}}[2] & \dots & \boldsymbol{R}_{\hat{a}}[M_B - 1] \\ \boldsymbol{R}_{\hat{a}}[-1] & \boldsymbol{R}_{\hat{a}}[0] & \boldsymbol{R}_{\hat{a}}[1] & \dots & \boldsymbol{R}_{\hat{a}}[M_B - 2] \\ \boldsymbol{R}_{\hat{a}}[-2] & \boldsymbol{R}_{\hat{a}}[-1] & \boldsymbol{R}_{\hat{a}}[0] & \dots & \boldsymbol{R}_{\hat{a}}[M_B - 3] \\ \vdots & \vdots & \vdots & \ddots & \vdots \\ \boldsymbol{R}_{\hat{a}}[-M_B + 1] & \boldsymbol{R}_{\hat{a}}[-M_B + 2] & \boldsymbol{R}_{\hat{a}}[-M_B + 3] & \dots & \boldsymbol{R}_{\hat{a}}[0] \end{bmatrix}
$$

$$
\tag{G.46}
$$

$$\boldsymbol{R}_{\bar{y}\bar{a}} \triangleq E\left[\bar{\boldsymbol{y}}^H[n]\bar{\boldsymbol{a}}[n]\right]$$

$$= \begin{bmatrix} \boldsymbol{R}_{y\hat{a}}[M_C - M_B] & \boldsymbol{R}_{y\hat{a}}[M_C - M_B + 1] & \dots & \boldsymbol{R}_{y\hat{a}}[M_C - 1] \\ \boldsymbol{R}_{y\hat{a}}[M_C - M_B - 1] & \boldsymbol{R}_{y\hat{a}}[M_C - M_B] & \dots & \boldsymbol{R}_{y\hat{a}}[M_C - 2] \\ \boldsymbol{R}_{y\hat{a}}[M_C - M_B - 2] & \boldsymbol{R}_{y\hat{a}}[M_C - M_B - 1] & \dots & \boldsymbol{R}_{y\hat{a}}[M_C - 3] \\ \vdots & \vdots & \ddots & \vdots \\ \boldsymbol{R}_{y\hat{a}}[-M_B + 1] & \boldsymbol{R}_{y\hat{a}}[-M_B + 2] & \dots & \boldsymbol{R}_{y\hat{a}}[0] \end{bmatrix}. \quad \text{(G.47)}$$

Finally, the elements in the matrices are matrix samples of the following cross-correlation functions:

$$\boldsymbol{R}_{ya}[m] \triangleq E\left[\boldsymbol{y}^H[n - m]\boldsymbol{a}[n]\right] \tag{G.48}$$

$$\boldsymbol{R}_{\hat{a}a}[m] \triangleq E\left[\hat{\boldsymbol{a}}^H[n - m]\boldsymbol{a}[n]\right] \tag{G.49}$$

$$\boldsymbol{R}_{y}[m] \triangleq E\left[\boldsymbol{y}^H[n - m]\boldsymbol{y}[n]\right] \tag{G.50}$$

$$\boldsymbol{R}_{\hat{a}}[m] \triangleq E\left[\hat{\boldsymbol{a}}^H[n - m]\hat{\boldsymbol{a}}[n]\right] \tag{G.51}$$

$$\boldsymbol{R}_{y\hat{a}}[m] \triangleq E\left[\boldsymbol{y}^H[n - m]\hat{\boldsymbol{a}}[n]\right]. \tag{G.52}$$

In order to be able to calculate the cross-correlations involving past decisions $\hat{\boldsymbol{a}}[n]$ in practice, it is customary to assume that all past decisions are correct, i.e. $\hat{\boldsymbol{a}}[n] = \boldsymbol{a}[n]$, $\forall n \in \mathbb{Z}$. Under this condition, one obtains

$$\boldsymbol{R}_{\hat{a}a}[m] = \boldsymbol{R}_a[m] \triangleq E\left[\boldsymbol{a}^H[n - m]\boldsymbol{a}[n]\right] \tag{G.53}$$

$$\boldsymbol{R}_{\hat{a}}[m] = \boldsymbol{R}_a[m] \tag{G.54}$$

$$\boldsymbol{R}_{y\hat{a}}[m] = \boldsymbol{R}_{ya}[m]. \tag{G.55}$$

Thus, in order to determine the optimal MMSE MIMO C-DFE filters, one only needs to know the autocorrelation functions of the input data $\boldsymbol{a}$, $\boldsymbol{R}_a$, and of the received signal $\boldsymbol{y}$, $\boldsymbol{R}_y$, as well as the cross-correlation function between these two quantities, $\boldsymbol{R}_{ya}$.

Let us finally approximate the number of operations required to determine the

forward and feedback filters. The solution expressed in the relations (G.36) and (G.37) suggests that it is necessary to evaluate the right hand side of Equation (G.36) for all $k \in \mathcal{I}_N$. Since $\boldsymbol{R}_{u,k}$ is a Hermitian $L_k \times L_k$-matrix (Equation (G.35)), an efficient method would be to perform a Cholesky factorization on $\boldsymbol{R}_{u,k}$ and backsubstitute with the elements of $\boldsymbol{r}_{au,k}^H$. However, as will be shown, only one Cholesky factorization is required.

Consider for the N-th user the correlation matrix $\boldsymbol{R}_{u,N}$. After performing a Cholesky factorization, one obtains

$$\boldsymbol{R}_{u,N} = \boldsymbol{U}_N^H \boldsymbol{U}_N \tag{G.56}$$

where $\boldsymbol{U}_N$ is an upper triangular $L_N \times L_N$-matrix. According to Equation (G.40), we note that $\boldsymbol{R}_{u,k}$ is the upper left submatrix of $\boldsymbol{R}_{u,N}$ of dimension $L_k \times L_k$:

$$\boldsymbol{R}_{u,k} = [\boldsymbol{R}_{u,N}]_{[1(1)L_k],[1(1)L_k]}, \quad \forall k \in \mathcal{I}_N. \tag{G.57}$$

It can then easily be shown that the $L_k \times L_k$ upper left submatrix of $\boldsymbol{U}_N$,

$$\boldsymbol{U}_k = [\boldsymbol{U}_N]_{[1(1)L_k],[1(1)L_k]}, \tag{G.58}$$

is the right Cholesky factor of $\boldsymbol{R}_{u,k}$, i.e.

$$\boldsymbol{R}_{u,k} = \boldsymbol{U}_k^H \boldsymbol{U}_k, \quad \forall k \in \mathcal{I}_N. \tag{G.59}$$

Hence, in order to obtain all equalizer parameters $\boldsymbol{p}_{k,c,\text{mmse}}^H$, $\forall k \in \mathcal{I}_N$, we need to perform only one Cholesky factorization, namely for $\boldsymbol{R}_{u,N}$. The Cholesky factors for all other correlation matrices $\boldsymbol{R}_{u,k}$ $(k = 1, 2, \ldots, N-1)$ are obtained simply by partitioning of $\boldsymbol{U}_N$, which does not involve any operations. The equalizer parameters are finally determined from Equation (G.36) by backsubstitution of $\boldsymbol{r}_{au,k}^H$ to the Cholesky factors $\boldsymbol{U}_k^H \boldsymbol{U}_k$ [97]. This results, without taking into account the number of calculations required for the determination of $\boldsymbol{R}_{u,N}$ and $\boldsymbol{r}_{au,k}^H$ $(\forall k \in \mathcal{I}_N)$, in a total

of approximately

$$\frac{1}{6} L_N^3 + \sum_{k=1}^{N} L_k^2 \text{ operations.} \tag{G.60}$$

The unit *operation* (op) has been defined as the combination of one complex multiplication and one complex addition.

Appendix H

Relationship between MMSE and Bias Coefficient

H.1 Relationship for the MMSE MIMO Linear Equalizer

This section provides a proof of Equation (4.129) for the MMSE MIMO LE.

Applying Equations (4.15) to (4.18) and performing a simple manipulation, the total transfer function from the data input to the equalizer output, $\boldsymbol{H}(D)$ (4.117), can be written in the form

$$\boldsymbol{H}(D) = \boldsymbol{I}_N - \boldsymbol{S}_a^{-1}(D)[\boldsymbol{S}_x(D) + \boldsymbol{S}_a^{-1}(D)]^{-1}. \tag{H.1}$$

Since the transmitted data sequences are mutually and temporally uncorrelated with unit variance, the spectrum of the input data is $\boldsymbol{S}_a(D) = \boldsymbol{I}_N$. Combining Equations (4.11) and (4.12), it is clear that the MMSE for user k, J_k, is given by the k-th diagonal element of the matrix

$$\boldsymbol{R}_e[0] = \int_0^1 [\boldsymbol{S}_x(e^{-j2\pi \check{f}}) + \boldsymbol{I}_N]^{-1} \, d\check{f}. \tag{H.2}$$

The bias coefficient may be obtained from the overall system transfer function

$\boldsymbol{H}(D)$. The system impulse response at time $n = 0$ is given by

$$\boldsymbol{H}[0] = \int_0^1 \boldsymbol{H}(e^{-j2\pi\check{f}}) \, d\check{f} \tag{H.3}$$

where $h_{kk}[0] = h_{kk}^{\text{re}}[0] + jh_{kk}^{\text{im}}[0]$ is the k-th diagonal element of $\boldsymbol{H}[0]$. Substituting Equation (H.1) into (H.3) and using (H.2), one obtains

$$\boldsymbol{H}[0] = \boldsymbol{I}_N - \boldsymbol{R}_e[0]. \tag{H.4}$$

The diagonal elements of the cross covariance matrix $\boldsymbol{R}_e[0]$ are real. Thus, all diagonal elements of $\boldsymbol{H}[0]$ are real, i.e. $h_{kk}[0] = h_{kk}^{\text{re}}[0]$. Since the k-th diagonal element of the matrix $\boldsymbol{R}_e[0]$ is equal to the MMSE for user k, it can be concluded that the bias coefficient of the MMSE MIMO LE is

$$h_{kk}^{\text{re}}[0] = 1 - J_{k,\text{le,mmse}}, \quad \forall k \in \mathcal{I}_N. \tag{H.5}$$

H.2 Relationship for the MMSE MIMO Decision-Feedback Equalizer

Equation (4.129) will now be proven for the MMSE MIMO DFE. The MMSE and bias coefficient expressions are identical for both the conventional and noise-predictive DFE's because both structures are completely equivalent. Thus, the C-DFE structure may be considered without loss of generality. The final result applies to both C-DFE and NP-DFE.

Let us again start with the total system transfer function $\boldsymbol{H}(D)$ from the system input to the output of the DFE forward filter (4.117). This equation may be manipulated using the expression for the MMSE MIMO DFE forward filter (4.57), (4.62), Equations (4.18), (4.61) and $\boldsymbol{S}_a(D) = \boldsymbol{I}_N$ in order to obtain

$$\boldsymbol{H}(D) = \boldsymbol{\Psi}(D) - \boldsymbol{\Psi}^{-H}(D^{-*})\boldsymbol{G}. \tag{H.6}$$

The total system impulse response at the time $n = 0$ is then

$$\boldsymbol{H}[0] = \int_0^1 \boldsymbol{H}(e^{-j2\pi \check{f}}) \, d\check{f}$$
$$= \boldsymbol{\Psi}[0] - \boldsymbol{\Omega}[0]\boldsymbol{G}, \tag{H.7}$$

where

$$\boldsymbol{\Omega}[0] \triangleq \int_0^1 [\boldsymbol{\Psi}^H(e^{-j2\pi \check{f}})]^{-1} \, d\check{f}. \tag{H.8}$$

Note that $\boldsymbol{\Psi}(D) = \boldsymbol{\Psi}[0] + \boldsymbol{\Psi}[1]D + \boldsymbol{\Psi}[2]D^2 + \dots$ is causal, and $\boldsymbol{\Psi}[0]$ is an upper triangular matrix with ones on the main diagonal. Thus, $\boldsymbol{\Psi}^H(D^{-*})$ is anticausal and may be written as

$$\boldsymbol{\Psi}^H(D^{-*}) = \boldsymbol{I}_N + \boldsymbol{\Theta}(D), \tag{H.9}$$

where $\boldsymbol{\Theta}(D)$ is also anticausal with a DC-coefficient matrix $\boldsymbol{\Theta}[0]$ that is lower triangular with zeros on the main diagonal. Based on Equation (H.9), the inverse of $\boldsymbol{\Psi}^H(D^{-*})$ can be developed into a series:

$$\left[\boldsymbol{\Psi}^H(D^{-*})\right]^{-1} = \boldsymbol{I}_N + \sum_{\nu=1}^{\infty} (-1)^\nu \boldsymbol{\Theta}^\nu(D). \tag{H.10}$$

Since $\boldsymbol{\Theta}(D)$ is anticausal and has a lower triangular DC-matrix with zeros on the main diagonal, $\boldsymbol{\Theta}^\nu(D) = [\boldsymbol{\Theta}(D)]^\nu$ is also anticausal and has a lower triangular DC-matrix with zeros on the main diagonal. As a result, $[\boldsymbol{\Psi}^H(D^{-*})]^{-1}$ has ones on the main diagonal for all D, and its DC-coefficient matrix $\boldsymbol{\Omega}[0]$ is lower triangular with ones on the main diagonal.

Let us now continue with some observations on Equation (H.7). Firstly, we note that the k-th diagonal element of $\boldsymbol{H}[0]$ is equal to $h_{kk}[0] = h_{kk}^{\text{re}}[0] + jh_{kk}^{\text{im}}[0]$. Secondly, $\boldsymbol{G}$ is a diagonal matrix with real elements. Thirdly, both $\boldsymbol{\Psi}[0]$ and $\boldsymbol{\Omega}[0]$ have ones on

the main diagonal. As a result, $h_{kk}[0]$ is given by

$$h_{kk}[0] = 1 - [\boldsymbol{G}]_{kk} \tag{H.11}$$

where $[\boldsymbol{G}]_{kk}$ is the k-th diagonal element of $\boldsymbol{G}$. Since the right hand side of the above equation is real, one finds $h_{kk}[0] = h_{kk}^{\mathrm{re}}[0]$. It is also known from Equation (4.65) that $[\boldsymbol{G}]_{kk}$ is equal to the MMSE J_k. Thus, the bias coefficient of the MMSE MIMO DFE is given by

$$h_{kk}^{\mathrm{re}}[0] = 1 - J_{k,\mathrm{c,mmse}}, \quad \forall k \in \mathcal{I}_N. \tag{H.12}$$

H.3 Relationship for the ZF MIMO Equalizers

Substituting Equations (4.51), (4.52) into (4.117) and using (4.16), it follows that the total transfer function of the ZF MIMO LE is $\boldsymbol{H}(D) = \boldsymbol{I}_N$. Hence, $\boldsymbol{H}[0] = \int_0^1 \boldsymbol{H}(e^{-j2\pi\check{f}}) \, d\check{f} = \boldsymbol{I}_N$ and the bias coefficients are $h_{kk}^{\mathrm{re}}[0] = 1$, $\forall k \in \mathcal{I}_N$.

For the ZF MIMO C-DFE, one may substitute Equations (4.109), (4.110) into (4.117) and apply (4.16) in order to obtain $\boldsymbol{H}(D) = \boldsymbol{\Psi}_x(D)$. Therefore, $\boldsymbol{H}[0] = \int_0^1 \boldsymbol{H}(e^{-j2\pi\check{f}}) \, d\check{f} = \boldsymbol{\Psi}_x[0]$. According to Section 4.3.3, $\boldsymbol{\Psi}_x[0]$ has ones on the main diagonal and it follows immediately that $h_{kk}^{\mathrm{re}}[0] = 1$, $\forall k \in \mathcal{I}_N$. The same relationship also holds for the ZF MIMO NP-DFE since this structure is equivalent to the C-DFE. In conclusion, the bias coefficients of all ZF MIMO equalizers are equal to unity, i.e.

$$h_{kk}^{\mathrm{re}}[0] = 1, \quad \forall k \in \mathcal{I}_N. \tag{H.13}$$

Appendix I

Algorithm for Matrix Spectral Factorization

The objective of this section is to describe a numerical algorithm which performs the matrix spectral factorization

$$\boldsymbol{Q}(D) = \boldsymbol{\Psi}(D)\boldsymbol{G}^{-1}\boldsymbol{\Psi}^H(D^{-*}) \tag{I.1}$$

under practical considerations such as stability and finite impulse responses. As in previous Chapters 4 and 5, $\boldsymbol{\Psi}(D)$ is a causal and stable $N \times N$ matrix function with $\boldsymbol{\Psi}(D) = \sum_{n=0}^{\infty} \boldsymbol{\Psi}[n]D^n$. $\boldsymbol{\Psi}[0]$ is constrained to be an upper triangular matrix with ones on the main diagonal. $\boldsymbol{G}^{-1}$ is a diagonal $N \times N$ matrix independent on D. If all of the following conditions are met, it will be possible to perform a matrix spectral factorization on the $N \times N$ matrix function $\boldsymbol{Q}(D)$ according to Equation (I.1) [43]:

- $\boldsymbol{Q}(D)$ is Hermitian, i.e. $\boldsymbol{Q}(D) = \boldsymbol{Q}^H(D^{-*})$,

- $\boldsymbol{Q}(D)$ is positive definite on the unit circle $D = e^{-j2\pi\check{f}}$, and

- $\boldsymbol{Q}(e^{-j2\pi\check{f}})$ is in the ring of absolutely convergent Fourier series.

All those conditions can be shown to be fulfilled for the matrix spectrum as defined in Equation (4.18).

Although it is generally possible to factorize $\boldsymbol{Q}(D)$ according to Equation (I.1), it is in most cases very difficult to find the purely causal factor $\boldsymbol{\Psi}(D)$ as polynomial expression in closed-form. Let us, therefore, instead focus on finding a finite impulse response (FIR) approximation[1] $\boldsymbol{\Psi}_{\text{FIR}}(e^{-j2\pi k/L})$ of $\boldsymbol{\Psi}(D)$, where

$$k \in \mathcal{S}_L, \tag{I.2}$$

$$\mathcal{S}_L \triangleq \{0; 1; 2; 3; \dots ; L-1\} \tag{I.3}$$

and L is an odd integer[2], which describes the length (number of samples) of the FIR approximation. Formally, the FIR approximation is obtained by evaluating the matrix functions $\boldsymbol{Q}(D)$ and $\boldsymbol{\Psi}(D)$ on the unit circle $D = e^{-j2\pi\check{f}}$ and then sampling them at L discrete frequencies $\check{f} = k/L, \ \forall k \in \mathcal{S}_L$.

The motivation for applying an FIR approximation is that numerical methods exist that determine $\boldsymbol{\Psi}(e^{-j2\pi k/L})$ given $\boldsymbol{Q}(e^{-j2\pi k/L})$, whereas finding the matrix polynomial $\boldsymbol{\Psi}(D)$ is usually very difficult and may be possible only in special cases. The method is justified because the FIR approximation can be made arbitrarily accurate by increasing the number of samples, L. In fact, in the limit $L \to \infty$, $\boldsymbol{\Psi}_{\text{FIR}}$ and $\boldsymbol{\Psi}$ are identical. Moreover, the FIR approximations of the causal and anticausal factors as well as their inverses are guaranteed to be stable. Thus, instead of solving (I.1), let us concentrate on performing the matrix spectral factorization

$$\boldsymbol{Q}(e^{-j2\pi\frac{k}{L}}) = \boldsymbol{\Psi}_{\text{FIR}}(e^{-j2\pi\frac{k}{L}})\boldsymbol{G}^{-1}\boldsymbol{\Psi}_{\text{FIR}}^{H}(e^{-j2\pi\frac{k}{L}}), \quad \forall k \in \mathcal{S}_L \tag{I.4}$$

where $\boldsymbol{\Psi}_{\text{FIR}}(e^{-j2\pi k/L})$ is a causal matrix sequence ($k \in \mathcal{S}_L$) with $\boldsymbol{\Psi}_{\text{FIR}}(e^{-j2\pi k/L}) = \sum_{n=0}^{(L-1)/2} \boldsymbol{\Psi}_{\text{FIR}}[n]e^{-j2\pi kn/L}$. $\boldsymbol{\Psi}_{\text{FIR}}[0]$ is constrained to be an upper triangular matrix with ones on the main diagonal. $\boldsymbol{G}^{-1}$ is a constant diagonal matrix.

---

[1] In conjunction with frequency-domain functions, the term "FIR approximation" has to be understood in the sense that the inverse Discrete Fourier Series (DFS) of $\boldsymbol{\Psi}_{\text{FIR}}(e^{-j2\pi k/L})$, $\boldsymbol{\Psi}_{\text{FIR}}[n] = \mathcal{F}_{dd}^{-1}\{\boldsymbol{\Psi}_{\text{FIR}}(e^{-j2\pi k/L})\}$, is a FIR matrix filter which approximates the inverse D-transform of $\boldsymbol{\Psi}(D)$, $\boldsymbol{\Psi}[n] = \mathcal{D}^{-1}\{\boldsymbol{\Psi}(D)\}$.

[2] For convenience, L should be an *odd* integer since this simplifies the numerical algorithms described subsequently.

In order to be able to apply the following algorithm, the formulation of the spectral factorization has to be changed slightly. It is easy to show that the matrix spectral factorization (I.4) is identical to

$$\boldsymbol{Q}(e^{-j2\pi\frac{k}{L}}) = \boldsymbol{\Phi}_{\mathrm{FIR}}(e^{-j2\pi\frac{k}{L}})\boldsymbol{W}\boldsymbol{\Phi}_{\mathrm{FIR}}^{H}(e^{-j2\pi\frac{k}{L}}), \quad \forall k \in \mathcal{S}_{L} \tag{I.5}$$

where $\boldsymbol{\Phi}_{\mathrm{FIR}}(e^{-j2\pi k/L})$ is a causal matrix sequence ($k \in \mathcal{S}_{L}$) with $\boldsymbol{\Phi}_{\mathrm{FIR}}(e^{-j2\pi k/L}) = \sum_{n=0}^{(L-1)/2} \boldsymbol{\Phi}_{\mathrm{FIR}}[n]e^{-j2\pi kn/L}$ and $\boldsymbol{\Phi}_{\mathrm{FIR}}[0] = \boldsymbol{I}_{N}$. $\boldsymbol{W}$ is a positive definite, Hermitian matrix. Hence, $\boldsymbol{W}$ can be decomposed via Cholesky factorization into $\boldsymbol{W} = \boldsymbol{J}\boldsymbol{G}^{-1}\boldsymbol{J}^{H}$, where $\boldsymbol{J}$ is an upper triangular matrix with ones on the main diagonal and $\boldsymbol{G}^{-1}$ is a real, diagonal matrix. It can now immediately be seen that the relationship between $\boldsymbol{\Psi}_{\mathrm{FIR}}$ and $\boldsymbol{\Phi}_{\mathrm{FIR}}$ is

$$\boldsymbol{\Psi}_{\mathrm{FIR}}(e^{-j2\pi\frac{k}{L}}) = \boldsymbol{\Phi}_{\mathrm{FIR}}(e^{-j2\pi\frac{k}{L}})\boldsymbol{J}, \quad \forall k \in \mathcal{S}_{L} \tag{I.6}$$

The iterative algorithm by Harris and Davis [43], which numerically performs a matrix spectral factorization (I.5) is described in the following two sections.

Section I.1 outlines the procedure exactly as described by Harris and Davis for a continuous-frequency notation. This formulation can not be computer programmed, however, its presentation is clearer and gives a better overview about the general algorithm. The difference between the equations presented in the next section and the ones of the original publication [43] is that the former are adapted to the notation of this dissertation.

Section I.2 describes the exact procedure for performing the matrix spectral factorization (I.5). This algorithm can be programmed on a digital computer. It has been used to determine all simulation results shown in this thesis which required a spectral factorization.

I.1 Algorithm for Continuous-Frequency Spectra

The objective is to find the causal factor $\boldsymbol{\Phi}(e^{-j2\pi\check{f}})$ of a given $N \times N$ matrix spectrum $\boldsymbol{Q}(e^{-j2\pi\check{f}})$ according to

$$\boldsymbol{Q}(e^{-j2\pi\check{f}}) = \boldsymbol{\Phi}(e^{-j2\pi\check{f}})\boldsymbol{W}\boldsymbol{\Phi}^H(e^{-j2\pi\check{f}}) \tag{I.7}$$

where $\boldsymbol{\Phi}(e^{-j2\pi\check{f}})$ is a causal matrix function with $\boldsymbol{\Phi}(e^{-j2\pi\check{f}}) = \sum_{n=0}^{\infty}\boldsymbol{\Phi}[n]e^{-j2\pi\check{f}n}$ and $\boldsymbol{\Phi}[0] = \boldsymbol{I}_N$. $\boldsymbol{W}$ is a positive definite, Hermitian matrix.

Harris and Davis [43] have described the following algorithm which performs the above matrix spectral factorization. It consists of an initialization step and an iteration that will be stopped if the approximation $\boldsymbol{\Phi}_m(e^{-j2\pi\check{f}})$ in the m-th step satisfies Equation (I.7) with sufficient accuracy. Since all matrix functions are periodic in $\check{f}$ with period 1, all steps have to be performed over the range $0 \leq \check{f} < 1$.

1. **Initialization.**

$$\boldsymbol{\Phi}_0(e^{-j2\pi\check{f}}) = \boldsymbol{I}_N. \tag{I.8}$$

2. **Iteration.** For each iteration, starting with $m = 1$, each of the following steps has to be performed in the order given:

Step 1: Calculate the matrix spectrum

$$\boldsymbol{A}_m(e^{-j2\pi\check{f}}) = \boldsymbol{\Phi}_{m-1}^{-1}(e^{-j2\pi\check{f}})\boldsymbol{Q}(e^{-j2\pi\check{f}})\boldsymbol{\Phi}_{m-1}^{-H}(e^{-j2\pi\check{f}}). \tag{I.9}$$

Step 2: Determine the causal part of $\boldsymbol{A}_m$, $\boldsymbol{A}_m^{0+}(e^{-j2\pi\check{f}})$:

- Perform an inverse Discrete-Time Fourier Transform (DTFT) on $\boldsymbol{A}_m(e^{-j2\pi\check{f}})$

$$\boldsymbol{A}_m[n] = \mathcal{F}_{dc}^{-1}\left\{\boldsymbol{A}_m(e^{-j2\pi\check{f}})\right\} = \int_0^1 \boldsymbol{A}_m(e^{-j2\pi\check{f}})e^{j2\pi\check{f}n}\,d\check{f}. \tag{I.10}$$

- Form the causal sequence $\boldsymbol{A}_m^{0+}[n]$ according to

$$\boldsymbol{A}_m^{0+}[n] = \begin{cases} \boldsymbol{A}_m[n], & \text{for } n \geq 0 \\ 0, & \text{for } n < 0. \end{cases} \tag{I.11}$$

- Perform a DTFT on $\boldsymbol{A}_m^{0+}[n]$

$$\boldsymbol{A}_m^{0+}(e^{-j2\pi\check{f}}) = \mathcal{F}_{dc}\left\{\boldsymbol{A}_m^{0+}[n]\right\} = \sum_{n=-\infty}^{\infty} \boldsymbol{A}_m^{0+}[n]e^{-j2\pi\check{f}n}. \tag{I.12}$$

Step 3: Determine $\boldsymbol{W}_m$ with

$$\boldsymbol{W}_m = \boldsymbol{A}_m[0]. \tag{I.13}$$

Step 4: Calculate the new approximation of the causal factor

$$\boldsymbol{\Phi}_m(e^{-j2\pi\check{f}}) = \boldsymbol{\Phi}_{m-1}(e^{-j2\pi\check{f}})\boldsymbol{A}_m^{0+}(e^{-j2\pi\check{f}})\boldsymbol{W}_m^{-1}. \tag{I.14}$$

Step 5: Determine the accuracy of the latest approximation $\boldsymbol{\Phi}_m(e^{-j2\pi\check{f}})$ and decide whether to stop the algorithm or to continue with another iteration. For this, calculate the error estimate

$$\varepsilon_{\infty,m} = \max_{0 \leq \check{f} < 1}\left\{\frac{1}{N}\left\|\boldsymbol{I}_N - \boldsymbol{Q}^{-1}(e^{-j2\pi\check{f}})\boldsymbol{\Phi}_m(e^{-j2\pi\check{f}})\boldsymbol{W}_m\boldsymbol{\Phi}_m^H(e^{-j2\pi\check{f}})\right\|_{\infty}\right\} \tag{I.15}$$

where $\|\boldsymbol{S}\|_\infty$ is the H_∞-norm of the matrix $\boldsymbol{S}$, i.e. the absolute value of the element of $\boldsymbol{S}$ that has the largest magnitude. If the error estimate $\varepsilon_{\infty,m}$ is smaller than a preselected value $\bar{\varepsilon}_\infty$, the algorithm will be discontinued and $\boldsymbol{\Phi}_m(e^{-j2\pi\check{f}})$ will be taken as sufficiently accurate approximation of the causal factor $\boldsymbol{\Phi}(e^{-j2\pi\check{f}})$. Otherwise, one will increment the step number m by one and proceed with Step 1 for another iteration.

I.2 Algorithm for Discrete-Frequency Spectra

This section describes the version of the algorithm by Harris and Davis which determines an FIR approximation for the causal factor of a matrix spectrum $\boldsymbol{Q}(D)$. The method works with discrete samples in both the time-domain and the frequency-domain. Therefore, it can be directly translated into computer language codes, which makes it useful for simulations.

Consider the given $N \times N$ matrix sequence $\boldsymbol{Q}(e^{-j2\pi k/L})$, which consists of L matrix samples ($k \in \mathcal{S}_L$). It may be directly available or it may be determined by evaluating $\boldsymbol{Q}(D)$ at the discrete points $D = e^{-j2\pi k/L}$. The following algorithm calculates an approximation of the causal factor $\boldsymbol{\Phi}_{\text{FIR}}(e^{-j2\pi k/L})$ ($\forall k \in \mathcal{S}_L$), which is defined by Equation (I.5).

Note that all of the following steps have to be performed for all values $k \in \mathcal{S}_L$.

1. **Initialization.**

$$\boldsymbol{\Phi}_{\text{FIR},0}(e^{-j2\pi \frac{k}{L}}) = \boldsymbol{I}_N. \tag{I.16}$$

2. **Iteration.** For each iteration, starting with $m = 1$, each of the following steps has to be performed in the order given:

Step 1: Calculate the matrix spectrum

$$\boldsymbol{A}_m(e^{-j2\pi \frac{k}{L}}) = \boldsymbol{\Phi}_{\text{FIR},m-1}^{-1}(e^{-j2\pi \frac{k}{L}})\boldsymbol{Q}(e^{-j2\pi \frac{k}{L}})\boldsymbol{\Phi}_{\text{FIR},m-1}^{-H}(e^{-j2\pi \frac{k}{L}}). \tag{I.17}$$

Step 2: Determine the causal part of $\boldsymbol{A}_m$, $\boldsymbol{A}_m^{0+}(e^{-j2\pi k/L})$:

- Perform an inverse Discrete Fourier Series (DFS) on $\boldsymbol{A}_m(e^{-j2\pi k/L})$. Note that this operation may be performed efficiently with an inverse Fast Fourier Transform (IFFT).

$$\boldsymbol{A}_m[n] = \mathcal{F}_{dd}^{-1}\left\{\boldsymbol{A}_m(e^{-j2\pi \frac{k}{L}})\right\} = \frac{1}{L}\sum_{k=0}^{L-1}\boldsymbol{A}_m(e^{-j2\pi \frac{k}{L}})e^{j2\pi \frac{nk}{L}}. \tag{I.18}$$

- Form the causal sequence $\boldsymbol{A}_m^{0+}[n]$ according to

$$\boldsymbol{A}_m^{0+}[n] = \begin{cases} \boldsymbol{A}_m[n], & \text{for } 0 \leq n < \frac{1}{2}(L+1) \\ 0, & \text{for } \frac{1}{2}(L+1) \leq n \leq L-1. \end{cases} \tag{I.19}$$

- Perform a DFS (or an FFT) on $\boldsymbol{A}_m^{0+}[n]$

$$\boldsymbol{A}_m^{0+}(e^{-j2\pi\frac{k}{L}}) = \mathcal{F}_{dd}\left\{\boldsymbol{A}_m^{0+}[n]\right\} = \sum_{n=0}^{L-1} \boldsymbol{A}_m^{0+}[n]e^{-j2\pi\frac{nk}{L}}. \tag{I.20}$$

Step 3: Determine $\boldsymbol{W}_m$ with

$$\boldsymbol{W}_m = \boldsymbol{A}_m[0]. \tag{I.21}$$

Step 4: Calculate the new approximation of the causal factor

$$\boldsymbol{\Phi}_{\mathrm{FIR},m}(e^{-j2\pi\frac{k}{L}}) = \boldsymbol{\Phi}_{\mathrm{FIR},m-1}(e^{-j2\pi\frac{k}{L}})\boldsymbol{A}_m^{0+}(e^{-j2\pi\frac{k}{L}})\boldsymbol{W}_m^{-1}. \tag{I.22}$$

Step 5: Determine the accuracy of the latest approximation $\boldsymbol{\Phi}_{\mathrm{FIR},m}(e^{-j2\pi\frac{k}{L}})$ and decide whether to stop the algorithm or to continue with another iteration. For this, calculate the error estimate

$$\varepsilon_{\infty,m} = \max_{k \in \mathcal{S}_L}\left\{\frac{1}{N}\left\|\boldsymbol{I}_N - \boldsymbol{Q}^{-1}(e^{-j2\pi\frac{k}{L}})\boldsymbol{\Phi}_{\mathrm{FIR},m}(e^{-j2\pi\frac{k}{L}})\boldsymbol{W}_m\boldsymbol{\Phi}_{\mathrm{FIR},m}^H(e^{-j2\pi\frac{k}{L}})\right\|_\infty\right\}. \tag{I.23}$$

where $\|\boldsymbol{S}\|_\infty$ is the H_∞-norm of the matrix $\boldsymbol{S}$, i.e. the absolute value of the element of $\boldsymbol{S}$ that has the largest magnitude. If the error estimate $\varepsilon_{\infty,m}$ is smaller than a preselected value $\bar{\varepsilon}_\infty$, the algorithm will be discontinued and $\boldsymbol{\Phi}_{\mathrm{FIR},m}(e^{-j2\pi k/L})$ will be taken as sufficiently accurate approximation of the causal factor $\boldsymbol{\Phi}_{\mathrm{FIR}}(e^{-j2\pi k/L})$. Otherwise, one will increment the step number m by one and proceed with Step 1 for another iteration.